MARTIN MARIETTA ENERGY SYSTEMS LIBRARIES

3 4456 0356584 4

NUREG/CR-2640
(ORNL/TM-7842)

cy. 44

ornl

OAK
RIDGE
NATIONAL
LABORATORY

UNION
CARBIDE

Facility Description—THTF MOD 3 ORNL PWR BDHT Separate-Effects Program

D. K. Felde
R. L. Durall
D. J. Fraysier
S. S. Gould
E. C. Keith
G. S. Mailen
L. J. Ott
A. G. Sutton
J. E. Wolfe

ORNL INFORMATION DIVISION
TECHNICAL LIBRARY
Document Reference Section
Building 9711-1, Y-12
LOAN COPY ONLY
Do NOT transfer this document to any other person. If you want others to see it, attach their names, return the document, and the Library will arrange the loan as requested.
UCN-1624 (3 12-79)

Prepared for the U.S. Nuclear Regulatory Commission
Office of Nuclear Regulatory Research
Under Interagency Agreements DOE 40-551-75 and 40-552-75

OAK RIDGE NATIONAL LABORATORY
CENTRAL RESEARCH LIBRARY
CIRCULATION SECTION
4500N ROOM 175
LIBRARY LOAN COPY
DO NOT TRANSFER TO ANOTHER PERSON.
If you wish someone else to see this report, send in name with report and the library will arrange a loan.
ORNL-118 (6-97)

OPERATED BY
UNION CARBIDE CORPORATION
FOR THE UNITED STATES
DEPARTMENT OF ENERGY

Printed in the United States of America. Available from
National Technical Information Service
U.S. Department of Commerce
5285 Port Royal Road, Springfield, Virginia 22161

Available from
GPO Sales Program
Division of Technical Information and Document Control
U.S. Nuclear Regulatory Commission
Washington, D.C. 20555

This report was prepared as an account of work sponsored by an agency of the United States Government. Neither the United States Government nor any agency thereof, nor any of their employees, makes any warranty, express or implied, or assumes any legal liability or responsibility for the accuracy, completeness, or usefulness of any information, apparatus, product, or process disclosed, or represents that its use would not infringe privately owned rights. Reference herein to any specific commercial product, process, or service by trade name, trademark, manufacturer, or otherwise, does not necessarily constitute or imply its endorsement, recommendation, or favoring by the United States Government or any agency thereof. The views and opinions of authors expressed herein do not necessarily state or reflect those of the United States Government or any agency thereof.

NUREG/CR-2640
ORNL/TM-7842
Dist. Category AN

Contract No. W-7405-eng-26

Engineering Technology Division

FACILITY DESCRIPTION – THTF MOD 3 ORNL PWR BDHT SEPARATE-EFFECTS PROGRAM

D. K. Felde
R. L. Durall
D. J. Fraysier
S. S. Gould
E. C. Keith
G. S. Mailen
L. J. Ott
A. G. Sutton
J. E. Wolfe

Manuscript Completed – September 17, 1982
Date Published – September 1982

Prepared for the
U.S. Nuclear Regulatory Commission
Office of Nuclear Regulatory Research
Under Interagency Agreements DOE 40-551-75 and 40-552-75

NRC FIN No. B0125

Prepared by the
OAK RIDGE NATIONAL LABORATORY
Oak Ridge, Tennessee 37830
operated by
UNION CARBIDE CORPORATION
for the
DEPARTMENT OF ENERGY

CONTENTS

Page

ACKNOWLEDGMENTS v

LIST OF FIGURES vii

LIST OF TABLES xv

ABSTRACT 1

1. INTRODUCTION 1

2. BASIC SYSTEM DESCRIPTION 3

3. THTF TEST SECTION AND BUNDLE 3 8

3.1 Test Section 8

3.2 Shroud-Box and Fluid Instrumentation 21

3.3 Bundle 3 FRSs 27

3.3.1 FRS radial dimensions and BN densities 34
3.3.2 FRS heating element electrical resistance 35
3.3.3 FRS surface emissivity 36

4. INSTRUMENTED SPOOL PIECES 40

5. TEST-SPECIFIC FACILITY DESCRIPTION 47

5.1 Original Bundle 49

5.1.1 Small-break LOCA-I test series 3.02.10C-H 49

5.2 First Bundle Modification 60

5.2.1 Upflow Film Boiling Test 3.03.6AR 69
5.2.2 Double-Ended Cold-Leg Break Test 3.05.5B 70

5.3 Second Bundle Modification 84

5.3.1 Upflow Film Boiling Test 3.06.6B 102
5.3.2 Steady-State Upflow Film Boiling Test 3.07.9 105
5.3.3 Upflow Film Boiling Test 3.08.6C 123
5.3.4 Small-break LOCA-II test series 3.09.10I-X 124
5.3.5 Intermediate-flow heat transfer test series 3.10.11A-H 126

6. INSTRUMENTATION AND DATA ACQUISITION SYSTEM 141

6.1 Instrumentation 141

6.1.1 Location 141
6.1.2 Sensors 141
6.1.3 Control and sequencing 167

6.2 Data Acquisition 167

6.2.1 Signal conditioning 169
6.2.2 50-Channel thermocouple display and alarm system .. 176
6.2.3 Multichannel analog strip-chart recorders 176
6.2.4 CCDAS 176

Page

6.3 Calibration 180

6.3.1 Pretest calibration 180
6.3.2 Posttest calibration 183
6.3.3 Periodic calibration 183
6.3.4 Special calibrations 184

REFERENCES 185

APPENDIX A. ESSENTIAL FEATURES 189

APPENDIX B. LOCATION AND NOMENCLATURE FOR FLUID THERMOCOUPLES IN THTF BUNDLE 3 229

APPENDIX C. FRS PROPERTY EVALUATION 237

APPENDIX D. INSTRUMENT UNCERTAINTY ANALYSIS FOR THE THTF LOOP 265

ACKNOWLEDGMENTS

In the conduct of a large experimental and analytical program, there are always a great many individuals whose contributions should be recognized. The dedicated efforts of the entire Blowdown Heat Transfer Program staff are reflected in this report. The authors express their sincere appreciation to the following personnel:

- assistance in design and development of electrical, electronics, instrument, and mechanical systems — A. F. Johnson, H. R. Payne, W. Ragan, Jr., R. D. Stulting, and B. J. Veazie
- assistance in design and development of fuel rod simulators — R. E. Dial, W. R. Finnell, R. W. McCulloch, and S. D. Snyder
- assistance in facility operations — R. E. Bohanan and A. N. Smith
- assistance in analysis of experimental system and components — T. M. Anklam, D. H. Cook, W. G. Craddick, R. D. Dabbs, R. C. Hagar, C. R. Hyman, D. G. Morris, C. B. Mullins, J. W. Teague, Jr., R. E. Textor, M. D. White, and G. L. Yoder with computational support from J. L. Bartley, R. M. Flanders, R. H. Greene, D. F. Hunt, D. G. Madewell, J. R. Robinson, and M. S. Thompson
- management support from H. W. Hoffman, F. R. Mynatt, and H. E. Trammell
- particular recognition to J. D. White, Program Manager during most of this activity, and to W. G. Craddick, who subsequently assumed this responsibility
- administrative and clerical support — M. C. Adair and N. R. Raulston

LIST OF FIGURES

Figure		Page
2.1	THTF in standard configuration	4
2.2	Simplified flow diagram of THTF in standard configuration	5
2.3	System line drawing of THTF in standard configuration (lines from rupture disks to PSS are not shown). (Microfiche copy of this drawing attached to back of report.)	6
3.1(a)	THTF test section	9
3.1(b)	Detail of THTF test section (partial). (Microfiche copy of this drawing attached to back of report.)	10
3.1(c)	Detail of THTF test section (partial). (Microfiche copy of this drawing attached to back of report.)	11
3.1(d)	Detail of THTF test section (partial). (Microfiche copy of this drawing attached to back of report.)	12
3.1(e)	Detail of THTF test section (partial). (Microfiche copy of this drawing attached to back of report.)	13
3.2	Detail of inlet plenum manifold. (Microfiche copy of this drawing attached to back of report.)	14
3.3	Detail of test section inlet plenum	15
3.4	Detail of subchannel thermocouple flange. (Microfiche copy of this drawing attached to back of report.)	17
3.5	Detail of shroud support and instrument flange. (Microfiche copy of this drawing attached to back of report.)	18
3.6	Detail of baffle plate assembly. (Microfiche copy of this drawing attached to back of report.)	19
3.7	Detail of volume plug and baffle plate assemblies. (Microfiche copy of this drawing attached to back of report.)	20
3.8	Schematic drawing of low-pressure-drop spacer-grid assembly used in THTF	22

Figure		Page
3.9	Axial location of critical points in THTF test section and Bundle 3	23
3.10	Location of fluid thermocouples in THTF Bundle 3	24
3.11	Subchannel thermocouple flange	25
3.12	Identification of THTF heater rods, subchannel locations, and instrument rods in THTF Bundle 3	26
3.13	Detail of thermocouple-array rod	27
3.14	Axial location of 19 sensing elements in INEL liquid level rod	28
3.15	Identification of THTF heater rods and axial thermocouple levels monitored by each rod in THTF Bundle 3	29
3.16	Cross section of THTF Bundle 3 FRS	30
3.17	Location of thermocouples in THTF Bundle 3	31
3.18	Special thermocouple locations in THTF Bundle 3	32
3.19	Example of FRS thermocouple nomenclature	33
3.20	Heated length electrical resistance for FRS-058B	36
4.1	Location and identification of instrumented spool pieces in THTF standard configuration	41
4.2	Original THTF spool-piece design (spool pieces SHI, SVI, SHO, and SVO in standard THTF configuration)	42
4.3	Recent spool-piece design (spool pieces BI1, BI2, and BO1 in standard THTF configuration). (Microfiche copy of this drawing attached to back of report.)	43
4.4	Turbine meter assembly (Flow Technology)	44
4.5	Appearance of three-bladed drag target in pipe	45
4.6	Diagram showing uniform density regions used in annular model for reduction of three-beam densitometer data	46
5.1	Location and identification of Metrascope thermocouples used for operational monitoring purposes	52
5.2	Small-break LOCA-I test configuration (3.02.10C-H)	53

Figure		Page
5.3	System line drawing of THTF in small-break LOCA-I test configuration. (Microfiche copy of this drawing attached to back of report.)	55
5.4	Test section pressure and differential pressure measurement locations for the small-break LOCA-I (3.02.10C-H) test series	56
5.5	Instrument application drawing for Test 3.02.10C-H	58
5.6	Identification of THTF heater rods, subchannel locations, and instrument rods in refurbished THTF Bundle 3 (March-July 1980)	61
5.7	Identification of THTF heater rods and axial thermocouple levels monitored by each rod in refurbished THTF Bundle 3 (March-July 1980)	62
5.8	Location of thermocouples in refurbished THTF Bundle 3 (March-July 1980)	63
5.9	Special thermocouple locations in refurbished THTF Bundle 3 (March-July 1980)	64
5.10	Location of fluid thermocouples in refurbished THTF Bundle 3 (March-July 1980)	66
5.11	(a) Axial location of pressure taps along THTF test section following first modification to bundle; (b) differential pressure measurement arrangement	67
5.12	Detail of construction of new pressure taps along test section	68
5.13	Schematic of special 2-in. spool piece used on external downcomer for upflow film boiling tests	71
5.14	THTF configuration for Test 3.03.6AR	72
5.15	Test section pressure and differential pressure instrumentation for Test 3.03.6AR	73
5.16	Instrument application drawings for Test 3.03.6AR	76
5.17	THTF configuration for Test 3.05.5B (standard configuration)	79
5.18	Test section pressure and differential pressure instrumentation for Test 3.05.5B	80

Figure		Page
5.19	Instrument application drawings for Test 3.05.5B	81
5.20	Identification of THTF heater rods, subchannel locations, and instrument rods in the modified Bundle 3 (August 1980 to present)	88
5.21	Identification of THTF heater rods and axial thermocouple levels monitored by each rod in the modified THTF Bundle 3 (August 1980 to present)	89
5.22	Schematic showing new thermocouple levels between primary levels E and G in modified THTF Bundle 3 (August 1980 to present)	90
5.23	Location of primary FRS thermocouples in modified THTF Bundle 3 (August 1980 to present)	91
5.24	Location of special FRS thermocouples (between primary levels F and G) in modified THTF Bundle 3 (August 1980 to present)	92
5.25	Location of special FRS thermocouples (between primary levels E and F) in modified THTF Bundle 3 (August 1980 to present)	93
5.26	Location of fluid thermocouples in modified THTF Bundle 3 (August 1980 to present)	96
5.27	Detail of new thermocouple-array rod	98
5.28	Schematic diagram of shroud-wall thermocouple locations ..	99
5.29	Detail of shroud-wall thermocouple assembly	100
5.30	Schematic diagram of the in-bundle gamma densitometer system	103
5.31	Detail of the in-bundle gamma densitometer source-detector radial geometry	104
5.32	THTF configuration for Test 3.06.6B	106
5.33	Test section pressure and differential pressure instrumentation for Test 3.06.6B	107
5.34	Instrument application drawings for Test 3.06.6B	111
5.35	THTF configuration for test series 3.07.9 and Test 3.08.6C	115

Figure		Page
5.36	Test section pressure and differential pressure instrumentation for test series 3.07.9 and Test 3.08.6C	116
5.37	Instrument application drawings for test series 3.07.9 and Test 3.08.6C	120
5.38	THTF configuration for test series 3.09.10I-X	127
5.39	System line drawing of the THTF in the small-break LOCA-II test configuration (test series 3.09.10I-X). (Microfiche copy of this drawing attached to back of report.)	128
5.40	Test section pressure and differential pressure instrumentation for test series 3.09.10I-X	129
5.41	Instrument application drawings for test series 3.09.10I-X	132
5.42	THTF configuration for test series 3.10.11A-H	134
5.43	Test section pressure and differential pressure instrumentation for test series 3.10.11A-H	135
5.44	Instrument application diagrams for test series 3.10.11A-H	138
6.1	Physical instrument hardware locations for primary piping system and test section in standard configuration. (Microfiche copy of this drawing attached to back of report.)	142
6.2	Physical instrument hardware locations for primary piping system and test section in standard configuration. (Microfiche copy of this drawing attached to back of report.)	143
6.3	Physical instrument hardware locations for primary piping system and test section in standard configuration. (Microfiche copy of this drawing attached to back of report.)	144
6.4	Physical instrument hardware locations for primary piping system and test section in standard configuration. (Microfiche copy of this drawing attached to back of report.)	145

Figure		Page
6.5	Physical instrument hardware locations for primary piping system and test section in standard configuration. (Microfiche copy of this drawing attached to back of report.)	146
6.6	Physical instrument hardware locations for primary piping system and test section in standard configuration. (Microfiche copy of this drawing attached to back of report.)	147
6.7	Physical instrument hardware locations for primary piping system and test section in standard configuration. (Microfiche copy of this drawing attached to back of report.)	148
6.8	Schematic diagram of the THTF data acquisition system (CCDAS)	168
6.9	Block diagram of CCDAS	177
A.1	Plan view of basement area of THTF	190
A.2	Plan view of first floor area of THTF	191
A.3	Schematic of THTF pressurizer	194
A.4	Critical flow nozzle and listing of available orifice sizes	201
A.5	Arrangement (out of system) of critical flow nozzle and rupture disk assembly	202
A.6	Rupture disks following a blowdown (end view)	203
A.7	Graham Heliflow heat exchanger	204
A.8	Bingham pump characteristics	208
A.9	THTF two-stage Bingham pump	209
A.10	Schematic of THTF fluid makeup system	210
A.11	THTF dc power system schematic. (Microfiche copy of this drawing attached to back of report.)	212
A.12	Identification of generator power supply distribution in THTF Bundle 3	213
A.13	Axial view of FRS and FRS dc power connections	215

Figure		Page
A.14	Identification of dc power lead-in length codes for THTF Bundle 3	216
A.15	Tabulation of FRS lead-in length code	216
A.16	FRS micarta sheet spacers	217
A.17	Detail of seal cooling systems. (Microfiche copy of this drawing attached to back of report.)	219
B.1	Location of fluid thermocouples in THTF Bundle 3	230
B.2	Subchannel thermocouples	231
B.3	Spacer-grid thermocouples	232
B.4	Typical installation of a shroud-box thermocouple	233
B.5	Shroud-box and thermocouple-array rod thermocouples	235
B.6	Cross section of thermocouple array rod illustrating protrusion of thermocouples from the rod	236
C.1	Cross section of THTF Bundle 3 FRS	237
C.2	Cross section of THTF Bundle 3 FRS with directional changes in the sublayer interfaces (uncycled FRS → cycled FRS)	241
C.3	Photograph of typical cross section of FRS-058B	241
C.4	ACA resistance measurement circuit	244
C.5	ACA resistance vs temperature for entire ACA of FRS-058B	245
C.6	ACA resistance vs temperature for entire ACA of FRS-058B (ACA heated by ramping sheath)	246
C.7	ACA resistance vs temperature for heated section of FRS-058B	247
C.8	ACA resistance vs temperature for heated section of FRS-058B	250
C.9	Inconel-600 electrical resistivity comparison	251
C.10	Inconel-600 electrical resistivity comparison	252

Figure		Page
C.11	FRS-058B heated length electrical resistance	253
C.12	FRS-058B terminal end electrical resistance	254
C.13	Circuit used in FRS emissivity determination	256
C.14	Free convection film heat transfer coefficient as a function of rod temperature	257
C.15	Heat generation in the heated length of FRS-026 (unpainted)	258
C.16	Heat generation in the heated length of FRS-026 (painted with Krylon paint, $\varepsilon \sim 0.98$ at >475 K)	259
C.17	Heat generation in the heated length of FRS-026 (painted with Deshler paint, $\varepsilon \sim 0.92$ at ~670 K)	260
C.18	Emissivity of FRS-026 surface after removal from the THTF	262
D.1	Amplifier	267
D.2	Generalized form for a large system	271
D.3	Error due to turbine linearity: characteristic curve	273
D.4	Typical densitometer calibration	276
D.5	Sensitivity calibration	281
D.6	Zero offset calibration	281
D.7	PDE-200 output from Test 101	282
D.8	Rod power schematic	285
D.9	Instrument reading as a function of response time assuming first-order lag	288
D.10	Instrument error as a function of DAS sampling assuming first-order lag	289

LIST OF TABLES

Table		Page
2.1	Summary of THTF design data	7
3.1	Internal dimensions and boron nitride densities of Bundle 3 FRSs (for the original and refurbished bundles)	34
3.2	Actual heated lengths and correction factor, β_i, for determining heating element electrical resistance for THTF FRSs	37
5.1	Summary of THTF Bundle 3 operating history	48
5.2	In-service thermocouple listing for original Bundle 3	50
5.3	Small-break LOCA test series summary	51
5.4	Primary flow instrumentation for Test 3.02.10C-H	57
5.5	In-service thermocouple listing for refurbished THTF Bundle 3 (March-July 1980)	65
5.6	THTF upflow film boiling data ranges — Test 3.03.6AR	69
5.7	Initial conditions for Test 3.03.6AR	70
5.8	Primary flow instrumentation for Test 3.03.6AR	74
5.9	Initial conditions for Test 3.05.5B	84
5.10	Primary flow instrumentation for Test 3.05.5B	85
5.11	Naming convention for super-level FRS thermocouples	94
5.12	In-service thermocouple listing for modified THTF Bundle 3 (August 1980)	95
5.13	Location of shroud-wall thermocouples relative to the core side of the shroud	101
5.14	Initial conditions for Test 3.06.6B	104
5.15	THTF upflow film boiling data ranges — Test 3.06.6B	105
5.16	Primary flow instrumentation for Test 3.06.6B	108
5.17	THTF steady-state upflow film boiling data ranges, test series 3.07.9a (a = test letter)	114

Table		Page
5.18	Primary flow instrumentation for test series 3.07.9 and 3.08.6C	117
5.19	Initial conditions for Test 3.08.6C	123
5.20	THTF upflow film boiling data ranges – Test 3.08.6C	123
5.21	THTF transient boiloff tests, November 1980 (preliminary)	125
5.22	THTF steady-state bundle uncovery tests, November 1980	126
5.23	THTF reflood tests, November 1980 (preliminary)	126
5.24	Primary flow instrumentation for test series 3.09.10I-X	130
5.25	Primary flow instrumentation for test series 3.10.11A-H	136
6.1	Primary loop instrumentation providing bounding condition measurements	149
6.2	THTF sensor description	151
6.3	Data sensor locations and systems characteristics	154
6.4	Detail of THTF primary instrumentation signal path-sensor to CCDAS	170
6.5	CCDAS subsystems and peripherals	178
6.6	Instrument calibration/verification intervals	181
A.1	Pressure-suppression tank characteristics	198
A.2	Spray circulation pump characteristics	199
A.3	PSS heat exchanger characteristics (Young No. SSF-606-ER-1P)	200
A.4	Specified operating and design characteristics of primary heat exchangers (Graham Heliflow No. 12-6C6C-225)	206
A.5	Specified operating and design characteristics of pump bypass heat exchanger (Graham Heliflow No. 9-6C6C-14S)	207
A.6	Tabulation of THTF heater rods and generators	213

Table		Page
A.7	Codes and standards applied to THTF	222
C.1	Bundle 3 FRS sublayer radii and thicknesses	238
C.2	Bundle 3 FRS sublayer radius and thickness uncertainties (1 standard deviation)	239
C.3	Stability statistics for loop-cycled rods	239
C.4	Cycled Bundle 3 FRS sublayer radii and thicknesses	240
C.5	Cycled Bundle 3 FRS sublayer radius and thickness uncertainties (1 standard deviation)	240
C.6	Internal dimensions and boron nitride densities of Bundle 3 FRSs (for the original and refurbished bundles)	243
D.1	Absolute error analysis	275
D.2	Least-squares best-fit line (RHO = A x DERHO + B)	276
D.3		289
D.4	Type code — Instrument Application Number Table	291
D.5	THTF instrument uncertainties — (nominal transient step function for Test 3.06.6B) (SI units)	296
D.6	THTF instrument uncertainties — (nominal transient step function for Test 3.06.6B) (English units)	303
D.7	THTF instrument uncertainties — (worst-case transient step function for Test 3.06.6B) (SI units)	310
D.8	THTF instrument uncertainties — (worst-case transient step function for Test 3.06.6B) (English units)	317

FACILITY DESCRIPTION – THTF MOD 3 ORNL PWR BDHT SEPARATE-EFFECTS PROGRAM

D. K. Felde
R. L. Durall D. J. Fraysier
S. S. Gould E. C. Keith
G. S. Mailen L. J. Ott
A. G. Sutton J. E. Wolfe

ABSTRACT

This report describes the Thermal-Hydraulic Test Facility (THTF) as modified for tests with Bundle 3, a 64-rod bundle of indirectly electrically heated fuel rod simulators. The report provides a description of the basic facility and instrumentation as well as a test-specific facility description for each of the primary tests run at the THTF during the operational period from June 1979 to February 1981. The primary tests include the Small-Break Loss-of-Coolant Accident (LOCA)-I Test Series (3.02.10C-H), the transient Upflow Film Boiling Tests (3.03.6AR, 3.06.6B, 3.08.6C), the Steady-State Upflow Film Boiling Test Series (3.07.9-), the Double-Ended Cold-Leg Break Test (3.05.5B), the Small-Break LOCA-II Test Series (3.09.10I-X), and the Intermediate-Flow Heat Transfer Test Series (3.10.11A-H). Two major modifications made to the bundle and test section over this period are also described.

1. INTRODUCTION

The Thermal-Hydraulic Test Facility (THTF) is a 7.5-MW(e) nonnuclear separate-effects test facility designed to provide thermal-hydraulic experimental data from an indirectly electrically heated fuel rod simulator (FRS) bundle over a wide range of hypothetical pressurized-water reactor (PWR) accident conditions. This report describes the facility and instrumentation systems that existed during the operational history of Bundle 3, from its installation in June 1979 to the final test run in February 1981.

The facility includes (1) a closed, recirculating, primary loop capable of providing a wide range of thermal-hydraulic operating conditions to the test section; (2) instrumentation, controls, and a computer-controlled data acquisition system (CCDAS) necessary for loop operation and test data analysis; (3) test section power supply up to 7.5 MW(e); and (4) a primary fluid blowdown system with pressure suppression. Because the THTF is primarily a separate-effects test facility, the loop components and primary piping system are designed to provide a range of mass flux, pressures, and temperatures of interest to the test section. Primary emphasis for instrumentation is focused on the test section, bundle, and test section boundary conditions. The approach taken in describing the facility follows the same reasoning.

Chapter 2 describes the basic system in the "standard" configuration as it was when Bundle 3 was initially installed. The test section and Bundle 3, as it was initially installed, are described in detail in Chap. 3. Chapter 4 describes the instrumented spool pieces that provide flow, pressure, and temperature measurements at the boundaries of the test section.

During the operating history of Bundle 3, major modifications were made to the test section, bundle, and loop piping. These changes were necessitated by both test-specific instrumentation and operational requirements in meeting test goals, as well as by a system component failure in one case (FRS O-ring seal assembly failure). Because significant modifications were made from test to test, test-specific facility and instrumentation descriptions for the primary tests run at the THTF are presented in Chap. 5. The two major modifications to the bundle and test section are described in detail in Chap. 5 with the test-specific facility descriptions subgrouped under the corresponding bundle and test section descriptions.

The instrumentation and CCDAS for the THTF are described in detail in Chap. 6. An uncertainty analysis for the instrumentation is presented in Appendix D.

Other appendices are included that provide additional detailed information on the system. Appendix A describes some of the primary "loop-side" components in greater detail than were discussed in Chap. 2. There is also a discussion of the protective features and quality assurance methods used in the operation and construction of the facility. Appendix B describes the nomenclature used for the fluid thermocouples in the bundle. Appendix C describes the methods by which some of the FRS physical properties were obtained.

A note on the figures and dimensions used in the report is appropriate at this time. The attempt was made wherever possible to provide SI units. Many of the figures used in this description, however, are photographs of engineering drawings that were in English units. It was not deemed necessary or practical to change the engineering drawings. Also, reductions of some engineering drawings were included in the main body of the report. Details on some of these drawings, however, are difficult to distinguish in the reduced form. For this reason, microfiche copies of figures noted in the main body are attached to the back cover of the report.

Some care should also be taken in using figures describing axial locations along the test section. The datum point established along the test section may vary depending on the source and typical use of the information.

2. BASIC SYSTEM DESCRIPTION

The THTF is a reasonably large nonnuclear test facility having a wide range of capabilities for thermal-hydraulic tests using electrical resistance heaters in a multirod geometry. The facility described in this report contains Bundle 3, an 8 x 8 array of 3.66-m (12-ft) heated length, 0.950-cm-diam (0.374-in.) indirectly electrically heated rods with a flat power profile. Four of the 64 rod positions in the array are occupied by unpowered instrument rods [1.02-cm diam (0.401 in.)]. Except for the solid bounding walls (shroud-box walls) surrounding the bundle, the 1.273-cm (0.501-in.) pitch array is dimensionally typical of late generation 17 x 17 PWR bundles. The bundle is mounted in a vertical test section and cooled by demineralized water with normal steady-state flow upward through the bundle. The all stainless steel primary piping system and pressurized water-cooled test section is designed for nominal subcooled operating temperatures, pressures, and flow rates of up to 616 K (1110°R), 17,200 kPa (2500 psig), and 3.8 x 10^{-2} m^3/s (600 gpm), respectively. The THTF is shown schematically in Fig. 2.1 and in the simplified flow diagram of Fig. 2.2.

The cooling water is circulated by a high-head high-capacity pump designed for a constant output of ~4.42 x 10^{-2} m^3/s (700 gpm) with a developed head of ~590 m (1940 ft). Fluid discharged from the pump flows through two control valves where excess pump head is dissipated and flow to the test section is adjusted by diverting a portion through the pump bypass line. Heat transferred to the coolant by the pump (600 hp) is removed by a small Graham "Heliflow" heat exchanger (Hx D) in the pump bypass line.

In the standard THTF configuration, flow conditions at the inlet and outlet boundaries of the test section are measured by "instrumented spool pieces." Four inlet and three outlet instrumented spool pieces are installed to provide both redundancy of measurements and measurements on both sides of the system rupture locations. The spool-piece instruments are designed to measure volumetric flow rate, average fluid density, momentum flux, fluid temperature, and pressure. The instrumented spool pieces are described in more detail in Chap. 4. During steady-state operation, primary flow passes through the inlet spool pieces, including the two installed on the external downcomer, through the inlet manifold, and enters the test section at the lower inlet plenum. Fluid flows upward through the bundle into the test section upper outlet plenum and then out of the test section and through the three outlet spool pieces. The energy added to the fluid by the bundle heater rods is removed by three Graham Heliflow heat exchangers (Hx A, Hx B, and Hx C), each having a rated capacity of 2.5 MW(t). Upon exit from the heat exchangers, the fluid returns to the pump suction.

A pressurizer is tied into the hot leg of the primary loop between the test section outlet spool pieces and the heat exchangers. With its 49 kW(e) of independent heat input, the pressurizer provides the primary pressure control for the loop while also serving as a surge tank for up to ~0.212 m^3 (7.5 ft^3) of fluid. An orifice restriction installed in the pressurizer connecting line is a variable test design parameter that controls the rate at which the relatively large pressurizer mass inventory enters the primary loop during transient blowdown-type tests.

ORNL–DWG 80–4545 ETD

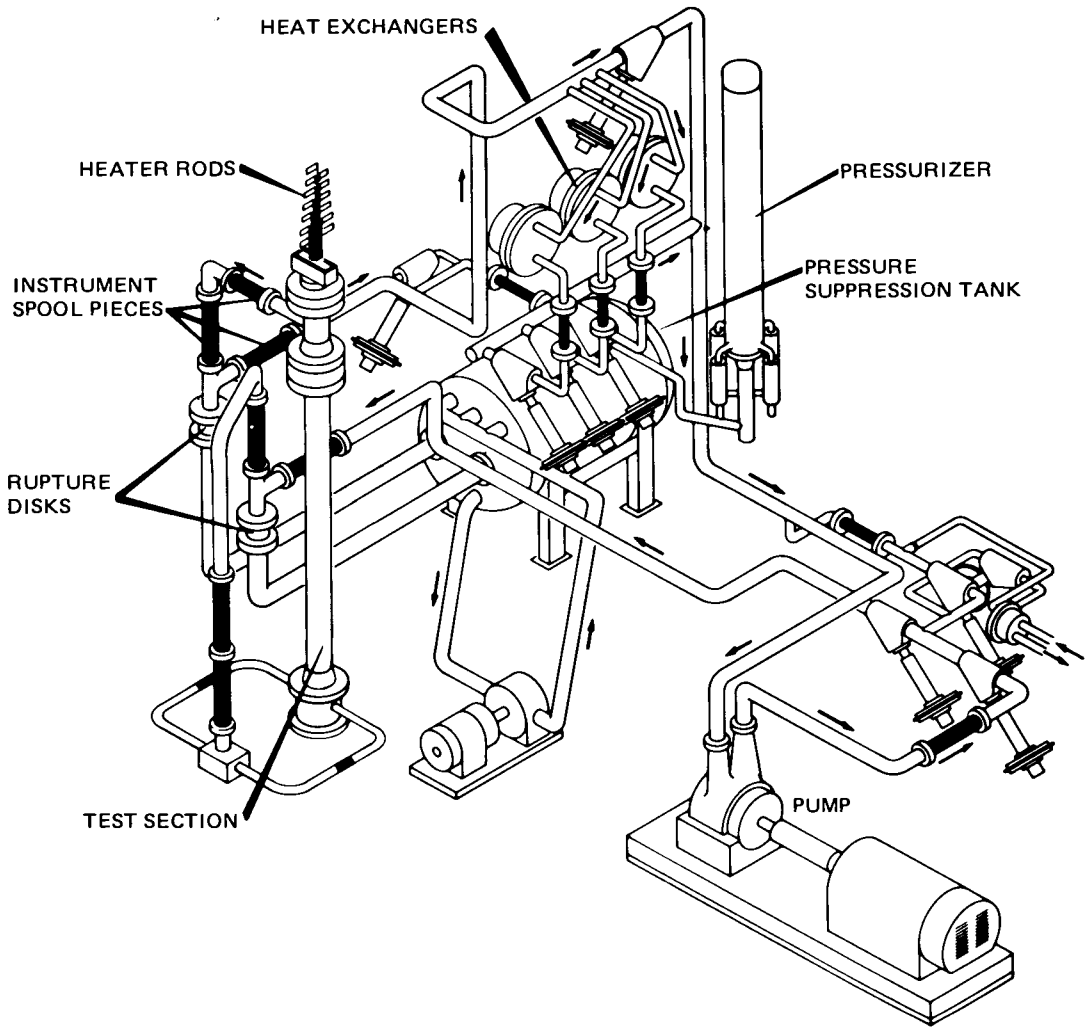

Fig. 2.1. THTF in standard configuration.

Rupture disk assemblies located near both the test section inlet and outlet are used for transient blowdown-type experiments to simulate inlet and exit pipe breaks. Appropriately sized critical flow orifices (a test design parameter) installed with the rupture disk assemblies control the mass letdown and depressurization rate of the system (along with applied bundle power during the blowdown and other initial system parameters). Either the inlet or outlet rupture disks, or both, may be used to initiate the transient. The primary loop fluid is discharged through either or both of these assemblies into the pressure-suppression system (PSS), where the shock produced by the blowdown is absorbed and cold water emerging from spray nozzles condenses the steam. The PSS consists of a 9.47×10^{-2} m^3/s (1500-gpm) pump that continuously recirculates the 1.97-m^3 (520-gal) water inventory of the 4.39-m^3 (1160-gal) pressure-suppression tank through 3 tubular spray lines, each containing 24 nozzles. The pressure-suppression tank is vented to the atmosphere through an 8-in. pipe.

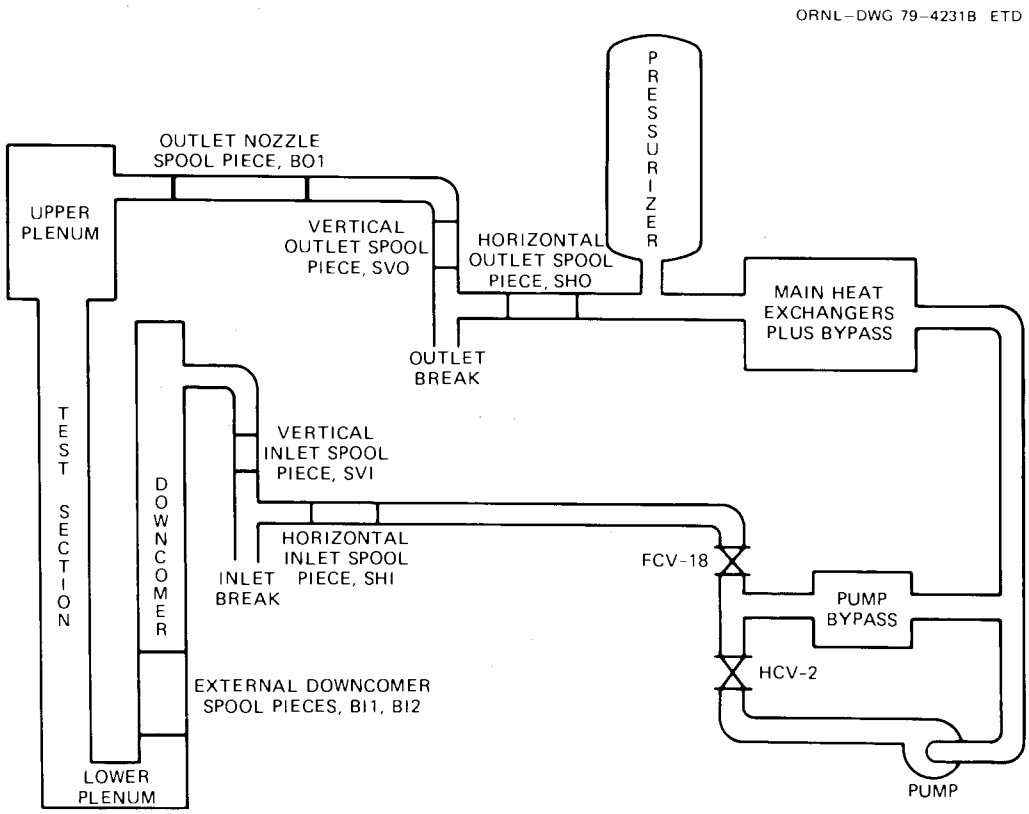

Fig. 2.2. Simplified flow diagram of THTF in standard configuration.

The loop piping is made up primarily of a special 4-in. Schedule-160 pipe having 1.27-cm (0.500-in.) wall thickness and an inside diameter of 8.89 cm (3.5 in.). Also used to some extent in bypass lines are 1- and 2-in. Schedule-80 stainless steel pipe. A system line drawing (Fig. 2.3) indicates pipe size and pipe run length for the system in its standard configuration (lines from the rupture disk assemblies to the PSS are not shown). Austenitic stainless steel material is used throughout the system to avoid corrosion and quality degradation of the high-purity demineralized water coolant. The piping system is assembled with a number of flanged disconnects to facilitate rearrangement and modification of the test loop configuration.

Power to the rod bundle is supplied by a dc power supply consisting of two double-ended motor-generator (MG) sets with each of four generators rated at 7140 A and 350 V dc. Power supplied to the rod bundle is control system limited, however, to ~7.5 MW (~125 kW/rod). These generators may be controlled jointly or separately, supplying up to 445 A and 280 V to each of the 60 powered heater rods in the 64-rod bundle. An extensive "crowbar" protection system, capable of isolating the generators from the heater rods, trips power in the event of an electrical malfunction or abnormality.

Adequate process instrumentation is provided for operational and safety control and monitoring purposes of the facility during testing. Panel-board-mounted indicators, recorders, and display/graphic terminals

ORNL-DWG 81-22799R ETD

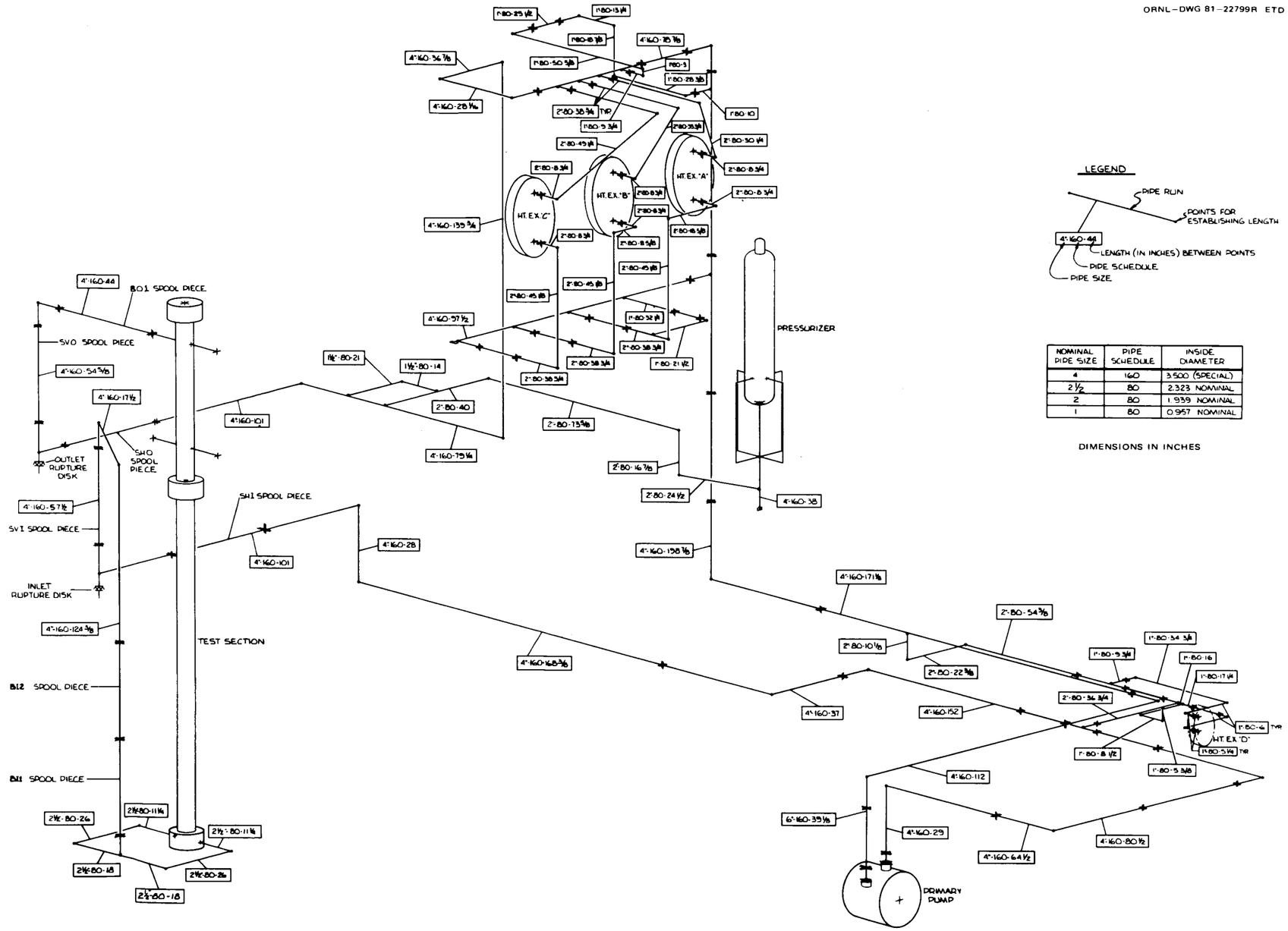

Fig. 2.3. System line drawing of THTF in standard configuration (lines from rupture disks to PSS are not shown). (Microfiche copy of this drawing attached to back of report.)

are also used for this instrumentation to provide readouts, aiding in facility operation. A high-speed CCDAS is used to record data at rates of up to 20,000 channels/s and store them on disk or tape for later retrieval. This system is described in more detail in Chap. 6.

A summary of THTF design data is presented in Table 2.1. The test section and bundle are described in more detail in Chap. 3. Other major system components discussed in this section will be described in greater detail in Appendix A.

Table 2.1. Summary of THTF design data

Component	Design data
Test section	
Heater rods	DC power, resistance heater
Number	60
Diameter, cm (in.)	0.950 (0.374)
Pitch, cm (in.)	1.273 (0.501)
Center of outside row to shroud-box wall, cm (in.)	0.733 (0.289)
Maximum rod power, kW(e)	125
Sheath couples per rod	12
Center couples per rod	4
Instrument rods	
Number	4
Diameter, cm (in.)	1.02 (0.401)
Shroud box	
Inside dimensions, cm (in.)	~10.37 x 10.37 (4.084 x 4.084)
Outside dimensions, cm (in.)	~15.45 x 14.183 (6.084 x 5.584)
Grid-spacer separation, cm (in.)	~60.96 (24.0)
Subchannel fluid thermocouples (upper end of heated length)	81
Primary loop	
Nomiual primary pipe sizes	
Special 4-in. Schedule-160	8.89-cm (3.5-in.) ID
2-in. Schedule-80	4.925-cm (1.939-in.) ID
1-in. Schedule-80	2.431-cm (0.957-in.) ID
Graham Heliflow heat exchangers	3
Heat removal capacity, each, MW(t)	2.5
Pressurizer	
Inside diameter, cm (in.)	26.67 (10.5)
Length, m (ft)	3.35 (11)
Heat input, steady state, kW(e)	30
Heat input, startup, kW(e)	49
Pump	
Type	Bingham 3 x 6 x 17 CJM
Stages	2
Capacity, m^3/s (gpm)	4.42×10^{-2} (700)
Head, m (ft)	~590 (1940)
Maximum pressure rating, kPa (psi)	2.06×10^4 (3000)
Maximum operating temperature, K (°R)	589 (1060)
Pump power, kW(e)	450
Total loop capabilities (design)	
Maximum generator dc power output, MW(e)	10
Maximum rod bundle power, MW(e)	7.5
Operating pressure, kPa (psia)	1.72×10^3–1.72×10^4 (250–2500)
Operating temperature, K (°R)	422–617 (760–1110)
Maximum loop flow, m^3/s (gpm)	5.68×10^{-2} (900)
Test section flow, m^3/s (gpm)	6.31×10^{-5}–3.79×10^{-2} (1-600)
Test section heated length, m (ft)	3.66 (12)
Normal test section flow direction	Vertical upflow

3. THTF TEST SECTION AND BUNDLE 3

This chapter describes the test section and Bundle 3 as it was initially installed in the THTF in June of 1979. The THTF Bundle 3 is one of the most extensively instrumented bundles ever used in light-water reactor safety research. Each FRS contains 16 thermocouples for a total of 960 thermocouples in the FRSs. Fluid thermocouples and other in-bundle instrumentation provide additional measurements necessary for assessing the thermal-hydraulic conditions in the bundle.

Significant modifications to the test section and bundle were made at two later periods during the operational history of Bundle 3. These modifications are described in Chap. 5, where test-specific system descriptions are presented. A detailed operating history of Bundle 3 is provided in Ref. 1.

As mentioned earlier, this chapter describes the system as it was initially installed. The test section and its integral components are described in Sect. 3.1. The shroud box, which forms the primary fluid boundary over the heated length of the FRSs, and its accompanying instrumentation are described in Sect. 3.2. The bundle FRSs are described in Sect. 3.3.

3.1 Test Section

The test section consists of a pressure container housing (test section barrel), shroud box, and the test bundle. The container incorporates the flanges and instrument taps necessary to accommodate the pressure boundary penetrations. The test bundle consists of the 64 rods (60 powered heater rods and 4 instrument rods) in an 8 x 8 square array. The shroud box enclosing the test bundle includes the spacer-grid supports and various types of instrumentation to monitor fluid conditions within the shroud box.

The test section barrel [Fig. 3.1(a)] consists primarily of two flanged sections of 10-in. Schedule-140 316 stainless steel pipe with a total overall length of ~6.1 m (20 ft). Support brackets are attached to the lower spool section, which is ~4.6 m (15 ft) long. The upper spool section is removable and considered as part of the test bundle (Bundle 3) and the shroud-box assembly. Grayloc flanges are used to permit quick coupling and uncoupling of the test section and the primary loop piping. Portions of the test section are shown in more detail in Figs. 3.1(b,c,d, and e).

The upper and lower test section container closures were fabricated with bolted blind flanges and sealed with conventional flexitallic gaskets. Seven gaskets were used between the surfaces of the seal plate flanges, the upper spool section, the subchannel thermocouple flange, the shroud support and instrument flange, the lower spool section, the inlet plenum, the nickel plate, and the bottom (blind) flange.

The nickel plate, sandwiched between the inlet plenum and the bottom flange, serves as both a heater rod anchor and a conductor of heater rod current. The portion of the dc generator circuit consisting of the heater rod anchor and the nickel flange is maintained at ground potential, and

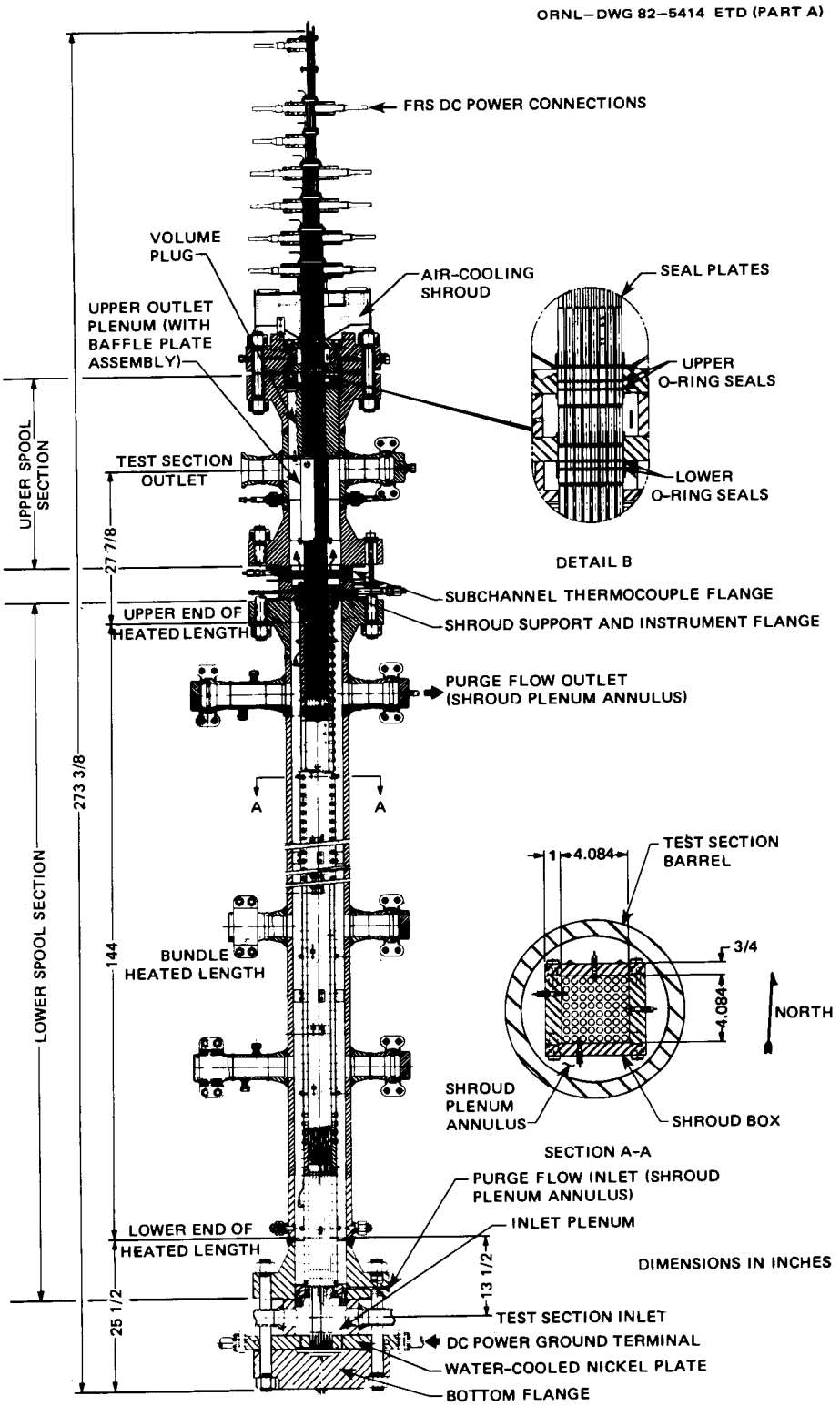

Fig. 3.1(a). THTF test section.

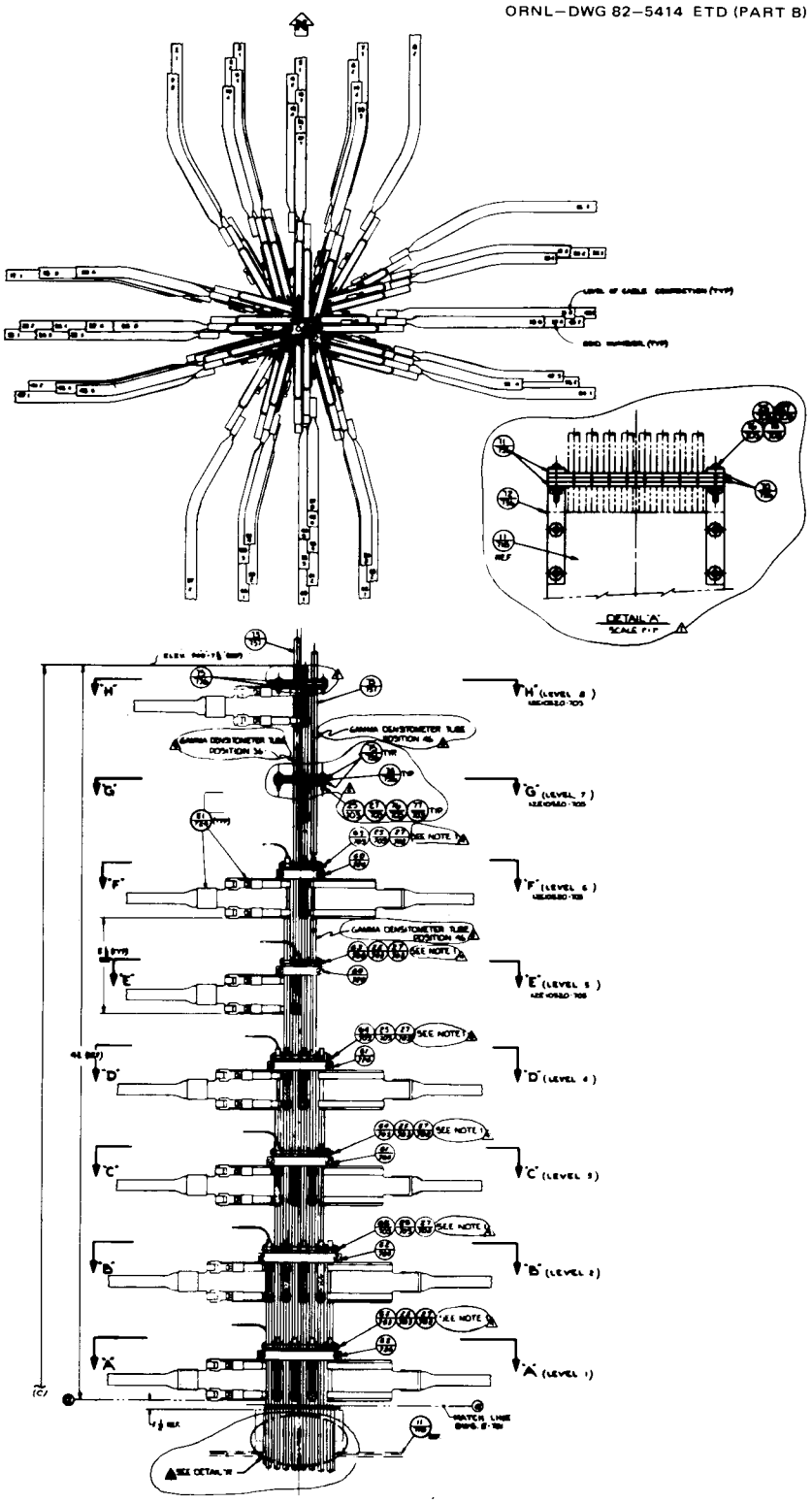

Fig. 3.1(b). Detail of THTF test section (partial). (Microfiche copy of this drawing attached to back of report.)

ORNL–DWG 82–5414 ETD (PART C)

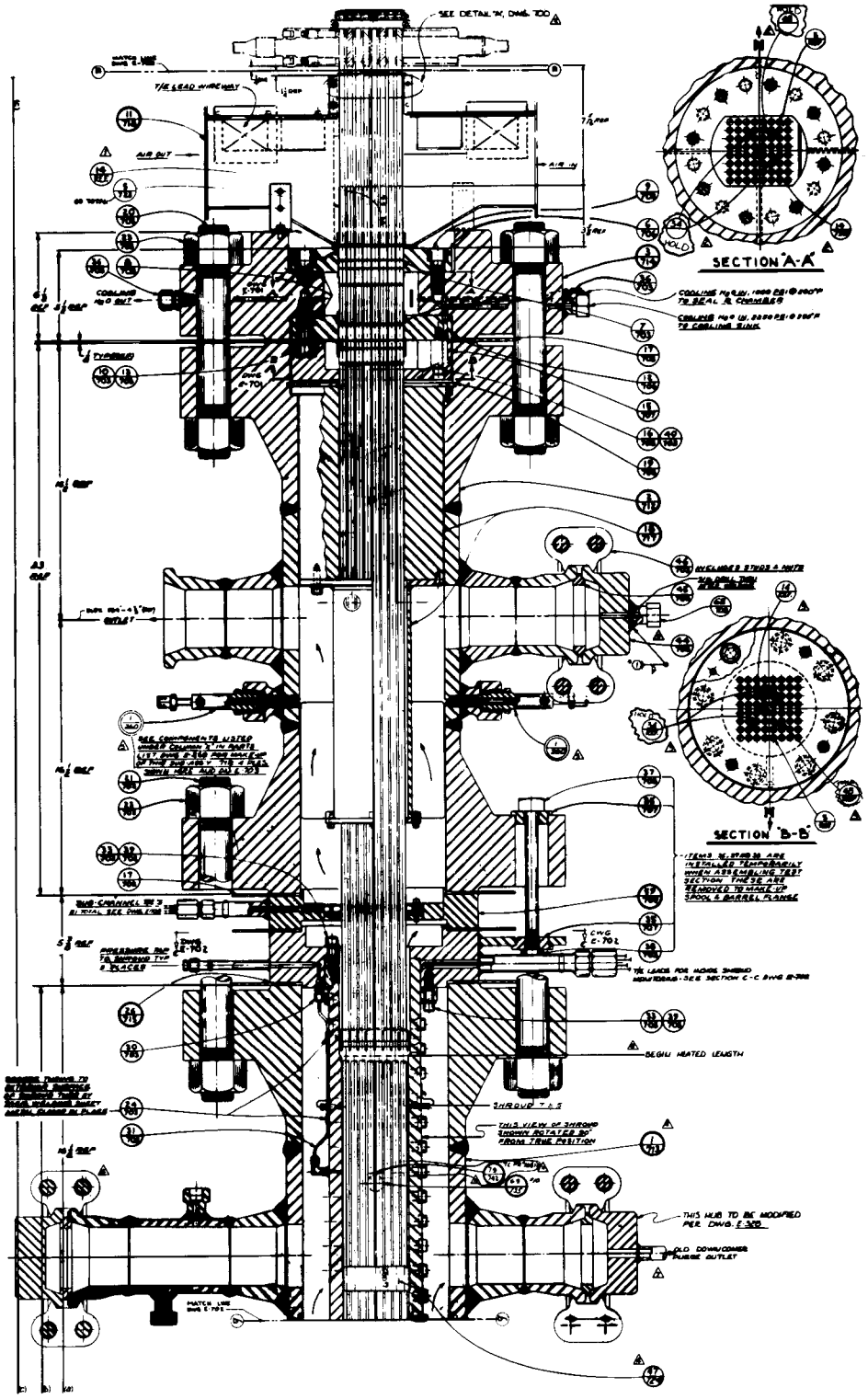

Fig. 3.1(c). Detail of THTF test section (partial). (Microfiche copy of this drawing attached to back of report.)

ORNL–DWG 82–5414 ETD (PART D)

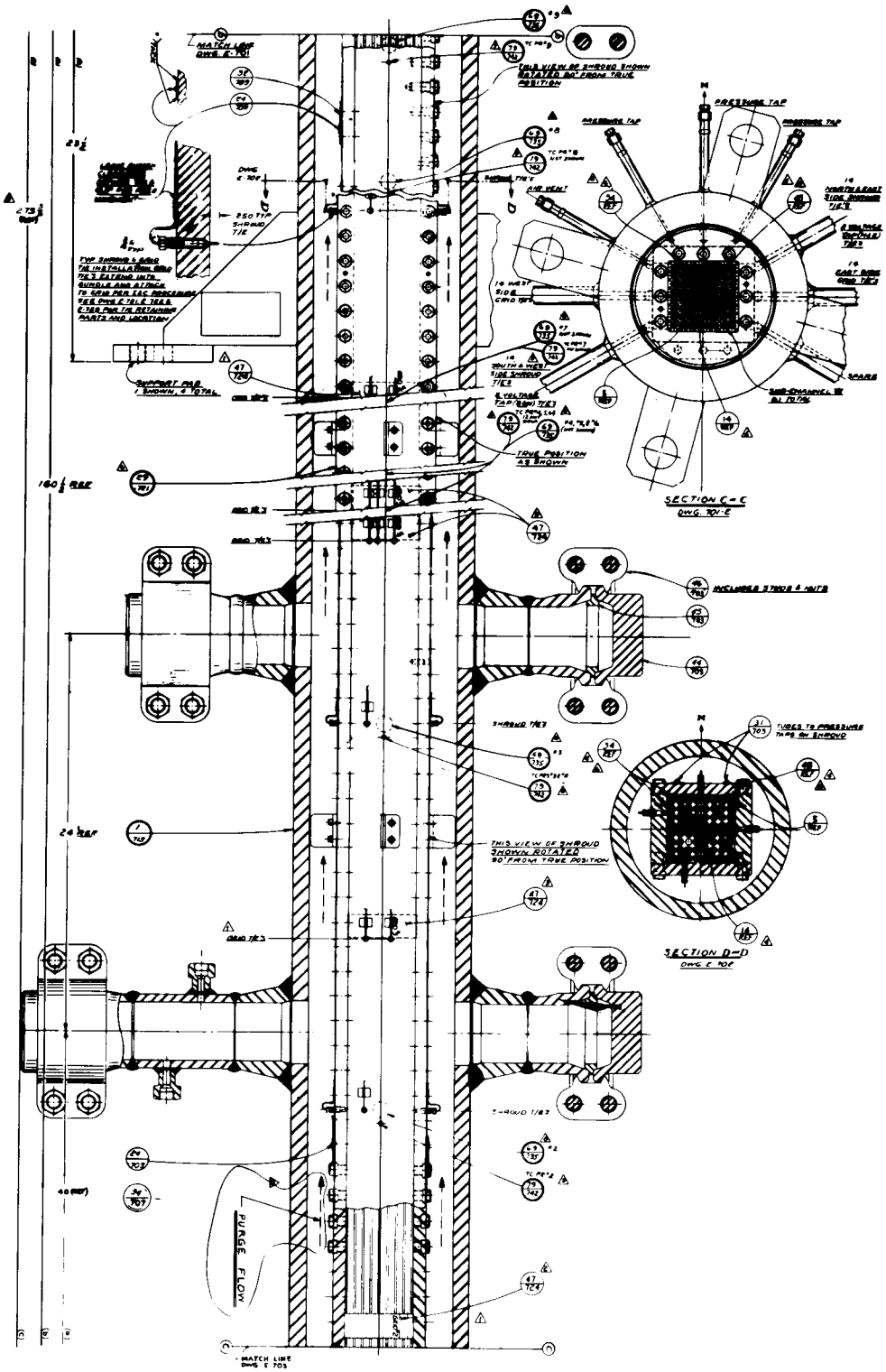

Fig. 3.1(d). Detail of THTF test section (partial). (Microfiche copy of this drawing attached to back of report.)

ORNL–DWG 82–5414 ETD (PART E)

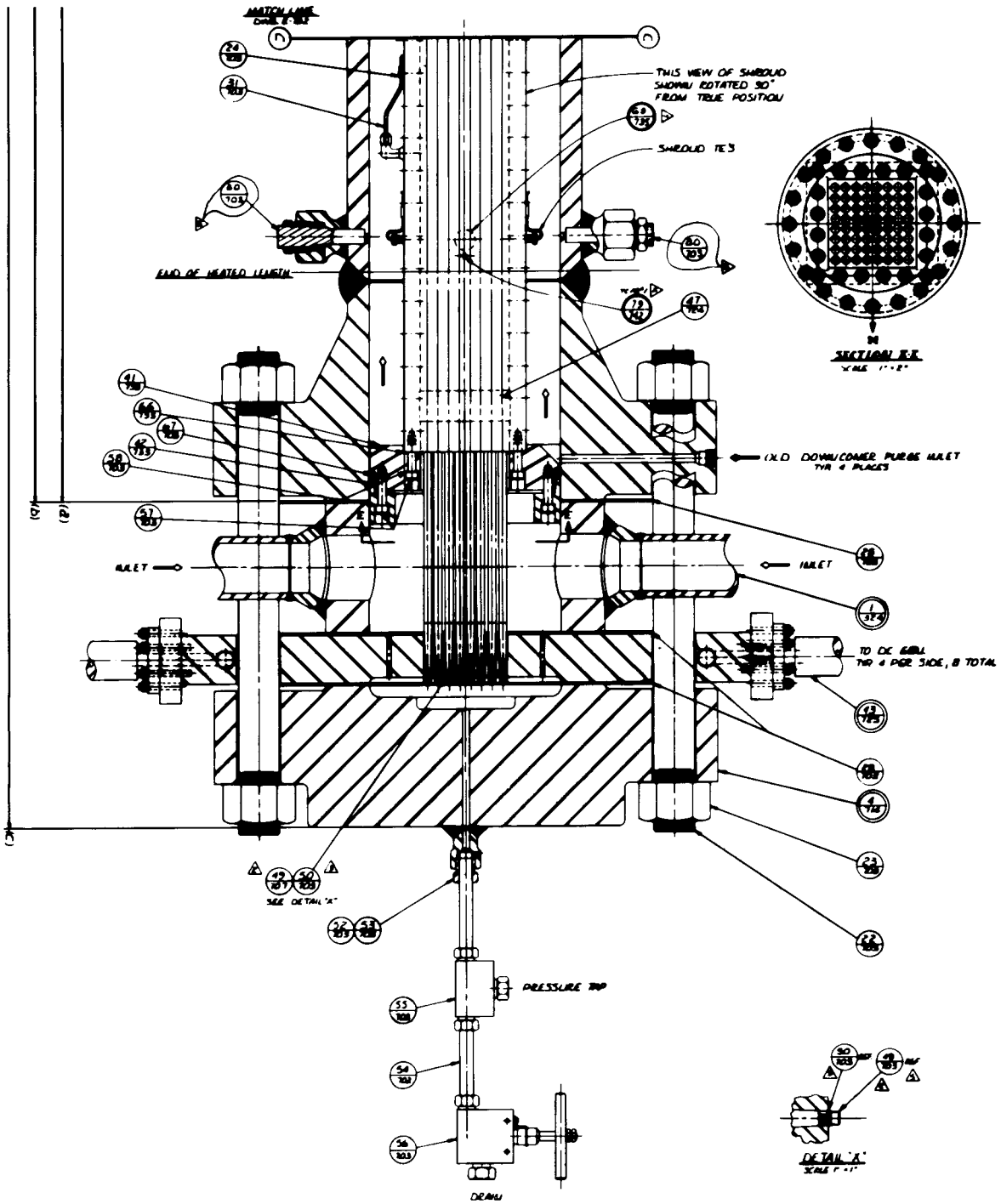

Fig. 3.1(e). Detail of THTF test section (partial). (Microfiche copy of this drawing attached to back of report.)

thus electrical isolation between the nickel flange and the test section is not required. Each heater rod, anchored in the nickel plate, is mated to a matching tapered socket and held in contact with a threaded fastener torqued to ~34.6 kg-m (250 ft-lb). A bundle total heater current of nearly 25,000 A requires cooling of the nickel plate. Passages drilled in the external portion of the plate share cooling with the eight water-cooled generator cables and current conducting copper pipe mounted to the nickel plate. Several internal passages, also supplied by generator cable cooling water, provide additional internal cooling.

The inlet plenum is located above the nickel plate and, for steady-state flow in the normal direction, forms the entrance region to the test bundle. The inlet plenum manifold shown in Fig. 3.2 joins the external downcomer to the test section inlet plenum. A detailed drawing of the inlet plenum dimensions is shown in Fig. 3.3.

The lower end of the shroud box is located ~5.72 cm (2.25 in.) above the seal made between the inlet plenum and lower spool section. A packing gland and seal assembly in this region also isolate the shroud plenum annulus (old downcomer) from the bundle flow. During Bundle 1 testing,[2] this annulus region was used as an internal downcomer for the primary test section flow. Because an external downcomer is used for Bundle 3 testing, this region is isolated from the primary test section flow. A purge flow is maintained through this shroud plenum annulus with primary water from the pump to provide thermal bounding conditions on the outside of the

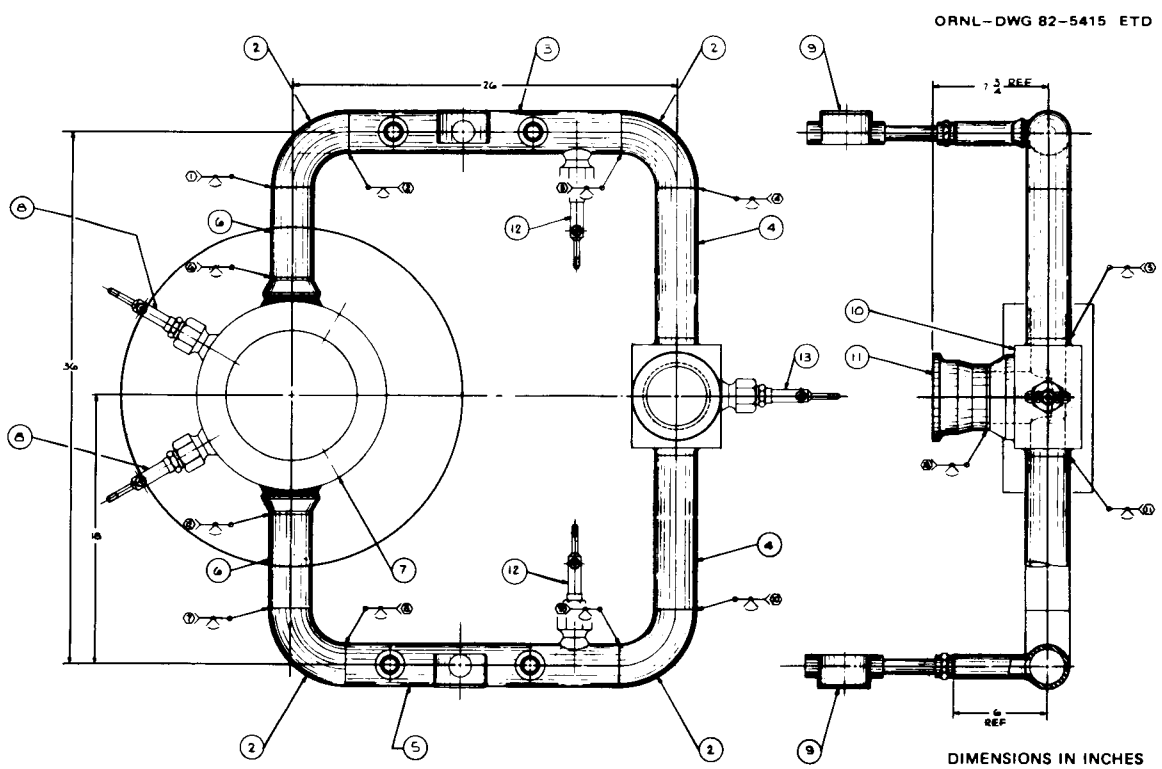

Fig. 3.2. Detail of inlet plenum manifold. (Microfiche copy of this drawing attached to back of report.)

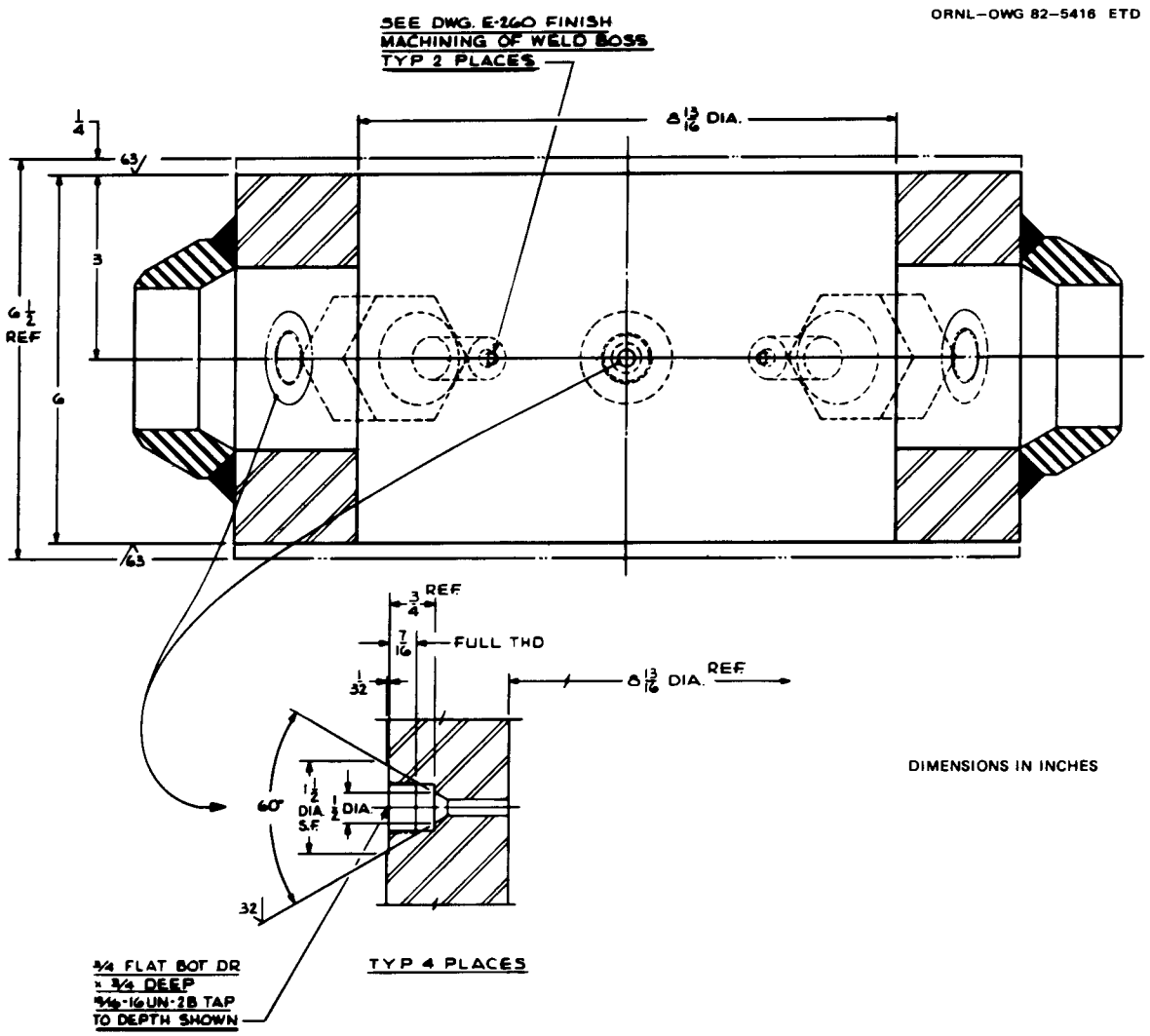

Fig. 3.3. Detail of test section inlet plenum.

shroud-box walls and to maintain an equalizing system pressure on both sides of the shroud box. Although the purge flow system is not shown in Figs. 2.1 and 2.2, it is indicated in the instrument application drawings shown later in Figs. 5.19(a–c).

The shroud box, which will be discussed in more detail later, is continuous over the heated length of the bundle. The upper end of the shroud box is mechanically attached to the shroud support and instrument flange (Fig. 3.1) that rests on the upper flange surface of the lower spool section. This flange also provides pressure penetrations for thermocouple leads and pressure instrumentation lines installed along the shroud-box walls.

The subchannel thermocouple flange is located between the shroud support and instrument flange and the upper spool section. This flange

provides both support for the subchannel fluid thermocouples and Conax-fitting pressure penetrations for the thermocouple leads. The subchannel thermocouples will be discussed in more detail later. Figure 3.4 shows details of the subchannel thermocouple flange.

The test section flow area expands above the upper end of the shroud box (beginning in the shroud support and instrument flange). This region, the upper outlet plenum, joins the test section outlet piping. The geometry in this region is complicated somewhat by the supports and instrumentation lead guide tubes present in the shroud support and instrument flange and the subchannel thermocouple flange. Drawings showing details are presented in Figs. 3.4 and 3.5.

The upper outlet plenum area in the upper spool section contains a baffle plate assembly. The assembly was installed to protect the FRSs from forces produced by the change in flow direction at the outlet flow nozzle during severe transients. The assembly is essentially a box surrounding the bundle with positioning fins extending over the lower-half of the box from the centers of the east and west sides. Figures 3.6 and 3.7 show the baffle plate assembly and also the volume plug located above the outlet flow nozzle. The volume plug is a solid steel plug with a lattice of holes machined through it allowing the FRSs and instrument rods to pass through. The holes are machined to fairly close tolerances to minimize penetration of test section fluid into the region above the test section outlet nozzle. Holes for the 0.950-cm-diam (0.374-in.) FRSs are drilled to ~1.02-cm diam (0.401-in.), while holes for the 1.02-cm-diam (0.401-in.) instrument rods are drilled to ~1.04-cm diam (0.410-in.).

The test bundle rods penetrate through seal plates at the top of the pressure container where each rod is sealed with two Viton O-rings in each of the two seal plates. A detail of the seal plate region is shown in Fig. 3.1. The space between the seal plates forms an intermediate-pressure chamber between the high pressure of the test section and the atmosphere. A closed outer-seal system with a pressurizer and circulating pump provides cooling water through the outer-seal area at the intermediate pressure (Appendix A.2.9).

The O-ring seal area also provides a sliding seal surface, allowing differential expansion between the heater rods and the test section container. The heater rods protrude another ~1.2 m (4 ft) above the seal flanges, thus making the overall test section assembly ~6.9 m (22.8 ft) in height. A forced air cooling shroud located above the seal plates provides additional cooling for the FRSs as they exit the test section.

The FRS dc power connections are made to individual rods at this upper end as they extend above the test section. The dc power system is described in more detail in Section A.2.8.2.

Other test section penetrations are associated with pressure measurements, temperature measurements, and additional nozzles originally fabricated to provide for possible future modifications to the test section. One of the nozzles (Fig. 3.1) is used as the outlet for the purge flow from the shroud plenum annulus (old downcomer) that was discussed earlier.

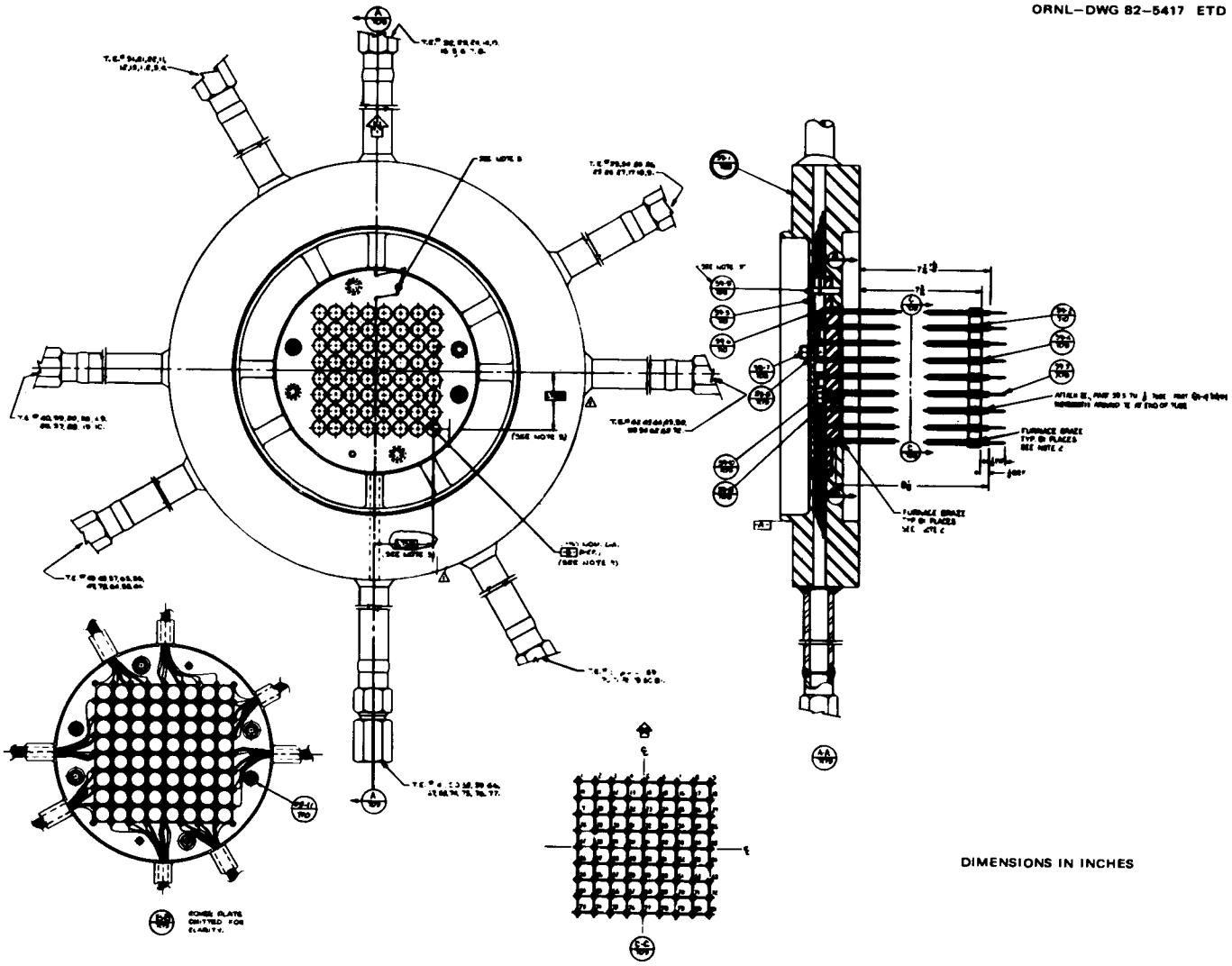

Fig. 3.4. Detail of subchannel thermocouple flange. (Microfiche copy of this drawing attached to back of report.)

ORNL–DWG 82–5418 ETD

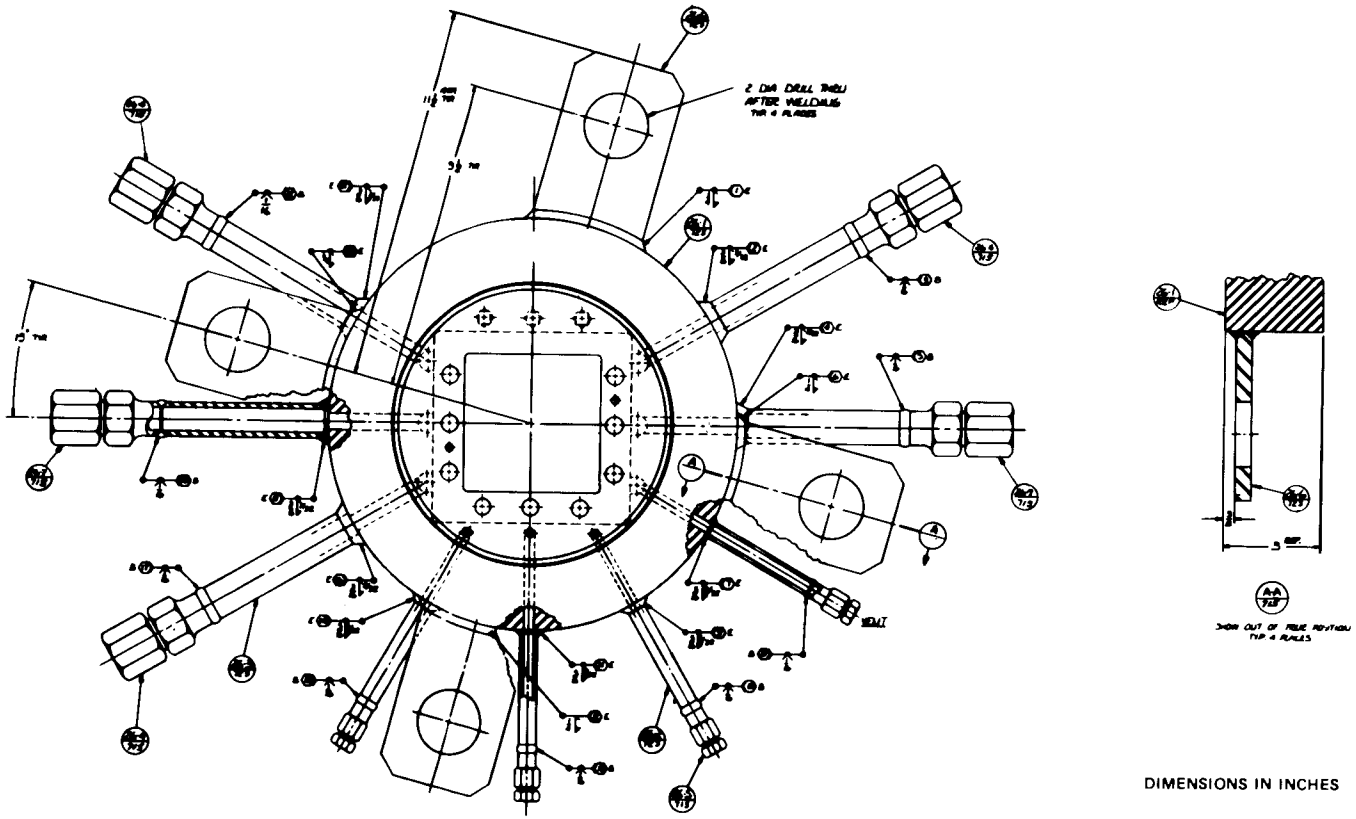

DIMENSIONS IN INCHES

Fig. 3.5. Detail of shroud support and instrument flange. (Microfiche copy of this drawing attached to back of report.)

ORNL–DWG 82–5419 ETD

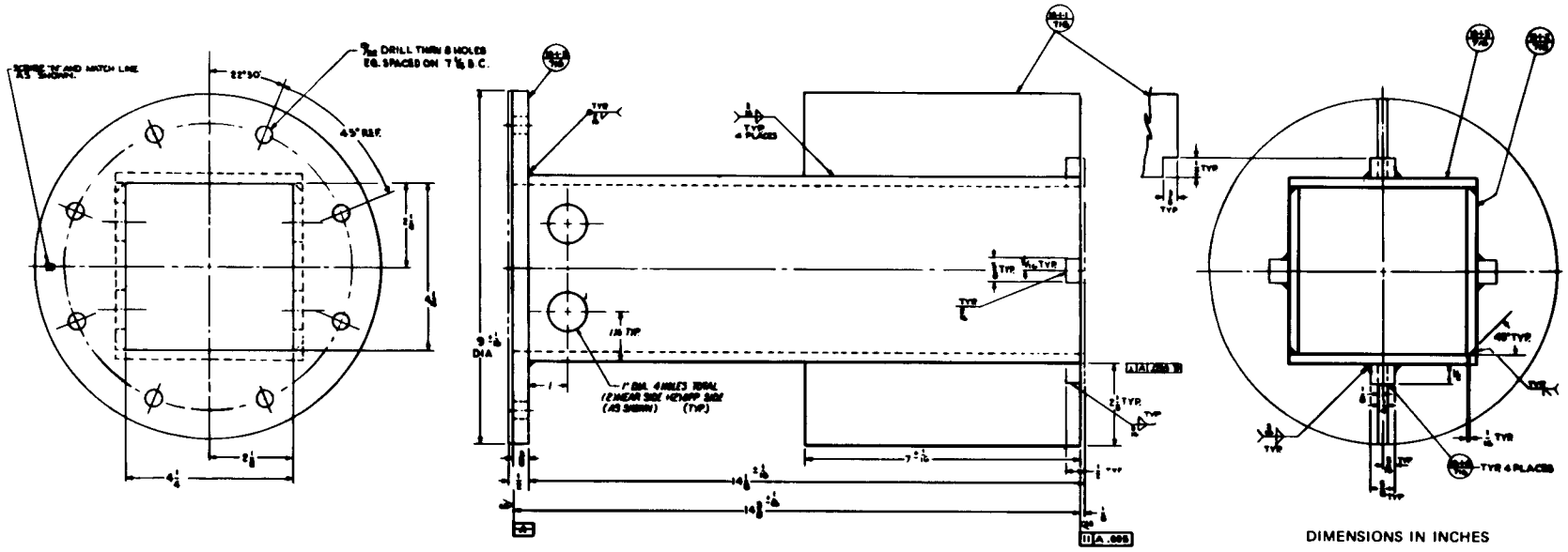

Fig. 3.6. Detail of baffle plate assembly. (Microfiche copy of this drawing attached to back of report.)

ORNL-DWG 82-5420 ETD

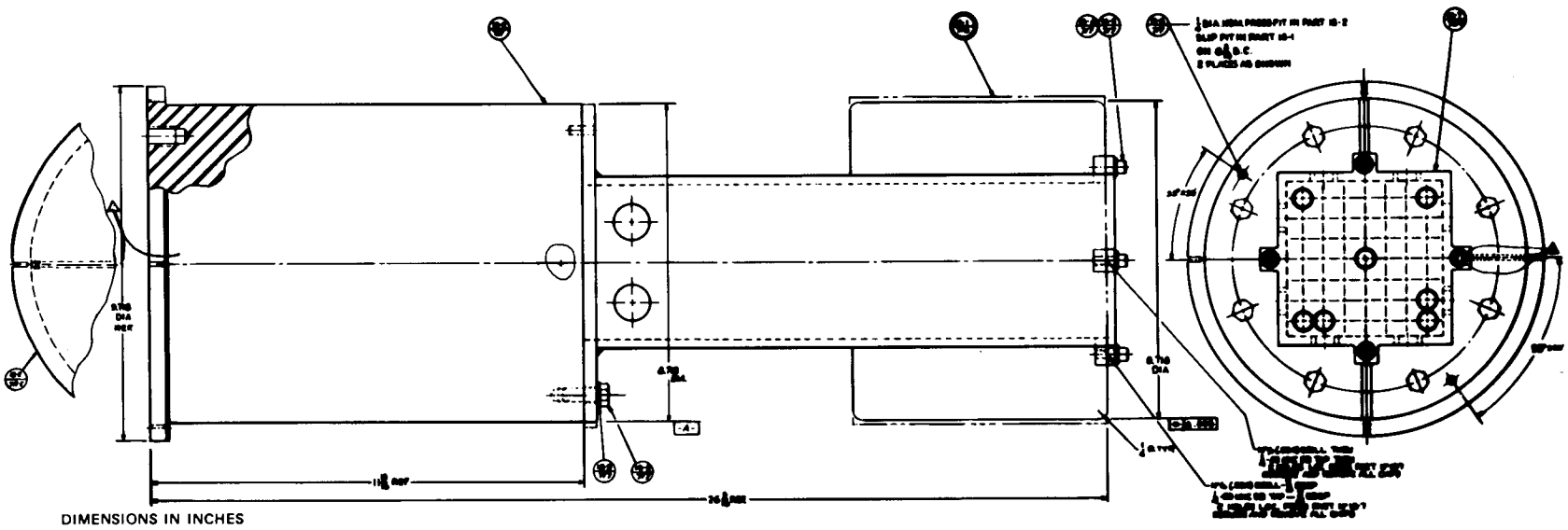

Fig. 3.7. Detail of volume plug and baffle plate assemblies. (Microfiche copy of this drawing attached to back of report.)

3.2 Shroud-Box and Fluid Instrumentation

As mentioned previously, the shroud box forms the primary test section flow boundary for the bundle along the heated length of the FRSs. As a result, the dimensions of the shroud box and associated components are very important to the thermodynamic and hydraulic analysis of the rod bundle behavior. The shroud-box inside dimensions are nominally 10.37 cm (4.084 in.) square. The shroud-wall thickness is 2.54 cm (1.0 in.) and 1.91 cm (0.75 in.) as shown in Fig. 3.1, fabricated from ASTM A240, 316 stainless steel plate. Because the heater rod diameters are 0.950 cm (0.374 in.) positioned on 1.273-cm (0.501-in.) centers in the 8 x 8 bundle array, the distance from the center of the outer row of rods to the shroud-box wall is 0.733 cm (0.289 in.).

The shroud box supports the spacer grids that, in turn, provide support to minimize heater rod buckling and to form bundle flow channels. Figure 3.8 is a schematic drawing of the low-pressure-drop spacer-grid assembly with integral spring spacers used in the THTF. Seven of these grids were installed at ~61.0-cm (24.0-in.) intervals along the shroud-box inside, positioned in the shroud box by 0.157-cm-deep (0.062-in.) slots into which the grid slides. The axial locations of the spacer grids along with the locations of other important test section parameters and instrumentation described later are shown in Fig. 3.9.

The shroud wall and spacer grids are instrumented with fluid thermocouples along the heated length of the bundle. The shroud thermocouples (1.57-mm OD) project ~0.64 cm (0.250 in.) into fluid subchannels from all four sides of the shroud box and at seven axial levels corresponding to the primary FRS thermocouple levels. The subchannels into which these thermocouples project and the locations of the other fluid thermocouples in the bundle are shown in Fig. 3.10. Because it is somewhat difficult to distinguish subchannels in Fig. 3.10, more detailed location figures and the naming convention for the bundle "fluid" thermocouples are presented in Appendix B. Spacer-grid thermocouples (1.02-mm OD) are attached to the six spacer grids located within the heated length. These thermocouples project ~0.68 cm (0.27 in.) below the spacer grids in the subchannels indicated in Fig. 3.10.

As mentioned earlier, a subchannel thermocouple flange located above the upper end of the shroud box allows fluid temperature measurements to be made at each flow subchannel (81 total) between heater rods. These thermocouple leads extend from the subchannel thermocouple flange into the shroud box to a position in the subchannels ~3.3 cm (1.3 in.) above the upper end of the bundle heated length. This distance (from the top of the heated length) varies somewhat for each of the bundle configurations because the average as-built heated length of the rods changes with the addition of the new rods. The average top of the heated length will be noted with the thermocouple locations for each bundle configuration (original bundle and two modifications). The thermocouple leads are supported by stiffening tubes that are anchored in the subchannel thermocouple flange and positioned in the shroud by a support grid. The thermocouple leads are then routed to one of eight exit seal nozzles via eight covered troughs that form spokes in the flange (Fig. 3.4). Flow from the test bundle is thus routed around the spokes and enters the test section

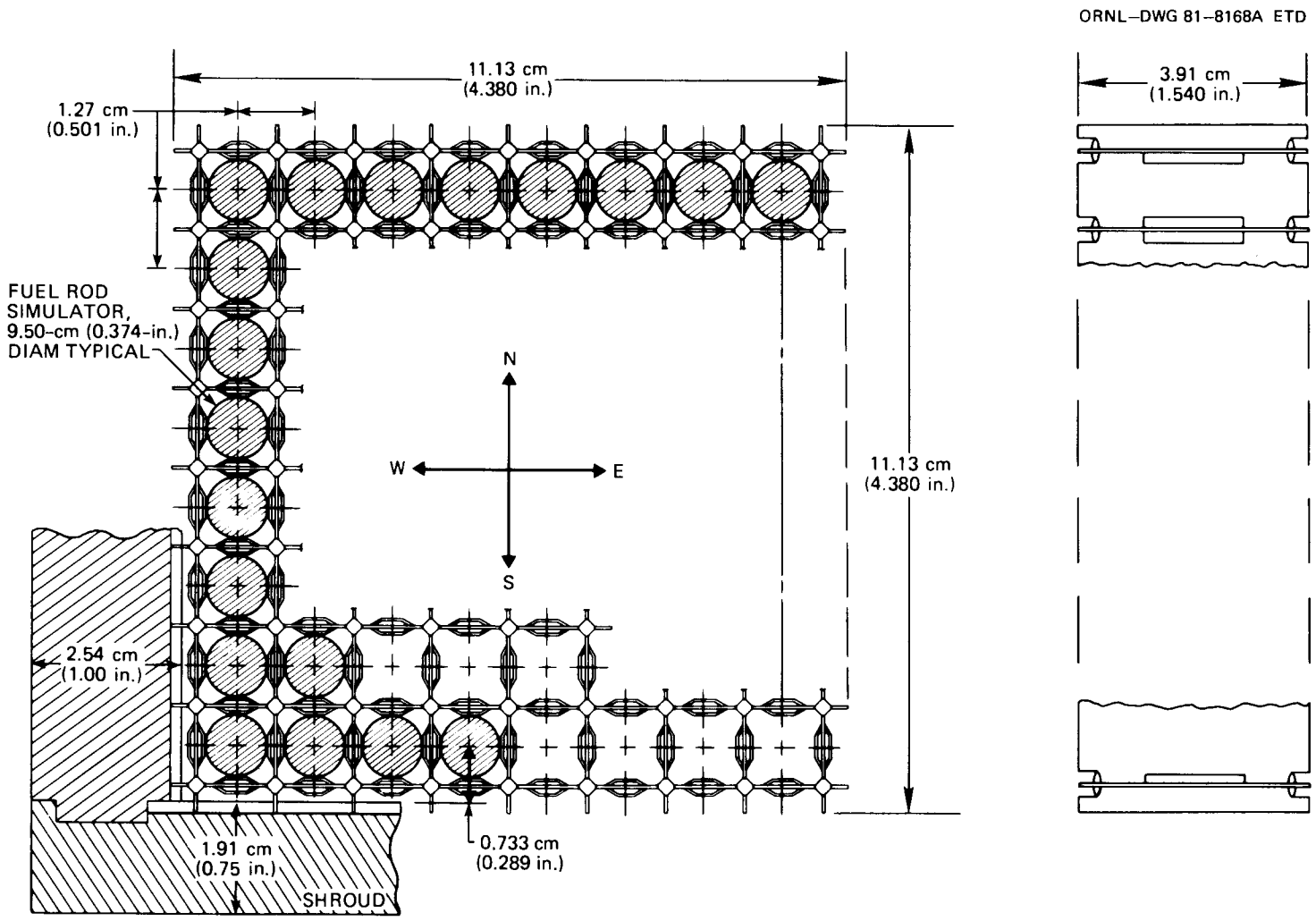

Fig. 3.8. Schematic drawing of low-pressure-drop spacer-grid assembly used in THTF.

ORNL–DWG 82–4715 ETD

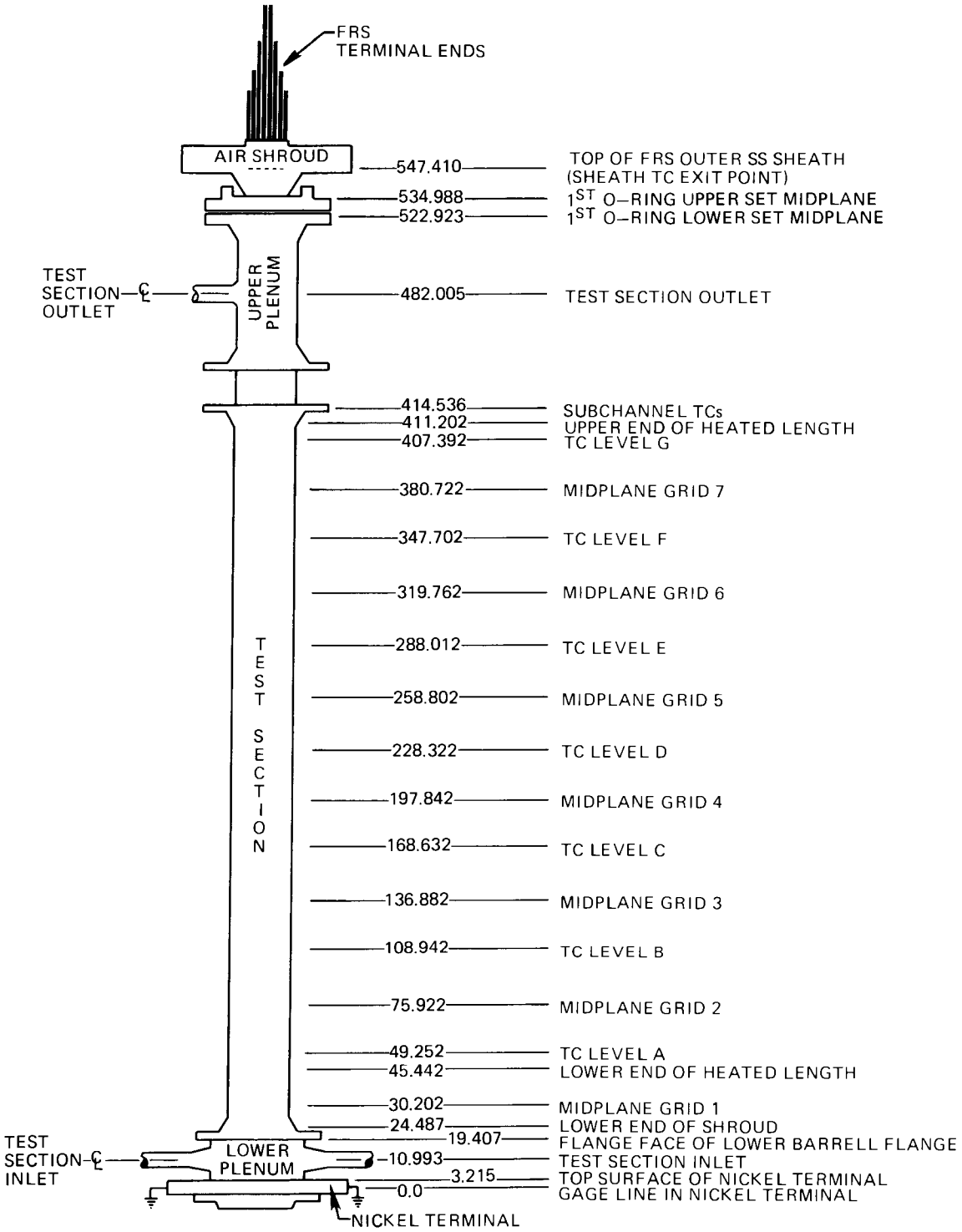

Fig. 3.9. Axial location of critical points in THTF test section and Bundle 3. All dimensions are in centimeters and are referenced to gage line in nickel terminal.

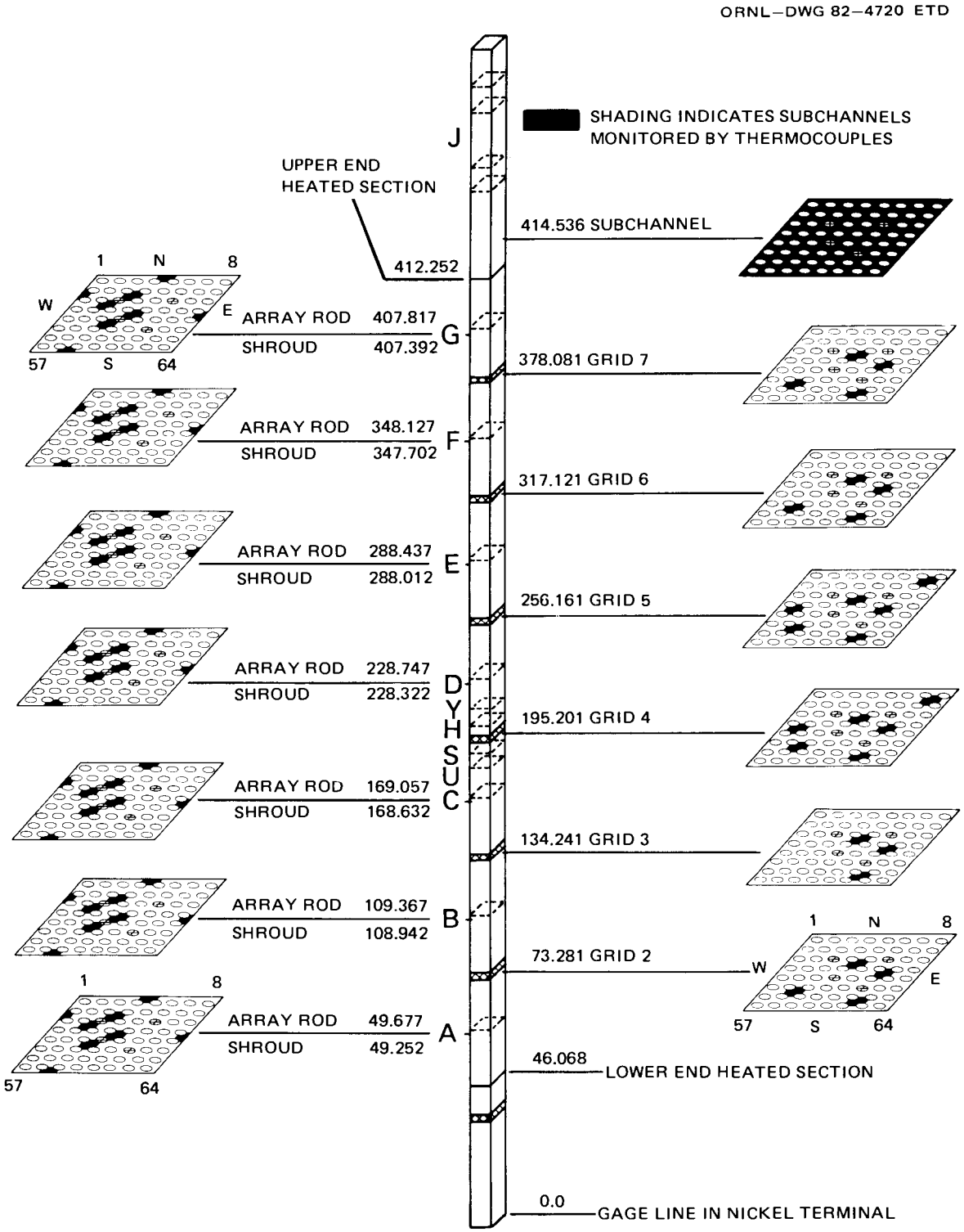

Fig. 3.10. Location of fluid thermocouples in THTF Bundle 3. All dimensions are in centimeters and are referenced to gage line in nickel terminal.

outlet plenum. A photograph of the subchannel thermocouple flange is shown in Fig. 3.11. A diagram identifying the bundle subchannels as well as the FRS and instrument rod locations is presented in Fig. 3.12. The subchannel thermocouples are 1.02-mm OD.

Two thermocouple-array rods provide additional fluid temperature measurements along the axial heated length of the bundle. Thermocouple-array

ORNL-PHOTO 7094-79

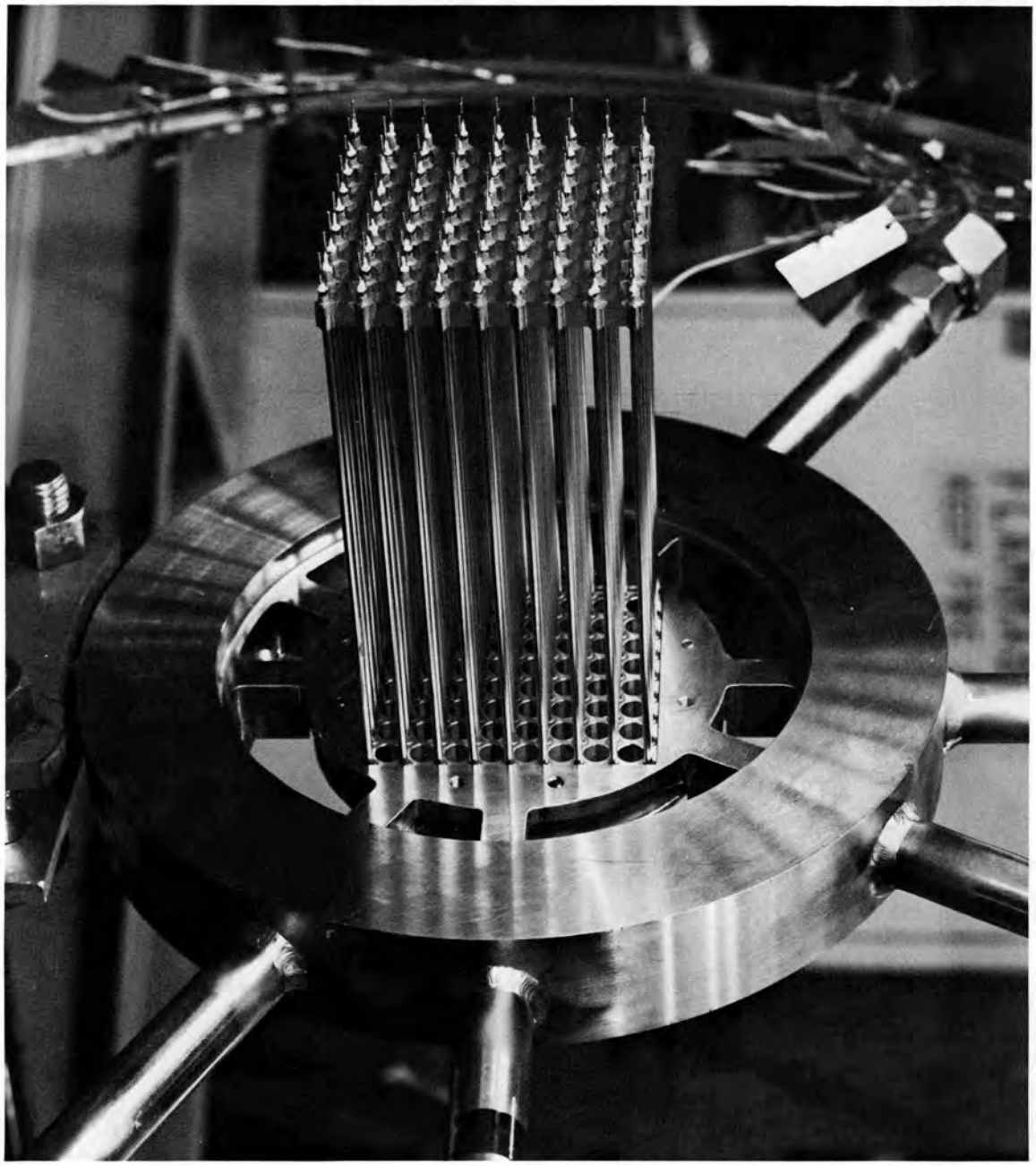

Fig. 3.11. Subchannel thermocouple flange.

ORNL–DWG 82–4713 ETD

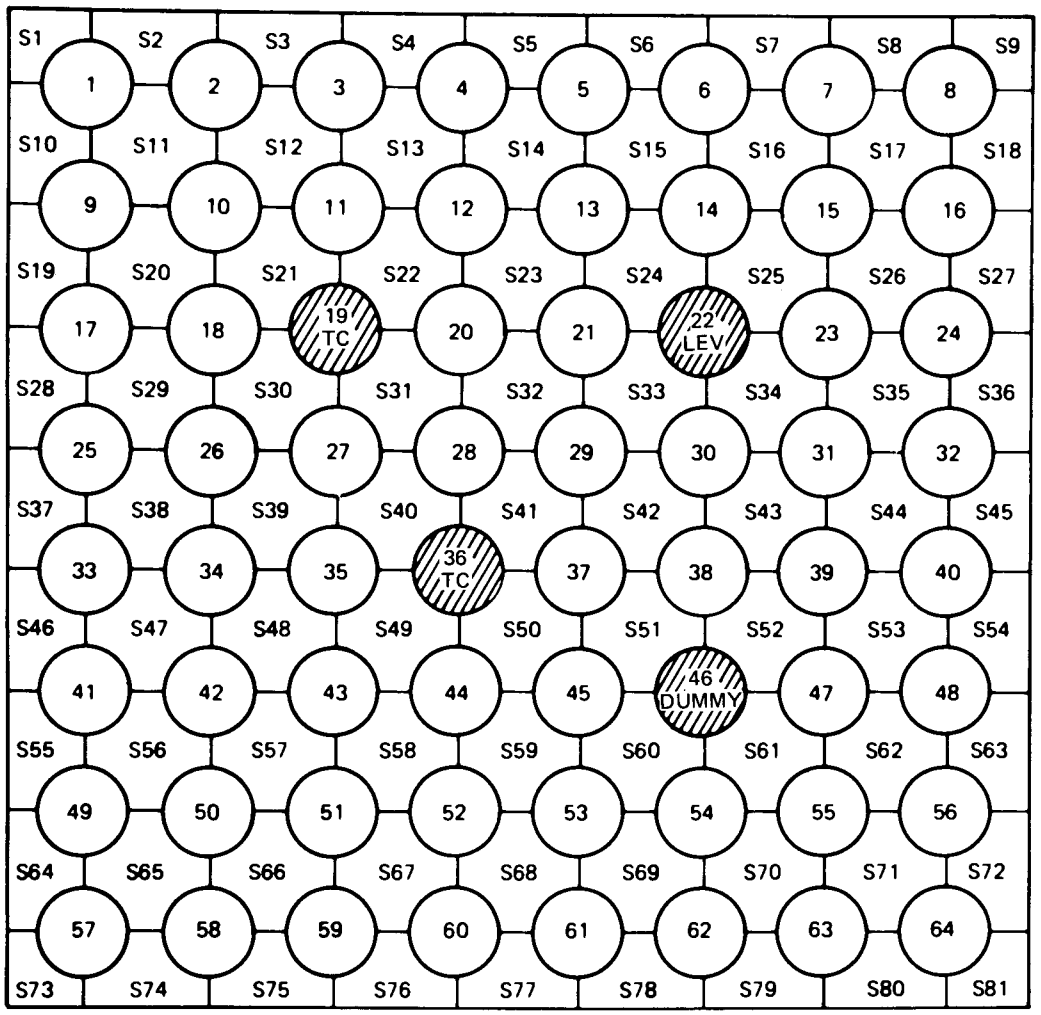

THERMOCOUPLE RODS 19 AND 36
LEVEL ROD 22
DUMMY ROD 46

INACTIVE RODS

Fig. 3.12. Identification of THTF heater rods, subchannel locations, and instrument rods in THTF Bundle 3.

rod thermocouples (1.02-mm OD) extend into the centers of the subchannels (Fig. 3.10) at the seven primary FRS thermocouple levels. Details of the thermocouple-array rods are shown in Fig. 3.13.

The remaining fluid instrumentation of note in Bundle 3 was a liquid level rod occupying position 22 in the grid. This liquid level detector system, purchased from EG&G Idaho, Inc., for use in the BDHT Program,[3] consists of an assembly of 19 sensing elements mounted in a probe (rod) plus an electronics package that provides signal conditioning, signal readout, and an output signal for the CCDAS. The probe sensing elements

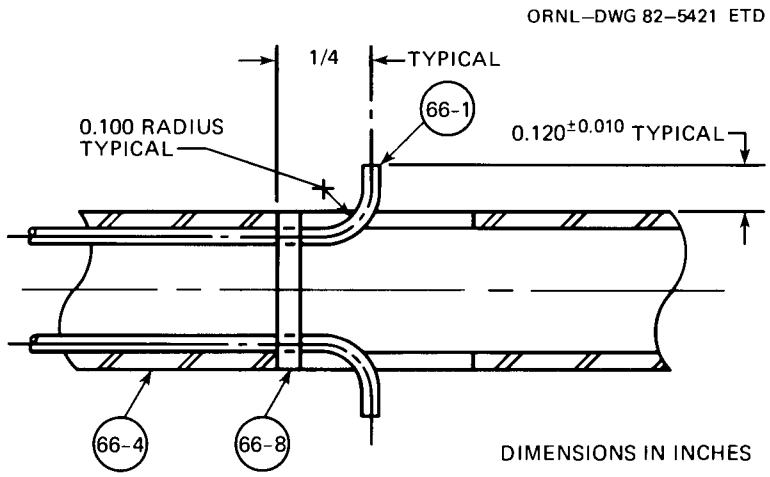

Fig. 3.13. Detail of thermocouple-array rod.

consist of small electrodes surrounded by cylindrical ground planes. The presence or absence of liquid at each sensing element is detected by measurement of a voltage that is a function of the electrical conductivity between the electrode and the ground plane. The axial location of these 19 sensing elements in Bundle 3 is presented in Fig. 3.14 (Ref. 4).

3.3 Bundle 3 FRSs

The original Bundle 3 was installed in the THTF test section on June 26, 1979. As mentioned earlier, the FRS test assembly was an 8 x 8 square array containing 60 FRSs 9.5-mm (0.374-in.) OD on a 12.73-mm (0.501-in.) square pitch with a 3.66-m (12-ft) heated length having a flat power profile. Four unpowered rods (two thermocouple rods, one level rod, and one dummy rod) had an OD of 10.2 mm (0.401 in.). A cross section of the bundle (identifying the FRSs, subchannel locations, and inactive rods) was given in Fig. 3.12. Each FRS contained 16 thermocouples in groups of 4 (1 centerline and 3 sheath) at each of 4 axial levels. The axial levels monitored by each rod are indicated in Fig. 3.15; these axial levels are denoted by alphabetic letters, and the major level nominal locations (A-G) were presented, along with other critical points, in Fig. 3.9.

Problem areas encountered in the Bundle 1 and 2 FRSs (Refs. 1 and 5) were essentially eliminated in the design and construction of the third bundle for the THTF. Bundle 3 FRSs (idealized cross section in Fig. 3.16) were constructed with a single outside sheath (rather than the dual sheath of Bundle 1 and 2), boron nitride (BN) insulator preforms to minimize eccentricity, BN-backfilled thermocouples, and multiple-sheath thermocouples per axial level (as compared to one in Bundle 1). The HEATING5[6] analysis of this FRS design showed the surface heat flux to be perturbed by the presence of the thermocouples by only ±2% of the mean flux, as compared to many times that amount in Bundles 1 and 2. X rays and cross sections of

ORNL–DWG 82–4721 ETD

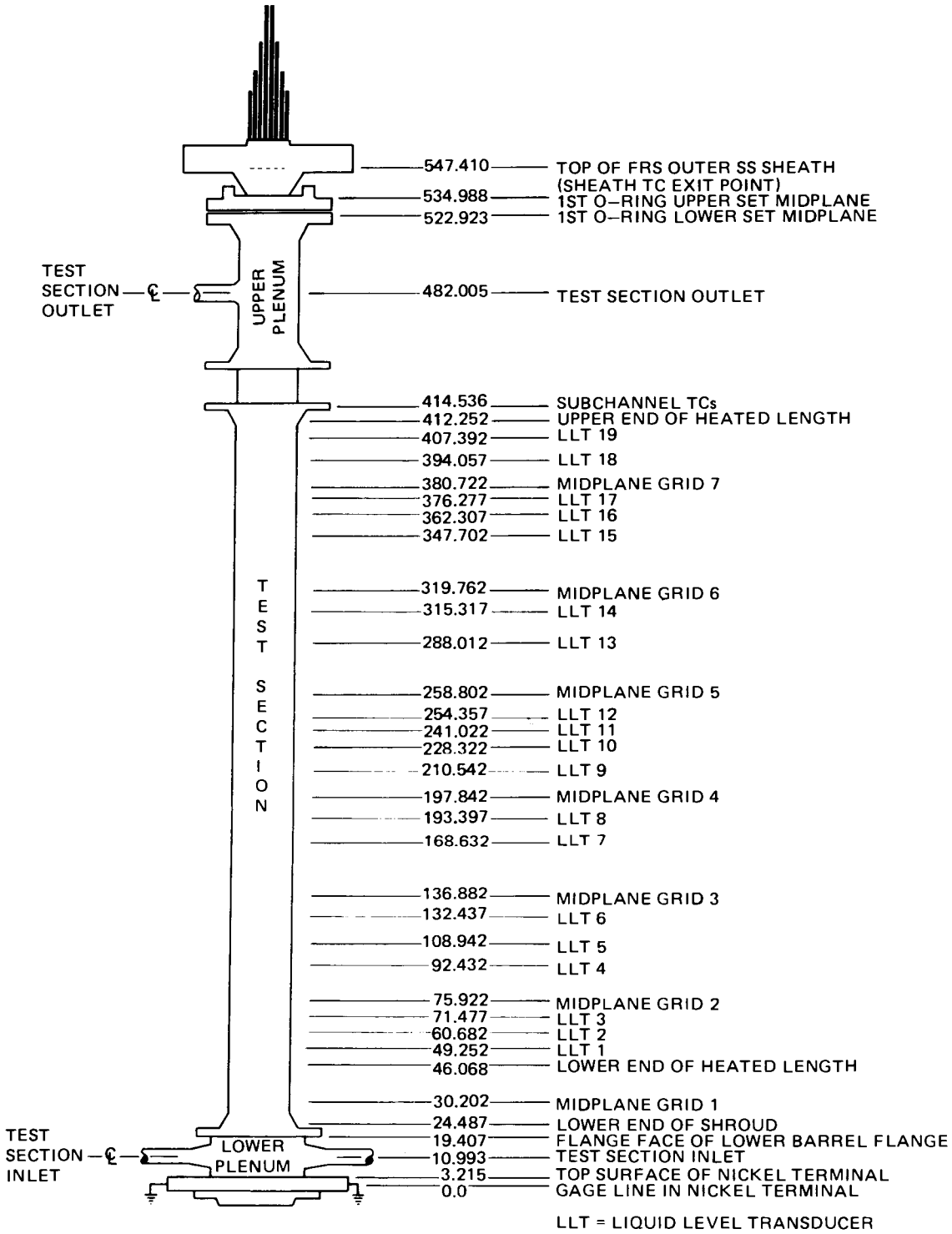

Fig. 3.14. Axial location of 19 sensing elements in INEL liquid level rod. All dimensions are in centimeters and are referenced to gage line in nickel terminal.

ORNL–DWG 82–4714 ETD

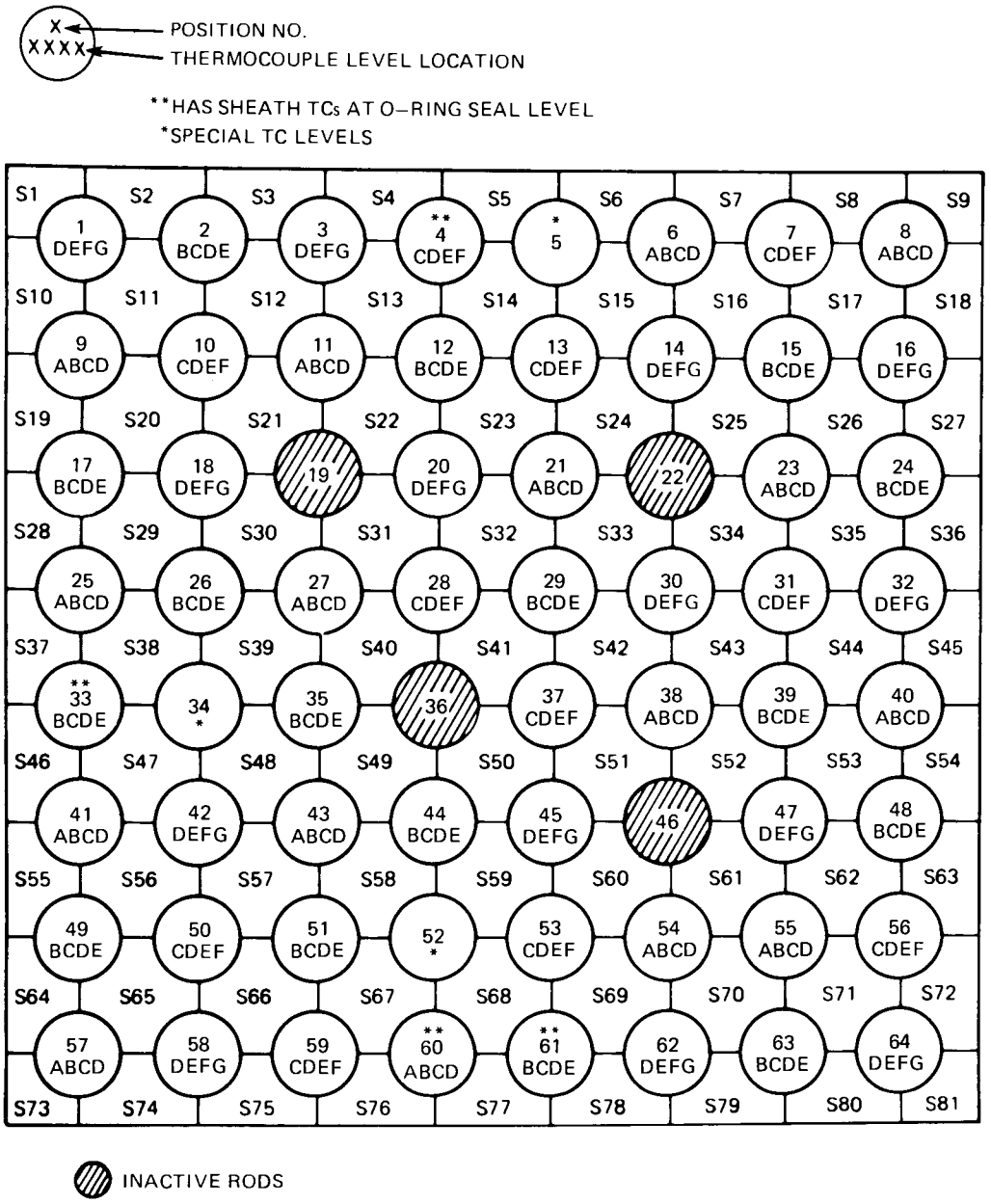

Fig. 3.15. Identification of THTF heater rods and axial thermocouple levels monitored by each rod in THTF Bundle 3.

prototypical Bundle 3 FRSs revealed negligible eccentricity. Furthermore, the Bundle 3 FRS incorporated a flat power profile (i.e., no changes in the power generation rate except at the ends of the 3.66-m heated length). These Bundle 3 FRSs were as nearly axisymmetric as possible using state-of-the-art manufacturing processes.[7]

The thermocouple level locations given in Fig. 3.9 are nominal or design values and do not represent the actual "as-built" locations of the

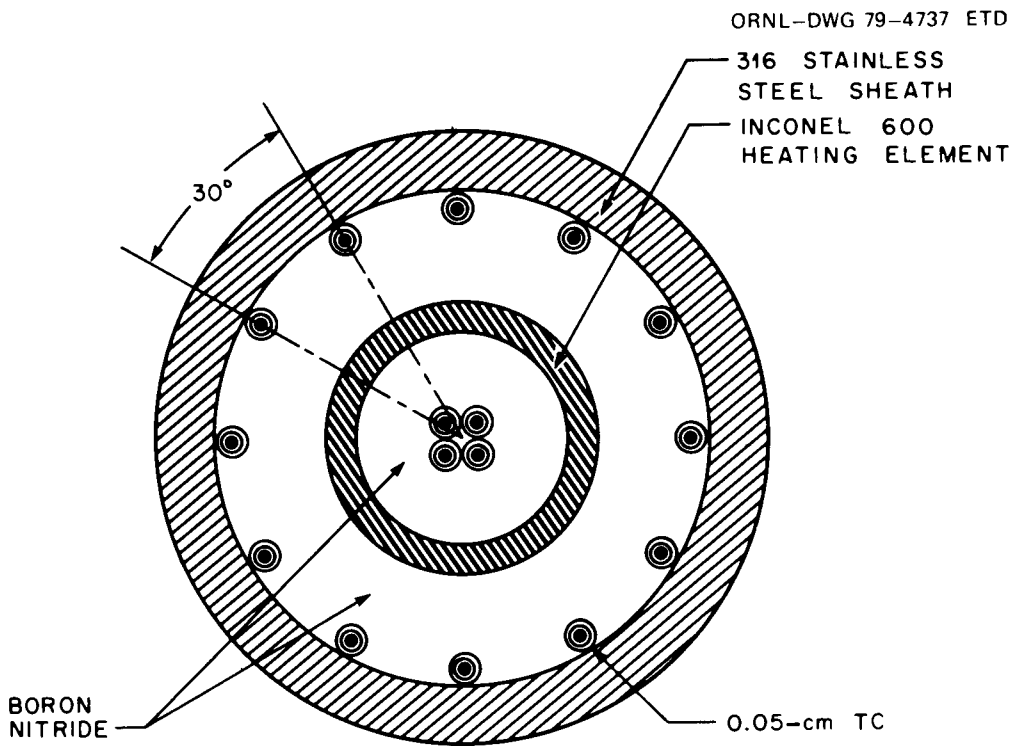

Fig. 3.16. Cross section of THTF Bundle 3 FRS.

FRS thermocouples. The location of each thermocouple in each FRS in Bundle 3 was determined individually from X rays.[8] The compilation of this data is presented graphically in Figs. 3.17 and 3.18. Figure 3.17 is a schematic of Bundle 3 giving the location of all primary-level FRS thermocouples (levels A–G) in the heated section. Figure 3.18 is a schematic of Bundle 3 illustrating the location of the special FRS thermocouples. These special locations include the Y, H, S, and U levels (grouped between C and D levels in the heated section of rods 5, 34, and 52) and O-ring thermocouples (designated as J level) in rods 4, 33, 60, and 61. Where applicable, locations are given as

$$\bar{X}\begin{cases} X_{max} \\ X_{min} \end{cases}, \quad S_X$$

where

$\bar{X}$ = statistical mean,
S_X = standard deviation about the mean,
X_{max} = maximum variation about the mean,
X_{min} = minimum variation about the mean.

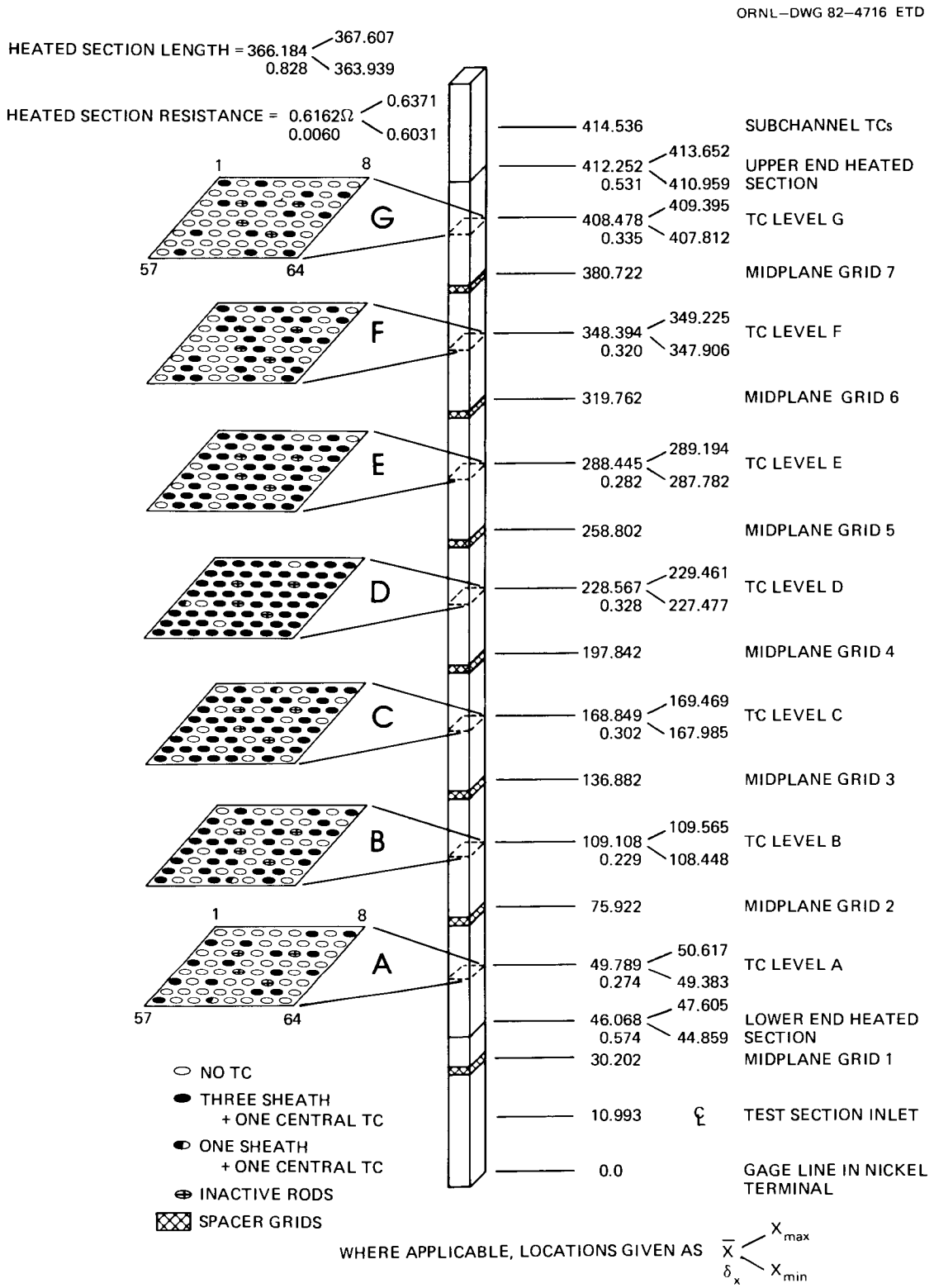

Fig. 3.17. Location of thermocouples in THTF Bundle 3. All dimensions are in centimeters and are referenced to gage line in nickel terminal.

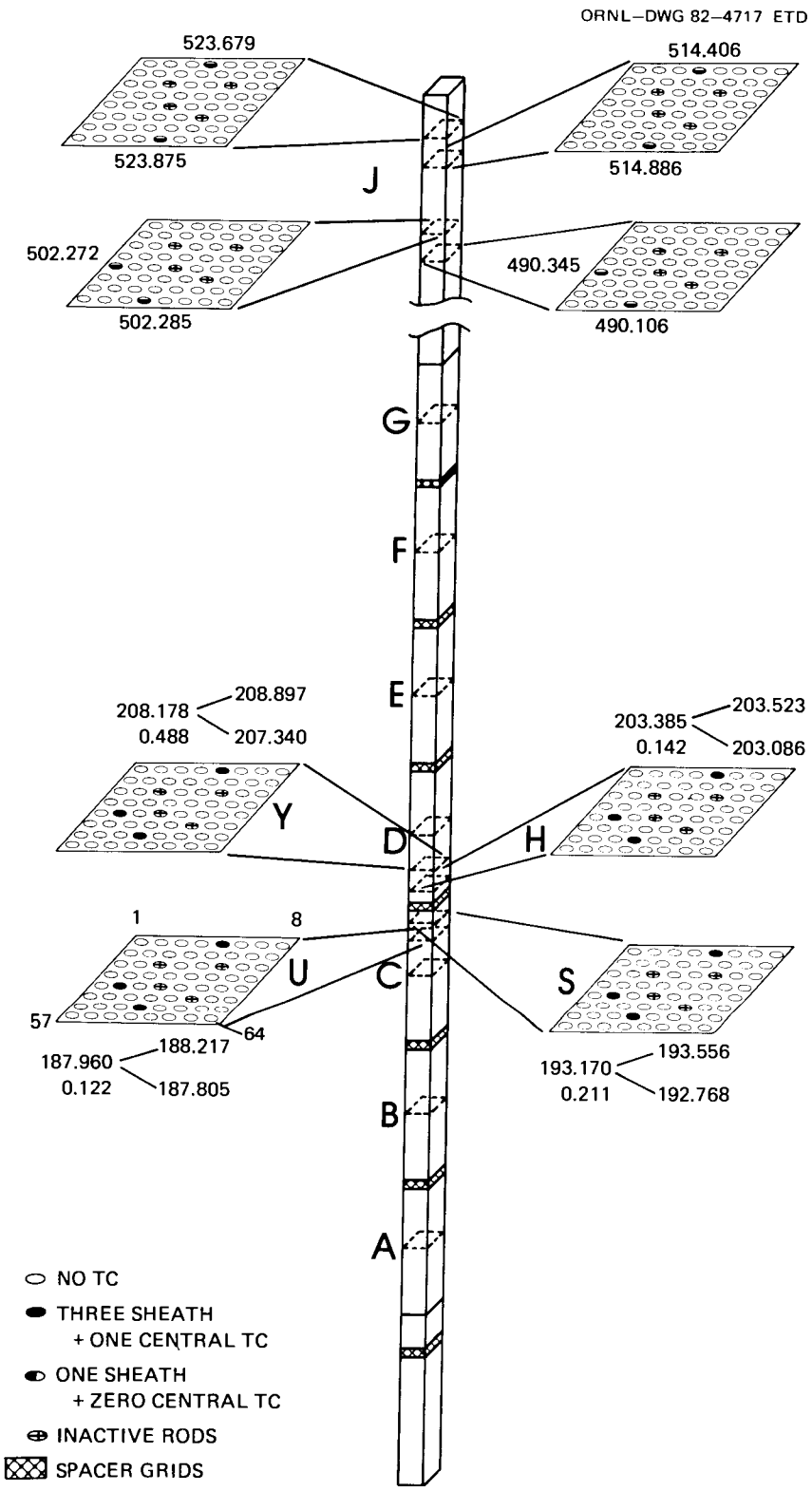

Fig. 3.18. Special thermocouple locations in THTF Bundle 3. All dimensions are in centimeters and are referenced to gage line in nickel terminal.

The nomenclature[9] for Bundle 3 FRS thermocouples takes the following form:

TE-3nnaℓ ,

where

nn = a number between 01 and 64 (inclusive) equal to the rod (grid) position number.

a = for sheath thermocouples, one of three letters (A, B, or C) designating the position of the thermocouple relative to the other two thermocouples in that rod at the designated level. The three thermocouples at a level are labeled A, B, and C in a clockwise direction as viewed from the top of the rod. The centerline thermocouple is designated by the letter M.

ℓ = the level of the thermocouple. A letter in the list A–G (heated section), J (O-ring area), or Y, H, S, and U (four levels grouped between C and D levels in the heated section).

An example of the FRS thermocouple naming convention applied to level F of rod 30 is given in Fig. 3.19.

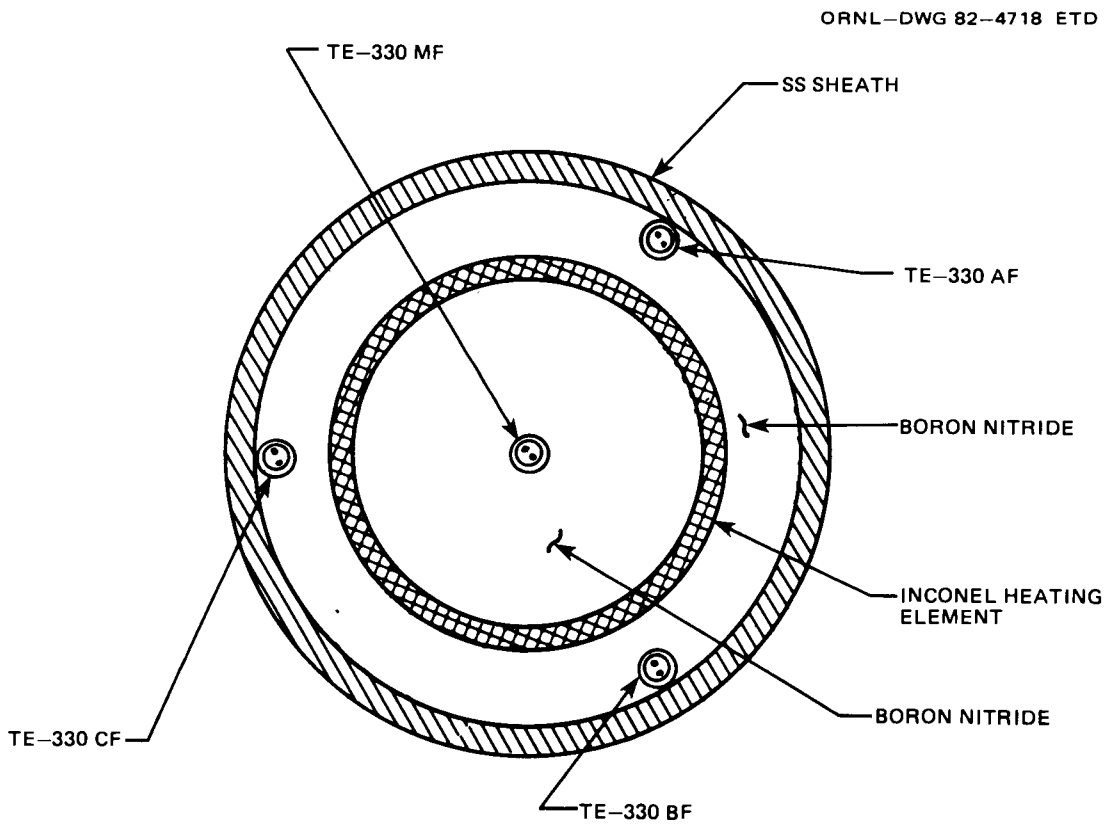

Fig. 3.19. Example of FRS thermocouple nomenclature.

3.3.1 FRS radial dimensions and BN densities

The radial dimensions of the FRSs are important for the analysis of bundle heat transfer data. Because the FRS temperature measurements are made internal to the rods, the FRS surface temperatures and surface heat fluxes are determined from the solution of the inverse heat conduction problem, which is accomplished at ORNL by the computer codes ORINC (Ref. 10) and ORMDIN (Ref. 11).

The final density of the BN material is also an important parameter in the solution of the inverse heat conduction problem. The densities are determined from BN mass inventories kept during the manufacturing process and the final dimensions of the FRSs.

The internal FRS radial dimensions and BN densities suggested for use in all thermal analyses of THTF Bundle 3 rod responses are indicated in Table 3.1. The FRS rods listed as "original or production FRS" are those initially installed in the bundle. The "preproduction FRS" and the "new FRS" are those installed during the two modifications to the bundle and are discussed in Chap. 5 in more detail.

The methodology used in determining the quantities listed in Table 3.1 is described in more detail in Appendix C.1. This appendix was taken from Ref. 1.

Table 3.1. Internal dimensions and boron nitride densities of Bundle 3 FRSs (for the original and refurbished bundles)

Sublayer	Preproduction FRS[a]	Original or production FRS	New FRS[b]
	Outer radius [mm (in.)]		
Stainless steel clad	4.7630 (0.18752)	4.7630 (0.18752)	4.7630 (0.18752)
Outer boron nitride	4.2997 (0.16928)	4.2997 (0.16928)	4.2997 (0.16928)
Heater element	3.1413 (0.12367)	3.1227 (0.12294)	3.1436 (0.12376)
Inner boron nitride	2.8090 (0.11059)	2.7882 (0.10977)	2.8116 (0.11069)
Thermocouple bundle	0.6652 (0.02619)	0.6652 (0.02619)	0.6652 (0.02619)
	Boron nitride density [g/cm³ (lb_m/ft³)]		
Core	2.139 (133.5)	2.158 (134.7)	2.154 (134.5)
Annulus	2.117 (132.1)	2.135 (133.3)	2.131 (133.1)

[a]Described in Sect. 5.2.

[b]Described in Sect. 5.3.

3.3.2 FRS heating element electrical resistance

The power generation rate in the FRS heating element is an important parameter in the thermal analysis of the rod bundle behavior. During preliminary analysis of the THTF tests, the ability to compute the power input to the THTF core was only marginally accurate. For instance, the summed EI product (i.e., the sum for all rods of the product of the rod current I and the generator voltage E) was ~3 to 10% greater than the observed power delivery to the core fluid. Also, if the power to each rod was computed using the rod current I and FRS heating element resistance R, where R is determined from literature data for Inconel-600 electrical resistivity and the cross-sectional area of the heating element, then the total power to the core was 2 to 4% greater than observed. These uncertainties in the computed power to each FRS (and the method of calculation) were unacceptable.

To improve the uncertainties, an FRS that had been removed from the THTF was sent to the FRS Technology Development Laboratory (TDL) to determine the in situ electrical resistance of the active component assembly [(ACA) – the FRS heating element] as a function of temperature. During the tests, the resistance as a function of temperature was behaving in a manner typical of alloys that can undergo order-disorder phenomenon. The results of the testing are presented in Appendix C.2, which is taken from Ref. 1.

As a result of these tests, a methodology for determining the resistance of the FRS heating element was obtained that significantly reduced the uncertainties with which the power generation rate could be determined. The ACA heated section electrical resistance per unit length as a function of temperature for the FRS rod tested (FRS-058B) is shown in Fig. 3.20. Using a correction factor β_i defined by

$$\beta_i = \frac{\text{heated length of rod i}}{\text{heated length of FRS-058B}} ,$$

the electrical resistance of rod i in the THTF core may be determined from Fig. 3.20 and β_i by

$$R_i = R_{FRS-058B} \times \beta_i ,$$

where R_i has units of ohms per unit length. The correction factor is necessary because of the dimensional changes in the heating element caused by the swaging process during fabrication of the FRSs. The actual "finished" cross section of the heating elements varies somewhat from rod to rod. Assuming that the initial heating elements were the same for each of the rods prior to the swaging process, then the measurement of the as-built heated length should be inversely proportional to the finished cross section of the heating element. Because the resistance is inversely proportional to the cross-sectional area, the correction factor is proportional to the ratio of the heated lengths.

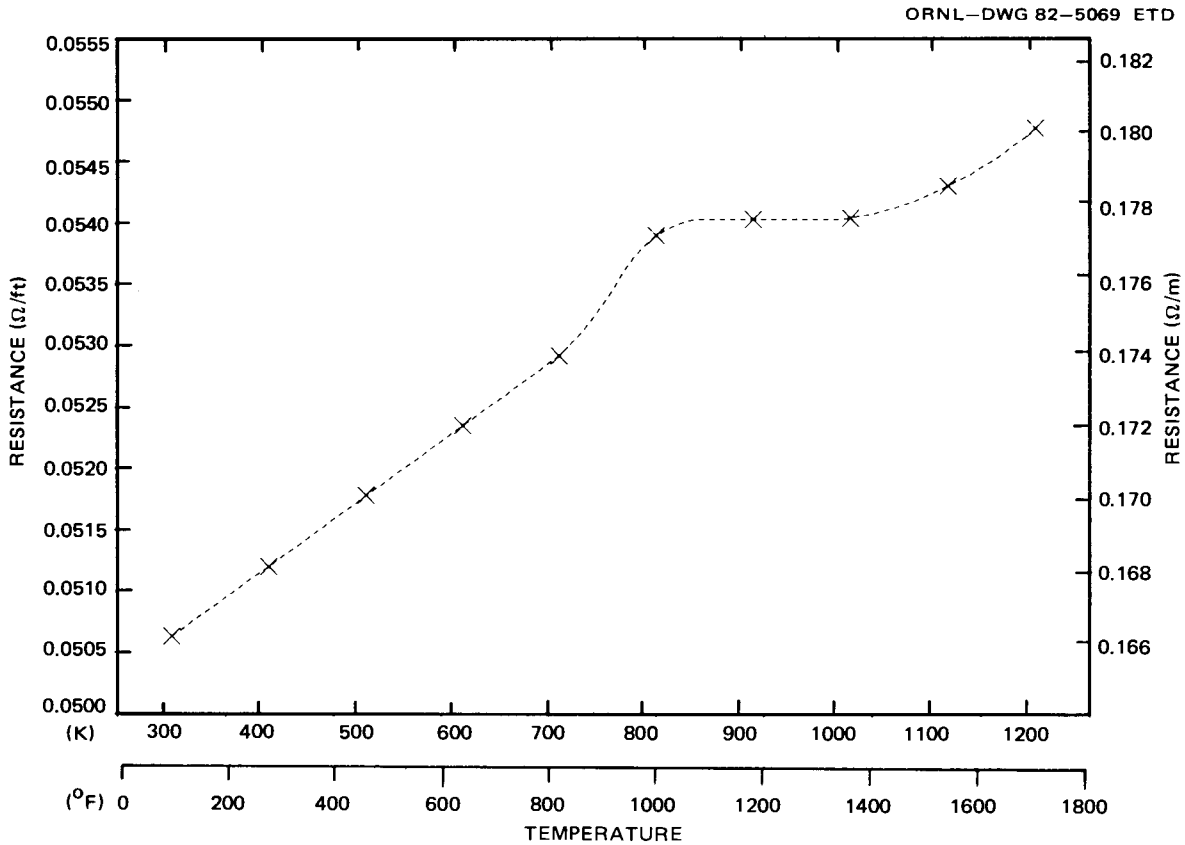

Fig. 3.20. Heated length electrical resistance for FRS-058B.

Using this method, the computed power input to the THTF core was ±1.0% of the observed power delivery to the core fluid. Table 3.2 lists the measured heated lengths and β_i for the original bundle as well as for the two modifications to the bundle.

3.3.3 FRS surface emissivity

In many of the tests conducted in the THTF during Bundle 3 operations, the radiative heat transfer from the rod surface was a significant mode of heat removal from the FRS. The determination of the radiant heat transfer component of the total heat transferred at the surface of the FRS requires that the rod surface emissivity be known. Estimates of the emissivity of stainless steel for different types of surfaces (i.e., polished-oxidized) can vary from 0.05 to 0.90. Also, the condition of the FRS cladding surface in the THTF does not necessarily fit in the literature categories and is dependent on its environment and operating history (i.e., possible chemical corrosion, surface deposition, and surface discoloration due to high temperature). To obtain an experimental value for the surface emissivity, an FRS from the THTF was tested in the FRS TDL.

Table 3.2. Actual heated lengths and correction factor, β_i, for determining heating element electrical resistance for THTF FRSs

Rod position	Original bundle		First modification		Second modification	
	Heated length (cm)	β_i	Heated length (cm)	β_i	Heated length (cm)	β_i
1	366.37	0.998	361.81	0.985[a,b]	363.17	0.989[a,c]
2	366.18	0.997	366.18	0.997	366.18	0.997
3	365.25	0.995	365.25	0.995	365.25	0.995
4	365.84	0.996	365.84	0.996	365.84	0.996
5	363.94	0.991	363.94	0.991	363.94	0.991
6	366.08	0.997	366.08	0.997	366.08	0.997
7	365.68	0.996	365.68	0.996	365.68	0.996
8	366.32	0.998	366.32	0.998	366.32	0.998
9	366.06	0.997	366.06	0.997	366.06	0.997
10	365.39	0.995	365.39	0.995	365.39	0.995
11	365.63	0.996	365.63	0.996	365.63	0.996
12	366.15	0.997	366.15	0.997	366.15	0.997
13	365.55	0.995	365.55	0.995	365.55	0.995
14	367.55	1.001	359.86	0.980[a,b]	365.57	0.995[a,c]
15	367.61	1.001	359.93	0.980[a,b]	366.06	0.997[a,d]
16	365.81	0.996	365.81	0.996	365.81	0.996
17	366.22	0.997	366.22	0.997	366.77	0.999[a,d]
18	366.31	0.997	366.31	0.997	366.31	0.997
19						
20	367.21	1.000	367.21	1.000	367.21	1.000
21	367.56	1.001	367.56	1.001	365.68	0.996[a,c]
22						
23	366.19	0.997	366.19	0.997	366.19	0.997
24	365.79	0.996	365.79	0.996	365.79	0.996
25	365.82	0.996	365.82	0.996	365.82	0.996
26	367.27	1.000	367.27	1.000	367.27	1.000
27	366.06	0.997	366.06	0.997	366.06	0.997
28	365.71	0.996	365.71	0.996	365.71	0.996
29	366.75	0.999	366.75	0.999	366.75	0.999
30	364.43	0.992	365.82	0.996[a,d]	365.82	0.996
31	366.65	0.998	366.65	0.998	366.65	0.998
32	367.01	0.999	367.01	0.999	367.01	0.999[e]
33	364.62	0.993	364.62	0.993	364.62	0.993
34	363.44	0.990	363.44	0.990	363.62	0.990[a,c]
35	365.56	0.995	365.56	0.995	365.56	0.995
36						
37	367.23	1.000	367.23	1.000	365.48	0.995[a,c]
38	366.22	0.997	366.22	0.997	364.61	0.993[a,c]
39	366.27	0.997	366.27	0.997	366.27	0.997
40	366.99	0.999	366.99	0.999	366.99	0.999
41	365.94	0.996	365.94	0.996	365.94	0.996
42	366.34	0.998	366.34	0.998	366.34	0.998

Table 3.2 (continued)

Rod position	Original bundle		First modification		Second modification	
	Heated length (cm)	β_i	Heated length (cm)	β_i	Heated length (cm)	β_i
43	364.88	0.994	364.88	0.994	364.88	0.994
44	366.68	0.999	366.68	0.999	366.68	0.999
45	363.92	0.991	363.92	0.991	363.92	0.991
46						
47	367.19	1.000	367.19	1.000	367.19	1.000
48	364.41	0.992	364.42	0.992[a,b]	364.42	0.992
49	366.78	0.999	366.78	0.999	366.78	0.999
50	366.06	0.997	366.06	0.997	365.58	0.996[a,c]
51	367.08	1.000	367.08	1.000	367.08	1.000
52	366.64	0.998	366.64	0.998	366.64	0.998
53	364.53	0.993	364.53	0.993	364.53	0.993
54	367.50	1.001	367.50	1.001	365.30	0.995[a,c]
55	365.85	0.996	365.85	0.996	365.85	0.996
56	365.55	0.995	362.19	0.986[a,b]	363.44	0.990[a,d]
57	366.47	0.998	366.47	0.998	366.47	0.998
58	362.82	0.988	362.82	0.988	362.82	0.988
59	365.92	0.996	365.92	0.996	365.92	0.996
60	366.58	0.998	361.99	0.986[a,b]	366.47	0.998[a,c]
61	367.23	1.000	367.23	1.000	367.23	1.000
62	363.76	0.991	362.31	0.987[a,b]	366.22	0.997[a,d]
63	366.48	0.998	366.48	0.998	366.48	0.998
64	366.23	0.997	366.23	0.997	366.23	0.997

[a]Replacement rod.

[b]Preproduction-type FRS (Table 3.1).

[c]New-type FRS (Table 3.1).

[d]Original-type FRS (Table 3.1).

[e]Rod 32 replaced prior to test 3.08.6C due to a failure of the original FRS. Heated length of new rod is 364.46 cm; β_i = 0.992. Rods not designated are original-type FRSs.

The details of the procedures used to determine the surface emissivity are presented in Appendix C.3, which was taken from Ref. 1. A least squares fit to the data results in an equation for the surface emissivity ε of

$$\varepsilon(T) = 0.25617 + 0.000348\ (T-616.67)\ ,$$

where T has units of K; or

$$\varepsilon(T) = 0.25617 + 0.000193\ (T-650)\ ,$$

where T has units of °F. For the temperature range of interest in the THTF (950–1150 K), the estimated surface emissivity is 0.372–0.442. As pointed out in Appendix C.3, the data used in determining the surface emissivity were taken at temperatures below 750 K so that the values used above this temperature are extrapolated estimates.

4. INSTRUMENTED SPOOL PIECES

Flow conditions at the boundaries of the test section are measured by "instrumented spool pieces" as input to the analysis of the rod bundle test data; these measurements include mass flux, pressure, and temperature.

A spool piece consists of a fluid thermocouple, an absolute pressure tap, a turbine meter for measuring volumetric flow or velocity v, a drag disk for measuring momentum flux ρv^2, and a gamma densitometer for measuring chordal average density ρ of the fluid – all contained within a flanged length of loop piping. Because the mass flux is not directly measured, it is necessary to use combinations of these instruments to determine mass flux. Homogeneous models may be used combining the turbine meter and gamma densitometer ρv, the drag disk and the gamma densitometer $\sqrt{\rho \times \rho v^2}$, and the turbine meter and drag disk $\rho v^2/v$ to obtain mass flux. Although the uncertainties obtained using the homogeneous models should be fairly small in single-phase flow, significant uncertainties may exist in two-phase flow where effects such as slip, void fraction, flow regime, and transient response affect the physical interpretation of the instrument output. Studies[12,13] on the uncertainties generated in using the homogeneous mass flux models in two-phase flow conditions are available.

As shown in Fig. 4.1, instrumented spool pieces are located at the inlet and outlet of the test section. Diagrams of the spool pieces are shown in Figs. 4.2 and 4.3. The four original spool pieces, SHI, SVI, SHO, and SVO, are designed with the densitometer positioned in the center of the spool piece (Fig. 4.2). A more recent design installed at BO1, BI1, and BI2 is shown in Fig. 4.3. In this latest design, the densitometer is located at the end of the spool piece. The design change was made to eliminate effects on the densitometer measurements due to flow and flow regime disturbances caused by interference-type instruments upstream of the densitometers.[14] The densitometer end of these spool pieces is generally oriented so that the densitometer is upstream of the other instruments for the expected direction of the two-phase flow. In the standard configuration, ORNL single-beam gamma densitometers are installed on the SHI, SVI, SHO, and SVO spool pieces. The BO1, BI1, and BI2 spool pieces use Measurements, Inc., three-beam gamma densitometers. The turbine meters installed in the spool pieces are five-bladed 3.5-in. Flow Technology turbine meters with ORNL electronics. A diagram showing the nominal dimension of the turbine meters is shown in Fig. 4.4. The drag disks are Ramapo Mark V strain-gage-type drag disk transducers with ORNL three-bladed full-flow drag disk targets. A diagram showing the target area for the flow is shown in Fig. 4.5. The fluid thermocouples are Nanmac type K and project into the center of the spool-piece flow area. Pressure cells used are Precise Sensor 0- to 20.7-MPa (0- to 3000-psig) pressure transducers.

As mentioned previously, three-beam gamma densitometers were installed on three of the spool pieces. A three-region annular model[15] was used to reduce the three-beam densitometer results to a composite density suitable for use in the mass flux models. The model solves for a uniform density for each region in Fig. 4.6 using the density indicated by each of the three beams and the length of each beam within each region.

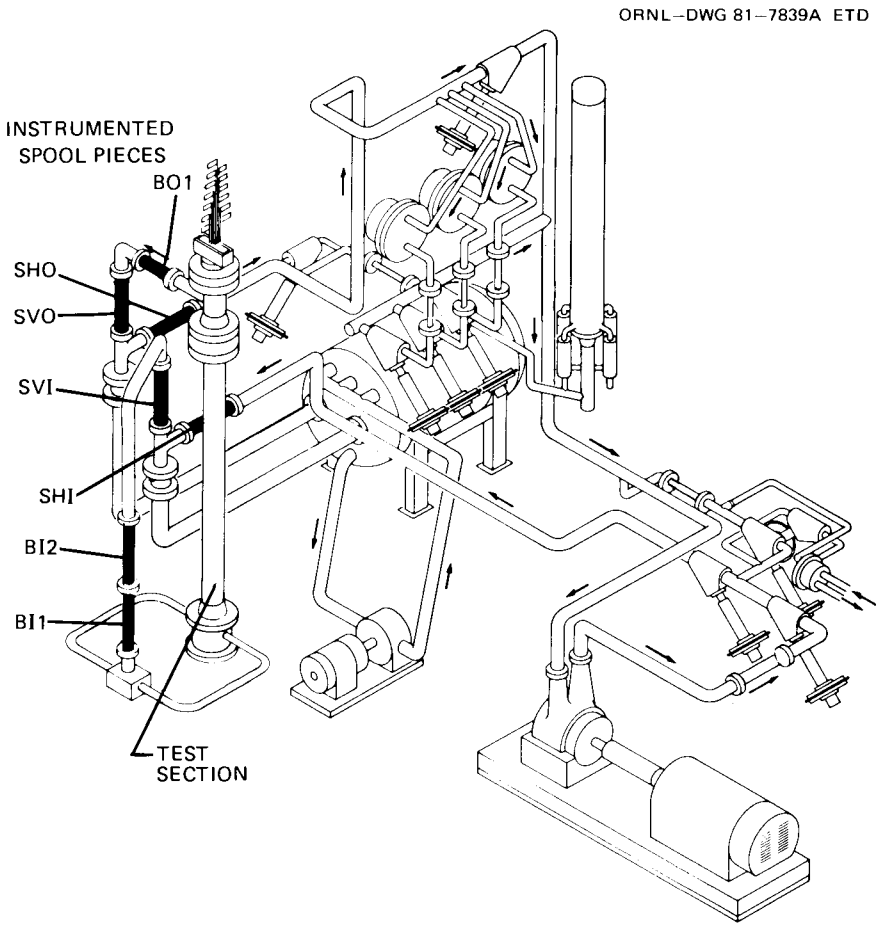

Fig. 4.1. Location and identification of instrumented spool pieces in THTF standard configuration.

The composite pipe density is then calculated as an area-weighted average of the three-region densities. The resulting equation for the composite density is

$$\bar{\rho}_{annular} = 0.3784\rho_A + 0.5117\rho_B + 0.1099\rho_C ,$$

where ρ_A, ρ_B, and ρ_C are the densities measured by the three beams (Fig. 4.6).

Various other models may be used for combining the three chordal density measurements, such as the stratified model.[14] However, air-water studies[14] indicate that little difference (~5%) is observed between the two models.

The individual instruments and their uncertainties are described in more detail in Chap. 6 and Appendix D.

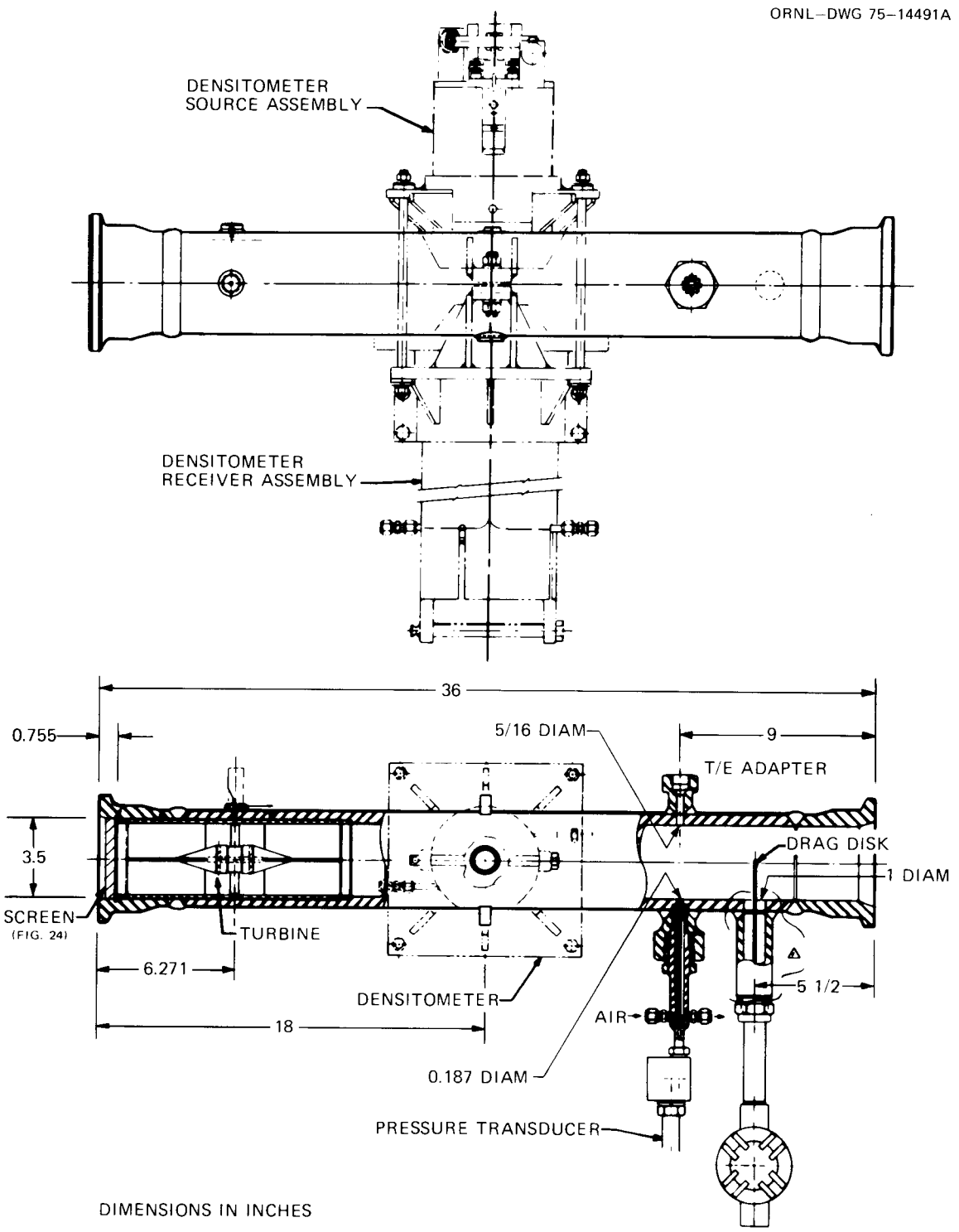

Fig. 4.2. Original THTF spool-piece design (spool pieces SHI, SVI, SHO, and SVO in standard THTF configuration).

ORNL-DWG 82-5422 ETD

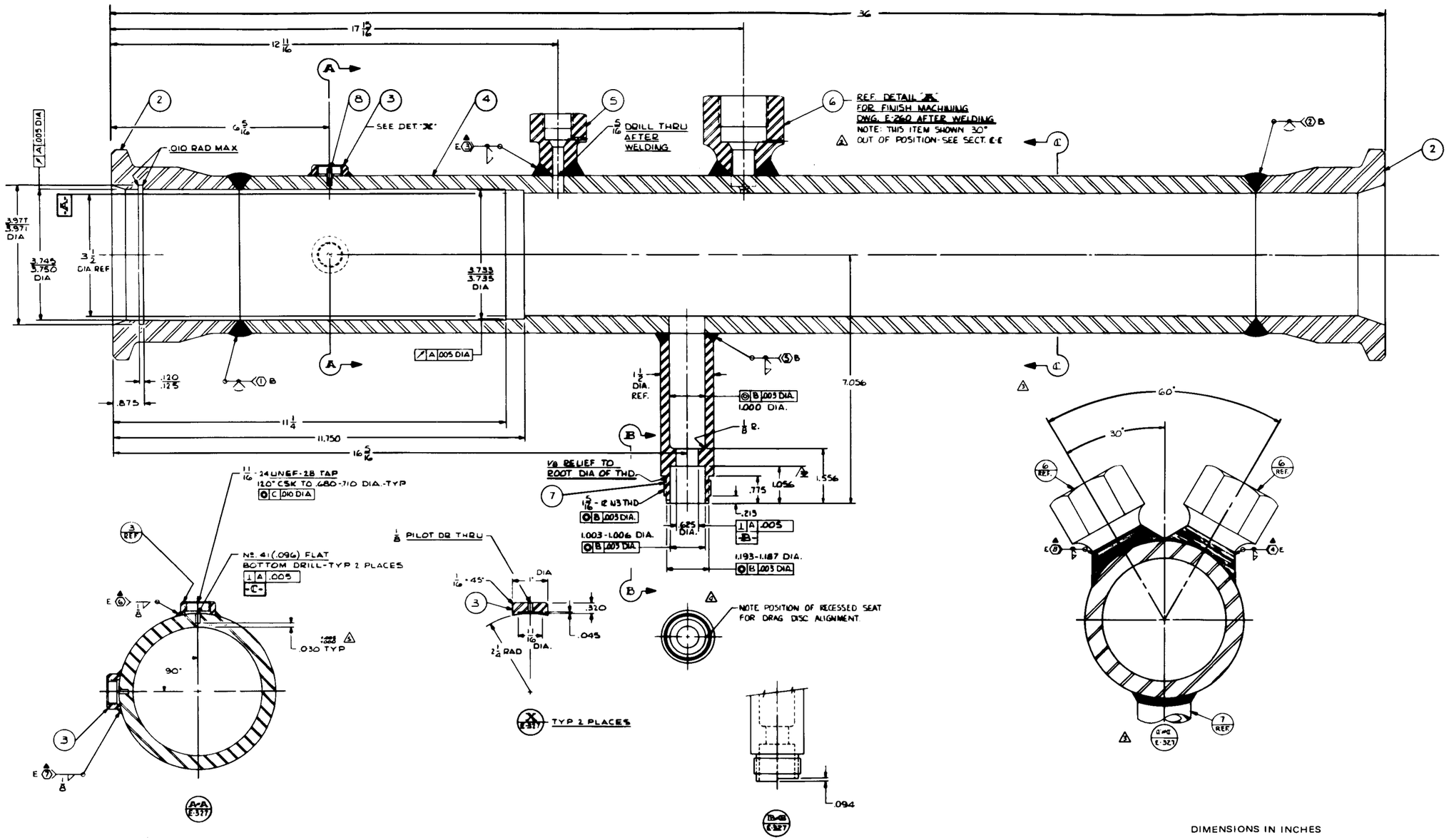

Fig. 4.3. Recent spool-piece design (spool pieces BI1, BI2, and BO1 in standard THTF configuration). (Microfiche copy of this drawing attached to back of report.)

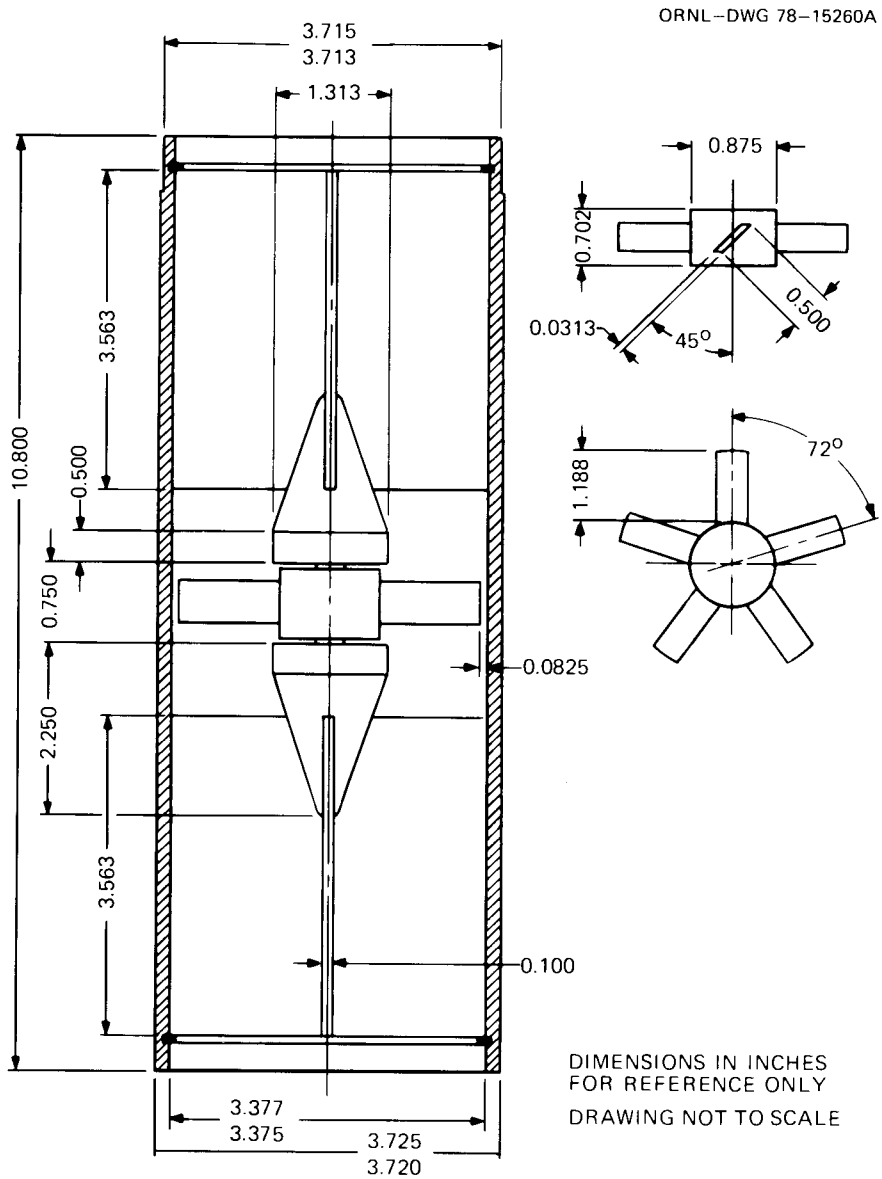

Fig. 4.4. Turbine meter assembly (Flow Technology).

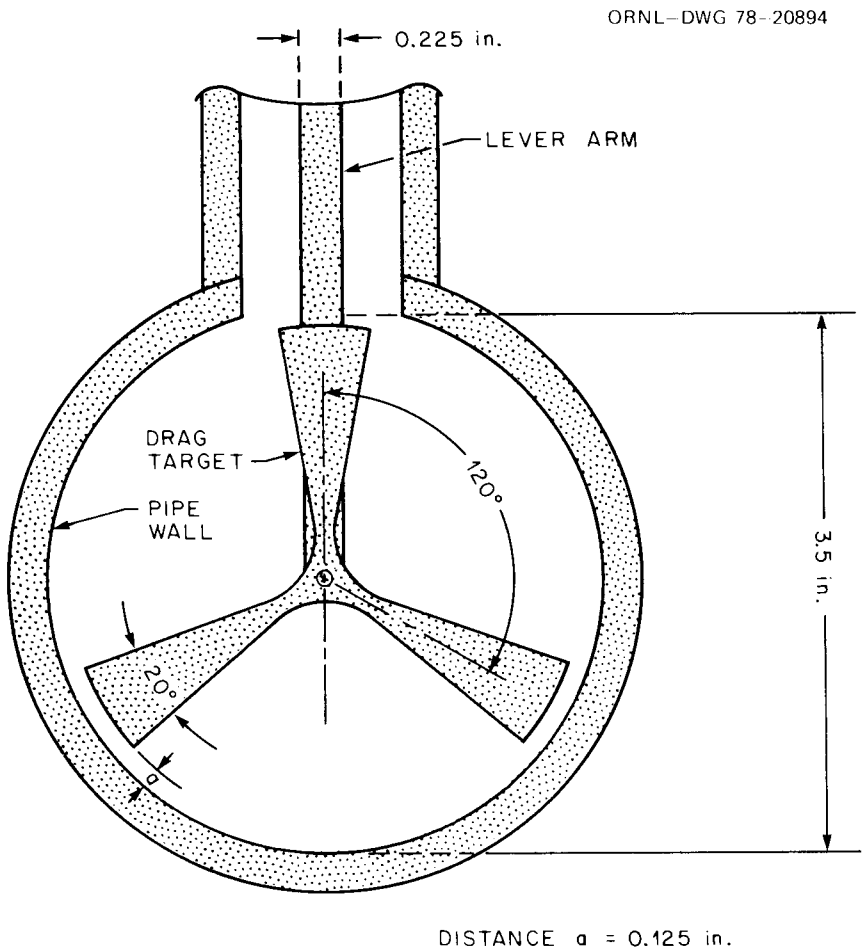

Fig. 4.5. Appearance of three-bladed drag target in pipe. View is looking downstream.

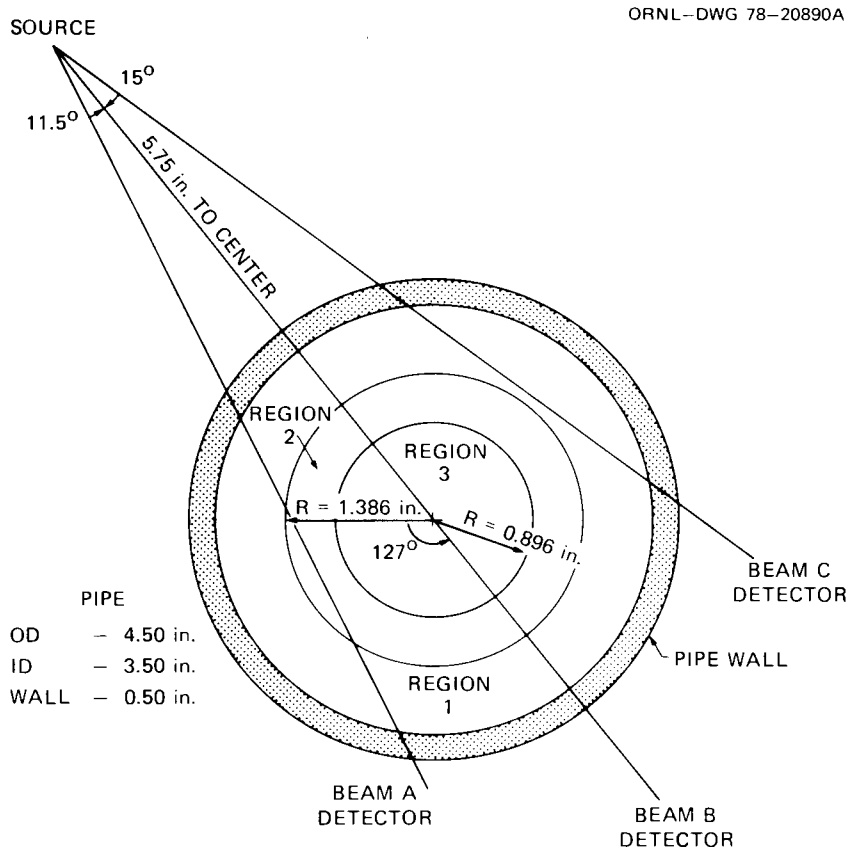

Fig. 4.6. Diagram showing uniform density regions used in annular model for reduction of three-beam densitometer data.

5. TEST-SPECIFIC FACILITY DESCRIPTION

Major modifications to the test section, bundle, and loop piping were made over the operating history of Bundle 3. The following chapter describes those modifications and provides test-specific descriptions for the primary tests run at the THTF. The descriptions of the tests are arranged chronologically with respect to the THTF Bundle 3 operating history and subgrouped according to the original bundle configuration and two subsequent modifications to the bundle. A complete history of Bundle 3 operations including shakedown and FRS calibration tests is presented in Ref. 1. A summary of the operations history is presented in Table 5.1.

The original bundle was used for only one primary set of tests, the small-break LOCA-I test series (3.02.10C-H). These tests were characterized by significantly lower power and mass flow rates than previous tests run at the THTF, and, as a result, significant loop-piping modifications were required. These tests are described in Sect. 5.1.1.

Following the small-break LOCA-I test series, attempts were made to reach full power with the bundle. However, these tests were not successful, because significant leakage through the O-ring seals providing the bundle pressure boundary was observed (presumably due to the high temperatures experienced during the small-break LOCA-I testing). As a result of the leakage, the O-ring seals required replacement. After the rods were removed to replace the O-rings, it was discovered that problems with the welds made in attaching the O-ring sets to the FRS rods had also caused damage to the FRS rods. The welds had punctured the sheaths, exposing the annular BN insulation to the system water. Operation of the rods, especially at high powers, eventually caused arcing and localized heating in the O-ring area. A new single-piece O-ring oversleeve was designed, fabricated, and installed on all of the FRSs. All but eight of the original Bundle 3 FRSs were repaired. A detailed description of the inspection and repair of the damaged FRSs is presented in Ref. 16. The eight permanently damaged rods were replaced with spare FRSs, seven of which were preproduction models of the Bundle 3 simulators (these will be described in more detail in Sect. 5.2). Instrument rod changes and the addition of pressure taps along the test section were also made during this period and will be discussed in more detail in Sect. 5.2.

Two primary tests were completed following these modifications, the Upflow Film Boiling Test 3.03.6AR and the Double-Ended Cold-Leg Break Test 3.05.5B. Test 3.03.6AR was a relatively slow, outlet-only break test aimed at obtaining transient heat transfer data for film boiling in rod bundle geometries. Test 3.05.5B was a relatively high-powered, double-ended blowdown aimed at (1) measuring times to departure-from-nucleate-boiling (DNB) in a hydraulic environment similar to that predicted to exist in a PWR during an LOCA and (2) to provide a benchmark for transient reactor analysis codes. Facility descriptions for these tests are presented in Sects. 5.2.1 and 5.2.2, respectively.

Following Test 3.05.5B, in July and August of 1980, the bundle and test section were again modified. The primary purpose this time was to improve instrumentation for the second series of upflow film boiling tests and small-break LOCA tests based on experience gained from initial testing. The modifications, which included (1) replacing most of the

Table 5.1. Summary of THTF Bundle 3 operating history

Event	Date
Initiation of Bundle 3 design and procurement	August 1978
Fabrication of Bundle 3 and FRS heater rods completed	June 1979
Bundle 3 installation at THTF site	September 1979
Isothermal blowdown test (3.01.5A)	October–November 1979
First Bundle 3 powered operation power-drop/ bundle-characterization test	November 1979
Small-break LOCA-I test series – 3.02.10A,B and 3.02.10C-H	December 1979 January 1980
Power-drop/bundle-characterization test	February 1980
First modification to Bundle 3, rebuild and repair of O-ring seal assemblies, installation of test section differential pressure taps	March–April 1980
Power-drop/bundle-characterization test	May 1980
Upflow Film Boiling (transient blowdown) Test (3.03.6AR)	May 1980
Downflow Film Boiling (transient blowdown) Test (3.04.7)	June 1980
Double-Ended Cold-Leg Break (transient blowdown) Test (3.05.5B)	July 1980
Second modification to Bundle 3, new FRS thermocouple levels, installation of shroud-box wall thermocouples, in-bundle gamma densitometers, and new thermocouple-array rods	July–August 1980
Upflow Film Boiling (transient blowdown) Test (3.06.6B)	August 1980
Steady-state upflow film boiling test series (3.07.9)	September–October 1980
Upflow Film Boiling (transient blowdown) Test (3.08.6C)	October 1980
Small-break LOCA-II test series (3.09.10I-X)	October–November 1980
Intermediate-flow heat transfer test series (3.10.11A-H)	December–February 1981

preproduction FRSs with new FRSs, (2) installing shroud-box wall thermocouples, and (3) installing new instrument rods, are described in Sect. 5.3.

Two transient Upflow Film Boiling Tests, 3.06.6B and 3.08.6C, and Steady-State Upflow Film Boiling Tests 3.07.9A–X were run in August and September of 1980. These tests are described in Sects. 5.3.1–5.3.3. Following these tests, the second series of small-break LOCA tests was run (3.09.10I–X); they are described in Sect. 5.3.4. These tests included boiloff, reflood, and steady-state uncovered bundle tests over similar parameter ranges as the small-break LOCA-I test series. The final test series, the Intermediate-Flow Heat Transfer Tests 3.10.11A–H, was completed in February of 1981. These tests were aimed at the mass flux and power ranges between those of the small-break LOCA test series and the steady-state upflow film boiling test series. They are described in Sect. 5.3.5.

5.1 Original Bundle

The original bundle was described previously in Chap. 3. In total there were 960 (720 sheath and 240 centerline) FRS thermocouples. Due to a limited number of FET multiplexers for the CCDAS, only ~60% of the total number of FRS thermocouples were monitored. The FRS thermocouples given in Table 5.2 were monitored by the CCDAS for the tests run on the original bundle. Additionally, 50 FRS thermocouples were monitored by a visual multichannel temperature indicator (Metrascope) in the THTF control room. These thermocouples provided a real time indication of the bundle conditions for operational purposes but were not available for the CCDAS. The location and names of these Metrascope thermocouples are indicated in Fig. 5.1.

5.1.1 Small-break LOCA-I test series 3.02.10C–H

The objective of the small-break LOCA-I test series was to experimentally investigate heat transfer and reflood under conditions similar to those expected in small-break LOCAs. These experiments[17–20] were designed to study the quasi-steady uncovered phase of a small-break LOCA and, in addition, to obtain qualitative data regarding the high-pressure reflooding of an uncovered core. Table 5.3 presents the range of parameters over which the tests were run.

Significant modifications were made to the THTF to meet the instrumentation and operational control requirements of these low-flow low-power tests. The 4-in. inlet and outlet piping of the standard configuration was replaced with 1/2- and 3/4-in. tubing to reduce the loop volume and facilitate the installation of low-flow controls and instrumentation. The reduced loop volume allowed the use of nitrogen overpressure in the pressurizer, which considerably simplified operation of the tests. With the smaller tubing on the outlet, the pressurizer volume was large enough to accommodate the system fluid displaced as steam was created in the upper bundle during uncovery. The smaller lines also aided in reducing energy

Table 5.2. In-service thermocouple listing for original Bundle 3

Rod	Sheath angle level	Center level
1	AE,[a] AG, BF, CD	MD,[b] ME, MF, MG
2	AB, AE, BC, CD	MB, MC, MD, ME
3	BE, BF, CD, CG	MD, ME, MF, MG
4	AC, BD, BE, CF	MC, MD, ME, MF
5	AS, BH, BU, CY	MH, MS, MU, MY
6	AB, BA, BC, BD	MA, MC, MD
7	AC, AF, CE	MC, MD, ME, MF
8	AA, BC, BD, CB	MB, MC, MD
9	AC, AA, CB, CD	MA, MB, MC, MD
10	AF, BE, CC, CD	MC, MD, ME, MF
11	CA, CB, CC, CD	MA, MB, MC, MD
12	BC, BD, BE, CB	MB, MC, MD, ME
13	BC, BF, CD, CE	MC, MD, ME, MF
14	AD, AE, AF, AG, BD, BE, BF, BG, CD, CE, CF	MD, ME, MF, MG
15	AB, AE, BC, CD	MB, MC, MD, ME
16	AD, BF, CE, CG	MD, ME, MF, MG
17	AE, CB, CC, CD	MB, MC, MD, ME
18	AD, AF, BE, BG	MD, ME, MF, MG
19	Rod 19 is unpowered	
20	AD, AE, AF, AG, BD, BE, BF, BG, CD, CE, CF, CG	MD, MF, MG
21	AA, AB, BC, CD	MA, MB, MD
22	Rod 22 is unpowered	
23	AD, BC, CB	MB, MC, MD
24	AC, BD, CB, CE	MC, MD, ME
25	AA, AB, AC, BA, BB, BC, BD, CA, CB, CC, CD	MA, MB, MC, MD
26	AC, BB, BD, CE	MB, MC, MD, ME
27	AA, AB, AC, AD, BA, BB, BC, BD, CA, CB, CC, CD	MA, MB, MC, MD
28	AC, AD, AE, AF, BC, BD, BE, BF, CC, CD, CE, CF	MC, MD, ME, MF
29	AB, AC, AD, AE, BB, BC, BD, BE, CB, CD, CE	MB, MC, MD, ME
30	BF, BG, CD, CE	MD, ME, MF, MG
31	AC, CD, CE, CF	MC, MD, ME, MF
32	AE, AD, AF, AG, BE, BG, CD, CE, CF, CG	MD, ME, MG
33	AC, AD, CB, CE	MB, MC, MD, ME
34	AH, AS, AU, AY, BH, BS, BU, BY, CH, CS, CU, CY	MH, MS, MY
35	AC, BB, BE, CD	MB, MC, MD, ME
36	Rod 36 is unpowered	
37	AE, BC, BD, CF	MC, MD, ME, MF
38	AB, BA, BC, BD	MA, MB, MC, MD
39	AC, BB, BD, BE	MB, MC, MD, ME
40	BC, BD, CA, CB	MA, MB, MC, MD
41	AB, BA, BD, CC	MA, MB, MC, MD
42	BD, BE, CF, CG	MD, ME, MF, MG
43	BA, BB, BC, CD	MA, MB, MC, MD
44	CB, CC, CD, CE	MB, MC, ME
45	AD, AE, AF, AG, BD, BE, BF, BG, CD, CE, CF, CG	MD, ME, MG
46	Rod 46 is unpowered	
47	AD, AE, AG, BF	MD, ME, MF, MG
48	BC, BD, CB, CE	MB, MC, MD, ME
49	CB, CC, CD, CE	MB, MC, MD, ME
50	AC, AD, AE, AF, BC, BD, BE, BF, CC, CD, CE, CF	MC, MD, ME, MF
51	AB, AE, BC, BD	MB, MC, MD, ME
52	AH, AS, AU, AY, BH, BS, BU, BY, CH, CS, CU, CY	MH, MS, MU, MY
53	AD, AE, AF, CC	MC, MD, ME, MF
54	AD, CA, CB, CC	MA, MB, MC, MD
55	AA, AD, BC, CB	MA, MB, MC, MD
56	AD, AF, BE, CC	MC, MD, ME, MF
57	AA, AB, AC, AD, BA, BB, BC, BD, CA, CB, CC, CD	MA, MB, MC, MD
58	BE, CD, CF, CG	MD, ME, MF, MG
59	AD, AE, CC, CF	MC, MD, ME, MF
60	AA, AB, AC, AD	MA, MB, MC, MD
61	AB, AC, AD, CE	MB, MC, MD
62	AD, AE, AF, CG	MD, ME, MF, MG
63	AD, BC, BE, CB	MB, MC, MD, ME
64	AD, AE, AF, AG, BD, BE, BF, BG, CD, CE, CF, CG	MD, MF, MG

[a]Thermocouple TE-301AE is a sheath thermocouple in rod 1 at angle A on level E.

[b]Thermocouple TE-301MD is a centerline thermocouple M in rod 1 at level D.

Table 5.3. Small-break LOCA test series summary

Power [kW/m (kW/ft)]	Pressure [MN/m^2 (psia)]	Maximum rod surface temperature [K (°F)]	Maximum steam temperature [K (°F)]	Maximum surface to steam ΔT [K (°F)]	Inlet temperature [K (°F)]	Outlet temperature [K (°F)]	Flooding rate [cm/s (in./s)]	Quench front velocity [cm/s (in./s)]		Initial collapsed liquid level [m (in.)]	Uncovery height [m (in.)]
								E-F	F-G		
1.050 (0.320)	6.96 (1010)	991 (1325)	889 (1140)	103 (185)	520 (476)	555 (540)	16.18 (6.37)	7.16 (2.82)	*a*	*b*	2.134 ± 0.3 (84 ± 12)
0.656 (0.200)	4.55 (660)	981 (1306)	813 (1003)	168 (303)	478 (400)	566 (560)	21.44 (8.44)	7.01 (2.76)	*a*	*b*	2.134 ± 0.3 (84 ± 12)
1.312 (0.400)	2.90 (420)	1024 (1383)	797 (975)	227 (408)	467 (381)	696 (794)	20.32 (8.00)		3.30 (1.30)	1.854 (73)	2.743 ± 0.3 (108 ± 12)
0.974 (0.297)	4.27 (620)	1044 (1419)	894 (1150)	149 (269)	464 (375)	714 (825)	16.00 (6.30)	7.16 (2.82)	4.90 (1.93)	1.740 (68.5)	2.134 ± 0.3 (84 ± 12)
1.444 (0.440)	4.27 (620)	1070 (1466)	846 (1064)	223 (402)	482 (408)	740 (872)	22.86 (9.00)		6.86 (2.70)	1.753 (69)	2.743 ± 0.3 (108 ± 12)
0.951 (0.290)	7.03 (1020)	1046 (1423)	879 (1122)	167 (301)	513 (464)	678 (761)	2.79 (1.10)		1.63 (0.64)	1.956 (77)	2.134 ± 0.3 (84 ± 12)
1.319 (0.402)	6.95 (1008)	1058 (1444)	839 (1050)	219 (394)	514 (466)	746 (883)	7.75 (3.05)	2.62 (1.03)	3.43 (1.35)	1.798 (70.8)	2.134 ± 0.3 (84 ± 12)
1.476 (0.450)	2.41 (350)	1047 (1425)	823 (1021)	224 (404)	460 (368)	658 (725)	5.84 (2.30)	2.31 (0.91)	2.69 (1.06)	1.313 (51.7)	2.134 ± 0.3 (84 ± 12)

[a]Not applicable.

[b]Not applicable because of injection of seal cooling water.

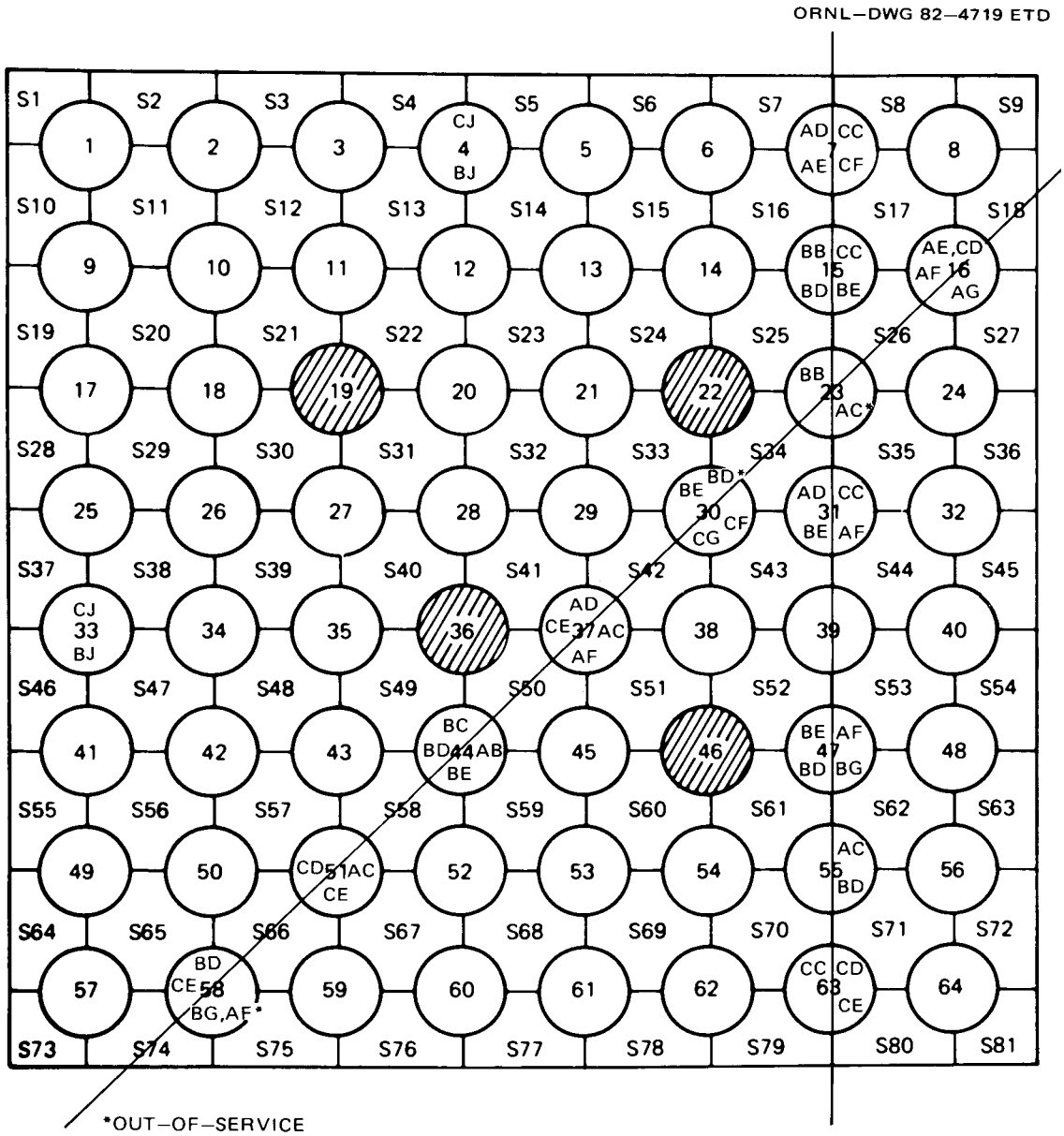

Fig. 5.1. Location and identification of Metrascope thermocouples used for operational monitoring purposes.

losses for these low-power tests. An isometric drawing of the small-break LOCA-I test configuration is shown in Fig. 5.2.

As mentioned previously, both steady-state uncovered bundle tests and reflood tests were run. Operation of the steady-state uncovered bundle tests involved setting the desired inlet flow rate and then increasing the bundle power, while letting down the system mass inventory and venting nitrogen overpressure in the pressurizer until the desired level of uncovered bundle was obtained (in actual practice, the level of

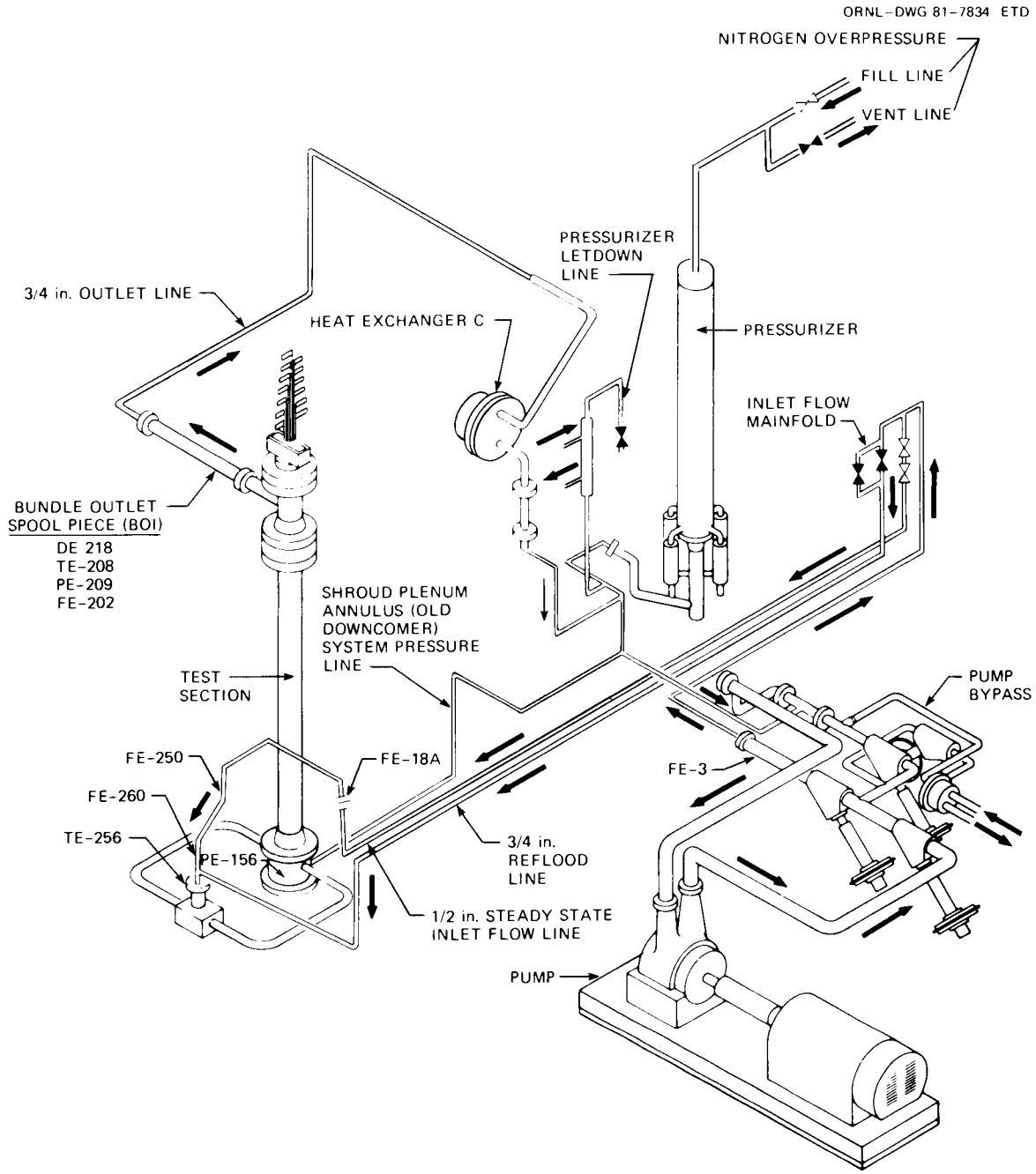

Fig. 5.2. Small-break LOCA-I test configuration (3.02.10C-H).

uncovery was generally dictated by FRS high-temperature limits). The mass inventory reduction and venting of the nitrogen from the pressurizer was necessary to accommodate the increased specific volume of the system mass inventory as steam was generated in the upper bundle. Mass inventory was letdown from the cold side of the loop through the pressurizer letdown line (Fig. 5.2). The reflood tests were run by simply increasing the

inlet flow to the test section when the bundle was in the uncovered state.

The inlet tubing configuration (Fig. 5.2) was designed to provide both a very low steady-state flow to the test section and a considerably higher flow for reflooding the test section. Most of the flow from the high-capacity pump was diverted through the pump bypass line by the large control valves on the pump supply. Flow to the test section leaving these control valves was routed to an inlet flow manifold. For the steady-state uncovery tests, flow controlled by valves in the inlet flow manifold was directed through the 1/2-in. inlet flow line containing an orifice flowmeter and two 1/2-in. turbine meters for measurement of the subcooled volumetric flow rate. For the reflood tests, valves at the inlet flow manifold were opened, allowing flow through the 3/4-in. inlet reflood line. Flow rates in this case were measured just downstream of the large flow control valves at the pump supply. Flow through both the steady-state and reflood lines merged at the test section inlet manifold, flowed up through the test section, and exited through a special 2-in. spool piece. This spool piece consisted of a single-beam gamma densitometer, a 2-in. drag disk, pressure sensor, temperature sensor, and a 2-in. turbine meter. Flow was routed from the outlet spool piece to the heat exchanger (condenser) by a run of 3/4-in. tubing. Flow then returned to the pump bypass through a length of 3/4-in. tubing. The shroud plenum annulus for this test did not have a purge flow; rather, the bottom of the shroud plenum annulus was simply connected by a 1/2-in. line to the cold side of the loop, maintaining the annulus at essentially the pressurizer pressure. A piping line drawing indicating piping size and run lengths for the small-break LOCA-I test series is shown in Fig. 5.3.

Additional differential pressure instrumentation was also added to the existing test section pressure taps for the small-break LOCA-I test series. Low-range differential pressure cells were added to measure collapsed liquid level across the bundle. Differential pressure measurements were also made across the shroud plenum annulus to aid in determining boundary conditions for the shroud-box walls. The measurement locations are indicated in Fig. 5.4. Note that test data from the differential pressure cells are the pressure differences measured at the cell itself and are not corrected for the static head of the cold reference leg. For correcting the measurements, a reference-leg fluid temperature of 302 K (85°F) may be assumed. An illustration of the typical relationship between the pressure taps and the differential pressure instrument is presented in Sect. 5.2.

A list of the primary instruments shown in Figs. 5.3 and 5.4 is presented in Table 5.4. The table describes the instrument type and range for the small-break LOCA-I test series. A more complete description of the instrumentation is presented in Chap. 6.

An instrument application drawing for the small-break LOCA-I test series is shown in Figs. 5.5(a and b). The drawings include both process and control instrumentation and CCDAS recorded instrumentation for this test series.

ORNL–DWG 82–5423 ETD

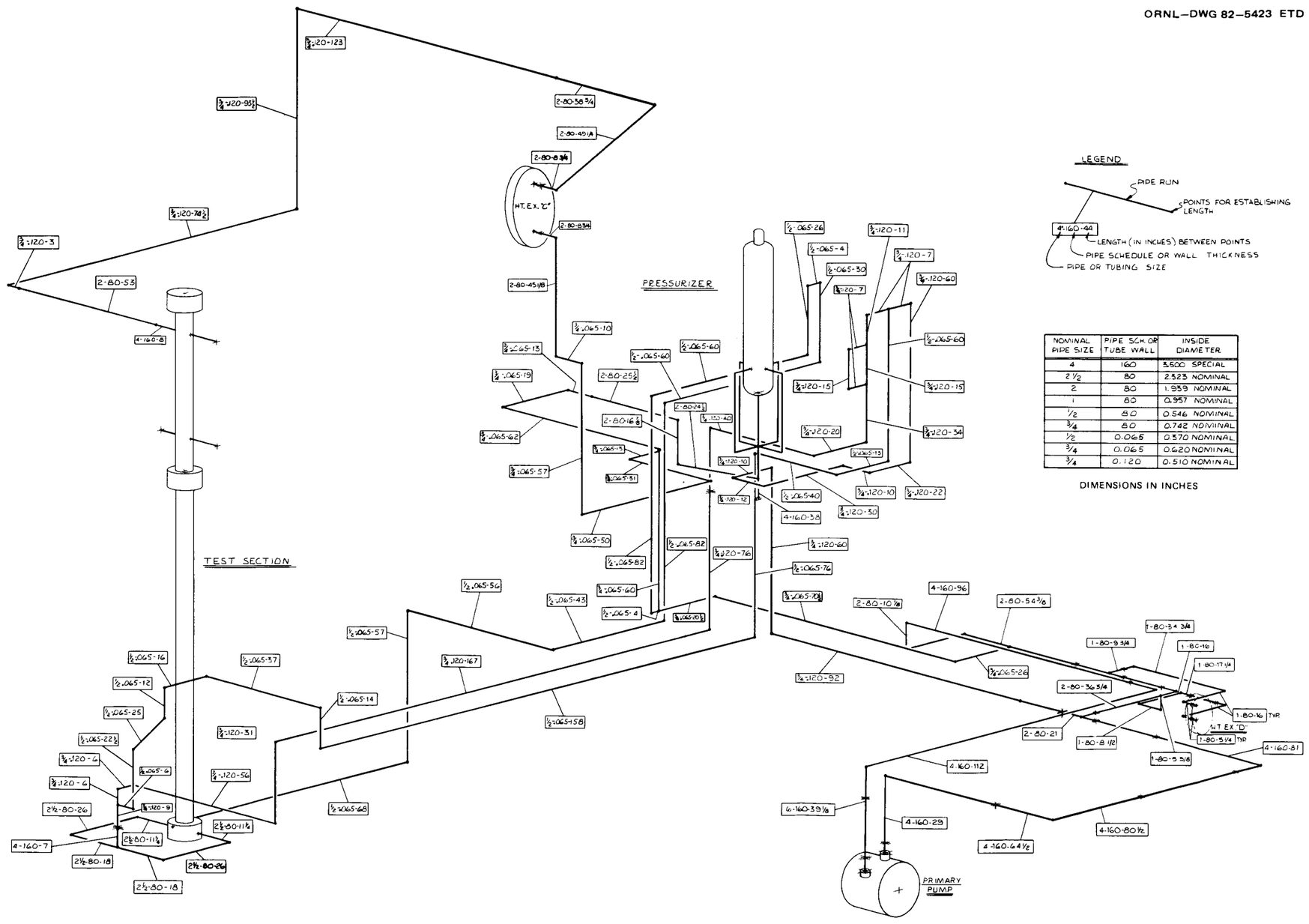

NOMINAL PIPE SIZE	PIPE SCH. OR TUBE WALL	INSIDE DIAMETER
4	160	3.600 SPECIAL
2 1/2	80	2.323 NOMINAL
2	80	1.939 NOMINAL
1	80	0.957 NOMINAL
1/2	80	0.546 NOMINAL
3/4	80	0.742 NOMINAL
1/2	0.065	0.370 NOMINAL
3/4	0.065	0.620 NOMINAL
3/4	0.120	0.510 NOMINAL

DIMENSIONS IN INCHES

Fig. 5.3. System line drawing of THTF in small-break LOCA-I test configuration. (Microfiche copy of this drawing attached to back of report.)

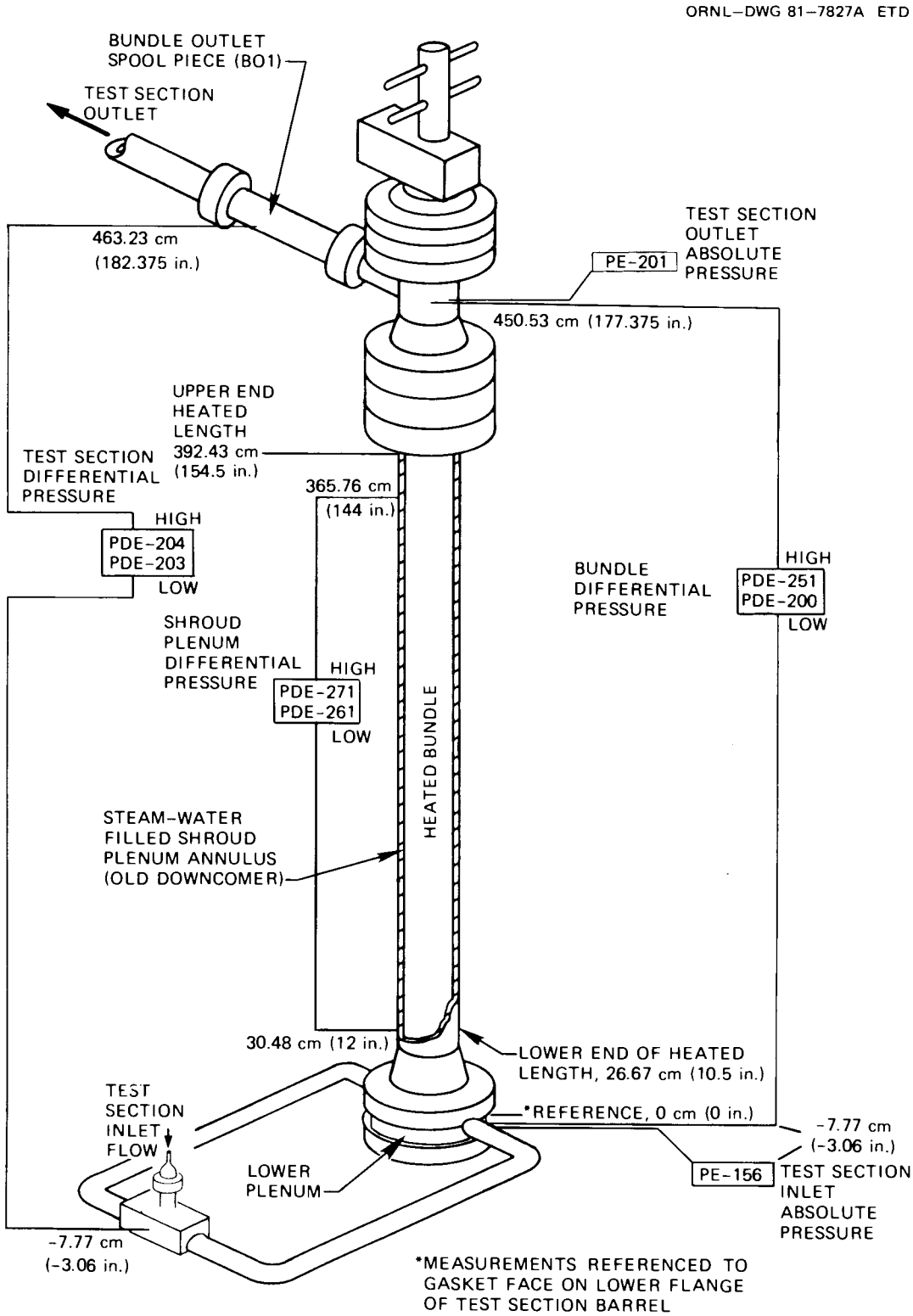

Fig. 5.4. Test section pressure and differential pressure measurement locations for the small-break LOCA-I (3.02.10C-H) test series.

Table 5.4. Primary flow instrumentation for Test 3.02.10C-H

Instrument application No.	Description	Instrument	Range
FE-3	2-in. inlet transient volumetric flow	2-in. Flow Technology turbine meter	$\pm 6.3 \times 10^{-4}$–3.54×10^{-3} m³/s ($\pm$10–56.2 gpm) range 1
FE-18A	Test section inlet steady-state volumetric flow	Orifice meter, 1/2-in. line, Foxboro differential pressure cell	0–1.7×10^{-4} m³/s (0–2.7 gpm)
FE-250	Bundle inlet volumetric flow 2	1/2-in. Flow Technology turbine meter	3.1×10^{-5}–3.1×10^{-4} m³/s (0.5–5 gpm)
FE-260	Bundle inlet volumetric flow 1	1/2-in. Flow Technology turbine meter	3.1×10^{-5}–3.1×10^{-4} m³/s (0.5–5 gpm)
TE-256	Test section inlet temperature	Nanmac fluid thermocouple	273–1309 K (32–1900°F)
PE-156	Test section inlet transient pressure	Precise Sensor absolute pressure transducer	0–2.07×10^4 kPa (0–3000 psig)
PE-201	Test section outlet transient pressure	Precise Sensor absolute pressure transducer	0–2.07×10^4 kPa (0–3000 psig)
DE-218	Bundle outlet spool density	Single-beam gamma densitometer (with 2-in. pipe adaptor)	0–1000 kg/m³ (0–62.4 lb_m/ft^3)
TE-208	Bundle outlet spool temperature	Nanmac fluid thermocouple	273–1309 K (32–1900°F)
PE-209	Bundle outlet spool transient pressure	Precise Sensor absolute pressure transducer	0–2.07×10^4 kPa (0–3000 psig)
FE-202	Bundle outlet spool volumetric flow	2-in. Flow Technology turbine meter	$\pm 6.3 \times 10^{-4}$–0.0284 m³/s ($\pm$10–450 gpm) range 4
PDE-200	Bundle transient differential pressure	100-in. BLH differential pressure transducer	$\pm$0–25 kPa ($\pm$0–100 in. of Std. H_2O)
PDE-251	Bundle transient differential pressure	6-psi Genisco differential pressure transducer	$\pm$0–41.4 kPa ($\pm$0–6 psid)
PDE-203	Test section transient differential pressure	50-psi BLH differential pressure transducer	$\pm$0–345 kPa ($\pm$0–50 psid)
PDE-204	Test section transient differential pressure	6-psi Genisco differential pressure transducer	$\pm$0–41.4 kPa ($\pm$0–6 psid)
PDE-261	Shroud plenum annulus transient differential pressure	500-in. BLH differential pressure transducer	$\pm$0–124 kPa ($\pm$0–500 in. of Std. H_2O)
PDE-271	Shroud plenum annulus transient differential pressure	6-psi Genisco differential pressure transducer	$\pm$0–41.4 kPa ($\pm$0–6 psid)

ORNL—DWG 82—5424 ETD (PART A)

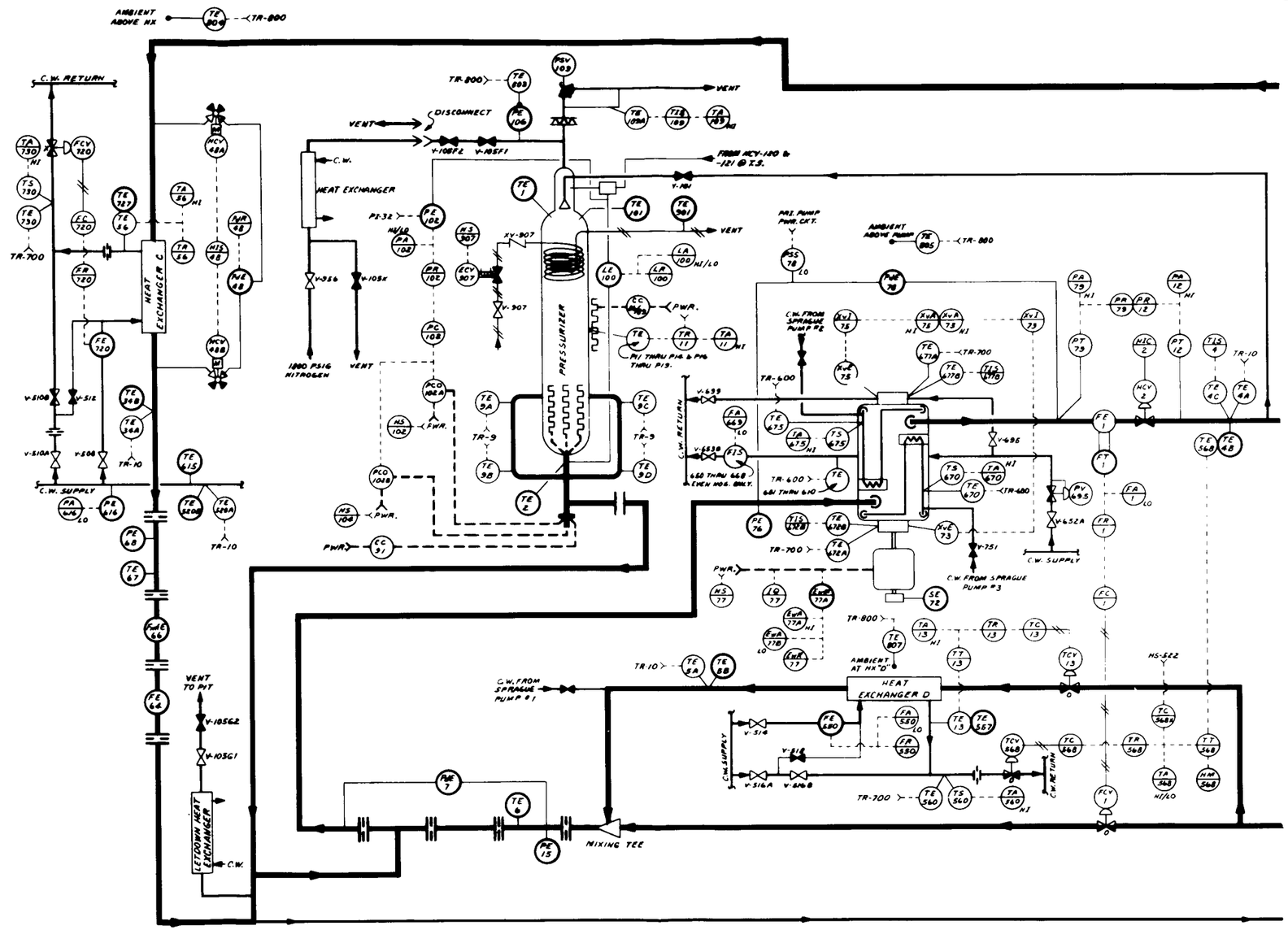

Fig. 5.5. Instrument application drawing for Test 3.02.10C-H.

ORNL-DWG 82-5424 ETD (PART B)

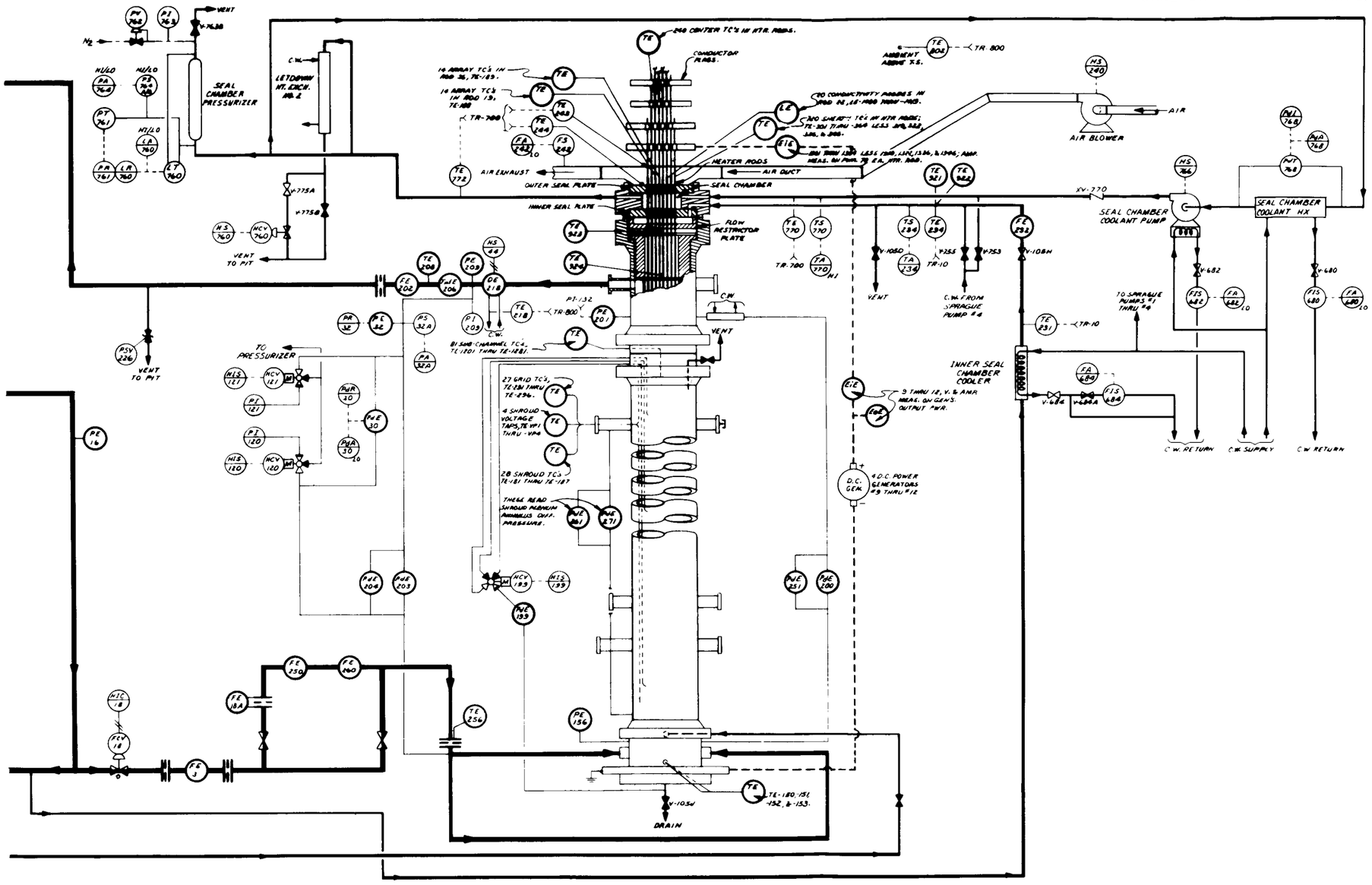

Fig. 5.5 (continued)

5.2 First Bundle Modification

The first modification to the bundle began in March 1980. As stated previously, eight of the original Bundle 3 FRSs had been severely damaged and could not be repaired by the FRS TDL. Therefore, these simulators were replaced with backup simulators. Seven of these replacement FRSs were preproduction models of the original Bundle 3 rods; these FRSs contain ten thermocouples (six sheath and four centerline) divided between four axial levels (level D has the normal contingent of one centerline and three sheath and the remaining three levels have a centerline-sheath pair only). The eight replacement rod positions are cross-hatched in Fig. 5.6. The axial levels monitored by each rod are indicated in Fig. 5.7.

A schematic[21] of the refurbished Bundle 3 giving the location of all primary-level (A–G) FRS thermocouples is presented in Fig. 5.8; also, the locations of the special FRS thermocouples (levels Y, H, S, U, and J) in the refurbished bundle are given in Fig. 5.9. The naming convention for these FRS thermocouples is the same as that in Sect. 3.3. As of May 2, 1980, those FRS thermocouples presented in Table 5.5 were monitored by the CCDAS.

The core fluid temperatures are also monitored by thermocouples; the axial and subchannel locations of all fluid thermocouples in the refurbished core are presented in the schematic in Fig. 5.10. The only changes in the locations given in Figs. 5.10 and 3.10 (and Appendix B) are the loss of the subchannels monitored by the thermocouple-array rod thermocouples in grid position 36 in the original bundle. One of the original thermocouple-array rods was damaged beyond repair and was replaced in the grid by a hollow instrument rod. A similar hollow instrument rod was installed in grid position 46. Both of these rods were designed to permit later installation of the in-bundle gamma densitometer system (described in Sect. 5.3).

The opportunity was also taken during this time to install additional pressure taps along the test section. This modification was primarily intended to provide improved collapsed liquid level and void fraction distribution measurements for the second small-break LOCA test series (Sect. 5.3.4). The axial locations of the pressure taps along the bundle are shown in Fig. 5.11(a). An illustration of the typical relative locations of the pressure taps and the differential pressure measurement instrument is shown in Fig. 5.11(b). A detail of the construction of the pressure taps and connecting lines is shown in Fig. 5.12. Lines extend horizontally through the test section barrel across the shroud plenum annulus to the flush wall taps drilled through the shroud-box wall. The lines coming off the test section are initially horizontal runs with copper cooling jackets installed around the lines [the lines are actually installed with a slight downward slope of ~1.27 cm (1/2 in.) over 46 cm (18 in.) of horizontal run to prevent drainage of water in the reference leg into the bundle as the bundle boils off]. Cooling of the horizontal leg coming immediately off of the test section prevents the boiling off of fluid in the line on the test section side of the cooling jackets from significantly affecting the cold reference leg of the differential pressure measurement. The reference legs turn downward on the other side of the cooling jackets and connect with the differential pressure instrument that is physically

ORNL–DWG 82–5048 ETD

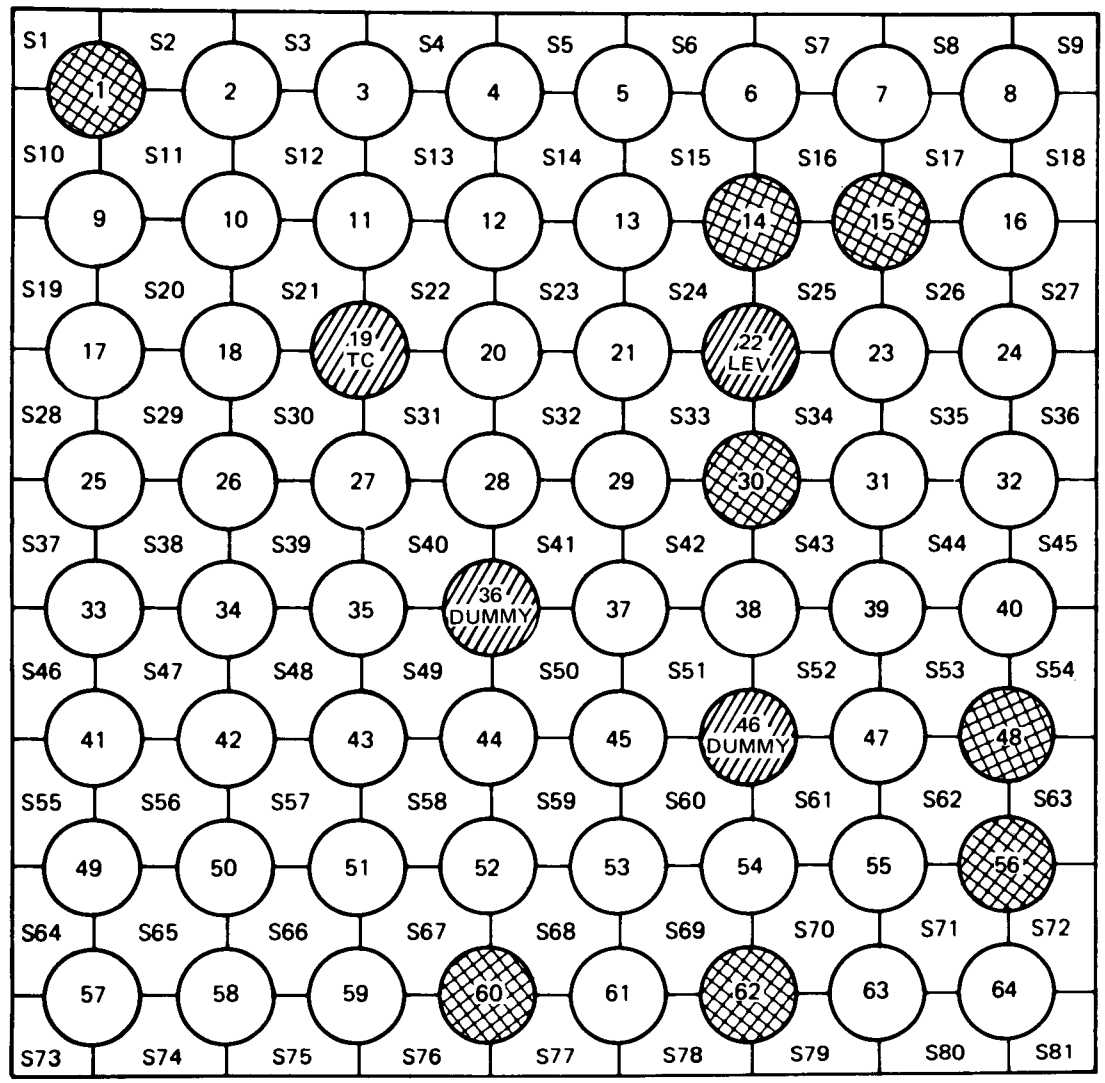

THERMOCOUPLE ROD 19

LEVEL ROD 22

DUMMY ROD 46 AND 36

INACTIVE RODS REPLACEMENT RODS

Fig. 5.6. Identification of THTF heater rods, subchannel locations, and instrument rods in refurbished THTF Bundle 3 (March–July 1980).

ORNL–DWG 82–5049 ETD

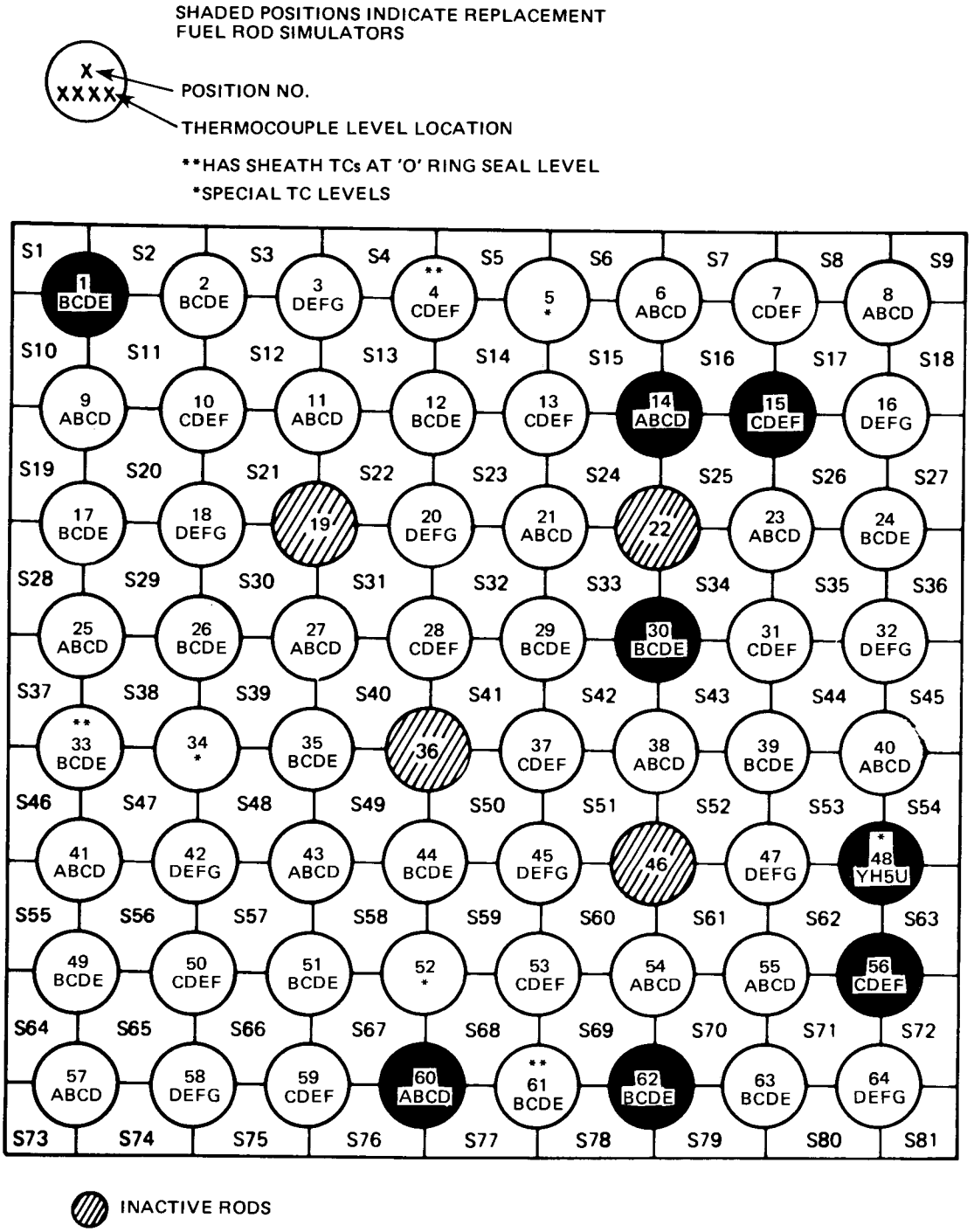

Fig. 5.7. Identification of THTF heater rods and axial thermocouple levels monitored by each rod in refurbished THTF Bundle 3 (March–July 1980).

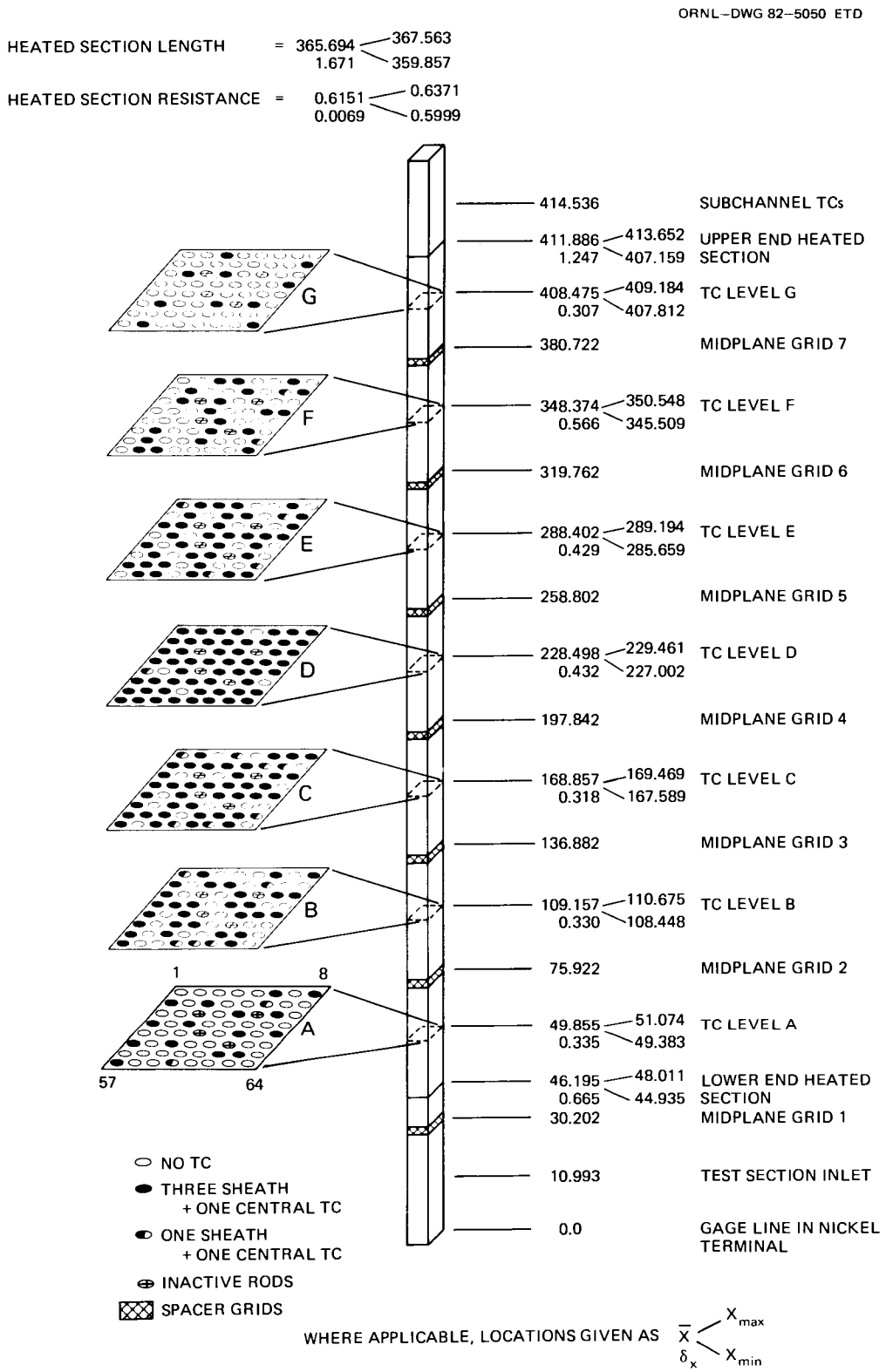

Fig. 5.8. Location of thermocouples in refurbished THTF Bundle 3 (March–July 1980). All dimensions are in centimeters and are referenced to gage line in nickel terminal.

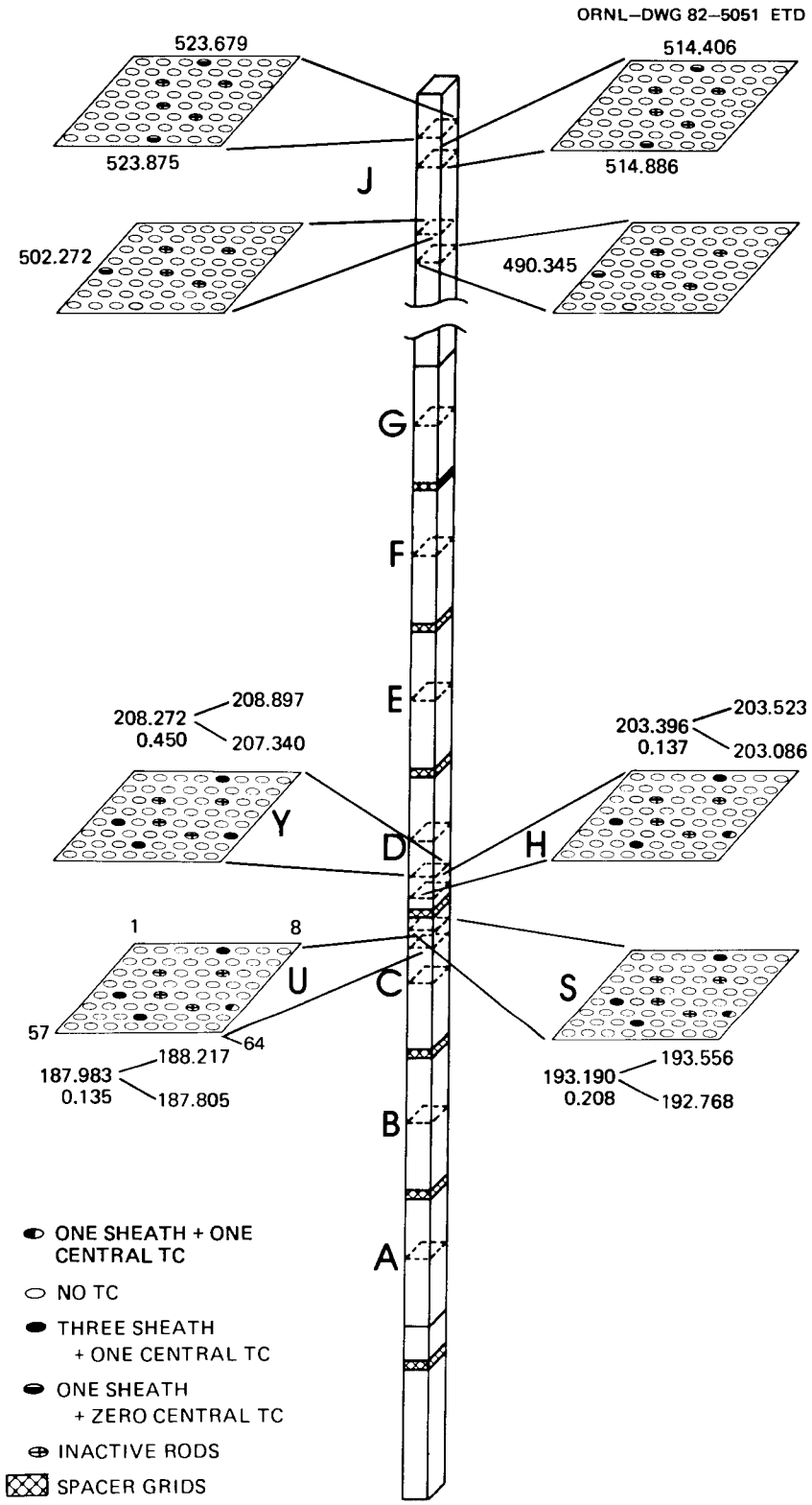

Fig. 5.9. Special thermocouple locations in refurbished THTF Bundle 3 (March–July 1980). All dimensions are in centimeters and are referenced to gage line in nickel terminal.

Table 5.5. In-service thermocouple listing for refurbished THTF Bundle 3 (March–July 1980)

Rod	Sheath angle level	Center level
1	AB, AD, AC, AE	MB, MC, MD, ME
2	AB, AD, AE, BC	MB, MC, MD, ME
3	BE, BF, CD, CG	MD, ME, MF, MG
4	AC, BD, BE, BF	MC, MD, ME, MF
5	AS, BH, BU, CY	MH, MS, MU, MY
6	AA, AB, BC, BD	MA, MC, MD
7	AC, AF, CE	MC, MD, ME, MF
8	BB, BC, BD, CB	MB, MC, MD
9	AC, BA, CB, CD	MA, MB, MC, MD
10	AF, BE, CC, CD	MC, MD, ME, MF
11	AA, AD, CB, CC	MA, MB, MC, MD
12	AD, AE, BC, CB	MB, MC, MD, ME
13	BC, BF, CD, CE	MC, MD, ME, MF
14	AA, AB, AC, BD	MA, MB, MC, MD
15	AC, AD, AE, AF	MC, MD, ME, MF
16	AD, BF, CE, CG	MD, ME, MF, MG
17	AE, CB, CC, CD	MB, MC, MD, ME
18	AD, AF, BE, BG	MD, ME, MF, MG
19	Rod 19 is unpowered	
20	AD, AE, AF, AG, BD, BE, BF, BG, CD, CE, CF, CG	MD, MF, MG
21	AA, AB, BC, CD	MA, MB, MD
22	Rod 22 is unpowered	
23	AA, AD, BC, CB	MB, MC, MD
24	AC, BD, CB, CE	MC, MD, ME
25	AA, AB, AC, BA, BB, BC, BD, CA, CB, CC, CD	MA, MB, MC, MD
26	AC, BB, BD, CE	MB, MC, MD, ME
27	AA, AB, AC, AD, BA, BB, BC, BD, CA, CB, CC, CD	MA, MB, MC, MD
28	AC, AD, AE, AF, BC, BD, BE, BF, CC, CD, CE, CF	MC, MD, ME, MF
29	AB, AC, AD, AE, BB, BC, BD, BE, CB, CD, CE	MB, MC, MD, ME
30	CB, CC, CD, CE	MB, MC, MD, ME
31	AC, CD, CE, CF	MF
32	AD, AF, AG, BE, BG, CD, CE, CF, CG	MD, ME, MG
33	AC, AD, CB, CE	MB, MC, MD, ME
34	AH, AS, AU, AY, BH, BS, BU, BY, CH, CS, CU, CY	MH, MS, MY
35	AC, BB, BE, CD	MB, MC, MD, ME
36	Rod 36 is unpowered	
37	AE, BC, BD, CF	MC, MD, ME, MF
38	AB, BA, BC, BD	MA, MB, MC, MD
39	AC, BB, BD, BE	MB, MC, MD, ME
40	BC, BD, CA, CB	MA, MB, MC, MD
41	AB, BA, BD, CC	MA, MB, MC, MD
42	BD, BE, CF, CG	MD, ME, MF, MG
43	BA, BB, BC, CD	MA, MB, MC, MD
44	CB, CC, CD, CE	MB, MC, ME
45	AD, AE, AF, AG, BD, BE, BF, BG, CD, CE, CF, CG	MD, ME, MG
46	Rod 46 is unpowered	
47	AD, AE, AG, BF	MD, ME, MF, MG
48	AH, AS, AU, AY	MH, MS, MU, MY
49	CB, CC, CD, CE	MB, MC, MD, ME
50	AC, AD, AE, AF, BC, BD, BE, BF, CC, CD, CE, CF	MC, MD, ME, MF
51	AB, AE, BC, BD	MB, MC, MD, ME
52	AH, AS, AU, AY, BH, BS, BU, BY, CH, CS, CU, CY	MH, MS, MU, MY
53	AD, AE, AF, CC	MC, MD, ME, MF
54	AD, CA, CB, CC	MA, MB, MC, MD
55	AA, AD, BC, CB	MA, MB, MC, MD
56	AC, AE, AF, CD	MC, MD, ME, MF
57	AA, AB, AC, AD, BA, BB, BC, BD, CA, CB, CC, CD	MA, MB, MC, MD
58	BE, CD, CF, CG	MD, ME, MF, MG
59	AD, AE, CC, CF	MC, MD, ME, MF
60	AB, AC, AD, CD	MA, MB, MC, MD
61	AB, AC, AD, CE	MB, MC, MD
62	AB, AC, AE, CD	MB, MC, MD, ME
63	AD, BC, BE, CB	MB, MC, MD, ME
64	AD, AE, AF, AG, BD, BE, BF, BG, CD, CE, CF, CG	MD, MF, MG

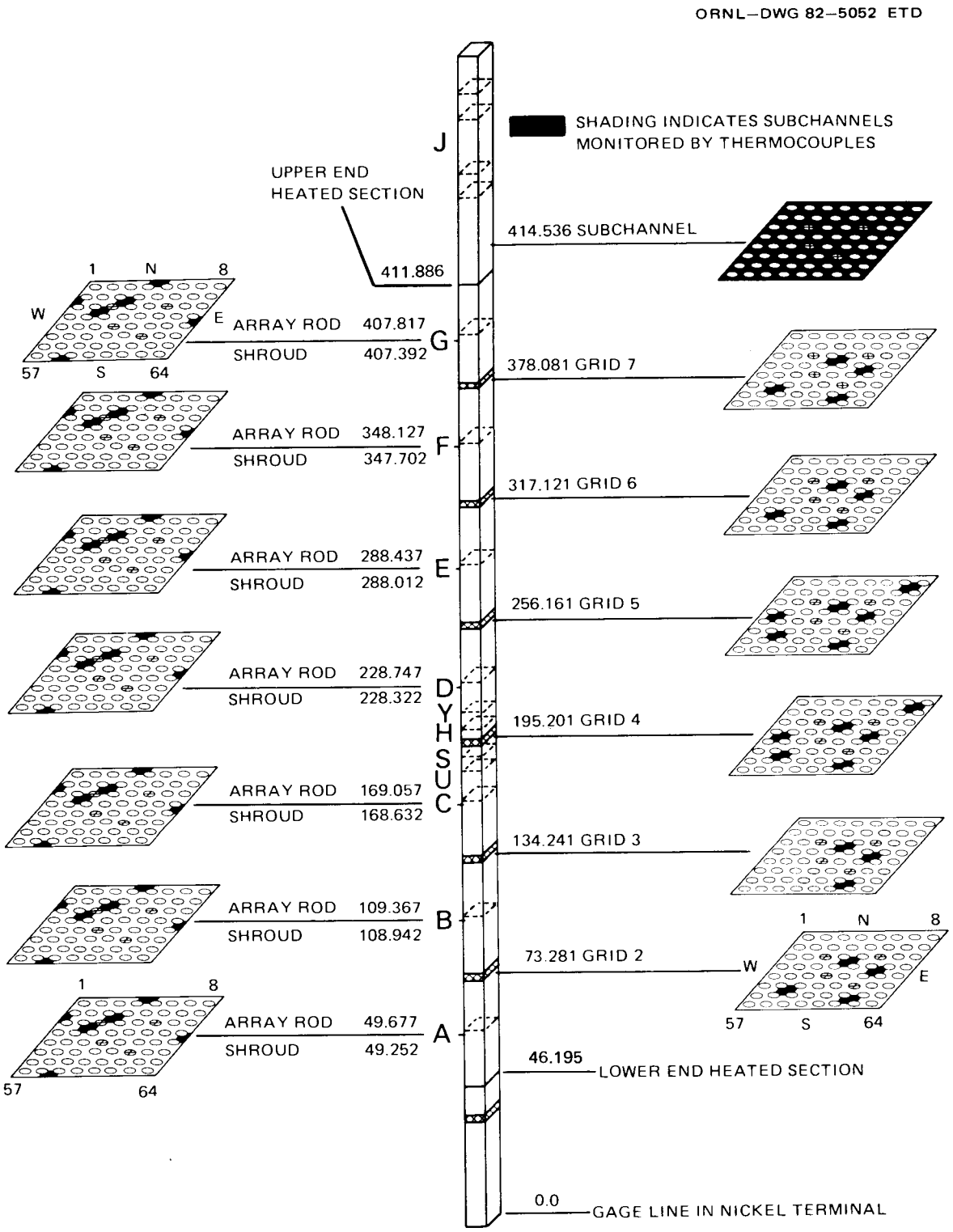

Fig. 5.10. Location of fluid thermocouples in refurbished THTF Bundle 3 (March–July 1980). All dimensions are in centimeters and are referenced to gage line in nickel terminal.

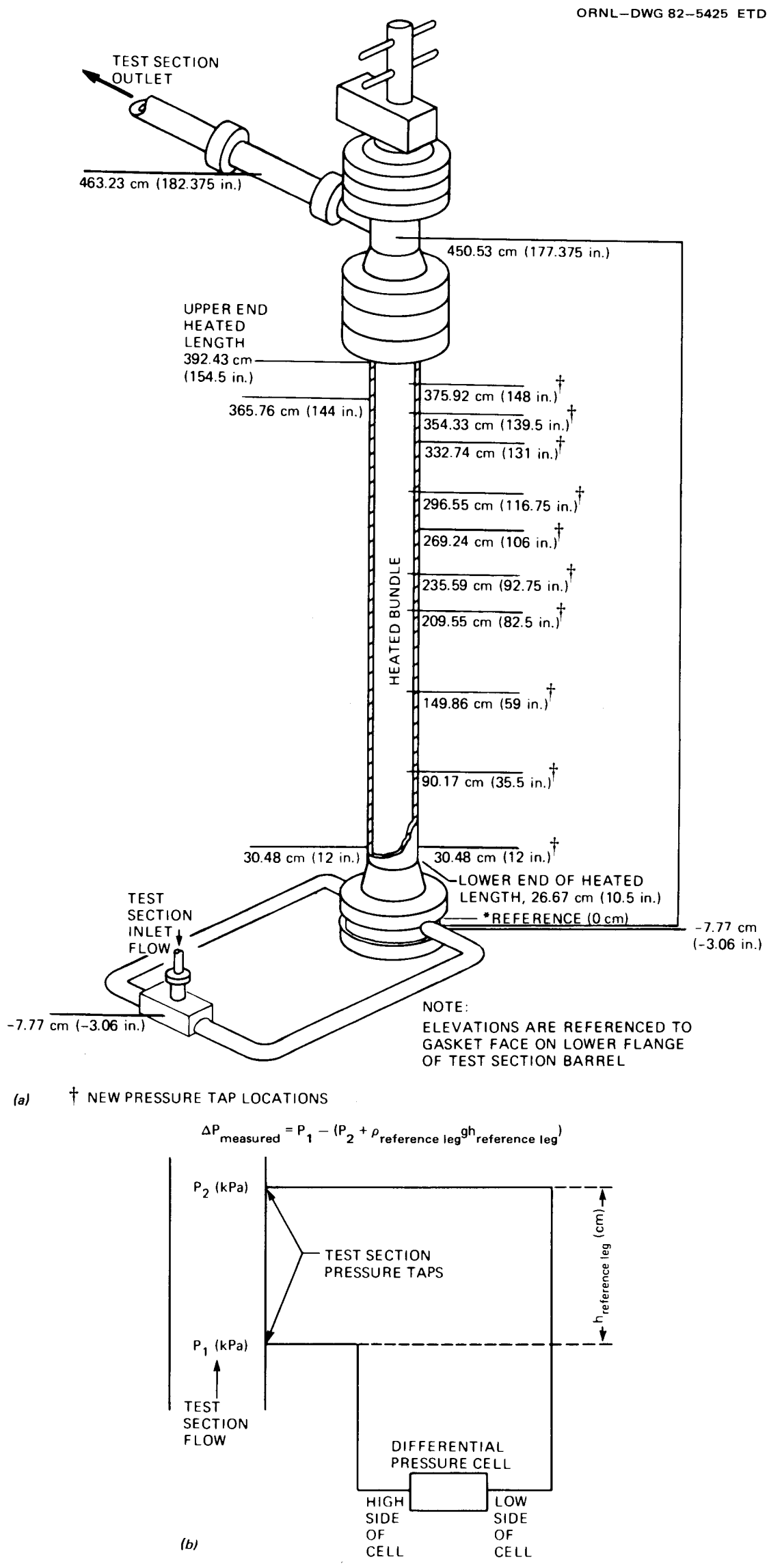

Fig. 5.11. (a) Axial location of pressure taps along THTF test section following first modification to bundle; (b) differential pressure measurement arrangement.

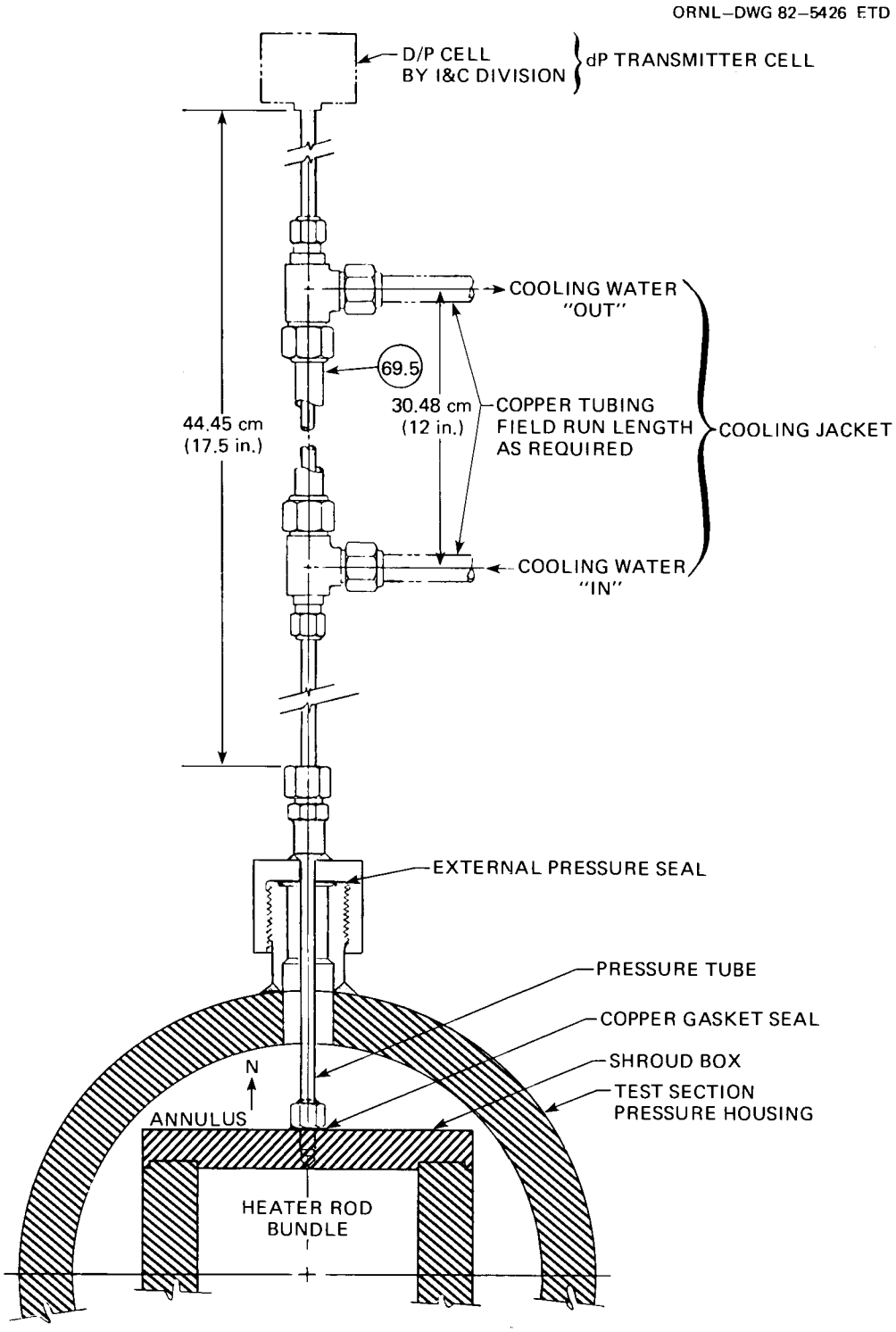

Fig. 5.12. Detail of construction of new pressure taps along test section.

located below the pressure taps of both lines. Fluid thermocouples were installed immediately downstream of the cooling jackets in two of the cold reference legs to provide temperature measurement and density determination of the reference-leg water [one in the line at 375.92 cm, TE-926, and one in the line at 209.55 cm, TE-925, in Fig. 5.11(a)]. Measurements taken during testing indicated temperatures of ~302 K (85°F) even when the bundle was uncovered below the pressure tap. Descriptions of the differential pressure instrumentation arrangements installed on the test section pressure tap locations are presented with the discussions of individual tests. (Note that installation of differential pressure instrumentation was not completed for Test 3.03.6AR.)

5.2.1 Upflow Film Boiling Test 3.03.6AR

Test 3.03.6AR (Refs. 22–25) was a single-ended outlet-only break transient blowdown test with a comparatively slow depressurization rate. The purposes of the experiment were to: (1) obtain transient heat transfer data for film boiling in rod bundle geometry to be used in assessing or developing film boiling heat transfer correlations for use in transient reactor analysis codes, (2) obtain data in the high-flow film boiling data ranges requested by the Nuclear Regulatory Commission Office of Nuclear Reactor Regulation, and (3) provide a benchmark for transient reactor analysis codes. The upflow film boiling data ranges are presented in Table 5.6, and the initial conditions prior to blowdown are presented in Table 5.7. The blowdown-type tests are run by bringing the system to the initial conditions and then initiating blowdown by rupturing the rupture disks. This test also included a power ramp at the initiation of blowdown. The initial power ramp was manually controlled until a desired set point was reached, at which time the power programmer automatically assumed control.

Table 5.6. THTF upflow film boiling data ranges – Test 3.03.6AR

	NRC requested	Obtained in Test 3.03.6AR
Mass flux, kg/s·m² (lb_m/h·ft²)	270–4070 (2×10^5–3×10^6)	203–543 (1.5×10^5–4×10^5)
Quality, %	0–100	30–100
Pressure, MN/m² (psi)	4.14–18.61 (600–2700)	5.17–9.7 (750–1400)
Heat flux, W/m² (Btu/h·ft²)	3×10^4–3×10^6 (10^4–10^6)	15.7×10^4–6.3×10^5 (5×10^4–2×10^5)

Table 5.7. Initial conditions for Test 3.03.6AR

Total bundle power, MW	3.96
Average rod power, kW	65.9
Flow	
Volumetric, m^3/s (gpm)	0.018 (285)
Mass, kg/s (lb_m/s)	14.1 (31.0)
Inlet temperature, K (°F)	540 (512)
Outlet temperature, K (°F)	590 (602)
Outlet pressure, MN/m^2 (psia)	14.1 (2065)

The loop test configuration was essentially that of the standard configuration described in Chap. 2. The only difference involved the replacement of the two 3.5-in. spool pieces on the external downcomer, BI1 and BI2, with a modular 2-in. spool piece (Fig. 5.13). The test was designed to provide subcooled inlet flow conditions over the important portions of the transient; however, significantly lower mass flow rates were also expected. The smaller diameter spool piece with the correspondingly smaller 2-in. turbine meters lowered the measurable volumetric flow range at the inlet from ~5.4×10^{-3} m^3/s (85 gpm) to 6.3×10^{-4} m^3/s (10 gpm).

An isometric drawing of the THTF with the location of the primary "bounding condition" instrumentation for the THTF is shown in Fig. 5.14. A schematic of the test section pressure and differential pressure measurement instrumentation is shown in Fig. 5.15. Table 5.8 indicates the type of instrument and nominal ranges for the instruments shown in Figs. 5.14 and 5.15. The instrument application drawings showing the complete system are presented in Figs. 5.16(a–c) for Test 3.03.6AR.

5.2.2 Double-Ended Cold-Leg Break Test 3.05.5B

Test 3.05.5B (Refs. 26 and 27) was a relatively high-powered double-ended blowdown loss-of-coolant experiment. The objectives of the test were: (1) to measure times to DNB in a hydraulic environment similar to that predicted to exist in a PWR during an LOCA and (2) to provide a benchmark for transient reactor analysis codes. The initial conditions for Test 3.05.5B are presented in Table 5.9.

The test was run in the standard configuration. An isometric drawing showing primary instrumentation is presented in Fig. 5.17. The test section pressure and differential pressure instrumentation arrangement is shown in Fig 5.18. Table 5.10 lists the instrument type and range for the instruments shown in Figs. 5.17 and 5.18. The instrument application drawings for Test 3.05.5B are presented in Figs. 5.19(a–c).

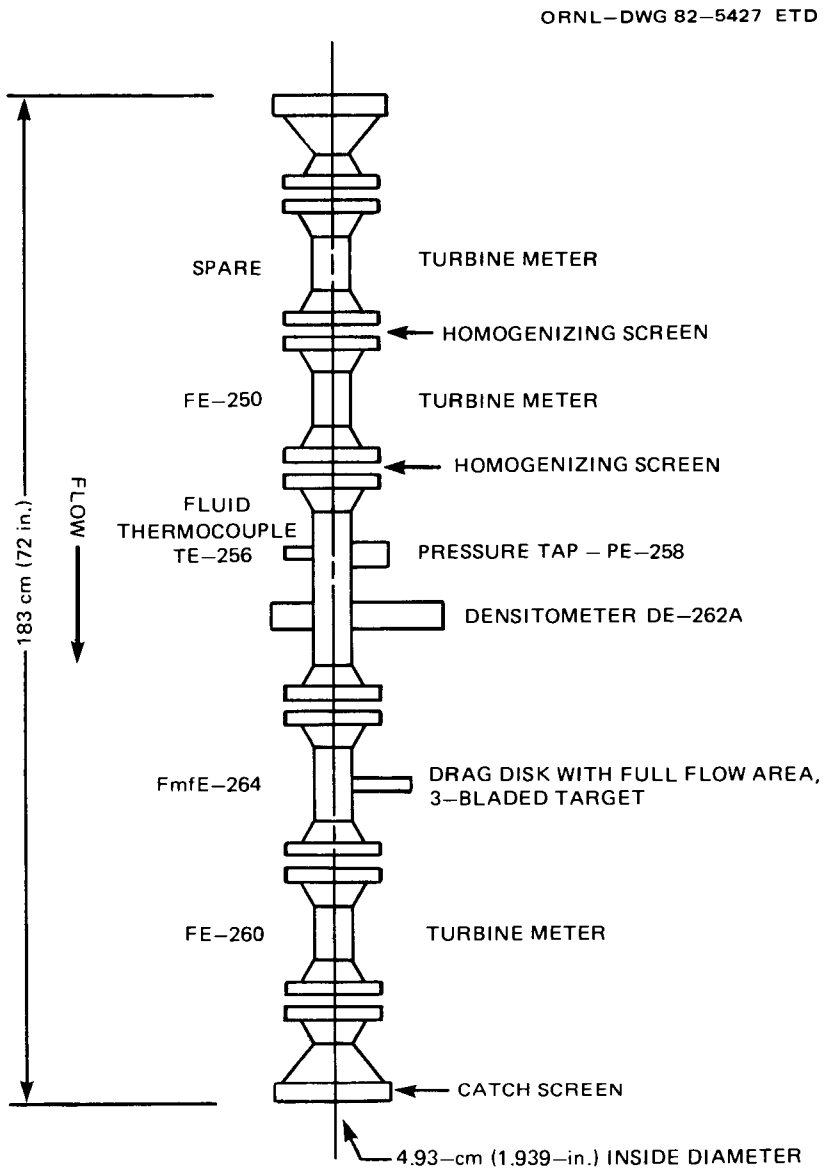

Fig. 5.13. Schematic of special 2-in. spool piece used on external downcomer for upflow film boiling tests.

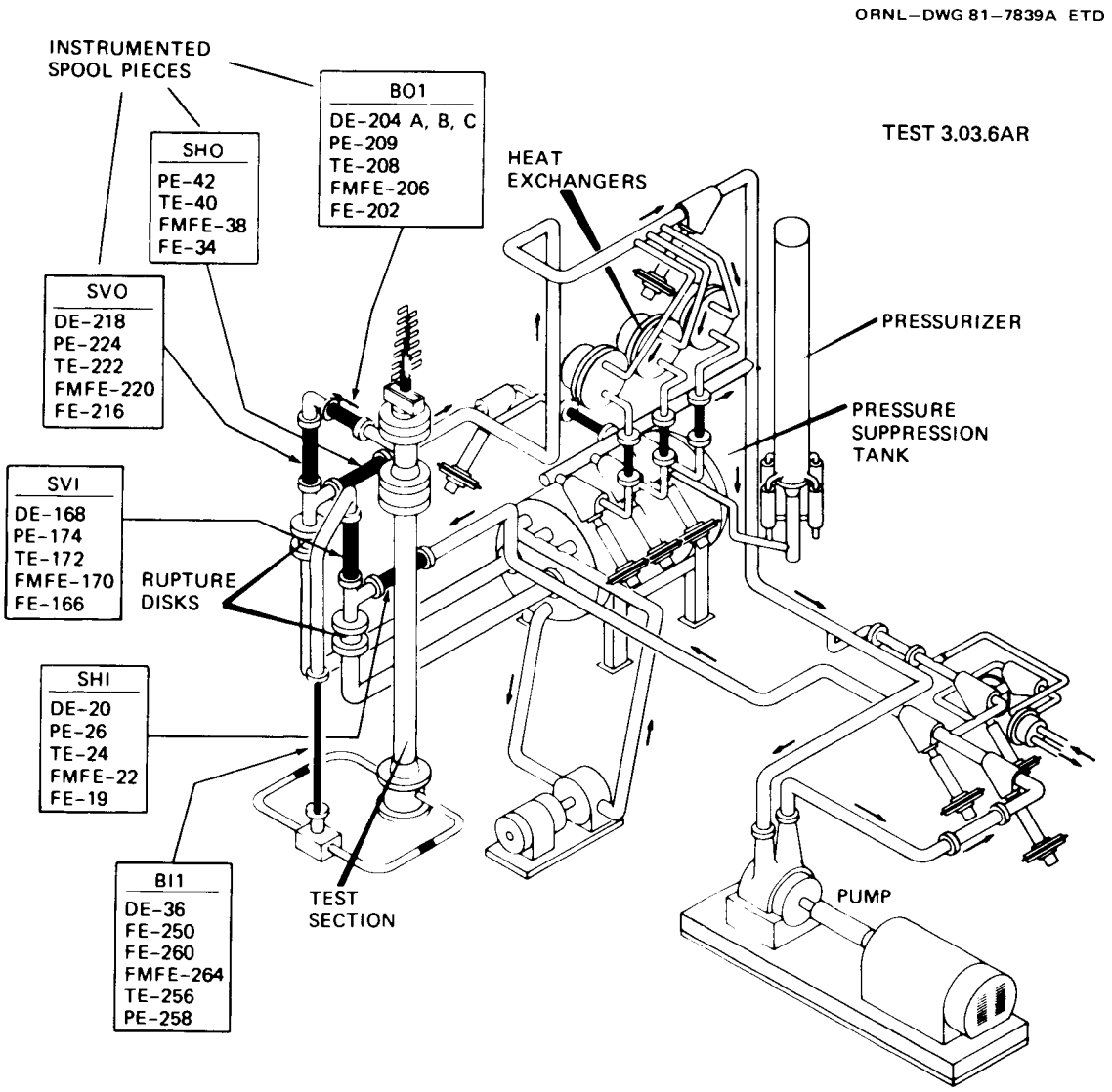

Fig. 5.14. THTF configuration for Test 3.03.6AR.

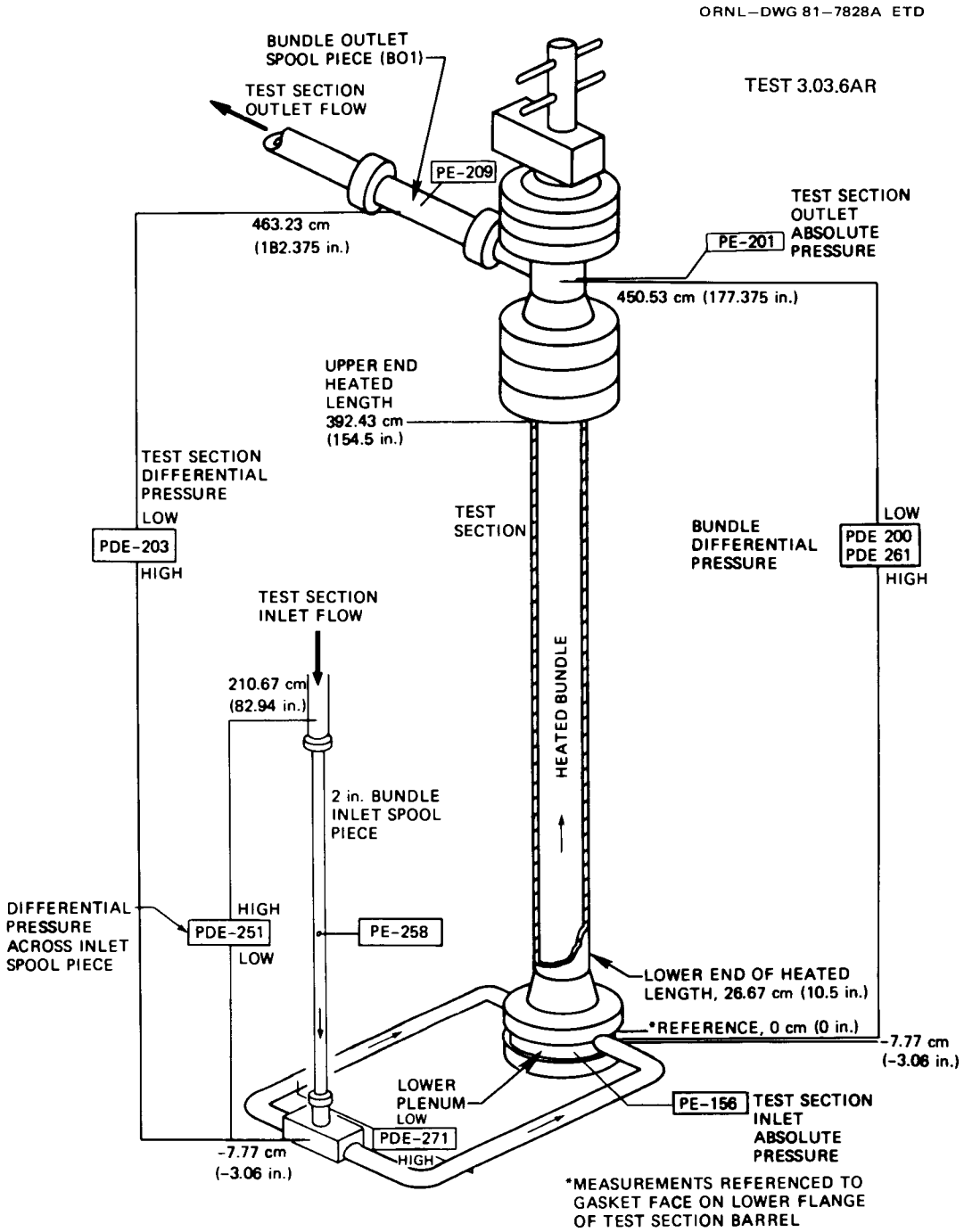

Fig. 5.15. Test section pressure and differential pressure instrumentation for Test 3.03.6AR.

Table 5.8. Primary flow instrumentation for Test 3.03.6AR

Instrument application No.	Description	Instrument	Range
DE-204A	Bundle outlet spool density	Three-beam gamma densitometer	0–1000 kg/m³ (0–62.4 lb_m/ft^3)
DE-204B			
DE-204C			
PE-209	Bundle outlet spool transient pressure	Precise Sensor absolute pressure transducer	0–2.07 x 10⁴ kPa (0–3000 psig)
TE-208	Bundle outlet spool temperature	Nanmac fluid thermocouple	273–1309 K (32–1900°F)
FMFE-206	Bundle outlet spool drag disk (momentum flux)	Ramapo drag disk, ORNL 3.5-in., 3-bladed full-flow target	±0–7.57 x 10⁴ kg/m·s² (±0–5.09 x 10⁴ $lb_m/ft\cdot s^2$)
FE-202	Bundle outlet spool volumetric flow	3.5-in. Flow Technology turbine meter	±0.005–0.113 m³/s (±80–1800 gpm)
PE-42	Horizontal outlet spool transient pressure	Precise Sensor absolute pressure transducer	0–2.07 x 10⁴ kPa (0–3000 psig)
TE-40	Horizontal outlet spool temperature	Nanmac fluid thermocouple	273–1309 K (32–1900°F)
FMFE-38	Horizontal outlet spool drag disk (momentum flux)	Ramapo drag disk, ORNL 3.5-in., 3-bladed full-flow target	±0–7.15 x 10⁴ kg/m·s² (±0–4.8 x 10⁴ $lb_m/ft\cdot s^2$)
FE-34	Horizontal outlet spool volumetric flow	3.5-in. Flow Technology turbine meter	±0.005–0.057 m³/s (±80–900 gpm) range 2
DE-218	Vertical outlet spool density	Single-beam gamma densitometer	0–1000 kg/m³ (0–62.4 lb_m/ft^3)
PE-224	Vertical outlet spool transient pressure	Precise Sensor absolute pressure transducer	0–2.07 x 10⁴ kPa (0–3000 psig)
TE-222	Vertical outlet spool temperature	Nanmac fluid thermocouple	273–1309 K (32–1900°F)
FMFE-220	Vertical outlet spool drag disk (momentum flux)	Ramapo drag disk, ORNL 3.5-in., 3-bladed full-flow target	±0–1.02 x 10⁵ kg/m·s² (±0–6.84 x 10⁴ $lb_m/ft\cdot s^2$)
FE-216	Vertical outlet spool volumetric flow	3.5-in. Flow Technology turbine meter	±0.005–0.113 m³/s (±80–1800 gpm) range 3
DE-168	Vertical inlet spool density	Single-beam gamma densitometer	0–1000 kg/m³ (0–62.4 lb_m/ft^3)
PE-174	Vertical inlet spool transient pressure	Precise Sensor absolute pressure transducer	0–2.07 x 10⁴ kPa (0–3000 psig)
TE-172	Vertical inlet spool temperature	Nanmac fluid thermocouple	273–1309 K (32–1900°F)
FMFE-170	Vertical inlet spool drag disk (momentum flux)	Ramapo drag disk, ORNL 3.5-in., 3-bladed full-flow target	±0–5.79 x 10⁴ kg/m·s² (±0–3.89 x 10⁴ $lb_m/ft\cdot s^2$)

Table 5.8 (continued)

Instrument application No.	Description	Instrument	Range
FE-166	Vertical inlet spool volumetric flow	3.5-in. Flow Technology turbine meter	±0.005–0.0284 m^3/s (±80–450 gpm) range 1
DE-20	Horizontal inlet spool density	Single-beam gamma densitometer	0–1000 kg/m^3 (0–62.4 lb_m/ft^3)
PE-26	Horizontal inlet spool transient pressure	Precise Sensor absolute pressure transducer	0–2.07 x 10^4 kPa (0–3000 psig)
TE-24	Horizontal inlet spool temperature	Nanmac fluid thermocouple	273–1309 K (32–1900°F)
FMFE-22	Horizontal inlet spool drag disk (momentum flux)	Ramapo drag disk, ORNL 3.5-in., 3-bladed full-flow target	±0–2.42 x 10^4 $kg/m \cdot s^2$ (±0–1.63 x 10^4 $lb_m/ft \cdot s^2$)
FE-19	Horizontal inlet spool volumetric flow	3.5-in. Flow Technology turbine meter	±0.005–0.0284 m^3/s (±80–450 gpm) range 1
DE-36	Bundle inlet spool density	Single-beam gamma densitometer	0–1000 kg/m^3 (0–62.4 lb_m/ft^3)
FE-250	Bundle inlet spool upper volumetric flow	2-in. Flow Technology turbine meter	±6.3 x 10^{-4}–0.0284 m^3/s (±10–450 gpm) range 4
FE-260	Bundle inlet spool lower volumetric flow	2-in. Flow Technology turbine meter	±6.3 x 10^{-4}–0.0284 m^3/s (±10–450 gpm) range 4
FMFE-264	Bundle inlet spool drag disk (momentum flux)	Ramapo drag disk, ORNL 2-in., 3-bladed full-flow target	±0–1.97 x 10^5 $kg/m \cdot s^2$ (±0–1.32 x 10^5 $lb_m/ft \cdot s^2$)
TE-256	Bundle inlet spool temperature	Nanmac fluid thermocouple	273–1309 K (32–1900°F)
PE-258	Bundle inlet spool pressure	Precise Sensor absolute pressure transducer	0–2.07 x 10^4 kPa (0–3000 psig)
PE-156	Test section inlet transient pressure	Precise Sensor absolute pressure transducer	0–2.07 x 10^4 kPa (0–3000 psig)
PE-201	Test section outlet transient pressure	Precise Sensor absolute pressure transducer	0–2.07 x 10^4 kPa (0–3000 psig)
PdE-200	Bundle transient differential pressure	50-psi BLH differential pressure transducer	±0–345 kPa (±0–50 psid)
PdE-261	Bundle transient differential pressure	500-in. BLH differential pressure transducer	±0–124 kPa (±0–500 in. of Std. H_2O)
PdE-203	Test section transient differential pressure	50-psi BLH differential pressure transducer	±0–345 kPa (±0–50 psid)
PDE-251	Bundle inlet spool differential pressure	50-psi BLH differential pressure transducer	±0–345 kPa (±0–50 psid)
PDE-271	Split downcomer transient differential pressure	6-psi Genisco differential pressure transducer	±0–41.4 kPa (±0–6 psid)

ORNL–DWG 82–5428 ETD (PART A)

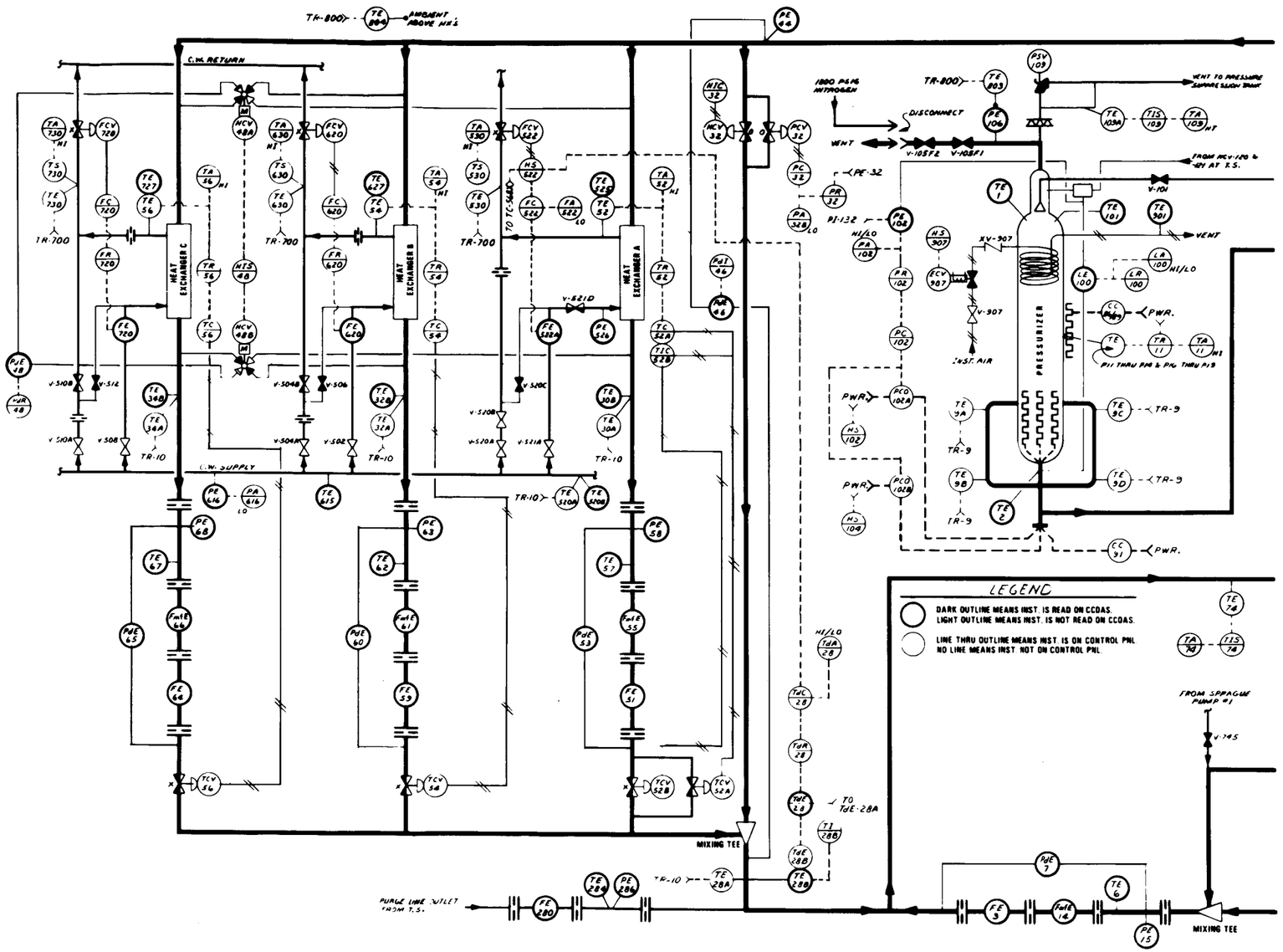

Fig. 5.16. Instrument application drawings for Test 3.03.6AR.

ORNL–DWG 82–5428 ETD (PART B)

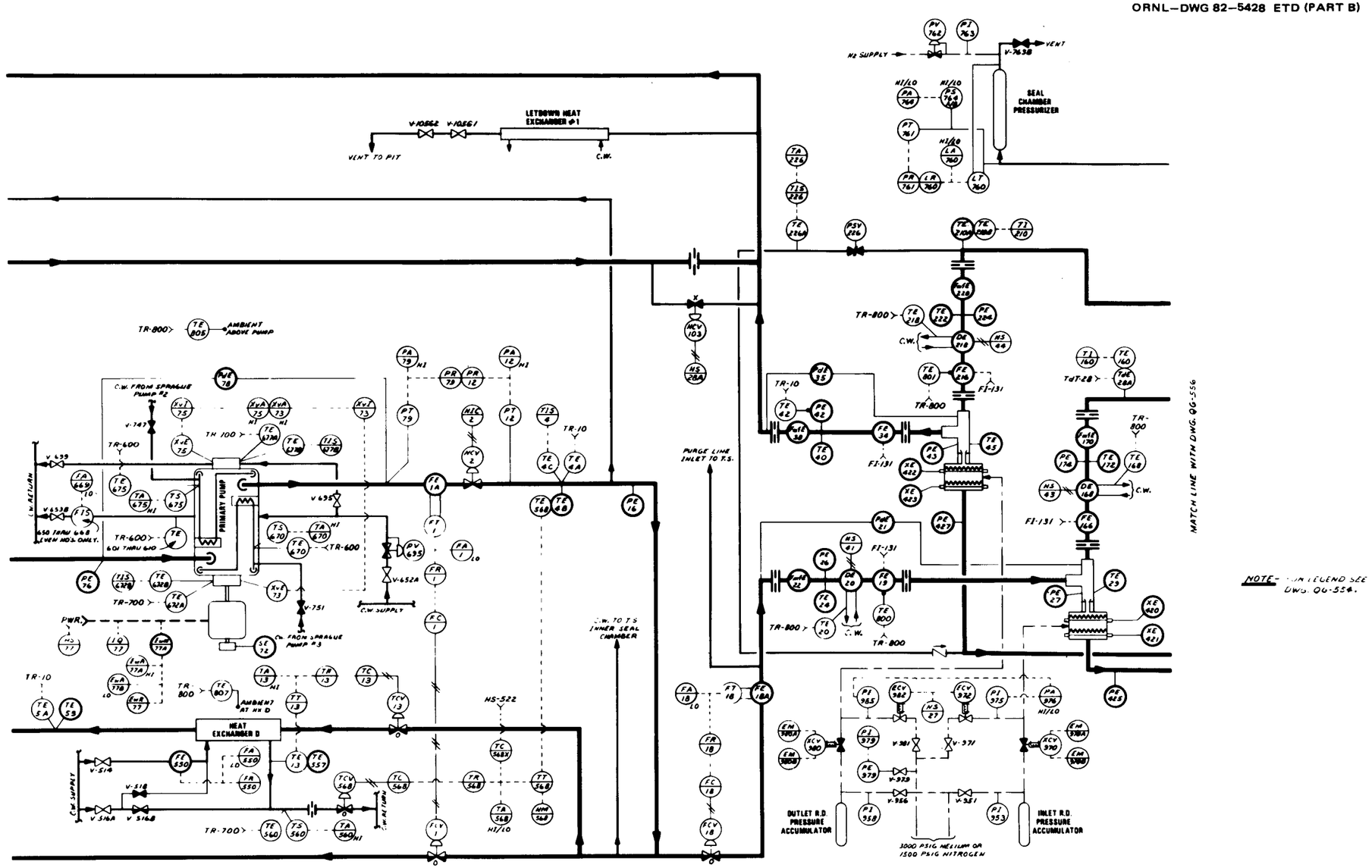

Fig. 5.16 (continued)

ORNL–DWG 82–5428 ETD (PART C)

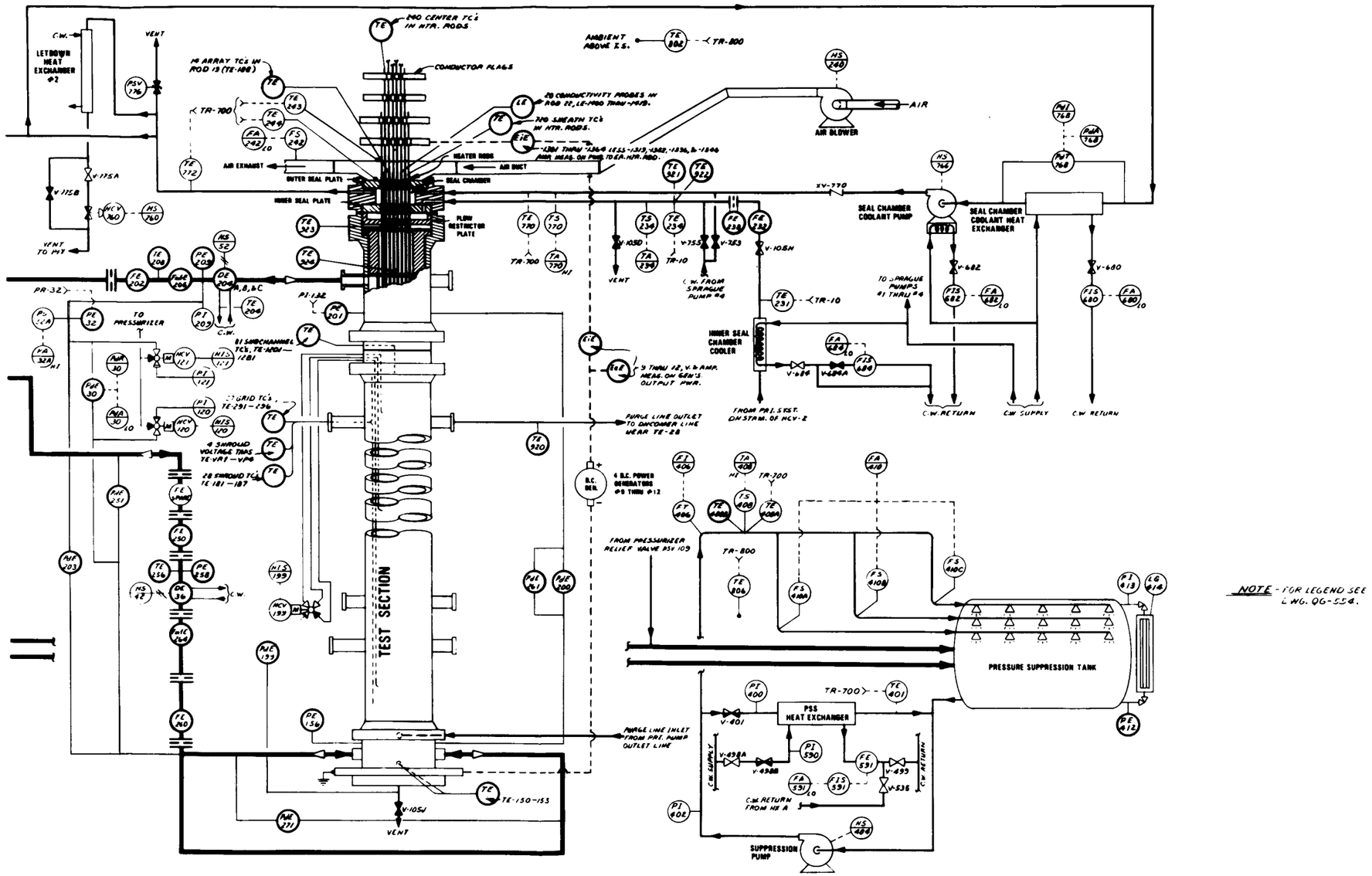

Fig. 5.16 (continued)

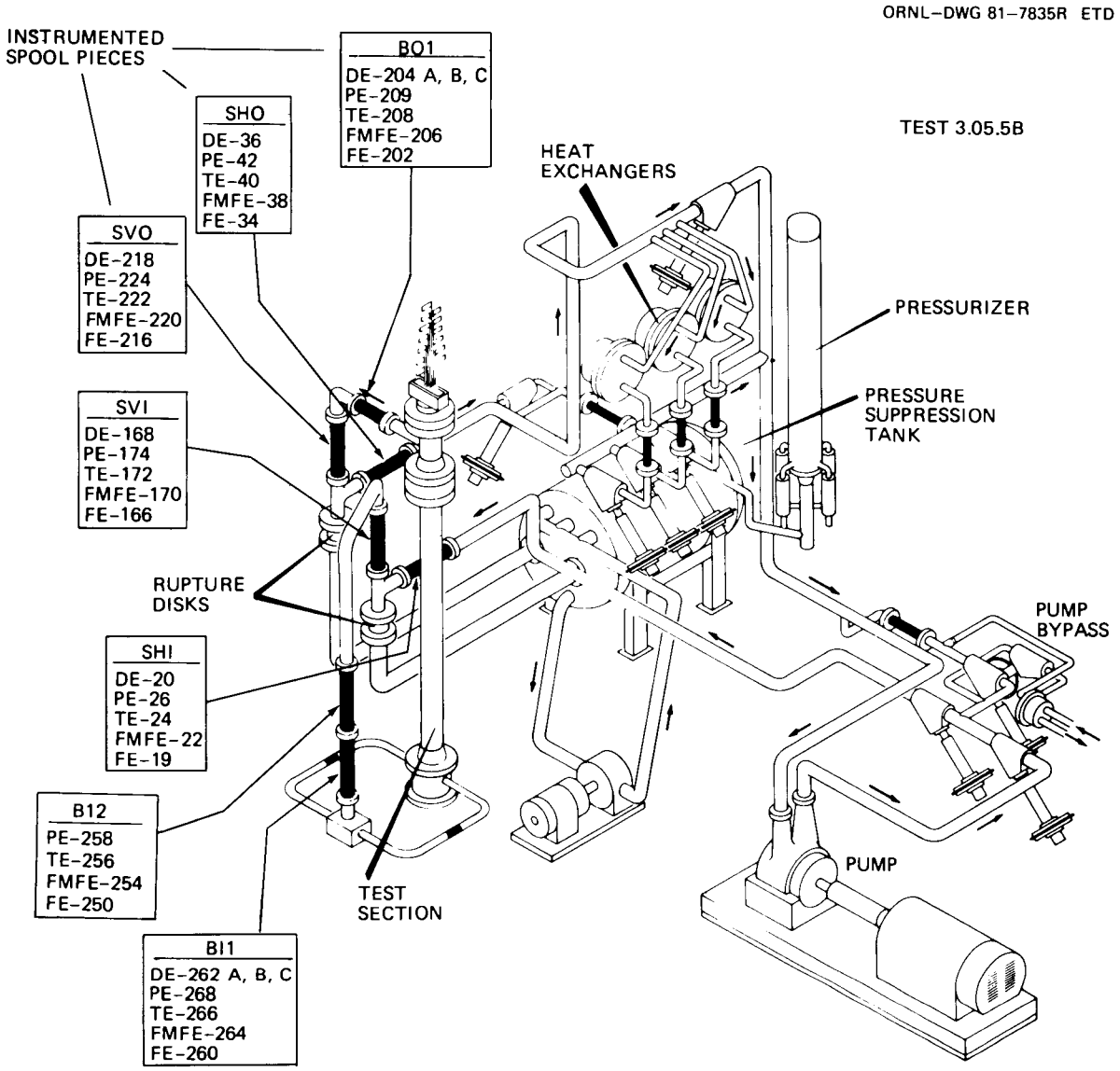

Fig. 5.17. THTF configuration for Test 3.05.5B (standard configuration).

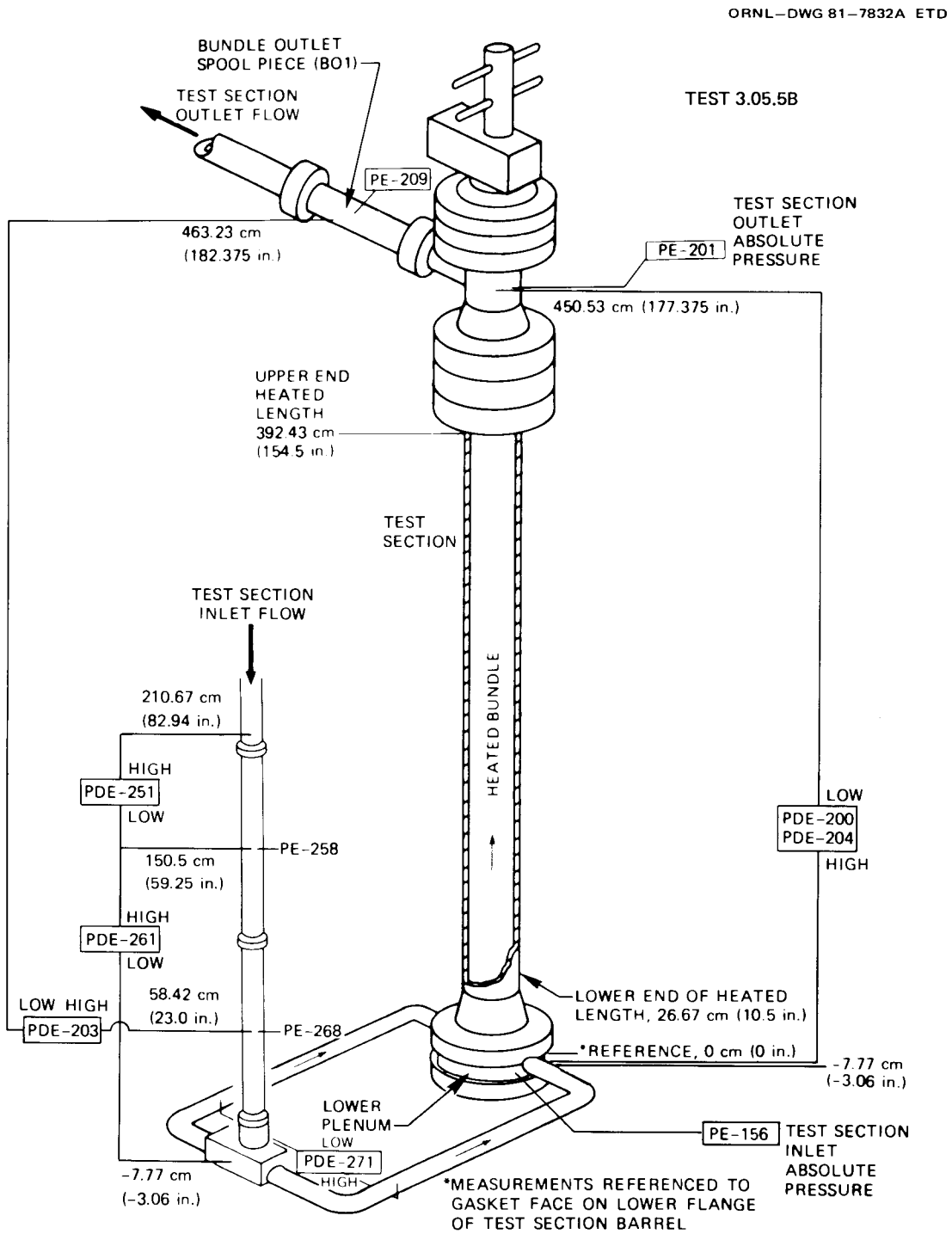

Fig. 5.18. Test section pressure and differential pressure instrumentation for Test 3.05.5B.

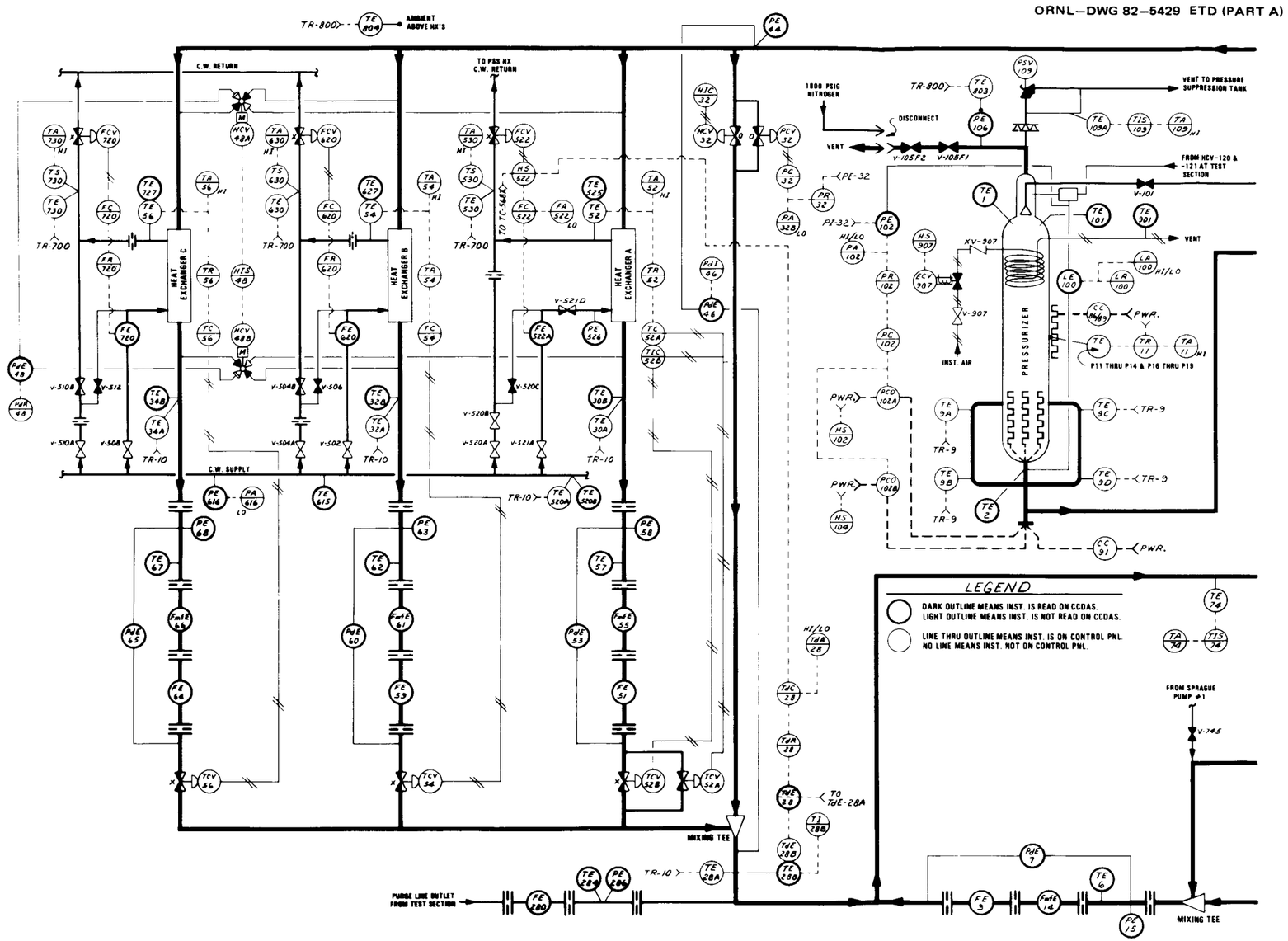

Fig. 5.19. Instrument application drawings for Test 3.05.5B.

ORNL—DWG 82—5429 ETD (PART B)

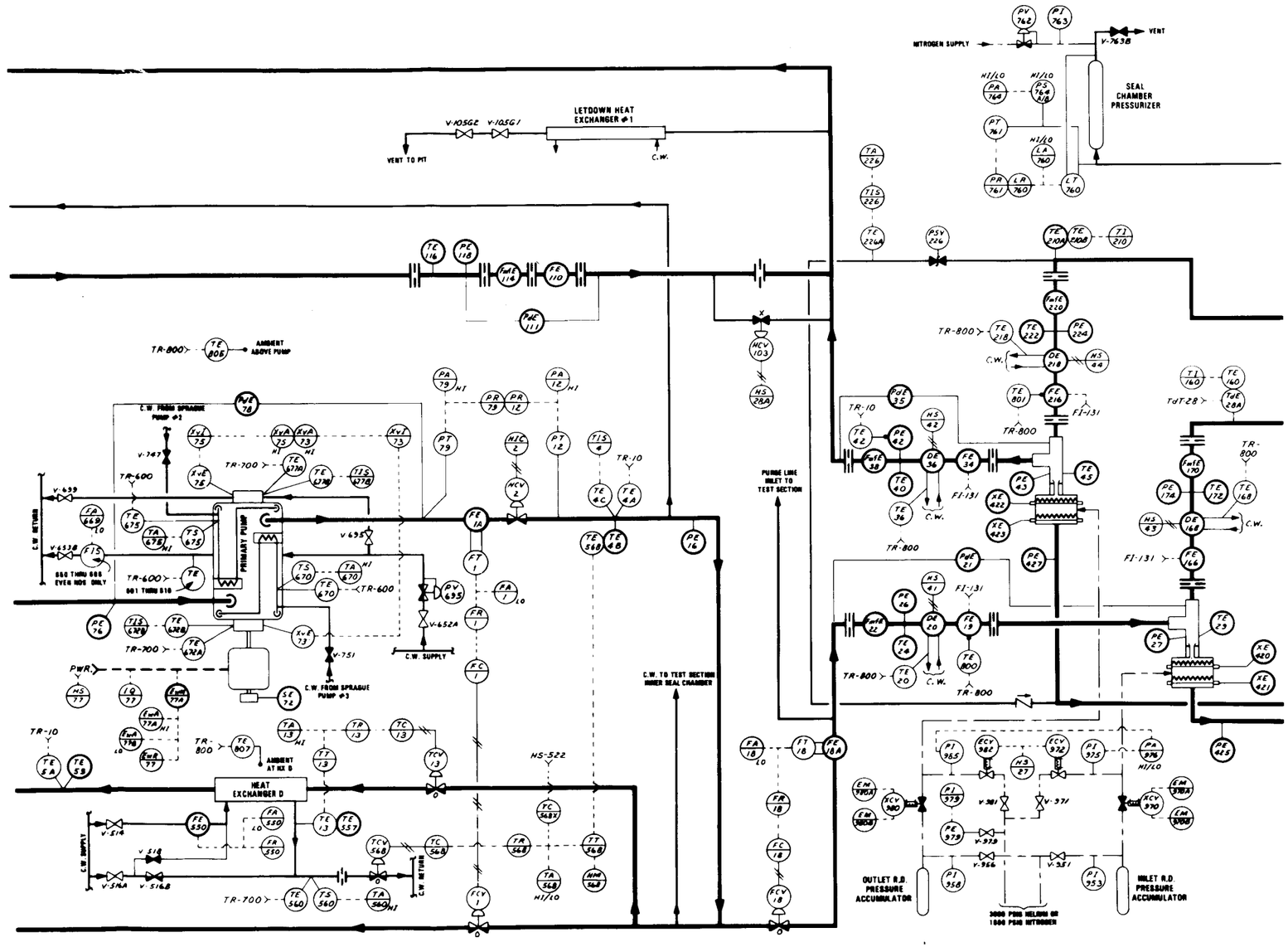

Fig. 5.19 (continued)

ORNL–DWG 82–5429 ETD (PART C)

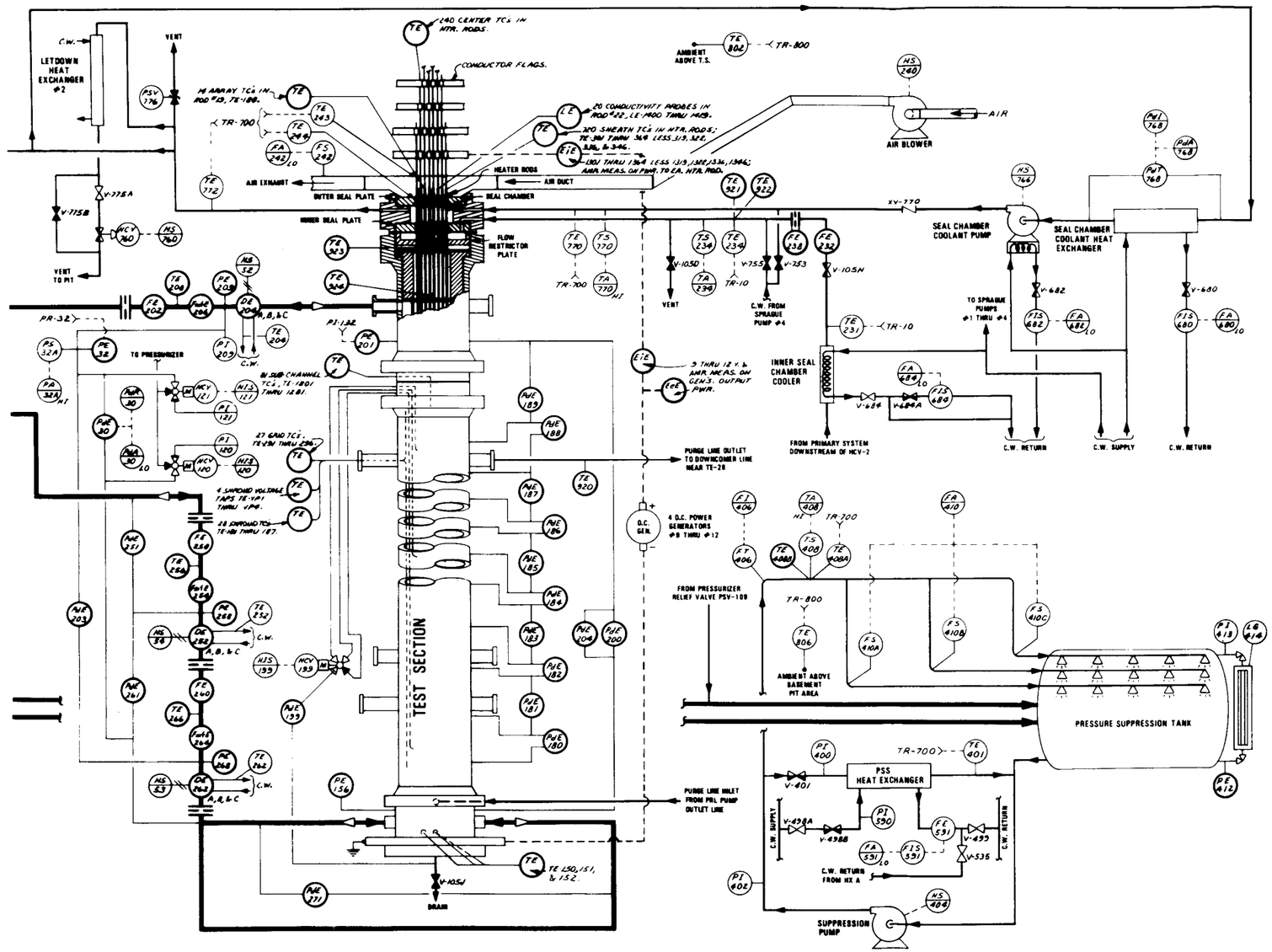

Fig. 5.19 (continued)

Table 5.9. Initial conditions for Test 3.05.5B

Total bundle power, MW	7.52
Average rod power, kW	125.3
Flow	
Volumetric, m^3/s (gpm)	0.032 (506)
Mass, kg/s (lb_m/s)	24.44 (53.88)
Inlet temperature, K (°F)	549.7 (529.7)
Outlet temperature, K (°F)	601.7 (623.4)
Outlet pressure, MN/m^2 (psia)	14.64 (2124)

5.3 Second Bundle Modification

The bundle and test section were modified again prior to the second series of upflow film boiling tests and the second series of small-break LOCA tests. The modifications were made primarily to improve the bundle instrumentation based on results from the initial test series. All but two of the preproduction FRS rods installed during the previous bundle modification were replaced by new FRS rods. The new rods provided an increased number of thermocouple levels in the upper bundle, which resulted in improved axially dependent heat transfer data and improved two-phase mixture level determination in the bundle. Thermocouples were installed in the shroud-box walls in response to apparent shroud-wall energy storage effects observed during the first small-break LOCA test series. New thermocouple-array rods were installed, replacing the remaining original thermocouple-array rod (rod position 19) and the INEL liquid level rod (rod position 22) in two of the instrumented rod positions. The in-bundle gamma densitometer system was installed for testing in the two other instrument rod positions (36 and 46).

Second modification. During the second modification to the bundle, ten new FRSs were fabricated and installed in Bundle 3 (the location of these FRSs is shown in Fig. 5.20). Additionally, FRSs 15, 56, and 62 were removed and replaced with the FRSs from positions 50, 34, and 17, respectively. Thus, only two of the replacement rods from the first refurbishment of the bundle were left (positions 30 and 48). The axial levels monitored by each rod are indicated in Fig. 5.21.

A schematic indicating the FRS levels is shown in Fig. 5.22. A schematic[28] of the refurbished Bundle 3 giving the location of all primary-level (A–G and Y, H, S, and U) FRS thermocouples is presented in Fig. 5.23. The location of special FRS thermocouples between primary levels F and G is illustrated in Fig. 5.24. Also, special FRS thermocouples are located between primary levels E and F as shown in Fig. 5.25. The naming convention for these special (or super-level) thermocouples is different from that given in Sect. 3.3 and illustrated in Table 5.11. As

Table 5.10. Primary flow instrumentation for Test 3.05.5B

Instrument application No.	Description	Instrument	Range
DE-204A	Bundle outlet spool density	Three-beam gamma densitometer	0–1000 kg/m³ (0–62.4 lb_m/ft^3)
DE-204B			
DE-204C			
PE-209	Bundle outlet spool transient pressure	Precise Sensor absolute pressure transducer	0–2.07 x 10⁴ kPa (0–3000 psig)
TE-208	Bundle outlet spool temperature	Nanmac fluid thermocouple	273–1309 K (32–1900°F)
FMFE-206	Bundle outlet spool drag disk (momentum flux)	Ramapo drag disk, ORNL 3.5-in., 3-bladed full-flow target	±0–5.64 x 10⁴ kg/m·s² (±0–3.79 x 10⁴ $lb_m/ft\cdot s^2$)
FE-202	Bundle outlet spool volumetric flow	3.5-in. Flow Technology turbine meter	±0.005–0.227 m³/s (±80–3600 gpm) range 4
DE-36	Horizontal outlet spool density	Single-beam gamma densitometer	0–1000 kg/m³ (0–62.4 lb_m/ft^3)
PE-42	Horizontal outlet spool transient pressure	Precise Sensor absolute pressure transducer	0–2.07 x 10⁴ kPa (0–3000 psig)
TE-40	Horizontal outlet spool temperature	Nanmac fluid thermocouple	273–1309 K (32–1900°F)
FMFE-38	Horizontal outlet spool drag disk (momentum flux)	Ramapo drag disk, ORNL 3.5-in., 3-bladed full-flow target	±0–1.88 x 10⁴ kg/m·s² (±0–1.26 x 10⁴ $lb_m/ft\cdot s^2$)
FE-34	Horizontal outlet spool volumetric flow	3.5-in. Flow Technology turbine meter	±0.005–0.113 m³/s (±80–1800 gpm) range 3
DE-218	Vertical outlet spool density	Single-beam gamma densitometer	0–1000 kg/m³ (0–62.4 lb_m/ft^3)
PE-224	Vertical outlet spool transient pressure	Precise Sensor absolute pressure transducer	0–2.07 x 10⁴ kPa (0–3000 psig)
TE-222	Vertical outlet spool temperature	Nanmac fluid thermocouple	273–1309 K (32–1900°F)
FMFE-220	Vertical outlet spool drag disk (momentum flux)	Ramapo drag disk, ORNL 3.5-in., 3-bladed full-flow target	±0–5.91 x 10⁴ kg/m·s² (±0–3.97 x 10⁴ $lb_m/ft\cdot s^2$)
FE-216	Vertical outlet spool volumetric flow	3.5-in. Flow Technology turbine meter	±0.005–0.227 m³/s (±80–3600 gpm) range 4
DE-168	Vertical inlet spool density	Single-beam gamma densitometer	0–1000 kg/m³ (0–62.4 lb_m/ft^3)

Table 5.10 (continued)

Instrument application No.	Description	Instrument	Range
PE-174	Vertical inlet spool transient pressure	Precise Sensor absolute pressure transducer	0–2.07 x 10^4 kPa (0–3000 psig)
TE-172	Vertical inlet spool temperature	Nanmac fluid thermocouple	273–1309 K (32–1900°F)
FMFE-170	Vertical inlet spool drag disk (momentum flux)	Ramapo drag disk, ORNL 3.5-in., 3-bladed full-flow target	±0–6.17 x 10^4 kg/m·s² (±0–4.15 x 10^4 lb_m/ft·s²)
FE-166	Vertical inlet spool volumetric flow	3.5-in. Flow Technology turbine meter	±0.005–0.057 m³/s (±80–900 gpm) range 2
DE-20	Horizontal inlet spool density	Single-beam gamma densitometer	0–1000 kg/m³ (0–62.4 lb_m/ft³)
PE-26	Horizontal inlet spool transient pressure	Precise Sensor absolute pressure transducer	0–2.07 x 10^4 kPa (0–3000 psig)
TE-24	Horizontal inlet spool temperature	Nanmac fluid thermocouple	273–1309 K (32–1900°F)
FMFE-22	Horizontal inlet spool drag disk (momentum flux)	Ramapo drag disk, ORNL 3.5-in., 3-bladed full-flow target	±0–4.34 x 10^4 kg/m·s² (±0–2.92 x 10^4 lb_m/ft·s²)
FE-19	Horizontal inlet spool volumetric flow	3.5-in. Flow Technology turbine meter	±0.005–0.113 m³/s (±80–1800 gpm) range 3
PE-258	Bundle inlet upper spool transient pressure	Precise Sensor absolute pressure transducer	0–2.07 x 10^4 kPa (0–3000 psig)
TE-256	Bundle inlet upper spool temperature	Nanmac fluid thermocouple	273–1309 K (32–1900°F)
FMFE-254	Bundle inlet upper spool drag disk (momentum flux)	Ramapo drag disk, 3.5-in., 3-bladed full-flow target	±0–1.59 x 10^4 kg/m·s² (±0–1.07 x 10^4 lb_m/ft·s²)
FE-250	Bundle inlet upper spool volumetric flow	3.5-in. Flow Technology turbine meter	±0.005–0.057 m³/s (±80–900 gpm) range 2
DE-262A	Bundle inlet lower spool density	Three-beam gamma densitometer	0–1000 kg/m³ (0–62.4 lb_m/ft³)
DE-262B			
DE-262C			
PE-268	Bundle inlet lower spool transient pressure	Precise Sensor absolute pressure transducer	0–2.07 x 10^4 kPa (0–3000 psig)

Table 5.10 (continued)

Instrument application No.	Description	Instrument	Range
TE-266	Bundle inlet lower spool temperature	Nanmac fluid thermocouple	273–1309 K (32–1900°F)
FMFE-264	Bundle inlet lower spool drag disk (momentum flux)	Ramapo drag disk, ORNL 3.5-in., 3-bladed full-flow target	±0–5.12 x 10^4 kg/m·s² (±0–3.44 x 10^4 lb_m/ft·s²)
FE-260	Bundle inlet lower spool volumetric flow	3.5-in. Flow Technology turbine meter	±0.005–0.057 m³/s (±80–900 gpm) range 2
PE-156	Test section inlet transient pressure	Precise Sensor absolute pressure transducer	0–2.07 x 10^4 kPa (0–3000 psig)
PE-201	Test section outlet transient pressure	Precise Sensor absolute pressure transducer	0–2.07 x 10^4 kPa (0–3000 psig)
PDE-200	Bundle transient differential pressure	50-psi BLH differential pressure transducer	±0–345 kPa (±0–50 psid)
PDE-204	Bundle transient differential pressure	500-in. BLH differential pressure transducer	±0–124 kPa (±0–500 in. of Std. H_2O)
PDE-203	Test section transient differential pressure	50-psi BLH differential pressure transducer	±0–345 kPa (±0–50 psid)
PDE-251	Bundle inlet upper spool differential pressure	50-psi BLH differential pressure transducer	±0–345 kPa (±0–50 psid)
PDE-261	Bundle inlet lower spool differential pressure	50-psi BLH differential pressure transducer	±0–345 kPa (±0–50 psid)
PDE-271	Split downcomer transient differential pressure	6-psi Genisco differential pressure transducer	±0–41.4 kPa (±0–6 psid)

ORNL–DWG 82–5053 ETD

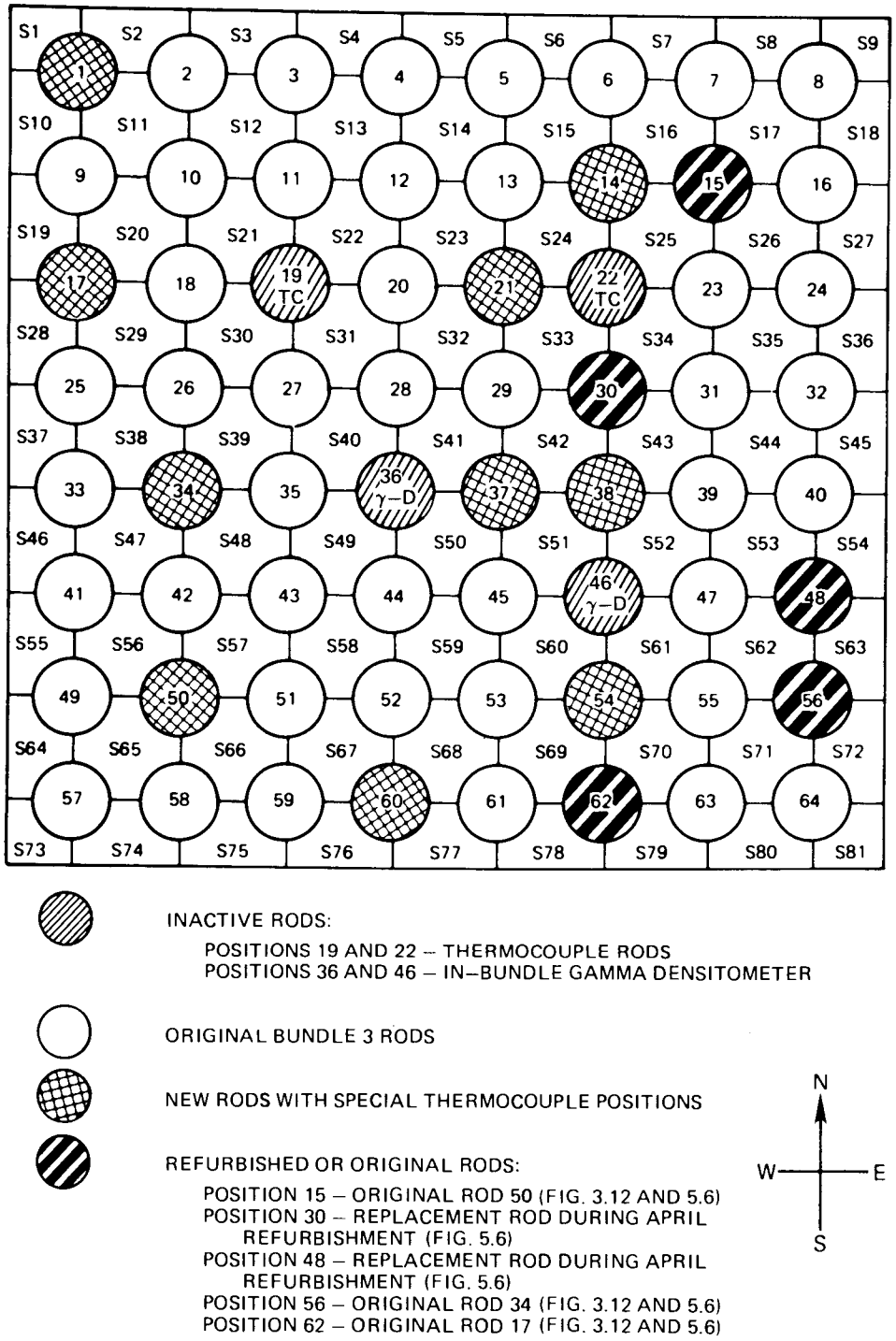

Fig. 5.20. Identification of THTF heater rods, subchannel locations, and instrument rods in the modified Bundle 3 (August 1980 to present).

ORNL-DWG 82-5054R ETD

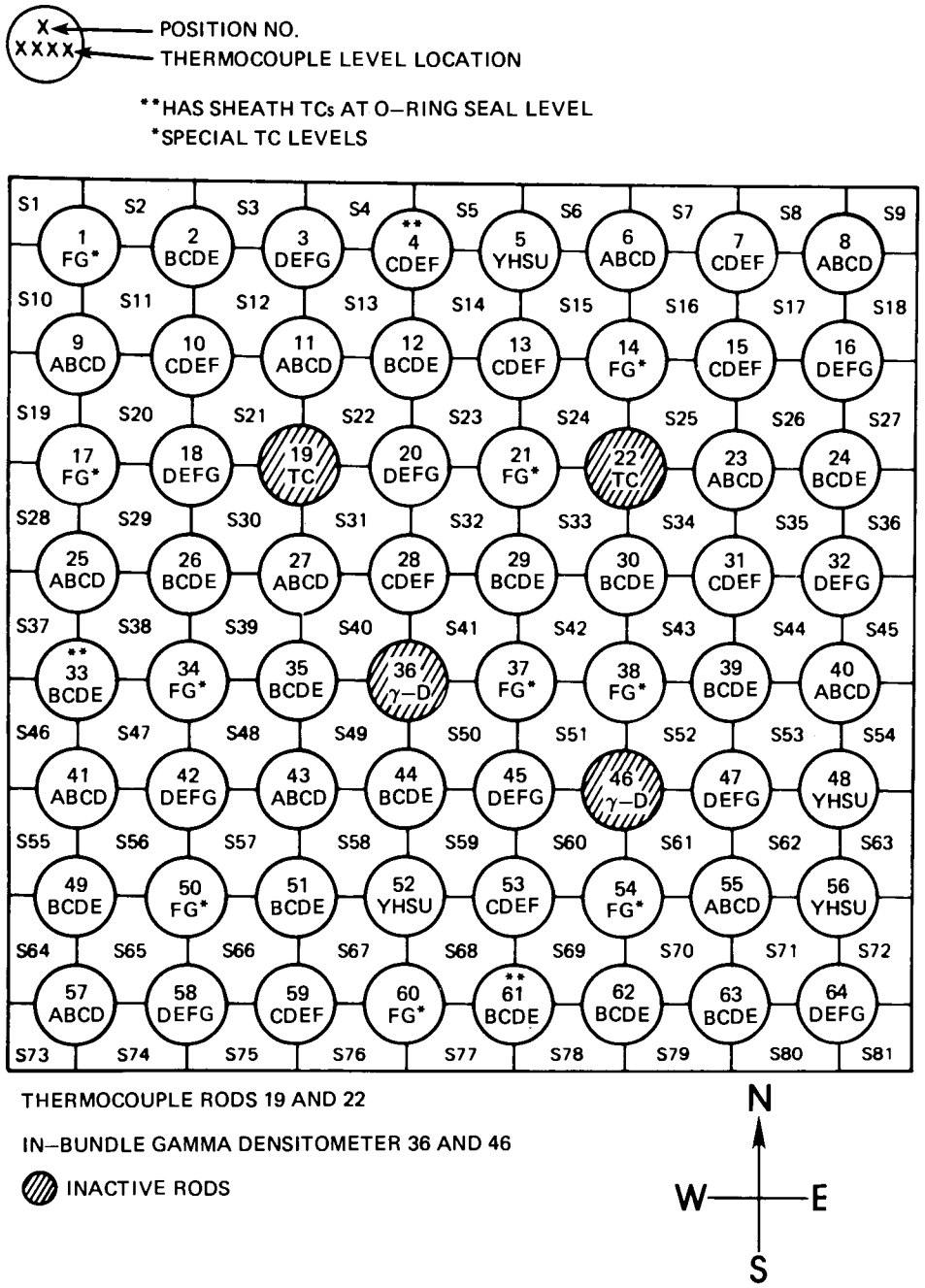

Fig. 5.21. Identification of THTF heater rods and axial thermocouple levels monitored by each rod in the modified THTF Bundle 3 (August 1980 to present).

ORNL–DWG 80–5646E ETD

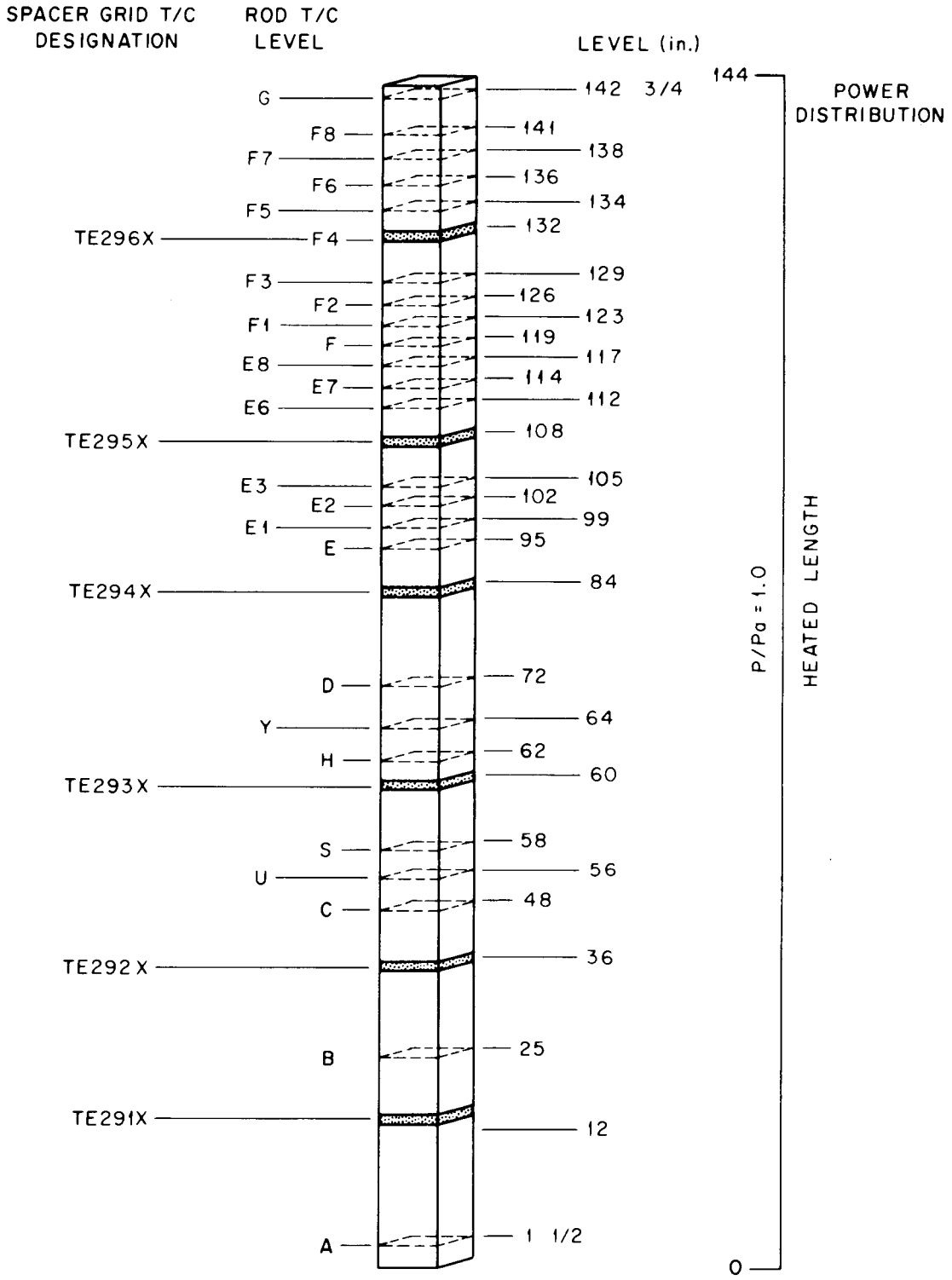

Fig. 5.22. Schematic showing new thermocouple levels between primary levels E and G in modified THTF Bundle 3 (August 1980 to present).

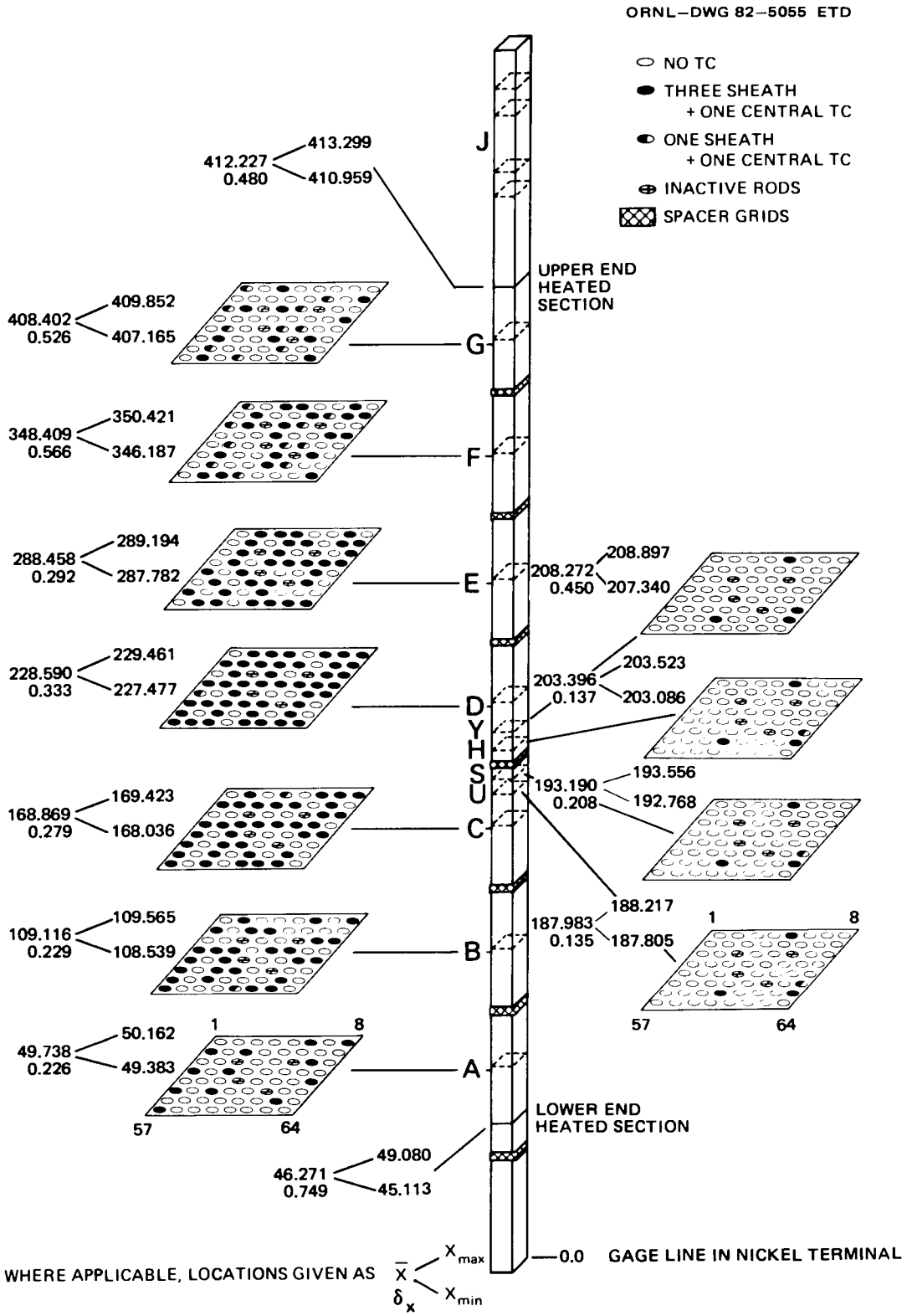

Fig. 5.23. Location of primary FRS thermocouples in modified THTF Bundle 3 (August 1980 to present). All dimensions are in centimeters and are referenced to gage line in nickel terminal.

ORNL–DWG 82–5056 ETD

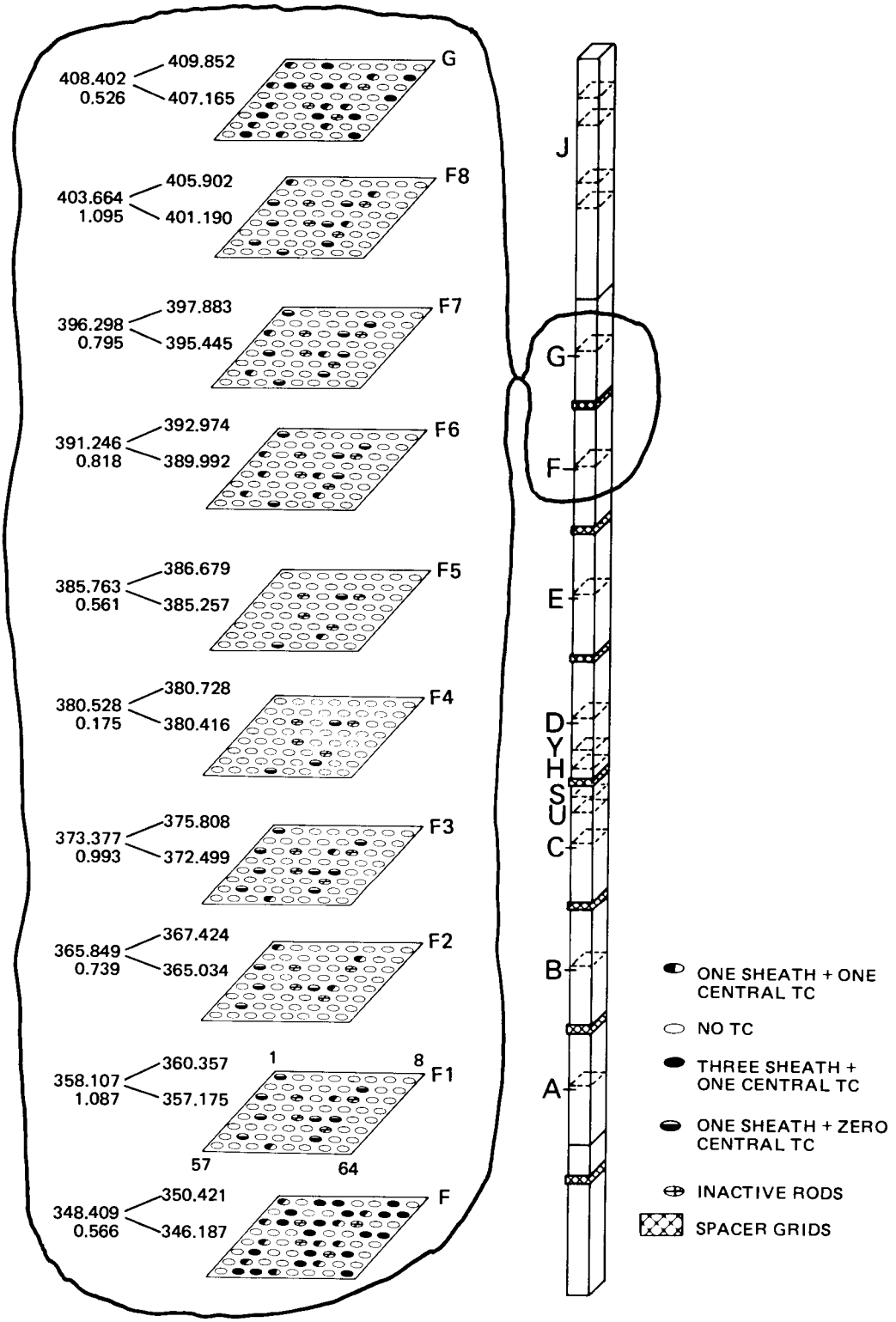

Fig. 5.24. Location of special FRS thermocouples (between primary levels F and G) in modified THTF Bundle 3 (August 1980 to present). All dimensions are in centimeters and are referenced to gage line in nickel terminal.

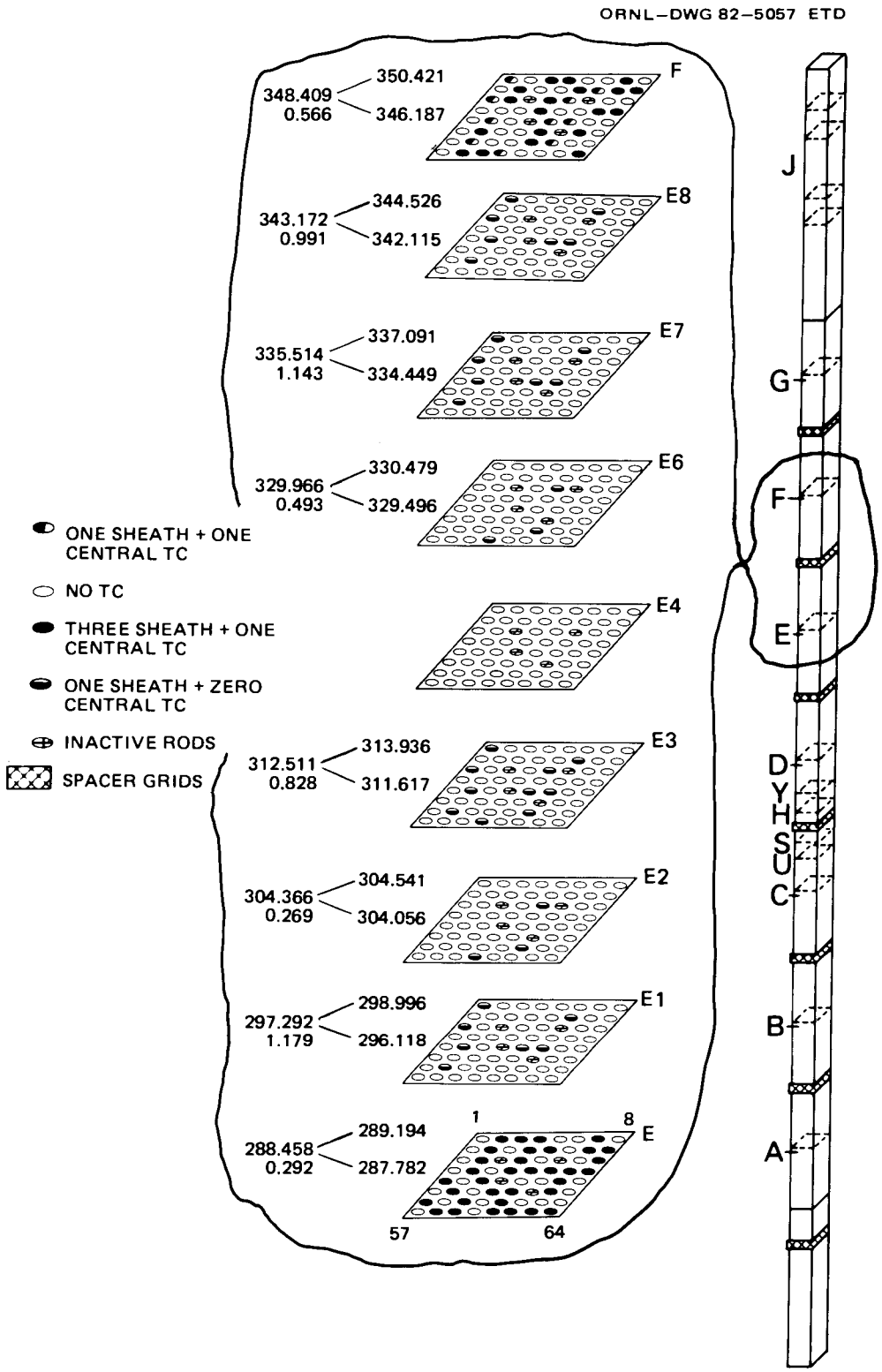

Fig. 5.25. Location of special FRS thermocouples (between primary levels E and F) in modified THTF Bundle 3 (August 1980 to present). All dimensions are in centimeters and are referenced to gage line in nickel terminal.

Table 5.11. Naming convention for super-level FRS thermocouples[a]

Level axial position[b] (cm)	al
297.292	E1
304.366	E2
312.511	E3
329.966	E6
335.514	E7
343.172	E8
358.107	F1
365.849	F2
373.377	F3
380.528	F4
385.763	F5
391.246	F6
396.298	F7
403.664	F8

[a]General form: TE-3nnal, where nn is a number between 01 and 64 equal to the rod or grid position number, and al is a combination of a letter (E or F) and a number (1-8). This combination is given along with the level axial position.

[b]Figures 5.4 and 5.5.

of August 29, 1980, those FRS thermocouples presented in Table 5.12 were monitored by the CCDAS.

The core fluid temperature measurement sites are indicated in Fig. 5.26. The location of subchannel, spacer-grid, and shroud fluid sites remains the same as in Figs. 3.10, 5.10, and Appendix B. The thermocouple-array rod that was in position 19 in the refurbished bundle was removed and discarded (it was theorized that the thermocouple extensions into the fluid were bent back into the rod during reassembly of the bundle during the first modification and, as a result, no longer measured the bulk fluid temperature). The original thermocouple-array rods were built into the bundle as it was being assembled, and the orientation and location of the thermocouples projecting into the subchannels were easily determined. The removal of the thermocouple-array rods through the spacer grids and then the reinsertion following installation of new O-rings during the first bundle modification possibly caused a disorientation of the thermocouples extending into the subchannel. The new design allowed installation of the

Table 5.12. In-service thermocouple listing for modified THTF Bundle 3 (August 1980)

Rod	Sheath angle level	Center level
1	AF, AG, E1, E3, E7, E8, F1, F2, F3, F6, F7, F8	MF, MG, M2, M8
2	AB, BC, AD, AE	MB, MC, MD
3	CD, BE, CE, BF, CG	MD, ME, MF, MG
4	AC, AD, BE, AF	MC, MD, ME, MF
5	BU, AS, BH, CY	MU, MS, MH, MY
6	AA, AB	MA
7	AC, BE, CE, AF, BF	MC, ME, MF
8	CB, BC, AD, CD	MB, MC, MD
9	CB, AC, CD	MB, MC
10	CC, BD, CD, BE, AF, BF, CF	MC, MD, ME
11	AA, AB, CC	MA, MC
12	CB, BC, CD, AE	MB, MC, MD, ME
13	BC, CD, AE, CE, BF, CF	
14	AF, AG, E1, E3, E7, E8, F2, F3, F6, F7, F8	MF, MG, M2, M8
15	AC, AD, BD, BE, CE, AF	MC, MD, ME, MF
16	AD, BE, CE, BF, BG, CG	MD, ME, MF, MG
17	AF, AG, E3, F1, F2, F3, F6, F7, F8	MF, MG, M6, M7
18	BD, CD, AE, BE, CE, AF, CF, AG, BG, CG	MD, ME, MF
19	Rod 19 is unpowered	
20	AD, BD, CD, AE, BE, CE, AF, BF, CF, AG, BG, CG	MD, MG
21	AF, AG, E2, E3, E6, F1, F3, F4, F5, F6, F7, F8	MF, MG, M1, M3
22	Rod 22 is unpowered	
23	AA, BC	
24	AB, AC, BD, AE, CE	MC, MD, ME
25	CA, CB, BC, CC, BD, CD	MA, MB, MC, MD
26	BB, AC, AD, BD, CD, AE, BE, CE	MC, MD, ME
27	BA, CB, AC, CC, AD, BD, CD	MB
28	AC, CC, AD, BD, CD, AE, CE, AF, BF, CF	MC, MD, ME, MF
29	CB, AC, BC, AD, BD, CD, AE, BE, CE	MB, MC, MD, ME
30	CB, AC, AD, AE, BE	MB, MC, ME
31	CD, CE, BF, CF	MF
32	CD, AE, CE, CF, CG	MD, ME, MG
33	AC, AD, AE, BE, CE	MC
34	AF, AG, E3, E7, E8, F1, F2, F3, F6, F7, F8	MF, M6
35	BB, BD, BE	MB, MD, ME
36	Rod 36 is unpowered	
37	AF, AG, E3, E7, E8, F1, F6, F7, F8	MF, MG, M6, M7
38	AF, AG, E1, E3, E7, E8, F1, F2, F3, F6, F7, F8	MF, MG, M2, M8
39	BB, AC, BD	MB, MC, MD
40	CA, CB, BC, BD	MA, MB, MC
41	AB	MB
42	BD, BE, BF, AG, BG, CG	
43	BA, BB, BC, AD, BD	
44	CB, CC, CD, AE, CE	MB, MC, ME
45	AD, BD, AE, BE, AF, BF, CF, AG, BG, CG	MD, ME, MG
46	Rod 46 is unpowered	
47	CF, CG	MF, MG
48	AH, AY	MH, MY
49	CB, CC, CD, AE, BE, CE	MB, MC, MD, ME
50	AG, E1, E3, E7, F1, F2, F3, F6, F7, F8	M6, M7
51	AB, BC, BD, AE, BE	MC
52	AU, BU, CU, AS, BS, CS, AH, BH, CH, AY, BY, CY	MU, MS, MH, MY
53	CC, AE, BE, BF	MC, ME
54	AF, AG, E2, E3, E6, F1, F3, F4, F5, F6, F7, F8	MF, MG, M5, M6
55	AA, CB, BC, CD	MA, MB, MC, MD
56	BU, BS, CH, AY	MS, MH
57	BA, CB, AC, BC, BD, CD	MA, MB, MC, MD
58	AD, CD, AE, BE, BF, CG	MD, ME, MF, MG
59	CC, AD, AE, BE, CE, AF, BF, CF	MC, ME, MF
60	AF, AG, E2, E3, E6, F3, F4, F5, F6, F7, F8	MF, MG, M3
61	AB, AC, AD, AE, BE, CE	MB, MC, MD
62	BB, AC, AD, CE	
63	CB, BC, AE, BE	MB, MC, ME
64	AD, BD, CD, AE, BE, AF, BF, CF, AG, CG	MD, MF, MG

ORNL–DWG 82–5058 ETD

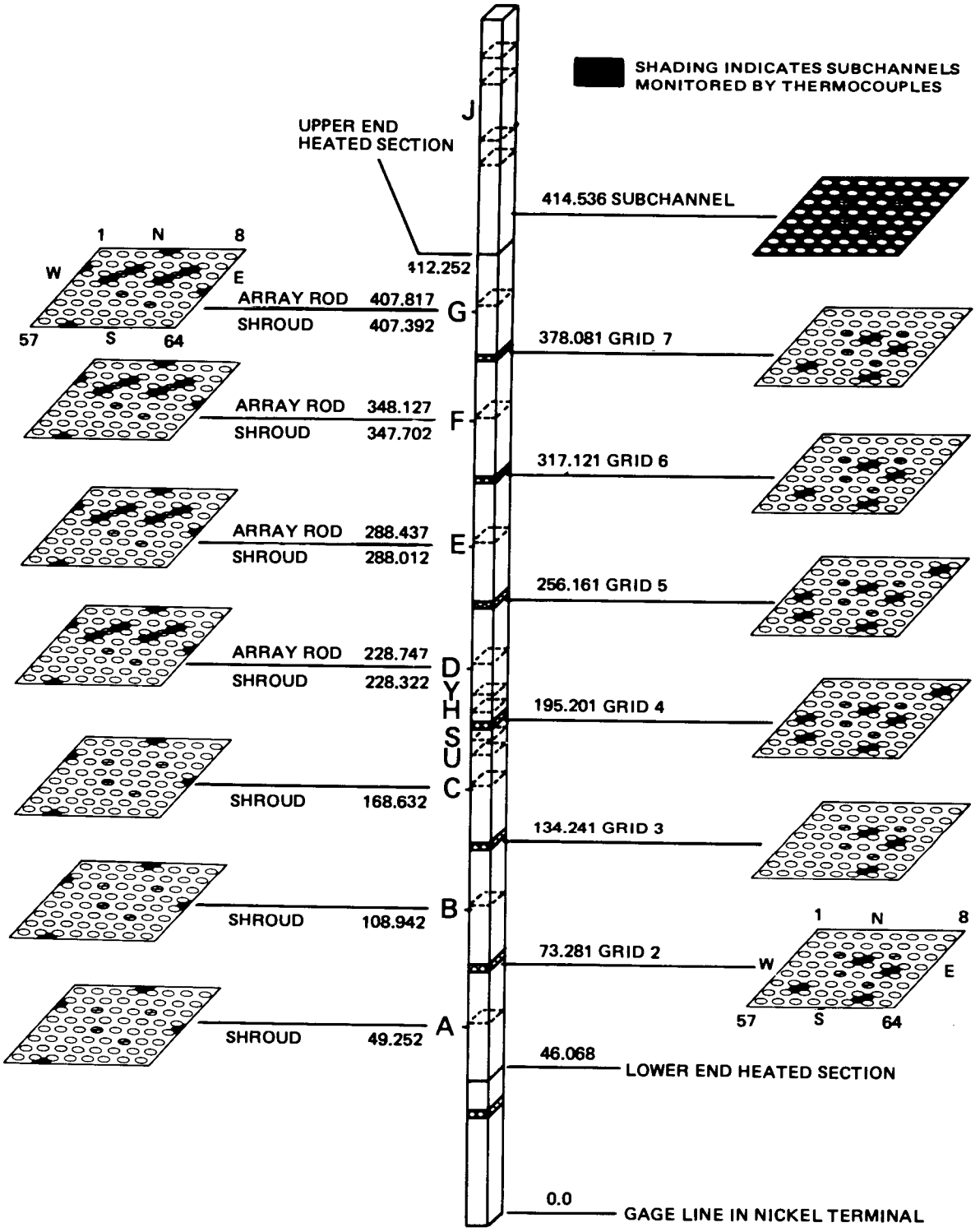

Fig. 5.26. Location of fluid thermocouples in modified THTF Bundle 3 (August 1980 to present). All dimensions are in centimeters and are referenced to gage line in nickel terminal.

thermocouple-array rod into the already assembled bundle. The thermocouples at each level in the thermocouple-array rod remain inside the rod until it is installed in the bundle. Once the rod is positioned in the bundle, the thermocouples are pulled into position from the upper end of the rod, with the thermocouples springing into the subchannel through slots in the rod wall as they are pulled up. A sliding component behind the thermocouples is machined to lock the thermocouples into the proper position. Figure 5.27 shows the thermocouple-array rod assembly. Bench tests indicated that the method worked well (in terms of the thermocouple springing into the proper position); however, because it is not possible to observe the thermocouples once they are in the bundle, absolute verification of their location in the subchannel is impossible. The intended design location for the 1.02-mm-diam (0.040-in.) thermocouples is the center of the subchannel. Thermocouples project from opposite sides of the instrument rod at thermocouple levels D, E, F, and G. The two new thermocouple-array rods were installed in the bundle in grid positions 19 and 22.

Shroud-wall thermocouples were installed during this modification period. The installation was the result of apparent wall heat-up effects observed during the small-break LOCA-I test series. The thermocouples were intended to provide both energy balance measurements and operational verification of steady-state conditions in the fairly massive shroud-box walls. Two thermocouples were installed at each of the 12 locations indicated in Fig. 5.28, 9 on the east side and 3 on the south side. The two thermocouples at each location, one on the bundle side and one on the shroud-plenum-annulus side of the shroud-box wall, provided a measurement of the temperature gradient across the wall.

Each shroud-wall thermocouple pair installed consisted of two 1.58-mm-diam (1/16-in.) thermocouples installed in a drilled cavity of a 5/16-24 UNF-2A stainless steel screw (Fig. 5.29). Each thermocouple was brazed to the screw and sealed at the test section barrel penetration with a Conax MHC-062-A-2-G 316 stainless steel fitting with Grafoil packing. Each shroud-wall thermocouple screw was 3.429 cm (1.350 in.) in length with two 0.1613-cm (0.0635-in.) holes drilled 0.1194 cm (0.047 in.) off center into the screw. One hole was drilled all the way through the screw, and the thermocouple was inserted flush with screw end. The second hole was drilled to a depth ~1.524 cm (0.600 in.) short of the screw end, and the thermocouple was inserted to the hole bottom.

Holes in the shroud-box wall were drilled to a depth of 2.286 cm (0.900 in.) on the east side where the total shroud-wall thickness is 2.54 cm (1.0 in.) and to a depth of 1.651 cm (0.650 in.) on the south side where the total shroud-wall thickness is 1.905 cm (0.750 in.). In all cases, the holes were bottom tapped, forming a smooth and flat surface to seat the shroud-wall screws. Each hole in the shroud-box wall was ~0.254 cm (0.100 in.) short of penetrating completely through the inner wall. However, actual dimensions varied from this nominal design value because the machining was done with the bundle and shroud box in place (in the test section). X-ray measurements of the thermocouple bead locations in the 5/16-in. screw combined with postmachining measurements of the tapped holes in the shroud-box wall result in the final dimensions indicated in Table 5.13 (measurements are referenced from the bundle side of the shroud-box wall). Note that at two positions (11 and 13) the outside

ORNL–DWG 82–5430 ETD

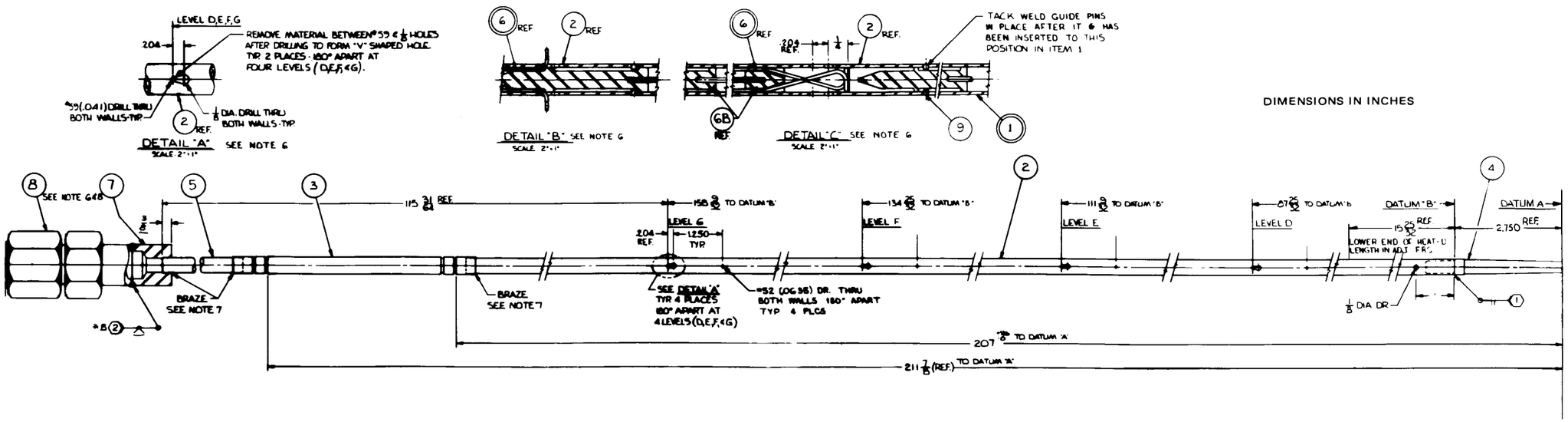

Fig. 5.27. Detail of new thermocouple–array rod.

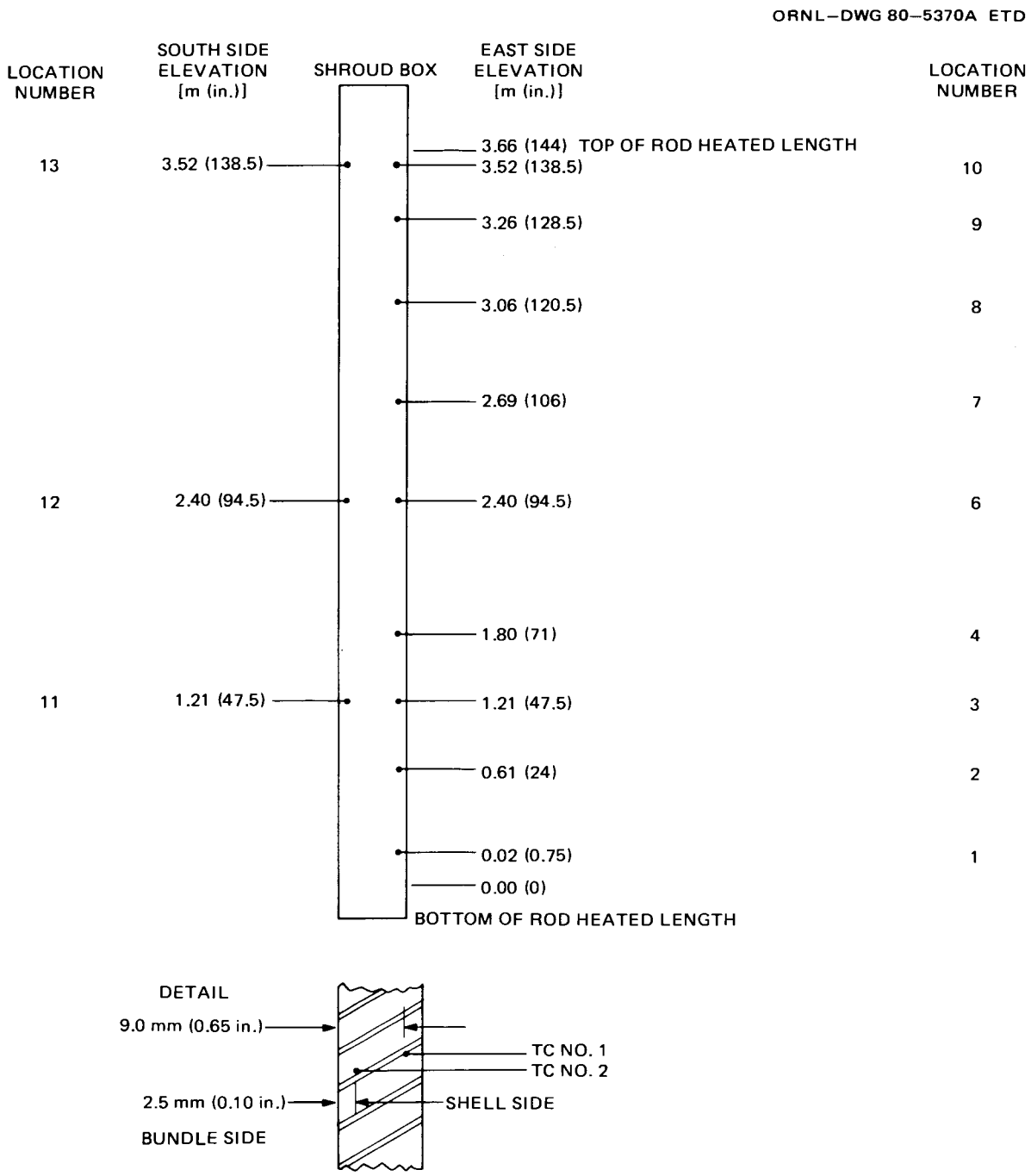

Fig. 5.28. Schematic diagram of shroud-wall thermocouple locations.

ORNL–DWG 82–5060 ETD

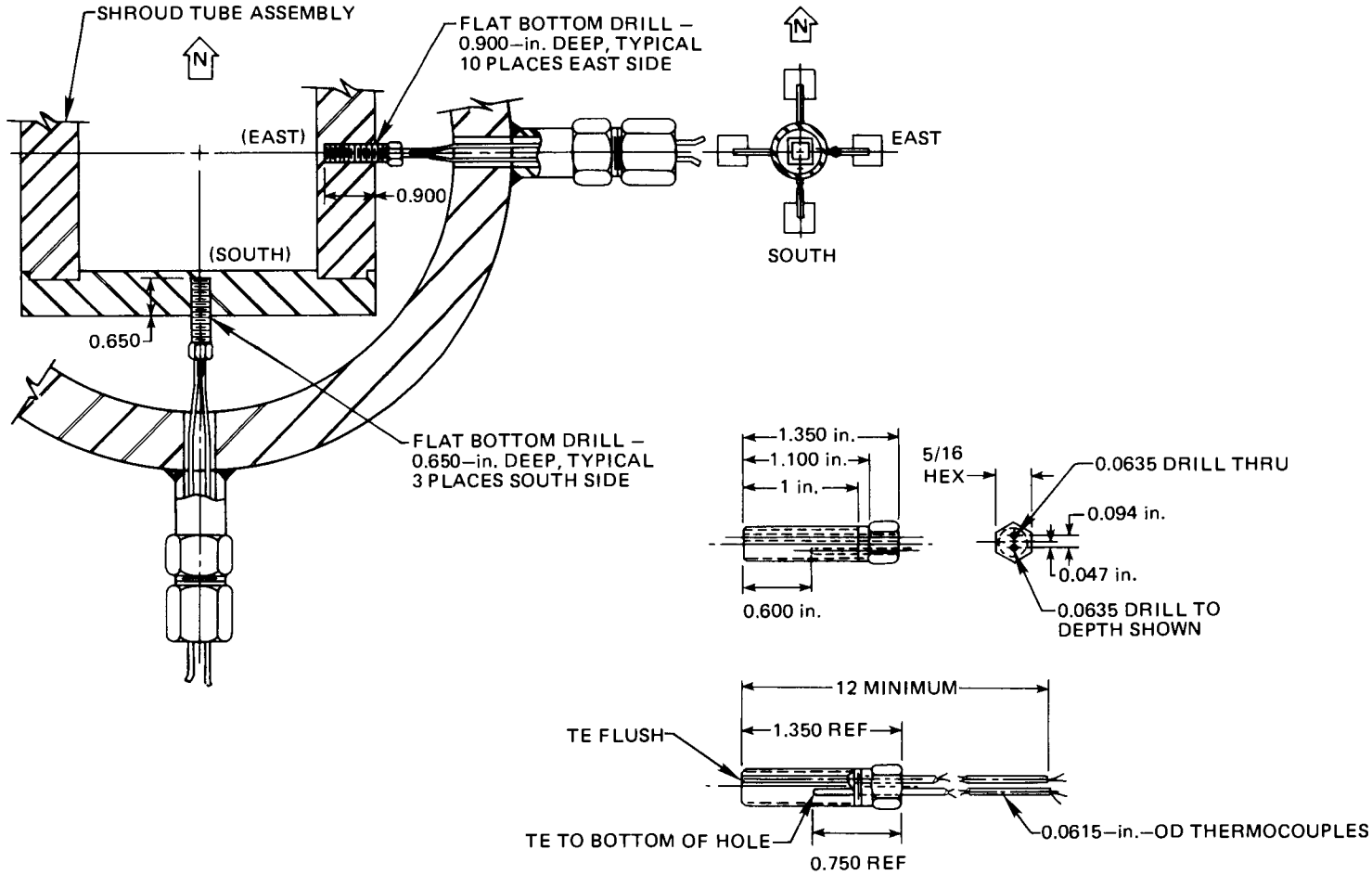

Fig. 5.29. Detail of shroud-wall thermocouple assembly.

Table 5.13. Location of shroud-wall thermocouples relative to the core side of the shroud

Location No.	Level and wall	Thermocouple assembly IAN	Location of inside thermocouple bead[a] [cm (in.)]	Location of outside thermocouple bead[b] [cm (in.)]
1	0E	TE-270AE[a] TE-270BE[b]	0.2769 (0.1090)	1.8669 (0.7350)
2	1E	TE-271AE TE-271BE	0.3376 (0.1329)	1.7777 (0.6999)
3	2E	TE-272AE TE-272BE	0.2875 (0.1132)	1.7976 (0.7077)
4	3E	TE-273AE TE-273BE	0.1575 (0.0620)	1.6576 (0.6526)
6	5E	TE-275AE TE-275BE	0.4394 (0.1730)	2.0594 (0.8108)
7	6E	TE-276AE TE-276BE	0.3744 (0.1474)	1.9042 (0.7497)
8	7E	TE-277AE TE-277BE	0.4061 (0.1599)	1.9461 (0.7662)
9	8E	TE-278AE TE-278BE	0.4544 (0.1789)	2.1245 (0.8364)
10	9E	TE-279AE TE-279BE	0.2032 (0.0800)	1.7033 (0.6706)
11	2S	TE-272AS TE-272BS	0.4747 (0.1869)	2.1549 (0.8484)[c]
12	5S	TE-275AS TE-275BS	0.2489 (0.0980)	1.7689 (0.6964)
13	9S	TE-279AS TE-279BS	0.4016 (0.1581)	1.9715 (0.7762)[c]

[a]Inside thermocouple.

[b]Outside thermocouple.

[c]Location of outside thermocouple is in the purge stream, not in the shroud wall.

bead is not in the shroud wall. The nomenclature used for these thermocouples has the following form:

TE-27abc ,

where TE-27 is the same for all positions, and

a = level (0–9),
b = the letter A and B (A indicates the inside thermocouple, and B indicates the outside thermocouple), and
c = the letter E (east wall) or S (south wall).

An in-bundle gamma densitometer system was installed for testing in the THTF during this modification period. The in-bundle gamma densitometer uses low-energy gamma sources and high-temperature ion chambers positioned in two of the instrumented rods. A line-of-sight path that crosses two subchannels exists between unheated instrument rod positions 36 and 46. The design concept is the determination of in-bundle void fraction by measurement of the variation in the attenuation of the source across the subchannel path length. A schematic diagram showing the system is presented in Fig. 5.30. A detail of the source-detector radial geometry is shown in Fig. 5.31. The annular source design was chosen to allow placement of two source-detector systems using only two instrument rod positions. For the instrument rod where the source is located above the detector (Fig. 5.30), the detector cable passes through the source annulus and out of the instrument rod tube. The source and detector assemblies in each of the rods are attached to a motor drive system for axial positioning. The two measurement sites are fixed with respect to each other, but variation of the axial position of the two measurement sites over the heated length of the bundle is made possible with the aid of the positioning motor drive. The system is described in more detail in Ref. 29 along with results from testing in the THTF. Figure 5.21 shows a cross section of the bundle indicating the locations of the instrument rods in the bundle.

5.3.1 Upflow Film Boiling Test 3.06.6B

The second transient upflow film boiling test, 3.06.6B, was run following completion of the modification.[24,25,30,31] The loop was in the same configuration as the first Upflow Film Boiling Test, 3.03.6AR, except for some instrumentation changes. The objectives of the experiment were the same as for Test 3.03.6AR (Sect. 5.2.1). The initial conditions for Test 3.06.6B prior to blowdown are presented in Table 5.14. The film boiling data ranges requested by NRC and obtained in Test 3.06.6B are presented in Table 5.15. An isometric drawing of the facility showing the primary loop instrumentation is presented in Fig. 5.32. The pressure and differential pressure instrumentation is shown in Fig. 5.33. Table 5.16 lists the type and ranges of the instrumentation shown in Figs. 5.32 and 5.33. The instrument application drawings for Test 3.06.6B are shown in Figs. 5.34(a–c).

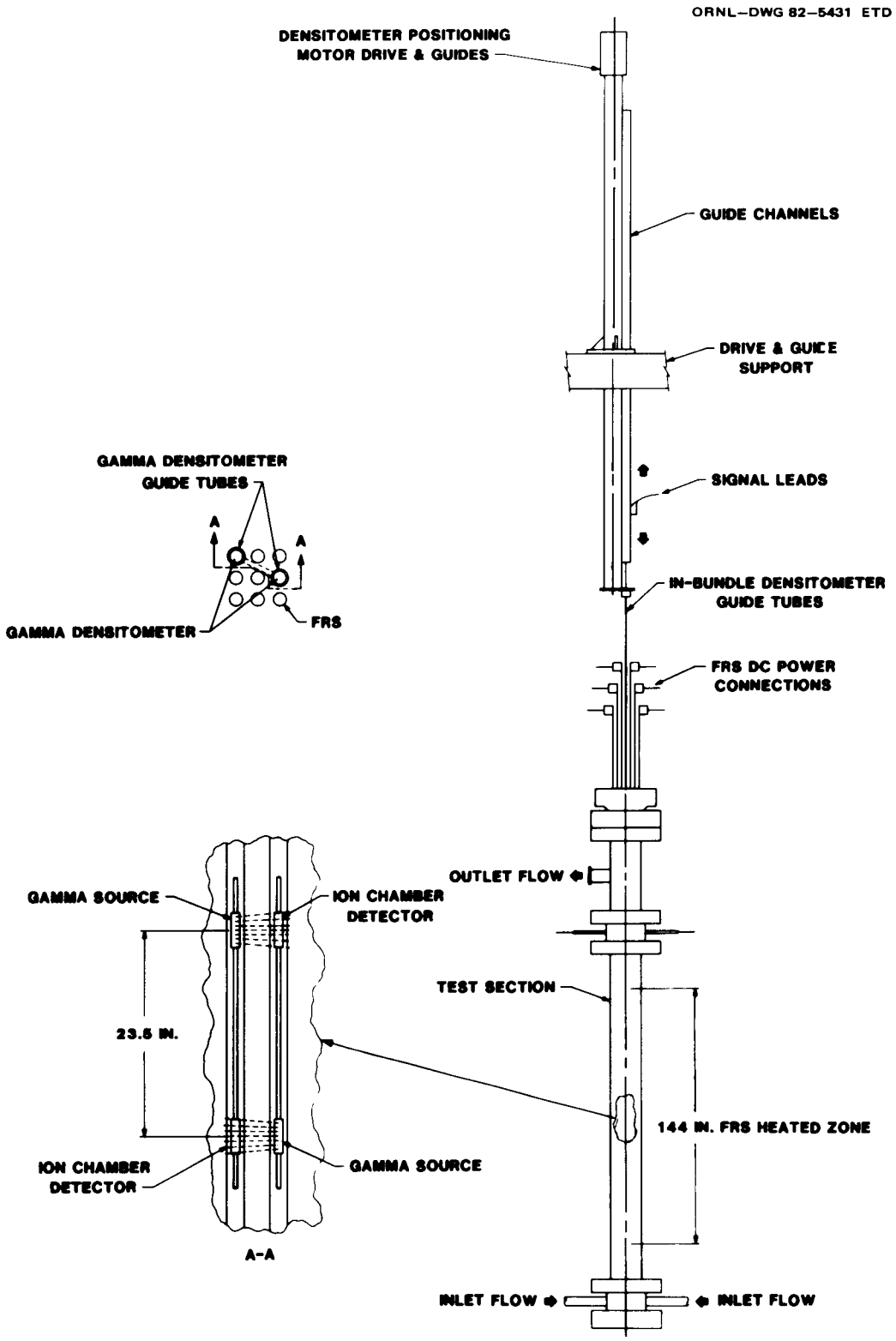

Fig. 5.30. Schematic diagram of the in-bundle gamma densitometer system.

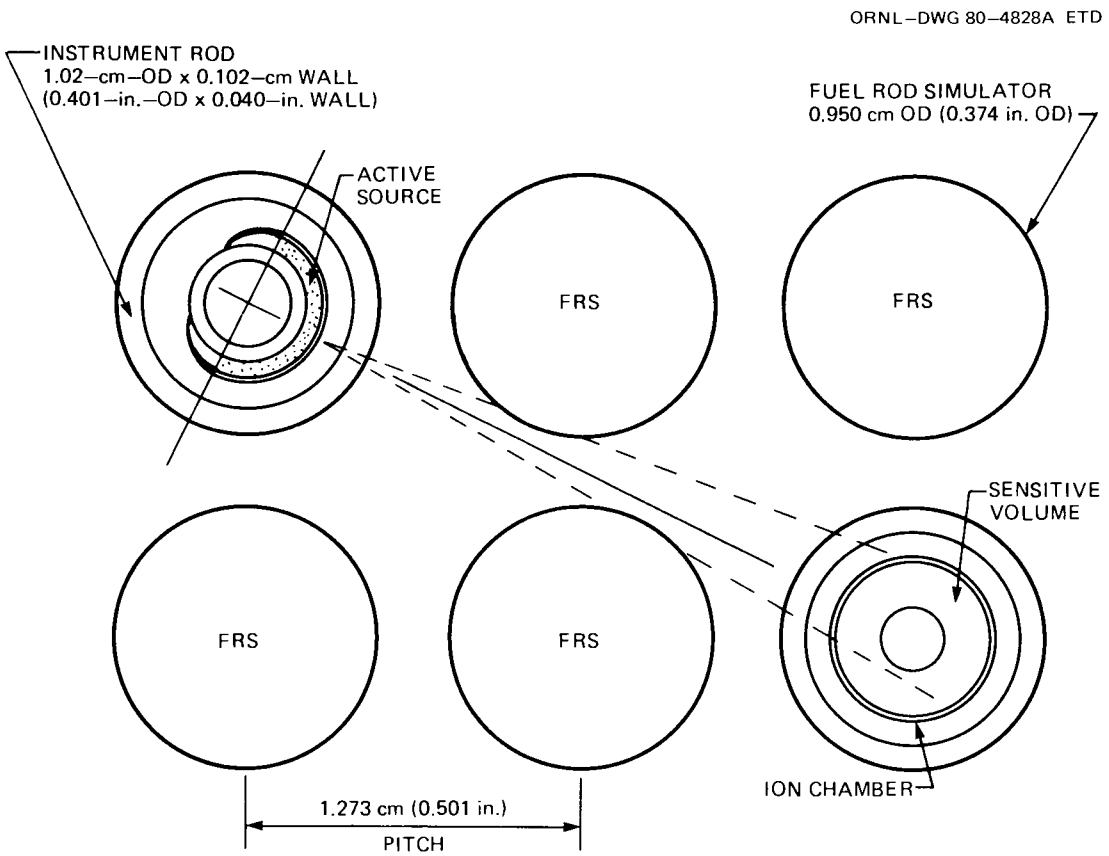

Fig. 5.31. Detail of the in-bundle gamma densitometer source-detector radial geometry.

Table 5.14. Initial conditions for Test 3.06.6B

Total bundle power, MW	2.26
Average rod power, kW	37.7
Flow	
Volumetric, m^3/s (gpm)	0.0079 (125)
Mass, kg/s (lb_m/s)	6.04 (13.3)
Inlet temperature, K (°F)	547 (526)
Outlet temperature, K (°F)	610.2 (638.7)
Outlet pressure, MN/m^2 (psia)	14.98 (2173)

Table 5.15. THTF upflow film boiling data ranges — Test 3.06.6B

	NRC requested	Obtained in Test 3.06.6B
Mass flux, kg/s·m² (lb_m/h·ft²)	270–4070 (2×10^5–3×10^6)	135–340 (1×10^5–2.5×10^5)
Quality, %	0–100	15–100
Pressure, MN/m² (psi)	4.14–18.61 (600–2700)	6.03–12.4 (875–1800)
Heat flux, W/m² (Btu/h·ft²)	3×10^4–3×10^6 (10^4–10^6)	15.7×10^4–4.7×10^5 (5×10^4–1.5×10^5)

5.3.2 Steady-State Upflow Film Boiling Test 3.07.9

A series of tests was run in the THTF providing steady-state rod bundle film boiling data over a range of flow conditions.[32–34] The test series data ranges are presented in Table 5.17. The system configuration was similar to the previous Upflow Film Boiling Tests, 3.03.6AR and 3.06.6B, except that the pressurizer connection with the loop was moved from the hot leg between the outlet spool pieces and the heat exchangers to the cold leg on the pump bypass line. An isometric drawing of the system is shown in Fig. 5.35. The pressurizer connection was moved primarily because of operating considerations. Once film boiling conditions are reached in the bundle, the line between the test section outlet and the heat exchangers is essentially high quality or superheated steam. Operation of the facility would be considerably more difficult with the pressurizer tied into that line.

The steady-state tests were operated in a manner similar to the small-break LOCA test series (Sect. 5.1.1). The inlet mass flow was set initially, and then the bundle power was increased while simultaneously reducing the mass inventory of the system. The level to which film boiling could be brought down to in the bundle was determined primarily by high-temperature limits on the FRS rods. The inlet flow was subcooled during these tests and provided good experimental boundary conditions for the bundle. The normal steam/water pressurizer was used for these tests. Although test operation would have been simplified in terms of obtaining desired conditions (i.e., pressure) more easily, the use of nitrogen overpressure (as was used in the small-break LOCA tests) was not possible for these tests due to the much larger outlet piping volume. A considerable mass of water was let down from the system as film boiling conditions in the bundle were obtained and the high-quality superheated steam displaced the subcooled liquid between the test section outlet and the heat exchangers (condensers). If nitrogen overpressure were used with the system containing a fairly low mass inventory, a loss of power with film boiling

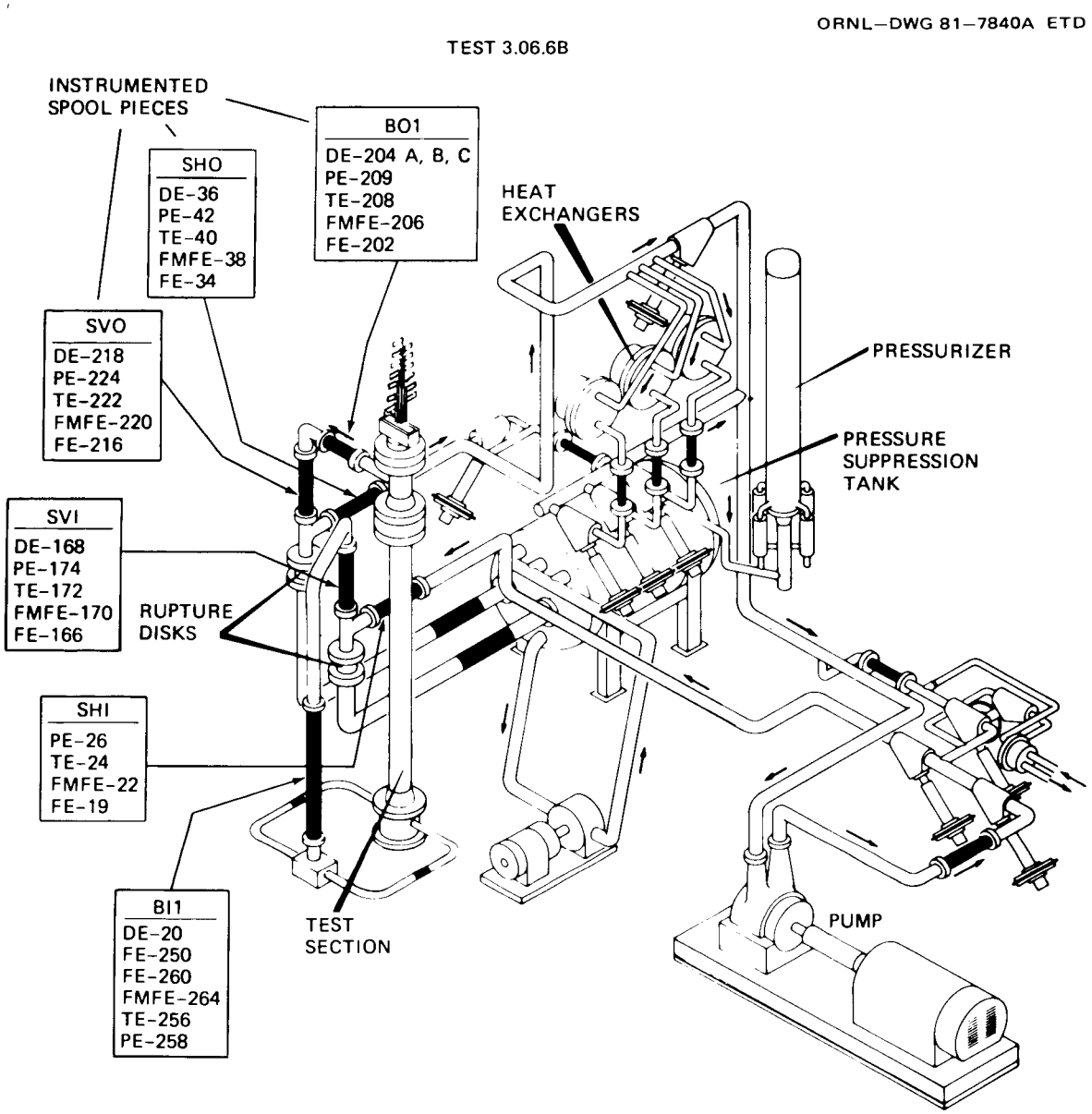

Fig. 5.32. THTF configuration for Test 3.06.6B.

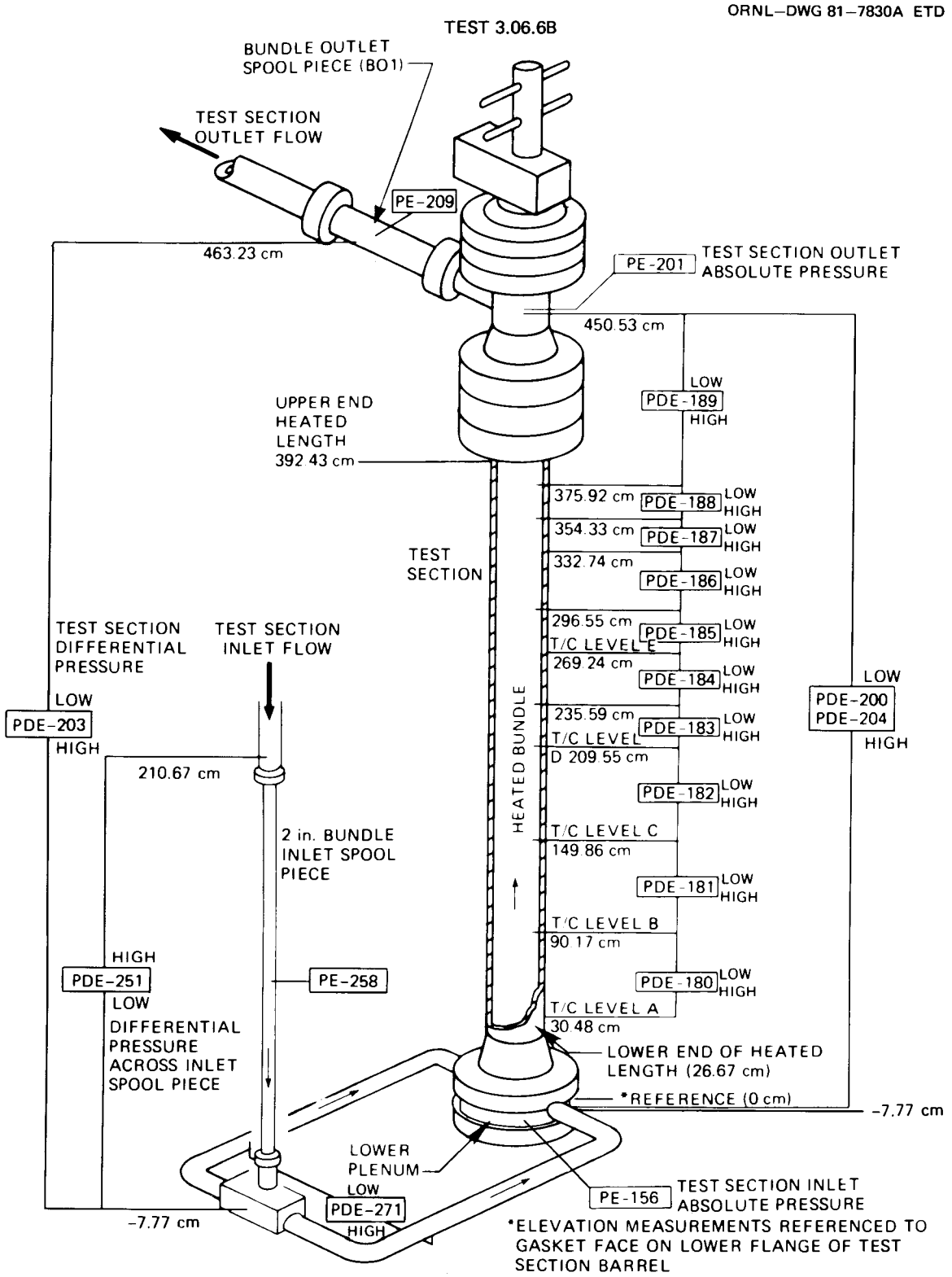

Fig. 5.33. Test section pressure and differential pressure instrumentation for Test 3.06.6B.

Table 5.16. Primary flow instrumentation for Test 3.06.6B

Instrument application No.	Description	Instrument	Range
DE-204A	Bundle outlet spool density	Three-beam gamma densitometer	0–1000 kg/m³ (0–62.4 lb_m/ft^3)
DE-204B			
DE-204C			
PE-209	Bundle outlet spool transient pressure	Precise Sensor absolute pressure transducer	0–2.07 x 10⁴ kPa (0–3000 psig)
TE-208	Bundle outlet spool temperature	Nanmac fluid thermocouple	273–1309 K (32–1900°F)
FMFE-206	Bundle outlet spool drag disk (momentum flux)	Ramapo drag disk, ORNL 3.5-in., 3-bladed full-flow target	±0–5.85 x 10⁴ kg/m·s² (±0–3.93 x 10⁴ $lb_m/ft\cdot s^2$)
FE-202	Bundle outlet spool volumetric flow	3.5-in. Flow Technology turbine meter	±0.005–0.227 m³/s (±80–3600 gpm) range 4
DE-36	Horizontal outlet spool density	Single-beam gamma densitometer	0–1000 kg/m³ (0–62.4 lb_m/ft^3)
PE-42	Horizontal outlet spool transient	Precise Sensor absolute pressure transducer	0–2.07 x 10⁴ kPa (0–3000 psig)
TE-40	Horizontal outlet spool temperature	Nanmac fluid thermocouple	273–1309 K (32–1900°F)
FMFE-38	Horizontal outlet spool drag disk (momentum flux)	Ramapo drag disk, ORNL 3.5-in., 3-bladed full-flow target	±0–2.09 x 10⁴ kg/m·s² (±0–1.41 x 10⁴ $lb_m/ft\cdot s^2$)
FE-34	Horizontal outlet spool volumetric flow	3.5-in. Flow Technology turbine meter	±0.005–0.113 m³/s (±80–1800 gpm) range 3
DE-218	Vertical outlet spool density	Single-beam gamma densitometer	0–1000 kg/m³ (0–62.4 lb_m/ft^3)
PE-224	Vertical outlet spool transient pressure	Precise Sensor absolute pressure transducer	0–2.07 x 10⁴ kPa (0–3000 psig)
TE-222	Vertical outlet spool temperature	Nanmac fluid thermocouple	273–1309 K (32–1900°F)
FMFE-220	Vertical outlet spool drag disk (momentum flux)	Ramapo drag disk, ORNL 3.5-in., 3-bladed full-flow target	±0–4.79 x 10⁴ kg/m·s² (±0–3.22 x 10⁴ $lb_m/ft\cdot s^2$)
FE-216	Vertical outlet spool volumetric flow	3.5-in. Flow Technology turbine meter	±0.005–0.227 m³/s (±80–3600 gpm) range 4

Table 5.16 (continued)

Instrument application No.	Description	Instrument	Range
DE-168	Vertical inlet spool density	Single-beam gamma densitometer	0–1000 kg/m³ (0–62.4 lb_m/ft^3)
PE-174	Vertical inlet spool transient pressure	Precise Sensor absolute pressure transducer	0–2.07 x 10⁴ kPa (0–3000 psig)
TE-172	Vertical inlet spool temperature	Nanmac fluid thermocouple	273–1309 K (32–1900°F)
FMFE-170	Vertical inlet spool drag disk (momentum flux)	Ramapo drag disk, ORNL 3.5-in., 3-bladed full-flow target	±0–5.32 x 10⁴ kg/m·s² (±0–3.57 x 10⁴ $lb_m/ft\cdot s^2$)
FE-166	Vertical inlet spool volumetric flow	3.5-in. Flow Technology turbine meter	±0.005–0.0284 m³/s (±80–450 gpm) range 1
PE-26	Horizontal inlet spool transient pressure	Precise Sensor absolute pressure transducer	0–2.07 x 10⁴ kPa (0–3000 psig)
TE-24	Horizontal inlet spool temperature	Nanmac fluid thermocouple	273–1309 K (32–1900°F)
FMFE-22	Horizontal inlet spool drag disk (momentum flux)	Ramapo drag disk, ORNL 3.5-in., 3-bladed full-flow target	±0–4.34 x 10⁴ kg/m·s² (±0–2.92 x 10⁴ $lb_m/ft\cdot s^2$)
FE-19	Horizontal inlet spool volumetric flow	3.5-in. Flow Technology turbine meter	±0.005–0.0284 m³/s (±80–450 gpm) range 1
DE-20	Bundle inlet spool density	Single-beam gamma densitometer	0–1000 kg/m³ (0–62.4 lb_m/ft^3)
FE-250	Bundle inlet spool upper volumetric flow	2-in. Flow Technology turbine meter	±6.3 x 10⁻⁴–0.0284 m³/s (±10–450 gpm) range 4
FE-260	Bundle inlet spool lower volumetric flow	2-in. Flow Technology turbine meter	±6.3 x 10⁻⁴–0.0284 m³/s (±10–450 gpm) range 4
FMFE-264	Bundle inlet spool drag disk (momentum flux)	Ramapo drag disk, ORNL 2-in., 3-bladed full-flow target	±0–2.06 x 10⁵ kg/m·s² (±0–1.38 x 10⁵ $lb_m/ft\cdot s^2$)
TE-256	Bundle inlet spool temperature	Nanmac fluid thermocouple	273–1309 K (32–1900°F)
PE-258	Bundle inlet spool pressure	Precise Sensor absolute pressure transducer	0–6.07 x 10⁴ kPa (0–3000 psig)
PE-156	Test section inlet transient pressure	Precise Sensor absolute pressure transducer	0–2.07 x 10⁴ kPa (0–3000 psig)
PE-201	Test section outlet transient pressure	Precise Sensor absolute pressure transducer	0–2.07 x 10⁴ kPa (0–3000 psig)

Table 5.16 (continued)

Instrument application No.	Description	Instrument	Range
PDE-200	Bundle transient differential pressure	50-psi BLH differential pressure transducer	±0–345 kPa (±0–50 psid)
PDE-204	Bundle transient differential pressure	6-psi Genisco differential pressure transducer	±0–41.4 kPa (±0–6 psid)
PDE-203	Test section transient differential pressure	50-psi BLH differential pressure transducer	±0–345 kPa (±0–50 psid)
PDE-251	Bundle inlet spool differential pressure	50-psi BLH differential pressure transducer	±0–345 kPa (±0–50 psid)
PDE-271	Split downcomer transient differential pressure	6-psi Genisco differential pressure transducer	±0–41.4 kPa (±0–6 psid)
PDE-180 to 189	Shroud-box differential pressure	Rosemount differential pressure transmitters	0–6.22 kPa (0–25 in. of Std. H_2O)

ORNL–DWG 82–5432 ETD (PART A)

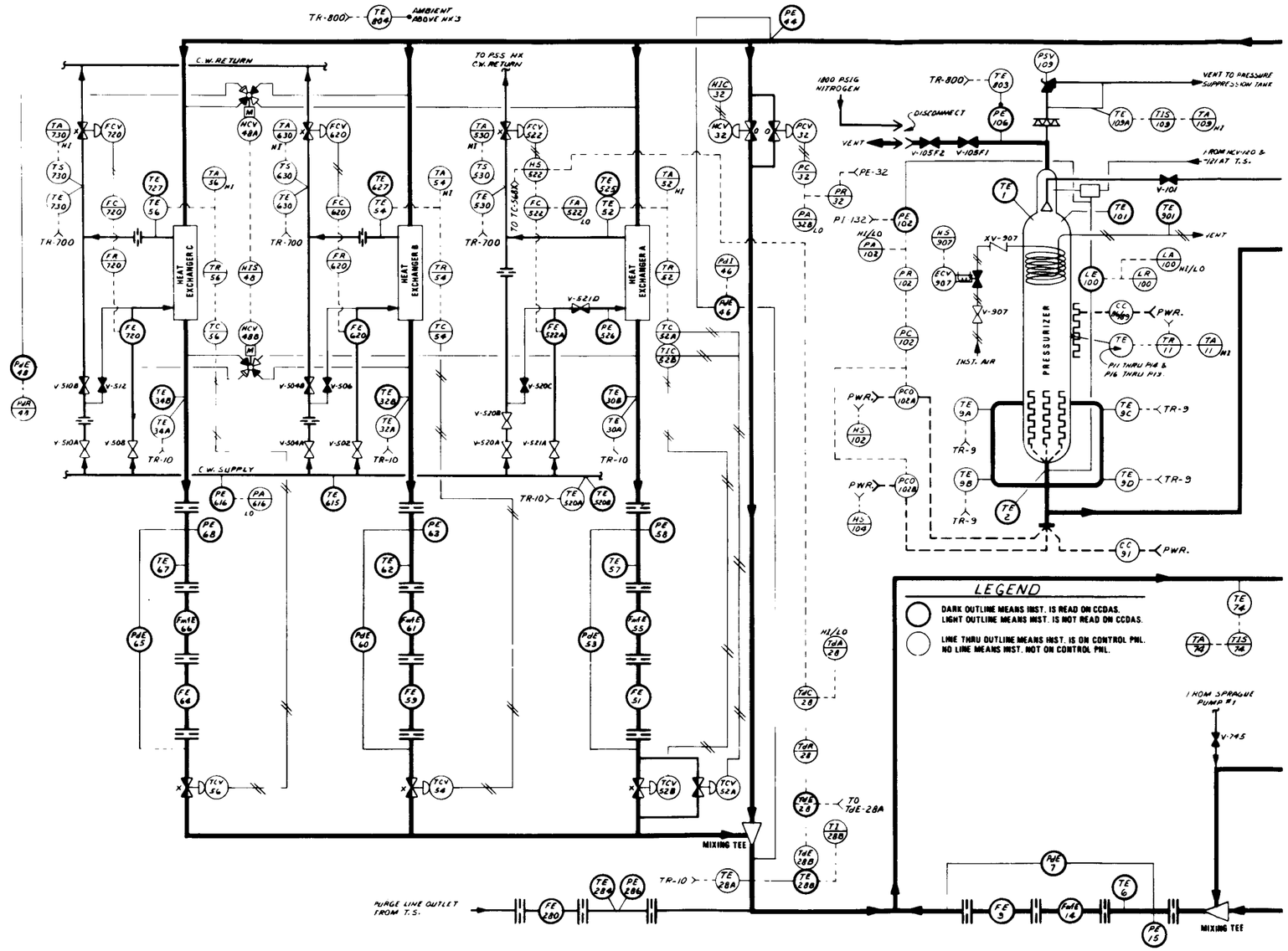

Fig. 5.34. Instrument application drawings for Test 3.06.6B.

ORNL–DWG 82–5432 ETD (PART B)

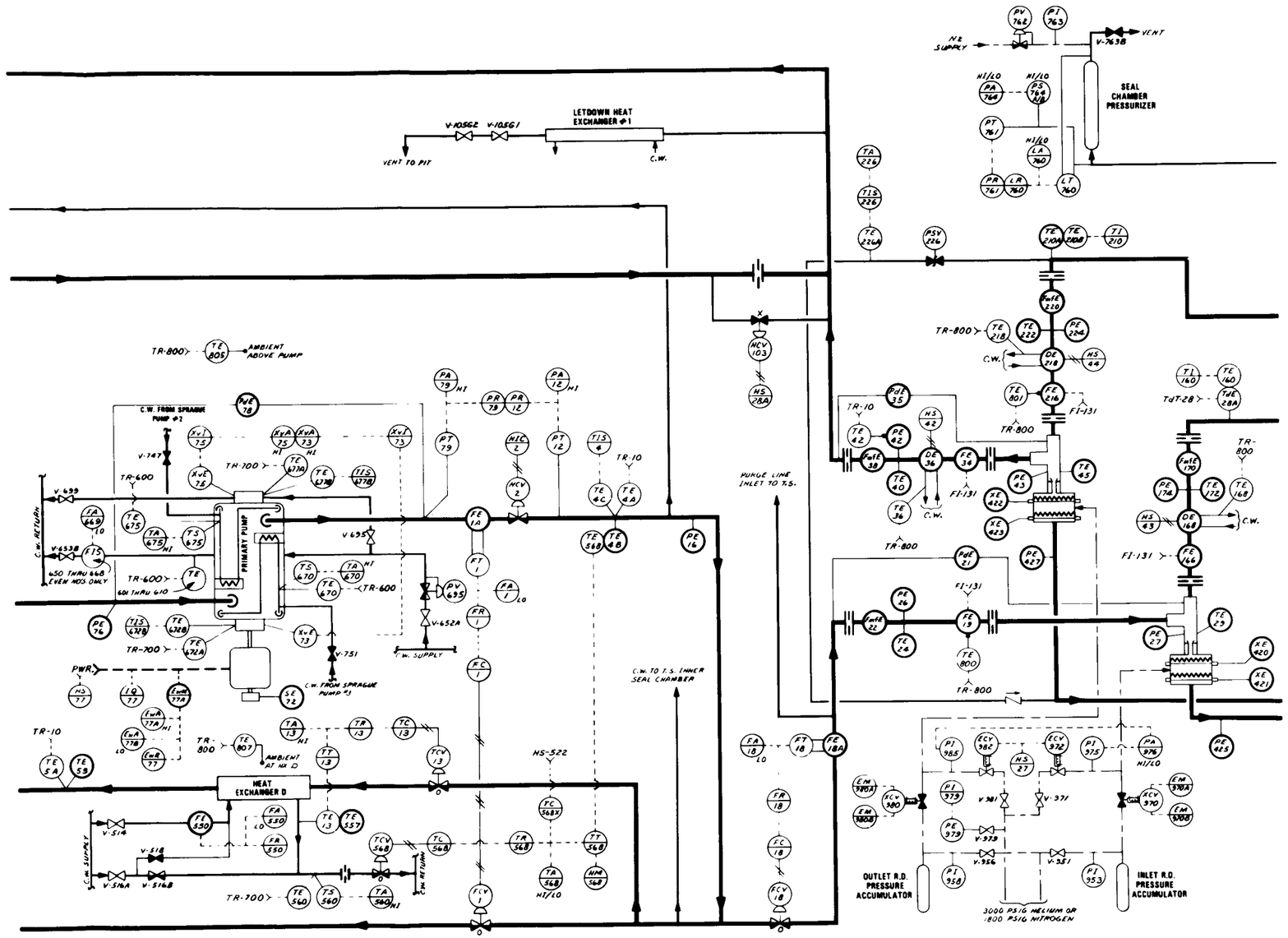

Fig. 5.34 (continued)

ORNL–DWG 82–5432 ETD (PART C)

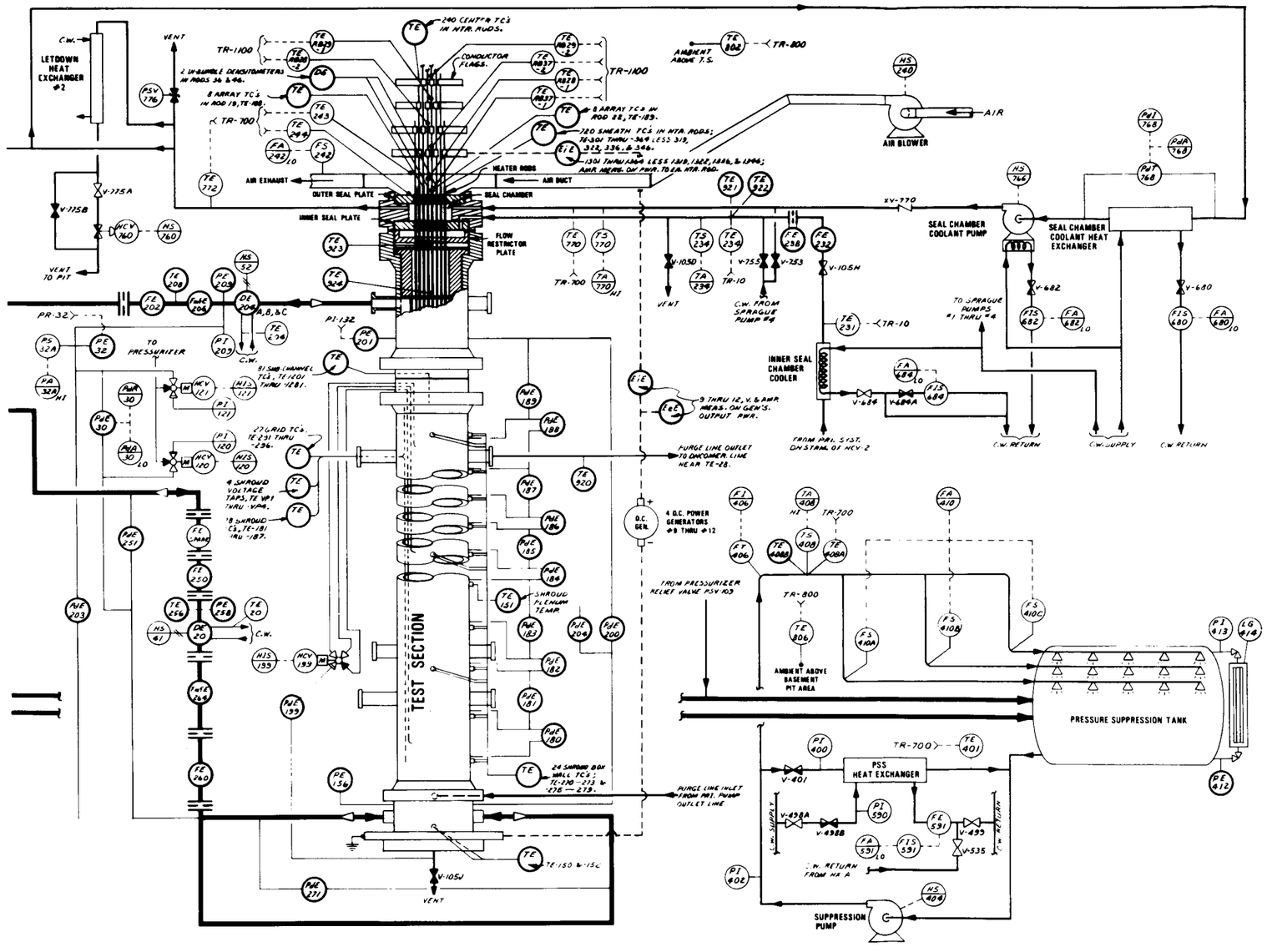

Fig. 5.34 (continued)

Table 5.17. THTF steady-state upflow film boiling data ranges, test series 3.07.9a (a = test letter)[a]

Date	Test (a)	Mass flux [kg/s·m² (lb_m/h·ft²)]	Heat flux [W/m² (Btu/h·ft²)]	Core exit quality	Pressure [MN/m² (psia)]
September 11	K	225 (1.7 x 10^5)	4.41 x 10^5 (1.4 x 10^5)	1.1	4.38 (635)
	H	257 (1.9 x 10^5)	4.10 x 10^5 (1.3 x 10^5)	1.08	8.89 (1290)
	I	362 (2.7 x 10^5)	5.68 x 10^5 (1.8 x 10^5)	1.09	9.19 (1332)
	L	529 (3.9 x 10^5)	7.88 x 10^5 (2.5 x 10^5)	1.005	8.30 (1203)
	M	657 (4.8 x 10^5)	8.82 x 10^5 (2.8 x 10^5)	0.94	8.57 (1242)
	N	800 (5.9 x 10^5)	9.45 x 10^5 (3.0 x 10^5)	0.82	8.52 (1234)
	O	307 (2.3 x 10^5)	5.36 x 10^5 (1.7 x 10^5)	1.09	5.98 (867)
	X	339 (2.5 x 10^5)	5.99 x 10^5 (1.9 x 10^5)	1.13	6.01 (872)
	P	520 (3.8 x 10^5)	8.19 x 10^5 (2.6 x 10^5)	1.02	6.03 (874)
September 18	Q	326 (2.4 x 10^5)	5.68 x 10^5 (1.8 x 10^5)	1.12	6.53 (947)
	R	366 (2.7 x 10^5)	6.46 x 10^5 (2.0 x 10^5)	1.13	6.57 (952)
October 1	T	240 (1.8 x 10^5)	3.15 x 10^5 (1.0 x 10^5)	1.03	11.89 (1723)
	U	242 (1.8 x 10^5)	3.15 x 10^5 (1.0 x 10^5)	1.01	11.69 (1694)
	V	250 (1.8 x 10^5)	3.15 x 10^5 (1.0 x 10^5)	0.99	12.04 (1745)
	G	248 (1.8 x 10^5)	3.15 x 10^5 (1.0 x 10^5)	1.0	12.54 (1818)
	W	257 (1.9 x 10^5)	3.78 x 10^5 (1.2 x 10^5)	1.17	12.55 (1820)
	F	255 (1.9 x 10^5)	3.78 x 10^5 (1.2 x 10^5)	1.18	12.62 (1830)
	C	334 (2.5 x 10^5)	5.67 x 10^5 (1.8 x 10^5)	1.32	12.46 (1805)
	D	517 (3.8 x 10^5)	6.93 x 10^5 (2.2 x 10^5)	1.05	12.75 (1847)
	E	593 (4.4 x 10^5)	6.93 x 10^5 (2.2 x 10^5)	0.95	13.2 (1908)
	J	733 (5.4 x 10^5)	7.56 x 10^5 (2.4 x 10^5)	0.82	13.37 (1937)
	B	705 (5.2 x 10^5)	9.14 x 10^5 (2.9 x 10^5)	1.04	12.76 (1849)

[a]Data ranges requested by NRC:

Mass flux 270–4070 kg/s·m² (2 x 10^5–3 x 10^6 lb_m/h·ft²),
Heat flux 3 x 10^4–3 x 10^6 W/m² (10^4–10^6 Btu/h·ft²), and
Pressure 4.14–18.61 MN/m² (600–2700 psia).

ORNL–DWG 81–7836A ETD

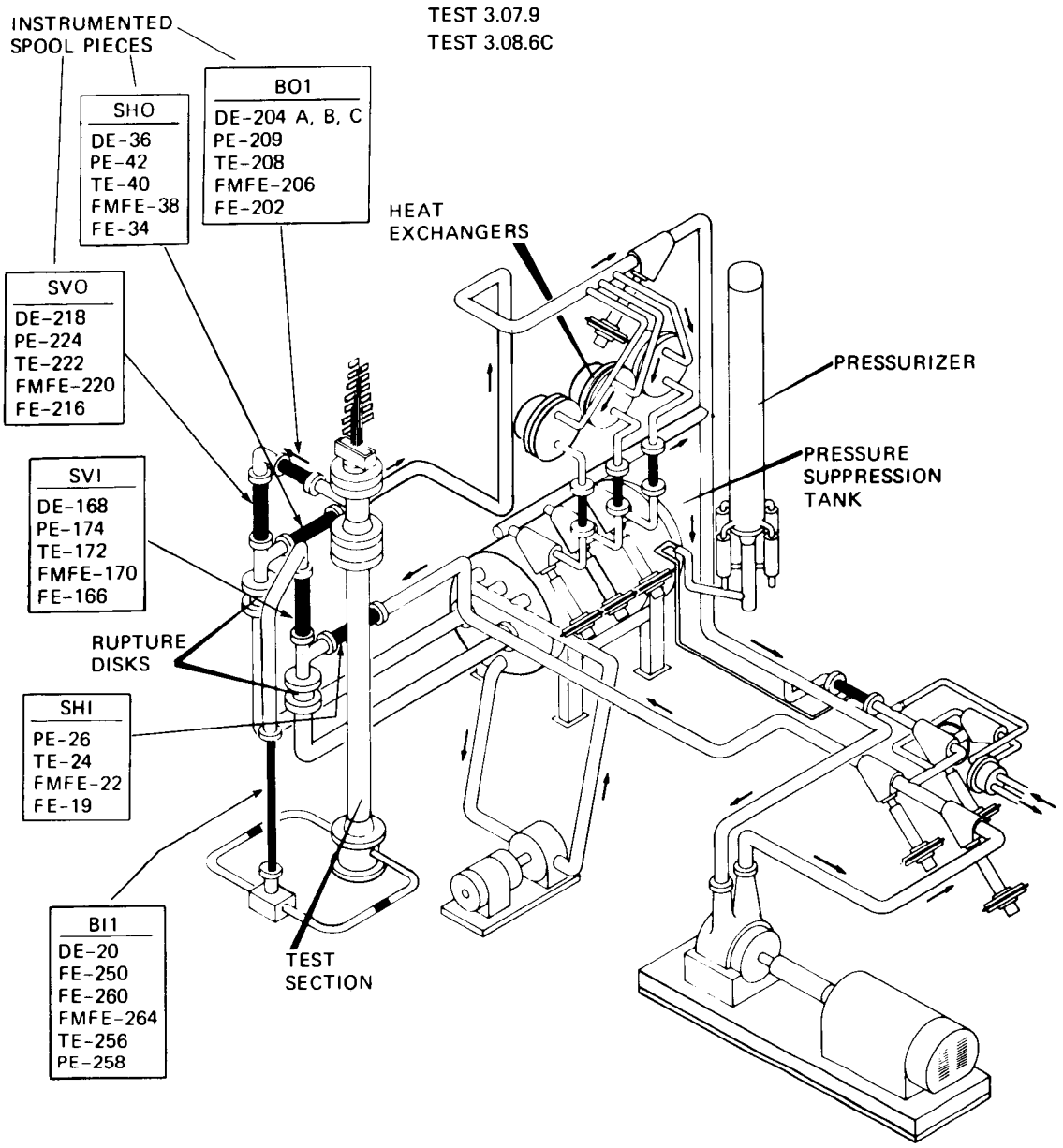

Fig. 5.35. THTF configuration for test series 3.07.9 and Test 3.08.6C.

conditions existing in the bundle (which did occur on several occasions) would have collapsed the steam volume and allowed nitrogen from the pressurizer to enter the system (as the mass inventory of the pressurizer drained into the loop).

The pressure and differential pressure instrumentation arrangement is shown in Fig. 5.36. Emphasis was placed on measurements across the upper

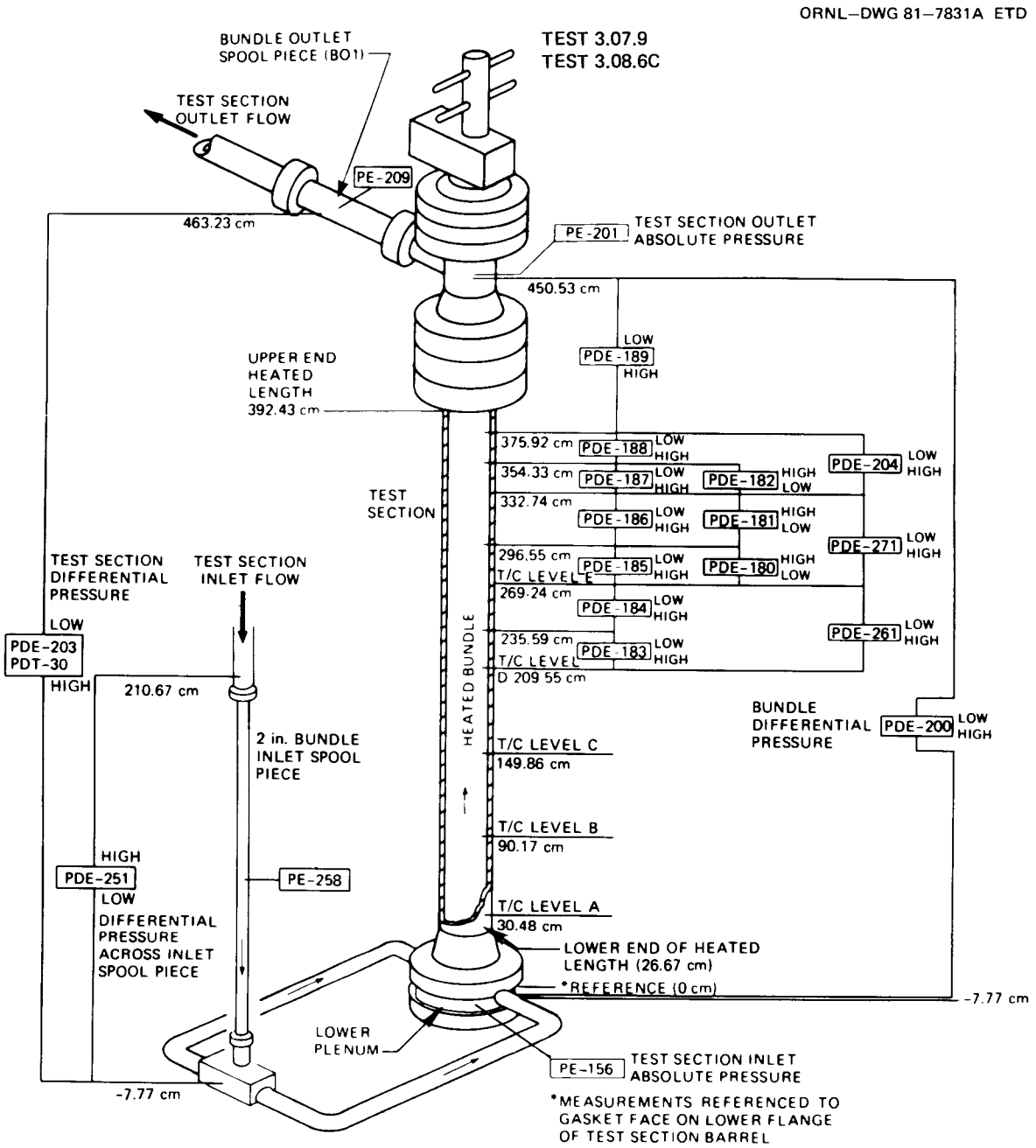

Fig. 5.36. Test section pressure and differential pressure instrumentation for test series 3.07.9 and Test 3.08.6C.

bundle. The available differential pressure cells were arranged across similar taps in certain cases to cover a range of conditions from static-pressure-dominated measurements to friction and form-loss-dominated measurements. A list of the instrument type and ranges for the instruments shown in Figs. 5.35 and 5.36 is presented in Table 5.18. An instrument application drawing is presented in Figs. 5.37(a–c).

Table 5.18. Primary flow instrumentation for test series 3.07.9 and 3.08.6C

Instrument application No.	Description	Instrument	Range
DE-204A	Bundle outlet spool density	Three-beam gamma densitometer	0–1000 kg/m³ (0–62.4 lb_m/ft^3)
DE-204B			
DE-204C			
PE-209	Bundle outlet spool transient pressure	Precise Sensor absolute pressure transducer	0–2.07 x 10⁴ kPa (0–3000 psig)
TE-208	Bundle outlet spool temperature	Nanmac fluid thermocouple	273–1309 K (32–1900°F)
FMFE-206	Bundle outlet spool drag disk (momentum flux)	Ramapo drag disk, ORNL 3.5-in., 3-bladed full-flow target	±0–4.96 x 10⁴ kg/m·s² (±0–3.34 x 10⁴ $lb_m/ft\cdot s^2$)
FE-202	Bundle outlet spool volumetric flow	3.5-in. Flow Technology turbine meter	±0.005–0.227 m³/s (±80–3600 gpm) range 4
DE-36	Horizontal outlet spool density	Single-beam gamma densitometer	0–1000 kg/m³ (0–62.4 lb_m/ft^3)
PE-42	Horizontal outlet spool transient	Precise Sensor absolute pressure transducer	0–2.07 x 10⁴ kPa (0–3000 psig)
TE-40	Horizontal outlet spool temperature	Nanmac fluid thermocouple	273–1309 K (32–1900°F)
FMFE-38	Horizontal outlet spool drag disk (momentum flux)	Ramapo drag disk, ORNL 3.5-in., 3-bladed full-flow target	±0–1.75 x 10⁴ kg/m·s² (±0–1.18 x 10⁴ $lb_m/ft\cdot s^2$)
FE-34	Horizontal outlet spool volumetric flow	3.5-in. Flow Technology turbine meter	±0.005–0.113 m³/s (±80–1800 gpm) range 3
DE-218	Vertical outlet spool density	Single-beam gamma densitometer	0–1000 kg/m³ (0–62.4 lb_m/ft^3)
PE-224	Vertical outlet spool transient pressure	Precise Sensor absolute pressure transducer	0–2.07 x 10⁴ kPa (0–3000 psig)
TE-222	Vertical outlet spool temperature	Nanmac fluid thermocouple	273–1309 K (32–1900°F)
FMFE-220	Vertical outlet spool drag disk (momentum flux)	Ramapo drag disk, ORNL 3.5-in., 3-bladed full-flow target	±0–4.31 x 10⁴ kg/m·s² (±0–2.89 x 10⁴ $lb_m/ft\cdot s^2$)
FE-216	Vertical outlet spool volumetric flow	3.5-in. Flow Technology turbine meter	±0.005–0.227 m³/s (±80–3600 gpm) range 4

Table 5.18 (continued)

Instrument application No.	Description	Instrument	Range
DE-168	Vertical inlet spool density	Single-beam gamma densitometer	0–1000 kg/m³ (0–62.4 lb_m/ft^3)
PE-174	Vertical inlet spool transient pressure	Precise Sensor absolute pressure transducer	0–2.07 x 10⁴ kPa (0–3000 psig)
TE-172	Vertical inlet spool temperature	Nanmac fluid thermocouple	273–1309 K (32–1900°F)
FMFE-170	Vertical inlet spool drag disk (momentum flux)	Ramapo drag disk, ORNL 3.5-in., 3-bladed full-flow target	±0–5.57 x 10⁴ kg/m·s² (±0–3.75 x 10⁴ $lb_m/ft\cdot s^2$)
FE-166	Vertical inlet spool volumetric flow	3.5-in. Flow Technology turbine meter	±0.005–0.0284 m³/s (±80–450 gpm) range 1
PE-26	Horizontal inlet spool transient pressure	Precise Sensor absolute pressure transducer	0–2.07 x 10⁴ kPa (0–3000 psig)
TE-24	Horizontal inlet spool temperature	Nanmac fluid thermocouple	273–1309 K (32–1900°F)
FMFE-22	Horizontal inlet spool drag disk (momentum flux)	Ramapo drag disk, ORNL 3.5-in., 3-bladed full-flow target	±0–4.34 x 10⁴ kg/m·s² (±0–2.92 x 10⁴ $lb_m/ft\cdot s^2$)
FE-19	Horizontal inlet spool volumetric flow	3.5-in. Flow Technology turbine meter	±0.005–0.0284 m³/s (±80–450 gpm) range 1
DE-20	Bundle inlet spool density	Single-beam gamma densitometer	0–1000 kg/m³ (0–62.4 lb_m/ft^3)
FE-250	Bundle inlet spool upper volumetric flow	2-in. Flow Technology turbine meter	±6.3 x 10⁻⁴–0.0284 m³/s (±10–450 gpm) range 4
FE-260	Bundle inlet spool lower volumetric flow	2-in. Flow Technology turbine meter	±6.3 x 10⁻⁴–0.0284 m³/s (±10–450 gpm) range 4
FMFE-264	Bundle inlet spool drag disk (momentum flux)	Ramapo drag disk, ORNL 2-in., 3-bladed full-flow target	±0–2.01 x 10⁵ kg/m·s² (±0–1.35 x 105 $lb_m/ft\cdot s^2$)
TE-256	Bundle inlet spool temperature	Nanmac fluid thermocouple	273–1309 K (32–1900°F)
PE-258	Bundle inlet spool pressure	Precise Sensor absolute pressure transducer	0–2.07 x 10⁴ kPa (0–3000 psig)

Table 5.18 (continued)

Instrument application No.	Description	Instrument	Range
PE-156	Test section inlet transient pressure	Precise Sensor absolute pressure transducer	0–2.07 x 10^4 kPa (0–3000 psig)
PE-201	Test section outlet transient pressure	Precise Sensor absolute pressure transducer	0–2.07 x 10^4 kPa (0–3000 psig)
PDE-200	Bundle transient differential pressure	50-psi BLH differential pressure transducer	±0–345 kPa (±0–50 psid)
PDE-204	Shroud-box differential pressure	6-psi Genisco differential pressure transducer	±0–41.4 kPa (±0–6 psid)
PDE-271	Shroud-box differential pressure	6-psi Genisco differential pressure transducer	±0–41.4 kPa (±0–6 psid)
PDE-261	Shroud-box differential pressure	6-psi Genisco differential pressure transducer	±0–41.4 kPa (±0–6 psid)
PDE-251	Bundle inlet spool differential pressure	50-psi BLH differential pressure transducer	±0–345 kPa (±0–50 psid)
PDE-203	Test section transient differential pressure	50-psi BLH differential pressure transducer	±0–345 kPa (±0–50 psid)
PDE-180 to 189	Shroud-box differential pressures	Rosemount differential pressure transmitters	0–6.22 kPa (0–25 in. of Std. H_2O)

ORNL–DWG 82–5433 ETD (PART A)

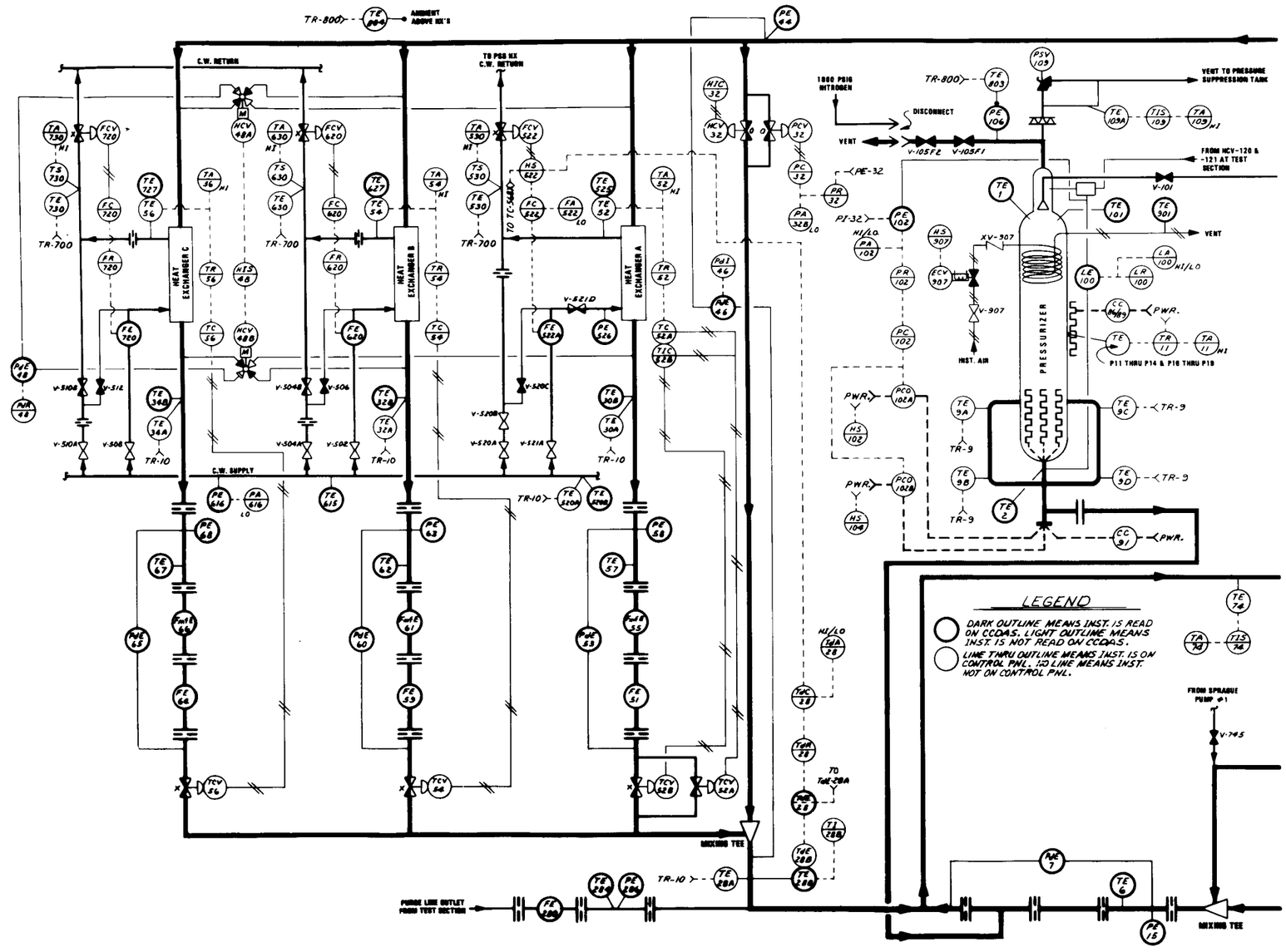

Fig. 5.37. Instrument application drawings for test series 3.07.9 and Test 3.08.6C.

ORNL–DWG 82–5433 ETD (PART B)

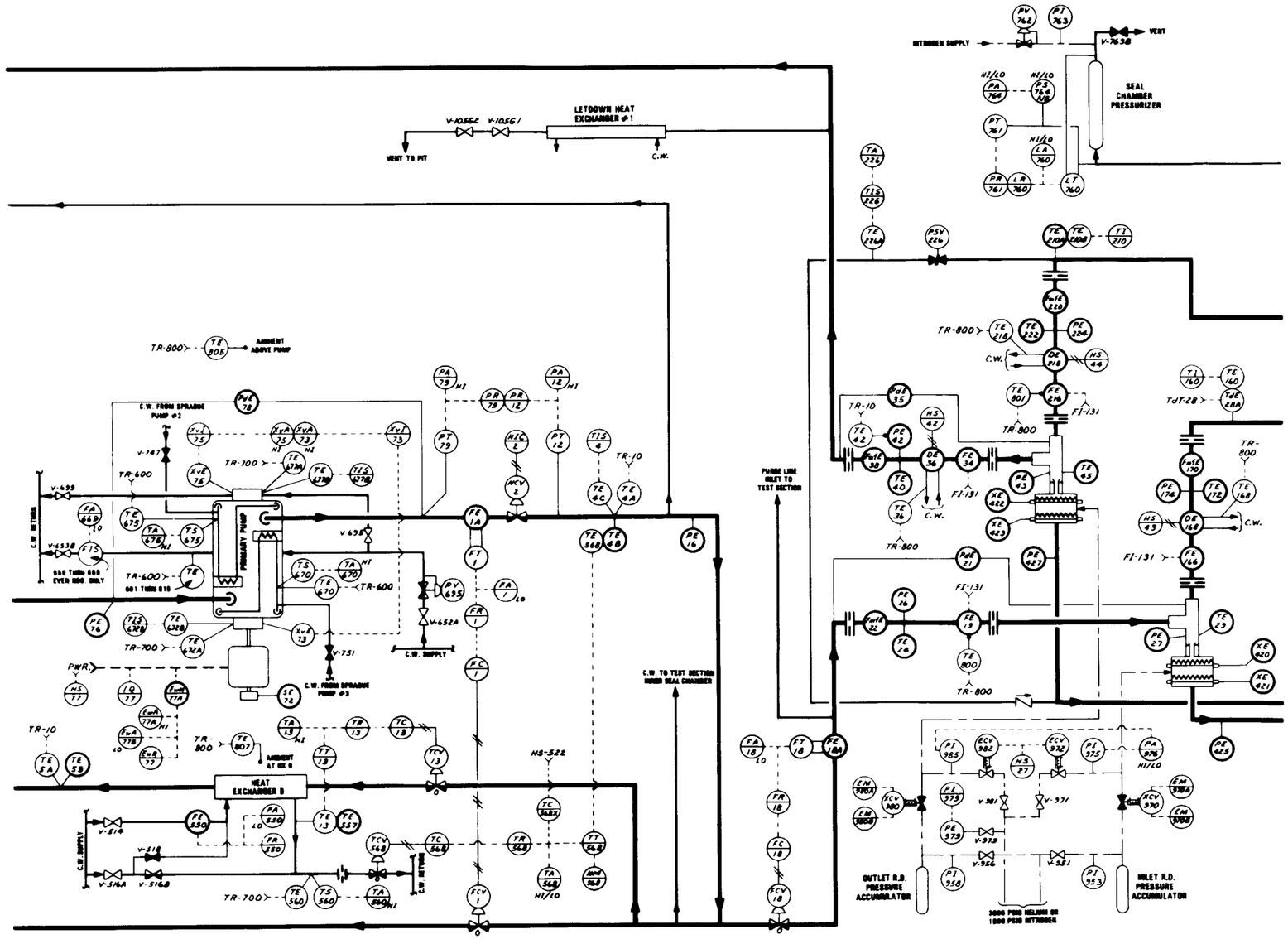

Fig. 5.37 (continued)

ORNL–DWG 82–5433 ETD (PART C)

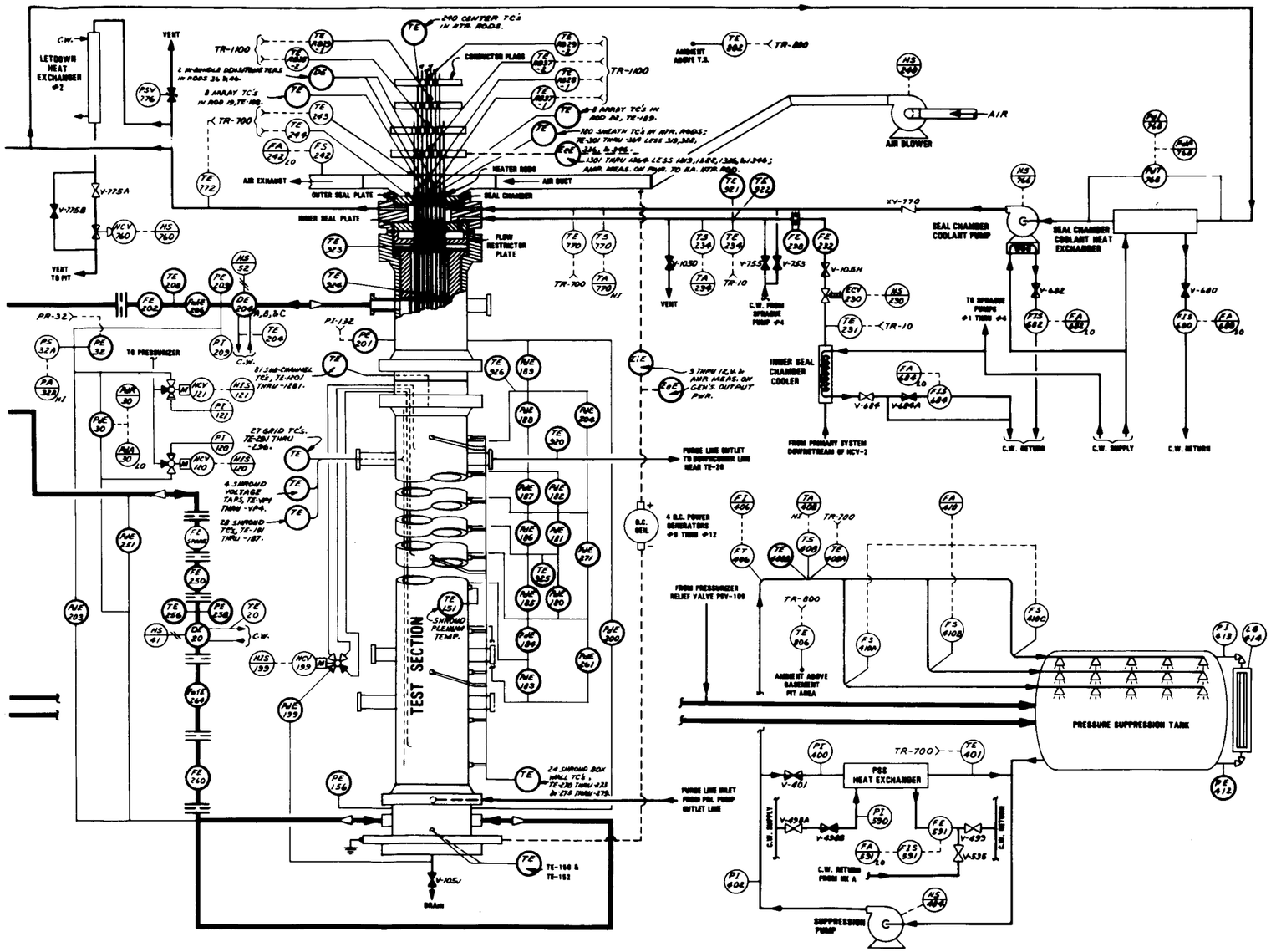

Fig. 5.37 (continued)

5.3.3 Upflow Film Boiling Test 3.08.6C

The final transient Upflow Film Boiling Test, 3.08.6C (Refs. 24, 25, 35, and 36) was run at the end of the steady-state upflow film boiling test series (3.07.9). For this reason, all of the system and instrumentation descriptions for Test 3.07.9 are applicable (Sect. 5.3.2). The test objectives were the same as in previous transient Upflow Film Boiling Tests 3.03.6AR and 3.06.6B. The initial conditions for the test prior to blowdown are presented in Table 5.19. The film boiling data ranges requested by NRC and obtained in Test 3.08.6C are given in Table 5.20.

Table 5.19. Initial conditions for Test 3.08.6C

Total bundle power, MW	2.4
Average rod power, kW	40.6
Flow	
Volumetric, m^3/s (gpm)	0.0082 (130)
Mass, kg/s (lb_m/s)	6.39 (14.1)
Inlet temperature, K (°F)	538 (519)
Outlet temperature, K (°F)	598 (618)
Outlet pressure, MN/m^2 (psia)	12.9 (1870)

Table 5.20. THTF upflow film boiling data ranges — Test 3.08.6C

	NRC requested	Obtained in Test 3.08.6C
Mass flux, $kg/s \cdot m^2$ ($lb_m/h \cdot ft^2$)	270–4070 (2×10^5–3×10^6)	200–1085 (1.5×10^5–8×10^5)
Quality, %	0–100	35–100
Pressure, MN/m^2 (psi)	4.14–18.61 (600–2700)	6.55–11.72 (950–1700)
Heat flux, W/m^2 ($Btu/h \cdot ft^2$)	3×10^4–3×10^6 (10^4–10^6)	4.73×10^5–1.1×10^6 (1.5×10^5–3.5×10^5)

5.3.4 Small-break LOCA-II test series 3.09.10I-X

The second series of small-break LOCA tests[37-39] was run both to repeat the testing carried out during the first test series with the improved instrumentation in the bundle and also to expand the types of tests and the test parameter ranges. Steady-state uncovered bundle tests and transient reflood tests were run in a manner similar to those of the small-break LOCA-I test series. In addition, transient boiloff tests were run. These tests involved setting the desired initial power and bundle conditions and then shutting off the inlet flow to the test section completely. Tests of this type with both controlled depressurization rates and constant pressure were run. A summary of the main features of the transient boiloff tests along with the test designations is presented in Table 5.21. The steady-state uncovered bundle tests are summarized in Table 5.22; the transient reflood tests are summarized in Table 5.23.

An isometric drawing of the small-break LOCA-II system configuration is shown in Fig. 5.38. The inlet piping is the same as that for the small-break LOCA-I test series. Instrumentation improvements were made on the outlet of the test section, however. An outlet orifice manifold was installed to provide accurate flow measurements when superheated steam conditions existed for flow ranges that were not measurable with the outlet turbine meter. The manifold was also installed as a backup in case the turbine meter failed in the expected high-temperature and high-quality steam environment. Also shown in Fig. 5.38 at the outlet is a shroud leakage bypass line. The initial attempt at running the second series of small-break LOCA tests failed because of an apparent leakage flow from inside the bundle to the shroud plenum annulus. This was discovered because of significant mass imbalances between the measured inlet and outlet flows at the test section. Posttest analysis indicated that large pressure differentials across the shroud-box wall resulted in steam leakage through the shroud (from the bundle to the shroud plenum annulus). The shroud plenum annulus was tied in with the pressurizer that is connected to the loop downstream of the heat exchangers. The small-diameter inlet and outlet piping causes considerable pressure drops, creating a large pressure differential between the shroud plenum annulus and the bundle. Modifications were made to eliminate the large pressure differentials. The shroud leakage line ties the shroud plenum annulus to the test section outlet flow. A valve installed in the shroud plenum annulus-pressurizer line allows isolation of the shroud plenum annulus from direct contact with the pressurizer. The transient reflood and boiloff tests were operated with the valve in the shroud plenum annulus-pressurizer line closed and the valve in the shroud leakage line at the outlet open. The steady-state uncovered bundle data scans were taken with both valves closed after equilibrium was attained.

A line drawing indicating piping sizes and run lengths for the small-break LOCA-II test configuration is shown in Fig. 5.39.

The test section pressure and differential pressure instrumentation arrangement for the small-break LOCA-II test series is shown in Fig. 5.40. Table 5.24 lists the types and ranges of the instruments indicated in Figs. 5.38 and 5.40. The instrument application drawings are shown in Figs. 5.41(a and b).

Table 5.21. THTF transient boiloff tests, November 1980 (preliminary)

Test	Test duration (s)	Average rod linear power [kW/m (kW/ft)]	Depressurization [MN/m² (psia)]		Maximum bundle uncovering (%)	
			Desired	Observed	Desired	Observed
3.09.10T	200	0.95 (0.29)	6.2–4.14 (900–600)	5.79–3.45 (840–500)	80	70
3.09.10U	60	1.90 (0.58)	7.93–6.2 (1150–900)	8.00–5.52 (1160–800)	70	70
3.09.10V	135	0.66 (0.20)	7.93–6.2 (1150–900)	7.58–5.52 (1100–800)	70	70
3.09.10W	100	0.62 (0.19)	7.93–6.2 (1150–900)	7.86–5.86 (1140–850)	70	45
3.09.10X	280	0.33 (0.10)	8.62 (1250)	8.55–8.34 (1240–1210)	60	70

Table 5.22. THTF steady-state bundle uncovery tests, November 1980

Test	Pressure [MN/m² (psia)]	Power [kW/m (kW/ft)]	Mixture level [m (ft)]	Maximum temperature [K (°F)]
3.09.10I	4.14 (600)	2.23 (0.68)	2.67 (8.75)	1050 (1430)
3.09.10J	4.14 (600)	0.98 (0.30)	2.92 (9.58)	905 (1170)
3.09.10K	4.14 (600)	0.36 (0.11)	2.13 (7.00)	989 (1320)
3.09.10L	7.58 (1100)	2.20 (0.67)	2.74 (9.00)	997 (1335)
3.09.10M	6.89 (1000)	1.05 (0.32)	2.54 (8.33)	1011 (1360)
3.09.10N	7.24 (1050)	0.49 (0.15)	2.13 (7.00)	1044 (1420)

Table 5.23. THTF reflood tests, November 1980 (preliminary)

Test	Pressure [MN/m² (psia)]	Power [kW/m (kW/ft)]	Flooding rate [cm/s (in./s)]
3.09.10O	4.14 (600)	1.97 (0.6)	15.24 (6)
3.09.10P	4.14 (600)	0.98 (0.3)	7.62 (3)
3.09.10Q	4.14 (600)	0.98 (0.3)	2.54 (1)
3.09.10R	7.58 (1100)	1.97 (0.6)	7.62 (3)
3.09.10S	7.58 (1100)	0.98 (0.3)	7.62 (3)

5.3.5 Intermediate-flow heat transfer test series 3.10.11A-H

The intermediate-flow heat transfer test series was aimed at obtaining heat transfer data over the range of mass flows and powers between those of the small-break LOCA-type tests and the steady-state upflow film boiling tests. Steady-state and boiloff tests were run for this series.

The loop configuration (Fig. 5.42) is essentially a combination of the two test configurations. The inlet piping configuration used for the small-break LOCA test series is combined with the 4-in. outlet piping of the standard configuration. A steam/water pressurizer is used for these tests for reasons previously explained in Sect. 5.3.2. The pressure and differential pressure instrumentation arrangement used for this test series is shown in Fig. 5.43. Table 5.25 lists the instrument type and ranges for the primary instruments indicated in Figs. 5.42 and 5.43. The instrument application drawings for Tests 3.10.11A-H are shown in Figs. 5.44(a-c). Note that a data report is not available for this test series, although the data tapes have been supplied to the INEL data bank.

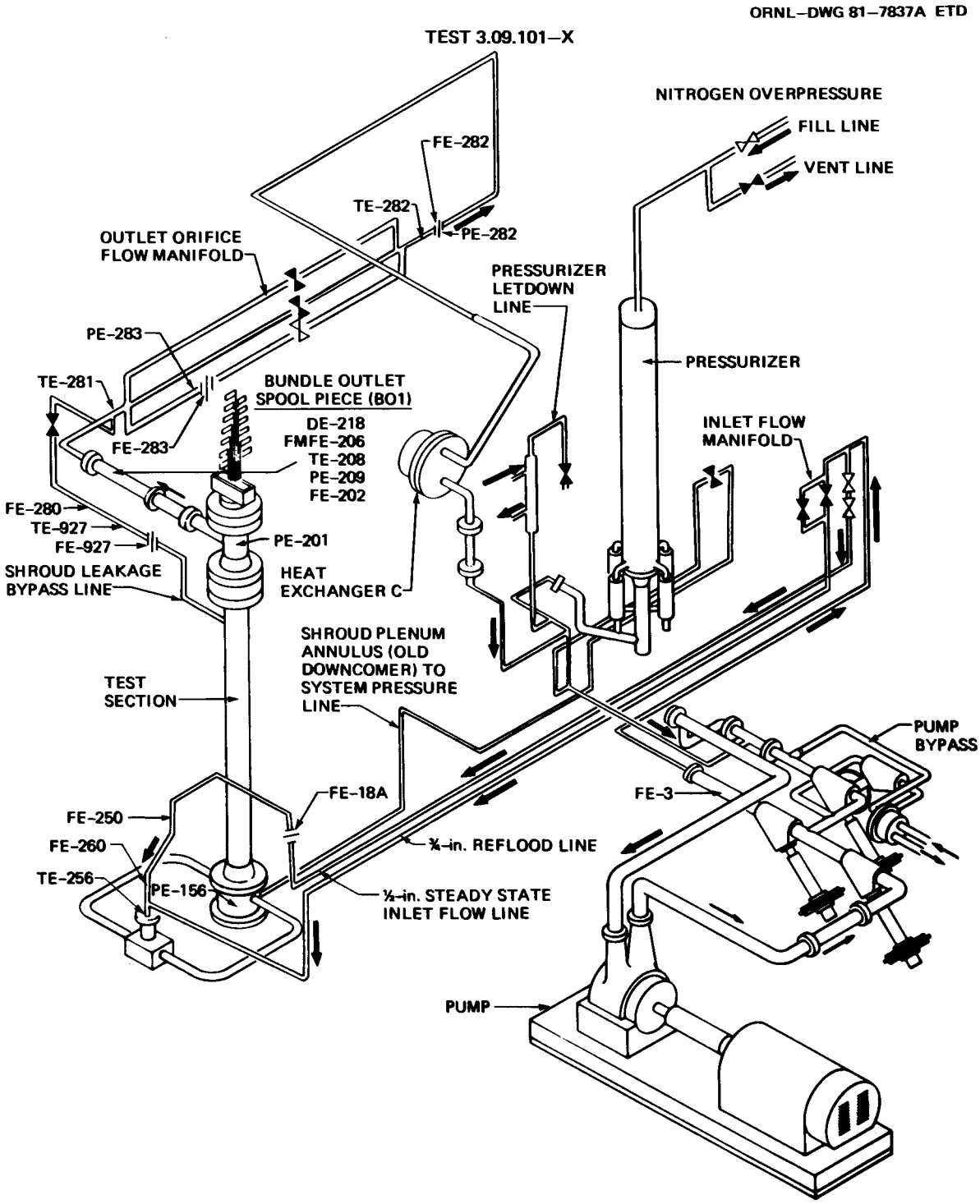

Fig. 5.38. THTF configuration for test series 3.09.10I-X.

ORNL–DWG 82–5434 ETD

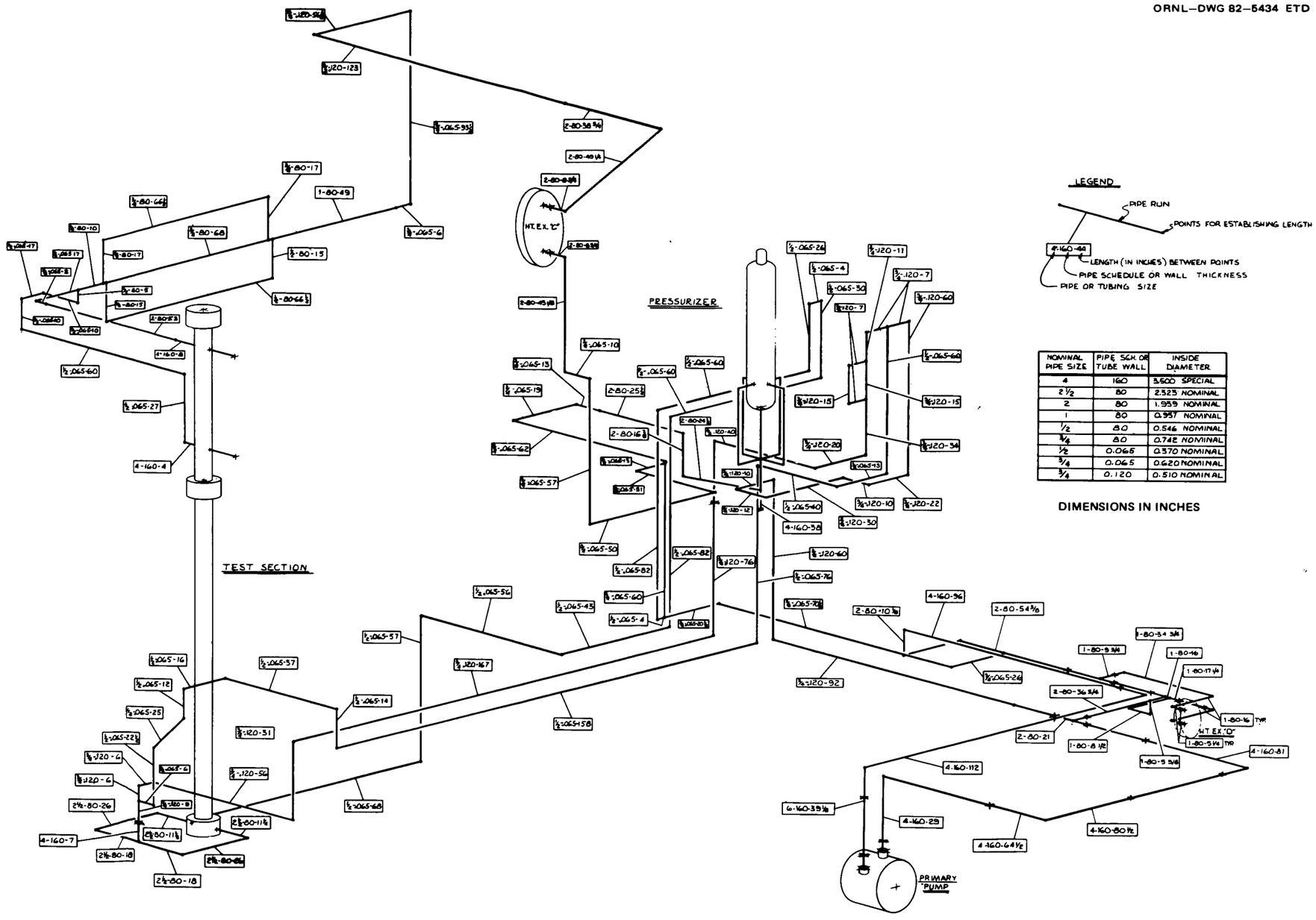

NOMINAL PIPE SIZE	PIPE SCH. OR TUBE WALL	INSIDE DIAMETER
4	160	3.600 SPECIAL
2 1/2	80	2.323 NOMINAL
2	80	1.939 NOMINAL
1	80	0.957 NOMINAL
1/2	80	0.546 NOMINAL
3/4	80	0.742 NOMINAL
1/2	0.065	0.370 NOMINAL
3/4	0.065	0.620 NOMINAL
3/4	0.120	0.510 NOMINAL

Fig. 5.39. System line drawing of the THTF in the small-break LOCA-II test configuration (test series 3.09.10I-X). (Microfiche copy of this drawing attached to back of report.)

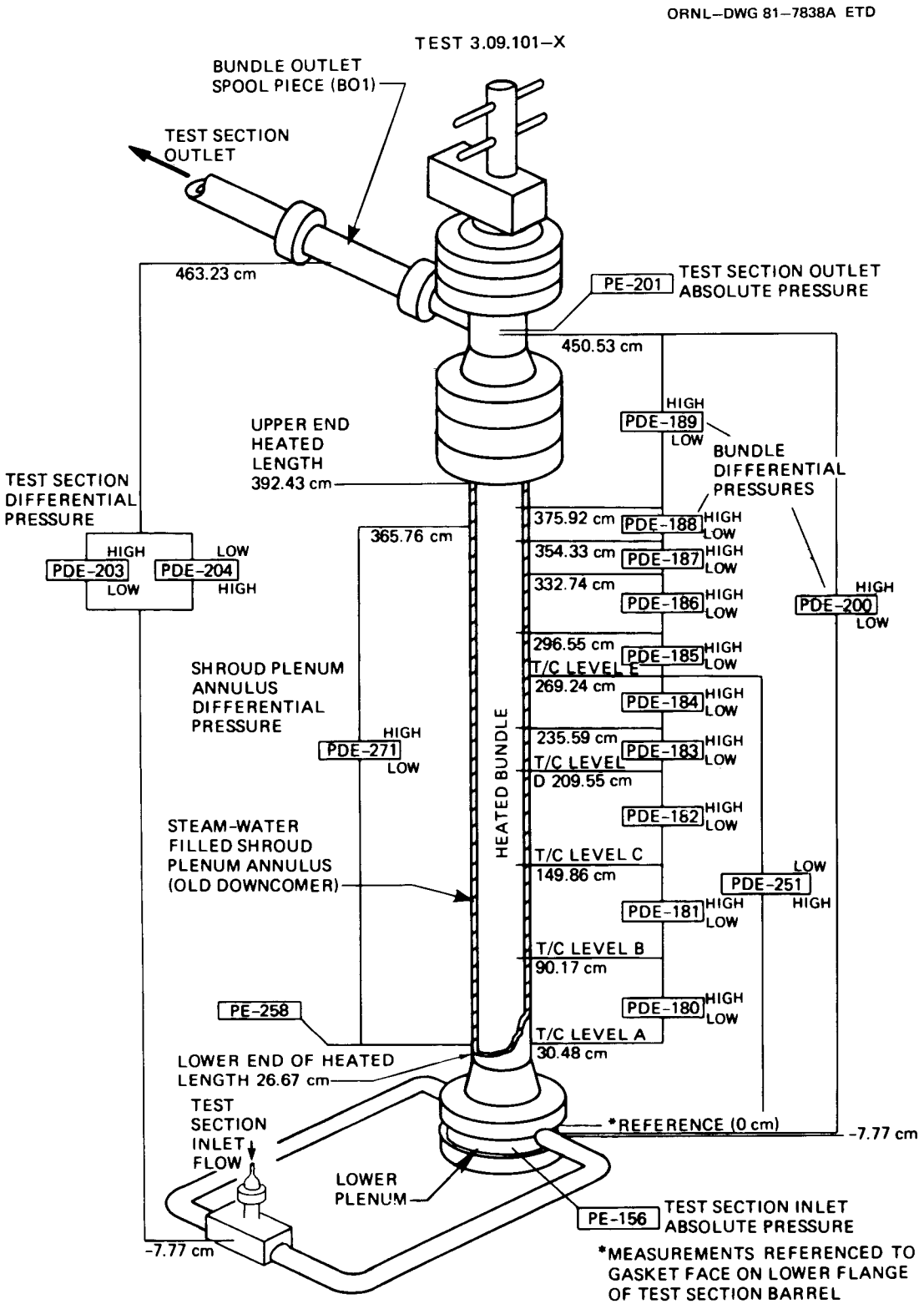

Fig. 5.40. Test section pressure and differential pressure instrumentation for test series 3.09.10I-X.

Table 5.24. Primary flow instrumentation for test series 3.09.10I-X

Instrument application No.	Description	Instrument	Range
FE-3	2-in. inlet transient volumetric flow	2-in. Flow Technology turbine meter	$\pm 6.3 \times 10^{-4}$–3.5×10^{-3} m³/s ($\pm$10–56.2 gpm) range 1
FE-18A	Test section inlet steady state volumetric flow	Orifice meter, 1/2-in. line, Foxboro differential pressure cell	0–1.7×10^{-4} m³/s (0–2.7 gpm)
FE-250	Bundle inlet volumetric flow 2	1/2-in. Flow Technology turbine meter	3.1×10^{-5}–3.1×10^{-4} m³/s (0.5–5 gpm)
FE-260	Bundle inlet volumetric flow 1	1/2-in. Flow Technology turbine meter	3.1×10^{-5}–3.1×10^{-4} m³/s (0.5–5 gpm)
TE-256	Test section inlet temperature	Nanmac fluid thermocouple	273–1309 K (32–1900°F)
PE-156	Test section inlet transient pressure	Precise Sensor absolute pressure transducer	0–2.07×10^{4} kPa (0–3000 psig)
PE-201	Test section outlet transient pressure	Precise Sensor absolute pressure transducer	0–2.07×10^{4} kPa (0–3000 psig)
DE-218	Bundle outlet spool density	Single-beam gamma densitometer (with 2-in. pipe adaptor)	0–1000 kg/m³ (0–62.4 lb_m/ft³)
FMFE-206	Bundle outlet spool drag disk (momentum flux)	Ramapo drag disk, ORNL 2-in., 3-bladed, full-flow target	$\pm$0–3.72×10^{4} kg/m·s² ($\pm$0–2.5×10^{4} lb_m/ft·s²)
TE-208	Bundle outlet spool temperature	Nanmac fluid thermocouple	273–1309 K (32–1900°F)
PE-209	Bundle outlet spool transient pressure	Precise Sensor absolute pressure transducer	0–2.07×10^{4} kPa (0–3000 psig)
FE-202	Bundle outlet spool volumetric flow	2-in. Flow Technology turbine meter	$\pm 6.3 \times 10^{-4}$–0.0284 m³/s ($\pm$10–450 gpm) range 4
TE-281	Low-range outlet orifice temperature	1/8-in.-OD sheathed thermocouple, type K	273–1309 K (32–1900°F)
PE-283	Low-range outlet orifice transient pressure	Precise Sensor absolute pressure transducer	0–2.07×10^{4} kPa (0–3000 psig)
FE-283	Low-range outlet orifice volumetric flow	Orifice flowmeter, 1/2-in. line, 100-in. Barton differential pressure transmitter	Density dependent 0–3.32×10^{-4} m³/s (0–5.2 gpm) for fluid density of 1000 kg/m³
TE-282	High-range outlet orifice temperature	1/8-in.-OD sheathed thermocouple, type K	273–1309 K (32–1900°F)

Table 5.24 (continued)

Instrument application No.	Description	Instrument	Range
PE-282	High-range outlet orifice transient pressure	Precise Sensor absolute pressure transducer	0–2.07 x 10^4 kPa (0–3000 psig)
FE-282	High-range outlet orifice volumetric flow	Orifice flowmeter, 1-in. line, Rosemount differential pressure transmitter (200 in.)	Density dependent 0–2.48 x 10^{-3} m^3/s (0–39.3 gpm) for fluid density of 1000 kg/m^3
FE-927	Shroud bypass line orifice volumetric flow	Orifice flowmeter, 1/2-in. line, 100-in. Barton differential pressure transmitter	Density dependent 0–1.35 x 10^{-4} m^3/s (0–2.1 gpm) for fluid density of 1000 kg/m^3
FE-927	Shroud bypass line temperature	1/8-in.-OD sheathed thermocouple, type K	273–1309 K (32–1900°F)
FE-280	Shroud bypass line volumetric flow	1/2-in. Flow Technology turbine meter	±6.3 x 10^{-5}–6.3 x 10^{-4} m^3/s (±1–10 gpm)
PDE-200	Bundle transient differential pressure	6-psi Genisco differential pressure transducer	±0–41.4 kPa (±0–6 psid)
PDE-203	Test section transient differential pressure	50-psi BLH differential pressure transducer	±0–345 kPa (±0–50 psid)
PDE-204	Test section transient differential pressure	6-psi Genisco differential pressure transducer	±0–41.4 kPa (±0–6 psid)
PDE-251	Shroud-box differential pressure across thermocouple level E and test section inlet level	6-psi Genisco differential pressure transducer	±0–41.4 kPa (±0–6 psid)
PDE-271	Shroud plenum annulus transient differential pressure	6-psi Genisco differential pressure transducer	±0–41.4 kPa (±0–6 psid)
PE-258	Shroud plenum annulus transient pressure	Precise Sensor absolute pressure transducer	0–2.07 x 10^4 kPa (0–3000 psig)
PDE-180 to 188	Shroud-box differential pressure	Rosemount differential pressure transmitter	0–6.22 kPa (0–25 in. of Std. H_2O)
PDE-189	Shroud-box differential pressure	Rosemount differential pressure transmitter	0–7.46 kPa (0–30 in. of Std. H_2O)

ORNL-DWG 82-5435 ETD (PART A)

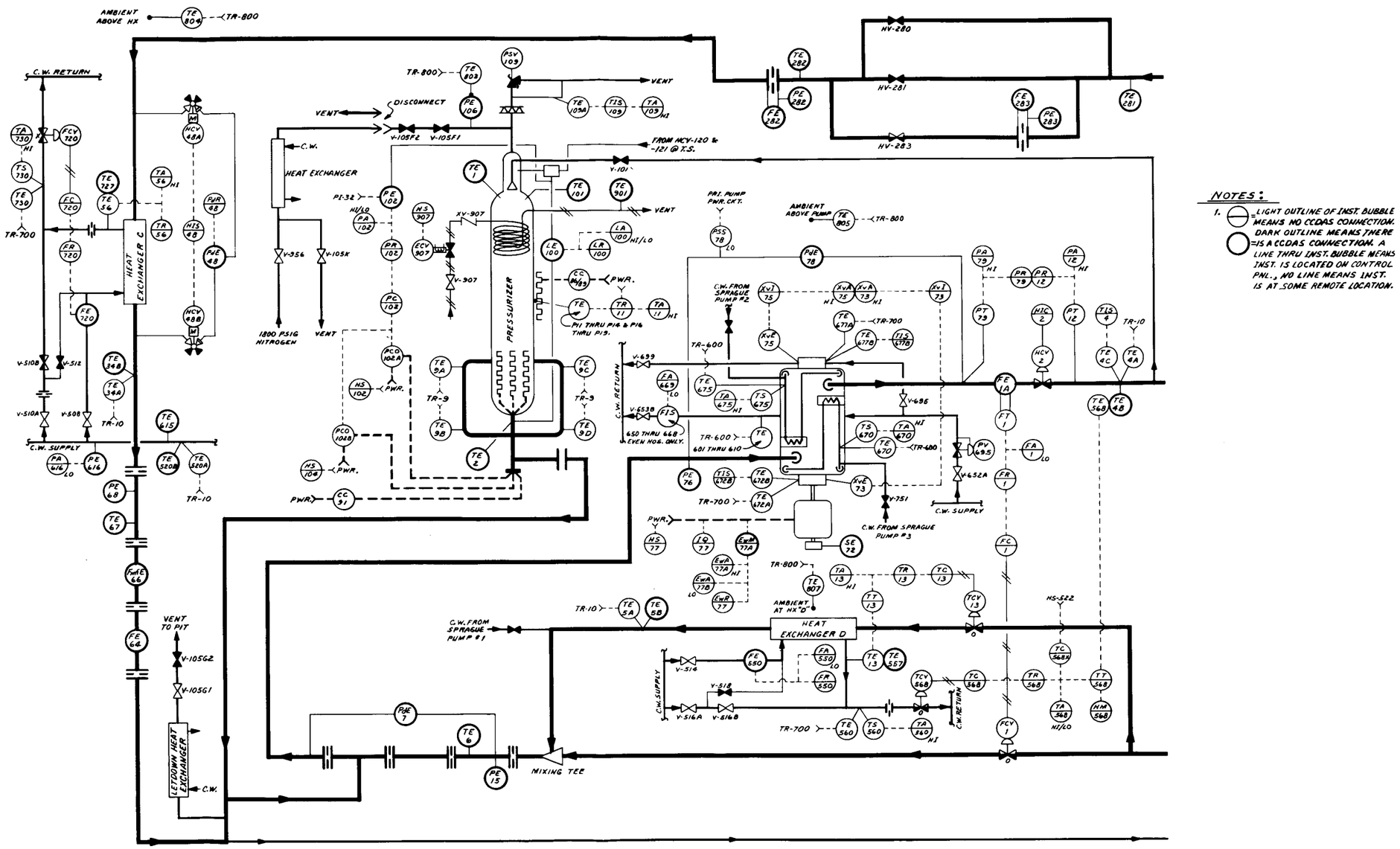

Fig. 5.41. Instrument application drawings for test series 3.09.10I-X.

ORNL–DWG 82–5435 ETD (PART B)

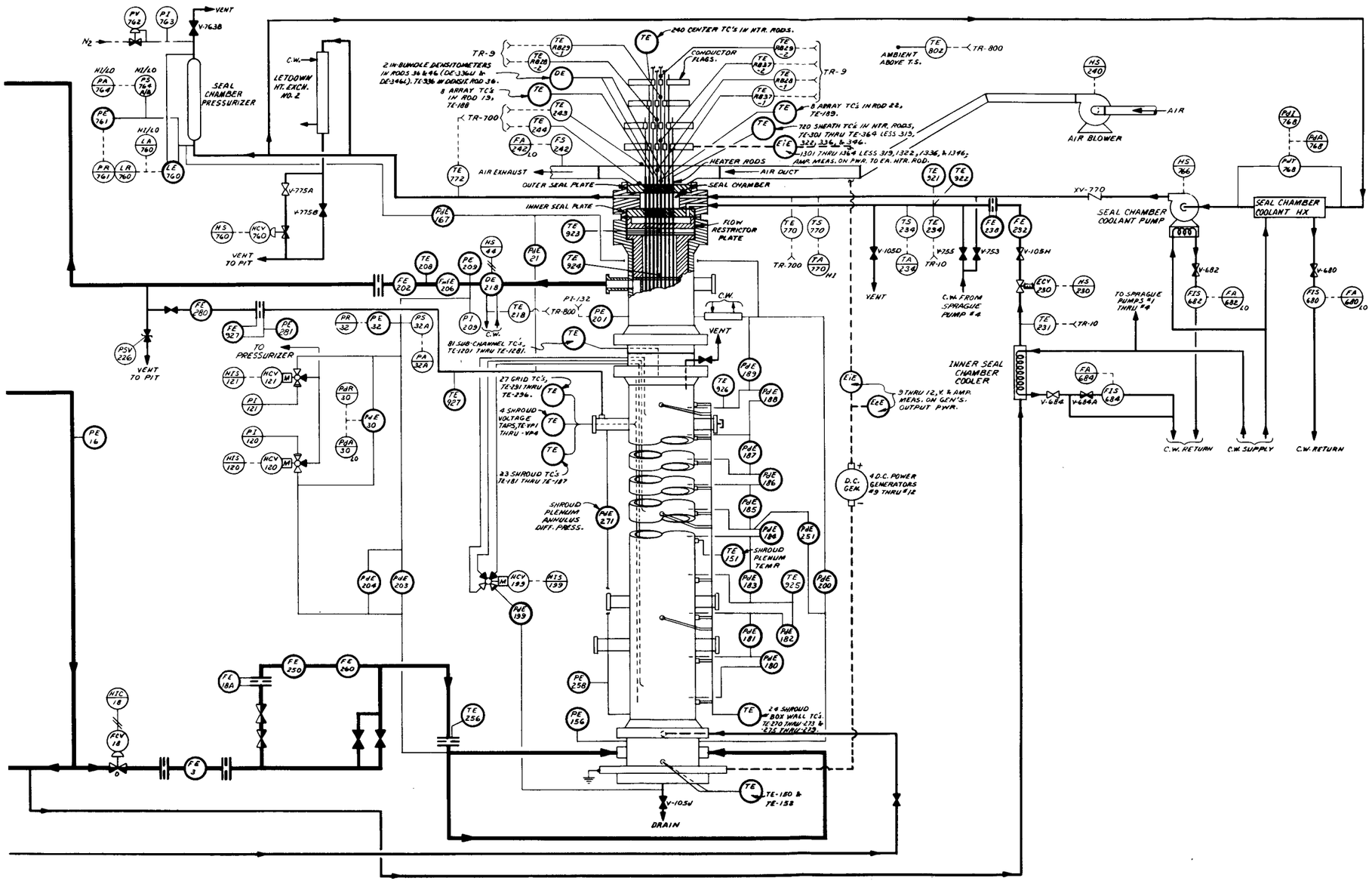

Fig. 5.41 (continued)

ORNL–DWG 81–7833A ETD

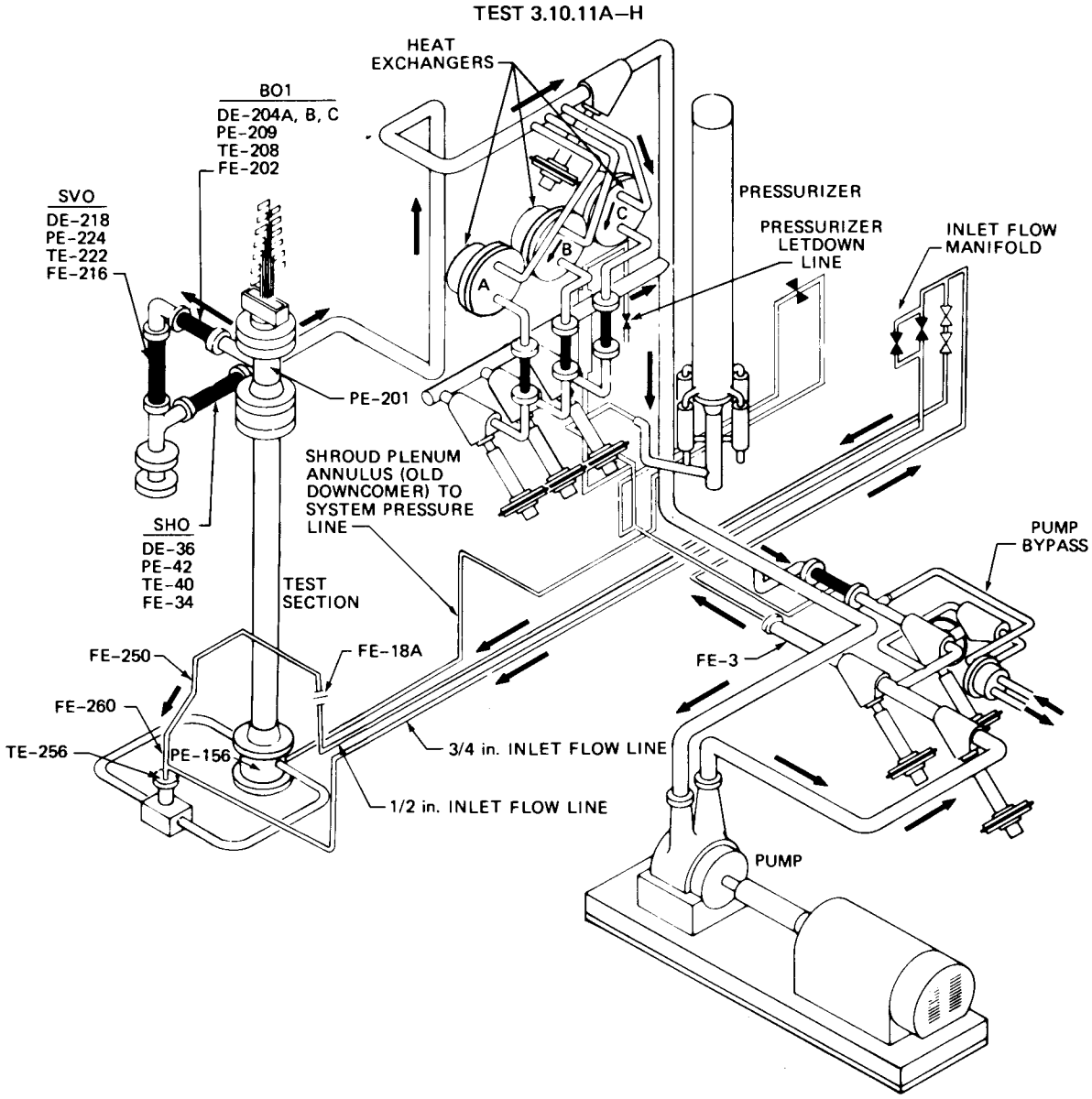

Fig. 5.42. THTF configuration for test series 3.10.11A–H.

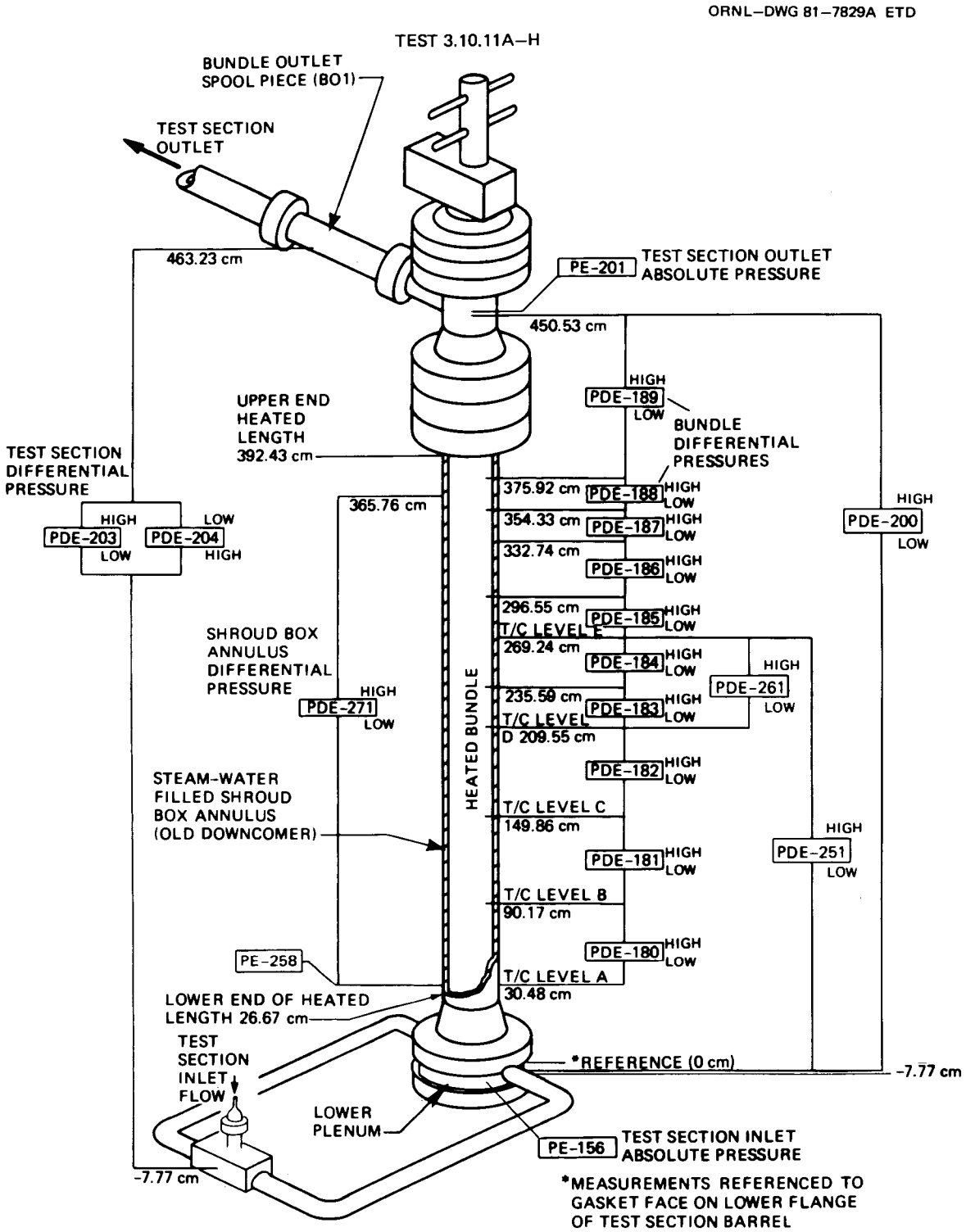

Fig. 5.43. Test section pressure and differential pressure instrumentation for test series 3.10.11A–H.

Table 5.25. Primary flow instrumentation for test series 3.10.11A-H

Instrument application No.	Description	Instrument	Range
DE-204A	Bundle outlet spool density	Three-beam gamma densitometer	0–1000 kg/m³ (0–62.4 lb_m/ft^3)
DE-204B			
DE-204C			
PE-209	Bundle outlet spool transient pressure	Precise Sensor absolute pressure transducer	0–2.07 x 10^4 kPa (0–3000 psig)
TE-208	Bundle outlet spool temperature	Nanmac fluid thermocouple	273–1309 K (32–1900°F)
FE-202	Bundle outlet spool volumetric flow	3.5-in. Flow Technology turbine meter	±0.005–0.227 m³/s (±80–3600 gpm) range 4
DE-36	Horizontal outlet spool density	Single-beam gamma densitometer	0–1000 kg/m³ (0–62.4 lb_m/ft^3)
PE-42	Horizontal outlet spool transient pressure	Precise Sensor absolute pressure transducer	0–2.07 x 10^4 kPa (0–3000 psig)
TE-40	Horizontal outlet spool temperature	Nanmac fluid thermocouple	273–1309 K (32–1900°F)
FE-34	Horizontal outlet spool volumetric flow	3.5-in. Flow Technology turbine meter	±0.005–0.227 m³/s (±80–3600 gpm) range 4
DE-218	Vertical outlet spool density	Single-beam gamma densitometer	0–1000 kg/m³ (0–62.4 lb_m/ft^3)
PE-224	Vertical outlet spool transient pressure	Precise Sensor absolute pressure transducer	0–2.07 x 10^4 kPa (0–3000 psig)
TE-222	Vertical outlet spool temperature	Nanmac fluid thermocouple	273–1309 K (32–1900°F)
FE-216	Vertical outlet spool volumetric flow	3.5-in. Flow Technology turbine meter	±0.005–0.227 m³/s (±80–3600 gpm) range 4
FE-3	2-in. inlet transient volumetric flow	2-in. Flow Technology turbine meter	±6.3 x 10^{-4}–3.54 x 10^{-3} m³/s (±10–56.2 gpm) range 1
FE-18A	Test section inlet steady-state volumetric flow	Orifice meter, 1/2-in. line, Foxboro differential pressure cell	Density dependent 0–1.7 x 10^{-4} m³/s (0–2.7 gpm) for density of 860 kg/m³

Table 5.25 (continued)

Instrument application No.	Description	Instrument	Range
FE-250	Bundle inlet volumetric flow 1	1/2-in. Flow Technology turbine meter	3.1×10^{-5}–3.1×10^{-4} m^3/s (0.5–5 gpm)
FE-260	Bundle inlet volumetric flow 2	1/2-in. Flow Technology turbine meter	3.1×10^{-5}–3.1×10^{-4} m^3/s (0.5–5 gpm)
TE-256	Test section inlet temperature	Nanmac fluid thermocouple	273–1309 K (32–1900°F)
PDE-200	Bundle transient differential pressure	200-in. Rosemount differential pressure transmitter	0–49.7 kPa (0–200 in. of Std. H_2O)
PDE-203	Test section transient differential pressure	50-psi BLH differential pressure transducer	±0–345 kPa (±0–50 psid)
PDE-204	Test section transient differential pressure	6-psi Genisco differential pressure transducer	±0–41.4 kPa (±0–6 psid)
PDE-251	Shroud-box differential pressure across T/C level E and test section inlet level	6-psi Genisco differential pressure transducer	±0–41.4 kPa (±0–6 psid)
PDE-261	Shroud-box differential pressure across T/C level D and E	6-psi Genisco differential pressure transducer	±0–41.4 kPa (±0–6 psid)
PDE-271	Shroud plenum annulus transient differential pressure	6-psi Genisco differential pressure transducer	±0–41.4 kPa (±0–6 psid)
PE-258	Shroud plenum annulus transient pressure	Precise Sensor absolute pressure transducer	0–2.07×10^4 kPa (0–3000 psig)
PDE-180 to 188	Shroud-box differential pressure	Rosemount differential pressure transmitter	0–6.22 kPa (0–25 in. of Std. H_2O)
PDE-189	Shroud-box differential pressure	Rosemount differential pressure transmitter	0–7.46 kPa (0–30 in. of Std. H_2O)
PE-156	Test section inlet transient pressure	Precise Sensor absolute pressure transducer	0–2.07×10^4 kPa (0–3000 psig)
PE-201	Test section outlet transient pressure	Precise Sensor absolute pressure transducer	0–2.07×10^4 kPa (0–3000 psig)

ORNL–DWG 82–5436 ETD (PART A)

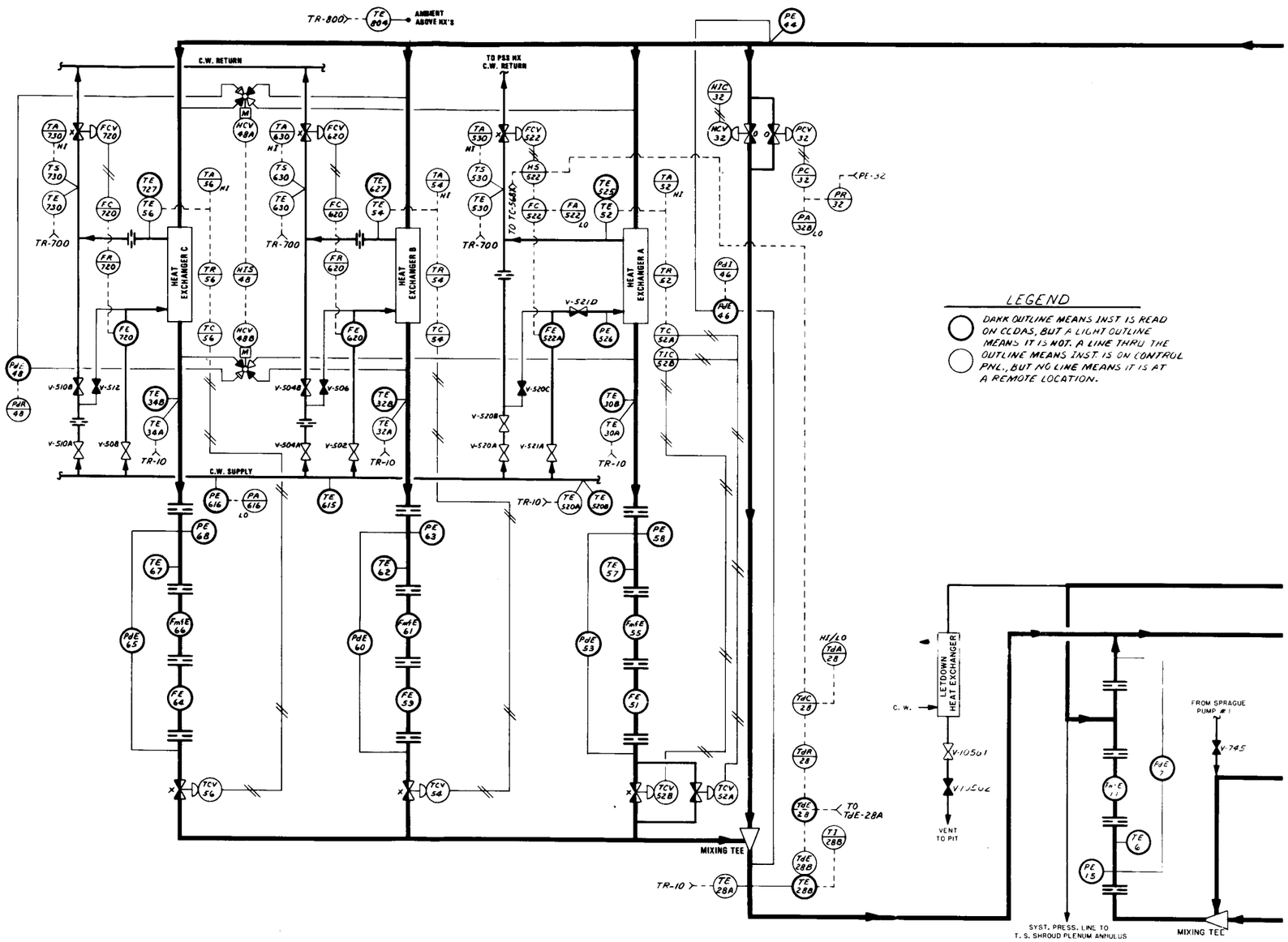

Fig. 5.44. Instrument application diagrams for test series 3.10.11A–H.

ORNL–DWG 82–5436 ETD (PART B)

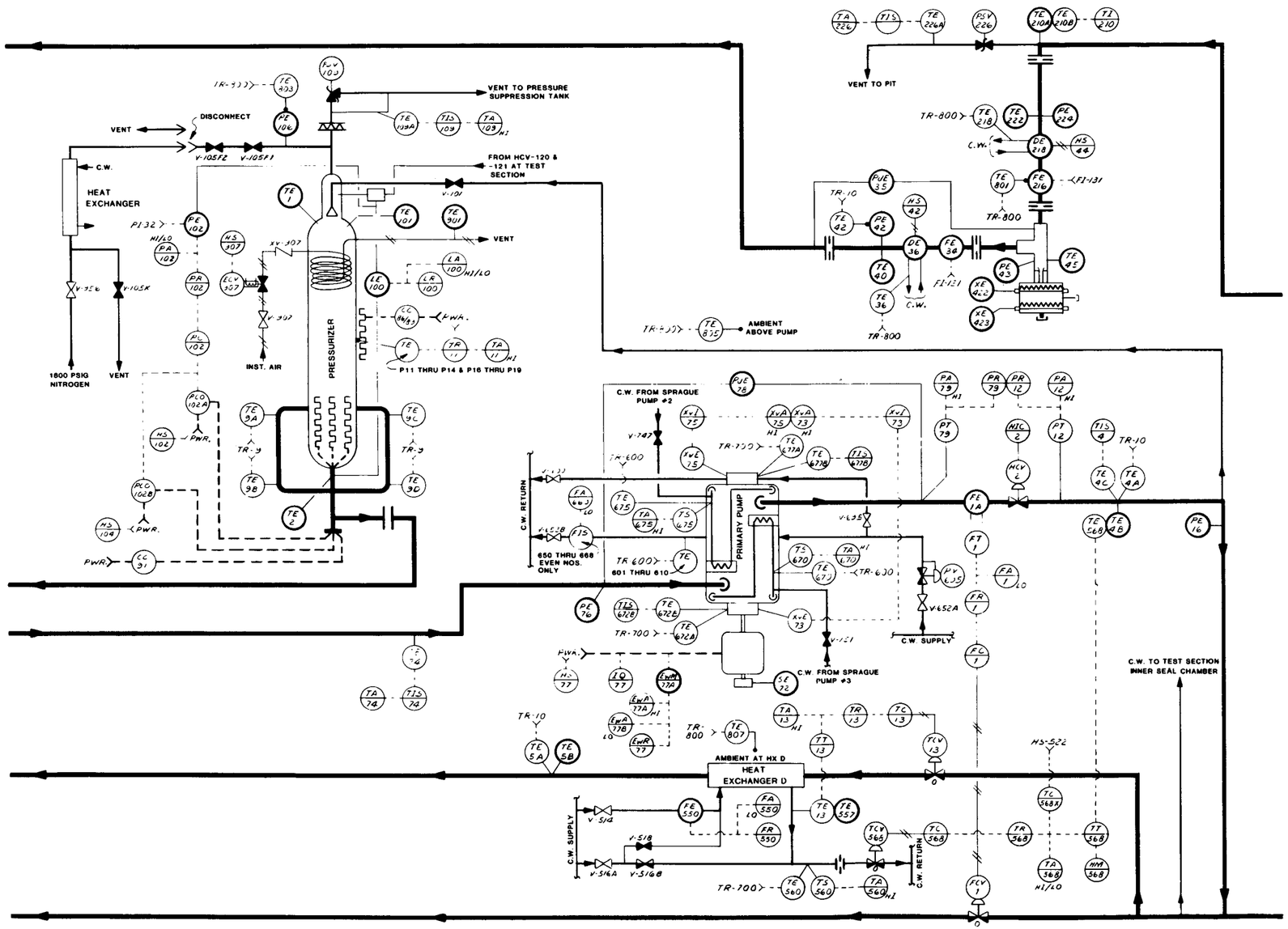

Fig. 5.44 (continued)

ORNL–DWG 82–5436 ETD (PART C)

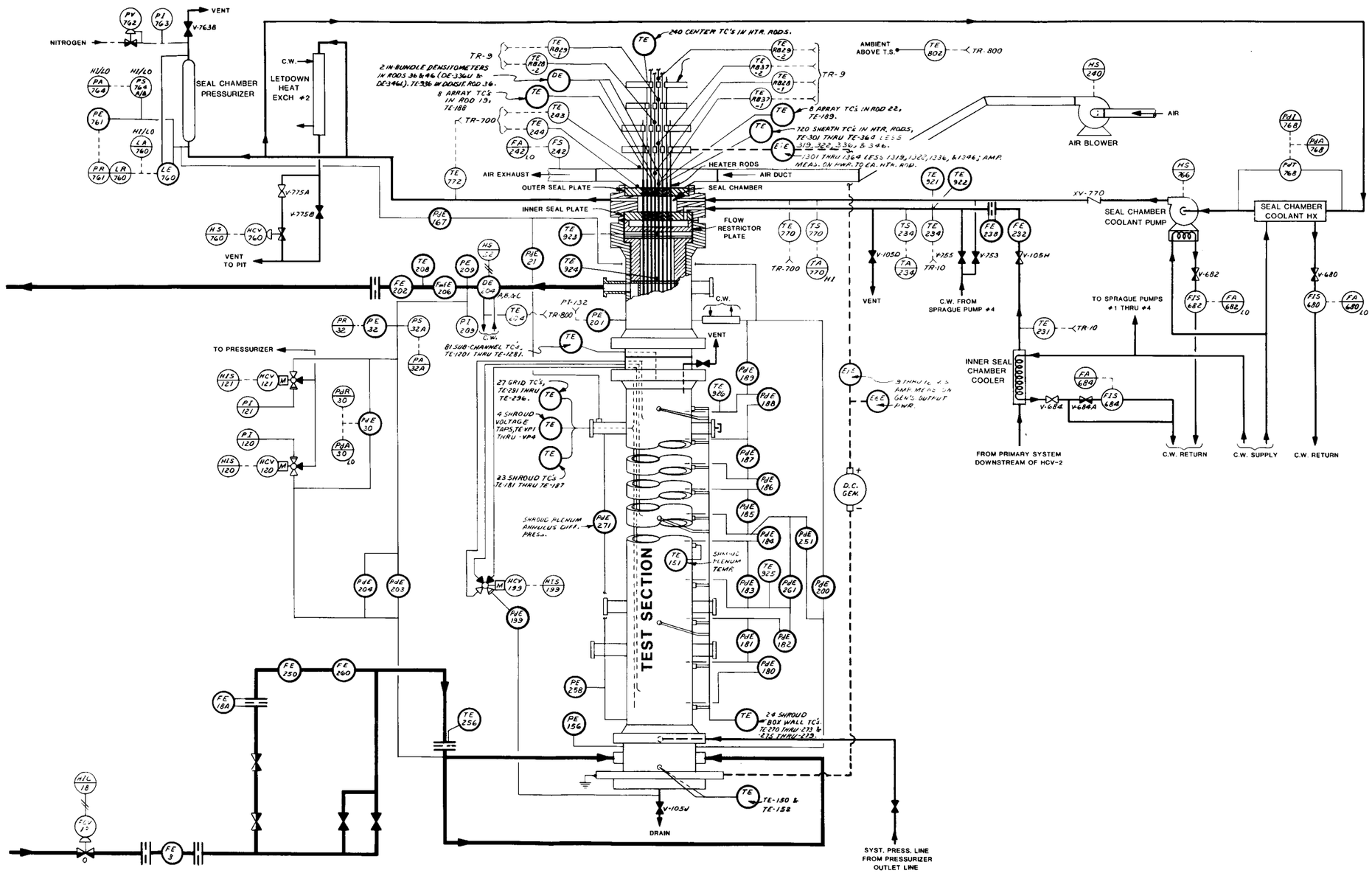

Fig. 5.44 (continued)

6. INSTRUMENTATION AND DATA ACQUISITION SYSTEM

6.1 Instrumentation

The THTF instrumentation system is designed to ensure the reliable and safe operation of the experimental facility. Instrument channels monitoring critical test parameters provide data needed for the determination of system behavior under steady-state and transient conditions. Additional instruments are installed in the test loop and associated secondary systems to provide operators with confidence that the facility is operating normally. The instrumentation system includes means for detecting out-of-limit and unsafe conditions, alerting the operators that such conditions exist, and initiating appropriate protective actions on detection of such conditions. Protective features are described in Appendix A.3.

6.1.1 Location

The THTF is instrumented to measure temperature, flow, fluid density, level, pressure, differential pressure, power, and time under both steady-state and transient conditions. Instrument application drawings for all of the primary tests were presented in Chap. 5. Physical instrument hardware locations for the primary piping system and test section in the standard configuration are illustrated in Figs. 6.1–6.7. Primary flow and test section bounding condition instrumentation was described in Chap. 5 for the primary tests run at the THTF. A listing by type of measurement of most of these instruments is presented in Table 6.1.

6.1.2 Sensors

The process variables important to facility operation are monitored by conventional-type instruments suited to the operating conditions. Most of the test variables are monitored by conventional-type instruments, except the gamma densitometers, bidirectional drag disks, bidirectional turbine meters, and fast-response pressure transducers.

Table 6.2 details the type of measurements, the sensor error, and required sensor response for all classes of primary measuring devices in the THTF. In the table, the "Type" column gives the class or principle of operation of the sensors, and the "Error" column gives the error band (2σ) for each type of sensor either as a percentage of full scale (% FS), percentage of reading (% Rdg), or an absolute value [such as 2 K (1.5°F)]. The "Required response" column defines the maximum time constant (i.e., time required for the output to change 63.2% of a step change in the measured variable) and minimum frequency acceptable for obtaining the desired data. Each type of sensor has an assigned code, as indicated in the "Designation;" these codes are designations used in Table 6.3 as a shorthand notation for the type of sensor used at each location. The "Type code" column gives the assigned instrument data base type code (ranges

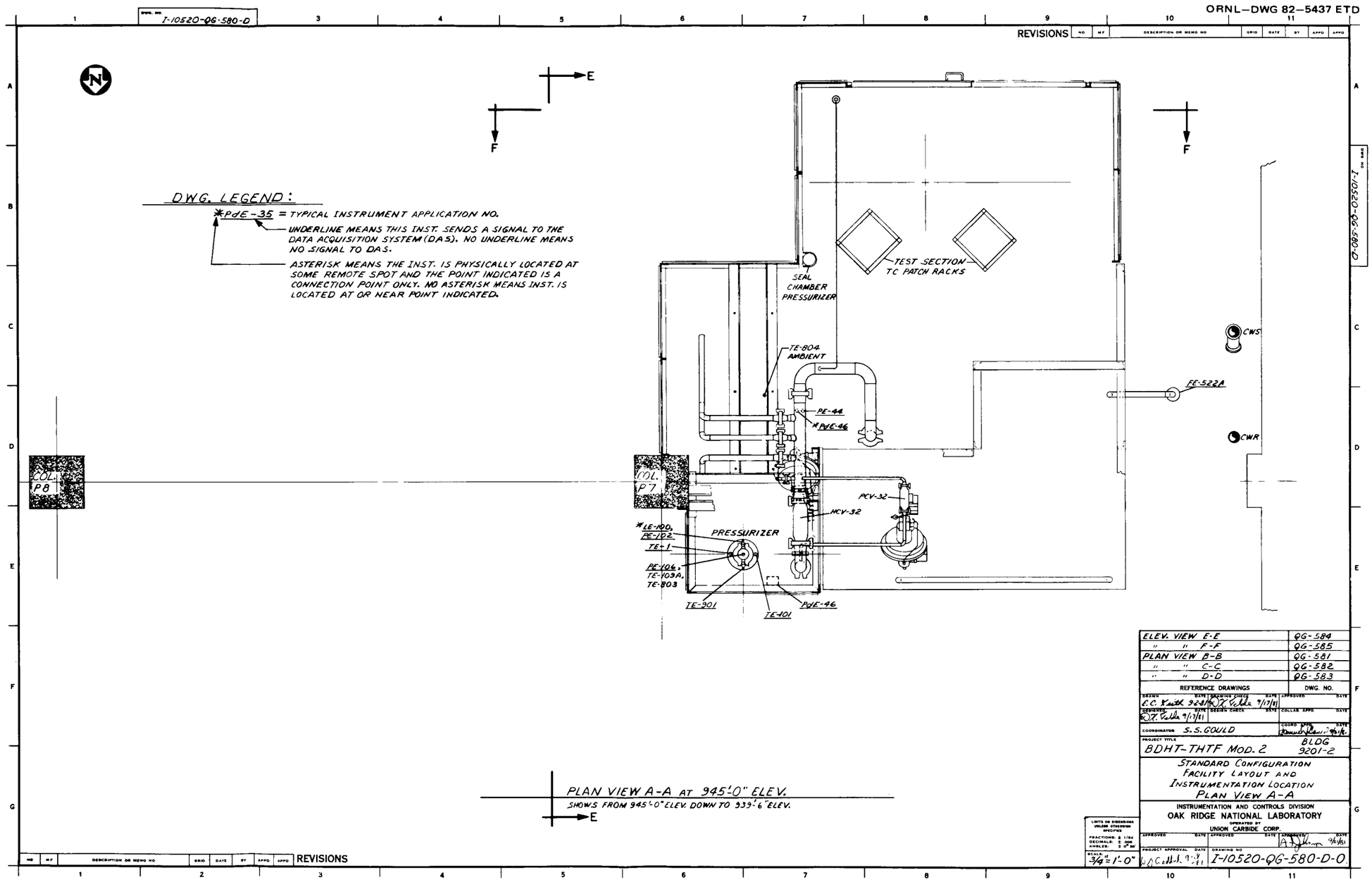

Fig. 6.1. Physical instrument hardware locations for primary piping system and test section in standard configuration. (Microfiche copy of this drawing attached to back of report.)

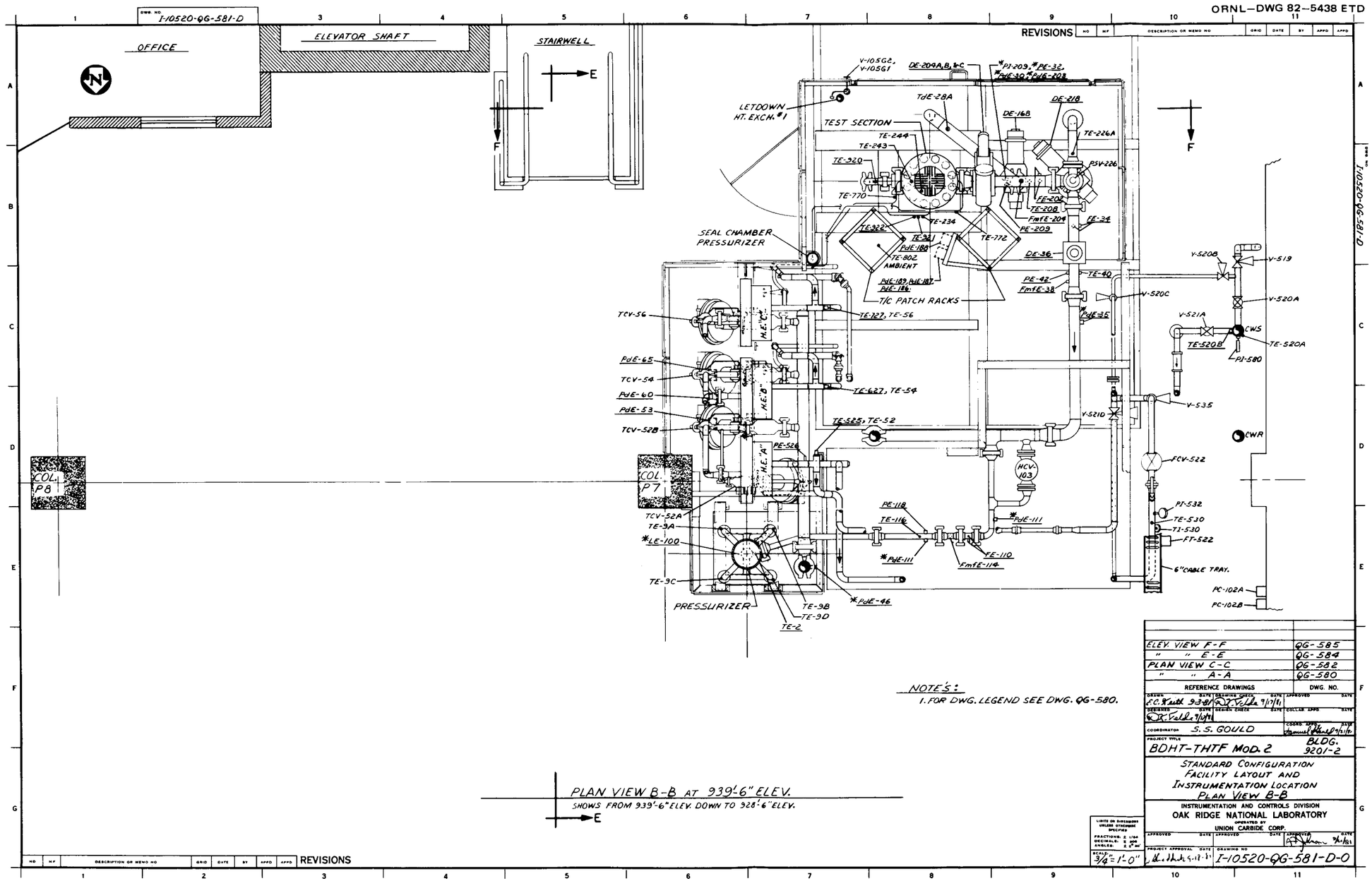

Fig. 6.2. Physical instrument hardware locations for primary piping system and test section in standard configuration. (Microfiche copy of this drawing attached to back of report.)

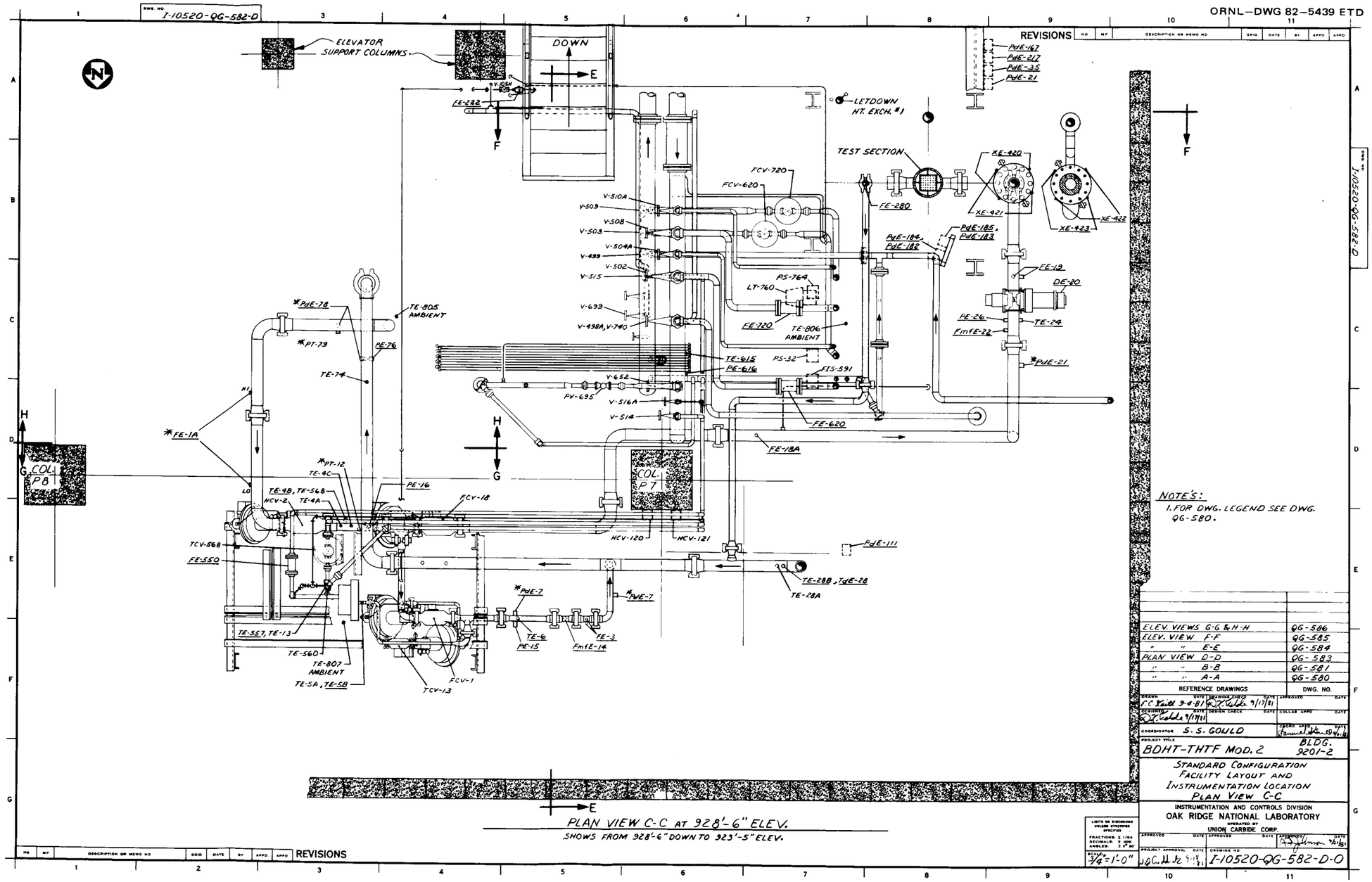

Fig. 6.3. Physical instrument hardware locations for primary piping system and test section in standard configuration. (Microfiche copy of this drawing attached to back of report.)

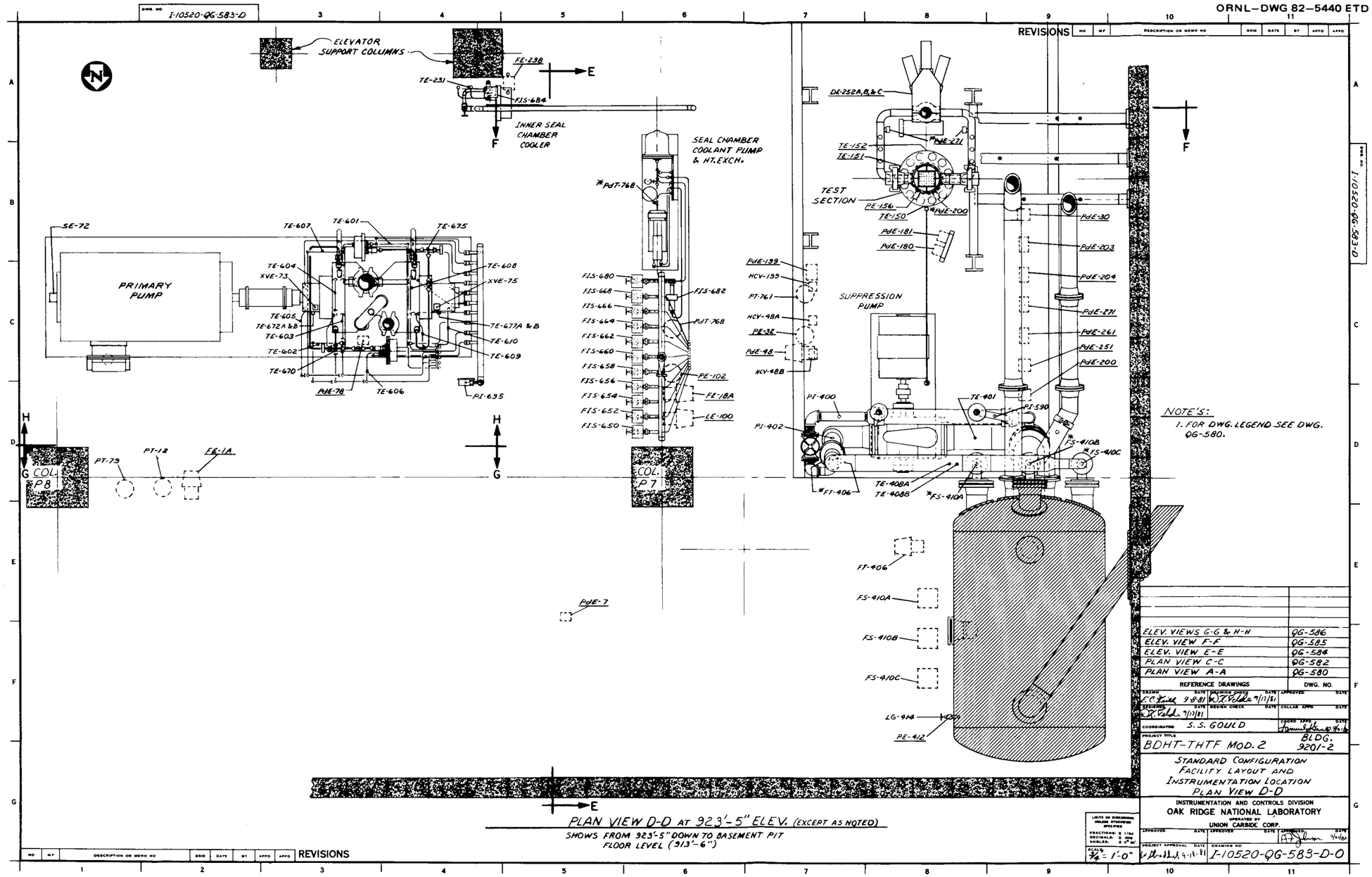

Fig. 6.4. Physical instrument hardware locations for primary piping system and test section in standard configuration. (Microfiche copy of this drawing attached to back of report.)

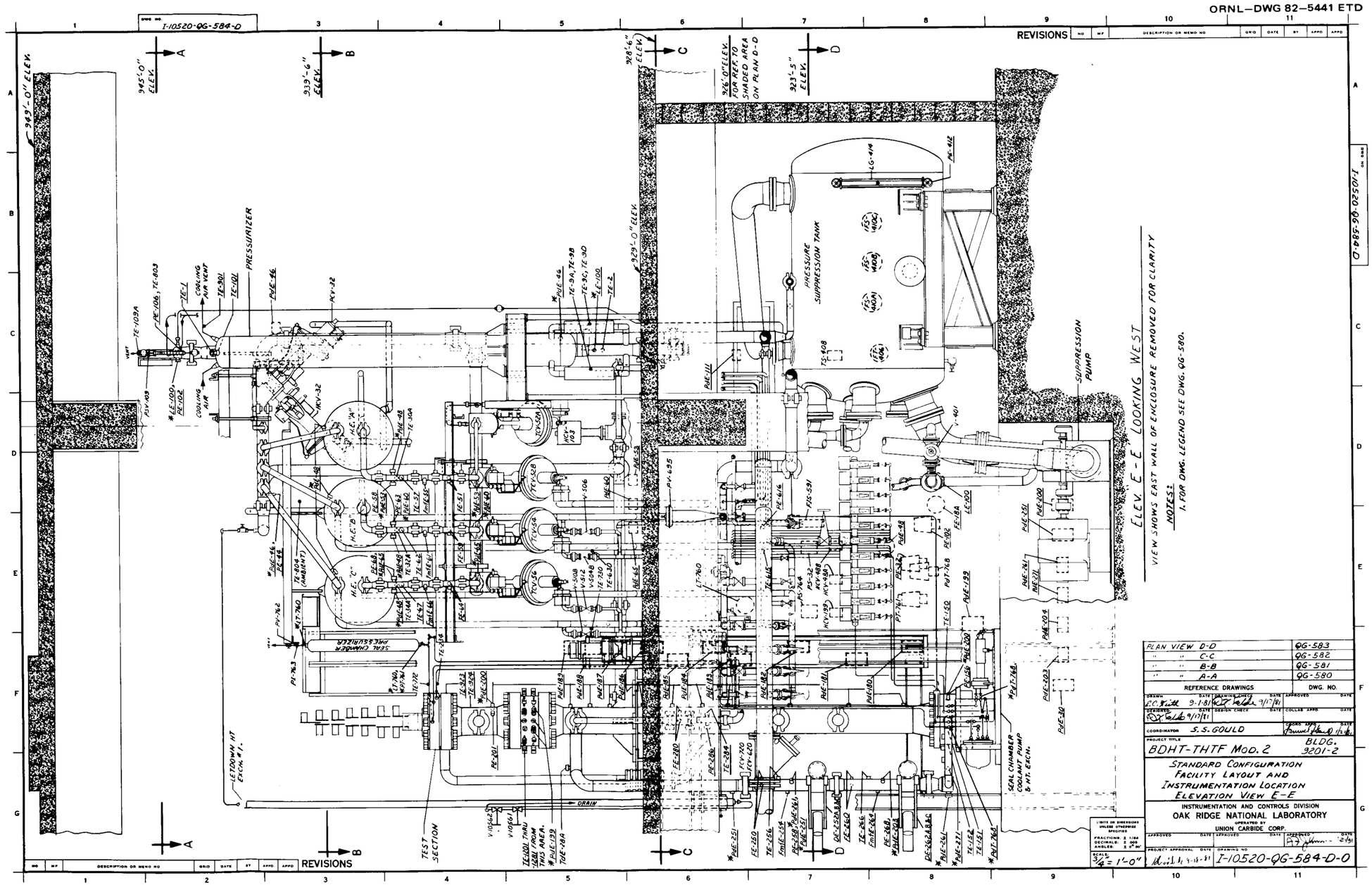

Fig. 6.5. Physical instrument hardware locations for primary piping system and test section in standard configuration. (Microfiche copy of this drawing attached to back of report.)

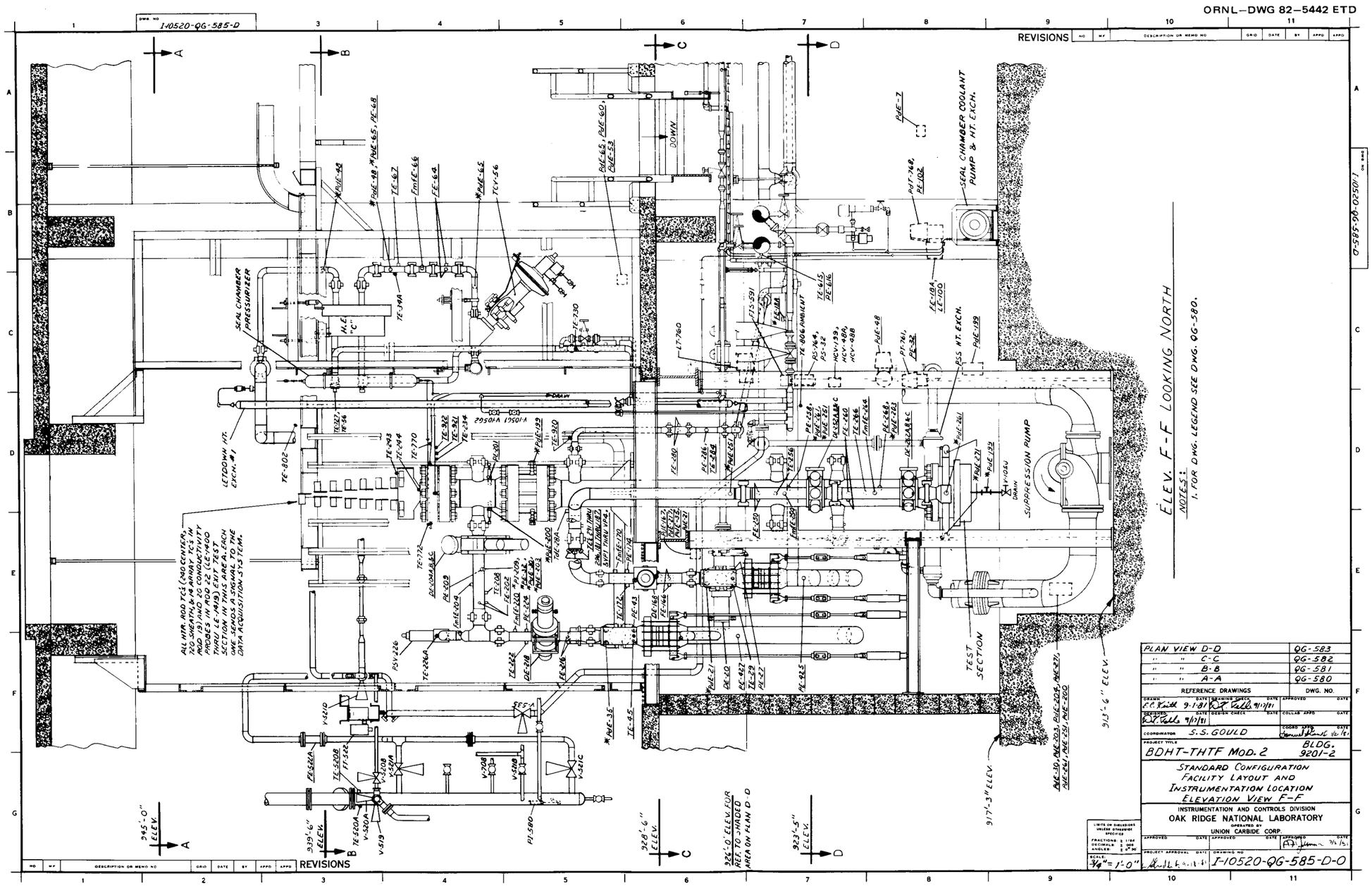

Fig. 6.6. Physical instrument hardware locations for primary piping system and test section in standard configuration. (Microfiche copy of this drawing attached to back of report.)

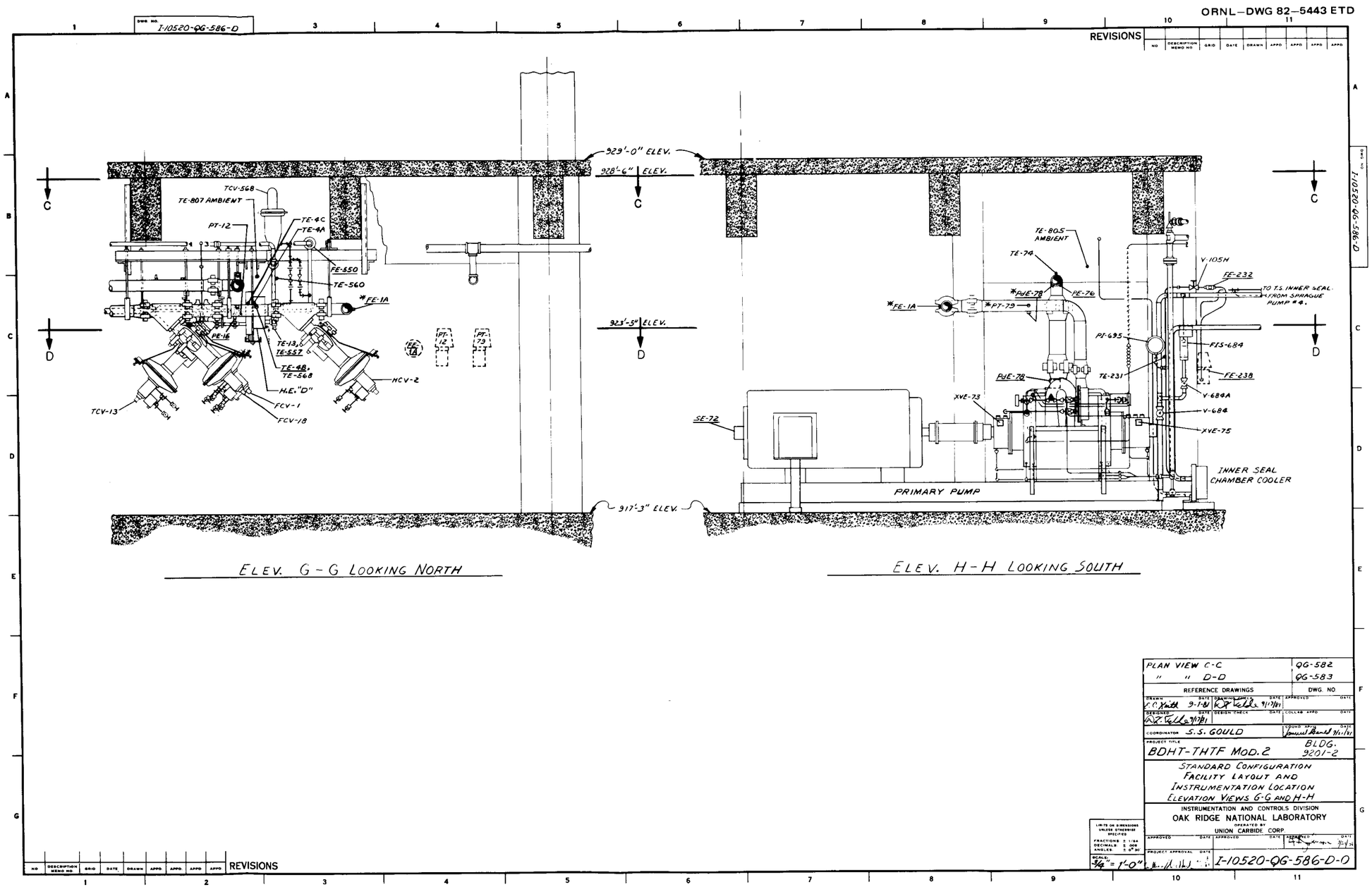

Fig. 6.7. Physical instrument hardware locations for primary piping system and test section in standard configuration. (Microfiche copy of this drawing attached to back of report.)

Table 6.1. Primary loop instrumentation providing bounding condition measurements

Instrument application No.	Location	Type	Measurement
			Density
DE-20	SHI	106	Standard horizontal inlet spool-piece
DE-36	SHO	106	Standard horizontal outlet spool-piece
DE-168	SVI	106	Standard vertical inlet spool-piece
DE-204A	BO1	106	Bundle outlet spool-piece (beam 1)
DE-204B	BO1	106	Bundle outlet spool-piece (beam 2)
DE-204C	BO1	106	Bundle outlet spool-piece (beam 3)
DE-218	SVO	106	Standard vertical outlet spool-piece
DE-252A	BI2	106	Bundle inlet upper spool-piece (beam 1)
DE-252B	BI2	106	Bundle inlet upper spool-piece (beam 2)
DE-252C	BI2	106	Bundle inlet upper spool-piece (beam 3)
DE-262A	BI1	106	Bundle inlet lower spool-piece (beam 1)
DE-262B	BI1	106	Bundle inlet lower spool-piece (beam 2)
DE-262C	BI1	106	Bundle inlet lower spool-piece (beam 3)
			Differential pressure[a]
PDE-180	TS	75	Shroud box (level A–B)
PDE-181	TS	75	Shroud box (level B–C)
PDE-182	TS	75	Shroud box (level C–D)
PDE-183	TS	75	Shroud box (level D–D/E)
PDE-184	TS	75	Shroud box (level D/E–E)
PDE-185	TS	75	Shroud box (level E–E/F)
PDE-186	TS	75	Shroud box (level E/F–F)
PDE-187	TS	75	Shroud box (level F–F/G)
PDE-188	TS	75	Shroud box (level F/G–G)
PDE-189	TS	80	Shroud box (level G–upper top)
PDE-200	BUN	28	Bundle transient
PDE-203	TS	28	Test section transient
PDE-204	TS	43	Bundle transient
PDE-251	BI1	43	Bundle inlet upper spool-piece
PDE-261	BUN	43	Bundle inlet lower spool-piece
PDE-271	SPO	43	Split downcomer transient
			Flow
FE-3	TSI	109	Test section inlet volumetric
FE-18A	TSI	108	Test section inlet steady-state volumetric
FE-19	SHI	109	Standard horizontal inlet spool-piece volumetric
FE-34	SHO	109	Standard horizontal outlet spool-piece volumetric
FE-166	SVI	109	Standard vertical inlet spool-piece volumetric
FE-202	BO1	109	Bundle outlet spool-piece volumetric
FE-216	SVO	109	Standard vertical outlet spool-piece volumetric
FE-250	BI1	109	Bundle inlet upper spool-piece volumetric
FE-260	BI2	109	Bundle outlet lower spool-piece volumetric
FE-280	SPO	109	Shroud plenum outlet bypass line volumetric
FE-282	TSO	107	Test section outlet manifold high-range volumetric
FE-283	TSO	107	Test section outlet manifold low-range volumetric
FE-927	SPO	107	Shroud plenum outlet bypass line volumetric

Table 6.1 (continued)

Instrument application No.	Location	Type	Measurement
			Momentum flux
FMFE-22	SHI	35	Standard horizontal inlet spool-piece
FMFE-38	SHO	35	Standard horizontal outlet spool-piece
FMFE-170	SVI	35	Standard vertical inlet spool-piece
FMFE-206	BO1	35	Bundle outlet spool-piece
FMFE-220	SVO	35	Standard vertical outlet spool-piece
FMFE-254	BI2	35	Bundle inlet upper spool-piece
FMFE-264	BI1	35	Bundle outlet lower spool-piece
			Level
LE-100	PZR	105	Pressurizer liquid
			Pressure
PE-26	SHI	23	Standard horizontal inlet spool-piece transient
PE-27	RDI	23	Inlet blowdown plenum transient
PE-42	SHO	23	Standard horizontal outlet spool-piece transient
PE-43	RDO	23	Outlet blowdown plenum transient
PE-106	PRZ	23	Pressurizer vapor transient
PE-156	TSI	23	Test section inlet transient
PE-174	SVI	23	Standard vertical inlet spool-piece transient
PE-201	TSO	23	Test section outlet transient
PE-209	BO1	23	Bundle outlet spool-piece transient
PE-224	SVO	23	Standard vertical outlet spool-piece transient
PE-258	BI1	23	Bundle inlet upper spool-piece transient
PE-268	BI1	23	Bundle inlet lower spool-piece transient
PE-282	TSO	23	Test section outlet manifold high-range transient
PE-283	TSO	23	Test section outlet manifold low-range transient
PE-425	RDI	23	Inlet blowdown line transient
PE-427	RDO	23	Outlet blowdown line transient
			Speed
SE-72	PPU	36	Primary pump
			Temperature
TE-24	SHI	6	Standard horizontal inlet spool-piece
TE-40	SHI	6	Standard horizontal outlet spool-piece
TE-172	SVI	6	Standard vertical inlet spool-piece
TE-208	BO1	6	Bundle outlet spool-piece
TE-222	SVO	6	Standard vertical outlet spool-piece
TE-256	BI1	6	Bundle inlet upper spool-piece
TE-266	BI1	6	Bundle inlet lower spool-piece
TE-281	TSO	6	Test section outlet manifold low-range
TE-282	TSO	6	Test section outlet manifold high-range
TE-927	SPO	6	Shroud plenum outlet bypass line

[a]Measurement locations may vary. See specific test description in Chap. 5.

Table 6.2. THTF sensor description

Measurement	Designation	Type code	Type	Error	Required response
			Temperature		
Rod sheath	TRS	1	0.51-mm-OD (0.020-in.)[a] type-K thermocouple	3.7 K (6.7°F) < 623 K (662°F) 1% Rdg[b] > 623 K (662°F)	12 ms (13 Hz)
Rod middle	TRM	2	0.51-mm-OD (0.020-in.)[a] type-K thermocouple	3.7 K (6.7°F) < 623 K (662°F) 1% Rdg > 623 K (662°F)	12 ms (13 Hz)
Subchannel	TSC	3	1.02-mm-OD (0.040-in.) type-K thermocouple	3.7 K (6.7°F) < 623 K (662°F) 1% Rdg > 623 K (662°F)	140 ms (1.1 Hz)
Shroud wall	TSW	4	1.57-mm-OD (0.060-in.) type-K thermocouple	3.7 K (6.7°F) < 623 K (662°F) 1% Rdg > 623 K (662°F)	350 ms (0.45 Hz)
Miscellaneous process	TMP	5	3.2-mm-OD (0.125-in.) type-K Namac thermocouple	3.7 K (6.7°F) < 623 K (662°F) 1% Rdg > 623 K (662°F)	870 ms (0.2 Hz)
Loop and process	TLP	6	6.4-mm-OD (0.250-in.) type-K thermocouple	3.7 K (6.7°F) < 623 K (662°F) 1% Rdg > 623 K (662°F)	18 ms (9 Hz)
Spacer grid	TSG	7	1.02-mm-OD (0.040-in.) type-K thermocouple	3.7 K (6.7°F) < 623 K (662°F) 1% Rdg > 623 K (662°F)	140 ms (1.1 Hz)
Array rod	TAR	8	1.02-mm-OD (0.040-in.) type-K thermocouple	3.7 K (6.7°F) < 623 K (662°F) 1% Rdg > 623 K (662°F)	140 ms (1.1 Hz)
O-ring	TOR	9	0.51-mm-OD (0.020-in.) type-K thermocouple	3.7 K (6.7°F) < 623 K (662°F) 1% Rdg > 623 K (662°F)	12 ms (13 Hz)
Shroud box	TSB	10	1.57-mm-OD (0.060-in.) type-K thermocouple	3.7 K (6.7°F) < 623 K (662°F) 1% Rdg > 623 K (662°F)	350 ms (0.45 Hz)
Base loop	TBL	71	Platinum, linearized resistance thermometer device	0.08 K (1.9°F) + 3/8% Rdg	10 s (0.016 Hz)
Loop differential	TLD	99	Platinum, linearized resistance thermometer device	3.8 K (6.8°F)	10 s (0.016 Hz)
Loop base	TLB	110	Platinum, linearized resistance thermometer device	0.08 K (1.9°F) + 3/8% Rdg	10 s (0.016 Hz)
			Pressure		
Operation	PBT		Bourdon tube gage	0.1% FS[c]	300 ms (0.53 Hz)
Fast response	PS1	23,29	Strain gage pressure element	1% FS	0.16 ms (1000 Hz)

Table 6.2 (continued)

Measurement	Designation	Type code	Type	Error	Required response
			Pressure (continued)		
Regular-response	PS2	25	Strain gage pressure element	1% FS	0.32 ms (500 Hz)
Miscellaneous pressure	PFB	24	Force balance pressure sensor	1% FS	300 ms (0.53 Hz)
			Differential pressure		
System	DPS	26-28, 41-43	Strain gage differential pressure element	2% FS minimum to 9.9% FS maximum	0.32 ms (500 Hz)
Shroud box	DPC	75,80	Capacitance differential pressure element	1.5% FS[d]	128 ms (1.25 Hz)
Operation	DPF	97,98	Force balance differential pressure element	2.0% FS	300 ms (0.53 Hz), 38 ms (4 Hz)
			Flow		
Fluid	FTM	95,96	Turbine flow meter (bidirectional)	4.1% Rdg[e]	1 ms (160 Hz) minimum to 18 ms (9 Hz) maximum
Fluid	FOP	107,108	Flow orifice plate with force balance differential pressure cell	2.5% FS	300 ms (0.53 Hz)
Fluid	FVT	109	Turbine flow meter	4.1% Rdg	1 ms (160 Hz) minimum to 18 ms (9 Hz) maximum
			Momentum flux		
Fluid	MF	35,40	Strain gage drag disk (bidirectional)	56% Rdg < 10% FS, 19% Rdg > 10% FS	16 ms (10 Hz)
			Density		
System	DGS	106	Gamma attenuation	10.4% FS	16 ms (10 Hz)
Bundle	DBG	111	Gamma attenuation	NA[f]	16 ms (10 Hz)

Table 6.2 (continued)

Measurement	Designation	Type code	Type	Error	Required response
			Voltage		
Generator	VG	33	Voltage divider	1.1% Rdg	50 ms (32 Hz)
			Current		
Rod	IR	31	Shunt	1.1% Rdg	50 ms (32 Hz)
Generator	IG	32	Shunt	1.1% Rdg	50 ms (32 Hz)
			Power		
Pump	PWR	34	Current and voltage transformers	0.5 kW or 0.3% Rdg, whichever is greater	150 ms (1 Hz)
			Initiation of blowdown		
Reference	BW	37	Time of rupture disk failure (To)	30 ms	20 ms (8 Hz)
			Liquid level		
System	LSF	105,113	Force balance differential pressure element	0.6% FS	300 ms (0.53 Hz)
Bundle	LBP	50	Experimental INEL level probe	NA	NA
			Speed		
Primary pump	SPP	36	Tachometer	20 rpm	150 ms (1 Hz)
			Position		
Densitometer (bundle)	ZBD	76,77	Potentiometer	0.5% Rdg	NA

[a]Special FRS couples are 0.38-mm-OD (0.015-in.) type-K thermocouples with 7-ms (23-Hz) response.

[b]% Rdg = percent of instrument reading.

[c]% FS = percent of instrument full-scale reading.

[d]For 37.5-kPa (150-in.) service the error is 1.1% FS with response of 74 ms (2.2 Hz).

[e]2.5% Rdg for flow turbine meter using flow technology signal conditioning.

[f]NA = not applicable.

Table 6.3. Data sensor locations and systems characteristics

Location/ measurement	Purpose	Instrument application No.	Sensor designation	Instrument type code	Range	Error	Required response [ms (Hz)]	Logging system
					Main pump			
Inlet pressure	I	PE-76	PS1	23	20,700 kPa (3000 psi)	1% FS	0.16 (1000)	CCDAS
Differential pressure	I, II	PDE-78	DPS	27	±6900 kPa (±1000 psi)	3.1% FS	0.32 (500)	CCDAS
Inlet fluid temperature	III	TE-74	TMP	5	273–1309 K (32–1900°F)	3.7 K < 623 K (6.7°F < 662°F) 1% Rdg > 623 K (662°F)	870 (0.2)	CCDAS
Pump flow	III	FE-1A	FOP	107	1E-4 m^3/s (800 gpm)	2.5% FS	300 (2)	CCDAS
Pump speed	III	SE-72	SPP	36	100–5400 rpm	20 rpm	150 (1)	CCDAS
Pump power	III	EWE-77A	PWR	34	750 kW	0.5 kW or 0.3% Rdg, whichever is greater	150 (1)	CCDAS
Pressure downstream	I, II	PE-16	PS1	23	20,700 kPa (3000 psi)	1% FS	0.16 (1000)	CCDAS
Fluid discharge temperature	II, III	TE-4B, 568	TLB	110	273–700 K (32–800°F)	0.08 K (1.9°F) + 3.8% Rdg	10^4 (0.016)	CCDAS
Outlet spool transient pressure	I	PE-88	PS1	23	20,700 kPa (3000 psi)	1% FS	0.16 (1000)	CCDAS
Outlet spool momentum flux	I	FMFE-84	MF	40	±0.2E5 $kg/m \cdot s^2$ (±1.4E4 $lb/ft \cdot s^2$) ±2.1E5 $kg/m \cdot s^2$ (±1.4E5 $lb/ft \cdot s^2$)	56% Rdg 19% Rdg	16 (10)	CCDAS
Outlet spool velocity	I	FE-232	FVT	109	±0.6E-4 m^3/s (±1 gpm) ±6.1E-4 m^3/s (±10 gpm)	2.5% Rdg	8 (20) 1 (160)	CCDAS
					Pressurizer			
Vapor space pressure	I	PE-106	PS1	23	20,700 kPa (3000 psi)	1% FS	0.16 (1000)	CCDAS
Vapor space temperature	I	TE-1	TLP	6	273–1309 K (32–1900°F)	3.7 K < 623 K (6.7°F < 662°F) 1% Rdg > 623 K (662°F)	18 (9)	CCDAS
Vapor space temperature	II	TE-101	TLB	110	273–700 K	0.08 K (1.4°F) + 3/8% Rdg	10^4 (0.016)	CCDAS
Outlet fluid temperature	I	TE-2	TLP	6	273–1309 K	3.7 K < 623 K (6.7°F < 662°F) 1% Rdg > 623 K (662°F)	18 (9) 18 (9)	CCDAS
Liquid level	IV	LE-100	LSF	105	3.81 m (150 in.)	0.6% FS	300 (0.53)	CCDAS, PR
Steam killer air vent temperature	IV	TE-901	TMP	5	273–1309 K (32–1900°F)	3.7 K < 623 K (6.7°F < 662°F) 1% Rdg > 623 K (662°F)	870 (0.2)	CCDAS
Velocity	I	FE-280	FVT	109	±0.6E-4 m^3/s (±1.0 gpm) ±6.1E-4 m^3/s (±10 gpm)	2.5% Rdg	8 (20) 1 (160)	CCDAS

Table 6.3 (continued)

Location/ measurement	Purpose	Instrument application No.	Sensor designation	Instrument type code	Range	Error	Required response [ms (Hz)]	Logging system
					Pump bypass heat exchanger			
Primary outlet temperature	III	TE-5B	TMP	5	273–1309 K (32–1900°F)	3.7 K < 623 K (6.7°F < 662°F) 1% Rdg > 623 K (662°F)	870 (0.2)	CCDAS
Secondary outlet temperature	II, III	TE-13,557	TLB	110	273–700 K (32–800°F)	0.08 K (1.9°F) + 3/8% Rdg	10^4 (0.016)	CCDAS, PR
Secondary flow	III	FE-550	FTM	96	±0.3E-3 m^3/s (±5 gpm) ±3.2E-3 m^3/s (±50 gpm)	4.1% Rdg	8 (20) 1 (160)	CCDAS, PR
					Main heat exchangers			
Primary upstream pressure	I	PE-44	PS1	23	20,700 kPa (3000 psi)	1% FS	0.16 (1000)	CCDAS
Primary bypass transient differential pressure	II	PDE-46	DPS	26	±1380 kPa (±200 psi)	3.1% FS	0.32 (500)	CCDAS
Primary steady-state differential pressure	III	PDE-48	DPF	97	166 kPa (24 psi)	2.0% FS	300 (0.53)	CCDAS, PR
Primary mixing tee temperature	III	TE-28B	TBL	71	273–700 K (32–800°F)	0.08 K (1.9°F) + 3/8% Rdg	10^4 (0.016)	CCDAS
Secondary outlet temperature	II, III	TE-52/525, TE-54/627, TE-56/727	TLB	110	273–700 K (32–800°F)	0.08 K (1.9°F) + 3/8% Rdg	10^4 (0.016)	CCDAS, PR
Secondary flow	III	FE-522, FE-620, FE-720	FTM	95	±0.9E-3 m^3/s (±15 gpm) ±9.5E-3 m^3/s (±150 gpm)	4.1% Rdg	11 (15) 1.2 (133)	CCDAS, PR
Secondary inlet pressure	III	PE-526	PS1	29	2400 kPa (350 psi)	1% FS	0.16 (1000)	CCDAS
Spool fluid pressure	I	PE-58, PE-63, PE-68	PS1	23	20,700 kPa (3000 psi)	1% FS	0.16 (1000)	CCDAS
Spool fluid temperature	I	TE-57, TE-62, TE-67	TLP	6	273–1309 K (32–1900°F)	3.7 K < 623 K (6.7°F < 662°F) 1% Rdg > 623 K (662°F)	18 (9)	CCDAS
Spool momentum flux	I	FMFE-55, FMFE-61, FMFE-66	MF	40	±0.2E5 $kg/m \cdot s^2$ (±1.4E4 $lb/ft \cdot s^2$) ±2.1E5 $kg/m \cdot s^2$ (±1.4E5 $lb/ft \cdot s^2$)	56% Rdg 19% Rdg	16 (10)	CCDAS

Table 6.3 (continued)

Location/ measurement	Purpose	Instrument application No.	Sensor designation	Instrument type code	Range	Error	Required response [ms (Hz)]	Logging system
					Main heat exchangers (continued)			
Spool velocity	I	FE-51,FE-59, FE-64	FVT	109	±1.3E-3 m³/s (±22 gpm) ±1.4E-2 m³/s (±225 gpm)	4.1% Rdg	13 (12) 2 (80)	CCDAS
Spool differential pressure	I	PDE-53, PDE-60 PDE-65	DPS	28	±345 kPa (±50 psi)	3.1% FS	0.32 (500)	CCDAS
					Test section			
Test bundle inlet pressure	I	PE-156	PS1	23	20,700 kPa (3000 psi)	1% FS	0.16 (1000)	CCDAS
Test bundle outlet pressure	I	PE-201	PS1	23	20,700 kPa (3000 psi)	1% FS	0.16 (1000)	CCDAS
Test bundle differential	I-III	PDE-200	DPS	28	±345 kPa (±50 psi)	3.1% FS	0.32 (500)	CCDAS
Shroud-box differential pressure	I	PDE-180 Series	DPC	75,80	37.5 kPa (150 in.) 6.25, 7.5 kPa (25, 30 in.)	1.5% FS 1.1% FS	131 (1.2) 74 (2.2)	CCDAS
Shroud-box differential cold-leg temperature	I	TE-925,926	TMP	5	273-1309 K (32-1900°F)	3.7 K < 623 K (6.7°F < 662°F) 1% Rdg > 623 K (662°F)	870 (0.2)	CCDAS
Volume plug temperature	I	TE-923,924	TMP	5	273-1309 K (32-1900°F)	3.7 K < 623 K (6.7°F < 662°F) 1% Rdg > 623 K (662°F)	870 (0.2)	CCDAS
Miscellaneous bundle differential pressure	III	PDE-199	DPS	43	±41 kPa (±6 psi)	3.9% FS	0.32 (500)	CCDAS
Fuel pin temperature	I-III	TE-300 Series (720 maximum)	TRS, TRM	1,2	273-1309 K (32-1900°F)	3.7 K < 623 K (6.7°F < 662°F) 1% Rdg > 623 K (662°F)	12 (13)	CCDAS, TI
Inlet line fluid temperature	I-III	TE-160	TLP	6	273-1309 K (32-1900°F)	3.7 K < 623 K (6.7°F < 662°F) 1% Rdg > 623 K (662°F)	18 (9)	CCDAS
Outlet line fluid temperature	I-III	TE-210A,B	TLP	6	273-1309 K (32-1900°F)	3.7 K < 623 K (6.7°F < 662°F) 1% Rdg > 623 K (662°F)	18 (9)	CCDAS, PR
Bundle inlet temperature	I	TE-150 Series (4 maximum)	TLP	6	273-1309 K (32-1900°F)	3.7 K < 623 K (6.7°F < 662°F) 1% Rdg > 623 K (662°F)	18 (9)	CCDAS

Table 6.3 (continued)

Location/ measurement	Purpose	Instrument application No.	Sensor designation	Instrument type code	Range	Error	Required response [ms (Hz)]	Logging system
				Test section (continued)				
Shroud-box temperature	I	TE-270 Series (24 maximum)	TSB	10	273–1309 K (32–1900°F)	3.7 K < 623 K (6.7°F < 662°F) 1% Rdg > 623 K (662°F)	18 (9)	CCDAS
Voltage across bundle	I–III	EEE-9–12	VG	33	300 V	1.1% Rdg	50 (3)	CCDAS
Individual rod current	I–III	E1E-1300 Series (60 maximum)	IR	31	800 A	1.1% Rdg	50 (3)	CCDAS
Individual generator current	I–III	EiE-9–12	IG	32	1000 A	1.1% Rdg	50 (3)	CCDAS
Outlet subchannel fluid temperature	I,II	TE-1200 Series (81 maximum)	TSC	3	273–1309 K (32–1900°F)	3.7 K < 623 K (6.7°F < 662°F) 1% Rdg > 623 K (662°F)	140 (1.1)	CCDAS
Outlet line pressure	II,III	PE-32	PFB	24	3400–27,000 kPa (500–3900 psi)	1% FS	300 (0.53)	CCDAS
Bundle density	I	DE-336U, 346L	DGB	111	1000 kg/m³ (62.4 lb/ft³)	104 kg/m³ (6.5 lb/ft³)	16 (10)	CCDAS
Densitometer temperature	I	TE-936	TMP	5	273–1309 K (32–1900°F)	3.7 K < 623 K (6.7°F < 662°F) 1% Rdg > 623 K (662°F)	870 (0.2)	CCDAS
Bundle density instrument position	I,III	ZE-336U, 346L	ZBD	76,77	0.59–3.92 m (23.5–155 in.) 0–3.33 m (0–131 in.)	0.5% Rdg	NA	CCDAS
Thermocouple-array rod temperature	I–III	TE-188, 189 Series	TAR	8	273–1309 K (32–1900°F)	3.7 K < 623 K (6.7°F < 662°F) 1% Rdg > 623 K (662°F)	140 (1.1)	CCDAS
Spacer-grid temperature	I–III	TE-290 Series	TSG	7	273–1309 K (32–1900°F)	3.7 K < 623 K (6.7°F < 662°F) 1% Rdg > 623 K (662°F)	140 (1.1)	CCDAS
Shroud-wall temperature	I–III	TE-180 Series	TSW	4	273–1309 K (32–1900°F)	3.7 K < 623 K (6.7°F < 662°F) 1% Rdg > 623 K (662°F)	350 (0.45)	CCDAS
Miscellaneous system differential pressure	I,III	PDE-203,204, 251,261,271	DPS	26–28, 41,43	±25 kPa (±100 in.) ±41 kPa (±6 psi) ±124 kPa (±500 in.) ±345 kPa (±50 psi)	2% FS minimum to 9.9% FS maximum	0.32 (500)	CCDAS

Table 6.3 (continued)

Location/ measurement	Purpose	Instrument application No.	Sensor designation	Instrument type code	Range	Error	Required response [ms (Hz)]	Logging system
				Test section (continued)				
Differential pressure	III	TDE-28	TLD	99	228–283 K (±50°F)	3.8 K (6.8°F)	10^4 (0.016)	CCDAS
Inlet flow	I–III	FE-18A	FOP	108	4.4E-2 m^3/s (700 gpm 1.7E-4 m^3/s (2.7 gpm)	2.5% FS	300 (0.53)	CCDAS
Inlet to outlet fluid differential pressure	II, III	PDE-30	DPF	98	345 kPa (50 psi)	2.0% FS	300 (0.53)	CCDAS
Bundle fluid level	I	LE-1400 Series	LBP	50	±10,000 mV	NA	NA	CCDAS
Downcomer temperature	III	TE-284	TMP	5	273–1309 K (32–1900°F)	3.7 K < 623 K (6.7°F < 662°F) 1% Rdg > 623 K (662°F)	870 (0.2)	CCDAS
Inlet seal coolant supply temperature	III	TE-921, 922	TMP	5	273–1309 K (32–1900°F)	3.7 K < 623 K (6.7°F < 662°F) 1% Rdg > 623 K (662°F)	870 (0.2)	CCDAS
Inlet seal fluid velocity	III	FE-238	FOP	108 107	1.7E-4 m^3/s (2.7 gpm) 1.0E-4 m^3/s (1.6 gpm)	2.5% FS	300 (0.5)	CCDAS
				Test section outlet manifold				
Fluid flow	I	FE-927	FOP	107	1.4E-4 m^3/s (2.1 gpm)	2.5% FS	300 (0.53)	CCDAS
Upstream fluid temperature	I	TE-281	TLP	6	273–1309 K (32–1900°F)	3.7 K < 623 K (6.7°F < 662°F) 1% Rdg > 623 K (662°F)	18 (9)	CCDAS
Downstream fluid temperature	I	TE-282	TLP	6	273–1309 K (32–1900°F)	3.7 K < 623 K (6.7°F < 662°F) 1% Rdg > 623 K (662°F)	18 (9)	CCDAS
High-range flow	I	FE-282	FOP	107	2.53E-3 m^3/s (39.3 gpm)	2.5% FS	300 (0.53)	CCDAS
Low-range flow	I	FE-283	FOP	107	3.3E-4 m^3/s (5.2 gpm)	2.5% FS	300 (0.53)	CCDAS
				Bundle inlet spools				
Fluid density	I	DE-252A–C DE-262A–C	DGS	106	1000 kg/m^3 (62.4 lb/ft^3)	10.4% FS	16 (10)	CCDAS
Pressure	I	PE-258 PE-268	PS1	23	20,700 kPa (3000 psi)	1% FS	0.16 (1000)	CCDAS
Fluid temperature	I	TE-256 TE-266	TLP	16	273–1309 K (32–1900°F)	3.7 K < 623 K (6.7°F < 662°F) 1% Rdg > 623 K (662°F)	18 (9)	CCDAS

Table 6.3 (continued)

Location/ measurement	Purpose	Instrument application No.	Sensor designation	Instrument type code	Range	Error	Required response [ms (Hz)]	Logging system
					Bundle inlet spools (continued)			
Momentum flux	I	FMFE-254 FMFE-264	MF	40	±0.2E5 kg/m·s² (±1.4E lb/ft·s²) ±2.1E5 kg/m·s² (±1.4E5 lb/ft·s²)	56% Rdg 19% Rdg	16 (10)	CCDAS
Velocity	I	FE-250 FE-260	FVT	109	±0.6E-2 m³/s (±100 gpm) ±6.1E-2 m³/s (±1000 gpm)	4.1% Rdg	18 (9) 2 (81)	CCDAS
					Standard vertical inlet spool			
Fluid density	I	DE-168	DGS	106	1000 kg/m³ (62.4 lb/ft³)	10.5% FS	16 (10)	CCDAS
Pressure	I	PE-174	PS1	23	20,700 kPa (3000 psi)	1% FS	0.16 (1000)	CCDAS
Fluid temperature	I	TE-172	TLP	6	273–1309 K (32–1900°F)	3.7 K < 623 K (6.7°F < 662°F) 1% Rdg > 623 K (662°F)	18 (9)	CCDAS
Momentum flux	I	FMFE-170	MF	35	±0.1E5 kg/m·s² (±0.7E4 lb/ft·s²) ±1.0E5 kg/m·s² (±7.0E4 lb/ft·s²)	56% Rdg 19% Rdg	16 (10)	CCDAS
Velocity	I	FE-166	FVT	109	±0.6E-2 m²/s (±100 gpm) ±6.1E-2 m²/s (±1000 gpm)	4.1% Rdg	18 (9) 2 (80)	CCDAS
Differential pressure	I	PDE-167	DPS	26	±1380 kPa (±200 psi)	3.1% FS	0.32 (500)	CCDAS
					Standard horizontal inlet spool			
Fluid density	I	DE-20	DGS	106	1000 kg [m³ (62.4 lb/ft³)]	10.4% FS	16 (10)	CCDAS
Pressure	I	PE-26	PS1	23	20,700 kPa (3000 psi)	1% FS	0.16 (1000)	CCDAS
Fluid temperature	I	TE-24	TLP	6	273–1309 K (32–1900°F)	3.7 K < 623 K (6.7°F < 662°F) 1% Rdg > 623 K (662°F)	18 (9)	CCDAS
Momentum flux	I	FMFE-22	MF	35	±0.1E5 kg/m·s² (±0.7E4 lb/ft·s²) ±1.0E5 kg/m·s² (±7.0E4 lb/ft·s²)	56% Rdg 19% Rdg	16 (10)	CCDAS
Velocity	I	FE-19	FVT	109	±0.6E-2 m³/s (±100 gpm) ±6.1E-2 m³ (±1000 gpm)	4.1% Rdg	18 (9) 2 (80)	CCDAS
Differential pressure	I	PDE-21	DPS	26	±1380 kPa (±200 psi)	3.1% Rdg	0.32 (500)	CCDAS

Table 6.3 (continued)

Location/ measurement	Purpose	Instrument application No.	Sensor designation	Instrument type code	Range	Error	Required response [ms (Hz)]	Logging system
					Bundle outlet spool			
Fluid density	I	DE-204A-C	DGS	106	1000 kg/m³ (62.4 lb/ft³)	10.4% FS	16 (10)	CCDAS
Pressure	I	PE-209	PS1	23	20,700 kPa (3000 psi)	1% FS	0.16 (1000)	CCDAS
Fluid temperature	I	TE-208	TLP	6	273–1309 K (32–1900°F)	3.7 K < 623 K (6.7°F < 662°F) 1% Rdg > 623 K (662°F)	18 (9)	CCDAS
Momentum flux	I	FMFE-206	MF	35	±0.1E5 kg/m·s² (±0.7E4 lb/ft·s²) ±1.0E5 kg/m·s² (±7.0E4 lb/ft·s²)	56% Rdg 19% Rdg	16 (10)	CCDAS
Velocity	I	FE-202	FVT	109	±0.6E-2 m³/s (±100 gpm) ±6.1E-2 m³/s (±1000 gpm)	4.1% Rdg	18 (9) 2 (80)	CCDAS
					Standard vertical outlet spool			
Fluid density	I	DE-218	DGS	106	1000 kg/m³ (62.4 lb/ft³)	10.4% FS	16 (10)	CCDAS
Pressure	I	PE-224	PS1	23	20,700 kPa (3000 psi)	1% FS	0.16 (1000)	CCDAS
Fluid temperature	I	TE-222	TLP	6	273–1309 K (32–1900°F)	3.7 K < 623 K (6.7°F < 662°F) 1% Rdg > 623 K (662°F)	18 (9)	CCDAS
Momentum flux	I	FMFE-220	MF	35	±0.1E5 kg/m·s² (±0.7E4 lb/ft·s²) ±1.0E5 kg/m·s² (±7.0E4 lb/ft·s²)	56% Rdg 19% Rdg	16 (10)	CCDAS
Velocity	I	FE-216	FVT	109	±0.6E-2 m³/s (±100 gpm) ±6.1E-2 m³/s (±1000 gpm)	4.1% Rdg	18 (9) 2 (80)	CCDAS
Differential pressure	I	PDE-217	DPS	26	±1380 kPa (±200 psi)	3.1% FS	0.32 (500)	CCDAS
					Standard horizontal outlet spool			
Fluid density	I	DE-36	DGS	106	1000 kg/m³ (62.4 lb/ft³)	10.4% FS	16 (10)	CCDAS
Pressure	I	PE-42	PS1	23	20,700 kPa (3000 psi)	1% FS	0.16 (1000)	CCDAS
Fluid temperature	I	TE-40	TLP	6	273–1309 K (32–1900°F)	3.7 K < 623 K (6.7°F < 662°F) 1% Rdg > 623 K (662°F)	18 (9)	CCDAS
Momentum flux	I	FMFE-38	MF	35	±0.1E5 kg/m·s² (±0.7E4 lb/ft·s²) ±1.0E5 kg/m·s² (±7.0E4 lb/ft·s²)	56% Rdg 19% Rdg	16 (10)	CCDAS

Table 6.3 (continued)

Location/ measurement	Purpose	Instrument application No.	Sensor designation	Instrument type code	Range	Error	Required response [ms (Hz)]	Logging system
					Standard horizontal outlet spool (continued)			
Velocity	I	FE-34	FVT	109	±0.6E-2 m³/s (±100 gpm) ±6.1E-2 m³/s (±1000 gpm)	4.1% Rdg	18 (9) 2 (80)	CCDAS
Differential pressure	I	PDE-35	DPS	26	±1380 kPa (±200 psi)	3.1% FS	0.32 (500)	CCDAS
					Pump bypass spool piece			
Pressure	I	PE-15	PS1	23	20,700 kPa (3000 psi)	1% FS	0.16 (1000)	CCDAS
Fluid temperature	I	TE-6	TLP	6	273–1309 K (32–1900°F)	3.7 K < 623 K (6.7°F < 662°F) 1% Rdg > 623 K (662°F)	18 (9)	CCDAS
Momentum flux	I	FMFE-14	MF	40	±0.2E5 kg/m·s² (±1.4E4 lb/ft·s²) ±2.1E5 kg/m·s² (±1.4E5 lb/ft·s²)	56% Rdg 19% Rdg	16 (10)	CCDAS
Velocity	I	FE-3	FVT	109	±1.3E-3 m³/s (±22 gpm) ±1.4E-2 m³/s (±225 gpm)	4.1% Rdg	13 (12) 2 (80)	CCDAS
					Pressurizer line spool piece			
Pressure	I	PE-118	SP1	23	20,700 kPa (3000 psi)	1% FS	0.16 (1000)	CCDAS
Fluid temperature	I	TE-116	TLP	6	273–1309 K (32–1900°F)	3.7 K < 623 K (6.7°F < 662°F) 1% Rdg > 623 K (662°F)	18 (9)	CCDAS
Momentum flux	I	FMFE-114	MF	40	±0.25E5 kg/m·s² (±1.4E4 lb/ft·s²) ±2.1E5 kg/m·s² (±1.4E5 lb/ft·s²)	56% Rdg 19% Rdg	16 (10)	CCDAS
Velocity	I	FE-110	FVT	109	±1.3E-3 m³/s (±22 gpm) ±1.4E-2 m³/s (±225 gpm)	4.1% Rdg	13 (12) 2 (80)	CCDAS
Differential pressure	I	PDE-111	DPS	28	±345 kPa (±50 psi)	3.1% FS	0.32 (500)	CCDAS
					Shroud plenum			
Inlet pressure	I	PE-276	PS1	23	20,700 kPa (3000 psi)	1% FS	0.16 (1000)	CCDAS
Outlet pressure	I	PE-286	PS1	23	20,700 kPa (3000 psi)	1% FS	0.16 (1000)	CCDAS
Fluid temperature	I	TE-920	TMP	5	273–1309 K (32–1900°F)	3.7 K < 623 K (6.7°F < 662°F) 1% Rdg > 623 K (662°F)	870 (0.2)	CCDAS
Velocity	I	FE-270	FVT	109	±0.6E-2 m³/s (±100 gpm) ±6.1E-2 m³/s (±1000 gpm)	4.1% Rdg	18 (9) 2 (80)	CCDAS

Table 6.3 (continued)

Location/ measurement	Purpose	Instrument application No.	Sensor designation	Instrument type code	Range	Error	Required response [ms (Hz)]	Logging system
					Shroud plenum (continued)			
Bypass temperature	I	TE-927	TMP	5	273-1309 K (32-1900°F)	3.7 K < 623 K (6.7°F < 662°F) 1% Rdg > 623 K (662°F)	870 (0.2)	CCDAS
Annulus pressure	I	PE-761	NA	105	1408 m (5.5E4 in.)	0.6% FS	300 (0.53)	CCDAS
Annulus level	I	LE-760	LSF	113	1.18 m (46 in.)	0.6% FS	300 (0.53)	CCDAS
					Pressure-suppression system			
Receiver pressure	I,III	PE-412	PS2	25	±1380 kPa (±200 psi)	1% FS	0.32 (500)	CCDAS
Recirculating fluid temperature	III	TE-408B	TMP	5	273-1309 K (32-1900°F)	3.7 K < 623 K (6.7°F < 662°F) 1% Rdg > 623 K (662°F)	870 (0.2)	CCDAS
Recirculating fluid flow	III	FT-406	FOP	NA	9.2E-2 m^3/s (1500 gpm)	8% FS	10^3 (0.16)	CCDAS
					Demineralized water			
Header pressure	III	PE-616	PS1	29	2400 kPa (350 psi)	1% FS	0.16 (1000)	CCDAS
6-in. header temperature	III	TE-615	TLB	110	273-700 K (32-800°F)	0.08 K (1.9°F) + 3/8% Rdg	10^4 (0.016)	CCDAS
4-in. header temperature	III	TE-520B	TMP	5	273-1309 K (32-1900°F)	3.7 K < 623 K (6.7°F < 662°F) 1% Rdg > 623 K (662°F)	870 (0.2)	CCDAS
Purification outlet temperature	III	TE-521	TMP	5	273-1309 K (32-1900°F)	3.7 K < 623 K (6.7°F < 662°F) 1% Rdg > 623 K (662°F)	870 (0.2)	CCDAS
					Blowdown lines			
Initiation of blowdown	I	XE-430A,B	BW	37	5000 mV	30 ms	20 (8)	CCDAS
Rupture disk buffer pressure	III	PE-979,989	PBT	NA	10,350 kPa (1500 psi)	0.5% FS	300 (0.53)	PI
Blowdown disk buffer pressure	III	PE-454,474 PE-425,427	PS1	23	20,700 kPa (3000 psi)	1% FS	0.16 (1000)	CCDAS
Blowdown line fluid velocity	III	FE-440,460	FVT	109	±0.6E-2 m^3/s (±100 gpm) ±6.1E-2 m^3/s (±1000 gpm)	4.1% Rdg	18 (9) 2 (80)	CCDAS
Plenum pressure	I	PE-27,43	PS1	23	20,700 kPa (3000 psi)	1% FS	0.16 (1000)	CCDAS
Plenum temperature	I	TE-29,45	TLP	6	273-1309 K (32-1900°F)	3.7 K < 623 K (6.7°F < 662°F) 1% Rdg > 623 K (662°F)	18 (9)	CCDAS

between 1 and 127 and classifies instruments as to manufacturer and sensor type, output, and range) as described in Appendix D.

Table 6.3 lists the measurements made in the THTF, the type, and the location. Many of the more routine operational measurements involved in ensuring reliable operation are not enumerated. Only those logged by the CCDAS and those necessary to establish base conditions in the facility at the beginning of a test are listed. The intended use of the data derived from each measurement is defined by a Roman numeral in the "Purpose" column; in the code for the application, I indicates primary transient and steady-state test analysis data, II indicates steady-state data prior to blowdown, and III indicates operational and base conditions data.

The next entries indicate the instrument application number of instruments associated with each measurement and the type of sensor used. The range, error, and required response are given for each measurement system (defined as the combination of a sensor, signal-conditioning equipment, and a readout of data-logging device). The "Error" column gives the total 2-σ error band for each system either as a percentage of full scale (% FS), percentage of reading (% Rdg), or an absolute value (such as 4°F). The "Required response" column is based on the assumption that each system, from sensor to readout, responds as a first-order system. This column defines the maximum time constant (i.e., time required for readout to indicate 63.2% change in response to a step change in the measured variable) and minimum frequency response acceptable for obtaining the desired data. The frequency f is defined by $f = 1/2\pi t$, where t is the system time constant. The column labeled "Logging system" gives the data logger or final readout device for each measurement; the code used in this column is data acquisition system (CCDAS), main control panel recorder (PR), main control panel indicator (PI), and multichannel temperature monitor (TS). More detailed descriptions of the various sensors, along with some considerations on their application in the THTF, will follow.

6.1.2.1 Temperature. Temperature measurements are required to (1) detect the onset of CHF and film boiling and permit calculation of heat transfer coefficients in the test bundle; (2) determine the subchannel fluid temperature distribution; (3) establish heat balances in the test section and heat exchangers; (4) monitor the liquid and steam space in the pressurizer; (5) detect pressurizer voiding during a transient; and (6) determine mass, energy, and momentum balances during a transient. Primary temperature measurements are taken to provide the following data:

1. cladding and centerline temperature of heater rods in test bundle,
2. subchannel fluid outlet temperature,
3. fluid temperatures at the inlet and outlet to the test section,
4. temperatures in the fluid adjacent to the heater rod shroud-box walls,
5. temperature of test section fluid at grid-spacer locations,
6. fluid temperature in the primary loop at the inlet and outlet of the heat exchangers,
7. temperature in the steam and water spaces of the pressurizer,
8. fluid temperature at the bottom of the pressurizer,
9. fluid temperature near each flow detection station,
10. temperature on the secondary side of the primary loop heat exchangers,

11. fluid temperature in the test section inlet plenum,
12. temperature of the shroud-box wall at nine levels, and
13. fluid temperature in the bundle along thermocouple-array rods.

Chromel-Alumel [sheathed, ungrounded-junction, and exposed-junction (Nanmac)] thermocouples and platinum resistance thermometers (RTDs) are used in this facility to measure temperature. The RTDs are used for precision steady-state measurement to establish base temperature conditions in the loop prior to blowdown and during steady-state tests. Associated with each RTD is the excitation and signal-conditioning equipment necessary to sense the resistance change with temperature. This auxiliary equipment consists either of a constant current source and readout of the emf across the RTD (for data signals) or of a Wheatstone bridge instrument with a current output proportional to the resistance change (for process control signals).

Stainless-steel-sheathed, magnesium-oxide-insulated Chromel-Alumel thermocouples are used extensively to obtain transient and steady-state test data; to reduce perturbations in heat flux and surface temperature measurements caused by the thermocouples in the FRS rods, ~0.08 cm (0.03 in.) of the magnesium oxide insulation was removed from the thermocouple sheath near the junction and replaced with boron nitride for all FRS thermocouples. Sheath couples in the indirect heaters have outside diameters of 20 mils [final special replacement rods installed during the bundle modification in August 1980 were swaged down to 15 mils (FRS rod numbers 1, 14, 17, 21, 34, 37, 38, 50, 54, and 60)]. Exposed-junction fluid thermocouples (Nanmac Corporation) are used in a few locations where very fast temperature transients (>10 Hz) must be measured. For routine monitoring of operation temperatures, 0.125-in.-OD sheathed thermocouples are installed. All thermocouples providing test data are of premium-grade material (error band being the greater of either 2°F or ±3/8% of reading) purchased in accordance with appropriate standards. Thermocouple cold-junction compensation is handled by multiterminal 150°F reference junction compensators.

6.1.2.2 Pressure and differential pressure. Transient pressure measurements are required to (1) detect the presence (or absence) of shock waves that may influence the test results, (2) determine the thermodynamic state of the fluid, (3) detect the presence of any unusual pressure difference condition across the test section, and (4) compare with calculated results derived from analytical models that describe the flow vs pressure-drop relationship of the loop and test section. Primary pressure measurements are made to obtain

1. bundle differential pressure,
2. test bundle inlet and outlet pressures,
3. heat exchanger inlet pressure,
4. heat exchanger differential pressure,
5. pump suction inlet pressure,
6. pump differential pressure,
7. pressurizer liquid level and steam pressure, and
8. pressure at each flow-measuring station.

Line pressure gauges and force-balance transmitters are used for normal monitor and control functions during pretest operations. For steady-state sensing prior to transient blowdown tests and for steady-state tests, Foxboro and Barton electronic force-balance transmitters, Heise precision Bourdon-tube gauges, and strain-gauge transducers are used. For sensing blowdown pressure transients, Precise Sensors, Inc., air-cooled, flush-diaphragm, strain-gauge transducers are used. These latter transducers have a frequency response cutoff at about 100,000 Hz. Frequency information above 1000 Hz is not needed, and no special effort is made to record data in the higher range. For sensing transient differential pressure, BLH Electronics, Inc., strain-gauge transducers are used. The manufacturer has stated that these transducers have a frequency cutoff at about 500 Hz. For measuring differential pressure along the test section between thermocouple levels, Rosemount capacitive-type cells were used.

Pressure gauges are complete in themselves and, as such, require no signal conditioning. Strain-gauge transducers require a source of excitation, a bridge completion network, and signal amplification; commercially available equipment satisfies all three of these requirements.

The strain-gauge pressure and differential pressure transducers have a specified static error band of $\pm 0.5\%$. (Static error band is the error band applicable at room conditions in the absence of any vibration, shock, or acceleration.) However, the overall accuracy of these transducers during the blowdown transient is degraded both by high operating temperatures and by the temperature transients. Typical manufacturer specifications for environmental conditions are a compensated temperature range of +75 to 600°F, a thermal zero shift of $<0.01\%$ FS/°F over the compensated range, and a thermal sensitivity shift of $<0.010\%$ FS/°F over the compensated temperature range. In view of these data, in the worst case, the overall error for these transducers could be as much as $\pm 11\%$ of full scale under blowdown conditions. Care in installation and operation is exercised to minimize this error; for example, air-cooled standoffs (water-filled pressure tap lines) are used to isolate the transducer from the loop temperature environment (the lines for the test section differential pressure measurements are water-cooled as described in Sect. 5.2). For pressure measurements, the transducer is mounted on the end of the standoff, thus operating at a temperature considerably below the temperature of the fluid in the system; for transient differential pressure measurements, the transducer is located equidistant (in terms of tap line length) between two such taps (the actual physical location of the transducer is below both taps). An example of the differential pressure measurement system was shown earlier in Fig. 5.11(b). The air cooling should also reduce flashing of the water in the differential pressure taps.

6.1.2.3 Flow. Transient and steady-state flow measurements are required to determine the mass, energy, and momentum balances of the fluid entering and leaving the test section. Critical measurement points use bidirectional sensors for measuring volumetric flow rates and momentum flux, because flow reversals may occur during certain transient blowdown-type tests. Flow measurements are taken to provide the following information:

1. primary flow at entry to inlet and outlet blowdown rupture disk assemblies;

2. primary flow at test section inlet or outlet, or in return line to pump;
3. pump discharge flow; and
4. heat exchanger primary or secondary coolant flow.

Both single-phase (liquid and steam) and two-phase (water and steam) flow measurements are required in the THTF.

Liquid volumetric flow, where no phase change is involved, is measured directly using turbine meters or indirectly through pressure drops across orifices or in pipe elbows. Turbine meters are installed where precision and wide ranges are required. Orifices (~3% accuracy) and pipe-elbow taps (5 to 10% accuracy) serve where a narrow range or less precision, respectively, is acceptable.

Momentum flux in instrumented spool pieces is measured by drag disks. The drag disk with its flow-obstructing target positioned in the flow stream develops a signal proportional to ρv^2 (the momentum flux), where ρ and v are the fluid density and velocity, respectively. The drag target is connected to a cantilevered beam, the forces on which are measured by strain gauges. The drag disk instruments used at the THTF have been found to be temperature sensitive; the signal offset due to temperature is a function of the temperature of the cantilevered beam at the strain gauges, in turn related to the fluid temperature, which varies during testing. Therefore, a correction factor based on preblowdown or pretest calibrations with temperature must be applied to the drag disk data. Further discussion on calibration is presented in Sect. 6.3.

Two-phase flow measurements using spool-piece instruments were discussed to some extent in Chap. 4. Mass flow may be obtained using various combinations of density, volumetric flow, and momentum flux measurements. The accuracy with which measurements can be made in two-phase flow is considerably less, however, than that of single-phase flow. Reference 12 presents a study of uncertainties in mass flow calculations for THTF instrumented spool pieces.

6.1.2.4 Density. The single-beam densitometer units designed and constructed at ORNL consist of a 25-Ci ^{137}Cs monoenergetic gamma source with associated collimator, ion chamber detector, and current amplifier. Depleted uranium is used for the collimator and source shield material in the THTF application to avoid cooling problems that would exist with lead.

The individual beams of the Measurements, Inc., three-beam gamma densitometers are similar to the ORNL single-beam densitometers. The three beams radiate from a common source of 25-Ci ^{137}Cs as shown in Fig. 4.6. Various models may be used for obtaining a composite pipe density from the three beams of the densitometer.

6.1.2.5 Power. In the dc power system, currents are sensed by instrument shunts, and voltage is measured using resistive voltage dividers. Isolation amplifiers with high common-mode tolerance are used on each current and voltage measurement channel to isolate the CCDAS from the dc power system. The voltage and current supplied by each of the four dc generators are measured separately. Furthermore, the current to each FRS is measured individually. Therefore, power input can be calculated on an individual FRS basis.

6.1.2.6 Time. The time of blowdown initiation (i.e., the moment at which the rupture disks are broken) is perceived by break wires located just downstream of the rupture disks. These wires are broken by the downward openings of the rupture disks, and the consequent interruption of the continuity signal defines time t = 0. The inlet and outlet break times are monitored separately. For double-ended blowdowns (simultaneous break in both inlet and outlet legs), the time difference between the inlet and outlet ruptures has been shown to be <10 ms.

6.1.2.7 Liquid level. Sight glasses are used for local indication of liquid levels in low-pressure applications where levels change only during drain or fill operations. In high-pressure applications involving frequent changes in liquid level or where automatic or manual level control is required (such as the pressurizer), electronic differential pressure transmitters are used to provide a continuous panel-board readout and/or a signal for controlling liquid level.

6.1.3 Control and sequencing

Several automatic analog control loops are provided for controlling the operation of the THTF. The facility may be operated manually or under automatic closed-loop control during steady-state or approach-to-blowdown operations. The primary controlled variables are the base loop pressure, the base loop temperature, the primary pump flow, the test section flow, and the test section outlet pressure. These control actions are exercised through various throttling valves in the primary and secondary systems and through some controllable power supplies. Power to the FRS bundle, supplied by dc MG sets, is manually controlled during steady-state operation.

Loop actions during blowdown, however, are controlled by automatic sequencing circuits. Blowdown is always initiated manually. At blowdown, all primary control valves are hydraulically locked. On detection of blowdown, simple control sequences can be programmed for the primary pump and bundle power. The primary pump can be programmed to shut off at blowdown or continue running for a predetermined time period following blowdown. Bundle power may be programmed to vary according to an arbitrary predetermined function of time using the automatic power programmer.

6.2 Data Acquisition

As shown in Fig. 6.8, the THTF DAS consists of (1) the data sensors and associated signal-conditioning equipment; (2) the CCDAS, consisting of two high-speed, computer-controlled data acquisition subsystems, the first accommodating 256 channels and the second 1024 channels; (3) a 50-channel thermocouple display and alarm system; and (4) multichannel analog strip-chart recorders.

Test data (steady-state and blowdown transient) are recorded on the CCDAS. Selected parameters not expected to vary widely during blowdown and all process control variables are registered on analog strip-chart recorders. In some cases, individual signals may be recorded in parallel on more than one system. Systems are not paralleled where the possibility

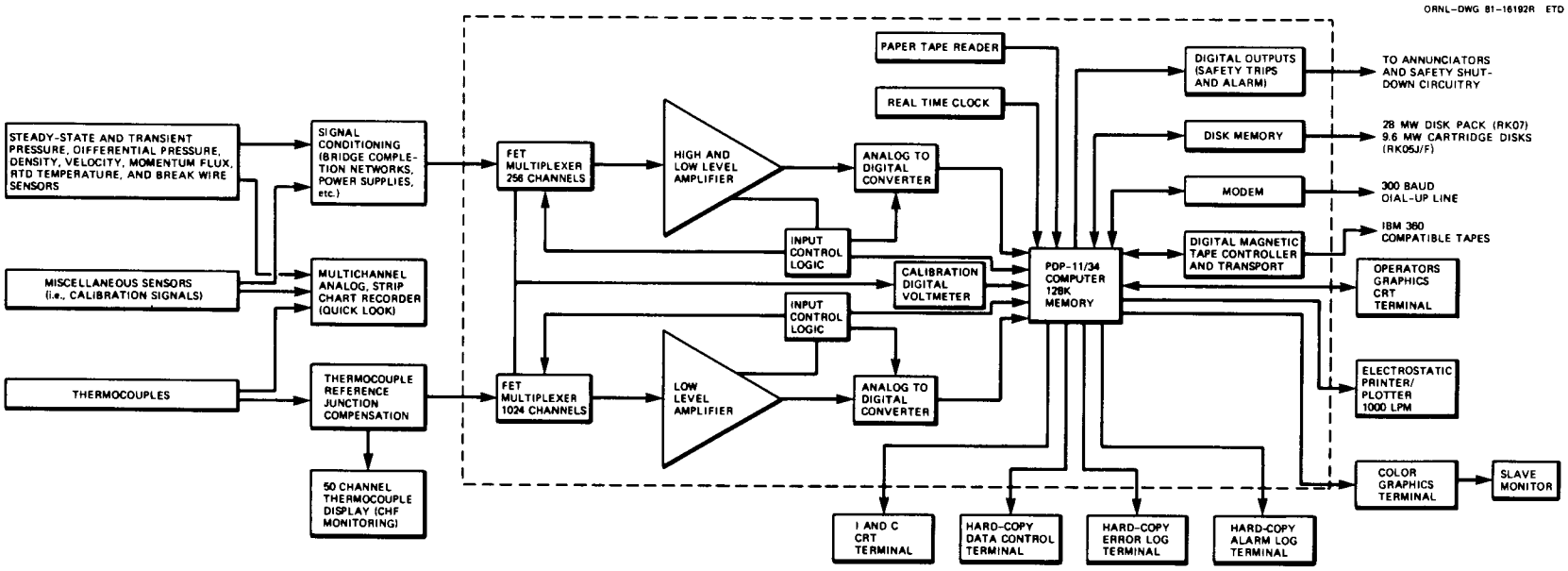

Fig. 6.8. Schematic diagram of the THTF data acquisition system (CCDAS).

of interaction exists; however, since all the DASs have high input impedance and the output impedance of most signal sources is low, interaction is not typically a problem.

All test data are recorded digitally on industry-compatible computer magnetic tape for archival storage as well as processing. On-site readout of data from the CCDAS is available via the various CCDAS consoles. The CCDAS assists in pre- and posttest checkout and calibration of process and signal-conditioning instrumentation. During a test, the CCDAS records and logs loop conditions for operator information. The CCDAS also serves as an element of the safety system by performing overtemperature checks of approximately 720 bundle thermocouples during approach to full power and the blowdown transient. An on-site "quick look" at recorded data is available through use of software routines that plot the data on the storage display unit and playback test data in video format on the color graphics console.

The time code generator is used to coordinate test data with respect to time for analytic purposes.

The analog strip-chart recorders are used primarily to obtain "quick look" data during steady-state experiments and, occasionally, for monitoring key variables during blowdown.

Additional details on system components are discussed in the following sections.

6.2.1 Signal conditioning

Much signal-conditioning equipment is required with the DASs; the types of conditioners required include (1) temperature reference ovens, (2) strain-gauge bridge completion and conditioning circuits, (3) voltage-isolation amplifiers, (4) frequency converters, (5) resistance converters, and (6) signal amplifiers.

The temperature reference ovens provide a cold-junction reference temperature for thermocouples. Since thermocouples constitute the bulk of the data sensors, most of the signal-conditioning equipment is of this type.

The strain-gauge bridge completion and conditioning equipment is associated with the strain-gauge-type transducers used for pressure, differential pressure, and drag disk measurements.

The voltage-isolation amplifiers isolate the data equipment from sensors having an excessively high common-mode voltage on the signal leads, such as the FRS current shunts.

The frequency converters alter the pulse output frequency of turbine meters to a proportional dc voltage signal.

The resistance converters are used with the resistance-type temperature sensors to convert resistance to a proportional dc signal.

Signal amplifiers provide conversion of low-level to high-level signals.

A detailed illustration of signal path from the primary instrument sensors through to the CCDAS is shown in Table 6.4. The first column, labeled "Sensors," establishes the primary sensor manufacturer, type, and model information. The column labeled "Signal conditioning" details the manufacturer, model, and type information of the next-in-line hardware

Table 6.4. Detail of THTF primary instrumentation signal path—sensor to CCDAS

Sensor	Signal conditioning	Signal to CCDAS	Remarks
	Temperature (TE)		
Sheath, 0.020-in. diam BN-backfilled Sheath, 0.015-in. diam BN-backfilled Center, 0.020-in. diam MGO-backfilled Center, 0.015-in. diam MGO-backfilled Shroud, 0.062-in. diam MGO-backfilled Thermocouple array rod, 0.040-in. diam MGO-backfilled Grid-spacer thermocouples, 0.040-in. diam MGO-backfilled Fast-response system thermocouples, 0.125-in. diam MGO-backfilled	Research, Inc., model RJ4081A-CS reference junction box (150°F)	−2.7–+40 mV	All type-K thermocouples; instrument type codes = 1–10
Rosemount Engineering Co. model 104WC-48-D	Rosemount Engineering Co. model 1442A-RD-B temperature transmitter with differential input	1,000–5,000 mV	Resistance thermometer device; instrument type code = 110
	Differential temperature (TDE)		
Rosemount Engineering Co. model 104WC-48-D	Rosemount Engineering Co. model 414L-3-A-G-B' resistance/EMF converter linear bridge	32–800 mV	Resistance thermometer device; instrument type code = 99
	Pressure (PE)		
Precise Sensors, model 111-1-3000-G-36-10-P (3-mV/V cell with 10-V excitation)	B&F model SY112-3, bridge completion network or Endevco model 4471.1A voltage-regulated bridge conditioner with Endevco model 4470 signal conditioner and Burr-Brown model 3640 differential input instrument amplifier with gain = 166.67	0–5,000 mV	Strain gauge pressure cell; instrument type code = 23

Table 6.4 (continued)

Sensor	Signal conditioning	Signal to CCDAS	Remarks
Foxboro model E11GM-HSAE2-ELSP pressure transmitter with zero elevation kit	Vishay Resistor Products style S105, 100-Ω, 3/4-W current-to-voltage signal converter	1,000–5,000 mV	Force balance pressure cell; instrument type codes = 24, 25
BLH Electronics, Inc., type DHF	Endevco model 4471.1A voltage-regulated bridge conditioner with Endevco model 4470 signal conditioner and Burr-Brown model 3620K/16 differential input instrument amplifier with gain = 166.67		
	Differential pressure (PDE)		
Foxboro model E13DH-HSAHZ or E11GM-HSAE2-ELSP	Vishay Resistor Products style S105, 100-Ω, 3/4-W current-to-voltage converter	1,000–5,000 mV	Force balance-type cell; instrument type code = 97, 105
BLH Electronics, Inc., type HMD, 1/4-in. FPT parts (2-mV/V cell with 10-V dc excitation)	B&F model SY112-3 bridge completion network or Endevco model 4471.1A voltage regulated bridge conditioner with Endevco model 4470 signal conditioner and Burr-Brown model 3620K/16 differential input instrument amplifier with gain = 250		Strain gauge differential pressure cell; instrument type code = 26, 41, 42
BLH Electronics, Inc., type HMD, 1/4-in FPT parts (2-mV/V cell with 10-V dc excitation)	B&F model SY112-3 bridge completion network or Endevco model 4471.1A voltage regulated bridge conditioner with Endevco model 4470 signal conditioner and Burr-Brown model 3620K/16 differential input instrument amplifier with gain = 250	0–5,000 mV	Strain gauge differential pressure cell; instrument type code = 26, 41, 42

Table 6.4 (continued)

Sensor	Signal conditioning	Signal to CCDAS	Remarks
BLH Electronics, Inc., type HHD, A.E. F-250-C H-P tube parts (3-mV/V cell with 10-V dc excitation)	B&F model SY112-3 bridge completion network Burr-Brown model 3620K/16 differential input instrument amplifier with gain = 166.67	0–5,000 mV	Strain gauge differential pressure cell; instrument type code = 27
BLH Electronics, Inc., type HMD (2-mV/V cell with 10-V dc excitation)	Endevco model 4471.1A voltage-regulated bridge conditioner with Endevco model 4470 signal conditioner Burr-Brown model 3620K/16 differential input instrument amplifier with gain = 250	0–5,000 mV	Strain gauge differential pressure cell; instrument type code = 28
Genisco Technology model PB 427B-101 (1-mV/V cell)	Endevco model 4471.1A voltage-regulated bridge conditioner with Endevco model 4470 signal conditioner Burr-Brown model 3620K/16 instrument amplifier gain = 500	0–5,000 mV	Strain gauge differential pressure cell; instrument type code = 43
Rosemount model 1151DP Alphaline	Vishay Resistor Products style S105, 250-Ω, 2-W current-to-voltage signal converter	1,000–5,000 mV	Capacitance-type cell; instrument type codes = 75, 78, 80
ITT Barton model 752-2	Vishay Resistor Products style S105, 250-Ω, 2-W current-to-voltage signal converter	1,000–5,000 mV	Bellows-type cell; instrument type code = 79
ITT Barton model 368/224	Vishay Resistor Products style S105, 100-Ω, 3/4-W current-to-voltage converter	1,000–5,000 mV	Bellows-type cell; instrument type code = 98

Table 6.4 (continued)

Sensor	Signal conditioning	Signal to CCDAS	Remarks
	Level (LE)		
Foxboro model E13DH-HSAH2	Vishay Resistor Products style S105, 100-Ω, 3/4-W current-to-voltage converter	1,000–5,000 mV	Force-balance-type cell; instrument type code = 105, 113
EG&G Idaho, Inc., liquid conductance sensor SK-10520-CB-RLH-025, -026	ORNL IR-PE-57 model Q-5659	0–10,000 mV	Instrument type code = 50
	Power (EWE)		
GE type JVM-2 potential transformer (20:1) with GE type JKM-3 current transformer (150:5)	Bristol-Weston model 878 thermal watt converter	0–40 mV	Power transmitter; instrument type code = 34
	Current (EIE)		
General Electric, Inc., catalog 50-140-014 current bus bar shunt (0–100 mV/800 A)	Burr-Brown model 3550/16 isolation amplifier with gain = 50	0–5,000 mV	FRS rod current shunt; instrument type code = 31
General Electric, Inc., catalog 50-140-021 current bus bar shunt (0–50 mV/1000 A)	Burr-Brown model 3550/16 isolation amplifier with gain = 100	0–5,000 mV	Generator current shunt; instrument type code = 32
ORNL drawing I-10520-QG-363 voltage divider network	Burr-Brown model 3550/16 isolation amplifier with gain = 3.5	0–5,000 mV	Generator voltage divider; instrument type code = 33
ORNL BDHT-THTF blowdown rupture disk assembly drawing I-10520-QG-350	ORNL BDHT-THTF breakwire detector drawings I-10520-QG-346 through 349	0–5,000 mV	Blowdown time marker; instrument type code = 37

Table 6.4 (continued)

Sensor	Signal conditioning	Signal to CCDAS	Remarks
	Rotational speed (SE)		
Kenco Instruments Co., Inc., model 51818-9421-7300-45760 tachometer-generator	Not applicable	89–4,806 mV	Tachometer-generator; instrument type code = 36
	Gamma densitometer (DE)		
ORNL model Q5666 (single beam) Measurements, Inc. (three-beam), model FM-4	ORNL model Q5233	0–1,000 mV	Single and triple beams; instrument type code = 106
	In-bundle gamma densitometer (DE)		
Reuter-Stokes model RS-C6-0202-2XX	ORNL model Q5233 signal conditioning	0–10,000 mV	Rod positions 36 and 46 of FRS bundle; instrument type code = 111
	Position (Ze)		
Beckman model E Helipot, 40-turn, 10,000-Ω potentiometer	ORNL model Q5782	0–10,000 mV	In-bundle gamma densitometer position indicator; instrument type code = 76, 77
	Drag disks (FMFE)		
Ramapo Instrument Co., Inc., model Mark V - 4PRBDX (2-mV/V with 5-V excitation)	Endevco model 4471.1A voltage-regulated bridge conditioner with Endevco model 4470 signal conditioner and Burr-Brown model 3620K/16 instrument amplifier with gain = 500	0–5,000 mV	Strain gauge momentum flux flow; instrument type code = 35, 40
	Turbine flowmeter (FE)		
Flow Technology model 1/2-in.-FT-6-8A5-LB 1/2-in.-FT-8-A10-LJC 2-in.-FT32G255-LB or LJC 3-1/2-in.-FT56I1000-LB or JLC	ORNL Electronic unit model Q5624-1	0–10,000 mV	Magnetic pickups are used to detect blade passage; instrument type code = 95, 96, 109

Table 6.4 (continued)

Sensor	Signal conditioning	Signal to CCDAS	Remarks
	Orifice plate flow (FE)		
ORNL concentric orifice with Foxboro model E13DH-HSAH2 or ITT Barton model 752-2 or Rosemount model 1151DP	Vishay Resistor Products style S105, 100-Ω, 3/4-W current-to-voltage converter	1,000–5,000 mV	Instrument type code = 107, 108, 112

used in the sensor/signal-conditioning pathway to the CCDAS. The column labeled "Signal to CCDAS" displays the signal range that is presented to the CCDAS analog front end from the signal-conditioning hardware. The "Remarks" column lists information such as primary sensor categories and the instrument type code information, which is intended to facilitate matching of sensor/signal conditioning information with the information listed in other instrument tables.

6.2.2 50-Channel thermocouple display and alarm system

A 50-channel Metrascope is used to provide additional display and overtemperature monitoring of bundle thermocouples. The Metrascope consists of type-K thermocouple reference junction compensation, a high-speed solid state [field effect transmitter (FET)] multiplexer, adjustable high and low limits for each channel, a cathode-ray tube (CRT) display of thermocouple temperatures and alarms, and associated control electronics. The Metrascope provides an alarm relay each for high- and low-temperature conditions occurring on any one channel. The high-alarm relay causes an alarm and trip of bundle power; the low-alarm relay is used only for indication of an open thermocouple and causes no control action.

The Metrascope, in conjunction with the CCDAS, will provide overtemperature monitoring of ~720 of the 1200 total bundle thermocouples.

6.2.3 Multichannel analog strip-chart recorders

One or more multichannel strip-chart recorders are provided for trend recording of key parameters during test operations. These recorders are used primarily for obtaining a quick look at, and observing trends in, selected parameters during steady-state experiments. A variety of instruments of this type are available at ORNL. The data recorded varies from test to test.

6.2.4 CCDAS

The CCDAS consists of a Digital Equipment Corporation (DEC) PDP-11/34 minicomputer and various peripheral devices and interfaces, as illustrated in the block diagram format of Fig. 6.9, with the individual components listed in Table 6.5. The minicomputer employs DEC's real time, multitasking executive software, RSX-11M, while all application software is written in FORTRAN.

The multiple cartridge disks are used as storage for the operating system, application programs, instrumentation data base, plots, and short data scans. The magnetic tape units are primarily used to record and process data acquired from the loop instrumentation during loop calibration, checkout, and testing operations. Because the units are industry compatible, the magnetic tapes are also used to interchange data and software programs with other computers. The high-speed analog input system consists of two data acquisition subsystems. The first subsystem is used to acquire data from the 256 loop instruments, while the second acquires data

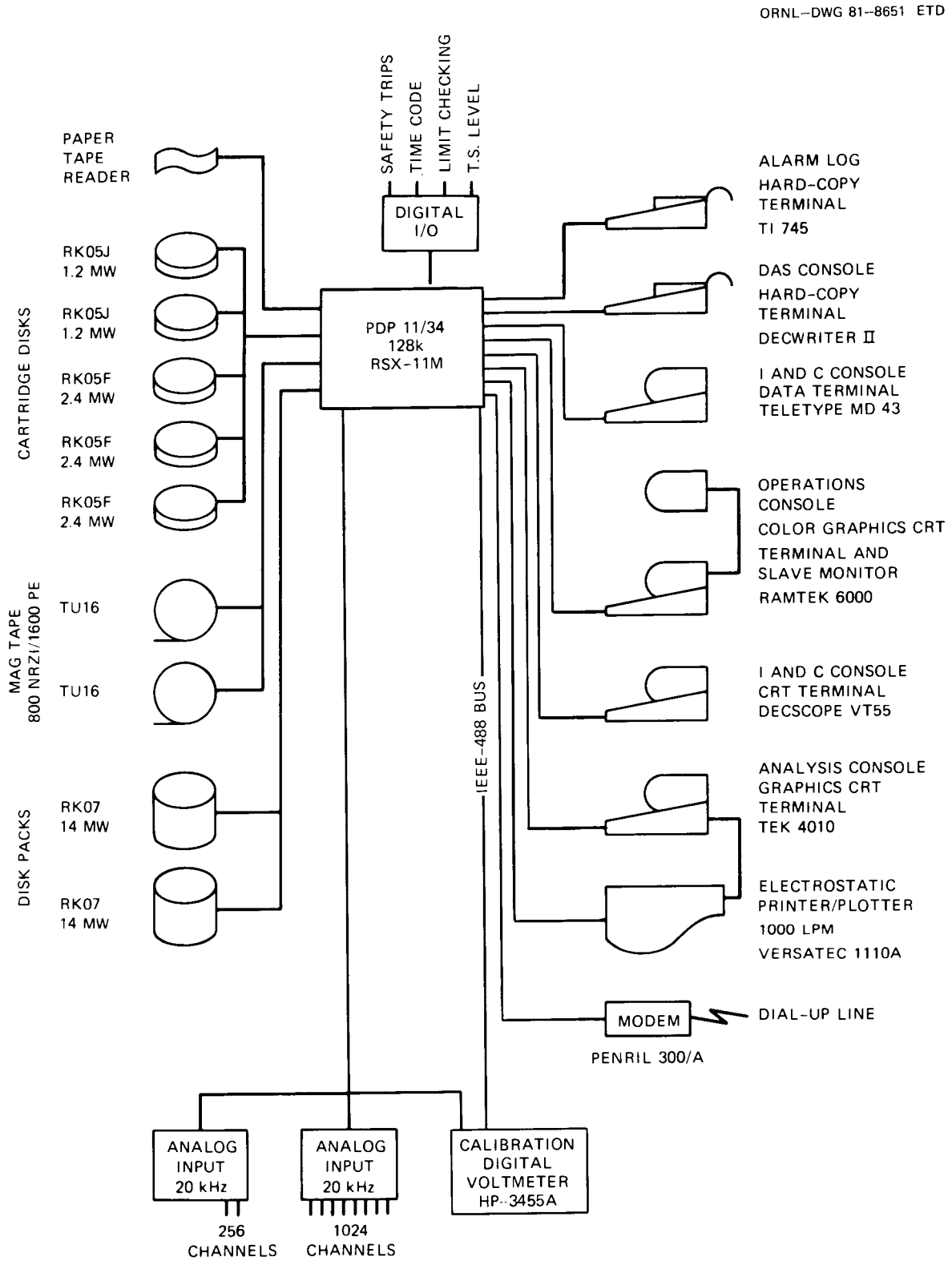

Fig. 6.9. Block diagram of CCDAS.

Table 6.5. CCDAS subsystems and peripherals

Item No.	Quantity	Description	Vendor
1	1	Computer, including 128 k-bytes of core memory, PDP-11/34	DEC
2	1	Operating system, RSX-11M (Fortran, Flex, Basic, Pascal languages used)	DEC
3	1	Programmable, real-time clock and time code generator and reader, model 9300	Datum
4	1	Power failure detector and automatic restart	DEC
5	8	Digital input or output 16-byte buffered channels	DEC
6	2	Magnetic tape controller and one transport system, model TU 16 — 9 channel	DEC
7	2	Cartridge disk controller and drive system, 1.2-MW capacity, RK05J	DEC
8	3	Cartridge disk controller and drive system, 2.4-MW capacity, RK05F	DEC
9	2	Disk pack controller and drive, 14-MW capacity, RK07	DEC
10	1	Paper tape reader	DEC
11	2	Analog input system, 1024-channel, model 2111 UDAM with model 140 UDAM controller	Datum
12	1	Calibration digital voltmeter, HP-3455A	HP
13	1	Modem, 300-baud dial-up line, model 300/A	Penril
14	1	Terminal, portable hardcopy, TI-745	TI
15	1	Terminal, console hardcopy, DECwriter II	DEC
16	1	Terminal, data hardcopy, model 43	Teletype
17	1	Terminal, color graphics CRT with slave monitor, model 6000	Ramtek, GBC
18	1	Terminal, graphics CRT, DECscope VT55	DEC
19	1	Terminal, plot graphics CRT, model 4010	Tectronix
20	1	Electrostatic printer and plotter, 10,001pm, model 1110A	Versatec

from up to 1024 bundle and loop thermocouples. The analog input system collects data at a maximum rate of 20,000 samples/s. Typically this corresponds to an individual channel frequency response of 10–20 Hz. The present software package allows the first subsystem to sample each of the 256 loop instruments five times as frequently as the second subsystem samples each of the 1024 bundle thermocouples; this allows every loop instrument to be sampled 100 times/s and bundle and loop thermocouples to be sampled 20 times/s. A custom computer interface for the analog input subsystems provides equally spaced data values at the full sampling rate while allowing hardware limit checking to be carried out concurrently on all thermocouples.

The multitasking executive software RSX-11M allows many operations to run simultaneously from the various terminal locations. From any CRT console, the operators can select real-time displays of any set of loop measurements (up to 48 instruments at a time) with hard copy available to facilitate operation, calibration, and checkout documentation. Periodic and on-demand logs can be initiated on any of the terminals generating hard copy results via the high-speed electrostatic line printer/plotter (1000 lines/min). The graphic CRT terminal can be used to rapidly view and edit plots of selected measurements, which can then be used to produce plots ready for preliminary data reporting following a test. Quick look data analysis and on-line instrumentation evaluation are supported during and immediately following test runs on this same CRT graphics terminal.

The number of process and data signals required to monitor and provide data from the THTF primary and secondary loops necessitated a computer-based DAS. The signals were recorded in digital form to facilitate analysis of tests, to monitor loop conditions prior to each test, and to effect on-site conversion of critical data to engineering units. The highest frequency component of these signals generally did not exceed 3 Hz; thus, the acquisition speed of the CCDAS (100 samples/s for 256 loop channels and 20 samples/s for 1024 bundle and loop thermocouples) is adequate. Most inputs are temperature signals from thermocouples located in the FRSs and in the test section coolant streams; the remainder of the signals come from sensing of flows, pressures, differential pressures, amperages, and voltages within the test bundle and in the coolant inlet and exit lines. Table 6.3 lists the signals recorded by this system.

The analog input system for the THTF is capable of scanning, digitizing, and recording signals from 2000 dc voltage sources in the ranges of 5 mV to 10.24 V. The system has a resolution of one part in +2048, an accuracy of 0.3% of full scale, and a scanning rate of 20,000 samples (channels) per second. The input signal multiplexers are easily field expandable in eight-channel increments to a total of 2048 channels. Data are recorded in real time on industry-compatible seven-track magnetic tape (high data-rate short scans are recorded on cartridge disk packs and later transferred to magnetic tape), along with time code information for correlation purposes.

To achieve the high scanning rate demanded on the system, FETs are used to switch the input signals. The FETs will not tolerate input signals with common-mode voltages >10 V peak to peak. Thus, isolation amplifiers are included in channels where signals have common-mode voltages that cannot be reduced below 10 V, such as those monitoring generator current.

In addition to acquiring and recording data, the CCDAS serves as a primary safety system. Simultaneously with data collection, the CCDAS performs high-limit checking on all designated analog channels and actuates alarm relays in the event of out-of-limit conditions. Approximately 720 bundle thermocouples connected to the CCDAS are continuously checked for overtemperature conditions during powered operation. The maximum delay between the occurrence of an out-of-limit condition and the actuation of the appropriate alarm relays is 350 ms for approach to power and 200 ms for the blowdown transient. To minimize the possibility of trips from noise, the alarm criterion is two successive samples during blowdown. The safety system activates an alarm when "X" number of signals are out of limits and activates the trip of bundle power when "Y" number of signals are out of limits where X and Y are chosen to reflect the safety margins required on a test-by-test basis. The high-limit set point for any channel is individually assigned at the time the instrument is placed in the instrument data base. A watchdog timer contact is also incorporated to monitor the integrity of the CCDAS and give an alarm if the computer should fail.

The CCDAS is a valuable tool for obtaining information required for the operation of the loop and evaluation of the instrumentation. In addition, the CCDAS is used for preliminary posttest evaluation of data to verify that test objectives were met and/or to identify problem areas to be remedied. The bulk of the data reduction and analysis is done at the central computing centers. The loop operator has the capability of requesting several different printed logs, each providing useful information on the current condition of any part of the loop. For example, one log prints the temperatures measured by all bundle thermocouples, while another log prints the current and voltage measurements on the dc power system. Preliminary plots of selected measurements can be generated on site from recorded data using the storage display unit (CRT). The data may be plotted either in engineering units or raw voltage. The CCDAS is used extensively in the pretest checkout and calibration of the loop instrumentation. Calibrations and procedures are discussed in the next section.

6.3 Calibration

All instrumentation channels in the THTF are calibrated either before every test run or on a periodic recall basis. In addition, special calibrations, some by independent testing laboratories, are performed as required. Table 6.6 summarizes the type and frequency of calibrations performed on the various classes of instruments.

6.3.1 Pretest calibration

Instrumentation channels that monitor critical test parameters are calibrated and/or functionally verified prior to each test run. This includes, in general, the CCDAS, the spool-piece instrumentation, and the pressure and differential pressure measurements positioned around the loop. All pretest calibration and checkout operations are performed in situ.

Table 6.6. Instrument calibration/verification intervals

Instrument channel	Calibration/verification type	Interval	Location
Pressure, transient (strain gauge transducer)	Calibration	Each test	In situ
Pressure, steady state (force balance transmitter)	Verification Calibration	Each test 24 months	In situ In situ
Pressure, precision (Bourdon-tube gauge)	Calibration	Each test	Laboratory
Temperature, loop steady state (platinum resistance thermometer)	Verification Calibration	Each test 24 months	In situ Laboratory
Temperature, loop transient (type-K thermocouples)	Verification Calibration	Each test 48 months	In situ Laboratory
Temperature, bundle transient (type-K thermocouples)	Verification Calibration	Each test At assembly	In situ Laboratory
Flow, loop transient (turbine meters)	Signal-conditioning calibration Transducer calibration	Each test At assembly	In situ Laboratory
Flow, HX secondary (turbine meters)	Signal-conditioning calibration Transducer calibration	24 months At assembly	In situ Factory
Flow, orifice (force balance transmitter)	Calibration	24 months	In situ
Flow, momentum flux (drag disk)	Calibration	Each test	In situ
Density (gamma densitometer)	Calibration	Each test	In situ
Level, pressurizer (force balance transmitter)	Calibration	24 months	In situ
Voltage, dc generator	Verification Calibration	Each test 12 months	In situ In situ
Current, dc generator	Verification Calibration	Each test 12 months	In situ In situ
Current, FRS	Verification Calibration	Each test 12 months	In situ In situ
Speed, primary pump	Verification Calibration	Each test 24 months	In situ Laboratory
Power, primary pump	Calibration	24 months	Laboratory
Working standard, voltage (DVM)	Calibration	6 months	Laboratory
Working standard, frequency (counter)	Calibration	6 months	Laboratory
Working standard, current loop (10–50 mA)	Calibration	6 months	Laboratory
Standard, pressure (Bourdon-tube gauge)	Calibration	12 months	Laboratory

The first to be calibrated is the CCDAS. Because the CCDAS employs low-level multiplexers (as opposed to amplifier-per-channel high-level multiplexers), calibration is accomplished, not on individual channels, but on a block of 128 instrument channels with a common amplifier assembly. Calibration signals are brought in on the first two channels of every 128-instrument-channel block, which serve as reference signals during calibration and as a monitor of long-term channel drift.

All loop pressure measurement channels are calibrated at ambient temperature over the full range from atmospheric to full operating pressure [usually 15.5 MPa (2250 psig)] as measured by the average of two Bourdon-tube Heise gauges that monitor the pressure at the test section inlet and outlet. Engineering units-conversion equation coefficients are calculated from these data using least-squares curve-fitting techniques. The calibration equation is of the form

$$P = C_0 + C_1V + C_2V^2 ,$$

where P is the computed pressure in kPa; V is the instrument signal in mV; and C_0, C_1, and C_2 are the zero-, first-, and second-order calibrated coefficients, respectively.

The differential pressure transducers exhibit a significant zero and span decalibration shift with applied static pressure. The differential pressure measurement channels are calibrated for zero shift over the full range from atmospheric to full operating pressure. Zero correction equation coefficients are then determined from the data. Span correction equation coefficients are determined by testing the transducers in the standards laboratory. The calibration data for each differential pressure transducer are fit to an equation of the form

$$\Delta P = (Ag \times P + Bg)[V - (Az \times P + Bz)] ,$$

where ΔP is the computed differential pressure, V is the instrument signal in mV, P is the pressure in kPa, Ag (1/mV) and Bg (kPa/mV) are calibrated gain coefficients, and Az (mV/kPa) and Bz (mV) are calibrated zero coefficients.

Both of the pressure and differential pressure instrument calibrations are carried out in part with the aid of calibration support software routines developed to facilitate instrument calibration by the THTF personnel.

Drag disk calibrations are generally made during heat-up of the facility in the early stages of a test run. Data are taken over a range of flow rates at two different temperatures [one at fairly low temperatures of ~338 K (150°F) and the other at ~450 K (350°F)]. The flow calibration data are used to determine the temperature corrections to be applied to the drag disk instruments. The drag disks, especially at the lower end of their range, are fairly sensitive to temperature changes. The drag disks are calibrated using the turbine meters (velocity V) and pressure- and temperature-deduced density ρ to obtain an "actual" momentum flux ρV^2_{actual}. A calibration equation is generated from a least-squares fit to the drag disk signal and corresponding actual momentum flux over a

range of momentum flux. The "measured" momentum flux ρV^2_{meas} is obtained by applying the calibration equation to the instrument signal. The calibration equation takes the form

$$\rho V^2_{meas} = A(IS - Z)^E ,$$

where IS is instrument signal (mV) and A, Z, and E are parameters determined by the least-squares fit. The value of E is generally near 1.0. The value of Z is the temperature offset determined from the calibration data taken at the two different temperatures.

Several parts of other instrument channels are calibrated prior to each test run. For example, the signal-conditioning electronics for the turbine flowmeters are calibrated using an internal calibration frequency source. The isolation amplifiers for monitoring the dc power system are nulled to eliminate any zero offsets. The constant current power supply of all RTDs is verified to be within limits prior to the test run.

6.3.2 Posttest calibration

Engineering units-conversion equation coefficients for the gamma densitometers are determined using data just prior to and just following blowdown. Empty pipe and background (source shutter closed) readings are taken ~10 min after blowdown while the loop is still at an elevated temperature. The measured temperature and pressure at steady state just prior to blowdown are then used to determine the water density from which the conversion coefficients are calibrated. For test runs that did not have blowdowns, "empty pipe" readings were obtained either prior to filling the loop with water or estimated from data scans taken when high-quality or superheated steam conditions existed in the spool pieces. The coefficient for converting the densitometer signal to engineering units is determined from the equation

$$\rho = K \ln \frac{V_E - V_o}{V - V_o} ,$$

where

ρ = density (kg/m³),
K = density factor (kg/m³),
V_E = empty pipe reading (mV),
V_o = background reading (mV),
V = instrument reading at density ρ (mV).

6.3.3 Periodic calibration

All instrumentation that is not completely calibrated prior to each test is entered into a programmed maintenance recall system. These

instruments are then calibrated on a periodic basis, as shown in Table 6.6. The periodicity of calibration depends on operating experience with the instrument, manufacturers' recommendations, and the importance of the measurement. The Working Standards used for field calibration of the instrumentation are also calibrated at regular programmed intervals.

All instrumentation is calibrated in situ as part of a complete instrument channel unless deemed impractical. In situ calibration eliminates errors caused by improper reinstallation and damage in transit. In those cases where the calibration cannot be accomplished in place, the instruments are removed and sent to the standards laboratory. All instruments removed for maintenance are recalibrated before being returned to service in the loop.

6.3.4 Special calibrations

Special calibrations are periodically performed on the instrumentation. These are for the most part one-time or infrequent calibrations that characterize new, experimental, or unfamiliar instrumentation. Special calibrations are also required to obtain data for performing error analysis on various instruments. Typically, special calibrations of THTF primary instrumentation are reported in technical manuals published at ORNL (Refs. 3 and 40).

REFERENCES

1. L. J. Ott, *Thermal-Hydraulic Test Facility Bundle 3 In-Core Instrumentation and Operating History*, ORNL/NUREG-75 (to be published).

2. *Project Description ORNL PWR Blowdown Heat Transfer Separate-Effects Program — Thermal-Hydraulic Test Facility (THTF)*, NUREG/CR-0104 (ORNL/NUREG/TM-218) (November 1978).

3. D. G. Thomas et al., *Quart. Prog. Rep. on Blowdown Heat Transfer Separate-Effects Program for October–December 1977*, ORNL/NUREG/TM-175 (April 1978).

4. D. H. Cook, Oak Ridge National Laboratory, BDHT Memorandum 2349 to J. D. White, Oak Ridge National Laboratory; Subject: Location of Critical Points in Bundle 3.

5. L. J. Ott, "Multidimensional Effects in the Thermal Response of Fuel Pin Simulators," *Proceedings of the ANS/ASME/NRS International Topical Meeting on Nuclear Reactor Thermal-Hydraulics*, Saratoga Springs, NY, October 5–8, 1980.

6. W. D. Turner, D. C. Elrod, and I. I. Siman-Tov, *HEATING5 — An IBM 360 Heat Conduction Program*, ORNL/CSD/TM-15 (March 1977).

7. R. W. McCulloch et al., *Fabrication Technology Development of Fuel Rod Simulators for Blowdown Heat Transfer Tests* (to be published).

8. L. J. Ott, Oak Ridge National Laboratory, BDHT Memorandum 2278 to BDHT Staff, July 26, 1979; Subject: Location of FRS Thermocouples in THTF Bundle 3.

9. B. J. Veazie, Oak Ridge National Laboratory, BDHT Memorandum 2327 to W. G. Craddick, Oak Ridge National Laboratory; Subject: THTF Bundle 3 — Thermocouple Nomenclature.

10. L. J. Ott and R. A. Hedrick, *ORINC — A One-Dimensional Implicit Approach to the Inverse Heat Conduction Problem*, ORNL/NUREG-23 (November 1977).

11. B. R. Bass, J. B. Drake, and L. J. Ott, *ORMDIN: A Finite Element Program for Two-Dimensional Nonlinear Inverse Heat Conduction Analysis*, NUREG/CR-1709 (ORNL/NUREG/CSD/TM-17) (December 1980).

12. N. C. J. Chen and D. K. Felde, *Two Phase Mass Flux Uncertainty Analysis for the Thermal Hydraulic Test Facility (THTF) Instrumented Spool Pieces*, ORNL/TM-7859 (May 1982).

13. K. G. Turnage, *Two-Phase Flow Measurements with Advanced Instrumented Spool Pieces*, NUREG/CR-1529 (ORNL/NUREG-72) (September 1980).

14. K. G. Turnage, C. E. Davis, and D. G. Thomas, *Advanced Two-Phase Flow Instrumentation Program Quart. Prog. Rep. for July–September 1978*, NUREG/CR-0686 (ORNL/NUREG/TM-309).

15. K. G. Turnage and P. A. Jallouk, *Advanced Two-Phase Instrumentation Program Quart. Prog. Rep. for April–June 1978*, NUREG/CR-0501 (ORNL/NUREG/TM-279).

16. R. W. McCulloch et al., *Analysis and Repair of Water-Contaminated Boron Nitride Insulation in BDHT-THTF Bundle 3 Fuel Rod Simulators*, NUREG/CR-2046 (ORNL/NUREG/TM-451) (June 1981).

17. T. M. Anklam et al., *ORNL Rod Bundle Heat Transfer Test Data. Volume 1. ORNL Small Break LOCA Test Series I: Experimental Data Report*, ORNL/NUREG/TM-407/V1 (April 1982).

18. T. M. Anklam, *ORNL Small-Break LOCA Heat Transfer Test Series 1: Rod Bundle Heat Transfer Analysis*, ORNL/NUREG/TM-445 (August 1981).

19. T. M. Anklam, *ORNL Small-Break LOCA Heat Transfer Test Series 1: High-Pressure Reflood Analysis*, ORNL/NUREG/TM-446 (August 1981).

20. T. M. Anklam, *ORNL Small-Break LOCA Heat Transfer Test Series 1: Two-Phase Mixture Level Swell Results*, ORNL/NUREG/TM-447 (August 1981).

21. T. M. Anklam and L. J. Ott, Oak Ridge National Laboratory, BDHT Memorandum 2403 to W. G. Craddick and J. D. White, Oak Ridge National Laboratory, May 2, 1980; Subject: Location of Thermocouples in FRSs (10) to be Fabricated by R. W. McCulloch.

22. C. B. Mullins, ORNL, personnal communication, November 1981.

23. C. B. Mullins et al., *ORNL Rod Bundle Heat Transfer Test Data. Volume 2. Thermal-Hydraulic Test Facility Experimental Data Report for Test 3.03.6AR – Transient Film Boiling in Upflow*, ORNL/NUREG/TM-407/V2 (April 1982).

24. D. G. Morris et al., *Transient Dispersed Flow Film Boiling of High Pressure Water in Rod Bundle Geometry*, AIChE Symposium Series 208(77), 282 (1981).

25. D. G. Morris et al., *An Analysis of Transient Film Boiling of High Pressure Water in a Rod Bundle*, ORNL/NUREG-85 (April 1982).

26. C. B. Mullins et al., *ORNL Rod Bundle Heat Transfer Test Data. Volume 6. Thermal-Hydraulic Test Facility Experimental Data Report for Test 3.05.5B – Double-Ended Cold-Leg Break Simulation*, ORNL/NUREG/TM-407/V6 (June 1982).

27. R. C. Hagar, *Oak Ridge National Laboratory PWR Blowdown Heat Transfer Separate-Effects Program Interim Report Test 3.05.5B*, ORNL/BDHT-2507 (October 1980).

28. L. J. Ott, Oak Ridge National Laboratory, BDHT Memorandum 2494 to BDHT Staff, Sept. 5, 1980; Subject: Location of Test Section FRS Thermocouples in the Rerefurbished THTF Bundle 3.

29. D. K. Felde, *Design Concept and Testing of an In-Bundle Gamma Densitometer for Subchannel Void Fraction Measurements in the THTF Electrically Heated Rod Bundle*, ORNL/TM-8064 (April 1982).

30. D. G. Morris, ORNL, personal communication, November 1981.

31. C. B. Mullins et al., *ORNL Rod Bundle Heat Transfer Test Data. Volume 3. Thermal-Hydraulic Test Facility Experimental Data Report for Test 3.06.6B – Transient Film Boiling in Upflow*, ORNL/NUREG/TM-407/V3 (May 1982).

32. C. B. Mullins, ORNL, personal communication, November 1981.

33. C. B. Mullins et al., *ORNL Rod Bundle Heat Transfer Test Data. Volume 7. Thermal-Hydraulic Test Facility Experimental Data Report for Test Series 3.07.9 – Steady-State Film Boiling in Upflow*, ORNL/NUREG/TM-407/V7 (May 1982).

34. G. L. Yoder et al., *Dispersed Flow Film Boiling in Rod Bundle Geometry – Steady-State Heat Transfer Data and Correlation Comparison*, ORNL-5822 (April 1982).

35. C. B. Mullins et al., *ORNL Rod Bundle Heat Transfer Test Data. Volume 5. Thermal-Hydraulic Test Facility Experimental Data Report for Test 3.08.6C – Transient Film Boiling in Upflow*, ORNL/NUREG/TM-407/V5 (May 1982).

36. D. G. Morris et al., *Dispersed Flow Film Boiling of High Pressure Water in a Rod Bundle*, ORNL/TM-7864 (to be published).

37. T. M. Anklam et al., *ORNL Rod Bundle Heat Transfer Test Data. Volume 4. ORNL Small Break LOCA Heat Transfer Test Series II: Experimental Data Report*, ORNL/NUREG/TM-407/V4 (May 1982).

38. T. M. Anklam et al., *Experimental Investigations of Uncovered Bundle Heat Transfer and Two-Phase Mixture Level Swell Under High Pressure, Low Heat Flux Conditions*, ORNL-5848 (April 1982).

39. C. R. Hyman et al., *Experimental Investigations of Bundle Boiloff and Reflood Under High Pressure, Low Heat Flux Conditions*, ORNL-5846 (April 1982).

40. *Quart. Prog. Rep. on Blowdown Heat Transfer Separate-Effects Program for January–March 1978*, NUREG/CR-0133 (ORNL/NUREG/TM-205) (1978).

Appendix A

ESSENTIAL FEATURES

The THTF is a complete and independent test facility with no interfacing requirements to systems other than building or plant-wide utilities. The physical configuration of the facility is primarily determined by the arrangement of major components as required by the available building space, the location of existing components and systems, economics and good practice in piping layouts, and the desired versatility of piping connections. The facility includes (1) a closed recirculating primary loop capable of providing a wide range of thermal-hydraulic operating conditions to the electrically heated test section; (2) instrumentation, controls, computer, and data acquisition systems necessary for loop operation and test data analysis; (3) test section power supply up to 7.5 MW(e); and (4) a primary fluid blowdown system with pressure suppression.

The primary loop includes the circulating pump, pressurizer, heat exchangers, and bypass piping, all connected with high-pressure, high-temperature quick-disconnect flanges. The system is designed for operation with subcooled water at 1.72×10^4 kPa (2500 psig) and 617 K (1110°R) except that (1) the pressurizer design is for 1.72×10^4 kPa (2500 psig) and 694.4 K (1250°R), (2) a section of the primary pump discharge piping is designed for 2.06×10^4 kPa (3000 psig) and 589 K (1060°R), and (3) the pump is limited to a 589 K (1060°R) maximum operating temperature. Further, pump design specifications limit temperature change rates during normal operation to 8.3 K/min (15°R/min) during heating and 13.9 K/min (25°R/min) during cooling. The pump and other flow components are also capable of withstanding abnormal, short-duration operations such as blowdowns where rapid temperature and pressure changes occur. All piping and components of the facility conform to the applicable codes and standards listed in Sect. A.3.3.

The facility was constructed by upgrading an existing facility built for steady-state or slow-transient critical heat flux (CHF) studies with pressurized water in a single heated tube or annulus. Presently, the circulating test coolant is high-purity demineralized water. The principal factor in material selection for the test facility was the avoidance of water contamination by corrosion products and/or other impurities. The ability to withstand repeated tests without damage imposes additional restraints on test section materials, especially for the heater rods. Complete descriptions of the THTF loop components, materials, and system integrity are given in Sects. A.2 and A.3.

A.1 Facility Location and Arrangement

The THTF and associated work areas occupy ~185 m² (2000 ft²) on the basement level and 419 m² (4500 ft²) on the first-floor level of the northwest end of Building 9201-2 in the Y-12 plant area. A plan view of the basement and first floor showing a general layout of equipment and work areas is shown in Figs. A.1 and A.2. The control room on the first-floor

ORNL–DWG 81–8166 ETD

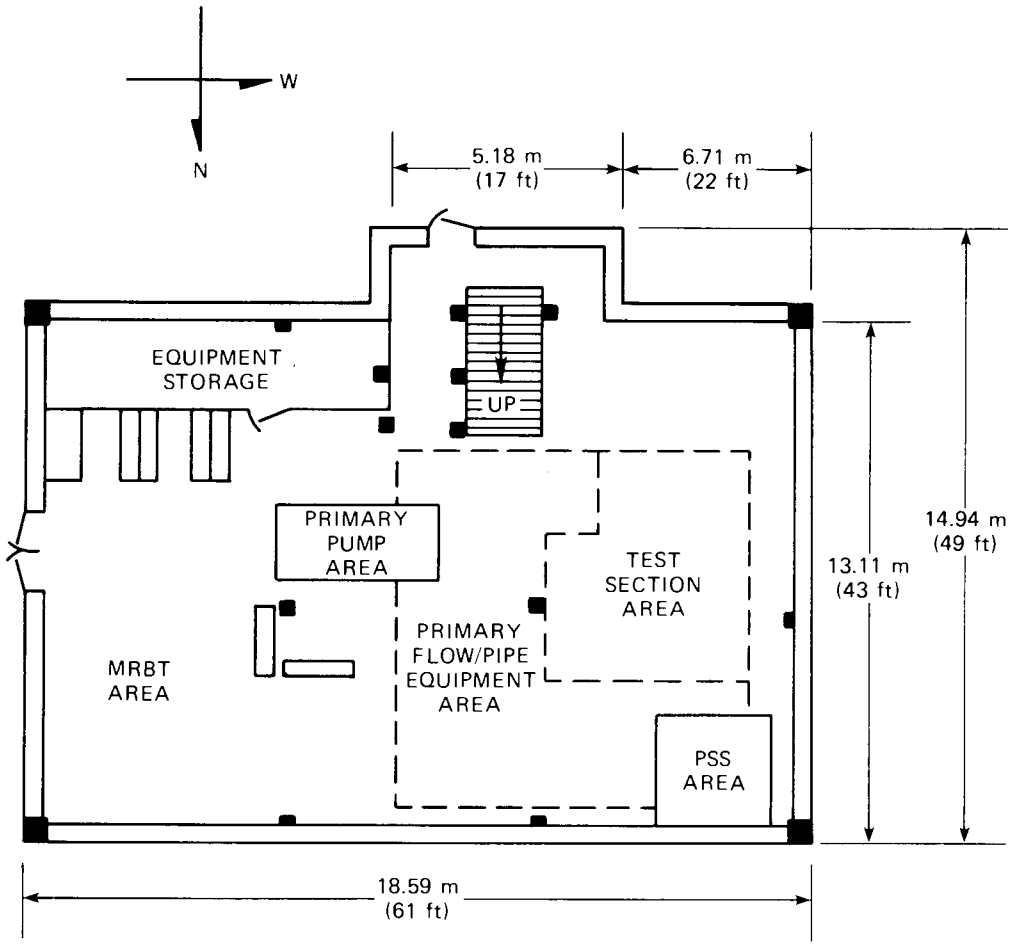

Fig. A.1. Plan view of basement area of THTF.

level contains all instrumentation and controls necessary for normal THTF loop operation, with associated computer and data acquisition equipment located in the adjacent computer room. Primary system piping is located southwest of the control panels on the first-floor area and in the northwest corner of the basement level. Piping layouts are compact, vertically oriented, and extend from the ground level of the basement to near the ceiling of the first floor. The test section and piping area on the first-floor level is entirely enclosed with a removable metal shield. The motor-generator and associated switch gear, interlocks, and controls are located in other areas of the building, external to the THTF work area, and are maintained by plant utilities staff.

The THTF multirod test section is mounted vertically through the first-floor level. The assembled test section pressure housing is ~6.1 m (20 ft) long and requires vertical clearances of ~1.5 m (5 ft) from the basement floor to the test section bottom closure for instrumentation and high-voltage negative dc power bus connections and ~10.1 m (33 ft) from

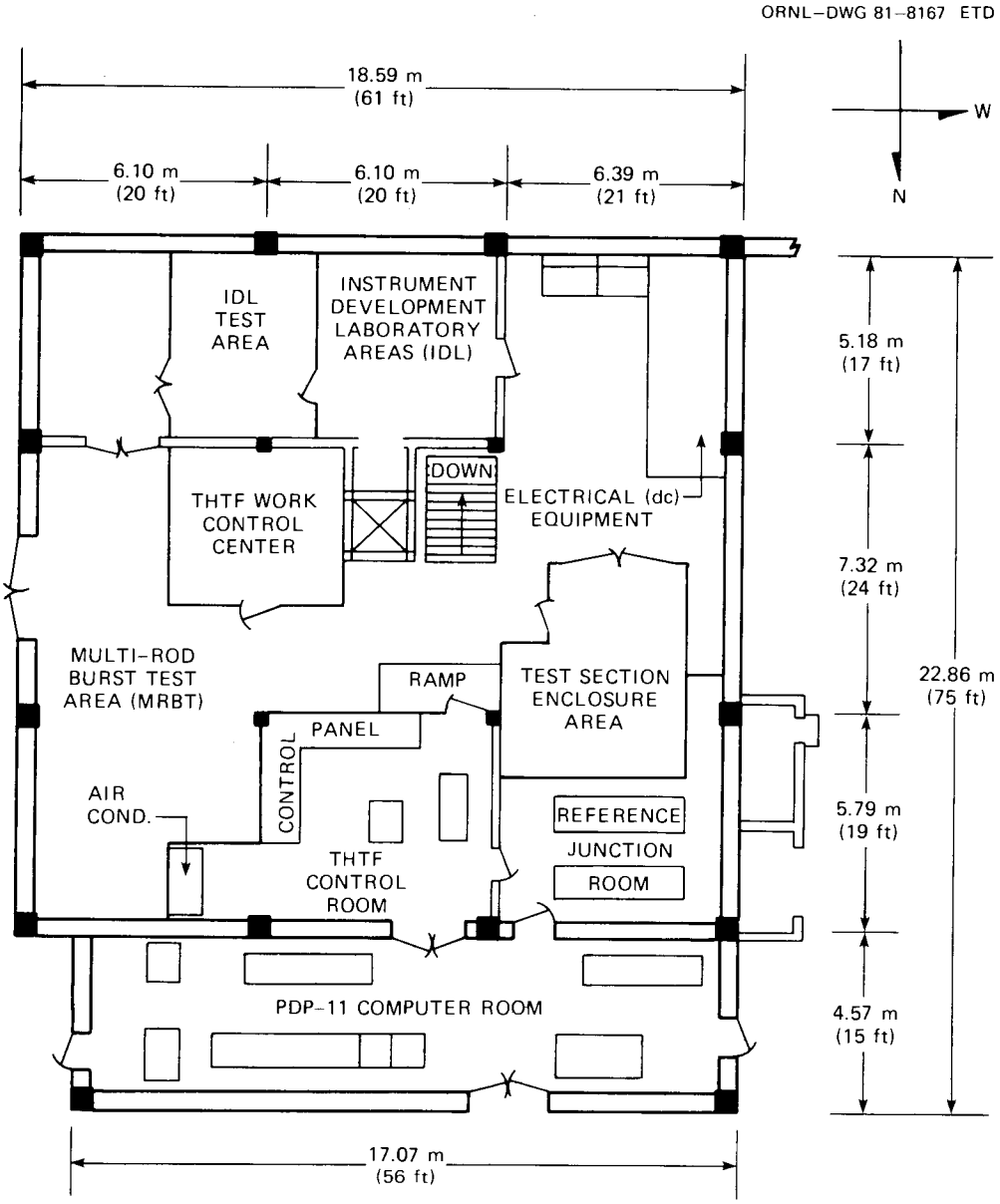

Fig. A.2. Plan view of first floor area of THTF.

the bottom housing closure to the overhead hoist for test section assembly, installation, or removal. Required clearances were obtained by constructing a 1.2-m-deep (4-ft) pit in the basement floor and by constructing an access hatch opening in the second-floor level (ceiling of first level) directly above the test section housing. The ceiling access and hoist mounted above it are used only during installation and removal of the test section heater rod assembly (Bundle 3), individual instruments, or FRS heater rods.

Equipment located in the basement area includes the primary circulation pump, components of the primary flow and bypass control loops, the

demineralized cooling water distribution station, PSS components, test section seal and cooling systems, and the lower end of the THTF test section. A large stockroom for spare parts, instruments, and maintenance equipment is located in the southeast corner, basement level, of the work area. The work control center located on the first-floor area is used for storage of equipment specification manuals, test data, and engineering drawings and for organization of facility maintenance and modification activities.

A.2 High-Pressure Primary System

A schematic flow diagram of the primary system referred to in this description was shown in the instrument application drawings for Test 3.05.5B [Figs. 5.19(a–c)]. This system consists of a closed loop that includes a circulation pump, an electrically heated pressurizer, a primary fluid makeup system, and heat exchangers to remove heat generated in the test section and by the pump. Primary fluid in the recirculating loop, also referred to as test section coolant, is high-purity demineralized water. Most of the piping used is special, heavy wall, type 347 stainless steel (reactor grade). Predominant pipe sizes are 1-in. Schedule-80, 2-in. Schedule-80, and special 4-in. nominal pipe having 1.27-cm (0.500-in.) wall thickness. In general, the piping is sized to limit the steady-state flow velocity to <9.15 m/s (30 ft/s). Most of the piping is joined by welding, but numerous mechanical connections are included to permit removal of valves, components, and special instrumentation for maintenance and to facilitate modifications to the system configuration. Grayloc flange connections, which are less massive than ring joint flanges and lend themselves to quick assembly and disassembly, are used.

The high-head high-capacity circulating pump operates at a constant output of ~4.42 x 10^{-2} m^3/s (700 gpm) with a developed head of ~590 m (~1940 ft). Because the available head is significantly larger than that required to make up pressure drop through loop components and piping, a remotely operated discharge throttling valve (HCV 2) and load orifices located throughout the system are provided to dissipate excess head. Flow in excess of test section requirements is routed to the parallel paths of the high-capacity bypass piping and back to the pump suction. One bypass leg contains heat exchanger D, which removes heat generated by the pump and throttling valve. Flow rate of primary fluid through this heat exchanger is variable and is controlled by the actions of temperature recorder controller alarm 13 and temperature control valve 13 to maintain pump discharge temperature at a set point. Flow rate to the test section is metered and controlled, so the balance of the pump discharge flows through the other bypass leg where control actions of FRCA 1 and FCV 1 maintain pump flow rate at a set point. Flow rate to the test section is metered and controlled by a fourth flow control station of nominal 100- to 600-gpm capacity consisting of an orifice flowmeter with output to flow recorder controller 18 and the flow control valve 18. Primary fluid, which is used as coolant for the electrically heated rod bundles in the test section, flows upward through the test section, through any combination of the three heat exchangers (A, B, or C) and bypass lines in parallel, and back to the primary pump suction.

The test section is connected to the primary piping and the PSS by four instrumented spools on the inlet and three instrumented spools on the outlet in series and immediately adjacent to the test section barrel (Figs. 2.1 and 2.2). Junctions with the PSS are located between two instrumented spool pieces on both the inlet and outlet of the test section to provide mass flow measurements of the complete system inventory following blowdown. A plenum is formed at these two junctions by 6-in. pipe ~0.305 m (1 ft) long to reduce hydraulic instability during blowdown. Also incorporated into the plenum design are a double rupture disk assembly to initiate blowdown, fast-response pressure instrumentation, a replaceable nozzle to control blowdown rate, and break wires to provide the timing mark for the instant of blowdown.

The double rupture disk assembly contains provisions to rupture either or both rupture disk assemblies simultaneously. The PSS described in Sect. A.2.2 is designed to absorb the thermal and mechanical energy of the high-velocity flashing liquid.

The heat removal section of this system (heat exchangers A, B, and C) is designed to remove heat transferred to the primary fluid from the electrically heated test section. Effluent from the test section can be routed through none, any, or all of the heat exchangers for versatility during system operational checks, startup, shutdown, and operation over a wide range of conditions. Each of the heat exchangers is manually controlled over a range of heat removal conditions by varying primary and secondary fluid flow rates under certain limitations. A bypass line that has manual flow control is also provided around these heat exchangers. Effluent from the heat removal section mixes with the bypass flow in a mixing tee. The mixing tee provides for absorbing severe temperature gradients and fluctuations in a non-pressure-containing thermal sleeve. The mixed effluent then flows to the pump suction.

The electrically heated pressurizer is connected to the system between the test section outlet and the heat exchangers. The connecting piping includes a horizontal line and a changeable restriction (orifice plate) to reduce mixing between the circulating fluid and the higher-temperature pressurizer fluid. A condenser coil installed in the steam volume permits rapid pressure reductions as required by the test program. Air can be used in the condenser coil to provide a wide variation in condensing rates. The pressurizer heaters may be automatically controlled to maintain set-point pressure. Other instrumentation is included to monitor temperature, pressure, and liquid level.

The remainder of this section describes some of the primary system components in more detail.

A.2.1 Pressurizer

The pressurizer (Fig. A.3) controls the base pressure in the primary system and is designed and installed to provide its contents a degree of thermal isolation from the primary loop so that it can operate at a temperature higher than that of the primary loop. This permits saturation temperature and pressure to be maintained in the pressurizer while water in the primary system is at a subcooled temperature. The pressurizer also

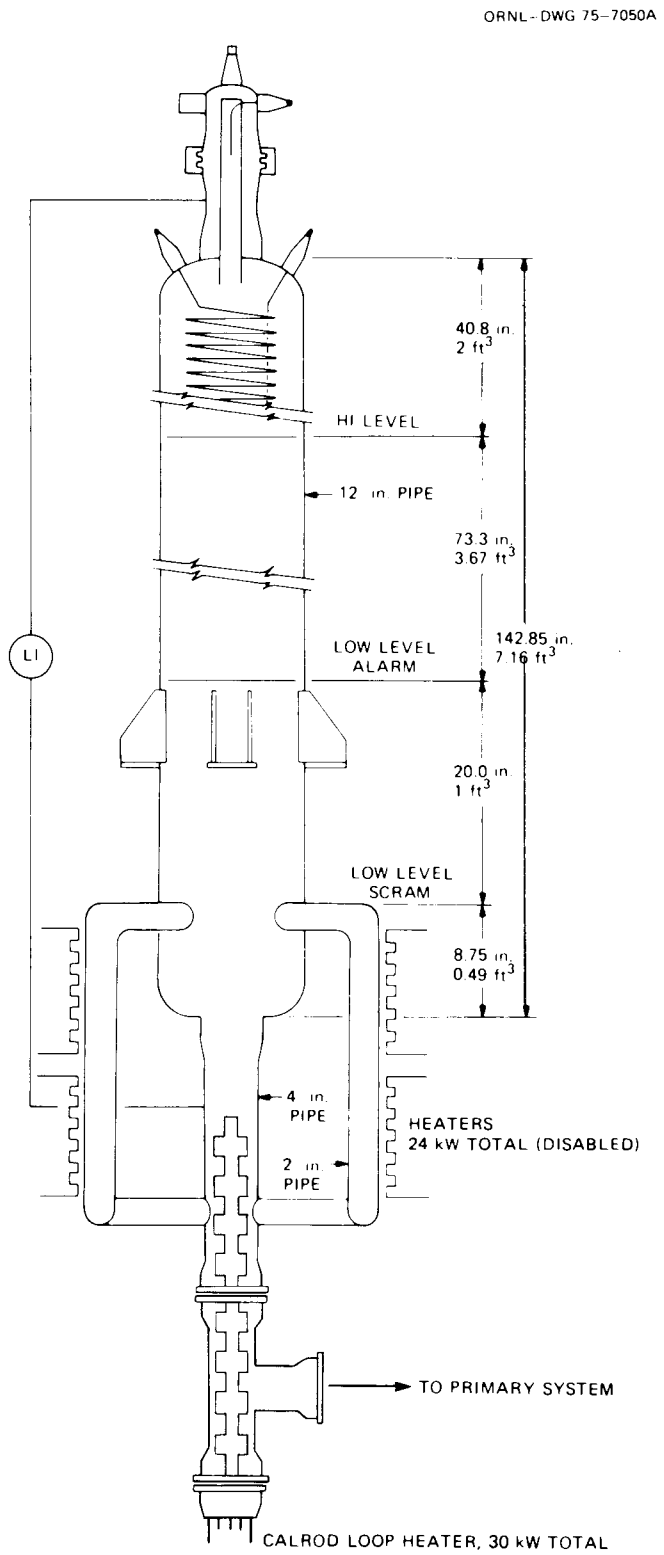

Fig. A.3. Schematic of THTF pressurizer.

serves as a surge tank; that is, its steam volume is sufficient to accommodate operational changes in specific volume of the water in the loop. These changes in specific volume result from temperature transients that occur during operation. However, the steam volume in the pressurizer is not sufficient to accommodate the very substantial increase in specific volume of water during startup. For instance, based on an initial filling of ~6.51 x 10^{-1} m^3 (23 ft^3) of water into the primary system at 101.1 kPa (14.7 psia) and 294.4 K (530°R), this volume will expand by ~34.5% or ~2.27 x 10^{-1} m^3 (8 ft^3) when heated and pressurized to the baseline operating conditions of 567 K (1020°R). This volume expansion exceeds the normal working volume range of the pressurizer, thus necessitating the letdown of excess inventory during the course of initial system heatup.

The main body of the pressurizer is of 12-in. Schedule-140, type 316 stainless steel pipe ~3.35 m (11 ft) long. It has four outboard heater legs near the pressurizer bottom, each equipped with 6-kW(e) clamshell heaters [24-kW(e) total capability], and five stainless steel Calrod immersion heating units rated at 6 kW(e) each [30-kW(e) total capability] located in the center opening of the pressurizer (Fig. A.3). A tee section located at the pressurizer bottom connects the pressurizer to the primary system while providing a port for adapting to a blank flange used to support the immersion heaters. To assist in loop startup, 19 kW(e) of manually controlled heat may be input on the pressurizer vessel walls. Once the desired pressurizer temperature and pressure are reached, these heaters are shut off. A relief valve located at the top of the pressurizer opens at 1136 kPa (2475 psi), thus providing a safety release of the pressurizer contents in the event that the heater controls inadvertently fail in the "full-on" position.

The heated legs of the pressurizer are made of 2-in. Schedule-80, type 347 stainless steel pipe. The outside surfaces of these pipes were machined down to a less-than-normal outer diameter for a close fit and good thermal conduction with the 50.8-cm-long (20-in.), 12.7-cm-OD (5-in.) clamshell heaters. A minimum wall thickness of 0.478 cm (0.188 in.), as required by the code, was maintained during machining operations.

Instrumentation is provided to protect the pressurizer in the event of malfunctioning controls or severe operating conditions. When the pressurizer water level drops to the elevation of the upper-leg nozzles, the heater power is automatically turned off. A low-level alarm actuates at an elevation 50.8 cm (20 in.) above these nozzles, providing an indication of a 2.83 x 10^{-2}-m^3 (1.0-ft^3) volumetric cushion between the alarm and trip (low-water-level heater power trip). The high-level-alarm point is 185.4 cm (73 in.) above the low-level-alarm point. The normal working volume range of the pressurizer is therefore ~0.105 x 10^{-2} m^3 (3.7 ft^3). A reserve volume above the high-water-level-alarm point contains ~5.66 x 10^{-2} m^3 (2 ft^3) of steam.

Degasification of water in the main loop, when needed, is effected by injecting a small stream of water from the loop into the top region of the pressurizer. A perforated internal tube is used to spray this injected water inside a thermal sleeve. The sleeve protects the outer wall of the pressurizer against thermal shock, which would result if the cooler injected water were allowed to impinge on the hotter wall. Noncondensable gases are evolved and accumulated in the steam volume at the pressurizer. These gases are manually vented from the pressurizer when the temperature

in the steam volume is observed to vary from the saturation temperature at the prevailing pressure.

For reducing the pressure when desired, a cooling coil is provided in the steam space at the top of the pressurizer. The coil is formed of 3/8-in.-OD by 0.065-in.-wall tubing to a diameter of 20.32 cm (8 in.) with 2.54-cm (1-in.) center-to-center spacing and has a developed length of ~7.0 m (23 ft). Air is used as the coolant inside the tubes. Additionally, depressurization may be accomplished by means of the water injection method described for degasification. By this latter means, cooler water from the main loop is injected directly into the pressurizer.

Connections are provided at the pressurizer for liquid-level instrument taps at the top and bottom of the vessel, along with connections for gas venting, relief valve, pressure instrumentation taps, water sampling, and letdown. The 4-in. tee located at the pressurizer bottom provides the connection to the primary loop piping. The 4-in. pipe is reduced to a 2-in. pipe that continues to the tie-in point located between the test section outlet and the main heat exchangers. This line is equipped with a flow-restricting orifice and a control valve capable of isolating the pressurizer from the primary loop.

The pressurizer is designed for operation at up to 1.7×10^4 kPa (2500 psig) at 672 K (1210°R). The highest metal temperature experienced by the heated walls of the pressurizer does not exceed 644 K (1160°R). The pressurizer is designed to meet the requirement of the ASME Boiler and Pressure Vessel Code, Sect. 3, Class 2.

A.2.2 PSS

The PSS functions to contain and condense the steam-water mixture resulting from a blowdown of the primary loop. A receiver tank with three spray headers and recirculating water forms a direct contact heat transfer and containment system that accepts the blowdown effluent from either or both of the blowdown lines connecting the primary loop. A bypass loop with a small heat exchanger removes the pump heat, maintaining the water temperature at <311 K (560°R) prior to blowdown [Fig. 5.19(c)]. It is mandatory that the spray system be in operation and ready to receive the loop contents before the primary temperature is increased by blowdown.

The pressure-suppression tank is ~1.5 m (5 ft) in diameter, is 2.4 m (8 ft) long, and has a volume of 4.4 m^3 (1160 gal). The primary loop inventory is estimated at 437.3 kg (962 lb_m) with a maximum heat content of 6.36×10^5 kJ (603,000 Btu). With all considerations of density changes and final tank level, the beginning tank inventory is set at 1.9 m^3 (509 gal). The final mixed-water temperatures, neglecting metal tank heat capacities, reach ~371 K (667°R). The pressure-suppression tank is connected to the atmosphere by a 20.3-cm-diam (8-in.) pipe that exits through the west wall of the pit into the subbasement area.

Blowdown reaction forces have been considered, and the necessary bracing and hydraulic snubbers are provided for in the design. The blowdown piping is sloped for drainage to prevent the collection of fluid, which might be propelled into the pressure-suppression tank during blowdown. Slug dispersers, which consist of a pyramid of concentric rings with a 10° dispersion angle, are also provided in each of the blowdown lines.

A.2.2.1 PSS receiver/reservoir tank. This tank serves two functions: (1) as a storage volume for cool water to be used for spray and (2) as a condenser with vapor space into which water is sprayed. Three spray manifolds, each containing 24 nozzles, are installed parallel to the tank axis in the upper-half of the horizontal tank. The manifolds are as close to the wall as possible (limited by a knuckle in the tank head), and the nozzles are aimed to direct spray horizontally or upward in an overlapping pattern. The blowdown lines enter the end of the pressure-suppression tank in the spray area above the water level. A disperser is provided on each of the blowdown lines in the unlikely event that a liquid slug is propelled into the tank by high-pressure vapor. The disperser is inserted into the tank at the blowdown line inlet so that it is replaceable if damaged. The disperser consists of a series of five concentric rings, each of a smaller diameter than the previous one and each having a 10° dispersion angle.

In the event of a failure of the spray system during blowdown, a 20.3-cm (8-in.) relief pipe extends through the wall adjacent to the tank and into an exclusion area. A resultant reaction force of up to 2.94×10^4 N (6600 lb_f) is possible if saturated steam at 688 kPa (100 psia) and sonic velocity are relieved through this line. Appropriate anchors are provided for the relief pipe and the tank to withstand these forces. The tank has three blind flange openings for inspection and cleaning in the event that some debris is carried over during blowdown. A 1-in. drain connection is in the bottom, and a sight gauge is provided for level indication. The main characteristics of the tank are summarized in Table A.1.

A.2.2.2 Spray circulation pump. The function of the pump is to circulate water from the receiver/reservoir tank and deliver it under pressure to the nozzles. This pump will be energized whenever the test facility is pressurized so that steam-condensing capability is provided should a blowdown rupture disk assembly accidentally rupture. The requirements of the pump, as contained in the purchasing specification, are summarized in Table A.2.

All wetted parts of the pump are cast iron, and the horizontal split casing has 125-lb ASA flanged connections. The electric motor driving the pump is of a totally enclosed design because the pump is located in a pit where flooding could occur.

A.2.2.3 Piping. The piping for spray circulation is 6-in. Schedule-40S except that between the pump suction and the reservoir, which is 10-in. Schedule-40S. The head loss is proportioned approximately as follows: (1) pipe and fittings 22.7 kPa (3.3 psi), (2) spray manifold 20.6 kPa (3.0 psi), and (3) nozzles 254.6 kPa (37 psi); this makes a total of 297.9 kPa (43.3 psi).

The blowdown piping and relief valve vent piping are considered part of the PSS because they operate at the same pressure. There are two blowdown lines of 6-in. Schedule-40 carbon steel, one from the test section inlet and one from the outlet, each beginning at the blowdown rupture disk assembly. The inlet blowdown line is 4.6 m (15 ft) long, and the outlet line is 5.5 m (18 ft) long. The blowdown lines are supported by their attachment to the plenum flange at one end and to the pressure-suppression tank at the other. Because the reaction forces during blowdown will be in

Table A.1. Pressure-suppression tank characteristics

Design pressure, kPa (psig)	−68.8 to +688 (−15 to +150)
Design temperature, K (°R)	617 (1110)
Operating pressure range, kPa (psig)	−67.4−459 (−14.7−100)
Operating temperature range, K (°R)	300−424 (540−763)
Hydrostatic test pressure, kPa (psig)	1033 (225)
Internal volume, m^3 (gal)	4.4 (1160)
Approximate size, m (in.)	1.52 OD by 2.69 long (60 OD by 106 long)
Maximum water inventory, m^3 (gal) at K (°R)	2.0 (522) at 311 (560)
Empty weight, kg (lb)	1591 (3500)
Material and grade	Carbon steel, ASTM A285 Grade C
Shell thickness, cm (in.)	1.77 (0.5)
Heads, cm (in.)	ASME flanged and dished (torispherical) 1.59 (0.625) minimum thickness
Design code	ASME Sect. VIII, Division 1
Connections	Bolted and gasketed flange
Spray manifolds, in.	3-1/2 (Schedule-40S pipe)
Nozzle features	
Flow rate, m^3/s at kPa (gpm at psi)	1.31×10^{-3} at 206.4 (20.8 at 30) 1.52×10^{-3} at 275.2 (24.0 at 40)
Hollow cone pattern, deg	90
Orifice diameter, cm (in.)	1.83 (0.72)
Median droplet diameter, μm at kPa (psi)	~2200 at 206.4 (30)

the upward direction, the plenum lower flanges are supported from below by pinned rods that allow horizontal movement. Analysis of blowdown forces indicated the need for shock suppression on the lower (test section inlet) of the two blowdown lines. A 12,500-lb, 5-in.-stroke hydraulic shock suppressor and a cross member are installed between the two tie rods and the main structural support.

The vent sides of the two relief valves on the pressurizer and test section outlet are tied into the PSS via the blowdown lines. The test section relief valve is located just above the outlet blowdown connection,

Table A.2. Spray circulation pump characteristics

Design capacity, m^3/s (gpm)	9.47×10^{-2} (1500)
Total head at design capacity, m (ft)	30.5 (100)
Pumped liquid	Demineralized water
Elevation of free surface above pump suction, m (ft)	~1.5 (~5)
Suction conditions	Flooded
Pump NPSH[a] at design capacity, m (ft)	~1.8 (~6)
Available NPSH at design capacity and saturated, m (ft)	~2 (~6.5)
Pump speed, rpm	1150
Pump rotation viewed from driven end	Counterclockwise
Maximum water temperature at inlet, K (°R)	424 (763)
Minimum water temperature at inlet, K (°R)	300 (540)

[a]Net pump suction head.

and its vent line (3-in. Schedule-40) bypasses the blowdown rupture disk station. Because this vent line will operate in a relatively cold condition, a bellows is provided to accommodate differential expansion between it and the test section outlet. Piping flexibility analysis indicated also that an expansion joint was needed on the inlet of the PSS circulating pump. This pump is short-coupled to the pressure-suppression tank by 10-in. Schedule-40 pipe and, during blowdown, must accommodate the temperature increase of the recirculating spray water.

A.2.2.4 PSS heat exchanger. The PSS pump supplies ~45 kW(t) of heat to the spray water. To keep the water cool during pump operation prior to blowdown, a heat exchanger is required. This unit, a Young Radiator Company No. SSF-606-ER-1P, was installed in a small bypass line between the discharge and suction of the spray circulation pump. The design value for the spray water was 311 K (560°R), but it was desirable to have the capability of using cooler spray to accommodate, for example, very rapid blowdowns. The Young heat exchanger was selected for this application because only 1.49 m^2 (16 ft^2) of the total exchanger area of 5.11 m^2 (55 ft^2) is required to maintain the spray water to 311 K (560°R) or less. The heat exchanger characteristics are presented in Table A.3.

A.2.3 Critical flow nozzle and blowdown rupture disk assembly

The blowdown rate is controlled by the critical flow nozzles located in the base of the plenum at the intersection between the loop and test section piping. The double-diaphragm blowdown rupture disks are located

Table A.3. PSS heat exchanger characteristics
(Young No. SSF-606-ER-1P)

Thermal duty, kW(t) (Btu/h)	45 (13,200)
Coolant and loop water flow rates, m^3/s (gpm)	3.16×10^{-3} (50)
Available cooling water temperature, K (°R)	300 (540)
Spray loop water temperature, K (°R)	311 (560)
Area required for 300 K (540°R) loop water, m^2 (ft^2)	3.8 (41)
Area required for 311 K (560°R) loop water, m^2 (ft^2)	1.5 (16)
Minimum pressure rating, kPa (psig)	1032 (150)
Minimum temperature rating, K (°R)	450 (810)
Total exchanger surface area, m^2 (ft^2)	5.11 (55.8)
Material	316 stainless steel
Tube size (OD x wall), cm (in.)	0.95 x 0.0635 (0.375 x 0.025)
Effective length, cm (in.)	137.2 (54)

just below the critical flow nozzle. To simulate the ratio of the pipe flow area to total core flow area of the PWRs, the total break size area required is 1.25 m^2 (0.0135 ft^2). The tests include test section inlet-outlet flow splits of 100 to 0% and all intermediate values. Thus, to cover the range of flow splits including 0% (no split or orifice) to 100%, nozzle diameters range up to 4.0 cm (1.57 in.). A drawing showing the critical orifice nozzle as well as a compilation of presently available nozzles is given in Fig. A.4. The blowdown rupture disk assembly is located just below the critical flow orifice nozzle, positioned between 6-in. weld neck flanges that form the coupling between the primary system and the blowdown lines. The nozzles are replaceable along with the rupture disk assembly to minimize the downtime between tests. A photograph showing the ruptured disks and the critical flow nozzle orientation (out of the system) is shown in Fig. A.5. A photograph of the rupture disks is shown in Fig. A.6 (postblowdown).

A.2.4 Heat exchangers A-D

Four heat exchangers (A-D) are used for primary fluid heat removal. All four are Graham Heliflow heat exchangers that feature a compact, spirally coiled tube bundle (Fig. A.7) and high-performance characteristics. Primary fluid at high temperature and pressure flows through the coil inside while cooling water (secondary fluid) flows through a shell

ORNL–DWG 82–5444 ETD

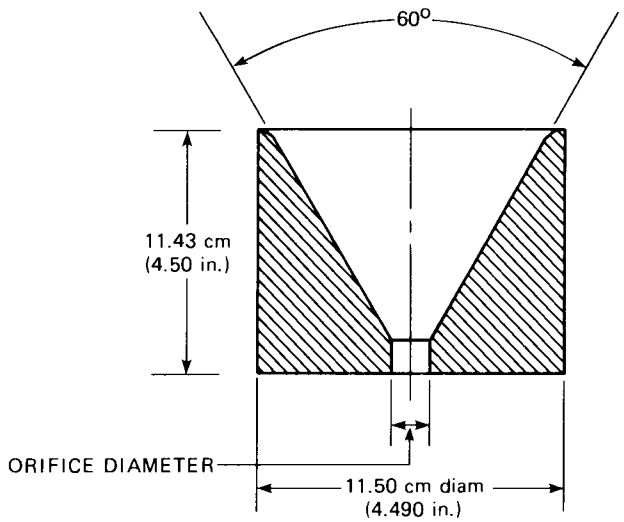

AVAILABLE ORIFICE SIZES

BREAK (%)	ORIFICE DIAMETER cm (in.)
100	4.00 (1.574)
85	3.68 (1.450)
70	3.34 (1.316)
60	3.09 (1.218)
50	2.82 (1.112)
40	2.53 (0.995)
35	2.36 (0.931)
32	2.26 (0.890)
30	2.19 (0.862)
28	2.12 (0.833)
25	2.00 (0.788)
20	1.78 (0.702)
10	1.26 (0.497)

Fig. A.4. Critical flow nozzle and listing of available orifice sizes.

enclosing the tubes. The bundle of tubes is slightly compressed between the shell base plate and casing to form a positive spiral circuit for shell-side fluid flow countercurrent to the direction of tube-side flow. The ends of the coiled tubes terminate in manifolds that project through the base plate. Pipe stubs for inlet and outlet shell-side flow are also attached to the casing end. The units are of all-welded construction except for the flanged connection joining the casing to the base plate. With the exception of bolts, gasket, and support bracket, all component parts of the heat exchangers are type 316 stainless steel.

The cooling water for each heat exchanger is supplied by an existing building-wide 9.47×10^{-1}-m^3/s (15,000-gpm), 1.72×10^3-kPa (250-psig)

ORNL PHOTO 6295–78

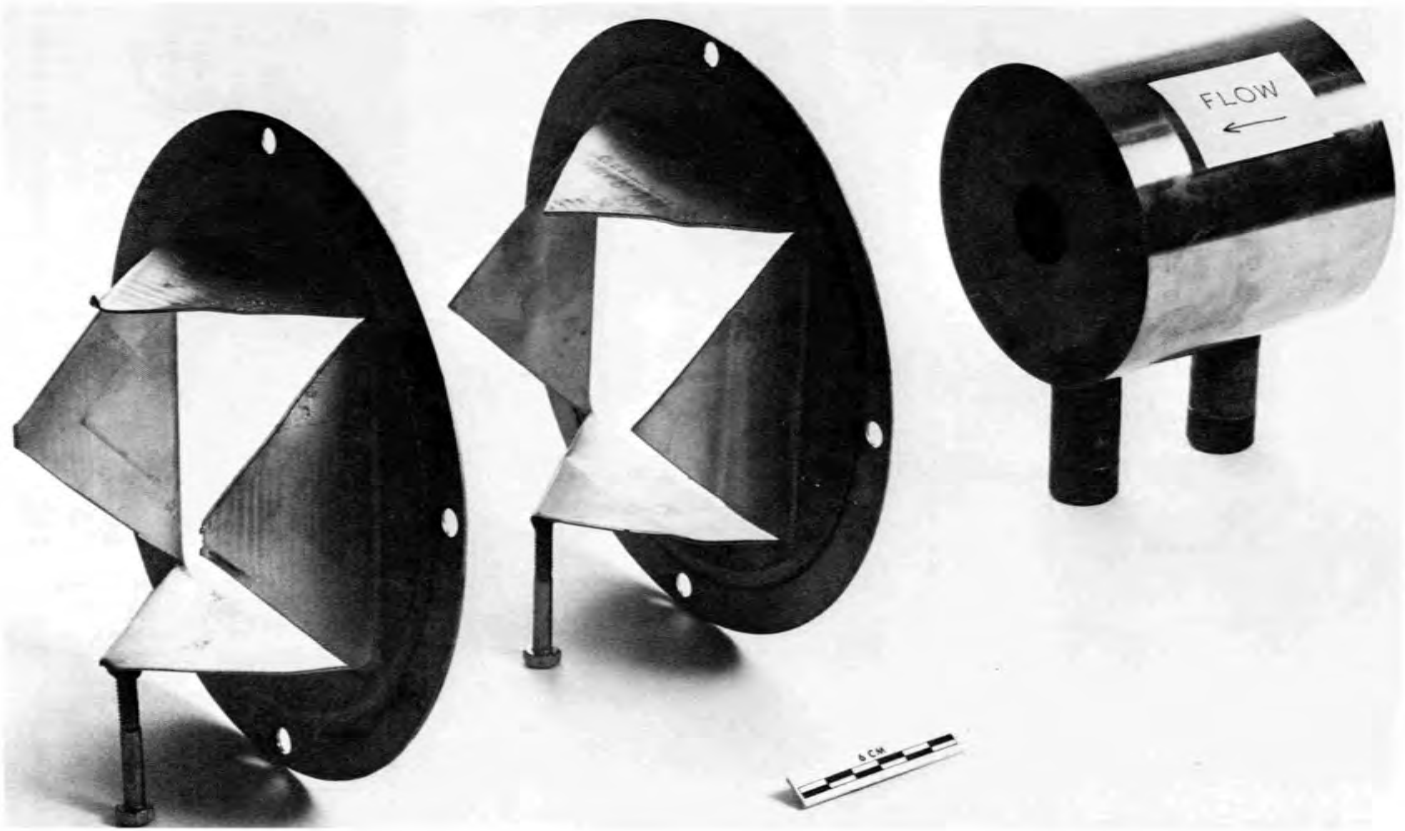

Fig. A.5. Arrangement (out of system) of critical flow nozzle and rupture disk assembly.

ORNL PHOTO 6709–77

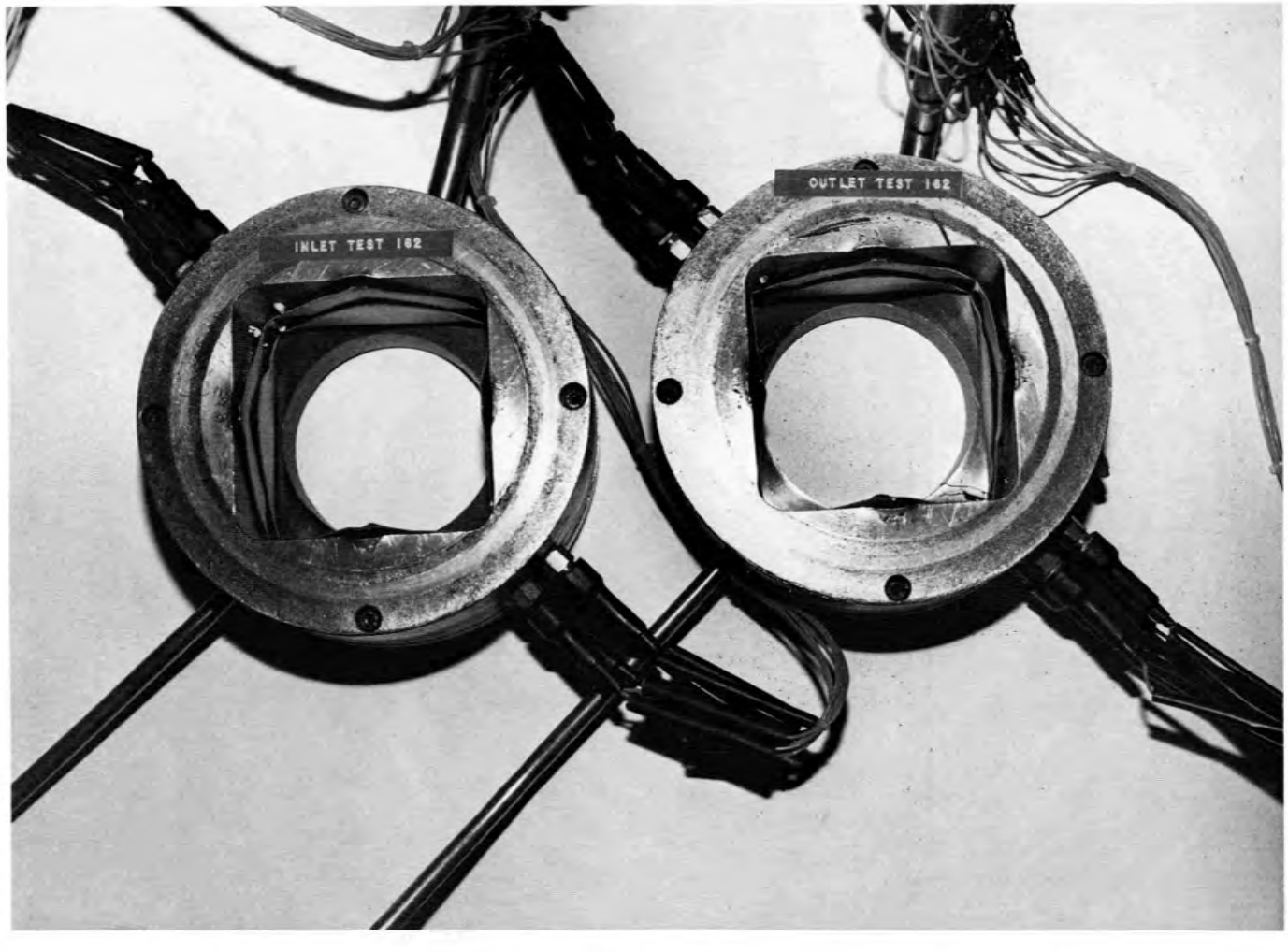

Fig. A.6. Rupture disks following a blowdown (end view).

ORNL PHOTO 3808–78A

Fig. A.7. Graham Heliflow heat exchanger.

recirculating demineralized water system. Heat is rejected to the atmosphere by a large plant cooling tower. The heat exchanger heat removal rate is adjustable over a wide range by variation of the cooling water flow rate. Heat exchangers A, B, and C remove heat generated in the test section, while the smaller heat exchanger D located in the pump bypass loop is used to maintain the temperature level of the loop and to remove heat generated by the primary circulation pump.

A.2.4.1 Main heat exchangers. Test section heat removal is accomplished by three identical heat exchangers (designated Hx A, B, and C) connected in parallel near the test section outlet. The load to each exchanger is controlled manually by three secondary fluid flow control valves, FCV 522, FCV 620, and FCV 720. The heat removal capacity of each exchanger is ~2.5 MW(t). Primary fluid flow to the heat exchangers is controlled by TCV 52, 54, and 56 used in conjunction with the bypass line flow control valve HCV 32 [Fig. 5.19(a)]. Details of specified operating and design characteristics of the primary heat exchangers are presented in Table A.4.

A.2.4.2 Pump bypass heat exchanger D. The pump bypass heat exchanger, denoted as Hx D in Fig. 5.19(b), is used to remove heat generated by the large primary pump and the throttling valve, maintaining or controlling the loop base temperature level. Secondary fluid flow is controlled by TCV 568, while primary fluid flow to the heat exchanger is controlled by the bypass flow control valve TCV 13. Operating and design characteristics of the pump bypass heat exchanger are presented in Table A.5.

A.2.5 Circulation pump

The high-head high-capacity circulation pump was originally purchased as a back-up unit for an Atomic Energy Commission (AEC) program at Battelle Northwest Laboratories (BNWL) and was made available to ORNL on an indefinite loan. The pump was intended for use in blowdown tests at BNWL and, except for excess discharge head, was well suited for the requirements of this program. The pump was designed and fabricated in the period 1965 to 1967 by the Bingham Pump Company, Portland, Oregon. A full-range cold hydraulic performance test and a 100-h hot test at 1.37×10^4 kPa (2000 psig), 589 K (1060°R), and 3.16×10^{-2} m^3/s (500 gpm), followed by disassembly and inspection, were completed by Bingham before delivery to BNWL, but the pump had not seen experimental service.

The Bingham 3 x 6 x 17 CJM pump (Serial No. 250920) is a two-stage, double-volute, horizontal, centerline-mounted, heavy-duty, centrifugal unit suitable for continuous operation at high system temperatures and pressures. Performance curves are shown in Fig. A.8, and a photograph of the pump is shown in Fig. A.9. This pump was specifically designed for high-pressure service and uses a stiff shaft to minimize deflection. The volute casing is radially split at each end with removable cover stuffing box units to enable disassembly without disturbing the connecting piping or the driver unit. All parts are machined to close tolerances, and rotating parts are dynamically balanced for smooth operation. The pump has babbitted journal bearings at each end of the shaft and a duplex ball thrust bearing on the outboard end. A self-contained oil-ring-type lubrication system, with oil level maintained by constant-level oilers, provides lubrication for the bearings.

Shaft seals are patented durametallic high-pressure units isolated from the high-temperature zones by an air gap. Seal cooling is accomplished by a closed internal system using a pumping disk on the pump shaft to circulate cooling water from the seal chamber through a heat exchanger and back to the seal. The two seal coolant heat exchangers

Table A.4. Specified operating and design characteristics of primary heat exchangers (Graham Heliflow No. 12-6C6C-225)

Parameters	Conditions	
	Tube side (primary fluid)	Shell side (secondary fluid)
Flow rate, kg/h (lb_m/h)	15,910 (35,000)	20,450 (45,000)
Maximum inlet temperature, K (°R)	617 (1110)	300 (540)
Maximum outlet temperature, K (°R)	481 (866)	406 (730)
Maximum pressure drop, kPa (psi)	68.8 (10)	82.6 (12)
Operating pressure, kPa (psig)	1.7×10^3–1.58×10^4 (250–2300)	1.4×10^3–1.7×10^3 (200–250)
Design pressure, kPa (psig)	1.7×10^4 (2500)	1.7×10^3 (250)
Hydrostatic test pressure, kPa (psig)	3.0×10^4 (4400)	3.3×10^3 (475)
Design temperature, K (°R)	617 (1110)	478 (860)
Nozzle pipe size	2-in. Schedule-80	2-in. Schedule-40
Number of coils	12	
Surface area, m^2 (ft^2)	3.3 (35.5)	
Coil diameter, cm (in.)	1.27 (0.5)	
Coil length, m (ft)	5.9 (19.25)	
Tube wall, cm (in.)	0.12 (0.049)	
Fluid	Demineralized water, liquid phase	Demineralized water, liquid phase
Total duty, MW(t) (Btu/h)	~2.5 (~8.54×10^6)	

Table A.5. Specified operating and design characteristics of pump bypass heat exchanger (Graham Heliflow No. 9-6C6C-14S)

Parameters	Conditions	
	Tube side (primary fluid)	Shell side (secondary fluid)
Flow rate, kg/h (lb_m/h)	6820 (15,000)	6820 (15,000)
Maximum inlet temperature, K (°R)	617 (1160)	300 (540)
Maximum outlet temperature, K (°R)	568 (1023)	348 (627)
Maximum pressure drop, kPa (psia)	34.4 (5)	192.7 (28)
Operating pressure, kPa (psig)	1.58×10^4 (2300)	1.4×10^3–1.7×10^3 (200–250)
Design pressure, kPa (psig)	1.7×10^4 (2500)	1.7×10^3 (250)
Hydrostatic test pressure, kPa (psig)	3.0×10^4 (4400)	3.3×10^3 (475)
Design temperature, K (°R)	617 (1110)	
Nozzle pipe size	1-in. Schedule-80	1-in. Schedule-40
Number of coils	9	
Surface area, m^2 (ft^2)	0.895 (9.63)	
Coil diameter, cm (in.)	1.27 (0.5)	
Coil length, m (ft)	2.49 (8.16)	
Tube wall, cm (in.)	0.12 (0.049)	
Fluid	Demineralized water, liquid phase	Demineralized water, liquid phase
Total duty, MW(t) (Btu/h)	0.38 (~1.3×10^6)	

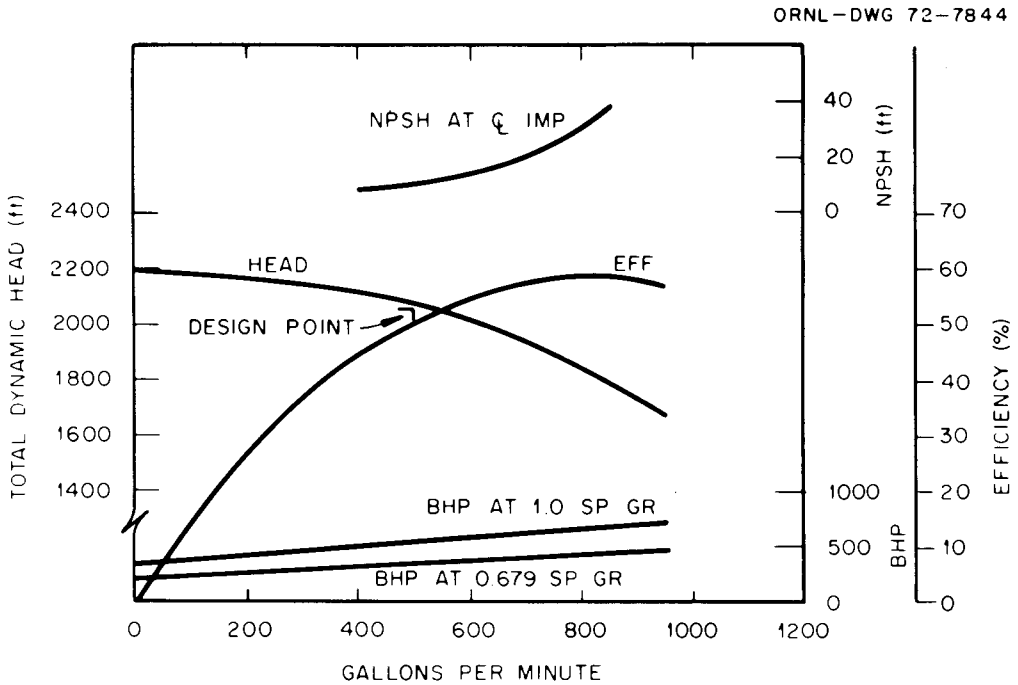

Fig. A.8. Bingham pump characteristics.

furnished with the pump are models 8 x 6C-12 Graham Heliflow units with a tube-side design pressure of 2.06 x 10^4 kPa (3000 psig) and hydrostatic test pressures of 3.09 x 10^4 kPa (4500 psig) on the tube side and 1.03 x 10^3 kPa (150 psig) on the shell side. Basic construction of the heat exchangers is the same as that of the system primary heat exchangers described in Sect. A.2.4. Water jackets are also located around the stuffing boxes, around the bearing mounts, in the bearing housing, and around the pump pedestal. Each of these cooling jackets is served by an external water supply at the following typical conditions:

Heat exchanger flow	3.16 x 10^{-4} m^3/s (5 gpm)
Pump pedestal flow	3.16 x 10^{-4} m^3/s (5 gpm)
Bearing housing flow	1.90 x 10^{-4} m^3/s (3 gpm)
Bearing bracket flow	1.26 x 10^{-4} m^3/s (2 gpm)
Stuffing box flow	3.16 x 10^{-4} m^3/s (5 gpm)
Maximum temperature rise	5.6–8.3 K (10–15°R)
Maximum inlet temperature	50.0–52.8 K (90–95°R)
Maximum pressure	1.03 x 10^3 kPa (150 psig)

Protective and surveillance instrumentation recommended by the manufacturer included vibration monitors on bearing housings and temperature indication of pump bearings, process fluid at the pump suction, inlet and outlet seal recirculation fluid, and inlet and outlet cooling water. In general, correct capacities and pressures indicate normal operation; unusual noise, vibration, or heat is a sign of developing trouble. Symptoms of seal deterioration would include increased seal leakage and increased

Y-12 PHOTO
157247

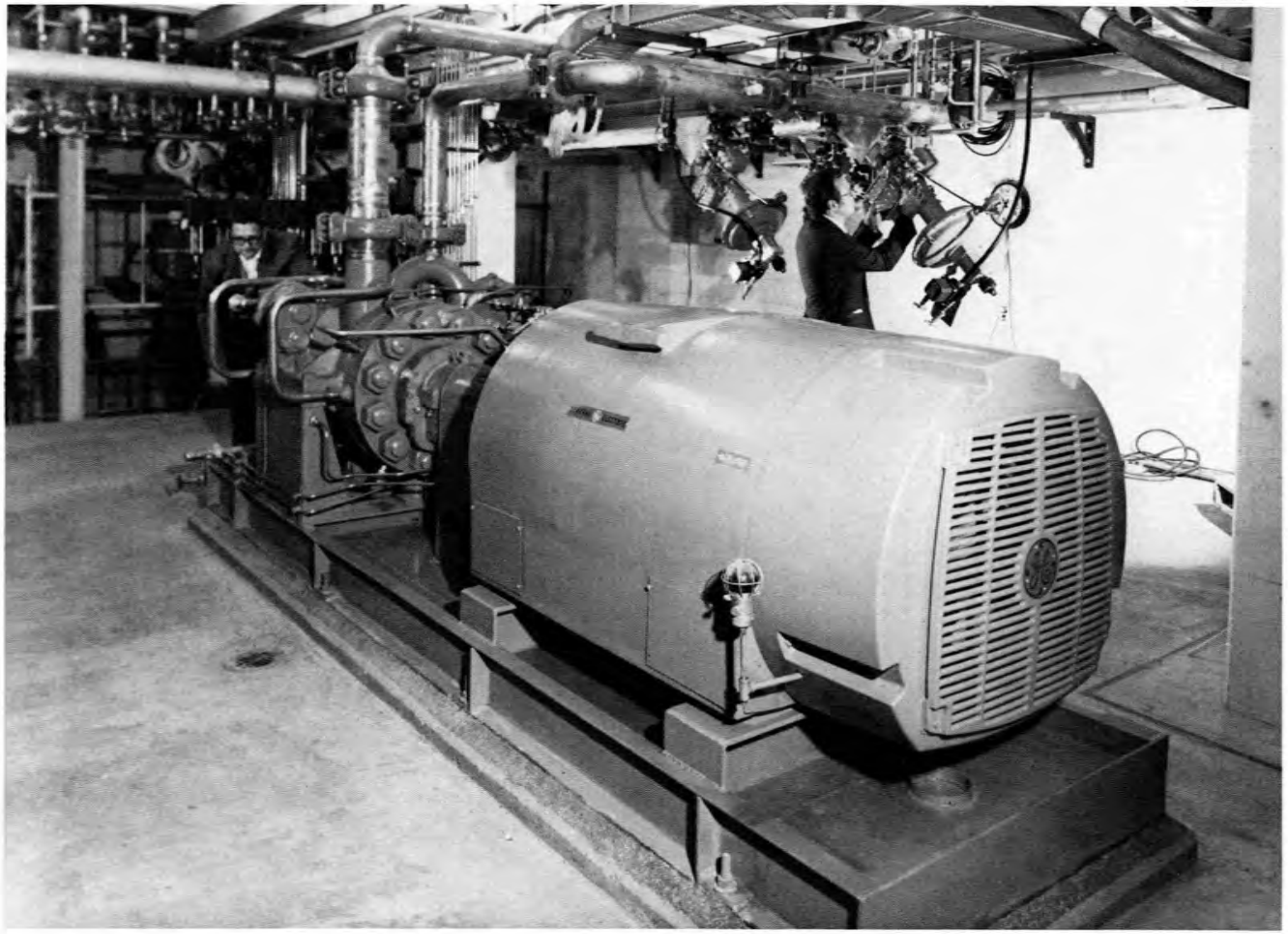

Fig. A.9. THTF two-stage Bingham pump.

temperature of the seal recirculation fluid, the seal heat exchanger cooling water, and the stuffing box cooling water.

A.2.6 Primary fluid makeup system

When the primary system is at operating temperature and pressure, significant leaks in the piping flanges and instrumentation flanges cannot be tolerated because they could damage the structural integrity of the facility. In the early phases of THTF operations, it became evident that a makeup system was essential because of leaks caused by loop thermal cycling and because of primary pump seal leakage. Thus, a simple system of four air-driven water pumps (Fig. A.10) was installed. The pumps receive their suction from the plant demineralized water system and discharge to any of five loop locations including the mixing tee in the pump bypass line, the inboard or outboard pump seal cavity, and the inner or

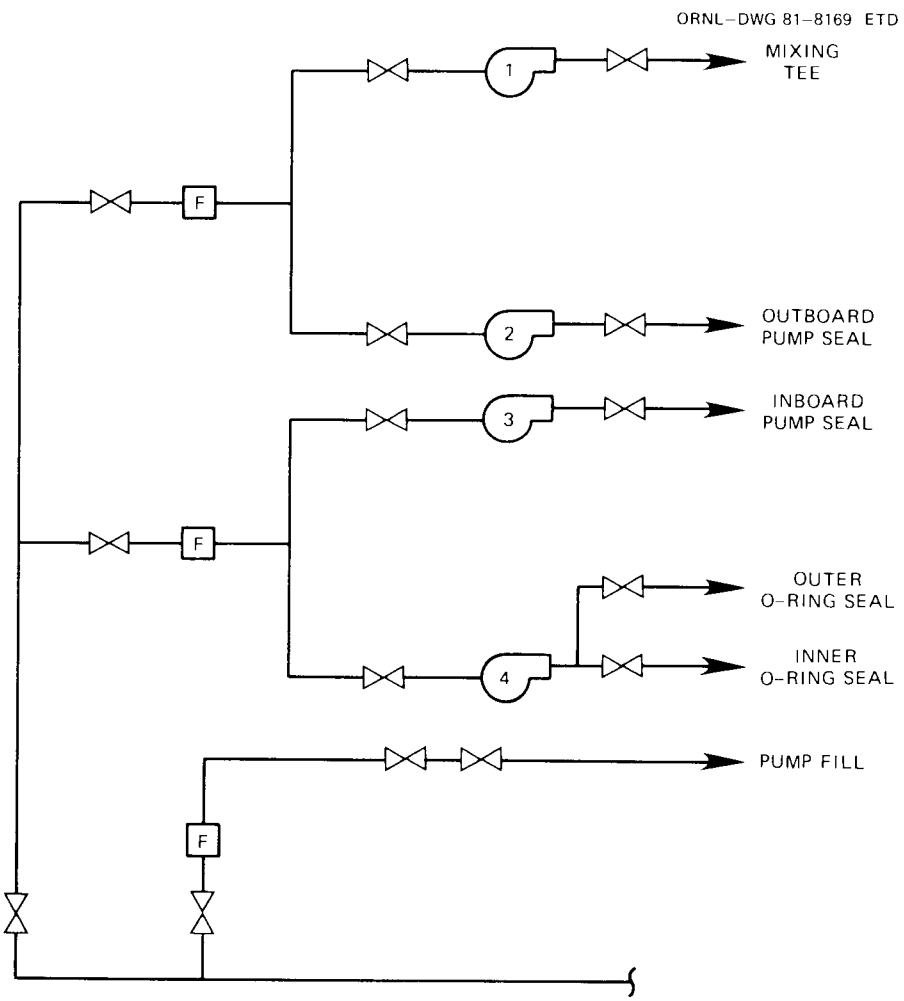

Fig. A.10. Schematic of THTF fluid makeup system.

outer O-ring seal area. Each pump is capable of delivering 4.23 x 10^{-5} m^3/s (0.67 gpm) of demineralized water to the primary loop while at high-pressure operating conditions.

A.2.7 Electrical (ac) power system

The ac electrical power system supplies power to equipment heaters, the primary circulating pump motor, the PSS pump motor, and instruments and controls. The 600-hp circulating pump motor is fed from a 2300-V circuit breaker located in a transformer vault room through three No. 2/0 5-kV cables. Thermal and overcurrent relays located at the switchgear provide motor protection. The pressure-suppression motor ($\leq$60 hp) is fed by a 460-V building power system. Instruments and equipment heaters are supplied by a 300-kVA, three-phase, 480-120/208-V transformer while control power is fed from a separate 5-kVA, 480-120/240-V transformer.

A.2.8 Electrical (dc) power system

The dc electrical power system supplies variable controlled power to the THTF (test section heaters) and to other non-BDHT experiments. Use of the dc power system is scheduled because each experiment program requires exclusive use of the MG units during operations. The dc power system must be capable of supplying 9 MW of power to the THTF at 30,000 A or 310 V.

The dc power system shown schematically in Fig. A.11 includes two MG units located in the northwest corner of Building 9201-2. Each unit consists of an ac synchronous motor coupled to two dc generators. The motors are rated at 700 hp and are fed from a 13.8 kV-area power supply. Each generator is rated at 7140 A, 350 V, and 2.5 MW(e) with a load rating of 125% for 2 h. Due to control system limitations, the generators supply a maximum of 125 kW(e) at ~280 V and 445 A to each of the 60 powered heater rods in the 64-rod Bundle 3. As presented in Fig. A.12 and itemized in Table A.6, each generator powers 15 single-ended indirect heater rods. Each rod is connected to the experiment housing and to the building ground grid, thus grounding the generator power system. The remaining 4 rods in the 64-rod bundle are nonpowered instrument rods (also at ground potential) described in detail in other sections of this report.

The generator output is connected to a single-pole 10,000-A circuit breaker with a 0.03-Ω bypass resistor connected in parallel with the breaker. Two 2.5- by 25.4-cm (1- by 10-in.) aluminum buses are routed to the disconnect switch location near the center of the building. The disconnect switches are interlocked to assign only one experiment to a generator at a time. Four water-cooled 1000 MCM cables connect the switches to the experiment equipment. A single-pole 10,000-A circuit breaker is provided for fast-disconnect operation.

A crowbar-type circuit is provided for each heater to minimize the damage to the heater in the event that a fault occurs. A fast-acting circuit detects a fault when the current to the heater reaches a preset value, and a silicon-controlled rectifier (SCR) is turned on to short-circuit the heater leads. The short-circuit path will divert the current

ORNL–DWG 82–5445 ETD

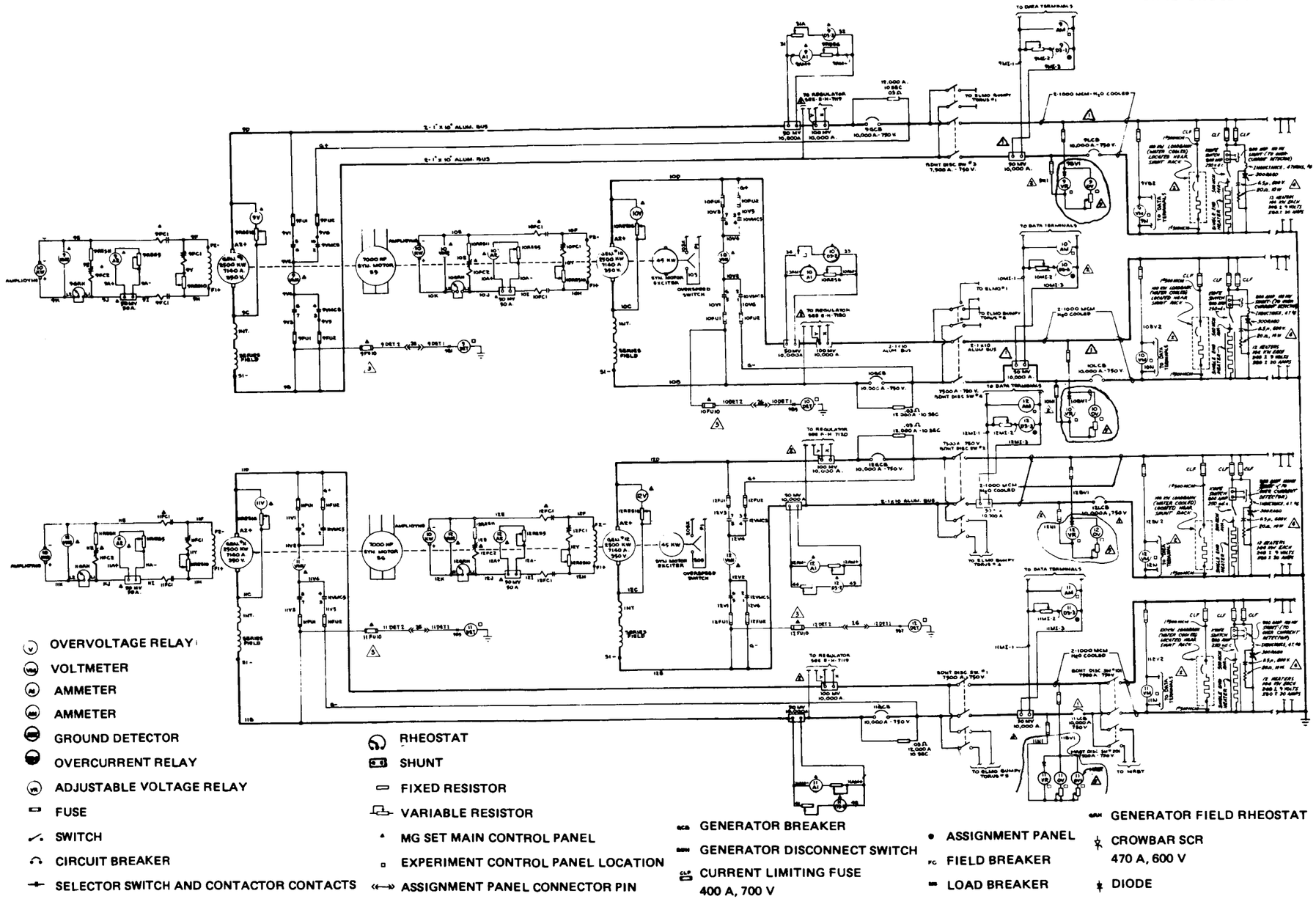

Fig. A.11. THTF dc power system schematic. (Microfiche copy of this drawing attached to back of report.)

ORNL–DWG 81–8170 ETD

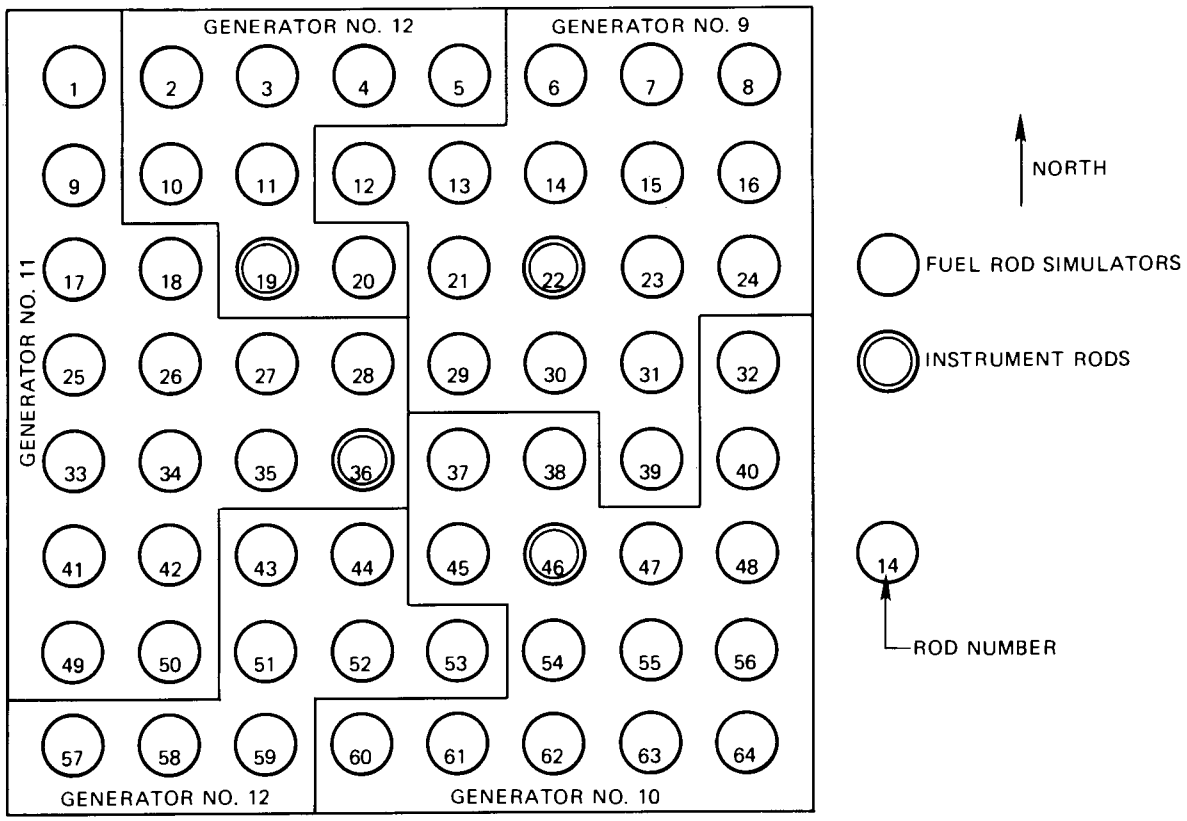

Fig. A.12. Identification of generator power supply distribution in THTF Bundle 3.

Table A.6. Tabulation of THTF heater rods and generators[a]

Generator No.											
9						10			11		12
Heater rods											
6	14	24	32	47	60	1	26	35	2	11	52
7	15	29	37	48	61	9	27	41	3	20	53
8	16	30	38	54	62	17	28	42	4	43	57
12	21	31	40	55	63	18	33	49	5	44	58
13	23	39	45	56	64	25	34	50	10	51	59

[a]Unpowered instrument rods 19, 22, 36, and 46.

from the faulted heater, thus reducing the current through the fault. The fuse limits the short-circuit current and isolates the fault from the generator circuit.

The crowbar circuit includes a shunt in each heater circuit to provide an input signal that is proportional to the heater current. An electronic-type detector unit compares the input signal with an adjustable signal that can be preset by the operator. When the heater current exceeds the preset value, a gating signal is produced to turn on the shorting SCR.

The generator outputs are program-controlled by a function generator located at the control panels and by voltage feedback signals from the generator leads. Signals from these sources are fed to a regulator that controls the amplidyne output and the generator shunt field excitation.

A.2.8.1 Cable coolant system. Power is supplied to the THTF bus from the generator distribution bus by water-cooled conductors. The length of cable run is such that excessive voltage drop (and cable heating) would result if the coolant were not provided. Each generator is provided with two water-cooled conductors for the supply and two for the return. Because the design for this system is standardized for the entire building's dc power distribution system and has been in operation several years, it is considered suitable for the intended purpose.

Demineralized water from the 9.47×10^{-1}-m^3/s (15,000-gpm), building-wide, recirculating cooling system is used for this purpose. Flow control valves and flow indicators are provided with interlocks and alarms to ensure that the cable coolant is circulating before the dc power can be turned on. Loss of coolant initiates automatic shutdown of the power supply.

A.2.8.2 Heater rod dc power connections. Each of the single-ended indirect heater rods has one lead connected to the heater sheath by an end enclosure that, in turn, is anchored in a 5.1-cm-thick (2-in.) nickel plate located at the test section bottom (Fig. A.13). The nickel plate and test section are connected to the building ground grid, thus grounding the heater rods and the system at this location. The upper heater ends extend from the top of the test section. The upper heater ends are of various lengths (Figs. A.14 and A.15) forming a "Christmas tree" pattern to facilitate connection of the positive dc power leads. The positive dc power is carried by 500 MCM cable to a copper connector lug capable of conducting 485 A that, in turn, is clamped to the upper heater rod ends. Each heater rod lead-in is electrically insulated by a single layer of fiberglass tape and separated by micarta sheet spacers (Fig. A.16). Plant equipment air is directed at the lead-in area to provide area cooling.

A.2.9 Test section seal cooling systems

The heater rods must be sealed while also allowing for expansion when heating current is applied. The provision for individual heater rod movement is necessary to allow for some expected test conditions calling for certain rods to be unheated or for radial power profiles where all rods will not operate at equal temperatures. The sealing is accomplished with dual elastomer O-rings in two seal plates. The seal plates form a chamber

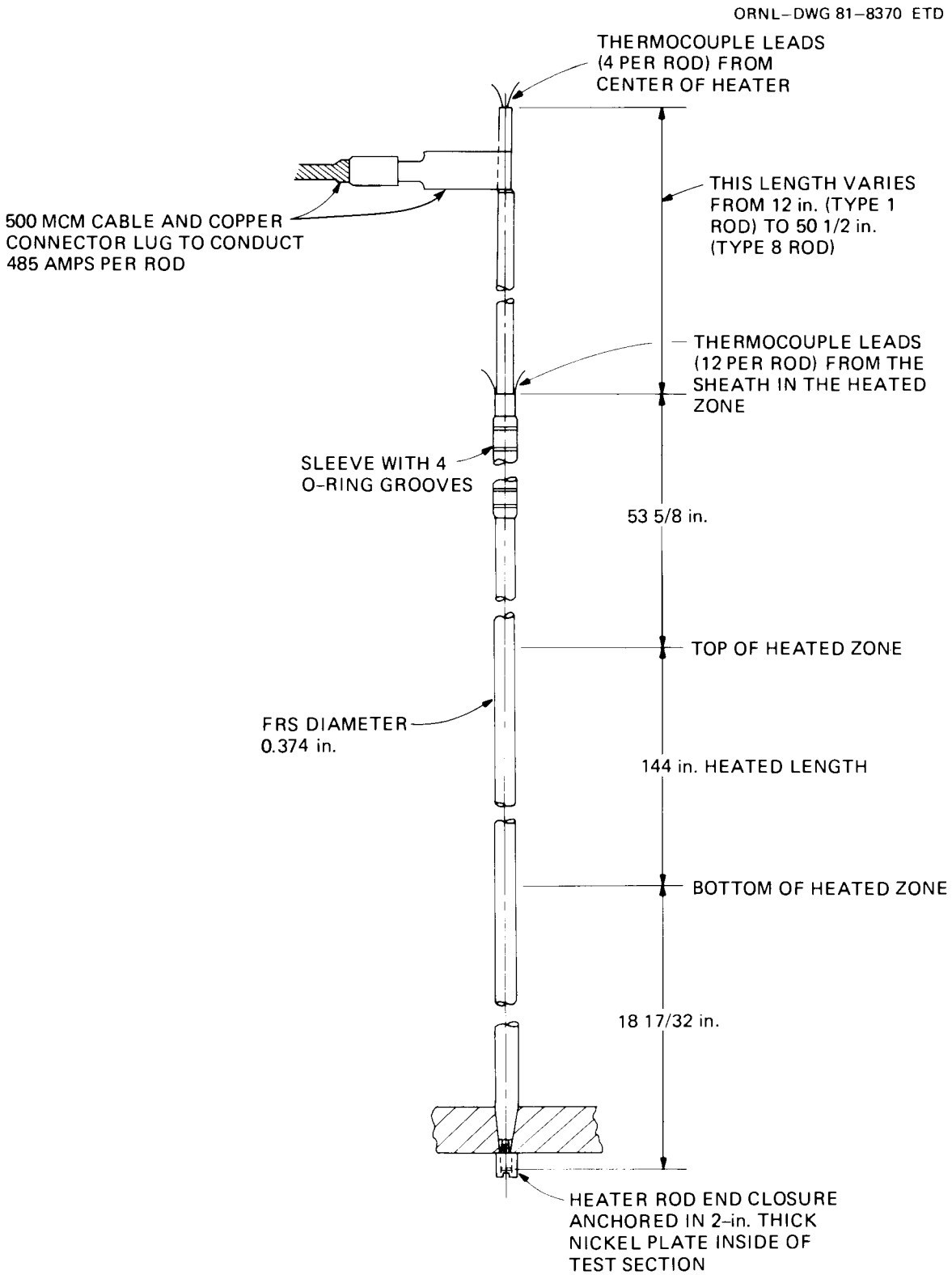

Fig. A.13. Axial view of FRS and FRS dc power connections.

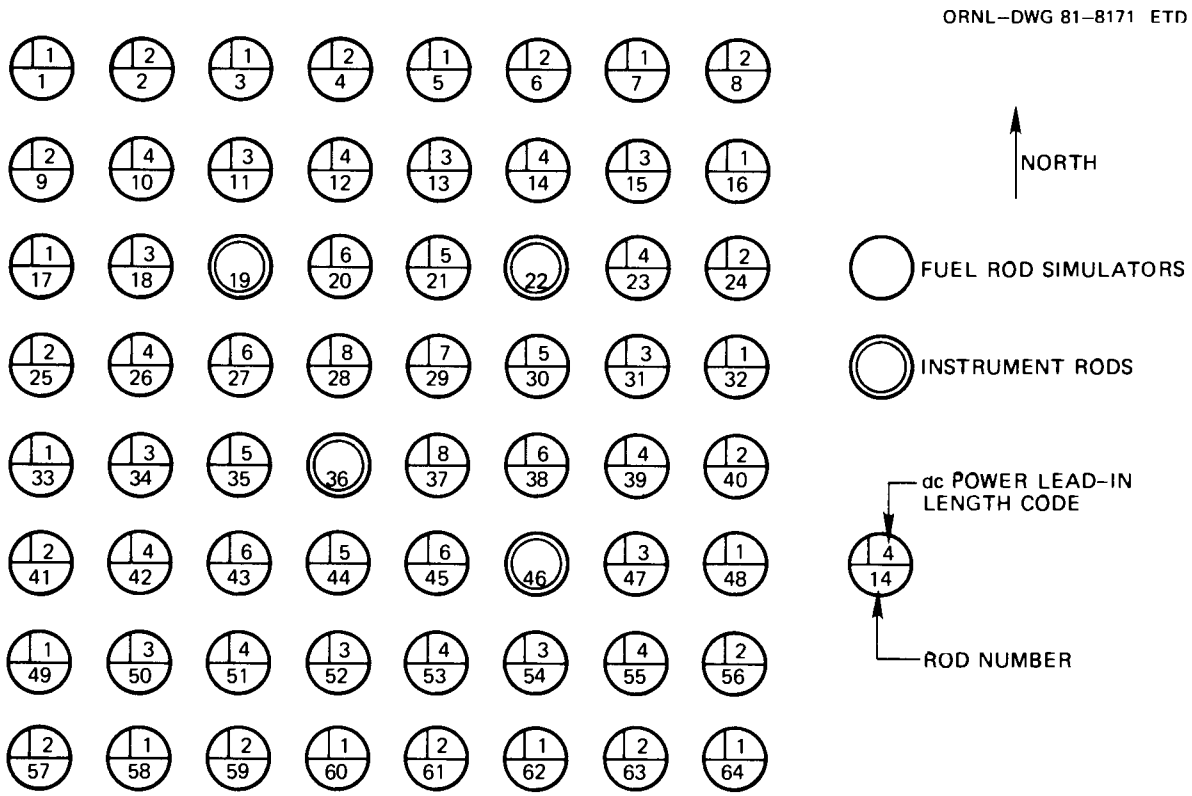

Fig. A.14. Identification of dc power lead-in length codes for THTF Bundle 3.

Lead-in length code	Length [cm (in.)]
1	30.5 (12.0)
2	44.5 (17.5)
3	58.4 (23.0)
4	72.4 (28.5)
5	86.4 (34.0)
6	100.3 (39.5)
7	114.3 (45.0)
8	128.3 (50.5)

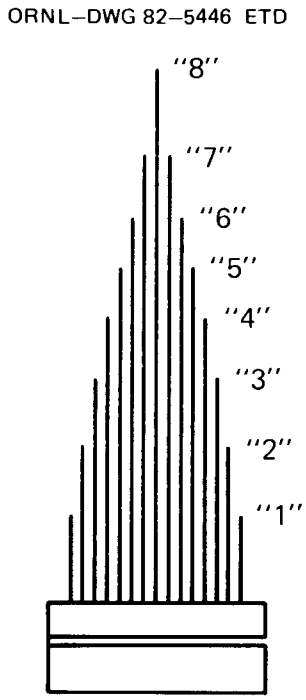

Fig. A.15. Tabulation of FRS lead-in length code.

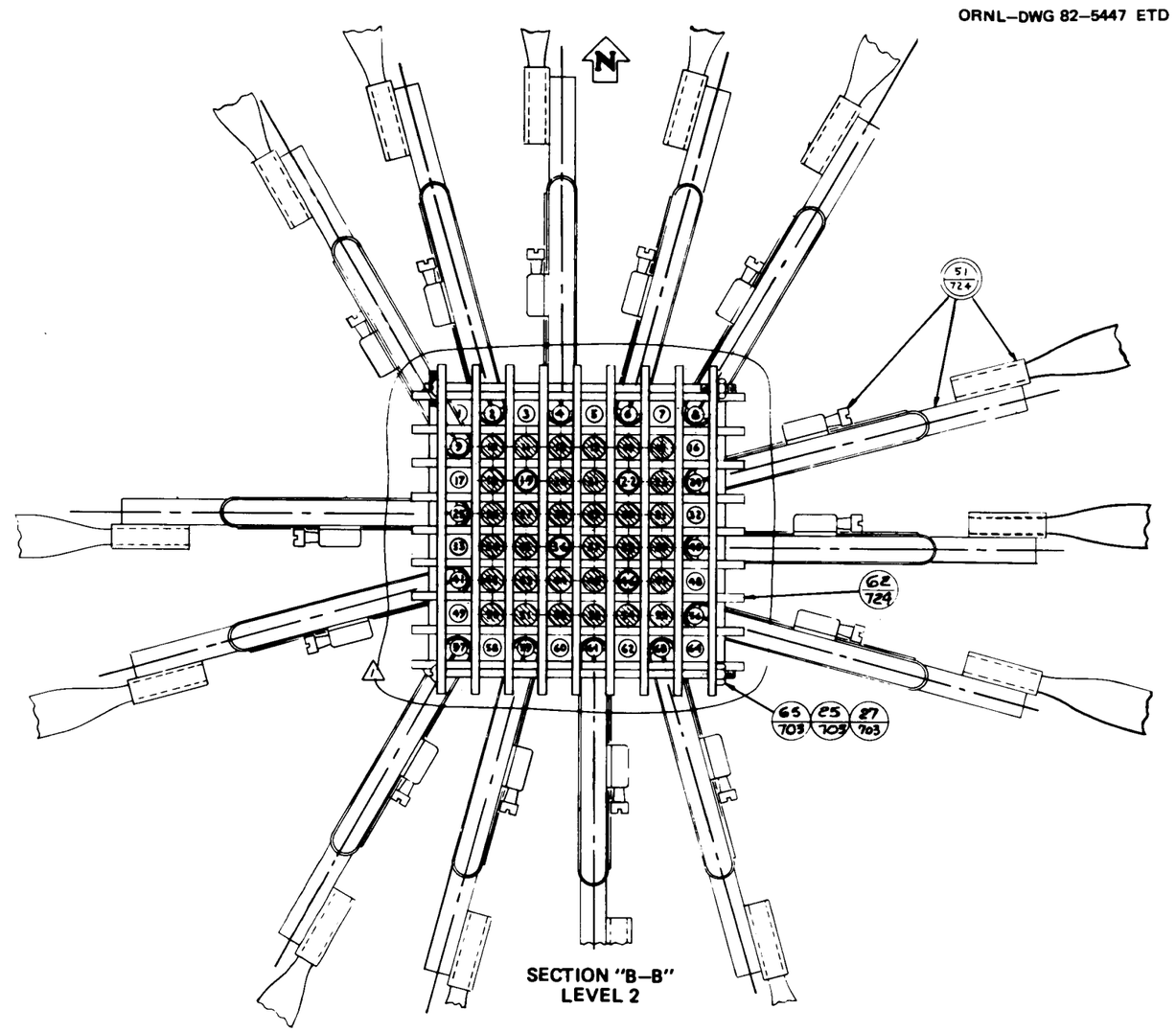

Fig. A.16. FRS micarta sheet spacers.

that is maintained at a buffer pressure between that of the test section and atmospheric.

The seal rings, made of Viton E 60 or of ethylene propylene material, must be maintained at temperatures <477 K (860°R) for necessary reliability. Due to the small copper cross section available in the lead-in conductor at this point, some heat is generated in the "unheated" portion of the rods extending through the seal area. Cooling is provided on all seal plate faces by three separate systems (Fig. A.17). Cooling above the top seal plate is provided by ducted air flowing across the rods. The chamber between the two seal plates is cooled by a small recirculating water system. The area below the lower seal plate is cooled by primary loop water obtained upstream of the test section and cooled by a small U-tube heat exchanger. The total heat generated by the heater lead-ins is ~1.5 kW/in. of rod bundle at 60 kW/rod.

The air cooling for the top seal plate is provided by a New York N 23P-15 blower with a capacity of 1500 ft^3/m at 42 in. H_2O. More than 15 m^2 (50 ft) of 6-in.-diam flexible duct and Schedule-10 pipe is used to supply air to the special air shroud around the 64-rod bundle and to exhaust the hot air to the subbasement area. The flow is split so that about two-thirds crosses the rod bundle and the remaining one-third exits parallel to the heater rods through slightly enlarged openings around the rods. This leakage air flow exiting the top of the air shroud provides cooling for the heater rod moisture barrier located just above the shroud. The air flow is designed to maintain the outer seal temperature at 450 K (810°R) or below.

Cooling water is circulated through the chamber between the seal plates by a low-pressure recirculating seal cooling system. This system consists of a small canned-rotor 1/4-hp pump, a 10-kW Borg-Warner heat exchanger (model CU 7254), a small pressurizer, and connecting tubing. A flow of ~3.16×10^{-4} m^3/s (5 gpm) is circulated through the seal chamber at ~340 K (610°R) and 6.9×10^3 kPa (1000 psig). Cooling water for the heat exchanger is provided by the demineralized cooling water system. This cooling system removes the heat generated in this portion of the rod bundle plus that conducted by the rods and the inner seal plate from the 505 K (910°R) temperature area below this plate.

The lower surface of the inner seal plate is cooled by a small flow [~1.26×10^{-4} m^3/s (2 gpm)] of high-pressure water from the primary loop obtained upstream of FCV-18. This primary loop water, which can run as high as 589 K (1060°R) during isothermal test operation, is cooled by a small jacketed U-tube heat exchanger to $\leq$450 K (810°R) before entering the test section at the upper flange. The flow is directed to a small plenum formed by the lower seal plate and a flow restrictor plate (volume plug). A small clearance between the heater rods and the flow restrictor plate ensures an even flow distribution around all 64 rods. After exiting the flow restrictor plate, the water rejoins the test section flow in the test bundle outlet plenum. This flow, in conjunction with the cooling water on the upper surface of this seal plate, is regulated to maintain the seal temperature below 478 K (860°R). Note that this flow is cut off prior to taking data scans, because the flow does drain into the top of the test section.

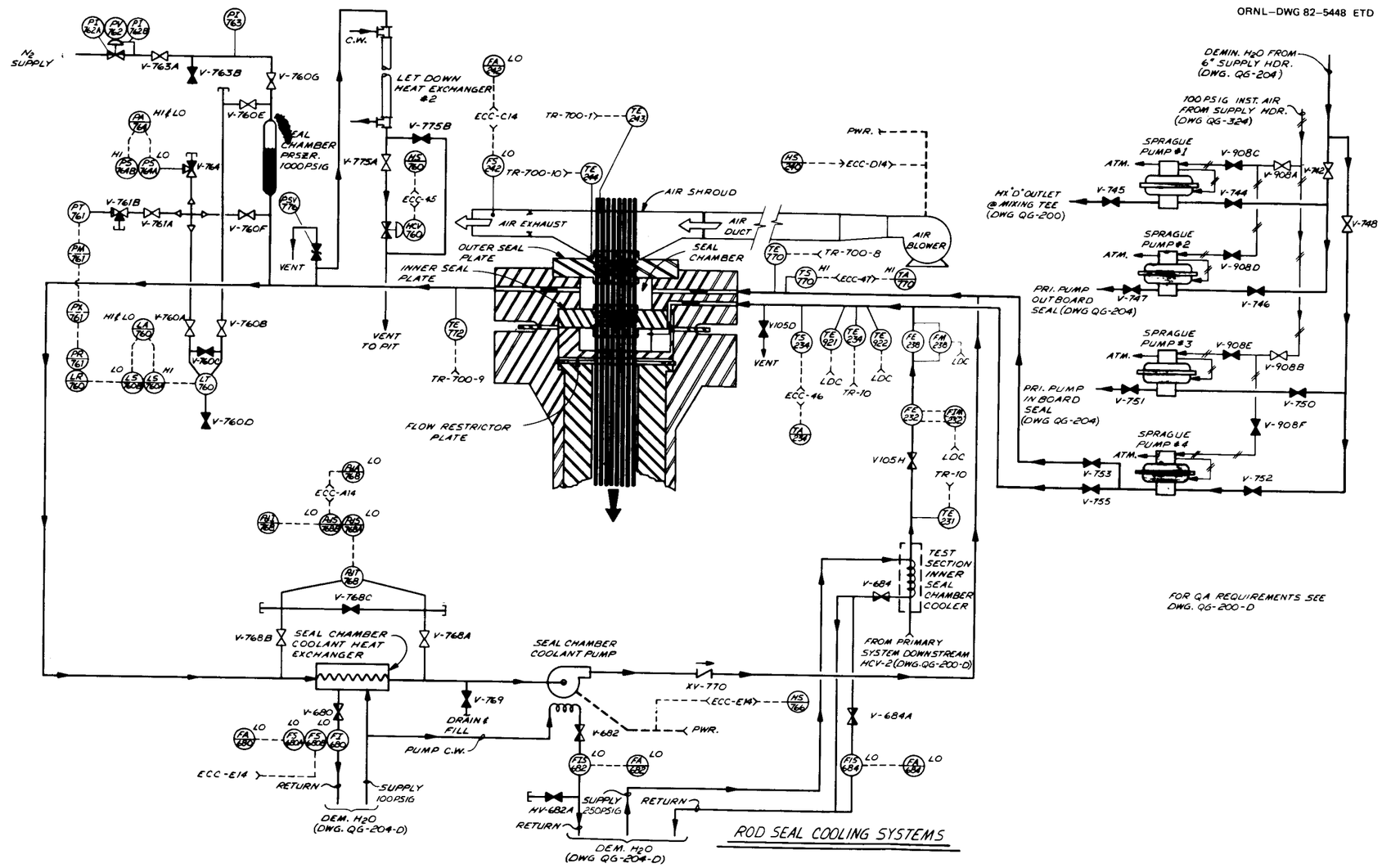

Fig. A.17. Detail of seal cooling systems. (Microfiche copy of this drawing attached to back of report.)

A.3 Protective Features and Quality Assurance

For protection of personnel and equipment, the instrumentation and controls for this facility include means for detecting out-of-limit and unsafe conditions, annunciators to alert the operators to the existence of such conditions, and interlocks to initiate appropriate protective actions on detection of such conditions.

A.3.1 General description

Many of the off-limit conditions have dual protective functions, both alerting the operator and shutting down the subsystem in which the condition exists. Where possible, two triggering levels are established. The primary level sets off the alarm bell and alerts the operator. In response to the alarm, the operator may initiate corrective action to return the system to normal operating range. A secondary level produces automatic shutdown in the event that the condition progresses farther off limit. Less critical circuits have only a single triggering device. In these cases, one set point applies for both operator alert and system trip.

The automatic shutdown system is designed to be fail-safe. Safety action is initiated by the interruption of control circuit power to the appropriate relays. In this way, loss of electrical control power will result in system shutdown. The facility air supply is interlocked with the system so that loss of air pressure will produce shutdown. Failure of the coolant systems to provide adequate cooling will initiate safety action.

A.3.2 Automatic shutdown systems

When a serious abnormal condition develops, prompt action is initiated automatically to trip the system involved, thus providing protection against damage to equipment. Interlocks are arranged in series so that shutdown will be actuated by any single off-limit condition.

A.3.2.1 Primary circulating pump. This device is heavily instrumented. Before pump startup is permissible, the instrument air supply system must be up to normal pressure, valve controllers must be powered, the primary system pressurizer must have reached a minimum pressure level, secondary cooling water flow must be adequate, and the PSS must be functioning normally. In addition to preventing pump startup, loss of instrument air pressure or controller power will trip the pump breaker. Overtemperature of the primary cooling system and pump bearings, overpressure in the primary piping, excessive pump vibration, or abnormal pump power will also initiate pump shutdown.

A.3.2.2 Primary system pressurizer. The pressurizer establishes and maintains the pressure of the primary system at the designed operating level. Power to the pressurizer heaters that are part of the automatic control circuit is interrupted under certain conditions. Low instrument

air supply pressure, lack of controller power, excessive pressurizer pressure, inadequate cooling water volume, high heater temperature, or the sensing of a blowdown will deenergize the heaters.

A.3.2.3 Test section power. For powered blowdown operations, the heater rod bundle will be in place in the test section. Protection of this assembly is accomplished by deenergizing the load breakers in the dc power supply when one of the following conditions is sensed:

1. low instrument air pressure,
2. loss of instrument power,
3. high primary coolant temperature,
4. low primary coolant flow into the test section,
5. low differential pressure across the test section,
6. insufficient test section outlet pressure,
7. primary pump deenergization,
8. low coolant flow in rod seal cooling system,
9. high rod seal cooling system temperature,
10. FRS high temperature,
11. excessive rate of change of bundle power,
12. high or low generator voltage,
13. low pressure of demineralized water supply, and
14. actuation of fire protection sprinkler system.

To provide additional safety for the FRS bundle, further protective features were incorporated into the automatic shutdown system. An independent power monitor system was designed and implemented to detect anomalies in the dc power system. The power monitor indicates an alarm if any imbalance is detected among the four dc generators or if a preset rate of power change is exceeded. The power monitor trips the bundle power if a second preset rate of power change is exceeded.

A.3.2.4 Blowdown initiation circuit. The blowdown initiation circuit contains interlocks that prevent blowdown until system operating conditions are satisfactory. Blowdown inhibit is in effect as long as (1) primary coolant flow through the test section is low, (2) rupture disk accumulator pressure is below the level required for successful blowdown, (3) control valve actuators are unlocked, or (4) the PPS is not operating properly.

A.3.3 Quality assurance, codes, and standards

The THTF was designed, fabricated, and operated as a quality level III–IV facility. (Quality levels are assigned from I to IV in order of decreasing quality assurance requirements.) Essentially, this means that the electrical, structural, and piping systems are quality level III and come under the jurisdiction of the various appropriate laboratory and industrial codes. Less critical portions, such as the demineralized cooling water system, are quality level IV, to which different standards apply.

The codes and standards selected for each component and/or subsystem in the THTF pressure boundary, along with major systems outside the pressure boundary, are summarized in Table A.7. Some of these codes and standards are discussed below.

Table A.7. Codes and standards applied to THTF

System or component	Quality level	Code or standard applied
High-pressure primary system		
Piping	III	Power Piping Code B 31.1.0
Valves	III	ASME Sect. III, Class 2, Spec. I-10520-QG-002-S-1
Heat exchangers	III	ASME Sect. VIII, Div. 1, Spec. M-10520-RM-001-X-0
Pump	III	See text (Sect. A.3.3.2)
Pressurizer	III	ASME Sect. III, Class 2, Spec. M-10520-RM-005-5-0
Test section container	III	ASME Sect. VIII, Div. 1
Heater rods	III	Spec. E-10520-RM-004-S-0
PPS		
Piping	III	Power Piping Code B 31.1.0
Tank	III	ASME Sect. VIII, Div. 1
Pump	III	See text (Sect. A.3.3.6)
Demineralized cooling water system piping	IV	UCC Tech. Spec. P-1.1, Subsection 107
Instrumentation and CCDAS	III	ORNL Instrumentation and Controls Division standards and procedures
Power supply system (dc)	III	National Electrical Code, NEMA, IEEE, and Underwriters Laboratories standards, ORNL standards and procedures
Support structure	IV	AISC specifications and standard practices

A.3.3.1 Codes and standards for heat exchangers. Heat removal capability over a wide range of operating conditions is required in the THTF. The method selected involves the use of three identical heat exchangers (A, B, and C) with appropriate valving to control the primary fluid flow rate through the exchangers and the cooling water flow rate. In addition, heat exchanger A has the means for controlling the cooling water temperature to minimize the log-mean temperature difference when operating with low heat removal rates at high primary fluid temperature levels.

Some unique features of the Heliflow heat exchangers, manufactured by Graham Manufacturing Company, Inc., are particularly advantageous for applications such as those encountered in the THTF. (See Sect. A.2.4 for a detailed description of the heat exchanger.) Normally, heat exchangers designed to operate at high system pressures require rather thick tube sheets to withstand the attendant pressure loadings. If significant temperature levels are involved, serious thermal stress problems may be encountered. These problems are alleviated in the Heliflow exchanger by replacement of the thick tube sheets with relatively thin tubing manifolds, with the tubes spirally wrapped around the inner manifold and terminating at a second manifold. Differential expansion resulting from temperature gradients along the tube length is easily accommodated by the spiral tube configuration. Additional benefits are derived from these two basic features. For example, the method of spiraling produces a well-defined secondary flow path so that the exchanger functions with either countercurrent or cocurrent flow without bypassing. Also, the spiral arrangement minimizes the space requirements for installation. This feature is particularly important to the THTF, because the additional heat removal equipment must be installed in a very limited space.

Based on the features discussed previously, Graham Heliflow heat exchangers have found wide application in the nuclear industry, and this type of unit was selected for the original THTF construction. Heat exchanger A was purchased in 1969 for that purpose in accordance with an ORNL specification covering design, fabrication, testing, and materials. The specification required that the unit be designed, constructed, and stamped in accordance with Sect. VIII, Div. 1 of the Code. This was considered adequate for the design criteria then applicable to the THTF (i.e., quasi-steady-state CHF research).

Early in the conceptual design of the modifications to increase the capability of the THTF to permit blowdown heat transfer test on 49-rod bundles (Bundle 1) operating at typical PWR conditions of power, flow, and temperature levels, sufficient detailed design was performed to ascertain that two heat exchangers (B and C) identical to A would satisfy the requirements and provide adequate flexibility in the test program. Specifications were written, and procurement of these long-delivery items was initiated.

Based on the technical and programmatic considerations discussed previously, the conclusion was reached that primary system heat exchangers (B and C) procured in accordance with Sect. VIII, Div. 1 of the ASME Code would be fully adequate to satisfy THTF requirements and goals. In addition to the primary system heat removal equipment, a small heat exchanger was required in the bypass flow loop around the main circulating pump. This exchanger (Hx D) was designed to remove the heat generated by the oversized pump and to aid in maintaining the base loop temperature level at the desired set point. Since the same considerations applicable to units B and C are appropriate to unit D, a small Heliflow heat exchanger was selected.

In all cases, the codes and standards used for design, fabrication, and operation of the 49-rod Bundle 1 were applicable and maintained for the 64-rod Bundle 3 described in this report.

A.3.3.2 Codes and standards for the circulating pump. The number of manufacturers that produce pumps suitable for the pressure, flow, and

heat requirements of the THTF is extremely limited. These manufacturers were contacted during the early conceptual design of the modifications to obtain approximate cost and delivery times for a pump having the desired capabilities. The determination was made that the cost of such a pump would be in the range of $100,000–150,000 with delivery in 20–30 months from the date of approval of drawings for fabrication. Both cost and delivery were unacceptable based on project funding and schedule considerations.

A high-head high-capacity circulating pump, which was originally purchased for an AEC blowdown test program at BNWL, was made available to ORNL on an indefinite loan. Except for an excess on the developed head, the pump is well suited for the requirements of the THTF blowdown test program. The pump was designed and fabricated in the period from 1965 to 1967 by the Bingham Pump Company of Portland, Oregon. Purchase order specifications were developed by BNWL based on its experience with previous pumps in blowdown test loops. Because of cancellation of the BNWL program, the pump was never put into service.

The pump purchase order specifications required that the pump be designed to operate at suction temperatures in the range 289 to 589 K (520 to 1060°R) and at suction pressures in the range 100–2500 psig.

Casing design conditions are 2.06×10^4 kPa (3000 psig) at 617 K (1110°R) to accommodate the developed head. No mention is made of an applicable code or of design stress values permitted in the structural components. However, Para. NC-3410 of Sect. III of the ASME Code permits the use of any design method of demonstrated adequacy for the service conditions. It is presumed that purchase of the pump from a reliable manufacturer and supplier of reactor-grade pumps would provide a design based on demonstrated adequacy.

Communication with individuals associated with specification and purchase of the pump gives some insight into the philosophy with which the specifications were developed in early 1965 in an era before adoption of detailed quality assurance requirements. The specifications were developed based on previous experience with the performance of pumps in blowdown services. (Note that a detailed idealized blowdown sequence is given as design criteria in the specifications.) The pump was believed to be urgently needed at the time the order was placed, and details of design, fabrication, and inspection were apparently left to the discretion of the manufacturer. The purchaser believed that possible faulty design or weaknesses present in the pump would appear quickly under operating conditions. Consequently, the specifications included testing, and acceptance was based on satisfactory performance during a 100-h test at 1.37×10^4 kPa (2000 psig), 589 K (1060°R), and 3.16×10^{-2} m^3/s (500 gpm). This test, in addition to a 3.10×10^4-kPa (4500-psig) hydrostatic test that was performed even though not required by the specifications, was taken as satisfactory evidence of structural integrity. A complete tabulation of materials used in the construction of the pump and most of the fabrication drawings are available. The drawings show weld details and note that the welds are to be liquid-penetrant inspected after the first and final passes and in between as required.

The manufacturer was contacted to determine if his records contained any information that might be used to infer the appropriate level of quality assurance built into the pump. The following quotation is taken

from the response to this request.

> There are no quality assurance documents available. Codes were not specifically made applicable except that it is our basic policy to design pumps to meet the requirements of ASME Section VIII. Liquid penetrant examinations were made as well as heat treatments to assure ourselves that pressure parts would pass the 4500 psi hydrostatic test and the 100 hour hot running test at 600°F. BNWL Inspection may have some inspection and test records which, if any, should be available to you with the pumps. Our file dates to the period 1965–1967 and reveals nothing more than the Hydrostatic Test and Performance Testing results possibly given to BNWL aside from the drawings and curves you have.

We believe that structural integrity of the pump has been adequately demonstrated for steady-state operation at THTF design conditions. For blowdown-type operation, only past experience is available for assurance of structural integrity and system reliability. A standby set of spare parts, as recommended by the manufacturer, has been purchased to facilitate maintenance. By maintaining a supply of parts, especially pump seals and bearings, repair and maintenance downtime has been minimized.

A.3.3.3 Codes and standards for the pressurizer. The THTF pressurizer serves the dual function of a pressurizing source for the facility and of an expansion volume to dampen pressure surges resulting from coolant expansion. The volume of the pressurizer is ~1.98×10^{-1} m^3 (7 ft^3). Calrod-type electrical immersion heaters provide heat to generate steam for maintaining system pressure at the desired level. The concept selected for the pressurizer is identical to that for a pressurizer used successfully at 2500 psi (at saturation temperature) in a large pressurized-water inpile loop facility at ORNL for a number of years. The major difference is that the length of the THTF pressurizer is increased to provide the necessary volume.

Even though ASME Sect. VIII would have been a satisfactory code from the standpoint of quality level III requirements, the pressurizer was designed and built to satisfy requirements of Sect. III, Class 2. Project management agreed to let ORNL fabrication shops use the pressurizer as a demonstration vessel for the purpose of acquiring an ASME nuclear stamp.

A.3.3.4 Codes and standards for the piping system. The piping system in the THTF high-pressure primary system contains pipes in the nominal size range of 1/2 to 6 in.; the major portion of the piping is nominal 4-in., while 6-in. Schedule-160 pipe is used for the pump suction. The exception is in reality a class exception because it includes 1/8- and 1/4-in. nominal pipe and high-pressure autoclave tubing, used as instrument connections and vent lines. Although this class of service is subject to system pressure, generally the temperature level is essentially ambient.

A significant quantity of suitable heavy wall piping and fittings was available at ORNL to satisfy the major system requirements, particularly in the larger size range. This material was purchased some years ago under stringent material specifications for highly corrosive service in a now-discontinued aqueous reactor program. The existing loop was

constructed from these materials, and we are confident that the quality is in excess of the requirements for piping systems. Material certifications (chemistry and physical properties) are either available in "dead storage" files or can be obtained from the manufacturer.

For the new construction, the use of piping and fittings available from existing stock was specified in those cases where the certification could be located or material upgraded. Piping and tubing not available from existing stock were purchased in accordance with ASME or ASTM material specifications.

Design, fabrication, installation, examination, and testing of the piping system were in accordance with the rules of the Power Piping Code B 31.1.0. Welding was accomplished in accordance with ORNL welding procedure WPS-302. Weld examination was made in accordance with ORNL inspection procedure MET-WR-201, except that X-ray porosity charts of Appendix IV of ASME Code Sect. VIII, Div. 1 were used.

A.3.3.5 Codes and standards for secondary coolant systems. Heat is rejected from the THTF primary coolant system to a secondary coolant system via four water-to-water heat exchangers. The secondary coolant is supplied to the heat exchangers from a 9.47 x 10^{-1}-m^3/s (15,000-gpm), building-wide, recirculating, demineralized water system operating at 1.72 x 10^3 kPa (250 psig). This system has been in operation for a number of years to provide cooling for a number of large experiments. Based on past experience, this system is considered highly reliable for supplying coolant to the many experimental facilities located within the building.

The new construction portions of the secondary cooling water system were designed, fabricated, and inspected at quality level IV and in accordance with UCC Tech. Spec. P-1.1, Subsect. 107, for Demineralized and Distilled Water Systems.

A.3.3.6 Codes and standards for the PSS. The THTF is designed with rupture disk assemblies located to simulate pipeline breaks. The rupture disk assemblies form the boundary between the high-pressure primary system and an energy-absorbing system [a recirculating spray condenser contained in a 4.39-m^3 (1160-gal) tank vented to the atmosphere through a 20.3-cm (8-in.) line]. Blowdown is initiated by causing the rupture disk to fail at a predetermined time.

The piping, valves, and other components in this system meet the ANSI Code for Pressure Piping Systems, B 31.1.0, Power Piping. The spray condenser was designed in accordance with Sect. VIII, Div. 1 of the ASME Code. Materials conform to ASTM material specifications appropriate to the service requirement.

A.3.3.7 Codes and standards for the test section housing. The test bundle array is placed in a pressure housing for test purposes. The housing has a number of penetrations and access ports to accommodate the necessary test bundle instrumentation. Coolant inlet and exit flow nozzles are provided at a number of locations to give flexibility in flow configuration. A number of unique problems were encountered with the requirements for the dc power connections to the individual heater rods at the upper end and the common connection to all heater rods at the lower end. The housing was fabricated in two longitudinal flanged sections to facilitate assembly and disassembly for bundle replacement. These aspects lead to a rather complicated housing with special considerations in regard to instrument penetrations and individual heater element penetrations necessitated by the experiment requirements.

Although some of these special considerations are outside the scope of the Code, the intent of the Code can provide guidance. The rules and intent of Sect. VIII were followed, with deviations as required to accommodate the particular requirements brought about by the nature of the experiment.

Materials were procured in accordance with appropriate ASME and ASTM material specifications.

A.3.3.8 Heater rods for the test section. Indirect-type heaters are used to simulate PWR fuel elements. An indirect heater is one in which heat is generated in an internal element that is electrically isolated from the heater sheath. The Quality Assurance Program Plan (Q-10520-RH-001-S-0) specifies a quality level of III for the heaters but with special inspection and assembly procedures to assure their functional operability. A heater specification (E-10520-RB-006-S-0) was written based on RDT Standard P 4-4T. The thermocouples were purchased to Specification IS 514, Thermocouple Material and Thermocouple Assembly, Chromel-P vs Alumel, stainless-steel-sheathed magnesium oxide insulated for the center couples and BN-backfilled junctions for the sheath couples, for specific use on the BDHT Program. All materials used for fabrication for Bundle 3 were procured by ORNL and assembled at the FRS TDL. Further details on standards, codes, and quality assurance procedures followed during the fabrication of Bundle 3 can be found in other reports.

Appendix B

LOCATION AND NOMENCLATURE FOR FLUID THERMOCOUPLES IN THTF BUNDLE 3

The location (axial and subchannel) of all fluid thermocouples monitored in the original THTF Bundle 3 is presented in Fig. B.1. These core fluid thermocouples can be subdivided into four distinct groups. The naming convention and location of these subgroups are given in the following four sections.

B.1 Subchannel Thermocouples

The subchannel thermocouple rake is located ~2.3 cm above the upper end of the heated section (414.5 cm above the gauge line). The naming convention takes the following form:

TE-12nn ,

where

nn = a number between 01-81 that equals the number of the subchannel in which it is located.

Figure B.2 indicates those subchannel thermocouples monitored by the CCDAS as of January 8, 1980.

B.2 Spacer-Grid Thermocouples

The spacer-grid fluid thermocouples are attached to core grids 2-7. The naming convention for these thermocouples has the following form:

TE-29na ,

where

n = a number 1-6 designating the spacer-grid level as follows:

Number	Between thermocouple levels	Actual Bundle 3 spacer-grid No.
1	A&B	2
2	B&C	3
3	C&D	4
4	D&E	5
5	E&F	6
6	F&G	7

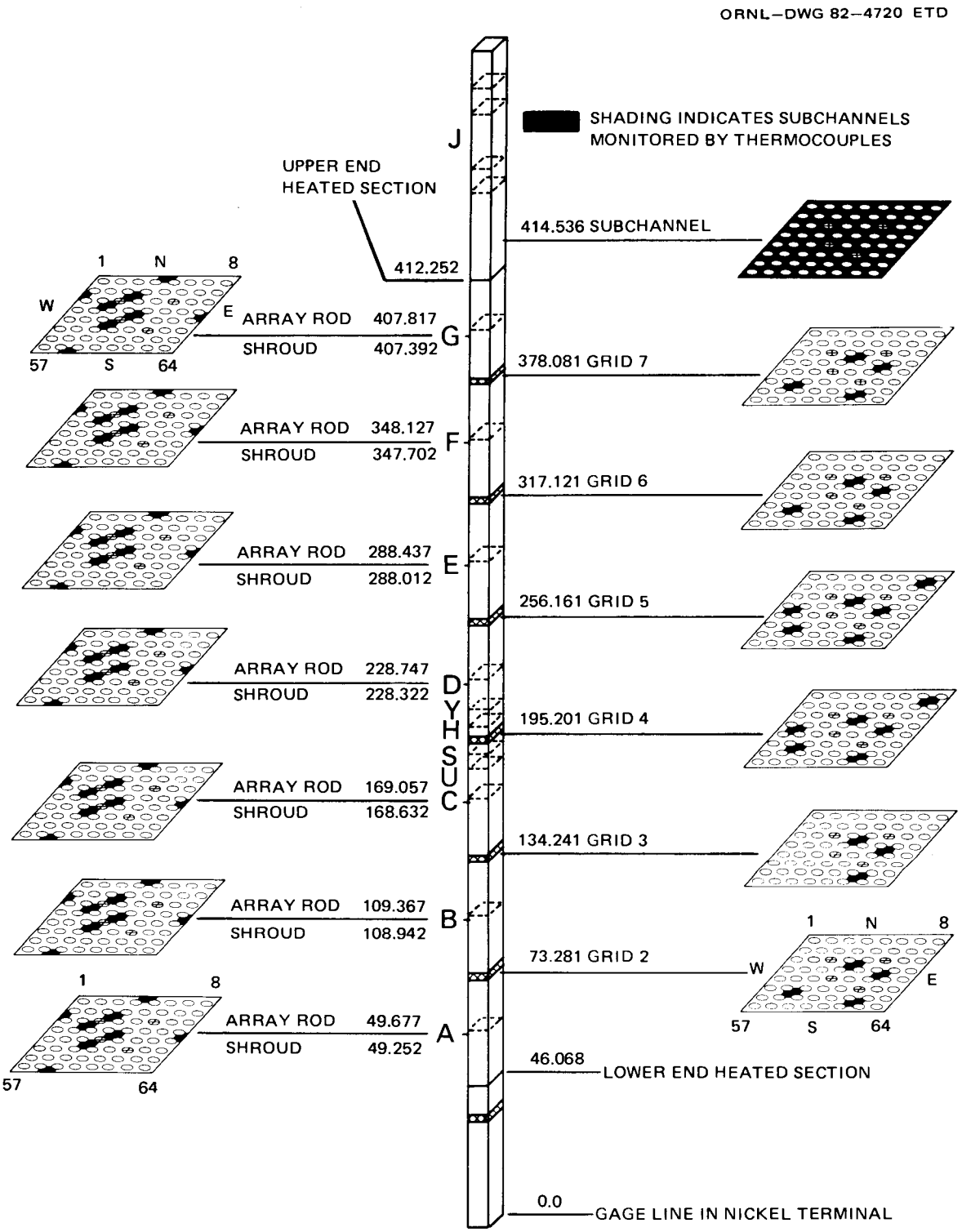

Fig. B.1. Location of fluid thermocouples in THTF Bundle 3. All dimensions are in centimeters and are referenced to the gage line in the nickel terminal.

ORNL–DWG 82–5078 ETD

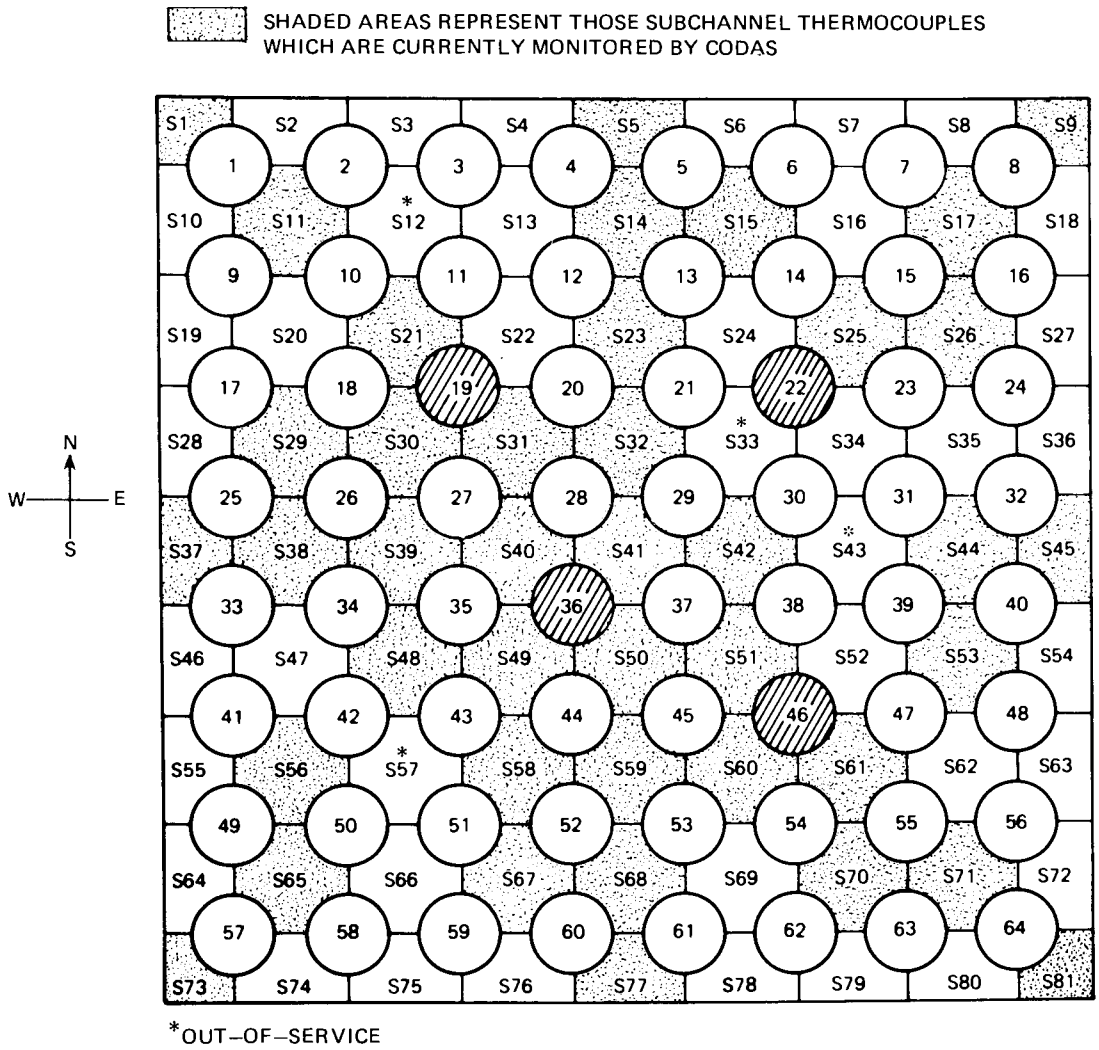

Fig. B.2. Subchannel thermocouples.

and

a = a letter "A–F" designating the subchannel into which the thermocouple is projecting, as follows:

Letter	Subchannel
A	32
B	43
C	57
D	70
E	17
F	38

Those fluid subchannels monitored by spacer-grid thermocouples are indicated in Figs. B.3(a–f).

ORNL–DWG 82–5079 ETD

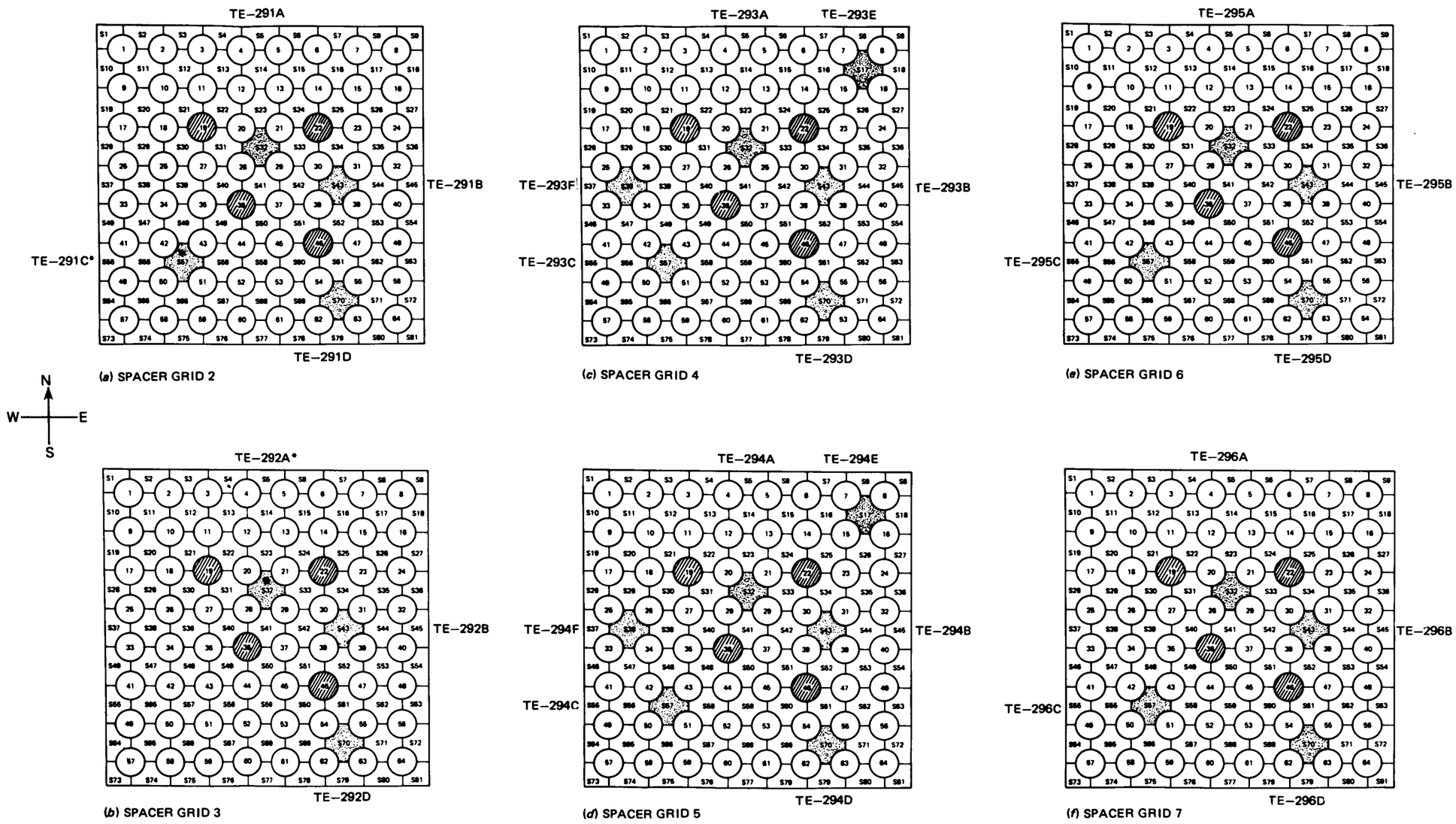

● INACTIVE RODS

*OUT–OF–SERVICE (NOT MONITORED BY CODAS)

Fig. B.3. Spacer–grid thermocouples.

B.3 Shroud-Box Thermocouples

Shroud-box thermocouples protrude through the shroud wall into the fluid in the wall subchannels. A typical installation is shown in Fig. B.4. The naming convention for these thermocouples has the following form:

TE-18na ,

where

n = a number 1–7 designating the level of the thermocouple in the shroud box as follows:

Number	Thermocouple level
181	A
182	B
183	C
184	D
185	E
186	F
187	G

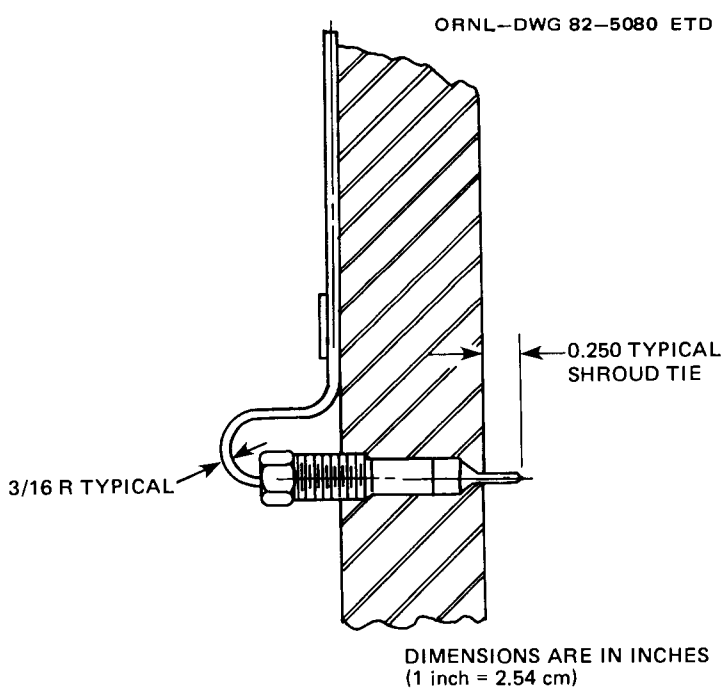

Fig. B.4. Typical installation of a shroud-box thermocouple. Dimensions are in inches (1 in. = 2.54 cm).

and

a = a letter designating the side of the box through which the thermocouple protrudes, N, E, S, or W, (whichever designates the compass direction most closely matching the direction the side faces).

Those fluid subchannels monitored by shroud-box thermocouples are shown in Fig. B.5(a–g).

B.4 Thermocouple-Array Rod Thermocouples

The thermocouple-array rods occupied grid positions 19 and 36 in the *original* Bundle 3. Each array rod contains 14 thermocouples, and, at each axial level in the core where there is a primary FRS thermocouple level, two of these thermocouples protrude from the rod into the fluid (as illustrated in Fig. B.6). The naming convention for these thermocouples has the following form:

TE-18nal ,

where

n = the number 8 or 9 designating in which grid position the thermocouple-array rod is located such that 8 denotes grid position 19 and 9 denotes grid position 36;

a = a letter A and B designating which of two subchannels associated with that rod the thermocouple protrudes into:

Rod grid position	A subchannel	B subchannel
19	22	30
36	41	49

1 = the thermocouple level A–G (same as FRS thermocouple level designations).

Those fluid subchannels monitored by the thermocouple-array rod thermocouples are indicated in Fig. B.5(a–g).

ORNL-DWG 82-5081 ETD

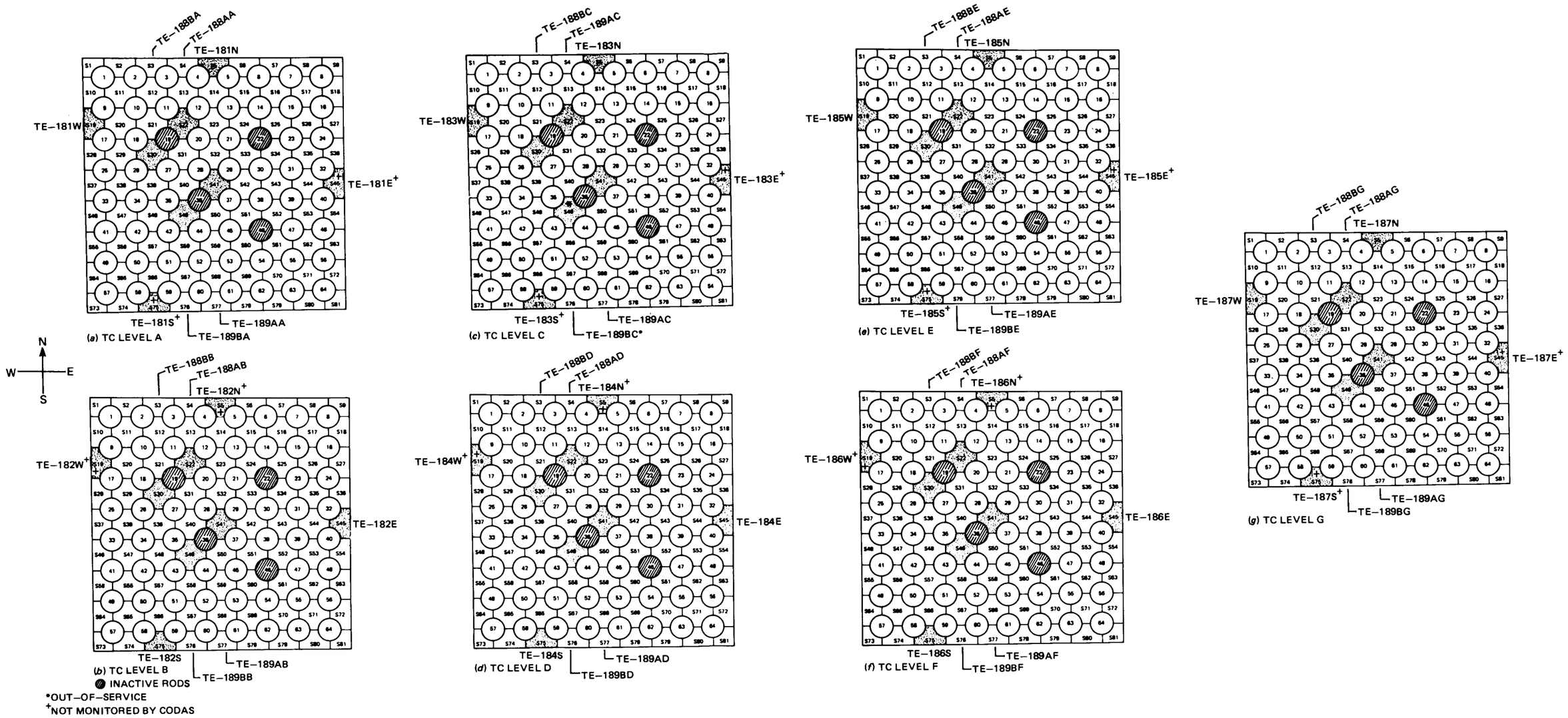

Fig. B.5. Shroud-box and thermocouple-array rod thermocouples.

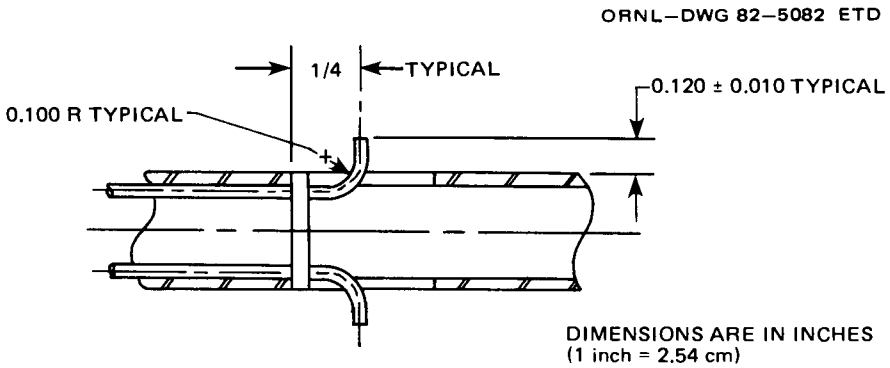

Fig. B.6. Cross section of thermocouple array rod illustrating protrusion of thermocouples from the rod. Dimensions are in inches (1 in. = 2.54 cm).

Appendix C

FRS PROPERTY EVALUATION

C.1 FRS Radial Dimensions

One of the primary requirements of the BDHT program is the determination of transient FRS surface temperatures and surface heat fluxes from the FRS internal sheath thermocouples (Fig. C.1) during a transient test in the THTF. This requires the solution of the inverse heat conduction problem, which is accomplished at ORNL by the computer codes ORINC (Ref. 1) and ORMDIN (Ref. 2). These codes along with the FRS calibration codes (ORTCAL) (Ref. 3) require that the FRS radial dimensions be known as precisely as possible. This should not imply that these codes would fail if these dimensions are not precise and accurate but that the uncertainties in the computed results would be less (hopefully) or at least could be estimated. Unfortunately, these dimensions are not readily available primarily because of the manufacturing technique used for the construction of the FRS. The best method to date to determine these dimensions is to (1) destructively cross-section an FRS, (2) mount and polish the cross sections, (3) photograph the cross sections at magnification, and (4) then make the measurements using a tool maker's microscope (at 100X magnification). The estimated accuracy of these measurements is

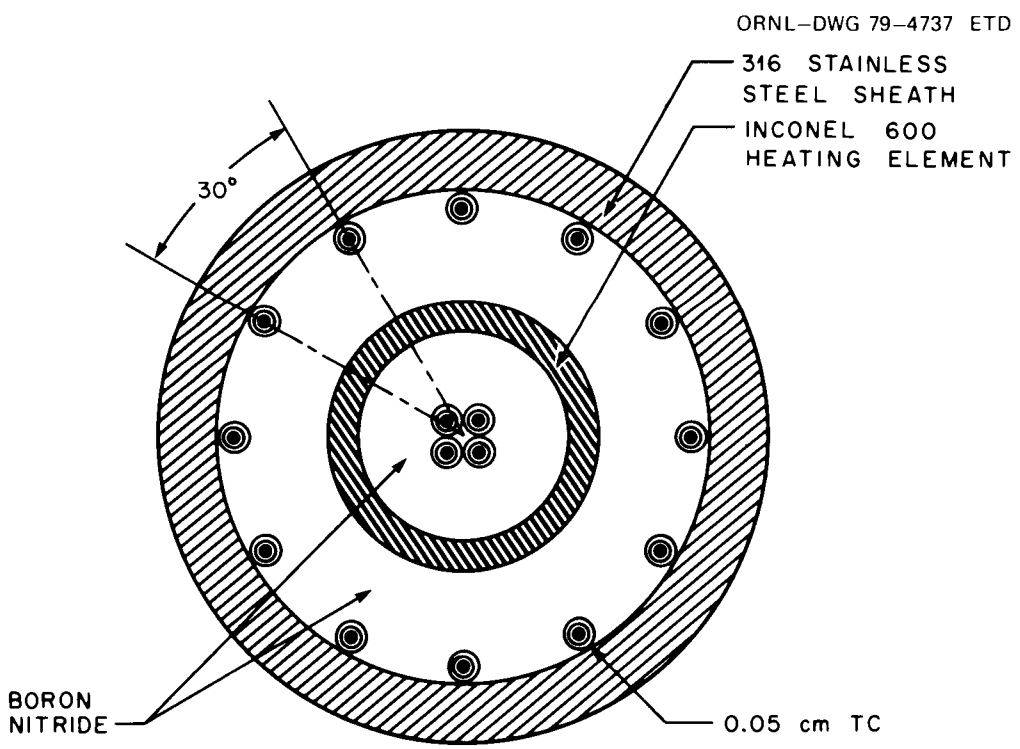

Fig. C.1. Cross section of THTF Bundle 3 FRS.

±0.0025 mm (0.0001 in.). Disadvantages to this method are that an expensive FRS is no longer available (except in 25-mm sections), and the assumption must be made that the cross-sectioned FRS is representative of the bundle.

Prior to the assembly of the original Bundle 3 (June 1979), BDHT FRS-038 was cross-sectioned and measured by the Y-12 Development Division Metallurgical Department.[4] FRS-038 (an original Bundle 3 FRS) was never placed in a BDHT loop and thus never power-cycled; in fact, this rod failed an electrical check during construction, which was the primary reason the rod was cross-sectioned. The electrical failure was caused by metal inclusions in the BN annular insulator that resulted in arcing between the heating element and the FRS cladding during the electrical check. Other than the metal inclusions, FRS-038 was typical of the original Bundle 3 FRSs (noncycled, that is). Table C.1 contains the results[5] of a statistical analysis performed on the FRS-038 measurements. The radial results (determined from diametric measurements) are independent of those for the thicknesses (the dimensions cross-check). Estimates of the uncertainties (one standard deviation) in the radii and thicknesses are included in Table C.2.

The dimensional stability of preproduction Bundle 3 FRSs is indicated in Table C.3. These measurements were compiled from four rods prior and subsequent to testing in the BDHT single-rod loop. Even though the diametric change in Table C.3 was small, it was decided to cross-section a THTF-cycled FRS when one became available.

Table C.1. Bundle 3 FRS sublayer radii and thicknesses

Sublayer	Outer radius [mm (in.)]	Thickness [mm (in.)]
	Heated length	
Stainless steel clad	4.7523 (0.1871)	0.4801 (0.0189)
Outer boron nitride	4.2723 (0.1682)	1.1557 (0.0455)
Heater element	3.1166 (0.1227)	0.3505 (0.0138)
Inner boron nitride	2.7661 (0.1089)	2.0523 (0.0808)
Thermocouple bundle	0.7137 (0.0281)	
	Terminal end	
Stainless steel clad	4.7371 (0.1865)	0.4724 (0.0186)
Outer boron nitride	4.2647 (0.1679)	1.1760 (0.0463)
Heater element	3.0886 (0.1216)	0.3556 (0.0140)
Copper tubing	2.7330 (0.1076)	0.8865 (0.0349)
Inner boron nitride	1.8466 (0.0727)	1.1303 (0.0445)
Thermocouple bundle	0.7163 (0.0282)	

Table C.2. Bundle 3 FRS sublayer radius and thickness uncertainties (1 standard deviation)

Sublayer	Outer radius uncertainty[a] [mm (in.)]	Thickness uncertainty[b] [mm (in.)]
	Heated length	
Stainless steel clad	0.0076 (0.0003)	0.0102 (0.0004)
Outer boron nitride	0.0102 (0.0004)	0.0356 (0.0014)
Heater element	0.0152 (0.0006)	0.0076 (0.0003)
Inner boron nitride	0.0152 (0.0006)	0.0406 (0.0016)
Thermocouple bundle	0.0356 (0.0014)	

[a]150 observations.

[b]300 observations.

Table C.3. Stability statistics for loop-cycled rods

Rod No.	Before loop testing [mm (in.)]		After loop testing [mm (in.)]		Change[a] (%)
	Mean value of rod diameter	Standard deviation	Mean value of rod diameter	Standard deviation	
40A	9.4945 (0.3738)	0.0127 (0.0005)	9.5352 (0.3754)	0.0178 (0.0007)	0.4
18A	9.4920 (0.3737)	0.0102 (0.0004)	9.5199 (0.3748)	0.0203 (0.0008)	0.3
10A	9.4996 (0.3740)	0.0076 (0.0003)	9.4996 (0.3740)	0.0102 (0.0004)	0.0
6A			9.5631 (0.3765)	0.0178 (0.0007)	

[a]Relative to rod diameter before testing.

After the refurbishment of Bundle 3 (July–August 1980), four FRSs formerly in grid positions 21, 37, 38, and 54 of the original Bundle 3 were placed in storage. These rods had experienced the first series of small-break LOCA tests and THTF testing during May and June 1980. One of these rods, FRS-058B (grid position 37) was acquired for testing in the FRS TDL (Sects. C.2 and C.3) and subsequent cross-sectioning and measurement by the Y-12 Development Division Metallurgical Department. FRS-058B should be representative of a cycled THTF rod, and the change in the rod's outer diameter (0.3–0.4%) agrees very well with the preproduction Bundle 3 rods (Table C.3) cycled in the BDHT single-rod facility.

Presented in Table C.4 are the internal dimensions for the cycled Bundle 3 FRS. (Sublayer radius and thickness uncertainties are included in Table C.5.) These dimensions are the result of a statistical analysis[6] performed on measurements[7] from BDHT FRS-058B. The radial results (determined from diametric measurements) are independent of those for the thicknesses.

Table C.4. Cycled Bundle 3 FRS sublayer radii and thicknesses

Sublayer	Outer radius [mm (in.)]	Thickness [mm (in.)]
Stainless steel clad	4.7630 (0.18752)	0.4636 (0.01825)
Outer boron nitride	4.2997 (0.16928)	1.1763 (0.04631)
Heater element	3.1227 (0.12294)	0.3345 (0.01317)
Inner boron nitride	2.7882 (0.10977)	2.1224 (0.08356)
Thermocouple bundle	0.6652 (0.02619)	

Table C.5. Cycled Bundle 3 FRS sublayer radius and thickness uncertainties (1 standard deviation)

Sublayer	Outer radius uncertainty[a] [mm (in.)]	Thickness uncertainty[b] [mm (in.)]
Stainless steel clad	0.0038 (0.00015)	0.0117 (0.00046)
Outer boron nitride	0.0056 (0.00022)	0.0310 (0.00122)
Heater element	0.0060 (0.00024)	0.0089 (0.00035)
Inner boron nitride	0.0078 (0.00031)	0.0615 (0.00242)
Thermocouple bundle	0.0580 (0.00229)	

[a]69 observations.

[b]138 observations.

Comparisons of the sublayer radii in Tables C.1 and C.4 show apparent dimensional changes. The direction of these diametric changes in the interfaces is indicated in Fig. C.2. Apparently, the FRS has stress-relieved itself. Considering the FRS manufacturing process, the relief is in the correct direction. Roughly, the manufacturing process takes the following scheme:

1. Four centerline thermocouples and a wire stiffener (Fig. C.3) are inserted in a stainless steel tube (~2 mm in diameter).
2. This assembly is inserted into an Inconel-600 tube, and BN preforms are slipped over the thermocouple bundle and crushed until the tube is full. It is now called the active component assembly (ACA).
3. The ACA is swaged (outer diameter reduced) in a hammer mill to a specified outer diameter.
4. The ACA is inserted in the stainless steel clad (a jig holds the ACA, clad, and sheath thermocouples in the proper positions), and grooved

ORNL–DWG 82–5061 ETD

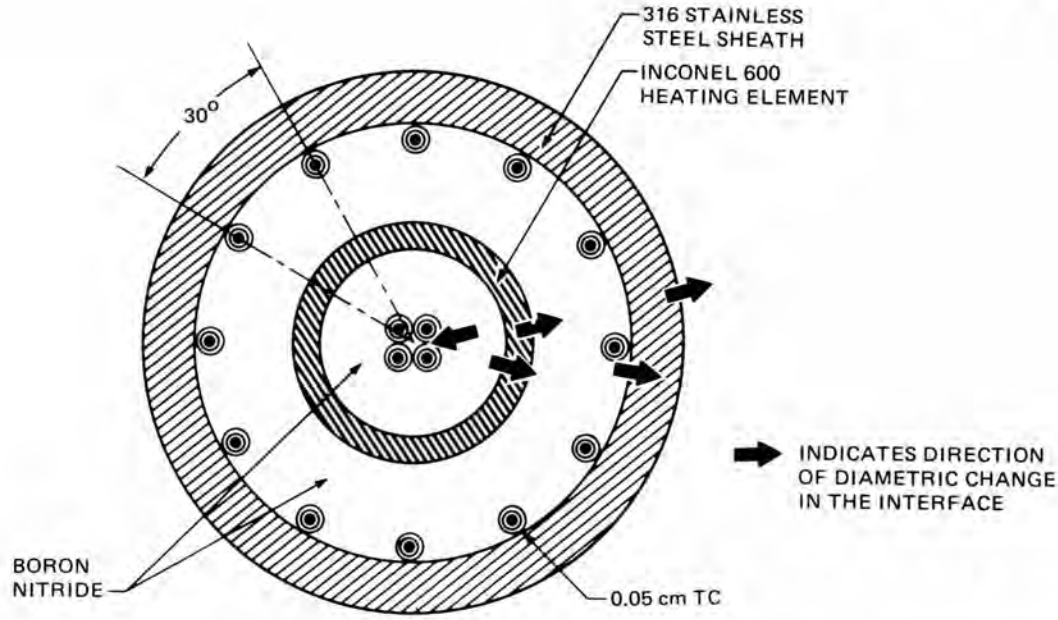

Fig. C.2. Cross section of THTF Bundle 3 FRS with directional changes in the sublayer interfaces (uncycled FRS → cycled FRS).

M&C PHOTO
MS–79–0235–44

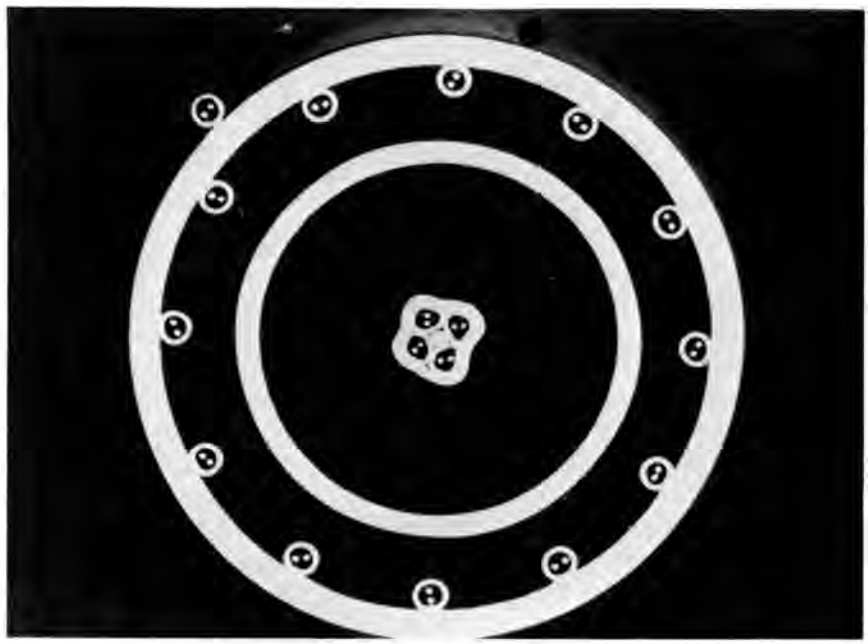

Fig. C.3. Photograph of typical cross section of FRS-058B.

BN preforms are slipped over the ACA and crushed until the assembly is full.

5. This completed assembly (FRS) is then swaged (outer diameter reduced) in a hammer mill until the outer diameter, the position of the sheath thermocouples, and active heated length are correct.

The procedure[8] is actually more complicated than outlined in the preceding paragraphs; but, generally the process follows this scheme. Thus, given the swaging process and the diametric reductions, expected stress relief would follow the directions shown in Fig. C.2.

During the construction of the FRS, a strict inventory (weight) of the BN preforms used in the ACA and the annular FRS region is maintained. Thus, given the final FRS dimensions (length and diametric), the BN density can be determined. Using the dimensions from Table C.1, the average BN core density for 61 rods was 2.215 g/cm³ (138.3 lb_m/ft^3) with a standard deviation of the observations of 0.013 g/cm³ (0.81 lb_m/ft^3); also, the average annular BN density was 2.175 g/cm³ (135.8 lb_m/ft^3) with a standard deviation of 0.019 g/cm³ (1.19 lb_m/ft^3). Now, using the cycled rod dimensions from Table C.4, the average BN core density was 2.158 g/cm³ (134.7 lb_m/ft^3) with a standard deviation of 0.013 g/cm³ (0.8 lb_m/ft^3), and the average annular BN density was 2.135 g/cm³ (133.3 lb_m/ft^3) with a standard deviation of 0.019 g/cm³ (1.19 lb_m/ft^3). Comparisons of the as-constructed FRS BN densities and the BN densities after rod thermal cycling show further evidence that the rods underwent stress relief.

The discussion on rod radial dimensions has dealt exclusively with the original Bundle 3 rods. The rods that were cross-sectioned for the data in Tables C.1 and C.4 were original Bundle 3 rods. However, as noted in Sect. 5.2 (and Fig. 5.6), during the first refurbishment of the bundle, seven of the original rods were replaced with "preproduction" models (these units contained only ten thermocouples, six sheaths, and four centerlines). Using the dimensions from Table C.1, it would be expected that the core BN density would be approximately the same as that of the production model with the annular density possibly less than that of the production model; this was observed to be the case. The cycled rod data in Table C.2 include those from a preprototype rod, two preproduction rods, and one production rod; thus, after cycling, these rods (and FRS-058B) exhibit similar diametric changes (~0.3–0.4%). Additionally, the new rods inserted in the bundle during the refurbishment phase (Sect. 5.3) were slightly different from the production models in that 0.4-mm (0.016-in.) thermocouples instead of 0.5-mm (0.020-in.) thermocouples were used. Neither a preproduction FRS nor a new FRS has ever been cross-sectioned, photographed, and measured. Therefore, no internal dimensions are available for these rods. However, given the facts that (1) the outer diametric changes are essentially the same, (2) the heating element (Inconel-600) electrical resistances per unit length are approximately equal, and (3) the assumption that the relative density difference between the core and annular BN is the same as the production FRS, the internal radial dimensions and BN densities of the preproduction FRSs and the new FRSs can be estimated from the dimensions in Table C.4. This has been done, and the dimensions (and BN densities) for the three rod types are given in Table C.6.

Table C.6. Internal dimensions and boron nitride densities of Bundle 3 FRSs (for the original and refurbished bundles)

Sublayer	Preproduction FRS	Original or production FRS	New FRS
	Outer radius [mm (in.)]		
Stainless steel clad	4.7630 (0.18752)	4.7630 (0.18752)	4.7630 (0.18752)
Outer boron nitride	4.2997 (0.16928)	4.2997 (0.16928)	4.2997 (0.16928)
Heater element	3.1413 (0.12367)	3.1227 (0.12294)	3.1436 (0.12376)
Inner boron nitride	2.8090 (0.11059)	2.7882 (0.10977)	2.8116 (0.11069)
Thermocouple bundle	0.6652 (0.02619)	0.6652 (0.02619)	0.6652 (0.02619)
	Boron nitride density [g/cm³ (lb_m/ft^3)]		
Core	2.139 (133.5)	2.158 (134.7)	2.154 (134.5)
Annulus	2.117 (132.1)	2.135 (133.3)	2.131 (133.1)

It is suggested that for all thermal analyses of THTF Bundle 3 rod response that the internal FRS radial dimensions and BN densities specified in Table C.6 be used.

C.2 FRS Heating Element Electrical Resistance

As mentioned in Sect. 3.3.1, accurate determination of the FRS radial dimensions is required for thermal analysis of the rods by ORINC, ORMDIN, and ORTCAL; however, the accuracy of the boundary conditions for these codes is much more important than the FRS radial dimensions.[9] The boundary conditions for ORINC and ORMDIN are the power generation rate in the heating element and the FRS sheath thermocouple response(s). The uncertainty in the BDHT FRS sheath thermocouple response is relatively well known; however, during preliminary analysis of the THTF tests, the ability to compute the power input to the THTF core was only marginally accurate. For instance, the summed EI product (i.e., the sum for all rods of the product of the rod current I and the generator voltage E) was ~3 to 10% greater than the observed power delivery to the core fluid. Also, if the power to each rod was computed by using the rod current I and FRS heating element resistance R, where R is determined from literature data for Inconel-600 electrical resistivity and the cross-sectional area of the heating element, then the total power to the core was 2 to 4% greater than observed. These uncertainties in the computed power to each FRS (and the method of calculation) were totally unacceptable. Therefore, after the refurbishment of Bundle 3 (July–August 1980), FRS-058B (rod in grid position 37 in the refurbished bundle) was sent to the FRS TDL for tests to

determine the in situ electrical resistance of the ACA (the FRS heating element) as a function of temperature.

S. D. Snyder of the Infrared Inspection Section of the FRS TDL has devised techniques for inspecting and characterizing FRSs.[10] The FRS is an electrical heating device, and, during its construction, the ability to measure accurately electrical parameters such as low and high resistance and leakage current is essential.[11] Low-resistance measurements are necessary to monitor the condition of the central heating element (the ACA). High-resistance and leakage-current measurements are necessary to determine the condition of the electrical insulation between the ACA and the sheath of the FRS and between the ACA and the FRS centerline thermocouples.

The circuit shown in Fig. C.4 was assembled to measure the low-resistance value of the ACA with an accuracy of ±0.5%. The FRS is heated to the desired temperature (as monitored by the FRS centerline thermocouples) by resistance heating of the FRS clad (the clad is electrically insulated from the ACA by the annular BN). Then, with the switch turned to position one, thus placing the dc voltmeter (DVM with a 0.1-mV sensitivity) across a 1.0000-Ω resistor, the power supply potential to the ACA is raised until the voltmeter reads 1.000 V. This establishes a 1.0000-A current through the ACA and resistor circuit. When the switch is moved to position two, the voltmeter reading is the ohmic value of the ACA resistance, because the current is 1.0000 A.

Using this technique, the ACA resistance curves vs temperature in Figs. C.5–C.7 were generated. A comparison of four different runs is

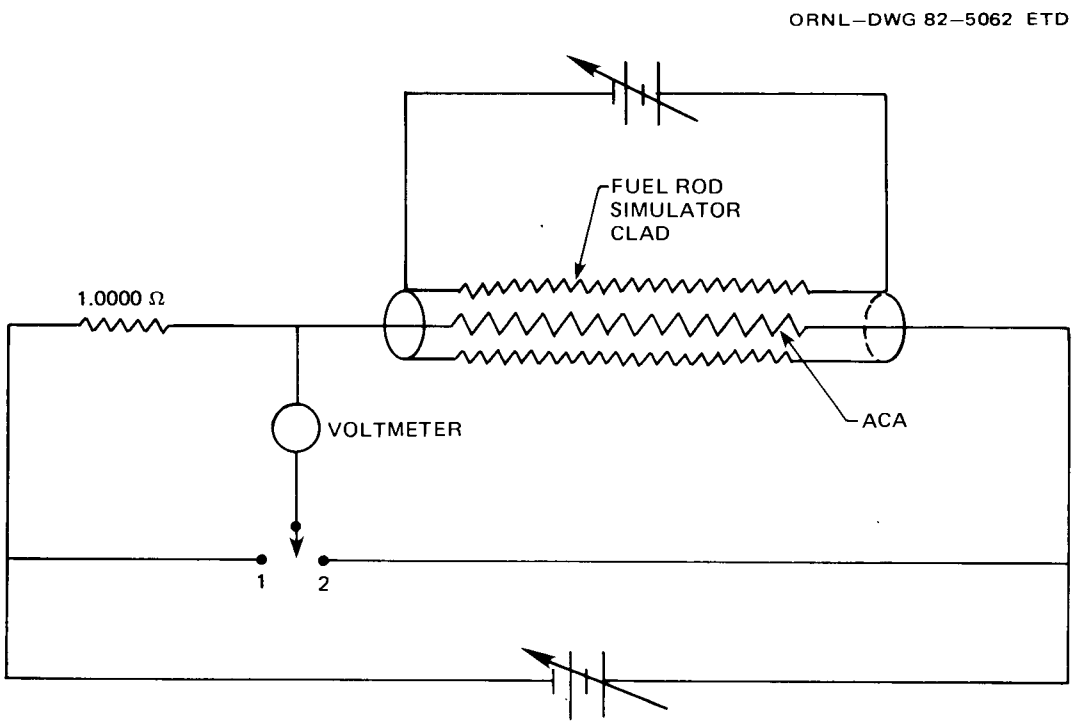

Fig. C.4. ACA resistance measurement circuit.

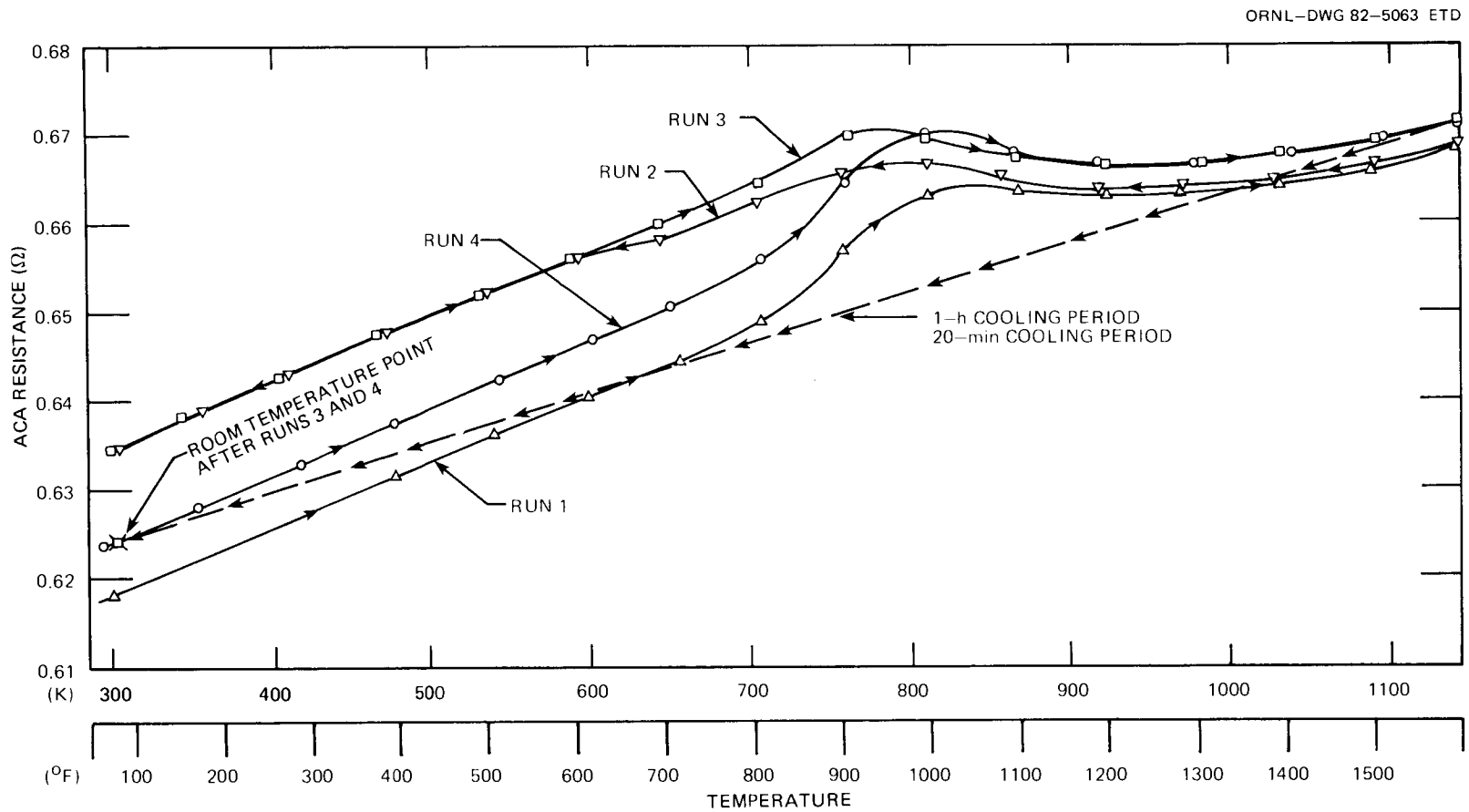

Fig. C.5. ACA resistance vs temperature for entire ACA of FRS-058B.

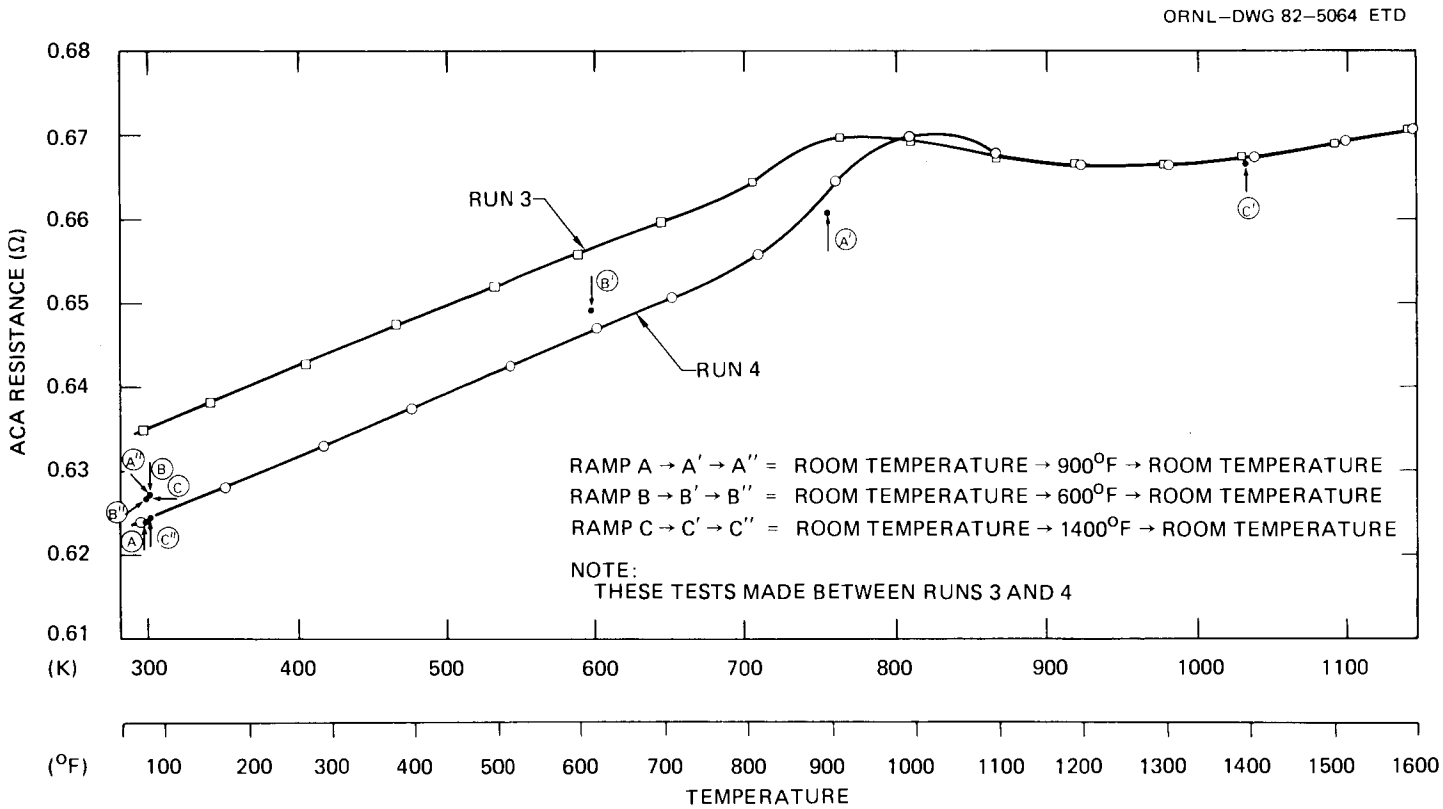

Fig. C.6. ACA resistance vs temperature for entire ACA of FRS-058B (ACA heated by ramping sheath).

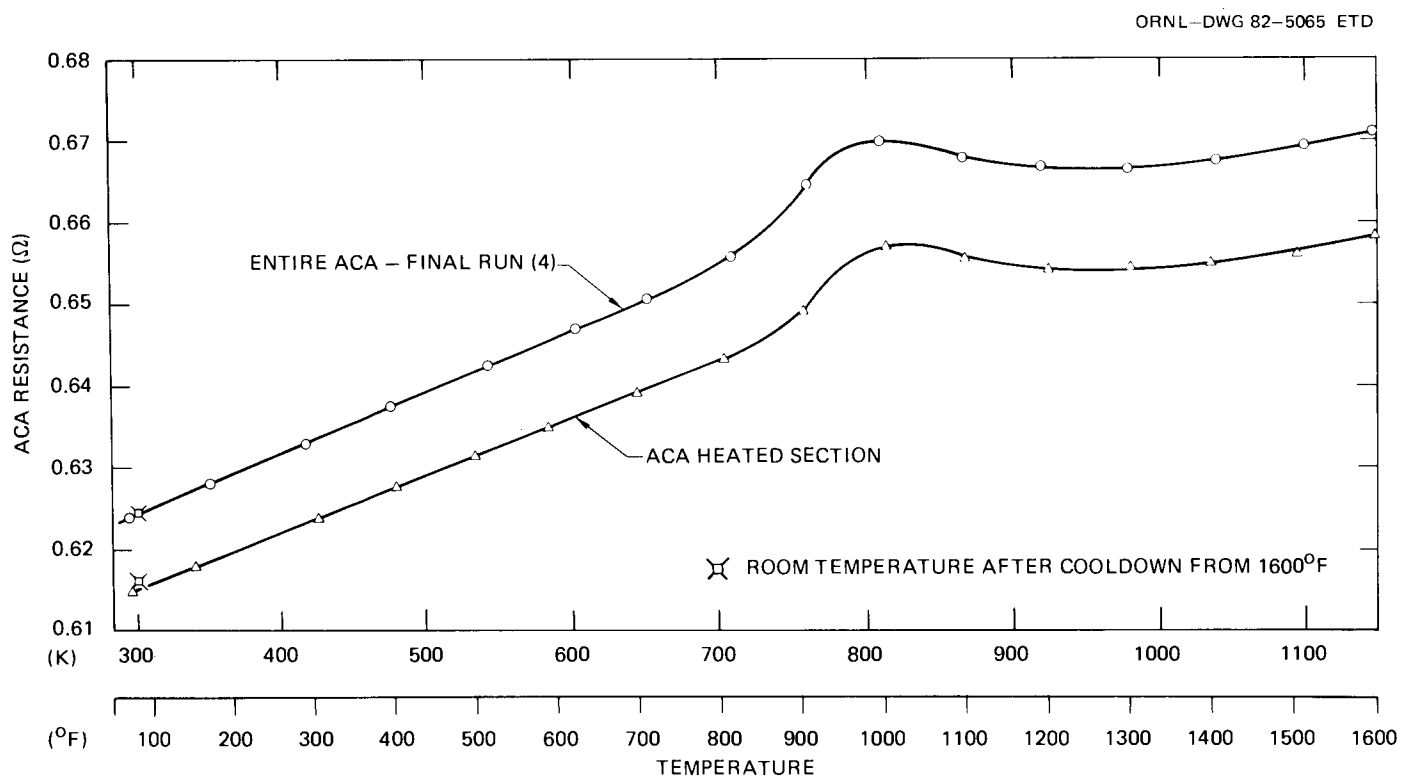

Fig. C.7. ACA resistance vs temperature for heated section of FRS-058B.

shown in Fig. C.5. None of the four separate runs duplicated each other, and the extreme spread was ~3%. To provide a reason for this nonrepeatability, it is necessary to look at the run sequence and time frame for the tests. Run 1 (Fig. C.5) was generated as the rod was heated up; the starting point (condition) of the rod was as it was received from the THTF. The data for run 2 were obtained as the rod cooled down (after run 1), and the time required to complete run 2 was ~1 d (i.e., it was a very slow cooldown). Two days elapsed between runs 2 and 3; after completion of the test, the power to the FRS sheath was turned off, and the rod cooled to room temperature in ~1 h. Several ramped heating tests were made between runs 3 and 4, and these are indicated in Fig. C.6. In these runs, the power to the sheath was turned on, the rod attained equilibrium conditions, data were taken, and then power was turned off. The cooling period in each case was 30 to 60 min. Run 4 was made after these ramp tests. The rod was cooled to room temperature in ~20 min by using a fan. Note that the ACA resistance at room temperature was repeatable when the rod had been previously cooled from >1000 K to room temperature in <1 h. Runs 1–4 and the ramp tests were made with the entire ACA; that is, the ACA consisted of the 3.672-m heated length *and* the terminal lead-in. After run 4, the terminal lead-in section of FRS-058B was cut off, leaving just the 3.672-m heated length. The final run and run 4 are shown in Fig. C.7. The difference between run 4 and the final run in Fig. C.7 is the resistance of the ACA terminal lead-in section.

The resistance behavior illustrated by Fig. C.5 is typical of alloys that can undergo the order–disorder phenomenon. The order–disorder phenomenon has been extensively studied for Chromel (a nickel–chromium alloy)[12] because it is a common thermoelement material (type K thermocouples). Some of the pertinent points follow:

1. Between 475 and 875 K, the nickel and chromium atoms in Chromel tend to occupy specific sites in the crystal lattice (the ordered state).
2. Above 875 K, the atoms are distributed randomly among the lattice sites (the disordered state).
3. A change from the ordered to the disordered state or vice versa is reversible.
4. The rate at and extent to which the ordered state is formed are time and temperature dependent.

McCulloch[13] has shown that the resistance change can approach +4% for Chromel. This background on Chromel has been given because the heating element in the BDHT rods consists of Inconel-600, which is a nickel, iron, and chromium alloy. Inconel-600 can undergo the same order–disorder phenomena as Chromel.

Referring to Fig. C.5, the resistance curves for runs 1 and 2 (run 2 data were generated over an ~8-h cool-down period after run 1) start diverging (as the temperature decreases) at ~875 K. The ordering process appears to be complete at ~575 K, and the two runs are essentially parallel below that temperature with approximately +3% change in the resistance at room temperature. Run 3 resistance should track the run 2 results up to ~575 K, and above that temperature it should be greater than run 2 (at the corresponding temperature) because the degree of ordering is greater. In all runs subsequent to run 2, some degree of ordering (approximately

+0.6% change in the resistance) appears even at temperatures >875 K. However, because the ordering is a time- and temperature-rate-controlled process with faster cooling periods (as following run 3), the degree of ordering (and the resulting change in resistance) is less. Little difference appears in the resulting resistance (approximately +0.6%) at room temperature after cooling periods of 20 min and 1 h. Also, it must be stated that the laboratory cooling environment for FRS-058B is totally different from that in the THTF. Following a typical test in the THTF, the rod would be steam-cooled or water-quenched at a rate three orders of magnitude faster than the best rate obtained in the Infrared Laboratory.

The resistance curve generated in run 1 is assumed to be typical of Bundle 3 FRSs in the THTF. Run 1, however, included the entire ACA. Knowing the resistance of the heated section and the terminal lead-in separately would be preferable. The primary resistance in the ACA in the terminal lead-in section is in copper sleeves inside and outside of the Inconel-600 tube, and this resistance can be determined from Fig. C.7. Thus, if the terminal end resistance is subtracted from the run 1 resistance curve, the resistance of the FRS-058B heated section as received from the THTF may be determined. This resistance and the curves in Fig. C.7 and run 1 are overlaid in Fig. C.8.

If the ACA heated-section electrical resistance (lower curve in Fig. C.8) is divided by the heated length (3.672 m for FRS-058B) and then multiplied by the heating element cross-sectional area (using dimensions from Table C.6), the in situ Inconel-600 electrical resistivity is obtained. This is compared with literature data[14] in Figs. C.9 and C.10. The ACA heated-section electrical resistance per unit length for FRS-058B is shown in Fig. C.11, and the ACA terminal end electrical resistance per unit length for FRS-058B is shown in Fig. C.12. Using a correction factor β_i defined by

$$\beta_i = \frac{\text{heated length of rod i}}{\text{heated length of FRS-058B}} ,$$

the electrical resistance of rod i in the THTF core can be determined from Fig. C.11 and β_i by

$$R_i = R_{FRS-058B} \times \beta_i ,$$

where R_i has units of ohm per unit length. The correction factor is necessary because of the dimensional changes in the heating element caused by the swaging process during fabrication of the FRSs. The actual "finished" cross section of the heating elements varies somewhat from rod to rod. Assuming that the initial heating elements were the same for each of the rods prior to the swaging process, then the measurement of the as-built heated length should be inversely proportional to the finished cross section of the heating element. Because the resistance is inversely proportional to the cross-sectional area, the correction factor is proportional to the ratio of the heated lengths.

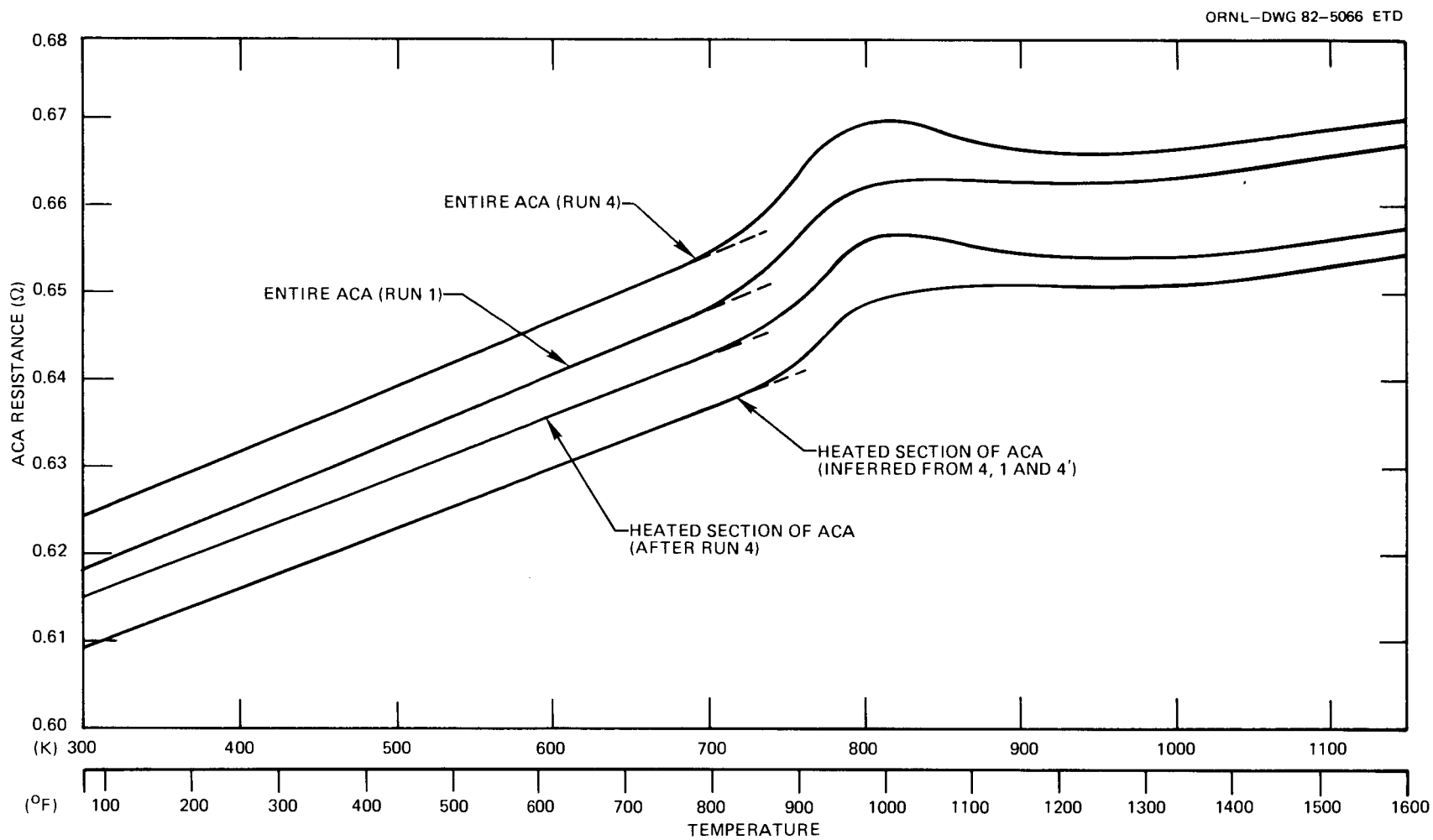

Fig. C.8. ACA resistance vs temperature for heated section of FRS-058B.

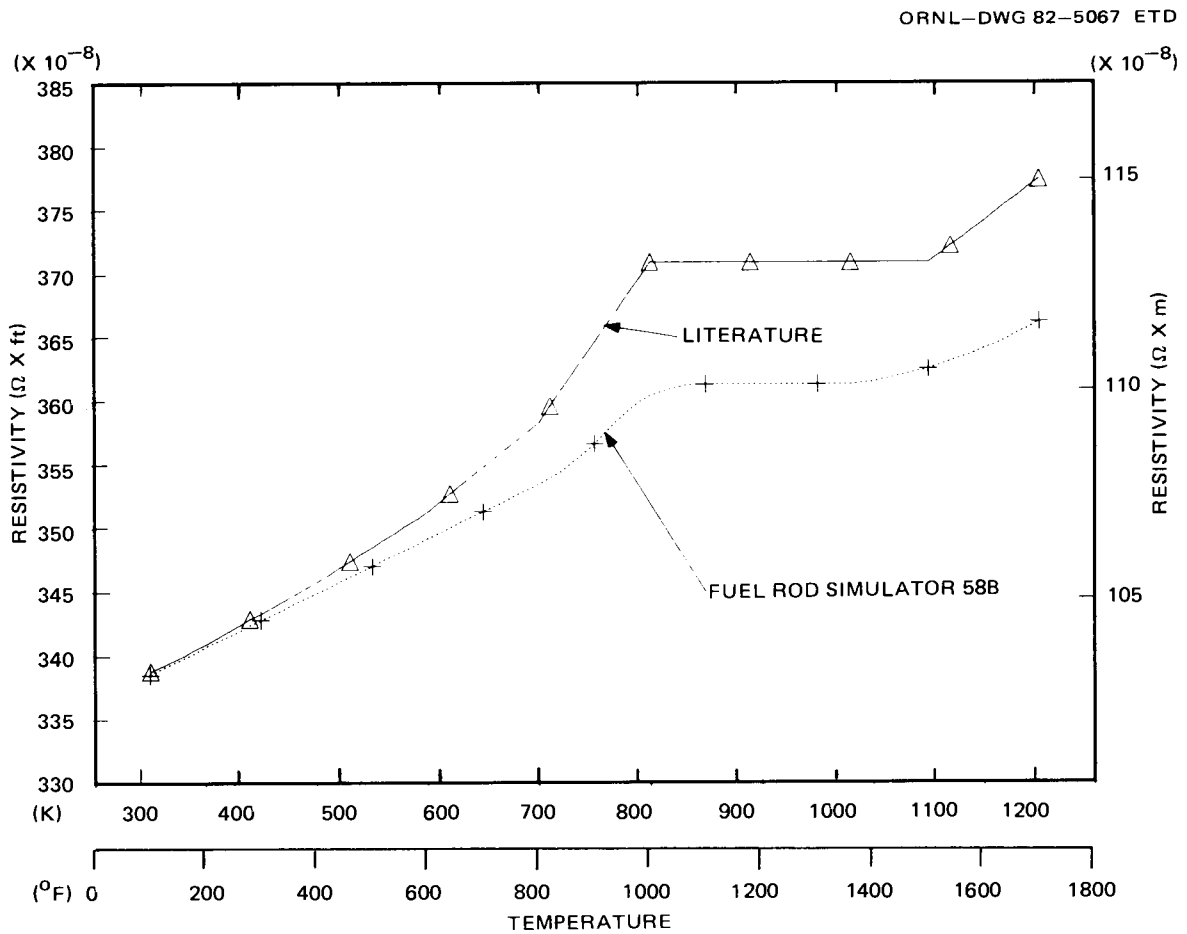

Fig. C.9. Inconel-600 electrical resistivity comparison.

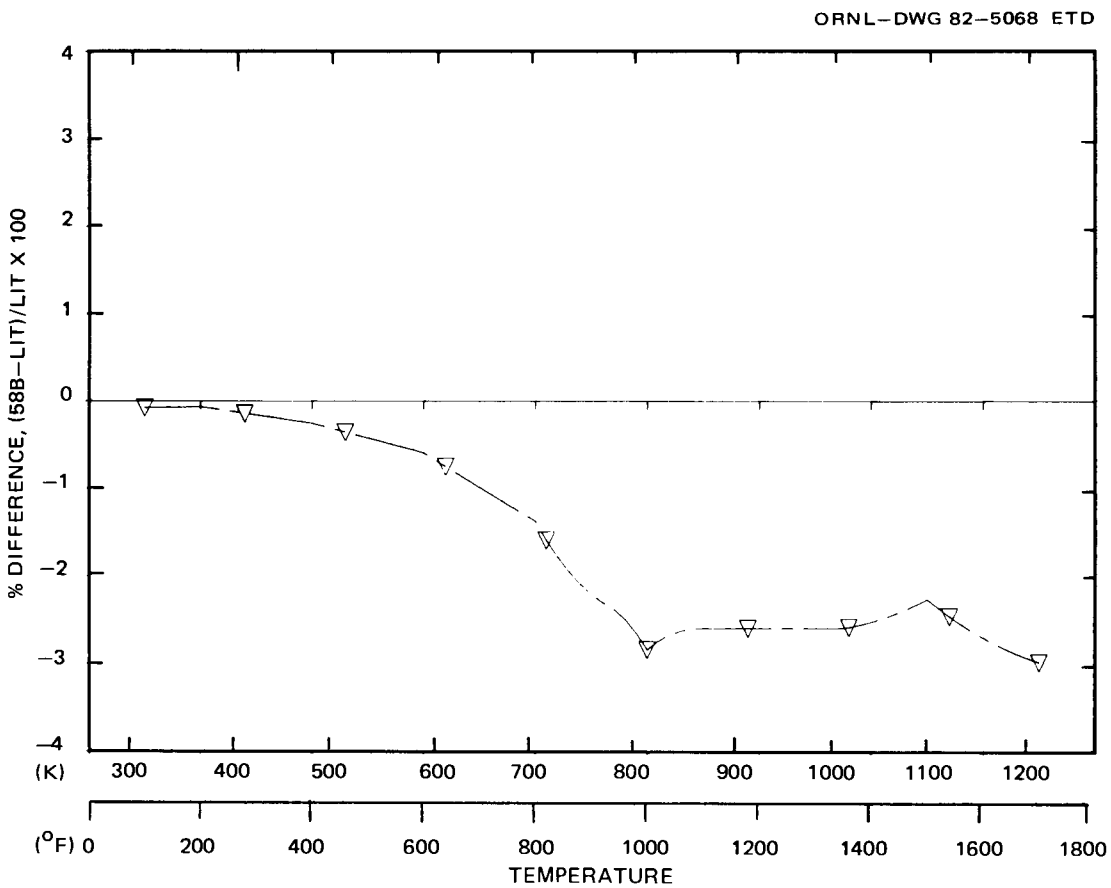

Fig. C.10. Inconel-600 electrical resistivity comparison.

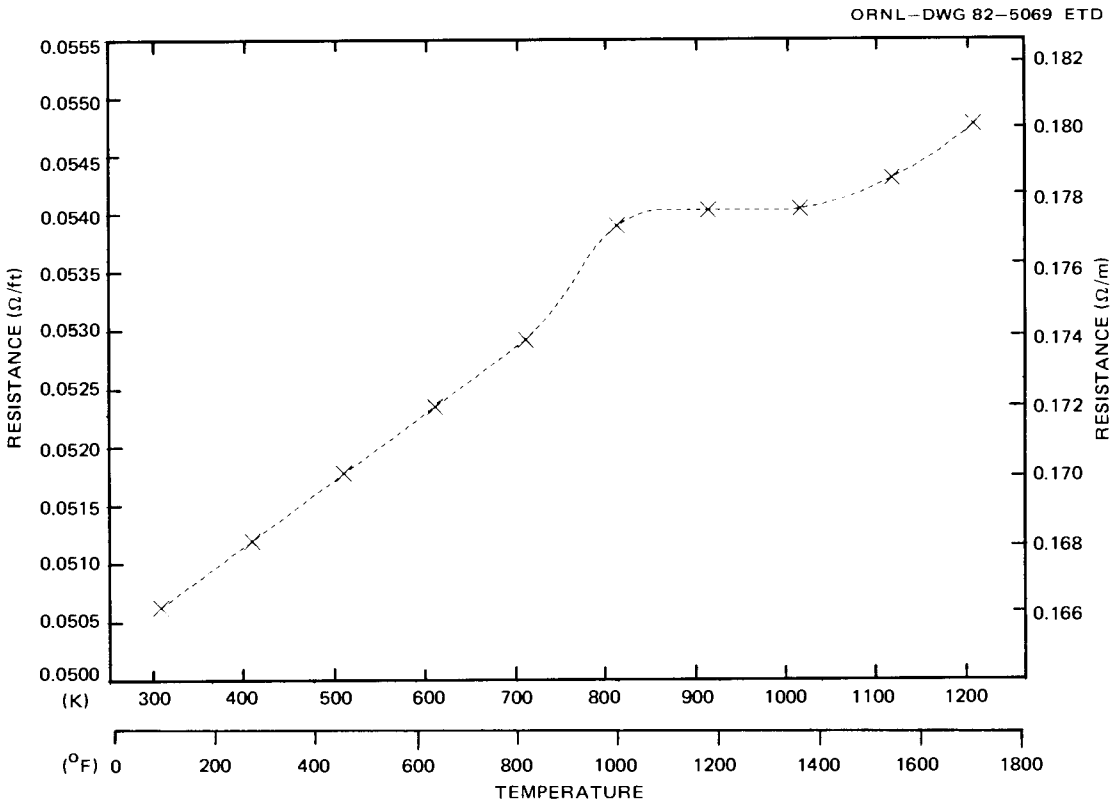

Fig. C.11. FRS-058B heated length electrical resistance.

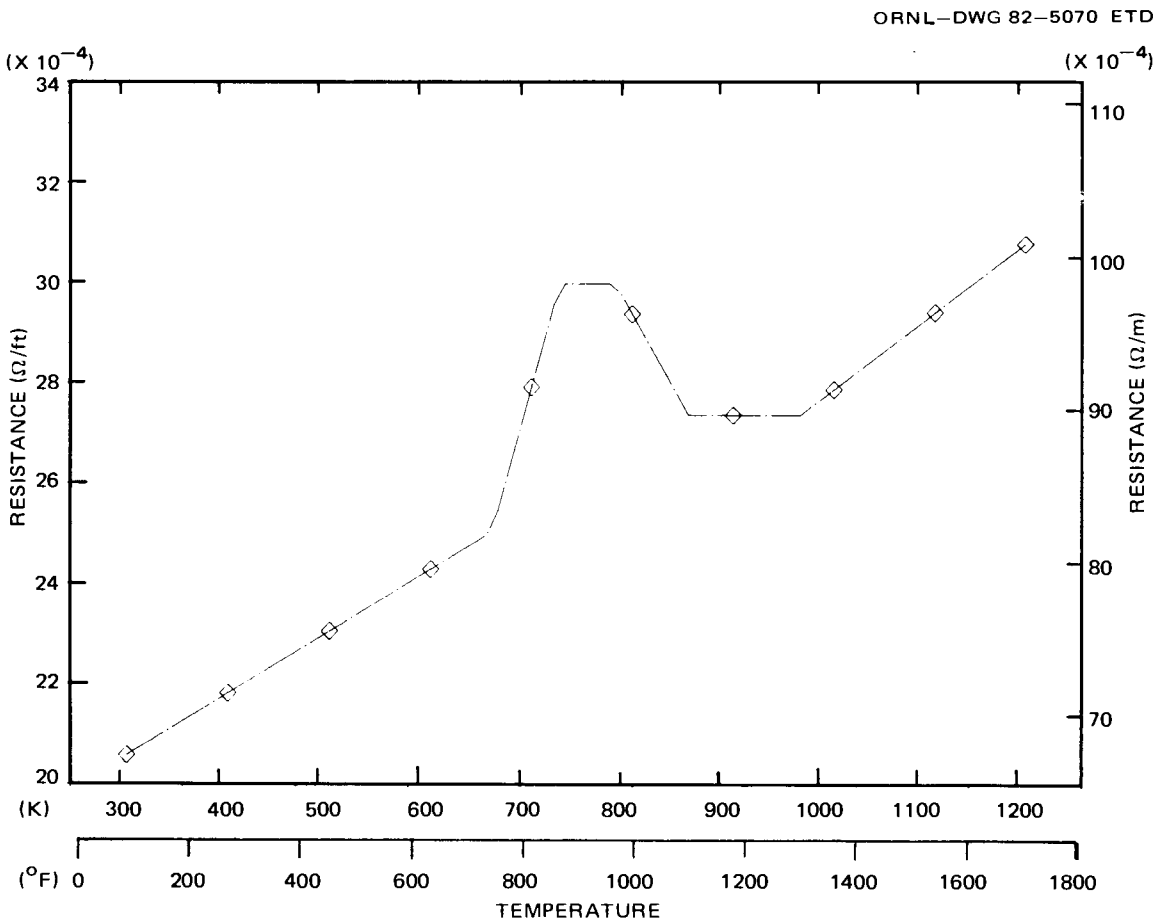

Fig. C.12. FRS-058B terminal end electrical resistance.

Using the in situ electrical resistance of the Inconel-600 (Fig. C.11) and the terminal end electrical resistance (Fig. C.12), the computed power input to the THTF core was ±1.0% of the observed power delivery to the core fluid.

C.3 FRS Surface Emissivity

In many of the tests conducted in the THTF during 1979 and 1980, radiative heat transfer from the rod surface was a significant mode of heat removal from the FRS. Specifically, in those tests in which the core was partially uncovered (i.e., the small-break LOCA tests and the steady-state film boiling tests), FRS surface temperatures reached 950 to 1150 K (1250 to 1610°F); at these temperatures, radiation from the surface becomes an important mode of heat transfer from the surface. Heat transfer at the surface occurs by two mechanisms acting in parallel; that is, the total heat transferred at the surface is the sum of the heat transferred by convection and by radiation:

$$q_{total} = q_{convection} + q_{radiation} \quad (C.1)$$

Because these tests (small-break LOCA and steady-state film boiling) are steady state, q_{total} is simply the power generated by the FRS, which can be calculated given the current to the rod and the rod resistance (Sect. C.2). If the objective of the test is to determine the convective component of the total heat transfer at the surface of the FRS, then the radiative component must be extracted from the total heat transferred. This determination of the radiant heat transfer requires that the rod surface emissivity be known. Estimates of the emissivity of stainless steel for different types of surfaces (i.e., polished or oxidized) can vary from 0.05 to 0.90. Also, the condition of the FRS cladding surface in the THTF does not necessarily fit in the literature categories and essentially is dependent on its environment and operating history (i.e., possible chemical corrosion, surface deposition, and surface discoloration due to high temperature). Because the facilities in the Infrared Inspection Section of the FRS TDL are available, it was decided to test one of the FRSs removed from the THTF during the bundle refurbishment in July–August 1980 to determine the surface emissivity.

S. D. Snyder used the circuit shown in Fig. C.13 [FRS-026 (grid position 15)] for the FRS emissivity determination. The procedure used is as follows:

1. Take the FRS as received from the THTF (i.e., no surface preparation), and place the rod in the circuit as shown in Fig. C.13.
2. Heat the FRS via resistance heating of the ACA to a desired temperature (as indicated by the FRS sheath and middle thermocouples), and determine the power to the rod and the rod temperature.

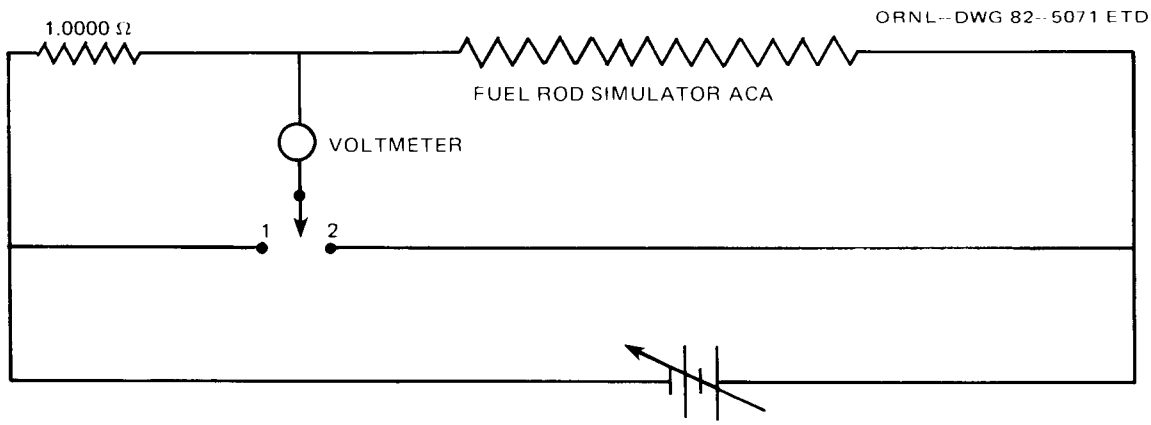

Fig. C.13. Circuit used in FRS emissivity determination.

3. Repeat step two by 55 K increments over the range from 300 to 750 K, and then shut off the power and cool the rod with a fan.
4. Paint the FRS black, and then repeat steps 1–3. (Two paints were used; each had a different temperature range over which it was applicable, and each had a known surface emissivity.)

These experiments could not be carried out in a vacuum, and as a result the total heat transferred at the surface (known) was the sum of the heat transferred by convection and radiation [Eq. (C.1)]. However, in the test apparatus, the convective heat transfer is via free (natural) convection to air that is adequately described by available correlations. The correlation used[15] is a Nusselt type of the form

$$\frac{hd}{K} = a[N_{Gr} \times N_{Pr}]^m , \qquad (C.2)$$

where the parameters a and m are dependent on the product of the Grashof number (N_{Gr}) and Prandtl number (N_{Pr}). For the specified temperature range, the free convective film heat transfer coefficient [h in Eq. (C.2)] is plotted vs the rod temperature in Fig. C.14. Thus, the convective heat transfer can be estimated by

$$q_{convection} = hA(T_{rod} - T_{sink}) , \qquad (C.3)$$

where h is defined by Eq. (C.2) and Fig. C.14, A is the surface area of the heated section of the FRS, and $T_{rod} - T_{sink}$ is the temperature difference between the rod and the surroundings. Then the radiant heat transfer is just the difference between the known power generation in the heated

ORNL–DWG 82–5072 ETD

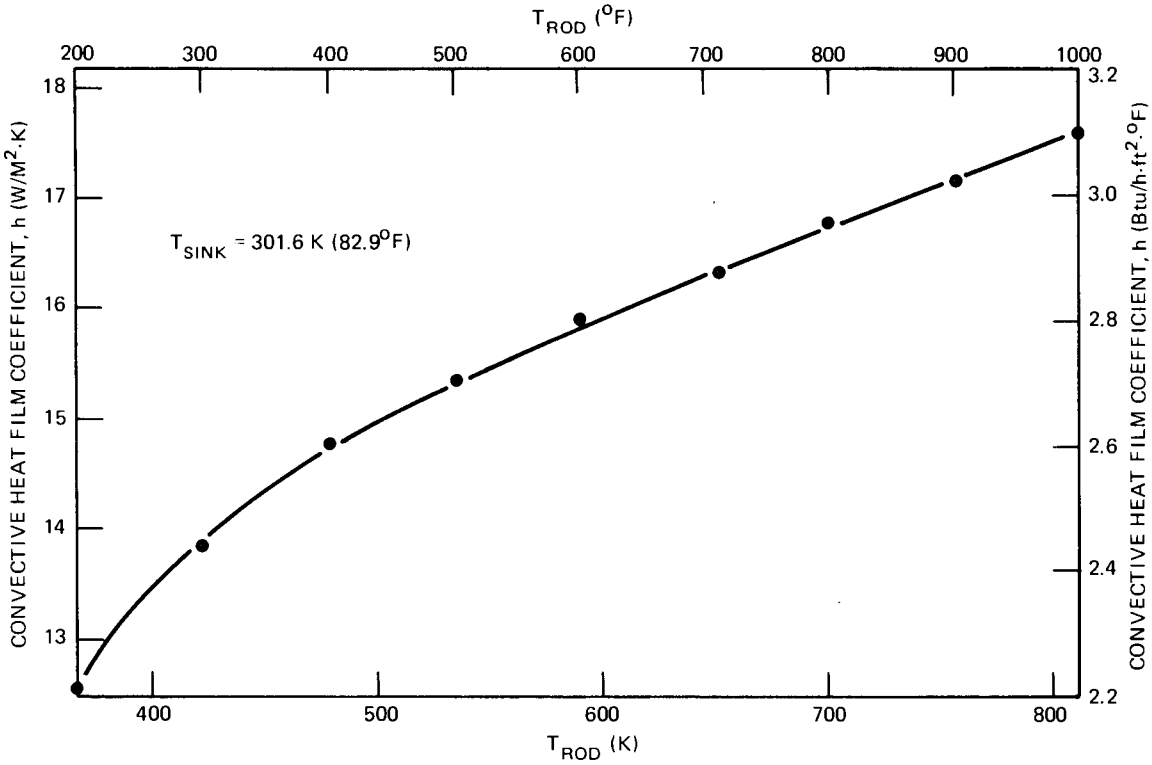

Fig. C.14. Free convection film heat transfer coefficient as a function of rod temperature.

section and the convective heat transfer; that is,

$$q_{radiation} = q_{total} - q_{convection} .$$

The heat transfer at the rod surface (total, convective, and radiative) for the three experimental runs is given in Figs. C.15–C.17. Run 2 was made with the rod painted with Krylon paint, which has an emissivity of 0.98 at temperatures >475 K; this paint turned to ash at ~700 K. Run 3 was made after painting the rod with Deshter paint, which has an emissivity of 0.92 at 670 K. A simplified formulation of radiant heat transfer is given by

$$q_{radiation} = \sigma A \varepsilon (T^4 - T^4_{sink}) . \qquad (C.4)$$

Given two surfaces (one with a known emissivity ε_1 and the second with an unknown emissivity ε_2) and letting

$$A_1 = A_2 ,$$

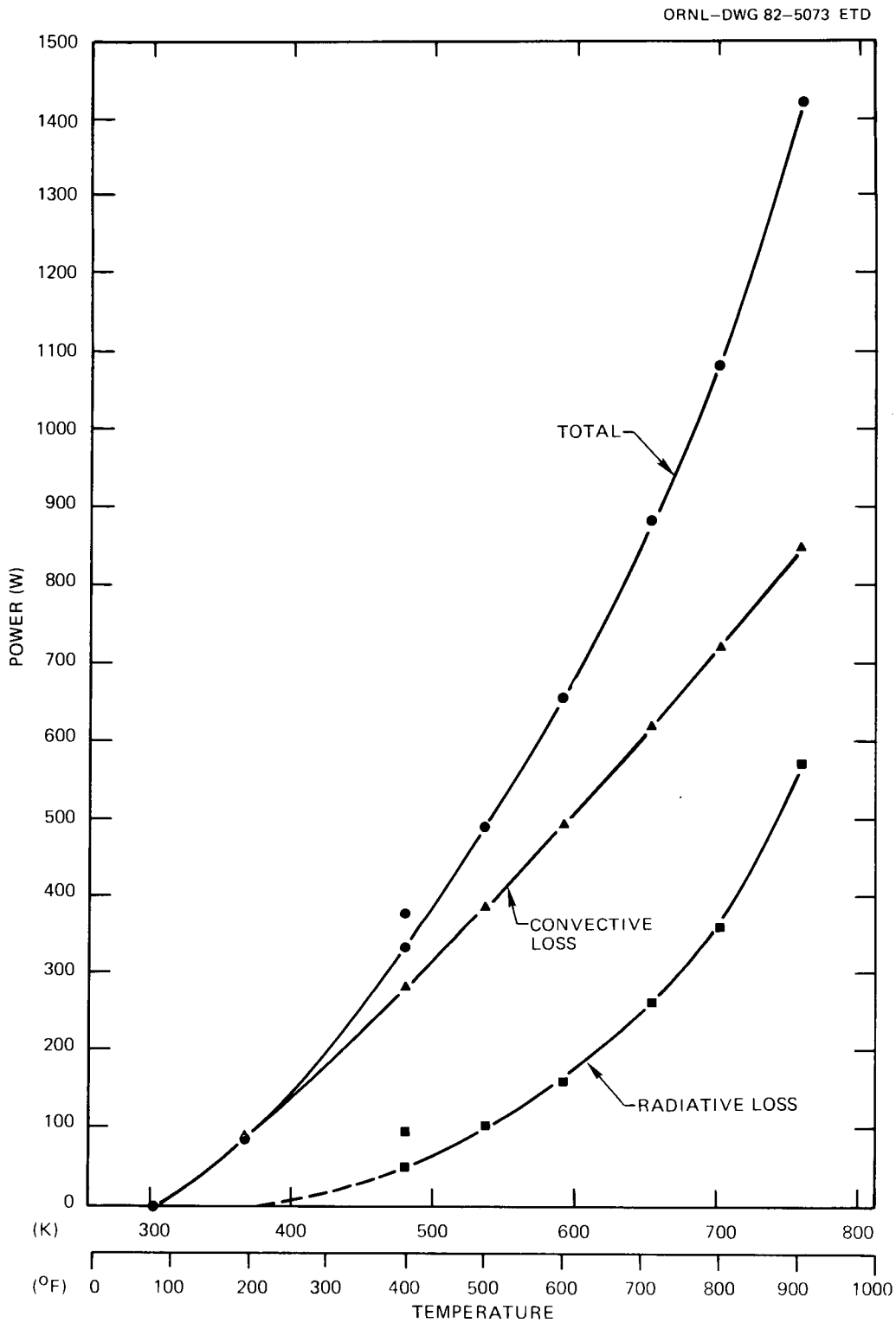

Fig. C.15. Heat generation in the heated length of FRS-026 (unpainted).

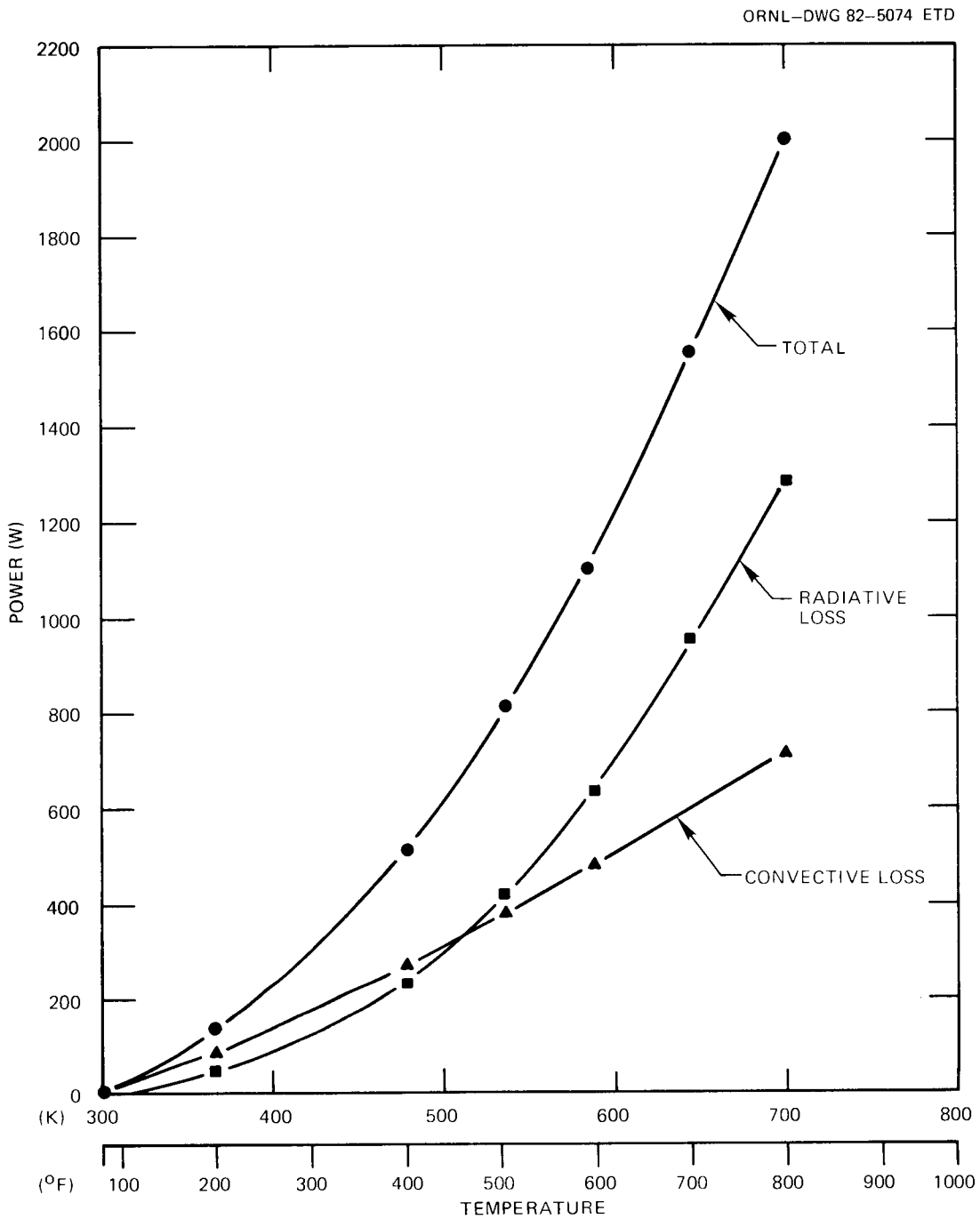

Fig. C.16. Heat generation in the heated length of FRS-026 (painted with Krylon paint, ε ~ 0.98 at >475 K).

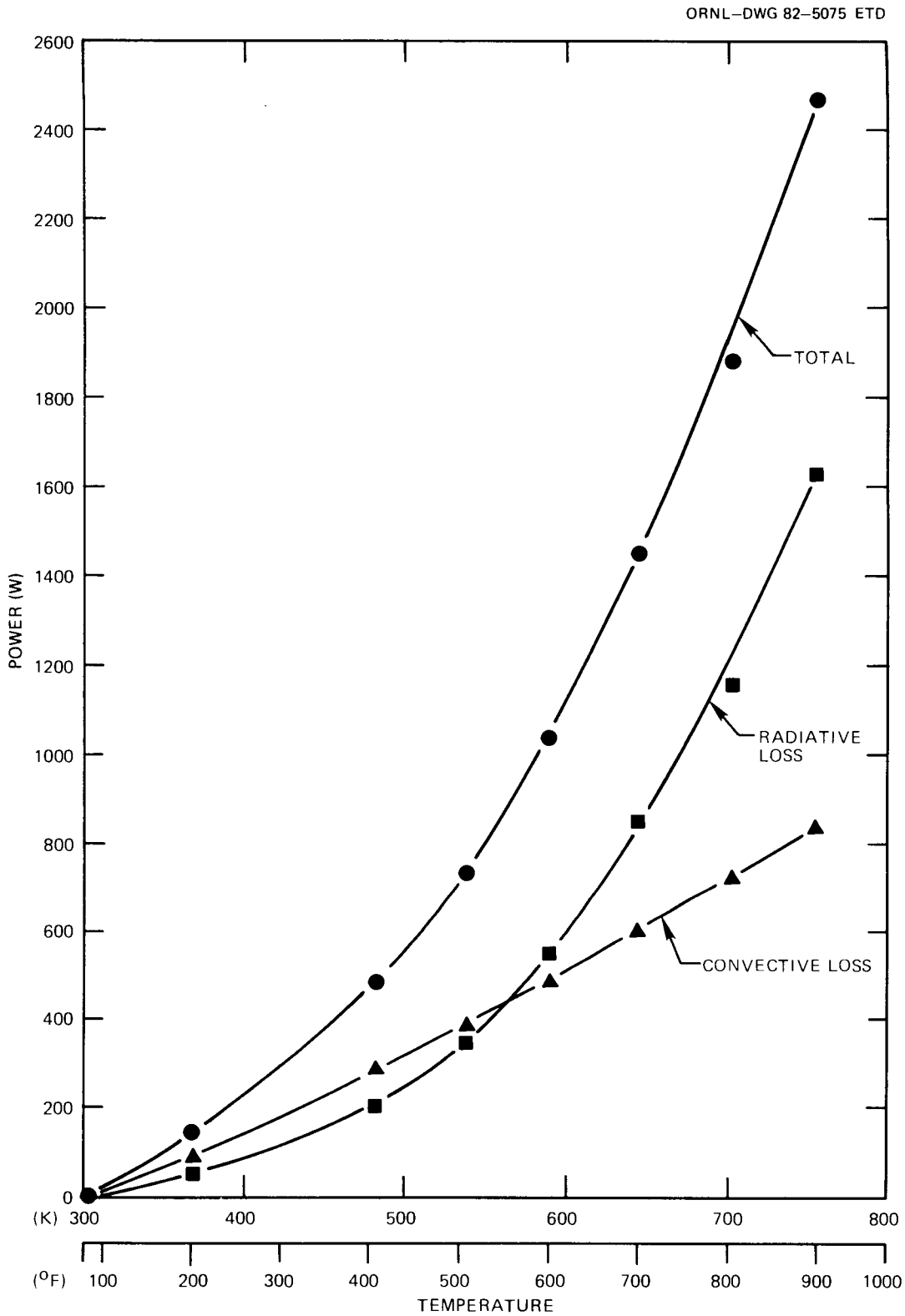

Fig. C.17. Heat generation in the heated length of FRS-026 (painted with Deshler paint, ε ~ 0.92 at ~670 K).

$$T_1 = T_2 ,$$

and

$$T_{sink_1} = T_{sink_2} ,$$

then

$$\frac{q_{r_1}}{q_{r_2}} = \frac{\varepsilon_1}{\varepsilon_2} ,$$

or

$$\varepsilon_2 = \varepsilon_1 \frac{q_{r_2}}{q_{r_1}} , \qquad (C.5)$$

where the radiative heat transfer q_{r_1} and q_{r_2} are known and the emissivity ε_1 is known. Thus, the emissivity of the unpainted rod (i.e., the FRS as received from the THTF) can be estimated as a function of rod temperature from the plots in Figs. C.15 and C.17 and the known[16] paint emissivities. The emissivity of the FRS-026 surface after removal from the THTF is shown in Fig. C.18. The best linear least-squares fit to the points in Fig. C.18 takes the following form:

$$\varepsilon(T) = 0.25617 + 0.000348\ (T - 616.67) , \qquad (C.6)$$

where T has units of K; or

$$\varepsilon(T) = 0.25617 + 0.000193\ (T - 650) , \qquad (C.7)$$

where T has units of °F. Using the available Infrared Inspection Section experimental apparatus, 750 K was approximately the maximum temperature to which the painted rods could be heated without oxidizing the paint (as noted, the Krylon paint oxidized at ~700 K). Therefore, for the range of temperatures of interest (i.e., 950–1150 K) an *extrapolation* of the experimental data must be made. *Remember* that it is an extrapolation beyond the range over which the data were gathered. For the temperature range of 950–1150 K, the estimated FRS surface emissivity in the THTF is 0.372–0.442.

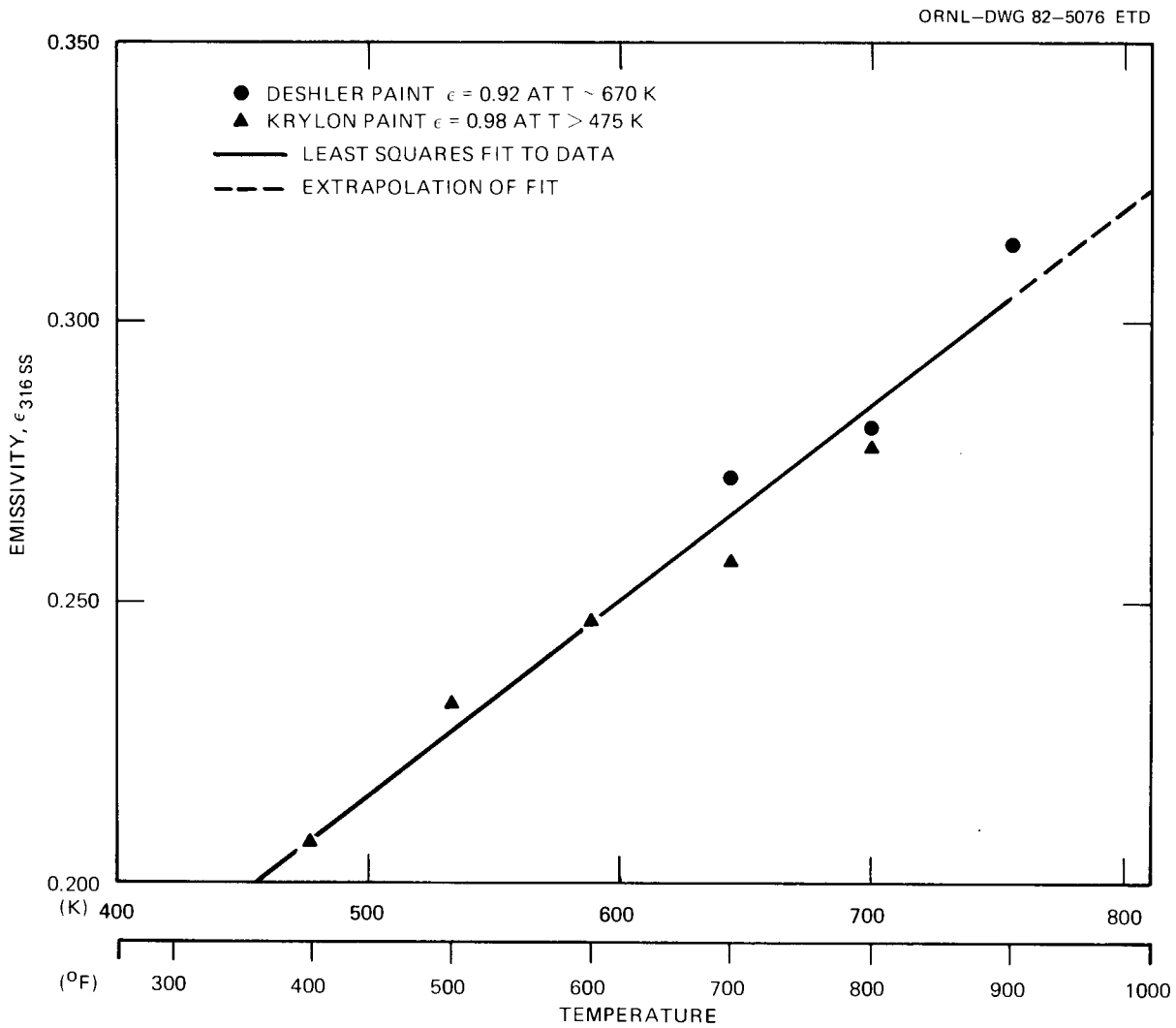

Fig. C.18. Emissivity of FRS-026 surface after removal from the THTF.

References

1. L. J. Ott and R. A. Hedrick, *ORINC — A One-Dimensional Implicit Approach to the Inverse Heat Conduction Problem*, ORNL/NUREG-23 (November 1977).

2. B. R. Bass, J. B. Drake, and L. J. Ott, *ORMDIN: A Finite Element Program for Two-Dimensional Nonlinear Inverse Heat Conduction Analysis*, NUREG/CR-1709 (ORNL/NUREG/CSD/TM-17) (December 1980).

3. L. J. Ott and R. A. Hedrick, *ORTCAL — A Code for THTF Heater Rod Thermocouple Calibration*, NUREG/CR-0342 (ORNL/NUREG-51) (February 1979).

4. R. L. Ludwig, ORNL, Letter MS-79-0235 to M. D. White, ORNL, June 1979; Subject: Measurement of Sections from BDHT FRS-038.

5. L. J. Ott and J. A. Smolen, ORNL, BDHT Memorandum 2287 to BDHT staff, August 8, 1979; Subject: Bundle 3 Fuel Rod Simulator Radial Dimensions.

6. L. J. Ott, ORNL, BDHT Memorandum 2522 to BDHT staff, December 9, 1980; Subject: Updated Bundle 3 Fuel Rod Simulator Radial Dimensions.

7. R. L. Ludwig, ORNL, Letter 80J-1120-195 to L. J. Ott, ORNL, November 20, 1980; Subject: Measurement of Sections from BDHT FRS-058B.

8. R. W. McCulloch et al., *Fabrication Technology Development of Fuel Rod Simulators for Blowdown Heat Transfer Tests* (to be published).

9. K. W. Childs, *Uncertainty in Calculated Surface Temperature and Surface Heat Flux of THTF Heater Rods*, NUREG/CR-1211 (ORNL/NUREG/CSD/TM-12) (December 1980).

10. S. D. Snyder et al., *Infrared Inspection and Characterization of Fuel Pin Simulators*, ORNL/NUREG/TM-55 (November 1976).

11. S. D. Snyder, "The Prevention and Cure of Diseased Fuel Rod Simulators — From Conception to Death — By Timely and Proper Inspection," paper presented at the International Symposium on Fuel Rod Simulators — Development and Application, Gatlinburg, Tennessee, October 22-24, 1980.

12. R. L. Anderson and T. G. Kollie, *Accuracy of Small Diameter Sheathed Thermocouples for the Core Flow Test Loop*, ORNL-5401 (April 1979).

13. R. W. McCulloch, ORNL, Letter to L. B. Thompson, NRC, January 25, 1980; Subject: Determination of a Recovery Anneal Process to Remove Coldwork from Type-K Small-Diameter Sheathed Thermocouples.

14. American Society for Metals, *Source Book on Industrial Alloy and Engineering Data*, Metals Park, Ohio, 1978.

15. J. H. Perry, *Chemical Engineers' Handbook*, Fourth Ed., McGraw-Hill Inc., New York, 1963.

16. S. D. Snyder, ORNL, personal communication to L. J. Ott, ORNL.

Appendix D

INSTRUMENT UNCERTAINTY ANALYSIS FOR THE THTF LOOP

Summary of Results

Two standard deviation uncertainty bands are described for critical instrumentation in the Thermal Hydraulic Test Facility (THTF). The analyzed instruments and their minimum, steady-state, 2σ error bands [root sum square (RSS), 95% confidence interval] include:

1.	Turbine flowmeter	4.1% reading
2.	Gamma densitometer	10.4% FS*
3.	Strain gage pressure cell	1.0% FS*
4.	Differential pressure cell	2.0% FS* min to 9.9% FS* max
5.	Thermocouples	3.7°C min to 10.3°C max
6.	Rod power instrumentation	1.1% reading
7.	Strain gage drag disk	56% reading below 10% FS* 19% reading above 10% FS*

Summary of Theory

The measure of the value of a group of n data points (x_i) with satistical significance is the mean ($\bar{x}$) or expected value given by

$$\bar{x} = \sum \frac{x_i}{n} , \tag{D.1}$$

where Σ is the usual sum from data point 1 to data point n. The standard measure of the dispersion of the data is the variance [σ^2 or V(x)] defined by

$$\sigma^2 = \sum \frac{(x_i - \bar{x})^2}{n} . \tag{D.2}$$

However, V(x) has dimensions of engineering units squared, which may be inconvenient. The square root of V(x), the standard deviation (σ), is usually reported. Furthermore, in normally distributed data with mean $\bar{x}$ and variance σ^2 (a good approximation for much variation in physical data),

---

*Full-scale values are found in Tables D.5–D.8 under instrument range.

statistical inferences may be drawn in terms of probabilities based on the measured values of $\bar{x}$ and σ as follows:

68% probability that $\bar{x} - \sigma < x_t < \bar{x} + \sigma$,

95% probability that $\bar{x} - 2\sigma < x_t < \bar{x} + 2\sigma$,

and

99.7% probability that $\bar{x} - 3\sigma < x_t < \bar{x} + 3\sigma$,

where x_t is the true value of the variable.

Brownlee has shown[1] that the variance of a linear function

$$Z = A_0 + A_1X_1 + A_2X_2 + \ldots A_nX_n$$

is a linear function of the variance of the variables as long as the correlation coefficients are zero, i.e., as long as they are physically unrelated. (Linearly independent variables have zero correlation coefficients, but linear independence is not a requirement.) That is,

$$V(Z) = A_iV(X_i) + A_2V(X_2) + \ldots A_nV(X_n) , \qquad (D.3)$$

where the A_i's are constants and the X_i's are independent variables.

Similarly, Scarborough has shown[2] that an analogous relation holds for a system where the independent variables are not linear:

$$Z = F(Y_1, Y_2 \ldots, Y_n) .$$

The variance of Z is given by

$$V(Z) = \left(\frac{\partial Z}{\partial Y_1}\right)^2 V(Y_1) + \left(\frac{\partial Z}{\partial Y_2}\right)^2 V(Y_2) + \ldots + \left(\frac{\partial Z}{\partial Y_n}\right)^2 V(Y_n) , \qquad (D.4)$$

where the correlation coefficients of the Y_i's are zero and the value of V(Y) is small compared to $(\partial Z/\partial Y_i)^2$. Notice that in situations where the standard deviation can be expressed legitimately as a percentage of the value of $\partial Z/\partial Y_i$, Eq. (D.4) can be rewritten as

$$\sigma\%(Z) = \sqrt{[\sigma\%(Y_1)]^2 + [\sigma\%(Y_2)]^2 + \ldots + [\sigma\%(Y_n)]^2} . \qquad (D.5)$$

The above equations can best be understood through the use of an illustrative example. Consider the amplifier of Fig. D.1. The uncertainty in the input voltage can be derived from the function $V_{in} = F(V_{out}, V_{offset}, GAIN)$, given the measured values for V_{out}, $V(V_{out})$, V_{offset}, $V(V_{offset})$, and GAIN, V(GAIN), when V_{in} is the input voltage, GAIN is the amplifier gain, and V_{offset} is the offset voltage.

Assuming the following data, the value of V_{in} is given by

$$V_{in} = \frac{V_{out} - V_{offset}}{GAIN}$$

and the variance in the input voltage can be found by applying Eq. (D.4) or (D.5):

$$V(V_{in}) = \frac{V(V_{out})}{GAIN^2} + \frac{V(V_{offset})}{GAIN^2} + \frac{V(GAIN)\ (V_{offset} - V_{out})^2}{GAIN^4}\ , \qquad (D.6)$$

where

$$V_{out}\ max = 20.0 \text{ volts},$$

$$V_{out} = 10.0 \text{ volts},$$

$$V(V_{out}) = (0.2 \text{ volts})^2 = (2\%)^2 \text{ reading},$$

$$V_{offset} = 0.5 \text{ volts},$$

$$V(V_{offset}) = (0.05 \text{ volts})^2 = (0.5\%)^2 \text{ reading},$$

$$GAIN = 200 \text{ volts/volt},$$

$$V(GAIN) = (1 \text{ volt/volt})^2 = (0.5\%)^2 \text{ reading},$$

$$V_{in} = \frac{(10.0 \text{ volts} - 0.5 \text{ volts})}{200} = 0.0475 \text{ volts},$$

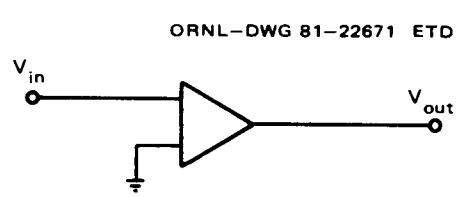

Fig. D.1. Amplifier.

$$V(V_{in}) = \frac{(0.2)^2}{(200)^2} + \frac{(0.05)^2}{(200)^2} + 1^2 \frac{(-9.5)^2}{(200)^4}$$

and

$$\sigma(V_{in}) = 10^{-3} \text{ volts or } 2.1\% \text{ reading} .$$

Because V_{in} is a function of V_{out}, V_{offset}, and GAIN in the form given above, it is reasonable to assume that stating the variances as percentages of the readings is equivalent to stating the variances as percentages of the respective partial differentials. In fact, this will always be reasonable as long as the variables are of the first order. The arithmetic for computing $\sigma(V_{in})$ becomes simply

$$\sigma(V_{in}) = \sqrt{(2\%)^2 + (0.5\%)^2 + (0.5\%)^2} = 2.1\% \text{ reading} .$$

Equation (D.4) or (D.5) applied to each major component of a complex information loop is often the only method available to arrive at an uncertainty value. However, in the case of the gamma densitometer and the strain gage pressure cell, in situ standards are available that allow direct measurement of the uncertainty. Heise gages are used as in situ standards for strain gage pressure cells. Pressure and temperature measurements in subcooled water can be used to determine density with steam tables for comparison with the gamma densitometers. Such a comparison is made using a linear regression analysis based on the method of Gauss.

The equation of a line in slope-intercept form is given by

$$y = Ax + B ,$$

where A is the slope ($\Delta y/\Delta x$) and B is the value of the y intercept.

The best-fit values of A and B can be found by minimizing the sum of the distances between the experimentally determined points and the best-fit line.

The pertinent equations are

$$A = \frac{\Sigma x_i \Sigma y_i - n \Sigma (x_i y_i)}{(\Sigma x_i)^2 - n \Sigma (x_i)^2} \tag{D.7}$$

and

$$B = \frac{\Sigma (x_i y_i) \Sigma x_i - \Sigma y_i \Sigma (x_i)^2}{(\Sigma x_i)^2 - n \Sigma (x_i)^2} , \tag{D.8}$$

where the x_i's are the values determined by the instrument under discussion and the y_i's are the corresponding values determined by the in situ standard. The uncertainty of the instrument values can then be defined analogously to Eq. (D.2):

$$\sigma = \sqrt{\sum \frac{(Y_i - y_i)}{n}} , \tag{D.9}$$

where the Y_i's are computed from the best-fit equation and the instrument values are y_i. A perfectly calibrated and properly operating instrument will have A = 1.0, B = 0, and $\sigma \ll$ reading.

Although the slope-intercept form of an equation is one of the easiest to interpret, it does have a disadvantage: A and B are not linearly independent variables, so drawing statistical inferences about A and B in terms of their variances is hindered. A solution to this problem is to solve for the best-fit line equation in the form

$$Y = \alpha(x - \bar{x}) + \beta . \tag{D.10}$$

The variances of α and β are then known to be

$$V(\alpha) = \frac{\sigma^2}{n} \tag{D.11}$$

and

$$V(\beta) = \frac{\sigma^2}{\Sigma(x_i - \bar{x})^2} , \tag{D.12}$$

as shown by Brownlee,[3] where σ is defined as in Eq. (D.9). We can still arrive at an estimate of V(A) and V(B) by modifying Eq. (D.10) to show

$$Y = \alpha x - \alpha\bar{x} + \beta ,$$

which implies α = A and B = $(-\alpha\bar{x} + \beta)$. Applying Eq. (D.4) yields

$$V(A) = \frac{\sigma^2}{n} \tag{D.13}$$

and

$$V(B) = \frac{\sigma^2}{n}\bar{x}^2 + \frac{\sigma^2}{\Sigma(x_i - \bar{x})^2} = \sigma^2 \left[\frac{x^2}{n} + \frac{1}{\Sigma(x_i - x)^2}\right] . \qquad (D.14)$$

Equations (D.2)–(D.5) and (D.9) should be applied with caution for several reasons.

Definitions for variance assume perfect knowledge. However, actual sampling procedures are limited to finite sample sizes, and formulas impose limits on the degrees of freedom by imposing constraints. To adjust for the limits to the number of degrees of freedom, Eq. (D.2) is modified to provide an estimator for the standard deviation denoted S such that

$$S = \sqrt{\frac{\Sigma(x_i - \bar{x})^2}{(n - 1)}} . \qquad (D.15)$$

Equation (D.9) becomes

$$S = \sqrt{\frac{\Sigma(Y_i - y_i)^2}{(n - 2)}} . \qquad (D.16)$$

Equations (D.15) and (D.16) are the proper equations to use in all sampling situations where the standard deviation is to be used as the measure of the uncertainty. Furthermore, the value for S should be substituted for the value of σ and S^2 for V(X) or V(Y) in each of the other equations where σ appears. Because of the common association between the standard deviation defined by Eqs. (D.15) and (D.16) with the symbol σ, the symbol σ will be used for S in the balance of this report. In a practical sense, where the standard deviation is reported as two significant figures, there is essentially no difference between σ and S [Eqs. (D.4) and (D.9) versus Eqs. (D.15) and (D.16)] as long as the number of data points is large.

A class of practical problems that arises in the actual error analysis is centered around the interpretation placed on uncertainties supplied by manufacturers. These uncertainties are often supplied as percentages in such a manner that it is difficult to determine whether it is reasonable to apply Eq. (D.5). Either it is difficult to determine how the stated error relates to the standard deviation, or it is difficult to determine whether the error can be applied as a percentage of the partial differentials required by Eq. (D.5). Furthermore, it is seldom stated whether the given uncertainties meet the required criterion of zero correlation coefficient. It is common for manufacturers to quote error bands as 2σ (95% confidence) or 3σ (99% confidence) though sometimes without assigning confidence limits. In this report it is conservatively assumed that the error reported by instrument manufacturers is 2σ. Unless otherwise stated, it is also assumed that a statement of error as a percent

with respect to the partial differentials of Eq. (D.5) is reasonable and that the correlation coefficient is zero for all variables.

The second class of problems relating to the uncertainty analysis dealt with multiple estimates of σ for a class of instruments where σ varied widely from instrument-to-instrument and from trial-to-trial. The method of choice was to use a value of σ large enough to include about 95% of the measured values. This was accomplished by using

$$\sigma \simeq \overline{\sigma} + \sigma(\sigma) \ .$$

That is, the value of the standard deviation used was the average value for all instruments and files read plus one standard deviation of σ. This is different from the probability statements above because σ is a span that includes zero to σ. Such a distribution cannot be normal in the sense that the probability statements require.

A generalized procedure for data analysis follows:

A common form for a large system is generalized in Fig. D.2. This system consists of a number of transducers (T_i), their associated signal conditioning equipment (S_i), and the data acquisition system (DAS). The DAS is understood to include both the hardware and the software. The standard deviations of the output signals are measured by reading the information from the magnetic tape written by the DAS and applying Eq. (D.2) or D.14) over an arbitrary length of time where the process is defined as being in a steady state. The measured value of the DAS output can then be incorporated with other measures of uncertainty using Eq. (D.5). If an in situ standard is going to be used to develop the total uncertainty directly, the data for the secondary standard need to be accessed and correlated in time and space with the instruments under consideration.

The development of software to perform the above estimates may be the most time-consuming part of the analysis. The software has to be able to perform the following functions for a magnetic-tape-based system:

1. Confirm that the tape is at the beginning.
2. Confirm that the tape density and number of tracks are system compatible.
3. Locate the instrument data base (IDB) and transfer the IDB to disk or core in a rapid access format.
4. Extract certain system constants from the IDB (record length, etc.).
5. Locate the scan table.
6. Use the scan table and instrument identifier code to determine the location of the desired instrument data in data records.
7. Locate the first data file of the type desired.

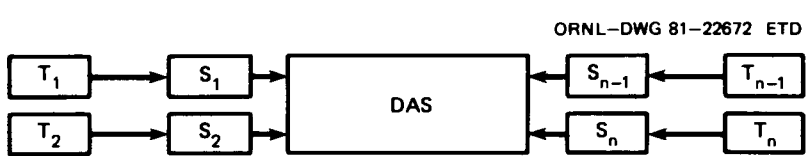

Fig. D.2. Generalized form for a large system.

8. Read a fixed number of records from the data file.
9. Store data in arrays or keep running totals for averaging.
10. Compute averages and standard deviations for steady-state data in the file.
11. Write the desired combinations of data, averages, and standard deviations to arrays.
12. Locate the next data file of the type desired and repeat steps 8–12 until end-of-tape is detected.
13. At end-of-tape, write the arrays to disk for later analysis.
14. At each tape operation, check for proper positioning.
15. Analyze data written to disk as required.

The following sections provide a detailed analysis of the critical instrumentation in the THTF loop. As stated above, the exact nature of the uncertainties is not always known. The RSS value of the uncertainty is the statistically defined one if variables are unrelated (correlation coefficient = 0) and the percentage uncertainty is given as a percent of partials required for Eq. (D.5). However, to the extent that the uncertainties stated do not comply with the assumptions, the more conservative strict sum of errors may need to be applied. Both the RSS value and the strict sum value are given in the text. The RSS values are reported in tabular form at the end of this Appendix. The superscript (*) is used to denote manufacturer derived data.

D.1 Turbine Flowmeter

The turbine flowmeter channel consists of a turbine flowmeter with integral magnetic pickup, an electronics package that conditions the signal to provide an output voltage proportional to flow rate, and the DAS, which converts the analog signal in volts to digital information and writes it onto magnetic tape. In operation, the turbine blade generates an electrical pulse as it passes the magnetic pickup. The ORNL electronics package senses this pulse and with 250 μs resets the count registers and begins accumulating the count until the next pulse disables the count. During the disabled period the count is passed to the digital-to-analog converter where it is converted to millivolt reading. The voltage divider then inverts the millivolt signal and outputs a voltage proportional to the angular velocity of the turbine blade, with 10-V full scale (FS) corresponding to 1200-Hz input signal from the flowmeter pickup. The DAS then converts the output of the ORNL electronics to a digital value and writes it onto magnetic tape. The identified sources of error in the turbine flowmeter are:

Channel noise (blade angle tolerance)	3.2%
Calibration uncertainty	2.4%
Inherent turbine linearity*	0.5%
ORNL electronics package	0.4%
A/D conversion at DAS*	0.3%
Effect of bearing change each run*	0.3%
Strict sum, 2σ error band	7.1%
RSS, 2σ error band	4.1%

The following items need to be considered when applying the above error bands to THTF data:

1. The above uncertainties are all reasonably expressed as a percent of reading. However, the value of turbine linearity quoted applies only over the range 10% rated FS through 100% rated FS. Below 10% rated FS, error bands increase rapidly (see Fig. D.3) as frictional drag becomes more significant, with a cutoff of useful information occurring near 6% of rated FS flow due to signal-to-noise problems in the electronics.

2. Random noise was measured for 30 records of data taken during Reactor Simulation Test 3.05.5B. When the standard deviation was computed for each of the 10 flowmeters without excessive channel noise, the average value (1.53% of reading) was found to agree very well with the predicted channel noise because of blade manufacturing tolerances (72° ± 1.56%). It would be optimistic, however, to conclude that this is the only source of random error. Data taken over a much wider range of flows would be needed to confirm this conclusion.

3. The calibration uncertainty was estimated from two different calibration laboratories (Flow Technology, Inc., and Measurements, Inc.) independently calibrating the same turbine flowmeters. The results of those calibrations indicated approximately 1.2% (as 1σ) differences from laboratory-to-laboratory. The supposed calibration uncertainty according to the laboratories was an order of magnitude smaller based on their NBS traceability standards. The reasons for the large difference were never satisfactorily determined. This comment applies solely to turbine meters located at the SVO, SVI, SHI, SHO, BI1, BI2, and BO1 spool pieces in the standard configuration (i.e., 3.5-in. turbine meters).

4. The most troublesome problems of interpreting flowmeter error are those that occur during two-phase flow. In a 1977 report[4] MPA Associates,

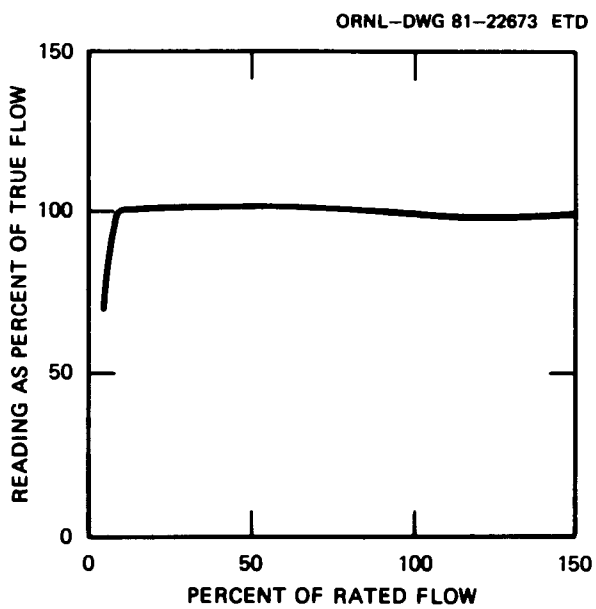

Fig. D.3. Error due to turbine linearity: characteristic curve.

Inc., investigated the possible errors due to slug flow, annular flow regimes, steam-water ratios, and differential two-phase velocities. This investigation was strictly theoretical, based on momentum exchange between the blade and the fluid. These analyses were based on steady-state flow, balancing the transverse momentum of one phase against that of the second. Assuming no net momentum exchange with the rotor, the turbine response was interpreted in light of the point effective radius (established as the calbration constant) in the presence of two phases with different flow regimes and different velocity profiles. The conclusion reached was that errors up to ±25% might be expected.

By assuming equal probabilities for the parameters investigated, it was determined that a 1σ error band of 10% might reasonably be expected. However, until experimental verification of both model and results can be obtained, it would only be prudent to use the above figures in a qualitative manner.

D.2 Gamma Densitometer

The gamma densitometers consist of a nearly monoenergetic ^{137}Cs gamma source, an ionization chamber to detect the gamma rays, an instrument amplifier, and the DAS. In use, the gamma rays pass through the steel pipe, through the water (in whatever phase) in the pipe, and into the ionization chamber. In the ionization chamber the gamma rays are converted into an electric current such that the current is proportional to the intensity of the impinging gamma rays. The instrument amplifier takes this current and converts it into a voltage that is proportional to the input current. At the DAS the voltage is converted to a digital value and stored on magnetic tape.

Given that the source approximates a point source, the density of the water (ρw) in the pipe should be given by

$$\rho w = \text{KFACTR} \ln \frac{V_p - V_o}{V - V_o} ,$$

where KFACTR is an experimentally determined constant that includes the effect of pipe diameter and the mass absorption coefficient of the water (including any dissolved salts), V_p is the output voltage when the pipe is empty, V_o is the output voltage with the source shielded (dark voltage or zero offset), and V is the output voltage when there is water in the pipe.

Due to the strong theoretical dependence of density error as a function of density, the 1σ error band was investigated as a statistical function of the density reading compared to an in situ standard based on the physical properties of the water in the pipe under known conditions of temperature and pressure and a steady-state, one-phase flow. Ten gamma densitometers in service during Test 3.05.5B were used as a basis of the study. The output voltage of each instrument was sampled 150 times in each of ten 3-s files. The output voltage was then used to compute the

water density using values of KFACTR, V_p, and V_o measured in a recent calibration run. Those densities were then compared to the expected densities based on water properties derived from the temperature and pressure instruments located adjacent to each gamma densitometer.

The measured uncertainty expressed as 1σ in kg/m^3 (and lb/ft^3) is shown in Table D.1. It was discovered, however, that at least part of the large variation in the uncertainties resulted from a systematic error that varied from instrument to instrument (see Fig. D.4, where the densitometer density is plotted against the water property density for DE-204B). Furthermore, the expected strong dependence of error on total density is not obvious over the range of data compared. Not all densitometers showed positive deviations from the standard as did DE-204B.

Table D.1. Absolute error analysis

Densitometer	σ (kg/m^3)	σ (lb/ft^3)
DE-20	18.9	1.18
DE-36	199.0	12.42
DE-168	3.6	0.22
DE-218	87.5	5.46
DE-204A	4.4	0.27
DE-204B	57.7	3.60
DE-204C	33.6	2.10
DE-262A[a]		
DE-262B	22.9	1.43
DE-262C	37.5	2.34
Average	52.0	3.20

[a]Probable equipment failure during test.

The data for each densitometer were fit to a straight line, densitometer calculated density to water property density, using linear regression analysis. The random error, expressed as 1σ, was then calculated for each gamma densitometer using Eq. (D.16), but Y_i is the best average value from the linear regression equation. The value of uncertainty was much more uniform from densitometer to densitometer (see Table D.2). A preliminary analysis of the calibration procedure indicates that it may be possible to recalibrate the densitometers analytically to remove the systematic error. Since the analysis performed on the experimental data does not use the densitometer responses, it was not deemed worthwhile to expend the effort required to perform this recalibration.

Since the density of water at room temperature is approximately 1×10^{-3} kg/m^3 (62.4 lb/ft^3), the above results can be summarized as

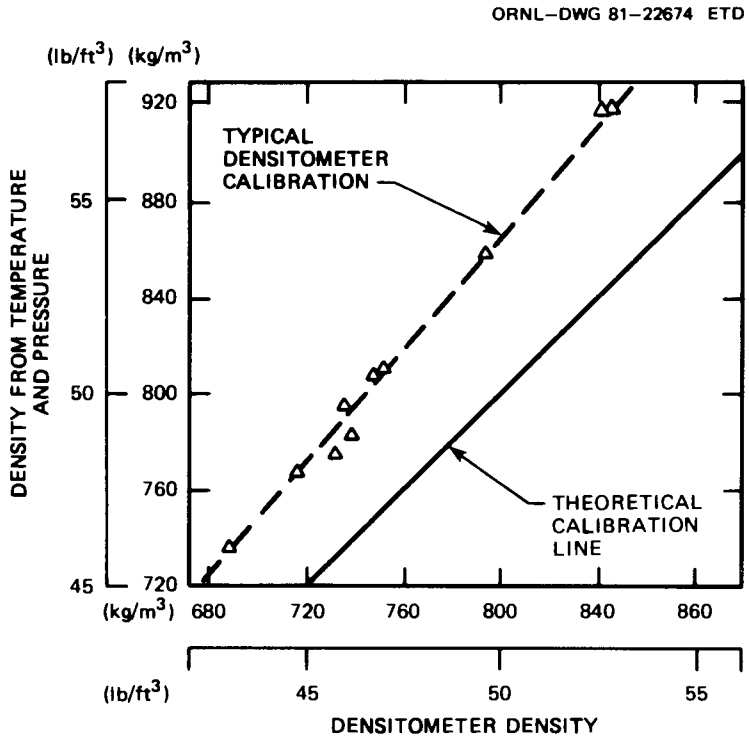

Fig. D.4 Typical densitometer calibration.

Table D.2. Least-squares best-fit line
(RHO = A x DERHO + B)

Densitometer	A	B	σ (kg/m³)	σ (lb/ft³)
DE-20	0.945	64.9	8.6	0.54
DE-36	0.131	745.0	9.7	0.61
DE-168	1.000	−0.4	0.9	0.06
DE-218	0.711	176.0	2.5	0.16
DE-204A	0.981	14.0	4.4	0.27
DE-204B	1.190	−85.9	6.0	0.37
DE-204C	1.010	24.8	12.4	0.77
DE-262A[a]				
DE-262B	0.740	246.0	5.3	0.33
DE-262C	1.160	−100.0	4.5	0.28
Average			5.8	0.36

[a]Probable equipment failure during test.

follows:

2σ error band under current operating procedures .... 10.4% FS

The following items need to be considered when applying the above error bands to THTF data analysis:

1. An analysis of data scatter indicates an average σ of 31 kg/m³ or 3.1% FS over 150 point data files. Therefore, individual points within a file have much higher uncertainties than those stated for files as a whole.
2. No other factor has been identified which would degrade the error bands beyond the steady-state, one-phase flow values listed above. However, it should be understood that the densities computed from densitometer voltages during transients and two-phase flow are time-and-path averaged values. Furthermore, a direct application of the above data to transient, two-phase flow is done at the risk of the data user until experimental verification can be obtained.

D.3 Strain Gage Pressure Cells

The pressure channel investigated consists of a strain gage pressure cell, an instrument amplifier, and the DAS. In operation, pressure on the diaphragm of the pressure cell causes a change of resistance in the foil strain gages attached to the diaphragm. The change in resistance in the gages causes a voltage output from the cell that is proportional to the applied pressure. This output is amplified by the instrument amplifier. The DAS converts the amplifier output to digital format and writes it onto magnetic tape.

The following errors were identified as contributing to the pressure cell uncertainty:

Nonlinearity (P-sensor)*	0.3% FS
Repeatability (P-sensor)*	0.1% FS
Hysteresis (P-sensor)*	0.1% FS
Tempco, gage factor (P-sensor)*	0.5% Reading
Tempco, zero offset (P-sensor)*	0.5% FS
Gain instability (instrument amplifier)* ...	0.1% Reading
Output offset (instrument amplifier)*	0.1% FS
DAS calibration*	0.3% Reading
Location of calibration standards	0.4% FS
Strict sum 2σ error band	2.5% FS
RSS 2σ error band	1.0% FS

The following items need to be considered when applying the above error bands to THTF data:

It is fairly obvious that the results of the in situ calibration run (see item 2 below) agree respectably with the 2σ error band determined above. The probable reason that in situ calibration errors are smaller than the theoretically determined value can be attributed primarily to

smaller than estimated temperature changes in actual operation for both gages and amplifiers. In the absence of contradictory experimental evidence, the 2σ error band for the strain gage pressure cells should be set at 1.0% FS or 200 kPa (29 psi).

1. The temperature effects were assumed to be operable over a range of only 56°C (100°F) in actual use. This seems like a reasonable assumption since the sensors themselves are installed at the end of a connecting tube ensuring cooling by ambient air flow and the instrument amplifier is mounted where ambient air flow should keep the temperature change within the 56°C (100°F) range. Channel noise was measured during Test 3.05.5B using Y_i [see Eq. (D.16)] as the average within a data file. Five instruments were sampled with 30 points per data file, 10 data files each. The 1σ value measured in this manner was quite variable, so that it was deemed expedient to select a value of σ large enough to include about 95% of the data.

2. The strain gage pressure cell does have a usable in situ standard for comparison. With data from a recent pressure cell calibration run, the standard deviation for system pressure was determined for six strain gage pressure instruments by comparing P-cell output converted to pressure using the measured calibration constants with the average reading of two Heise bourdon tube gages accurate to 20 kPa (3 psi). The results of that comparison are:

Instrument	σ (kPa)	σ (psi)	σ (% FS)
PE-26	37.2	5.4	0.18
PE-42	66.2	9.6	0.32
PE-44	18.6	2.7	0.09
PE-76	43.4	6.3	0.21
PE-106	47.6	6.9	0.23
PE-156	91.0	13.2	0.44
Average	51.0	7.4	0.24
Plus location of calibration standard	40.0	5.8	0.18
Total 2σ value	130.0	18.9	0.6

3. The in situ calibration uses the average reading of two Heise gages as system pressure. These gages may be separated by 8.53 m (26 ft) vertically. The result of the difference in static water pressure can produce an offset of ~40 kPa (5.8 psi) (1σ) depending on the location of the specific instrument.

4. The DAS seems to be the limiting factor in instrument response time, including the response time of the transducer itself since pressure waves should reach the diaphragm much faster than the normal sample rate. No other source of error has been identified to degrade the error band established for steady-state, one-phase flow. However, the application of the above error bands to transient or two-phase flow without corroborating data might be overly optimistic, and any such use is the responsibility of the data user.

D.4 Differential Pressure (dp) Cells

The strain gage dp cell (A, B, C) instruments are very similar to the strain gage pressure cells above, except that they have lower full-scale capability.

A. The identified sources of error in the BLH strain gage (1380 and 6870 kPa or 200 and 1000 psi, respectively) dp cell are

Bench calibration (note 1)	2.4% FS
Tempco, gage factor (P-sensor)*	0.1% FS
Tempco, zero offset (P-sensor)*	0.1% FS
Gain instability (instrument amplifier)* ...	0.1% FS
Output offset (instrument amplifier)*	0.1% FS
A/D inaccuracy (DAS)*	0.3% FS
Random noise (note 2)	2.0% FS
Strict sum 2σ error band	5.1% FS
RMS 2σ error band	3.1% FS

B. The identified sources of error in the BLH strain gage (1380 kPa or 200 psi) (pit) dp cell are

Bench calibration (note 1)	2.4% FS
Tempco, gage factor (P-sensor)*	0.5% Reading
Tempco, zero offset (P-sensor)*	0.5% FS
Gain instability (instrument amplifier)* ...	0.1% Reading
Output offset (instrument amplifier)*	0.1% FS
A/D inaccuracy (DAS)*	0.3% Reading
Random noise (note 2)	9.6% FS
Strict sum 2σ error band	13.5% FS
RMS 2σ error band	9.9% FS

C. The identified sources of error in the GENISCO (41 kPa or 6 psi) strain gage dp cell

Static pressure offset	2.6% FS
Zero balance*	2.0% FS
Linearity, hysteresis*	0.4% FS
Tempco, sensitivity*	0.3% FS
Tempco, zero offset*	0.3% FS
Noise (note 1)	2.0% FS
A/D conversion DAS*	0.3% FS
Strict sum 2σ error band	7.9% FS
RSS 2σ error band	3.9% FS

D. The identified sources of error in the ITT Barton (25 kPa or 100 in.) dp cell are

Transduction accuracy*	0.25% FS
Static pressure effect*	0.4% FS

Tempco, zero offset*	0.2% FS
Tempco, sensitivity*	0.2% FS
Noise	2.0% FS
DAS*	0.3% FS
Strict sum 2σ error band	3.4% FS
RSS 2σ error band	2.1% FS

E. The identified sources of error in the Rosemount Capacitance dp cell are (see note 4)

	6.2 and 7.4 kPa (25 and 30 in.)	37 and 50 kPa (150 and 200 in.)
Transduction accuracy	0.25% FS	0.25% FS
Tempco, combined*	0.95% FS	0.14% FS
Static pressure offset	1.0% FS	1.0% FS
Stability*	0.25% FS	0.25% FS
Noise	0.2% FS	0.2% FS
DAS*	0.3% FS	0.3% FS
Strict sum 2σ error band	3.0% FS	2.1% FS
RSS 2σ error band	1.5% FS	1.1% FS

F. The identified sources of error in the FOXBORO force balance dp cell are

Transduction accuracy*	0.25% FS
Noise	2.0% FS
DAS	0.3% FS
Strict sum 2σ error band	2.6% FS
RSS 2σ error band	2.0% FS

The following items need to be considered in evaluating the above 2σ error bands:

Note 1. Bench calibration data were substituted for the values of nonlinearity, repeatability, and hysteresis since bench data were available and indicated significantly larger error bands for strain gage dp cells. The dp sensors in use show a dependence on system pressure for both gain and offset (see Figs. D.5 and D.6). The approach has been to use a calibration equation based on a linear regression calibration of both gain and zero offset in the form

$$P_{dp} = (PAg + Bg)[V - (PAz + Bz)] ,$$

where P_{dp} is the differential pressure measured by the dp cell; Ag, Bg, Az, and Bz are the calibration coefficients; V is the sensor output voltage; and P is the system pressure. However, the linear correlation of system pressure and constants Ag, Bg, Az, and Bz is not high enough to make the correlation better than 1.2% (as 1σ) overall.

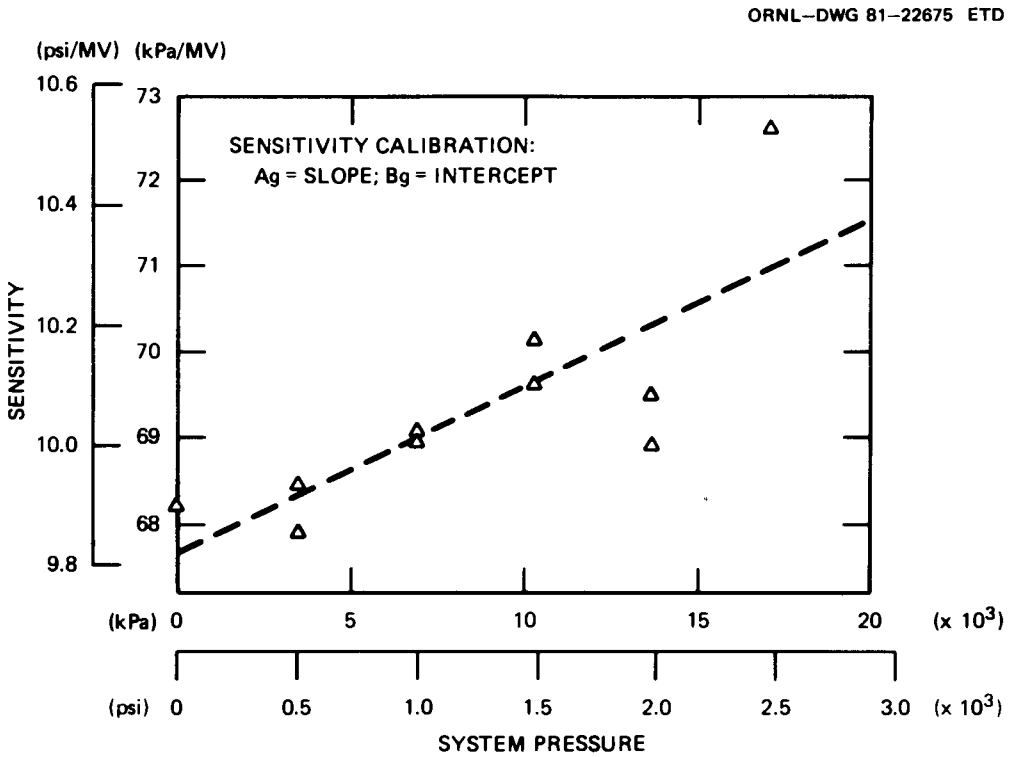

Fig. D.5. Sensitivity calibration.

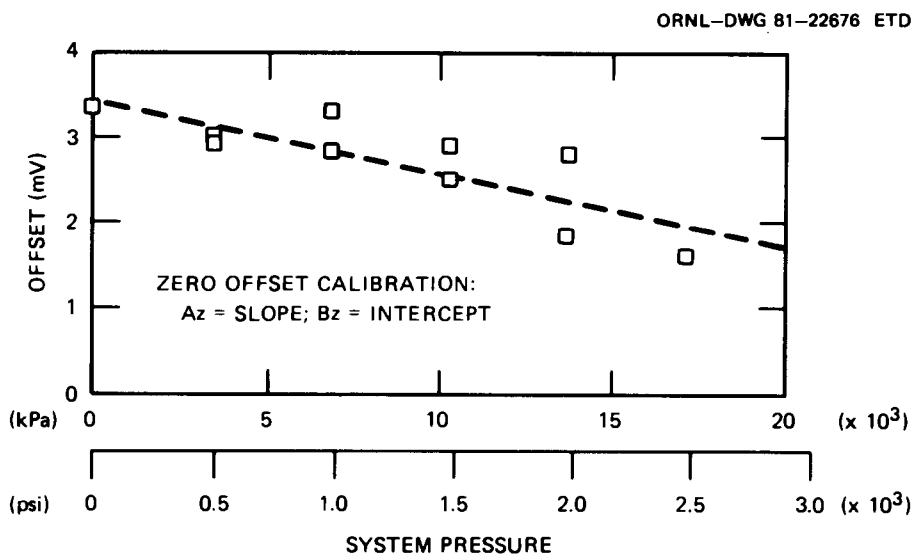

Fig. D.6. Zero offset calibration.

Note 2. When the error band for the BLH strain gage dp cells was checked using digital data from Reactor Simulation Test 3.05.5B, an average value of σ equivalent to 1.0% FS was measured using 13 PDE's in service prior to blowdown. The average output was used as the standard.

Note 3. When the strain gage dp cells are used as pit dp cells, they are connected to different parts of the system by long lines of small diameter tubing. Analysis of Test 101 showed that resonant ringing could account for an increase in the noise level (as 1σ) to 4.8% FS just prior to blowdown and up to 65% FS after blowdown when the 28-Hz (the measured resonant frequency) notch filter is used as a standard (see Fig. D.7).

Note 4. An in situ calibration of the Rosemount dp cells was made during steady-state scans for the Small Break LOCA II tests of October and November 1980. The uncertainty estimate used water properties as a basis of known differential pressure. The results indicated an average 1σ uncertainty of ±0.05 kPa (0.2 in.) (0.8% FS).

Note 5. Temperature coefficients were applied over a range of 15°C (27°F).

Note 6. No parameter was identified that would degrade error bands beyond those listed above during two-phase flow. However, extension of the stated error bands to two-phase flow or transient conditions without supporting experimental evidence is done at the data user's risk.

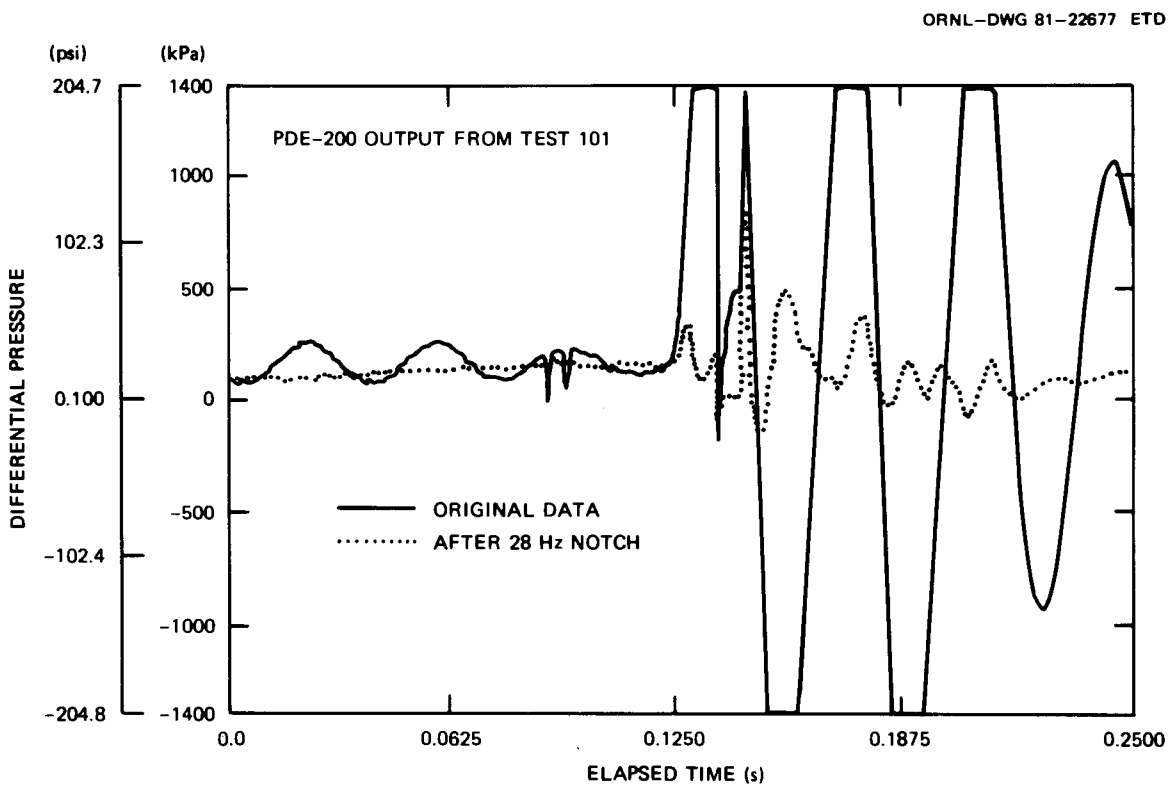

Fig. D.7. PDE-200 output from Test 101.

D.5 Thermocouple Temperature Instruments

The thermocouple instruments consist of Chromel-Alumel thermocouples, a "cold-junction" reference box, and the DAS.

The following error sources were identified for thermocouple instruments:

	Minimum value (°C)	(°F)	Above 350°C (660°F)
Thermocouple material*	2.2	4.0	0.76%
Random noise	0.5	1.0	
DAS calibration	1.8	3.2	0.46%
Reference junction calibration	2.2	4.0	2.2°C (4.0°F)
Reference junction controller	0.16	0.3	0.16°F (0.3°F)
Strict sum 2σ error band	6.9	12.4	(See below)
RSS 2σ error band	3.7	6.7	(See below)

Conversion of the above percentage values to degrees centigrade above 350°C (660°F) results in the following:

Temperature (°C)	(°F)	2σ Error band (°C)	(°F)	2σ Error band strict sum (°C)	(°F)
350	662	3.7	6.7	7.4	13.3
400	752	4.2	7.6	8.3	14.9
450	842	4.7	8.5	9.1	16.4
500	932	5.1	9.2	10.0	18.0
550	1022	5.6	10.1	10.8	19.4
600	1112	6.1	11.0	11.7	21.1
650	1202	6.6	11.9	12.5	22.5
700	1292	7.1	12.8	13.4	24.1
750	1382	7.6	13.7	14.2	25.6
800	1472	8.0	14.4	15.1	27.8
850	1562	8.5	15.3	15.9	28.6
900	1652	9.0	16.2	16.8	30.2

The following items need to be considered when applying the above error band estimates to THTF data:

1. The reference junction box calibration error was determined by analyzing long-term calibration data from February 4, 1976, to February 10, 1981, and includes any offset from the mean set-point value of 2.666 mV. Reference junction box anomalies were discovered during a 7-day steady-state period. Controller errors up to 0.08°C (0.14°F) were observed for periods of approximately 1-h duration. Operating four units continuously over 7 days, the average error was determined to be less than 0.006°C (0.01°F).

2. Random noise was determined by analyzing the data from Reactor Simulation Test 3.05.5B for five Type Code = 6 and nine Type Code = 1 thermocouples in operation during that test for steady-state, one-phase flow conditions. Because of considerable scatter from instrument-to-instrument and file-to-file, a value of σ large enough to include approximately 95% of all data was chosen. In an effort to provide a conservative estimate, it was assumed that the noise at higher temperatures would be proportional to the millivolt signal above 350°C (660°F).

3. Data Acquisition System calibration was checked after a test calibration with the voltage output compared with a 32.0-mV input signal.

4. A thermocouple that had been in service at the THTF facility was analyzed by R. L. Anderson[5] of the I&C standards lab to determine the effect of nickel crystal reordering. The results indicate that errors from 1.2°C (2.2°F) [near 150°C (1300°F)] to 16.3°C (29.3°F) [near 900°C (1650°F)] may be expected in addition to the above values. However, the recent history of a specific thermocouple coupled with its end-to-end temperature gradient makes it difficult to extrapolate to all THTF thermocouples. The effect of crystal reordering would be to produce readings higher than actually experienced at the junction.

5. An isothermal scan taken during Test 3.06.6B was used to compare the output of 615 thermocouples believed to be operational. The measured standard (2σ) deviation of 4.0°C (7.2°F) agrees closely with the RSS estimated value of 3.7°C (6.7°F) (2σ).

D.6 Rod Power Instrumentation

The rod power instrumentation consists of two operational amplifiers, a calibrated low resistance shunt, and the DAS (see Fig. D.8). Amplifier 1 reads the voltage across the rod itself. V_1 is the output from the voltage divider. Amplifier 2 reads the voltage across the shunt. The current in the rod is then inferred using Ohm's law such that

$$I = V_2/R_s ,$$

where I is the current in amps, V_2 is the potential across the shunt in volts, and R_s is the resistance of the shunt in ohms.

The following items were identified as probable sources of error when determining rod power:

R_s	Calibration inaccuracy*	0.26% Reading
R_s	Temperature coefficiency*	0.2% Reading
V_2	Nonlinearity*	0.01% Reading
V_2	Channel noise	0.72% Reading
V_2	Tempco, gain*	0.02% Reading
V_2	Tempco, offset*	0.03% FS

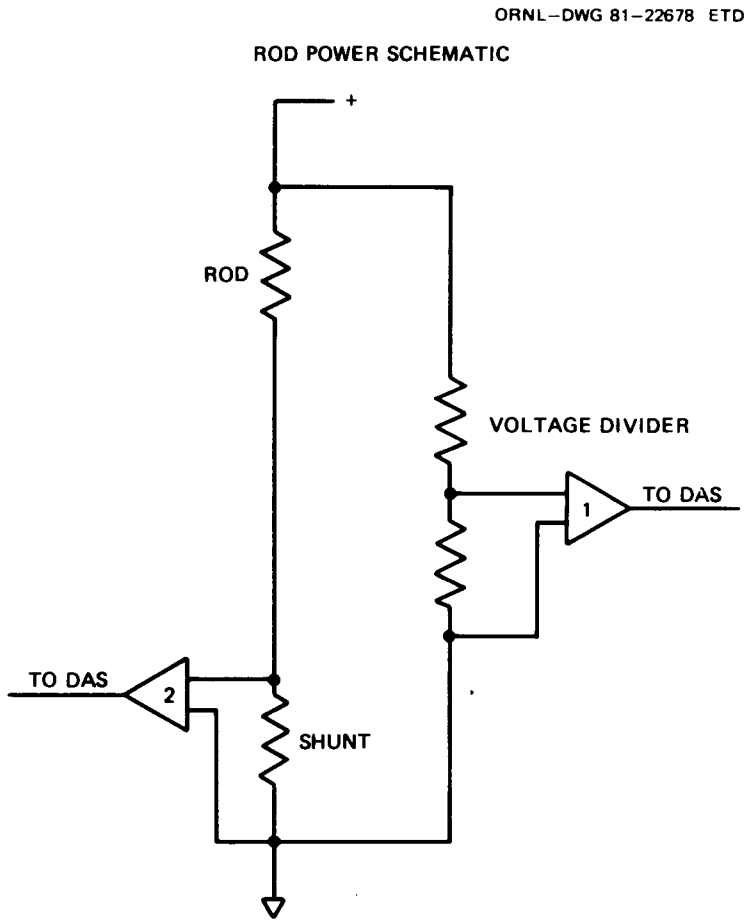

Fig. D.8. Rod power schematic.

V_2	DAS calibration inaccuracy*	0.30% Reading
V_1	Nonlinearity*	0.01% Reading
V_1	Channel noise	0.7% Reading
V_1	Tempco, gain*	0.02% Reading
V_1	Tempco, offset*	0.03% Reading
V_1	DAS calibration inaccuracy*	0.30% Reading
	Strict sum 2σ error band	2.6% Reading
	RSS sum 2σ error band	1.1% Reading

The following items need to be considered when applying the above error bands to THTF rod power data:

1. Temperature changes at the amplifiers were assumed to be less than or equal to 20°C (36°F). The temperature changes at the shunt were assumed to be less than or equal to 40°C (72°F). The temperature changes

chosen may be excessively large resulting in larger than necessary error bands.

2. No error source was identified that would degrade the steady-state, 2σ error band beyond those listed above.

3. Because of matched voltage divider temperature coefficients and the current calibration procedures, the error contributed by the voltage dividers is considered negligible. However, channel noise was measured at low power, so that the values used might be unnecessarily conservative. Furthermore, the resistance of the shunt is very much less than the rod, so that the voltage drop across the rod is essentially unaffected by the shunt.

D.7 Strain Gage Drag Disks

An analysis of steady-state, single-phase drag disk uncertainties based on subcooled flow calibrations from four THTF tests is presented. The data are from pretest drag disk calibrations performed on the same day of the test during heatup to blowdown conditions for Tests 3.04.7, 3.05.5B, 3.06.6B, and 3.08.6C.

The drag disks are calibrated using the turbine flowmeters (velocity, V) and pressure- and temperature-deduced density (ρ) to obtain an in situ standard momentum flux $[(\rho V^2)_{std}]$. A calibration equation is generated from a least-squares fit to the drag disk signal corresponding to the momentum flux over a range of momentum fluxes. The measured momentum flux $[(\rho V^2)_{meas}]$ is obtained by applying the calibration equation to the instrument signal. The calibration equation takes the form:

$$(\rho V^2)_{meas} = A(IS - Z)^E ,$$

where IS is the instrument signal in millivolts and A, Z, and E are calibration parameters determined by the least-squares fit. The value of E is generally near 1.0.

An estimate of the uncertainty in the drag disk instrument is made by comparing the in situ standard to the instrument-measured momentum flux. The errors are formulated in terms of percent of actual momentum flux, which is approximately equivalent to percent of reading. For each data point, the percent error is calculated from

$$\% \text{ error} = \frac{(\rho V^2)_{std} - (\rho V^2)_{meas}}{(\rho V^2)_{std}}$$

Two different drag disk instrument ranges and two different geometries (2-in. and 4-in. spool piece configurations) resulted in three different instrument measurement ranges. It was observed that values of σ

for the three different types of drag disks (target and geometry) agree well with each other. It would appear reasonable to combine the data for all three types and to report average uncertainties. However, separate uncertainty estimates are made for instrument signals below 10% of maximum range due to a pronounced temperature effect that is especially noticeable at the lower readings. This effect is caused by the strain gage elements being in close thermal contact with the fluid. The value of Z in the calibration equation is a temperature correction term based on calibration runs taken at two different temperatures. The attempted temperature compensation is not very accurate at low signal values.

The resulting uncertainty bands for strain gage drag disks are:

2σ error band below 10% FS	56% reading
2σ error band above 10% FS	19% reading

The following items need to be considered when applying the above error bands to THTF data:

1. Percentage error estimates for the drag disks were compared with the subcooled data immediately preceding blowdown for the tests from which the calibration data were obtained. Average error values of 9.2% of readings (1σ) above 10% FS and 30% of readings (1σ) below 10% FS tend to support the uncertainty bands derived from calibration runs.
2. The strain gage transducer elements are exposed to the temperature environment of the loop. Temperatures significantly outside of the temperature range used during calibration will degrade the accuracy of the instrument further, especially below 10% FS.

D.8 Transient Response and Transient Errors

It is generally understood that no instrument responds infinitely fast to changes in the physical parameters being measured. That is, if the environment were to change suddenly from 200 arbitrary units to 400 arbitrary units, an instrument would initially read some value near 200 units and would approach a reading of 400 units asymptotically. A good approximation for many instruments is first-order lag (see Fig. D.9) defined by

$$V_r = V_o + (1 - e^{-T/\tau})(V_f - V_o) \ .$$

That is, the value indicated by the instrument (V_r) is equal to the original value (V_o) plus the value of the step function ($V_f - V_o$) multiplied by an exponential delay factor, where T is the elapsed time and τ is the 63.2% instrument response time, and V_f is the final value of the step function. Instrument error as a function of time would be represented by the area between V_f and the instrument reading line.

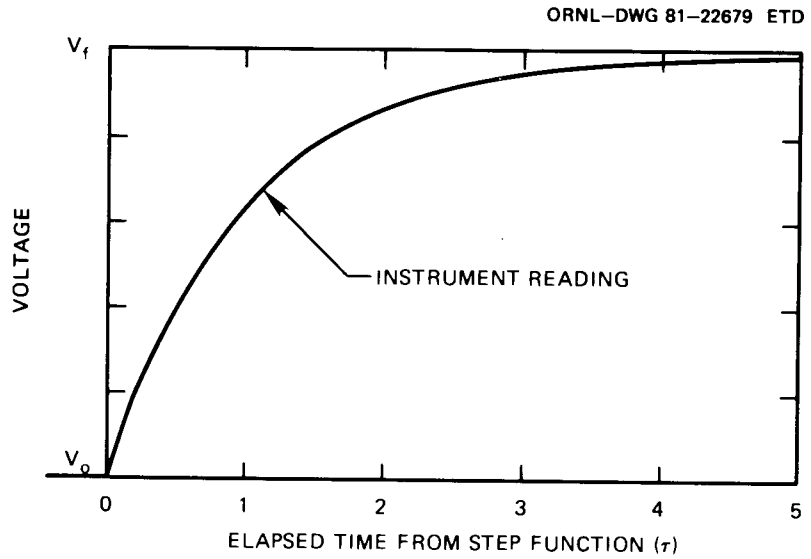

Fig. D.9. Instrument reading as a function of response time assuming first-order lag.

An additional problem in the THTF uncertainty analysis is introduced because the signal is sampled over discrete time intervals instead of continuously. It may be difficult to identify the exact starting point of a step function. If the step change in physical parameter occurs very near in time to the DAS sample (relative to the instrument response time), the instrument reading at that point will be in error by the total value of the change. If the DAS samples five or more response times after the step function, less than a one percent error (expressed as percent of the step function) will result.

Some arbitrariness is required, therefore, to provide a consistent definition of transient error. The method chosen was to assume that the step function occurred midway between two DAS sampling intervals (n and n + 1 in Fig. D.10). The error is measured at each sample point as the distance in engineering units between the modeled instrument reading and the assumed final value of the physical parameter V_f (vertical dashed lines in Fig. D.10). The uncertainty is expressed as the average of all the errors observed during an averaging interval (typically, 150 or 500 ms). The size of the step function and the length of the averaging interval were chosen with test conditions in mind.

As an example, let us consider the errors in the reading of a gamma densitometer (Sect. D.2) as a function of time. The response time on the ionization chamber is estimated at 16 ms. Assuming that the observed density decreases instantly from 750 kg/m (46.8 lb/ft) to 0 (a worst-case, blowdown situation), the errors observed at the DAS and the average error for a 100-ms averaging interval reported are shown in Table D.3.

The following items need to be considered when applying transient uncertainty values in the appendices to THTF data:

1. Although first-order lag modeling is appropriate for most instruments, it is at best a close approximation to the true instrument response.

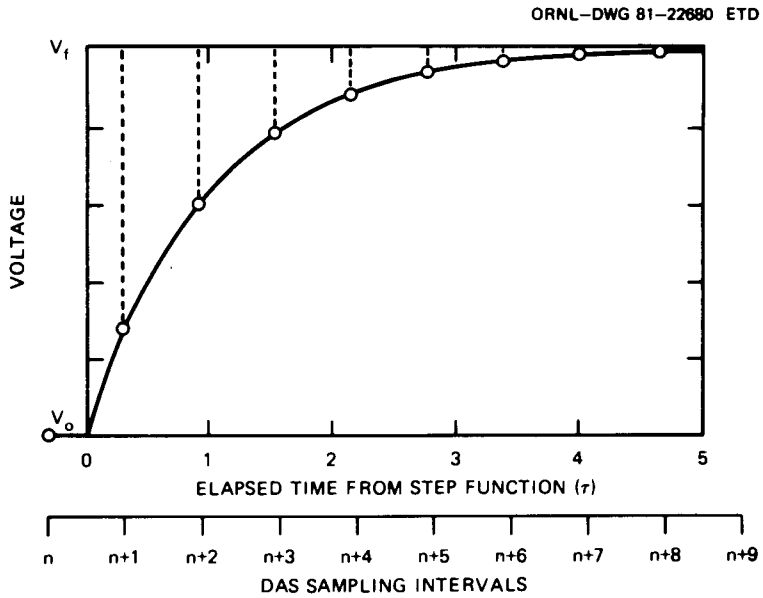

Fig. D.10. Instrument error as a function of DAS sampling assuming first-order lag.

Table D.3

DAS interval n + 1n = 0.01 s	Error (kg/m^3)	Error (lb/ft^3)
1	549	34.2
2	249	18.3
3	157	9.8
4	84	5.3
5	45	2.8
6	24	1.5
7	13	0.8
8	7	0.4
9	4	0.2
10	2	0.1
Average	118	7.4

2. The instrument response times are estimates. When these estimates are known from averages, the standard deviation is large, indicating wide variation from instrument-to-instrument. As a result, a particularly slow instrument of a given type might show errors a factor of 2 or more worse than the average would indicate.

3. The average uncertainty values noted in the tables are extremely sensitive to the averaging interval chosen. Average errors that appear

insignificant over a 500-ms averaging interval may well become significant over a 150-ms interval. A careful analysis of Table D.3 is illustrative in this light.

4. Step functions were chosen that were thought to be either representative or worst-case possibilities on a test-by-test basis. It is possible, however, that steps more severe than those chosen may have occurred.

D.9 General Comments

1. All of the above error bands were derived assuming that the specified instrument was in nominal working condition and had been recently calibrated using normal THTF calibration techniques. The error bands will not apply to defective instruments.

2. The error bands stated apply only to those items covered in the above discussion. Although every attempt has been made for the examination to be exhaustive and for the results to be conservatively stated, there is always the possibility that excessive instrument noise or out-of-spec components will cause actual readings to be outside of the given error limits (stated as 2σ).

3. The error bands given herein represent the experimenter's best judgment of the applicable uncertainties. Two points should be noted, however. First, the estimation of transient contributions to the uncertainty involves a number of assumptions and judgments. These have been documented in Sect. D.8, and the steady-state and transient contributions to the uncertainty have been listed separately in the tables to facilitate the reader who wishes to use his own estimates of the transient contribution to uncertainty if he chooses. Second, most of the data available on specific sources of instrument errors were obtained in single-phase flow. Thus, the experimenters had to rely primarily on engineering judgment to combine and extrapolate this data to two-phase flow. In most cases there is no experimental, two-phase flow data that can be used to verify the resulting uncertainty estimates.

D.10 Steady-State and Transient Instrument Uncertainties

Table D.4 provides a cross reference for instrument application numbers (IAN) and type codes. The first column provides the type code as an integer between 1 and 113, the second column lists the form of the IAN, and the "Remarks" column provides additional information to properly correlate type code to IAN for all instruments.

Tables D.5–D.8 provide a summary listing of steady-state and transient error bands by test. Tables D.5 and D.7 have values stated in SI units. Table D.6 is the English unit version of Table D.5; Table D.8 is the English unit version of Table D.7.

The first column in each table gives a brief instrument description. The second column provides the instrument type code. (Use Table D.4 to

Table D.4. Type Code — Instrument Application Number Table

Type Code	I.A.N	Remarks
1	TE-3nnal	Special FRS Sheath Thermocouples [0.38 mm//0.015 inch] nn = 01, 14, 17, 21, 34, 37, 38, 50, 54, or 60 a = A, E, or F 1 = 1, 2, 3, 4, 5, 6, 7, 8; or E, F, or G
1	TE-3nnal	Regular FRS Sheath Thermocouples [0.51 mm//0.020 inch] nn = 01-64 (except 19,22,36,46) and (excluding 01, 14, 17, 21, 34, 37, 38, 50, 54, 60 for tests 3.06.6B, 3.08.6C, 3.07.9, 3.09.10I-X and Mothball) a = A, B, or C 1 = A, B, C, D, E, F, G, H, U, or Y
2	TE-3nnM1	Special FRS Middle Thermocouples [0.38 mm//0.015 inch] nn = 01, 14, 17, 21, 34, 37, 38, 50, 54, or 60 M = M 1 = 1, 2, 3, 4, 5, 6, 7, 8; or E, F, or G
2	TE-3nnM1	Regular FRS Middle Thermocouples [0.51 mm//0.020 inch] nn = 01-64 (except 19, 22, 36, 46) and (excluding 01, 14, 17, 21, 34, 37, 38, 50, 54, 60 for tests 3.06.6B, 3.08.6C, 3.07.9, 3.09.10I-X and Mothball) M = M 1 = A, B, C, D, E, F, or G
3	TE-12nn	Subchannel Thermocouples nn = 01-81
4	TE-18na	Shroud Wall Thermocouples n = 1, 2, 3, 4, 5, 6, or 7 a = N, E, S, or W
5	TE-xxx	Miscellaneous and Process Thermocouples xxx = 5B, 408B, 520B, 521, 901, 920, 921, 922, 923, 924, 925, 926, 927, or 936
6	TE-xxx	Loop and Process Thermocouples xxx = 1, 2, 6, 24, 29, 40, 45, 57, 62, 67, 116, 150, 151, 152, 153, 172, 208, 212, 222, 228, 256, 266, 281, 282, 284
7	TE-29na	Spacer Grid Thermocouples n = 1, 2, 3, 4, 5, or 6 a = A, B, C, D, E, or F

Table D.4 (continued)

Type Code	I.A.N	Remarks
8	TE-18na1	Array Rod Thermocouples n = 8 or 9 a = A or B 1 = A, B, C, D, E, F, or G
9	TE-361-aJ	O-ring Area Thermocouples a = A, B, or C J = J
10	TE-nab	Shroud Box Thermocouples n = 0, 1, 2, 3, 4, 5, 6, 7, 8, or 9 a = A or B b = E or S
23	PE-xxx	Strain Gage Pressure Cells [20700 kPa//3000 psi] xxx = 15, 16, 26, 27, 42, 43, 44, 58, 63, 68, 76, 88, 106, 118, 156, 174, 201, 209, 224, 258, 268, 276, 281, 282, 283, 286, 425, 427, 454, 474
24	PE-32	Force Balance Pressure Cell [both ranges]
25	PE-102	Strain Gage Pressure Cell [1380 kPa//200 psi]
26	PDE-xxx	Strain Gage dP Cell [± 1380 kPa//± 200 psi] xxx = 35, 46, 167, 217 21 except for tests 3.09.10I-X and 3.10.10 60 except for test 3.05.5B
27	PDE-78	Strain Gage dP Cell [± 6900 kPa//1000 psi]
28	PDE-xxx	Strain Gage dP cell [± 345 kPa//± 50 psi] xxx = 7, 53, 65, 111, 203 21 only for tests 3.09.10I-X and 3.10.10 60 only for test 3.05.5B 200 except for 3.02.10C-H and Mothball 251 except for 3.02.10C-H and 3.09.10I-X
29	PE-nnn	Strain Gage Pressure Cell [2400 kPa//350 psi] nnn = 526 or 616
31	EIE-13nn	FRS Heater Rod Currents nn = 01-64 (excluding 19, 22, 36, 46)
32	EIE-xx	Generator Currents xx = 9, 10, 11, 12

Table D.4 (continued)

Type Code	I.A.N	Remarks
33	EEE-xx	Generator Voltage xx = 9, 10, 11, 12
34	EWE-77A	Primary Pump Power
35	FMFE-xxxx	Momentum Flux Flow (Drag Disk) [9 cm//3.5 inch spool piece] xxx = 22, 38, 170, 220 206 except for 3.09.10I-X 254, 264 only for 3.05.5B
36	SE-72	Primary Pump Speed
37	XE-430a	Break Wire Detector a = A or B
40	FMFE-xxx	Momentum Flux Flow (Drag Disk) [5 cm//2 inch spool piece] xxx = 14, 55, 61, 66, 114, 154, 155 206 only for 3.09.10I-X 254, 264 except for 3.04.5B
41	PDE-200	Strain Gage dP Cell [± 25 kPa//± 100 inches water] only for tests 3.02.10C-H
42	PDE-204 PDE-261	Strain Gage dP Cell [± 125 kPa//± 500 inches water] only for test 3.05.5B except for 3.08.6C, 3.07.9, 3.09.10I-X, and Mothball
43	PDE-nnn	Strain Gage dP Cell [± 41 kPa//± 6 psi] nnn = 199, 271 204 except for 3.05.5B 251 only for 2.02.10C-H 261 only for 3.08.6C, 3.07.9, 3.09.10I-X, Mothball
50	LE-14nn	Experimental INEL Level Prone nn = 01 through 19
71	TE-28B	Linearized Resistance Thermometer Device
75	PDE-nnn	Capacitive dP Cell nnn = 180 through 188 189 except on 3.09.10I-X and Mothball set at 0-6.2 kPa (0-30 inches) except for 3.05.5B set at 0-37.5 kPa (0-150 inches) only for 3.05.5B

Table D.4 (continued)

Type Code	I.A.N	Remarks
76	ZE-336U ZE-346L	Inbundle Gamma Densitometer Position Indicator except for 3.09.10I-X and Mothball
77	ZE-346L	Inbundle Gamma Densitometer Position Indicator only for 3.09.10I-X and Mothball
78	PDE-251	Capacitance dP Cell [25 kPa//100 inches] only for 3.09.10I-X
79	PDE-200	Capacitance dP Cell [50 kPa//200 inches] only for Mothball
80	PDE-189	Capacitance dP Cell [7.5 kPa//30 inches] only for 3.09.10I-X and Mothball
95	FE-nnn	Turbine Flowmeter—Heat Exchanger Secondary Flow nnn = 522, 620, 720
96	FE-550	Turbine Flowmeter—Heat Exchanger Secondary Flow
97	PDE-48	Force Balance dP Cell [166 kPa//24 psi]
98	PDE-30	Force Balance dp Cell [345 kPa//50 psi]
99	TDE-28	Differential Temperature
105	PDE-761 LE-100	Force Balance dP Cell
106	DE-xxx	Single Beam Gamma Densitometer xxx = 20, 36, 168, 218 Triple Beam Gamma Densitometer xxx = 204A, 204B, 204C, 252A, 252B, 252C, 262A, 262B, 262C
107	FE-xxx	Orifice Place/Force Balance Flowmeter xxx = 1A [0-5.0E-2 m^3/s or 0-800 gpm] 238 [0-1.0E-4 m^3/s or 0-1.6 gpm] only 3.09.10I-X Orifice Place/Capacitance Flowmeter xxx = 282 [0-2.5E-3 m^3/s or 0-39.3 gpm] 283 [0-3.3E-4 m^3/s or 0-5.2 gpm] 927 [0-1.4E-4 m^3/s or 0-2.1 gpm]

Table D.4 (continued)

Type Code	I.A.N	Remarks
		Orifice Plate/Force Balance Flowmeter
108	FE-18A	[4.4E-2 m^3/s or 700 gpm] except for 3.01.10C-H, 3.09.10I-X and Mothball
	FE-18A	[1.7E-4 m^3/s or 2.7 gpm] only for 3.01.10C-H, 3.09.10I-X and Mothball
	FE-238	except for 3.09.10I-X
		Instrument Spool Piece Turbine Flowmeter
109	FE-xxx	[3E-4 m^3/s or 5 gpm] xxx = 250, 260 only for tests 3.01.10C-H, 3.09.10I-X, and Mothball
		[6E-4 m^3/s or 10 gpm] xxx = 232, 280
		[1.4E-2 m^3/s or 225 gpm] xxx = 3, 51, 59, 64, 110,
		[1.4E-2 m^3/s or 225 gpm] xxx = 250, 260 except for 3.01.10C-H, 3.05.5B, 3.09.10I-X, and Mothball
		[1.4E-2 m^3/s or 225 gpm] xxx = 202 only for tests 3.01.10C-H, 3.09.10I-X
		[6E-2 m^3/s or 1000 gpm] xxx = 19,34,166,216,440,460
		[6E-2 m^3/s or 1000 gpm] xxx = 250, 260 for 3.05.5B
		[6E-2 m^3/s or 1000 gpm] xxx = 202 except for tests 3.01.10C-H, 3.09.10I-X
		Resistance Thermometer Device
110	TE-xxx	xxx = 4B, 101, 210A, 525, 557, 615, 627, 727
		Inbundle Gamma Densitometer
111	DE-xxx	xxx = 336U, 346L
		Orifice Plate/Force Balance Flowmeter
112	FE-238	same as type code 107 FE-238
113	LE-760	Force Balance dP Cell

Table D.5. THTF instrument uncertainties — (nominal transient step function for Test 3.06.6B) (SI units)

THTF Instrument Error Bands						
Instrument Description	Type Code	Instrument Range	Steady State Error	Transient Error	Estimated Response Time	Assumed Value of Step Fn.
Rod Sheath Thermocouple 0.38 mm OD	1	273 K 1309 K	3.7K < 623 K 10.3 K	0.8 K[a]	7 ms	300 K
Rod Sheath Thermocouple 0.51 mm OD	1	273 K 1309 K	3.7K < 623 K 10.3 K	3.8 K[a]	12 ms	300 K
Rod Middle Thermocouple 0.36 mm OD	2	273 K 1309 K	3.7K < 623 K 10.3 K	0.8 K[a]	7 ms	300 K
Rod Middle Thermocouple 0.51 mm OD	2	273 K 1309 K	3.7K < 623 K 10.3 K	3.8 K[a]	12 ms	300 K
Bundle Subcnn Thermocouple 1.02 mm OD	3	273 K 1309 K	3.7K < 623 K 10.3 K	2.7 K	140 ms	10 K
Shroud Box Thermocouple 1.57 mm OD	4	273 K 1309 K	3.7K < 623 K 10.3 K	5.3 K	350 ms	10 K
System Thermocouple 3.2 mm OD	5	273 K 1309 K	3.7K < 623 K 10.3 K	7.6 K	870 ms	10 K
System (Nanmac) Thermocouple 6.4 mm OD	6	273 K 1309 K	3.7K < 623 K 10.3 K	0.3 K	18 ms	10 K
Spacer Grid Thermocouple 1.02 mm OD	7	273 K 1309 K	3.7K < 623 K 10.3 K	2.7 K	140 ms	10 K
Array Rod Thermocouple 1.02 mm OD	8	273 K 1309 K	3.7K < 623 K 10.3 K	2.7 K	140 ms	10 K

Table D.5 (continued)

THTF Instrument Error Bands						
Instrument Description	Type Code	Instrument Range	Steady State Error	Transient Error	Estimated Response Time	Assumed Value of Step Fn.
Rod Sheath Thermocouple 0.51 mm OD	9	273 K 1309 K	3.7K < 623 K 10.3 K	3.8 K[a]	12 ms	300 K
Shroud Box Thermocouple 1.57 mm OD	10	273 K 1309 K	3.7K < 623 K 10.3 K	5.3 K	350 ms	10 K
Strain Gage Pressure Cell	23	20700 kPa	200 kPa	N.S.[j]	0.16 ms	200 kPa
Force Balance Pressure Cell	24	3400 kPa 17000 kPa	100 kPa	157 kPa	300 ms	200 kPa
Force Balance Pressure Cell	24	3400 kPa 27000 kPa	160 kPa	157 kPa	300 ms	200 kPa
Strain Gage Pressure Cell	25	1380 kPa	17 kPa	N.S.	0.32 ms	200 kPa
Strain Gage D.P. Cell	26	±1380 kPa	43 kPa	N.S.	0.32 ms	200 kPa
Strain Gage D.P. Cell	27	±6900 kPa	210 kPa	N.S.	0.32 ms	1.7 kPa
Strain Gage[g] D.P. Cell	28	±345 kPa	11 kPa	N.S.	0.32 ms	1.7 kPa
Strain Gage Pressure Cell	29	2400 kPa	24 kPa	N.S.	0.16 ms	200 kPa
Rod Heater Current	31	800 amp	0.85% Rdg	4.7 amp	50 ms	15 amp
Generator Current	32	1000 amp	0.85% Rdg	32 amp	50 ms	100 amp
Generator Voltage	33	300 volt	0.76% Rdg	3.8 volt	50 ms	12 volt

Table D.5 (continued)

THTF Instrument Error Bands						
Instrument Description	Type Code	Instrument Range	Steady State Error	Transient Error	Estimated Response Time	Assumed Value of Step Fn.
Primary Pump Power	34	750 kW	greater of 0.5 kW or 0.3% Rdg	6.3 kW	150 ms	10 kW
Strain Gage Drag Disk	35	±0.1E5 kg/ms² ±1.0E5 kg/ms²	56% Rdg 19% Rdg	157 kg/ms²	16 ms	150 kg/ms
Primary Pump Speed	36	100 rpm 5400 rpm	20 rpm	13 rpm	150 ms	20 rpm
Breakwire Detector	37	5 volt	30 ms	N.A.[k]	20 ms	N.A.
Strain Gage Drag Disk	40	±0.3E4 kg/ms² ±3.0E4 kg/ms²	56% Rdg 17% Rdg	47 kg/ms²	16 ms	1500 kg/ms²
Strain Gage D.P. Cell	41	±25 kPa	0.8 kPa	N.S.	0.32 ms	1.7 kPa
Strain Gage D.P. Cell	42	±125 kPa	4 kPa	N.S.	0.32 ms	1.7 kPa
Strain Gage D.P. Cell	43	±41 kPa	2 kPa	N.S.	0.32 ms	1.7 kPa
Level[i] Indicator	50	±10 volt	***	***	***	***
RTD	71	273 K 700 K	1.1 K 2.7 K	9.9 K	10 sec	10 K
Capacitive D.P. Cell	75	6.2 kPa	0.1 kPa	0.15 kPa	131 ms	0.25 kPa
Capacitive D.P. Cell	75	37.5 kPa	0.4 kPa	0.11 kPa	74 ms	0.25 kPa
Position Indicator	76	3.92 m	0.5% Rdg	N.A.	N.A.	N.A.
Position Indicator	77	3.33 m	0.5% Rdg	N.A.	N.A.	N.A.

Table D.5 (continued)

THTF Instrument Error Bands						
Instrument Description	Type Code	Instrument Range	Steady State Error	Transient Error	Estimated Response Time	Assumed Value of Step Fn.
Capacitive D.P. Cell	78	25 kPa	1.3 kPa	0.9 kPa	110 ms	1.7 kPa
Capacitive D.P. Cell	79	50 kPa	0.5 kPa	0.7 kPa	68 ms	1.7 kPa
Capacitive D.P. Cell	80	7.5 kPa	0.1 kPa	0.15 kPa	125 ms	0.25 kPa
Turbine[f] Flowmeter	95	0.9E-3 m^3/s 9.5E-3 m^3/s	4.1% Rdg	1.3E-4 m^3/s	11 ms 1.2 ms	6.3E-4 m^3/s
Turbine[f] Flowmeter	96	0.3E-3 m^3/s 3.2E-3 m^3/s	4.1% Rdg	1.3E-4 m^3/s	8 ms 1 ms	6.3E-4 m^3/s
Force Balance D.P. Cell	97	166 kPa	1 kPa	1.3 kPa	300 ms	1.7 kPa
Capacitive D.P. Cell	98	345 kPa	0.1 kPa	0.4 kPa	38 ms	1.7 kPa
Differential Temperature	99	228 K 283 K	3.8 K	9.9 K	10 sec	10 K
Liquid Level	105	3.81 m	0.023 m	0.16 m	300 ms	0.2 m
Liquid Level	105	1408 m	8 .5 m	0.16 m	300 ms	0.2 m
Gamma Densitometer	106	1000 kg/m^3	104 kg/m^3	5 kg/m^3	16 ms	50 kg/m^3
Orifice[c] Flowmeter	107	1.0E-4 m^3/s	2.5E-6 m^3/s	7.9E-6 m^3/s	300 ms	1E-5 m^3/s
Orifice[c] Flowmeter	107	1.35E-4 m^3/s	3.4E-6 m^3/s	1.1E-5 m^3/s	300 ms	1.4E-5 m^3/s
Orifice[c] Flowmeter	107	3.32E-4 m^3/s	8.3E-6 m^3/s	2.6E-5 m^3/s	300 ms	3.3E-5 m^3/s

Table D.5 (continued)

THTF Instrument Error Bands						
Instrument Description	Type Code	Instrument Range	Steady State Error	Transient Error	Estimated Response Time	Assumed Value of Step Fn.
Orifice[c] Flowmeter	107	2.48E-3 m^3/s	6.2E-5 m^3/s	2.0E-4 m^3/s	300 ms	2.5E-4 m^3/s
Orifice[c] Flowmeter	107	5.0E-2 m^3/s	1.3E-3 m^3/s	3.9E-3 m^3/s	300 ms	5E-3 m^3/s
Orifice[d] Flowmeter	108	1.7E-4 m^3/s	4.2E-6 m^3/s	1.3E-5 m^3/s	300 ms	1.7E-5 m^3/s
Orifice[e] Flowmeter	108	4.4E-2 m^3/s	1.1E-3 m^3/s	3.5E-3 m^3/s	300 ms	4.4E-3 m^3/s
Turbine[f,h] Flowmeter	109	±0.3E-4 m^3/s ±3.0E-4 m^3/s	4.1% Rdg	3.1E-6 m^3/s	8 ms 1 ms	1.5E-4 m^3/s
Turbine[f,h,b] Flowmeter	109	±0.6E-4 m^3/s ±6.1E-4 m^3/s	2.5% Rdg	N.A.	8 ms 1 ms	N.A.
Turbine[f,h,l] Flowmeter	109	±1.3E-3 m^3/s ±1.4E-2 m^3/s	4.1% Rdg	1.3E-4 m^3/s	13 ms 2 ms	6.3E-4 m^3/s
Turbine[f,h,l] Flowmeter	109	±0.6E-2 m^3/s ±6.1E-2 m^3/s	4.1% Rdg	1.3E-4 m^3/s	18 ms 2 ms	1.3E-3 m^3/s
RTD	110	273 K 700 K	1.1 K 2.7 K	9.9 K	10 sec	10 K
Inbundle Gamma Densitometer	111	1000 kg/m^3	104 kg/m^3	5 kg/m^3	16 ms	50 kg/m^3
Orifice[c] Flowmeter	112	1.0E-4 m^3/s	2.5E-6 m^3/s	7.9E-6 m^3/s	300 ms	1E-5 m^3/s
Liquid Level	113	1.18 m	0.007 m	0.16 m	300 ms	0.20 m

Table D.5 (continued)

Documentation of Steady-State and Transient Error Bands

Steady-State Error Bands: Two-standard deviations compared to in-situ standard or twice the root-sum-square of uncertainties, whichever is applicable.

Transient Error Bands: Assuming first-order lag function, response times (TAU), and step function (Vf − Vo) indicated--the average error seen by the DAS assuming the step function occurred midway between DAS samples. The averaging interval is 500 ms for thermocouples and 150 ms for all other instruments.

Total Error: The total error due to steady state error and transient error is the sum of the steady state and transient error bands.

Footnotes:

a. Error bands apply to the environment as sensed at the surface of the thermocouple sheath. Larger errors may occur when data is modelled to provide temperatures at other points. Transient response is estimated by using the response time (25 ms or less) prior to swaging the sheath (0.71 mm swaged to 0.51 mm OD), then scaling using the rule: response time is inversely proportional to the outside diameter squared (OD**2 scaling). An additional 7% improvement in response time was allowed for packing of the boron nitride during swaging. The smaller thermocouples (0.51 mm swaged to 0.38 mm OD) were estimated from the values of the larger thermocouples by first scaling the 25 ms response time to the unswaged 0.51 mm diameter using OD**2 scaling, then applying OD**2 scaling and the 7% improvement for packing to the swaged 0.38 mm OD.

b. This instrument is fitted with Flow Technology electronics that time 10-blade passings. Averaging improves the steady-state error bands but degrades transient response.

c. Range applies specifically to instruments calibrated in subcooled liquid at a density of 1000 kg/m**3.

d. Range applies specifically to instruments calibrated in subcooled liquid at a density of 860 kg/m**3.

e. Range applies specifically to instruments calibrated in subcooled liquid at a density of 750 kg/m**3.

f. Error bands apply specifically to instruments calibrated in subcooled liquid. Extended range electronics provide readings out to 0.227 m^3/s for the 8.89E-2 meter diameter models; 0.028 m^3/s for the 5.08E-2 meter diameter models, but the error bands apply only to 150% of nominal maximum range.

g. Strain gage D.P. Cells used as pit cells are connected to different segments of the test section by long lines. These long lines induce resonant oscillations in the instrument that increase the steady-state errors bands to 35 kPa, and the transient error bands to 400 kPa.

h. The turbine flowmeters (type code 109) have a flow range such that:
-3.0E-4<Flow<-0.3E-4 .OR. 0.3E-4<Flow<3.0E-4,
-6.1E-4<Flow<-0.6E-4 .OR. 0.6E-4<Flow<6.1E-4,
-1.4E-3<Flow<-0.1E-3 .OR. 0.1E-3<Flow<1.4E-3,
-6.1E-2<Flow<-0.6E-2 .OR. 0.6E-2<Flow<6.1E-2,

i. The INEL level probe is an experimental device, and as such, does not have well documented error bands.

j. No significant error over a 500 ms averaging interval.

k. N.A. implies not applicable.

l. Flow Technology supplies calibration constants over the ranges 6.3E-4 to 1.9E-2 m^3/s and 5.0E-33 to 6.3E-2 m^3/s respectively. The uncertainty bands for these instruments should approach the quoted values for these ranges, but special care may be required. See the section on turbine flowmeters in the critical instruments section.

Table D.5 (continued)

Basis for Steady-State and Transient Error Bands by Type Code		
Type Code	Steady State	Transient
1	Critical instrument	Manufacturer's spec, OD**2 scaling
2	Critical instrument	Manufacturer's spec, OD**2 scaling
3	Critical instrument	Work of Carroll and Sheppard
4	Critical instrument	Work of Carroll and Sheppard
5	Critical instrument	Work of Carroll and Sheppard
6	Critical instrument	Manufacturer's spec
7	Critical instrument	Work of Carroll and Sheppard
8	Critical instrument	Work of Carroll and Sheppard
9	Critical instrument	Manufacturer's spec, OD**2 scaling
10	Critical instrument	Work of Carroll and Sheppard
23	Critical instrument	Table B.2 of Ref. 6
24	Manufacturer's spec	Table B.2 of Ref. 6
25	Bench Cal. + DAS	Table B.2 (inferred) of Ref. 6
26	Critical instrument	Table B.2 of Ref. 6
27	Critical instrument	Table B.2 of Ref. 6
28	Critical instrument	Table B.2 of Ref. 6
29	Critical instrument	Table B.2 (inferred) of Ref. 6
31	Critical instrument	Table B.2 (inferred) of Ref. 6
32	Inferred (type code 31)	Table B.2 (inferred) of Ref. 6
33	Critical instrument	Table B.2 (inferred) of Ref. 6
34	Manufacturer's spec	Manufacturer's spec
35	Critical instrument	Table B.2 of Ref. 6
36	Bench Cal. + DAS	Inferred (type code 34)
37	From test 3.03.6AR	From test 3.03.6AR
40	Critical instrument	Table B.2 of Ref. 6
43	Critical instrument	Table B.2 (inferred) of Ref. 6
50	**********	**********
71	Bench Cal. & specs	Table B.2 of Ref. 6
75	Critical instrument	Manufacturer's spec
76	Engineering judgement	N.A.
77	Engineering judgement	N.A.
78	Critical instrument	Inferred (type code 75)
79	Inferred (type code 75)	Inferred (type code 75)
80	Inferred (type code 75)	Inferred (type code 75)
95	Inferred (type code 109)	Work of N. Chen
96	Inferred (type code 109)	Work of N. Chen
97	Critical instrument	Table B.2 of Ref. 6
98	Critical instrument	Inferred (typed code 75)
99	Inferred (type code 71)	Inferred (type code 71)
105	Manufacturer's spec	Table B.2 (inferred) of Ref. 6
106	Critical instrument	Work of R. Shipp (manufacturer's spec)
107	In-situ calibration	Table B.2 (inferred) of Ref. 6
108	Inferred (type code 107)	Table B.2 (inferred) of Ref. 6
109	Critical instrument	Work of N. Chen
110	Bench Cal. & specs	Table B.2 of Ref. 6
111	Inferred (type code 106)	Inferred (type code 109)
112	Inferred (type code 107)	Table B.2 (inferred) of Ref. 6
113	Manufacturer's spec	Table B.2 (inferred) of Ref. 6

Table D.6. THTF instrument uncertainties — (nominal transient step function for Test 3.06.6B) (English units)

THTF Instrument Error Bands						
Instrument Description	Type Code	Instrument Range	Steady State Error	Transient Error	Estimated Response Time	Assumed Value of Step Fn.
Rod Sheath Thermocouple 0.015 inch OD	1	32 F 1900 F	6.7F < 662 F 18.5 F	1.4 F[a]	7 ms	540 F
Rod Sheath Thermocouple 0.020 inch OD	1	32 F 1900 F	6.7F < 662 F 18.5 F	6.8 F[a]	12 ms	540 F
Rod Middle Thermocouple 0.015 inch OD	2	32 F 1900 F	6.7F < 662 F 18.5 F	1.4 F[a]	7 ms	540 F
Rod Middle Thermocouple 0.020 inch OD	2	32 F 1900 F	6.7F < 662 F 18.5 F	6.8 F[a]	12 ms	540 F
Bundle Subchn Thermocouple 0.040 inch OD	3	32 F 1900 F	6.7F < 662 F 18.5 F	4.9 F	140 ms	18 F
Shroud Box Thermocouple 0.062 inch OD	4	32 F 1900 F	6.7F < 662 F 18.5 F	9.5 F	350 ms	18 F
System Thermocouple 0.125 inch OD	5	32 F 1900 F	6.7F < 662 F 18.5 F	13.7 F	870 ms	18 F
System (Nanmac) Thermocouple 0.25 inch OD	6	32 F 1900 F	6.7F < 662 F 18.5 F	0.5 F	18 ms	18 F
Spacer Grid Thermocouple 0.040 inch OD	7	32 F 1900 F	6.7F < 662 F 18.5 F	4.9 F	140 ms	18 F
Array Rod Thermocouple 0.040 inch OD	8	32 F 1900 F	6.7F < 662 F 18.5 F	4.9 F	140 ms	18 F

Table D.6 (continued)

THTF Instrument Error Bands						
Instrument Description	Type Code	Instrument Range	Steady State Error	Transient Error	Estimated Response Time	Assumed Value of Step Fn.
Rod Sheath Thermocouple 0.020 inch OD	9	32 F 1900 F	6.7F < 662 F 18.5 F	6.8 F[a]	12 ms	540 F
Shroud Box Thermocouple 0.062 inch OD	10	32 F 1900 F	6.7F < 662 F 18.5 F	9.5 F	350 ms	18 F
Strain Gage Pressure Cell	23	3000 psi	29 psi	N.S.[j]	0.16 ms	30 psi
Force Balance Pressure Cell	24	500 psi 2500 psi	15 psi	23 psi	300 ms	30 psi
Force Balance Pressure Cell	24	500 psi 3900 psi	23 psi	23 psi	300 ms	30 psi
Strain Gage Pressure Cell	25	200 psi	2.5 psi	N.S.	0.32 ms	30 psi
Strain Gage D.P. Cell	26	±200 psi	6.2 psi	N.S.	0.32 ms	30 psi
Strain Gage D.P. Cell	27	±1000 psi	30 psi	N.S.	0.32 ms	0.25 psi
Strain Gage[g] D.P. Cell	28	±50 psi	1.6 psi	N.S.	0.32 ms	0.25 psi
Strain Gage Pressure Cell	29	350 psi	3.5 psi	N.S.	0.16 ms	30 psi
Rod Heater Current	31	800 amp	0.85% Rdg	24 amp	50 ms	75 amp
Generator Current	32	1000 amp	0.85% Rdg	95 amp	50 ms	300 amp
Generator Voltage	33	300 volt	0.76% Rdg	32 volt	50 ms	100 volt

Table D.6 (continued)

THTF Instrument Error Bands						
Instrument Description	Type Code	Instrument Range	Steady State Error	Transient Error	Estimated Response Time	Assumed Value of Step Fn.
Primary Pump Power	34	750 kW	greater of 0.5 kW or 0.3% Rdg	6.3 kW	150 ms	10 kW
Strain Gage Drag Disk	35	±0.7E4 lb/fts² ±7.0E4 lb/fts²	56% Rdg 19% Rdg	106 lb/fts²	16 ms	1000 lb/fts²
Primary Pump Speed	36	100 rpm 5400 rpm	20 rpm	13 rpm	150 ms	20 rpm
Breakwire Detector	37	5 volt	30 ms	N.A.[k]	20 ms	N.A.
Strain Gage Drag Disk	40	±1.4E4 lb/fts² ±1.4E5 lb/fts²	56% Rdg 19% Rdg	106 lb/fts²	16 ms	1000 lb/fts²
Strain Gage D.P. Cell	41	±100 inch	3.2 inch	N.S.	0.32 ms	6.8 inch
Strain Gage D.P. Cell	42	±500 inch	16 inch	N.S.	0.32 ms	6.8 inch
Strain Gage D.P. Cell	43	±6 psi	0.3 psi	N.S.	0.32 ms	0.25 psi
Level[i] Indicator	50	±10 volt	***	***	***	***
RTD	71	32 F 800 F	2.0 F 4.9 F	17.8 F	10 sec	18 F
Capacitive D.P. Cell	75	25 inch	0.4 inch	0.6 inch	131 ms	1.0 inch
Capacitive D.P. Cell	75	150 inch	16 inch	0.4 inch	74 ms	1.0 inch
Position Indicator	76	155 inch	0.5% Rdg	N.A.	N.A.	N.A.
Position Indicator	77	131 inch	0.5% Rdg	N.A.	N.A.	N.A.

Table D.6 (continued)

THTF Instrument Error Bands						
Instrument Description	Type Code	Instrument Range	Steady State Error	Transient Error	Estimated Response Time	Assumed Value of Step Fn.
Capacitive D.P. Cell	78	±100 inch	5.2 inch	3.6 inch	110 ms	6.8 inch
Capacitive D.P. Cell	79	200 inch	2.0 inch	2.8 inch	68 ms	6.8 inch
Capacitive D.P. Cell	80	30 inch	0.4 inch	0.6 inch	125 ms	1.0 inch
Turbine[f] Flowmeter	95	15 gpm 150 gpm	4.1% Rdg	2.0 gpm	11 ms 1.2 ms	100 gpm
Turbine[f] Flowmeter	96	5 gpm 50 gpm	4.1% Rdg	2.0 gpm	8 ms 1 ms	100 gpm
Force Balance D.P. Cell	97	24 psi	0.15 psi	0.2 psi	300 ms	0.25 psi
Capacitive D.P. Cell	98	50 psi	2.6 psi	0.06 psi	38 ms	0.25 psi
Differential Temperature	99	±50 F	6.8 F	17.8 F	10 sec	18 F
Liquid Level	105	150 inch	0.9 inch	6.2 inch	300 ms	7.9 inch
Liquid Level	105	5.5E4 inch	336 inch	6.2 inch	300 ms	7.9 inch
Gamma Densitometer	106	62.4 lb/ft^3	6.5 lb/ft^3	0.33 lb/ft^3	16 ms	3 lb/ft^3
Orifice[c] Flowmeter	107	1.6 gpm	4E-2 gpm	0.13 gpm	300 ms	0.16 gpm
Orifice[c] Flowmeter	107	2.1 gpm	0.054 gpm	0.17 gpm	300 ms	0.22 gpm
Orifice[c] Flowmeter	107	5.3 gpm	0.13 gpm	0.41 gpm	300 ms	0.52 gpm

Table D.6 (continued)

THTF Instrument Error Bands						
Instrument Description	Type Code	Instrument Range	Steady State Error	Transient Error	Estimated Response Time	Assumed Value of Step Fn.
Orifice[c] Flowmeter	107	39.3 gpm	9.8 gpm	3.2 gpm	300 ms	4.0 gpm
Orifice[c] Flowmeter	107	800 gpm	21 gpm	62 gpm	300 ms	80 gpm
Orifice[d] Flowmeter	108	2.7 gpm	0.067 gpm	0.21 gpm	300 ms	0.27 gpm
Orifice[e] Flowmeter	108	700 gpm	17.4 gpm	0.55 gpm	300 ms	70 gpm
Turbine[f,h] Flowmeter	109	±0.5 gpm ±5.0 gpm	4.1% Rdg	0.05 gpm	8 ms 1 ms	2.4 gpm
Turbine[f,h,b] Flowmeter	109	±1.0 gpm ±10 gpm	2.5% Rdg	N.A.	8 ms 1 ms	N.A.
Turbine[f,h,l] Flowmeter	109	±22 gpm ±225 gpm	4.1% Rdg	0.2 gpm	13 ms 2 ms	10 gpm
Turbine[f,h,l] Flowmeter	109	±100 gpm ±1000 gpm	4.1% Rdg	0.2 gpm	18 ms 2 ms	10 gpm
RTD	110	32 F 800 F	2.0 F 4.9 F	17.8 F	10 sec	18 F
In-bundle Gamma Densitometer	111	62.4 lb/ft³	6.5 lb/ft³	0.3 lb/ft³	16 ms	3 lb/ft³
Orifice[c] Flowmeter	112	1.6 gpm	0.04 gpm	0.13 gpm	300 ms	0.16 gpm
Liquid Level	113	46 inch	0.3 inch	6.2 inch	300 ms	7.9 inch

Table D.6 (continued)

Documentation of Steady-State and Transient Error Bands

Steady-State Error Bands: Two-standard deviations compared to in-situ standard or twice the root-sum-square of uncertainties, whichever is applicable.

Transient Error Bands: Assuming first-order lag function, response times (TAU), and step function (Vf − Vo) indicated--the average error seen by the DAS assuming the step function occurred midway between DAS samples. The averaging interval is 500 ms for thermocouples and 150 ms for all other instruments.

Total Error: The total error due to steady state error and transient error is the sum of the steady state and transient error bands.

Footnotes:

a. Error bands apply to the environment as sensed at the surface of the thermocouple sheath. Larger errors may occur when data is modelled to provide temperatures at other points. Transient response is estimated by using the response time (25 ms or less) prior to swaging the sheath (0.028 inch swaged to 0.020 inch OD), then scaling using the rule: response time is inversely proportional to the outside diameter squared (OD**2 scaling). An additional 7% improvement in response time was allowed for packing of the boron nitride during swaging. The smaller thermocouples (0.020 inch swaged to 0.015 inch) were estimated from the values of the larger thermocouples by first scaling the 25 ms response time to the unswaged 0.020 inch diameter using OD**2 scaling, then applying OD**2 scaling and the 7% improvement for packing to the swaged 0.015 inch OD.

b. This instrument is fitted with Flow Technology electronics that time 10-blade passings. Averaging improves the steady-state error bands but degrades transient response.

c. Range applies specifically to instruments calibrated in subcooled liquid at a density of 62.4 lb/ft**3.

d. Range applies specifically to instruments calibrated in subcooled liquid at a density of 53.7 lb/ft**3.

e. Range applies specifically to instruments calibrated in subcooled liquid at a density of 46.8 lb/ft**3.

f. Error bands apply specifically to instruments calibrated in subcooled liquid. Extended range electronics provide readings out to 3600 gpm for the 3.5 inch diameter models; 445 gpm for the two inch diameter models, but the error bands apply only to 150% of nominal maximum range.

g. Strain gage D.P. Cells used as pit cells are connected to different segments of the test section by long lines. These long lines induce resonant oscillations in the instrument that increase the steady-state errors bands to 5 psi, and the transient error bands to 60 psi in the interval immediately following blowdown.

h. The turbine flowmeters (type code 109) have a flow range such that:
-5.0<Flow<-0.5 .OR. 0.5<Flow<5.0,
-10.0<Flow<-1.0 .OR. 1.0<Flow<10.0,
-225<Flow<-22 .OR. 22<Flow<225,
-1000<Flow<-100 .OR. 100<Flow<1000.

i. The INEL level probe is an experimental device, and as such, does not have well documented error bands.

j. No significant error over the averaging interval.

k. N.A. implies not applicable.

l. Flow Technology supplies calibration constants over the ranges 10 to 300 gpm and 80 to 1000 gpm respectively. The uncertainty bands for these instruments should approach the quoted values for these ranges, but special care may be required. See the section on turbine flowmeters in the critical instruments section.

Table D.6 (continued)

Basis for Steady-State and Transient Error Bands by Type Code		
Type Code	Steady State	Transient
1	Critical instrument	Manufacturer's spec, OD**2 scaling
2	Critical instrument	Manufacturer's spec, OD**2 scaling
3	Critical instrument	Work of Carroll and Sheppard
4	Critical instrument	Work of Carroll and Sheppard
5	Critical instrument	Work of Carroll and Sheppard
6	Critical instrument	Manufacturer's spec
7	Critical instrument	Work of Carroll and Sheppard
8	Critical instrument	Work of Carroll and Sheppard
9	Critical instrument	Manufacturer's spec, OD**2 scaling
10	Critical instrument	Work of Carroll and Sheppard
23	Critical instrument	Table B.2 of Ref. 6
24	Manufacturer's spec	Table B.2 of Ref. 6
25	Bench Cal. + DAS	Table B.2 (inferred) of Ref. 6
26	Critical instrument	Table B.2 of Ref. 6
27	Critical instrument	Table B.2 of Ref. 6
28	Critical instrument	Table B.2 of Ref. 6
29	Critical instrument	Table B.2 (inferred) of Ref. 6
31	Critical instrument	Table B.2 (inferred) of Ref. 6
32	Inferred (type code 31)	Table B.2 (inferred) of Ref. 6
33	Critical instrument	Table B.2 (inferred) of Ref. 6
34	Manufacturer's spec	Manufacturer's spec
35	Critical instrument	Table B.2 of Ref. 6
36	Bench Cal. + DAS	Inferred (type code 34)
37	From test 3.03.6AR	From test 3.03.6AR
40	Critical instrument	Table B.2 of Ref. 6
43	Critical instrument	Table B.2 (inferred) of Ref. 6
50	**********	**********
71	Bench Cal. & specs	Table B.2 of Ref. 6
75	Critical instrument	Manufacturer's spec
76	Engineering judgement	N.A.
77	Engineering judgement	N.A.
78	Critical instrument	Inferred (type code 75)
79	Inferred (type code 75)	Inferred (type code 75)
80	Inferred (type code 75)	Inferred (type code 75)
95	Inferred (type code 109)	Work of N. Chen
96	Inferred (type code 109)	Work of N. Chen
97	Critical instrument	Table B.2 of Ref. 6
98	Critical instrument	Inferred (typed code 75)
99	Inferred (type code 71)	Inferred (type code 71)
105	Manufacturer's spec	Table B.2 (inferred) of Ref. 6
106	Critical instrument	Work of R. Shipp (manufacturer's spec)
107	In-situ calibration	Table B.2 (inferred) of Ref. 6
108	Inferred (type code 107)	Table B.2 (inferred) of Ref. 6
109	Critical instrument	Work of N. Chen
110	Bench Cal. & specs	Table B.2 of Ref. 6
111	Inferred (type code 106)	Inferred (type code 109)
112	Inferred (type code 107)	Table B.2 (inferred) of Ref. 6
113	Manufacturer's spec	Table B.2 (inferred) of Ref. 6

Table D.7. THTF instrument uncertainties — (worst-case transient step function for Test 3.06.6B) (SI units)

THTF Instrument Error Bands						
Instrument Description	Type Code	Instrument Range	Steady State Error	Transient Error	Estimated Response Time	Assumed Value of Step Fn.
Rod Sheath Thermocouple 0.38 mm OD	1	273 K 1309 K	3.7K < 623 K 10.3 K	0.8 K[a]	7 ms	300 K
Rod Sheath Thermocouple 0.51 mm OD	1	273 K 1309 K	3.7K < 623 K 10.3 K	3.8 K[a]	12 ms	300 K
Rod Middle Thermocouple 0.38 mm OD	2	273 K 1309 K	3.7K < 623 K 10.3 K	0.8 K[a]	7 ms	300 K
Rod Middle Thermocouple 0.51 mm OD	2	273 K 1309 K	3.7K < 623 K 10.3 K	3.8 K[a]	12 ms	300 K
Bundle Subchn Thermocouple 1.02 mm OD	3	273 K 1309 K	3.7K < 623 K 10.3 K	4.1 K	140 ms	15 K
Shroud Box Thermocouple 1.57 mm OD	4	273 K 1309 K	3.7K < 623 K 10.3 K	8.0 K	350 ms	15 K
System Thermocouple 3.2 mm OD	5	273 K 1309 K	3.7K < 623 K 10.3 K	11.4 K	870 ms	15 K
System (Nanmac) Thermocouple 6.4 mm OD	6	273 K 1309 K	3.7K < 623 K 10.3 K	0.4 K	18 ms	15 K
Spacer Grid Thermocouple 1.02 mm OD	7	273 K 1309 K	3.7K < 623 K 10.3 K	4.1 K	140 ms	15 K
Array Rod Thermocouple 1.02 mm OD	8	273 K 1309 K	3.7K < 623 K 10.3 K	4.1 K	140 ms	15 K

Table D.7 (continued)

THTF Instrument Error Bands						
Instrument Description	Type Code	Instrument Range	Steady State Error	Transient Error	Estimated Response Time	Assumed Value of Step Fn.
Rod Sheath Thermocouple 0.51 mm OD	9	273 K 1309 K	3.7K < 623 K 10.3 K	3.8 K[a]	12 ms	300 K
Shroud Box Thermocouple 1.57 mm OD	10	273 K 1309 K	3.7K < 623 K 10.3 K	8.0 K	350 ms	15 K
Strain Gage Pressure Cell	23	20700 kPa	200 kPa	N.S.[j]	0.16 ms	700 kPa
Force Balance Pressure Cell	24	3400 kPa 17000 kPa	100 kPa	550 kPa	300 ms	700 kPa
Force Balance Pressure Cell	24	3400 kPa 27000 kPa	160 kPa	550 kPa	300 ms	700 kPa
Strain Gage Pressure Cell	25	1380 kPa	17 kPa	N.S.	0.32 ms	700 kPa
Strain Gage D.P. Cell	26	±1380 kPa	43 kPa	N.S.	0.32 ms	5.1 kPa
Strain Gage D.P. Cell	27	±6900 kPa	210 kPa	N.S.	0.32 ms	5.1 kPa
Strain Gage[g] D.P. Cell	28	±345 kPa	11 kPa	N.S.	0.32 ms	5.1 kPa
Strain Gage Pressure Cell	29	2400 kPa	24 kPa	N.S.	0.16 ms	700 kPa
Rod Heater Current	31	800 amp	0.85% Rdg	4.7 amp	50 ms	15 amp
Generator Current	32	1000 amp	0.85% Rdg	32 amp	50 ms	100 amp
Generator Voltage	33	300 volt	0.76% Rdg	3.8 volt	50 ms	12 volt

Table D.7 (continued)

THTF Instrument Error Bands						
Instrument Description	Type Code	Instrument Range	Steady State Error	Transient Error	Estimated Response Time	Assumed Value of Step Fn.
Primary Pump Power	34	750 kW	greater of 0.5 kW or 0.3% Rdg	6.3 kW	150 ms	10 kW
Strain Gage Drag Disk	35	±0.1E5 kg/ms² ±1.0E5 kg/ms²	56% Rdg 19% Rdg	157 kg/ms²	16 ms	1500 kg/ms²
Primary Pump Speed	36	100 rpm 5400 rpm	20 rpm	13 rpm	150 ms	20 rpm
Breakwire Detector	37	5 volt	30 ms	N.A.[k]	20 ms	N.A.
Strain Gage Drag Disk	40	±0.2E5 kg/ms² ±2.1E5 kg/ms²	56% Rdg 19% Rdg	157 kg/ms²	16 ms	1500 kg/ms²
Strain Gage D.P. Cell	41	±25 kPa	0.8 kPa	N.S.	0.32 ms	5.1 kPa
Strain Gage D.P. Cell	42	±125 kPa	4 kPa	N.S.	0.32 ms	5.1 kPa
Strain Gage D.P. Cell	43	±41 kPa	2 kPa	N.S.	0.32 ms	5.1 kPa
Level[i] Indicator	50	±10 volt	***	***	***	***
RTD	71	273 K 700 K	1.1 K 2.7 K	14.9 K	10 sec	15 K
Capacitive D.P. Cell	75	6.2 kPa	0.1 kPa	0.5 kPa	131 ms	0.75 kPa
Capacitive D.P. Cell	75	37.5 kPa	0.4 kPa	0.3 kPa	74 ms	0.75 kPa
Position Indicator	76	3.92 m	0.5% Rdg	N.A.	N.A.	N.A.
Position Indicator	77	3.33 m	0.5% Rdg	N.A.	N.A.	N.A.

Table D.7 (continued)

THTF Instrument Error Bands						
Instrument Description	Type Code	Instrument Range	Steady State Error	Transient Error	Estimated Response Time	Assumed Value of Step Fn.
Capacitive D.P. Cell	78	25 kPa	1.3 kPa	2.7 kPa	110 ms	5.1 kPa
Capacitive D.P. Cell	79	50 kPa	0.5 kPa	2.1 kPa	68 ms	5.1 kPa
Capacitive D.P. Cell	80	7.5 kPa	0.1 kPa	0.4 kPa	125 ms	0.75 kPa
Turbine[f] Flowmeter	95	0.9E-3 m^3/s 9.5E-3 m^3/s	4.1% Rdg	1.3E-6 m^3/s	11 ms 1.2 ms	6.3E-4 m^3/s
Turbine[f] Flowmeter	96	0.3E-3 m^3/s 3.2E-3 m^3/s	4.1% Rdg	1.3E-6 m^3/s	8 ms 1 ms	6.3E-4 m^3/s
Force Balance D.P. Cell	97	166 kPa	1 kPa	4 kPa	300 ms	5.1 kPa
Capacitive D.P. Cell	98	345 kPa	0.1 kPa	1.3 kPa	38 ms	5.1 kPa
Differential Temperature	99	228 K 283 K	3.8 K	9.9 K	10 sec	10 K
Liquid Level	105	3.81 m	0.023 m	0.16 m	300 ms	0.2 m
Liquid Level	105	1408 m	8.5 m	0.16 m	300 ms	0.2 m
Gamma Densitometer	106	1000 kg/m^3	104 kg/m^3	8 kg/m^3	16 ms	80 kg/m^3
Orifice[e] Flowmeter	107	1.0E-4 m^3/s	2.5E-6 m^3/s	7.9E-6 m^3/s	300 ms	1E-5 m^3/s
Orifice[e] Flowmeter	107	1.35E-4 m^3/s	3.4E-6 m^3/s	1.1E-5 m^3/s	300 ms	1.4E-5 m^3/s
Orifice[e] Flowmeter	107	3.32E-4 m^3/s	8.3E-6 m^3/s	2.6E-5 m^3/s	300 ms	3.3E-5 m^3/s

Table D.7 (continued)

THTF Instrument Error Bands						
Instrument Description	Type Code	Instrument Range	Steady State Error	Transient Error	Estimated Response Time	Assumed Value of Step Fn.
Orifice[c] Flowmeter	107	2.48E-3 m^3/s	6.2E-5 m^3/s	2.0E-4 m^3/s	300 ms	2.5E-4 m^3/s
Orifice[c] Flowmeter	107	5.0E-2 m^3/s	1.3E-3 m^3/s	3.9E-3 m^3/s	300 ms	5E-3 m^3/s
Orifice[d] Flowmeter	108	1.7E-4 m^3/s	4.2E-6 m^3/s	1.3E-5 m^3/s	300 ms	1.7E-5 m^3/s
Orifice[e] Flowmeter	108	4.4E-2 m^3/s	1.1E-3 m^3/s	3.5E-3 m^3/s	300 ms	4.4E-3 m^3/s
Turbine[f,h] Flowmeter	109	±0.3E-4 m^3/s ±3.0E-4 m^3/s	4.1% Rdg	3.1E-6 m^3/s	8 ms 1 ms	1.5E-4 m^3/s
Turbine[f,h,b] Flowmeter	109	±0.6E-4 m^3/s ±6.1E-4 m^3/s	2.5% Rdg	N.A.	8 ms 1 ms	N.A.
Turbine[f,h,l] Flowmeter	109	±1.3E-3 m^3/s ±1.4E-2 m^3/s	4.1% Rdg	2.7E-5 m^3/s	13 ms 2 ms	1.3E-3 m^3/s
Turbine[f,h,l] Flowmeter	109	±0.6E-2 m^3/s ±6.1E-2 m^3/s	4.1% Rdg	6.7E-5 m^3/s	18 ms 2 ms	3.2E-3 m^3/s
RTD	110	273 K 700 K	1.1 K 2.7 K	14.9 K	10 sec	15 K
In-bundle Gamma Densitometer	111	1000 kg/m^3	104 kg/m^3	8 kg/m^3	16 ms	80 kg/m^3
Orifice[c] Flowmeter	112	1.0E-4 m^3/s	2.5E-6 m^3/s	7.9E-6 m^3/s	300 ms	1E-5 m^3/s
Liquid Level	113	1.18 m	0.007 m	0.16 m	300 ms	0.20 m

Table D.7 (continued)

Documentation of Steady-State and Transient Error Bands

Steady-State Error Bands: Two-standard deviations compared to in-situ standard or twice the root-sum-square of uncertainties, whichever is applicable.

Transient Error Bands: Assuming first-order lag function, response times (TAU), and step function (Vf − Vo) indicated—the average error seen by the DAS assuming the step function occurred midway between DAS samples. The averaging interval is 500 ms for thermocouples and 150 ms for all other instruments.

Total Error: The total error due to steady state error and transient error is the sum of the steady state and error bands.

Footnotes:

a. Error bands apply to the environment as sensed at the surface of the thermocouple sheath. Larger errors may occur when data is modelled to provide temperatures at other points. Transient response is estimated by using the response time (25 ms or less) prior to swaging the sheath (0.71 mm swaged to 0.51 mm OD), then scaling using the rule: response time is inversely proportional to the outside diameter squared (OD**2 scaling). An additional 7% improvement in response time was allowed for packing of the boron nitride during swaging. The smaller thermocouples (0.51 mm swaged to 0.38 mm OD) were estimated from the values of the larger thermocouples by first scaling the 25 ms response time to the unswaged 0.51 mm diameter using OD**2 scaling, then applying OD**2 scaling and the 7% improvement for packing to the swaged 0.38 mm OD.

b. This instrument is fitted with Flow Technology electronics that time 10-blade passings. Averaging improves the steady-state error bands but degrades transient response.

c. Range applies specifically to instruments calibrated in subcooled liquid at a density of 1000 kg/m**3.

d. Range applies specifically to instruments calibrated in subcooled liquid at a density of 860 kg/m**3.

e. Range applies specifically to instruments calibrated in subcooled liquid at a density of 750 kg/m**3.

f. Error bands apply specifically to instruments calibrated in subcooled liquid. Extended range electronics provide readings out to 0.227 m^3/s for the 8.89E-2 meter diameter models; 0.028 m^3/s for the 5.08E-2 meter diameter models, but the error bands apply only to 150% of nominal maximum range.

g. Strain gage D.P. Cells used as pit cells are connected to different segments of the test section by long lines. These long lines induce resonant oscillations in the instrument that increase the steady-state errors bands to 35 kPa, and the transient error bands to 400 kPa.

h. The turbine flowmeters (type code 109) have a flow range such that:
-3.0E-4<Flow<-0.3E-4 .OR. 0.3E-4<Flow<3.0E-4,
-6.1E-4<Flow<-0.6E-4 .OR. 0.6E-4<Flow<6.1E-4,
-1.4E-3<Flow<-0.1E-3 .OR. 0.1E-3<Flow<1.4E-3,
-6.1E-2<Flow<-0.6E-2 .OR. 0.6E-2<Flow<6.1E-2

i. The INEL level probe is an experimental device, and as such, does not have well documented error bands.

j. No significant error over a 500 ms averaging interval.

k. N.A. implies not applicable.

l. Flow Technology supplies calibration constants over the ranges 6.3E-4 to 1.9E-2 m^3/s and 5.0E-3 to 6.3E-2 m^3/s respectively. The uncertainty bands for these instruments should approach the quoted values for these ranges, but special care may be required. See the section on turbine flowmeters in the critical instruments section.

Table D.7 (continued)

Basis for Steady-State and Transient Error Bands by Type Code		
Type Code	Steady State	Transient
1	Critical instrument	Manufacturer's spec, OD**2 scaling
2	Critical instrument	Manufacturer's spec, OD**2 scaling
3	Critical instrument	Work of Carroll and Sheppard
4	Critical instrument	Work of Carroll and Sheppard
5	Critical instrument	Work of Carroll and Sheppard
6	Critical instrument	Manufacturer's spec
7	Critical instrument	Work of Carroll and Sheppard
8	Critical instrument	Work of Carroll and Sheppard
9	Critical instrument	Manufacturer's spec, OD**2 scaling
10	Critical instrument	Work of Carroll and Sheppard
23	Critical instrument	Table B.2 of Ref. 6
24	Manufacturer's spec	Table B.2 of Ref. 6
25	Bench Cal. + DAS	Table B.2 (inferred) of Ref. 6
26	Critical instrument	Table B.2 of Ref. 6
27	Critical instrument	Table B.2 of Ref. 6
28	Critical instrument	Table B.2 of Ref. 6
29	Critical instrument	Table B.2 (inferred) of Ref. 6
31	Critical instrument	Table B.2 (inferred) of Ref. 6
32	Inferred (type code 31)	Table B.2 (inferred) of Ref. 6
33	Critical instrument	Table B.2 (inferred) of Ref. 6
34	Manufacturer's spec	Manufacturer's spec
35	Critical instrument	Table B.2 of Ref. 6
36	Bench Cal. + DAS	Inferred (type code 34)
37	From test 3.03.6AR	From test 3.03.6AR
40	Critical instrument	Table B.2 of Ref. 6
43	Critical instrument	Table B.2 (inferred) of Ref. 6
50	**********	**********
71	Bench Cal. & specs	Table B.2 of Ref. 6
75	Critical instrument	Manufacturer's spec
76	Engineering judgement	N.A.
77	Engineering judgement	N.A.
78	Critical instrument	Inferred (type code 75)
79	Inferred (type code 75)	Inferred (type code 75)
80	Inferred (type code 75)	Inferred (type code 75)
95	Inferred (type code 109)	Work of N. Chen
96	Inferred (type code 109)	Work of N. Chen
97	Critical instrument	Table B.2 of Ref. 6
98	Critical instrument	Inferred (typed code 75)
99	Inferred (type code 71)	Inferred (type code 71)
105	Manufacturer's spec	Table B.2 (inferred) of Ref. 6
106	Critical instrument	Work of R. Shipp (manufacturer's spec)
107	In-situ calibration	Table B.2 (inferred) of Ref. 6
108	Inferred (type code 107)	Table B.2 (inferred) of Ref. 6
109	Critical instrument	Work of N. Chen
110	Bench Cal. & specs	Table B.2 of Ref. 6
111	Inferred (type code 106)	Inferred (type code 109)
112	Inferred (type code 107)	Table B.2 (inferred) of Ref. 6
113	Manufacturer's spec	Table B.2 (inferred) of Ref. 6

Table D.8. THTF instrument uncertainties — (worst-case transient step function for Test 3.06.6B) (English units)

THTF Instrument Error Bands						
Instrument Description	Type Code	Instrument Range	Steady State Error	Transient Error	Estimated Response Time	Assumed Value of Step Fn.
Rod Sheath Thermocouple 0.015 inch OD	1	32 F 1900 F	6.7F < 662 F 18.5 F	1.4 F[a]	7 ms	540 F
Rod Sheath Thermocouple 0.020 inch OD	1	32 F 1900 F	6.7F < 662 F 18.5 F	6.8 F[a]	12 ms	540 F
Rod Middle Thermocouple 0.015 inch OD	2	32 F 1900 F	6.7F < 662 F 18.5 F	1.4 F[a]	7 ms	540 F
Rod Middle Thermocouple 0.020 inch OD	2	32 F 1900 F	6.7F < 662 F 18.5 F	6.8 F[a]	12 ms	540 F
Bundle Subchn Thermocouple 0.040 inch OD	3	32 F 1900 F	6.7F < 662 F 18.5 F	7.4 F	140 ms	27 F
Shroud Box Thermocouple 0.062 inch OD	4	32 F 1900 F	6.7F < 662 F 18.5 F	14.4 F	350 ms	27 F
System Thermocouple 0.125 inch OD	5	32 F 1900 F	6.7F < 662 F 18.5 F	20.5 F	870 ms	27 F
System (Nanmac) Thermocouple 0.25 inch OD	6	32 F 1900 F	6.7F < 662 F 18.5 F	0.7 F	18 ms	27 F
Spacer Grid Thermocouple 0.040 inch OD	7	32 F 1900 F	6.7F < 662 F 18.5 F	7.4 F	140 ms	27 F
Array Rod Thermocouple 0.040 inch OD	8	32 F 1900 F	6.7F < 662 F 18.5 F	7.4 F	140 ms	27 F

Table D.8 (continued)

THTF Instrument Error Bands						
Instrument Description	Type Code	Instrument Range	Steady State Error	Transient Error	Estimated Response Time	Assumed Value of Step Fn.
Rod Sheath Thermocouple 0.020 inch OD	9	32 F 1900 F	6.7F < 662 F 18.5 F	6.8 F[a]	12 ms	540 F
Shroud Box Thermocouple 0.062 inch OD	10	32 F 1900 F	6.7F < 662 F 18.5 F	14.4 F	350 ms	27 F
Strain Gage Pressure Cell	23	3000 psi	29 psi	N.S.[j]	0.16 ms	100 psi
Force Balance Pressure Cell	24	500 psi 2500 psi	15 psi	79 psi	300 ms	100 psi
Force Balance Pressure Cell	24	500 psi 3900 psi	23 psi	79 psi	300 ms	100 psi
Strain Gage Pressure Cell	25	200 psi	2.5 psi	N.S.	0.32 ms	100 psi
Strain Gage D.P. Cell	26	±200 psi	6.2 psi	N.S.	0.32 ms	100 psi
Strain Gage D.P. Cell	27	±1000 psi	30 psi	N.S.	0.32 ms	0.7 psi
Strain Gage[g] D.P. Cell	28	±50 psi	1.6 psi	N.S.	0.32 ms	0.7 psi
Strain Gage Pressure Cell	29	350 psi	3.5 psi	N.S.	0.16 ms	100 psi
Rod Heater Current	31	800 amp	0.85% Rdg	24 amp	50 ms	75 amp
Generator Current	32	1000 amp	0.85% Rdg	95 amp	50 ms	300 amp
Generator Voltage	33	300 volt	0.76% Rdg	32 volt	50 ms	100 volt

Table D.8 (continued)

THTF Instrument Error Bands						
Instrument Description	Type Code	Instrument Range	Steady State Error	Transient Error	Estimated Response Time	Assumed Value of Step Fn.
Primary Pump Power	34	750 kW	greater of 0.5 kW or 0.3% Rdg	6.3 kW	150 ms	10 kW
Strain Gage Drag Disk	35	±0.7E4 lb/fts² ±7.0E4 lb/fts²	56% Rdg 19% Rdg	106 lb/fts²	16 ms	1000 lb/fts²
Primary Pump Speed	36	100 rpm 5400 rpm	20 rpm	13 rpm	150 ms	20 rpm
Breakwire Detector	37	5 volt	30 ms	N.A.[k]	20 ms	N.A.
Strain Gage Drag Disk	40	±1.4E4 lb/fts² ±1.4E5 lb/fts²	56% Rdg 19% Rdg	106 lb/fts²	16 ms	1000 lb/fts²
Strain Gage D.P. Cell	41	±100 inch	3.2 inch	N.S.	0.32 ms	20.5 inch
Strain Gage D.P. Cell	42	±500 inch	16 inch	N.S.	0.32 ms	20.5 inch
Strain Gage D.P. Cell	43	±6 psi	0.3 psi	N.S.	0.32 ms	0.7 psi
Level[i] Indicator	50	±10 volt	***	***	***	***
RTD	71	32 F 800 F	2.0 F 4.9 F	26.8 F	10 sec	27 F
Capacitive D.P. Cell	75	25 inch	0.4 inch	2.0 inch	131 ms	3 inch
Capacitive D.P. Cell	75	150 inch	1.6 inch	1.2 inch	74 ms	3 inch
Position Indicator	76	155 inch	0.5% Rdg	N.A.	N.A.	N.A.
Position Indicator	77	131 inch	0.5% Rdg	N.A.	N.A.	N.A.

Table D.8 (continued)

THTF Instrument Error Bands						
Instrument Description	Type Code	Instrument Range	Steady State Error	Transient Error	Estimated Response Time	Assumed Value of Step Fn.
Capacitive D.P. Cell	78	±100 inch	5.2 inch	10.9 inch	110 ms	20.5 inch
Capacitive D.P. Cell	79	200 inch	2.0 inch	8.4 inch	68 ms	20.5 inch
Capacitive D.P. Cell	80	30 inch	0.4 inch	1.6 inch	125 ms	3 inch
Turbine[f] Flowmeter	95	15 gpm 150 gpm	4.1% Rdg	2.0 gpm	11 ms 1.2 ms	100 gpm
Turbine[f] Flowmeter	96	5 gpm 50 gpm	4.1% Rdg	2.0 gpm	8 ms 1 ms	100 gpm
Force Balance D.P. Cell	97	24 psi	0.15 psi	0.6 psi	300 ms	0.7 psi
Capacitive D.P. Cell	98	50 psi	2.6 psi	0.2 psi	38 ms	0.7 psi
Differential Temperature	99	±50 F	6.8 F	17.8 F	10 sec	18 F
Liquid Level	105	150 inch	0.9 inch	6.2 inch	300 ms	7.9 inch
Liquid Level	105	5.5E4 inch	336 inch	6.2 inch	300 ms	7.9 inch
Gamma Densitometer	106	62.4 lb/ft^3	6.5 lb/ft^3	0.5 lb/ft^3	16 ms	5 lb/ft^3
Orifice[c] Flowmeter	107	1.6 gpm	4E-2 gpm	0.13 gpm	300 ms	0.16 gpm
Orifice[c] Flowmeter	107	2.1 gpm	0.054 gpm	0.17 gpm	300 ms	0.22 gpm
Orifice[c] Flowmeter	107	5.3 gpm	0.13 gpm	0.41 gpm	300 ms	0.52 gpm

Table D.8 (continued)

THTF Instrument Error Bands						
Instrument Description	Type Code	Instrument Range	Steady State Error	Transient Error	Estimated Response Time	Assumed Value of Step Fn.
Orifice[c] Flowmeter	107	39.3 gpm	9.8 gpm	3.2 gpm	300 ms	4.0 gpm
Orifice[c] Flowmeter	107	800 gpm	21 gpm	62 gpm	300 ms	80 gpm
Orifice[d] Flowmeter	108	2.7 gpm	0.067 gpm	0.21 gpm	300 ms	0.27 gpm
Orifice[e] Flowmeter	108	700 gpm	17.4 gpm	0.55 gpm	300 ms	70 gpm
Turbine[f,h] Flowmeter	109	±0.5 gpm ±5.0 gpm	4.1% Rdg	0.05 gpm	8 ms 1 ms	2.4 gpm
Turbine[f,h,b] Flowmeter	109	±1.0 gpm ±10 gpm	2.5% Rdg	N.A.	8 ms 1 ms	N.A.
Turbine[f,h,l] Flowmeter	109	±22 gpm ±225 gpm	4.1% Rdg	0.4 gpm	13 ms 2 ms	21 gpm
Turbine[f,h,l] Flowmeter	109	±100 gpm ±1000 gpm	4.1% Rdg	1.1 gpm	18 ms 2 ms	50 gpm
RTD	110	32 F 800 F	2.0 F 4.9 F	26.8 F	10 sec	27 F
In-bundle Gamma Densitometer	111	62.4 lb/ft^3	6.5 lb/ft^3	0.5 lb/ft^3	16 ms	5 lb/ft^3
Orifice[c] Flowmeter	112	1.6 gpm	0.04 gpm	0.13 gpm	300 ms	0.16 gpm
Liquid Level	113	46 inch	0.3 inch	6.2 inch	300 ms	7.9 inch

Table D.8 (continued)

Documentation of Steady-State and Transient Error Bands

Steady-State Error Bands: Two-standard deviations compared to in-situ standard or twice the root-sum-square of uncertainties, whichever is applicable.

Transient Error Bands: Assuming first-order lag function, response times (TAU), and step function (Vf − Vo) indicated—the average error seen by the DAS assuming the step function occurred midway between DAS samples. The averaging interval is 500 ms for thermocouples and 150 ms for all other instruments.

Total Error: The total error due to steady state error and transient error is the sum of the steady state and transient error bands.

Footnotes:

a. Error bands apply to the environment as sensed at the surface of the thermocouple sheath. Larger errors may occur when data is modelled to provide temperatures at other points. Transient response is estimated by using the response time (25 ms or less) prior to swaging the sheath (0.028 inch swaged to 0.020 inch OD), then scaling using the rule: response time is inversely proportional to the outside diameter squared (OD**2 scaling). An additional 7% improvement in response time was allowed for packing of the boron nitride during swaging. The smaller thermocouples (0.020 inch swaged to 0.015 inch) were estimated from the values of the larger thermocouples by first scaling the 25 ms response time to the unswaged 0.020 inch diameter using OD**2 scaling, then applying OD**2 scaling and the 7% improvement for packing to the swaged 0.015 inch OD.

b. This instrument is fitted with Flow Technology electronics that time 10-blade passings. Averaging improves the steady-state error bands but degrades transient response.

c. Range applies specifically to instruments calibrated in subcooled liquid at a density of 62.4 lb/ft**3.

d. Range applies specifically to instruments calibrated in subcooled liquid at a density of 53.7 lb/ft**3.

e. Range applies specifically to instruments calibrated in subcooled liquid at a density of 46.8 lb/ft**3.

f. Error bands apply specifically to instruments calibrated in subcooled liquid. Extended range electronics provide readings out to 3600 gpm for the 3.5 inch diameter models; 445 gpm for the two inch diameter models, but the error bands apply only to 150% of nominal maximum range.

g. Strain gage D.P. Cells used as pit cells are connected to different segments of the test section by long lines. These long lines induce resonant oscillations in the instrument that increase the steady-state errors bands to 5 psi, and the transient error bands to 60 psi in the interval immediately following blowdown.

h. The turbine flowmeters (type code 109) have a flow range such that:
-5.0<Flow<-0.5 .OR. 0.5<Flow<5.0,
-10.0<Flow<-1.0 .OR. 1.0<Flow<10.0,
-225<Flow<-22 .OR. 22<Flow<225,
-1000<Flow<-100 .OR. 100<Flow<1000.

i. The INEL level probe is an experimental device, and as such, does not have well documented error bands.

j. No significant error over the averaging interval.

k. N.A. implies not applicable.

l. Flow Technology supplies calibration constants over the ranges 10 to 300 gpm and 80 to 1000 gpm respectively. The uncertainty bands for these instruments should approach the quoted values for these ranges, but special care may be required. See the section on turbine flowmeters in the critical instruments section.

Table D.8 (continued)

Basis for Steady-State and Transient Error Bands by Type Code		
Type Code	Steady State	Transient
1	Critical instrument	Manufacturer's spec, OD**2 scaling
2	Critical instrument	Manufacturer's spec, OD**2 scaling
3	Critical instrument	Work of Carroll and Sheppard
4	Critical instrument	Work of Carroll and Sheppard
5	Critical instrument	Work of Carroll and Sheppard
6	Critical instrument	Manufacturer's spec
7	Critical instrument	Work of Carroll and Sheppard
8	Critical instrument	Work of Carroll and Sheppard
9	Critical instrument	Manufacturer's spec, OD**2 scaling
10	Critical instrument	Work of Carroll and Sheppard
23	Critical instrument	Table B.2 of Ref. 6
24	Manufacturer's spec	Table B.2 of Ref. 6
25	Bench Cal. + DAS	Table B.2 (inferred) of Ref. 6
26	Critical instrument	Table B.2 of Ref. 6
27	Critical instrument	Table B.2 of Ref. 6
28	Critical instrument	Table B.2 of Ref. 6
29	Critical instrument	Table B.2 (inferred) of Ref. 6
31	Critical instrument	Table B.2 (inferred) of Ref. 6
32	Inferred (type code 31)	Table B.2 (inferred) of Ref. 6
33	Critical instrument	Table B.2 (inferred) of Ref. 6
34	Manufacturer's spec	Manufacturer's spec
35	Critical instrument	Table B.2 of Ref. 6
36	Bench Cal. + DAS	Inferred (type code 34)
37	From test 3.03.6AR	From test 3.03.6AR
40	Critical instrument	Table B.2 of Ref. 6
43	Critical instrument	Table B.2 (inferred) of Ref. 6
50	**********	**********
71	Bench Cal. & specs	Table B.2 of Ref. 6
75	Critical instrument	Manufacturer's spec
76	Engineering judgement	N.A.
77	Engineering judgement	N.A.
78	Critical instrument	Inferred (type code 75)
79	Inferred (type code 75)	Inferred (type code 75)
80	Inferred (type code 75)	Inferred (type code 75)
95	Inferred (type code 109)	Work of N. Chen
96	Inferred (type code 109)	Work of N. Chen
97	Critical instrument	Table B.2 of Ref. 6
98	Critical instrument	Inferred (typed code 75)
99	Inferred (type code 71)	Inferred (type code 71)
105	Manufacturer's spec	Table B.2 (inferred) of Ref. 6
106	Critical instrument	Work of R. Shipp (manufacturer's spec)
107	In-situ calibration	Table B.2 (inferred) of Ref. 6
108	Inferred (type code 107)	Table B.2 (inferred) of Ref. 6
109	Critical instrument	Work of N. Chen
110	Bench Cal. & specs	Table B.2 of Ref. 6
111	Inferred (type code 106)	Inferred (type code 109)
112	Inferred (type code 107)	Table B.2 (inferred) of Ref. 6
113	Manufacturer's spec	Table B.2 (inferred) of Ref. 6

cross reference to IANs.) The third column provides the nominal instrument range. The fourth and fifth columns give the steady-state and transient error bands, respectively. The sixth and seventh columns provide the estimated response time and step function values used to estimate the transient uncertainty value.

The transient errors shown are derived from test-specific step functions used in the transient error analysis described previously. Nominal and worst-case step functions refer to a step size that is characteristic of transient phenomena occurring during the specific test. The nominal and worst-case step functions shown in this report are for Test 3.06.6B. Transient error estimates for other tests are included in their respective test data reports.

The English version tables are intended for reference only. Exact correspondence of entries will be limited by significant figure rounding.

The values quoted for both steady-state and transient errors are estimates based on several assumptions. It is the responsibility of the data user to ascertain the appropriateness of these assumptions when using the included error bands for THTF data analysis.

References

1. K. A. Brownlee, *Statistical Theory and Methodology in Science and Engineering*, p. 80, John Wiley and Sons, Inc., New York, 1965.

2. J. B. Scarborough, *Numerical Mathematical Analysis*, 3rd Ed., p. 429, The John Hopkins Press, Baltimore, 1955.

3. K. A. Brownlee, *Statistical Theory and Methodology in Science and Engineering*, p. 340, John Wiley and Sons, Inc., New York, 1965.

4. Unpublished report, *Summary Two and Three Dimensional Analysis of Turbine Flowmeter Response in Two-Phase Flow*, MPR Associates, Inc. (October 11, 1977).

5. Internal memo from R. L. Anderson, I&C Division ORNL, to B. J. Veazie, *Error in BDHT Thermocouple*, June 18, 1980.

6. *Project Description ORNL PWR Blowdown Heat Transfer Separate-Effects Program - Thermal-Hydraulic Test Facility (THTF)*, NUREG/CR-0104 (ORNL/NUREG/TM-218) (November 1978).

NUREG/CR-2640
ORNL/TM-7842
Dist. Category AN

Internal Distribution

1. T. M. Anklam
2-3. W. G. Craddick
4. R. L. Duraall
5-9. D. K. Felde
10-14. D. K. Fraysier
15. D. S. Griffith
16-20. S. S. Gould
21. T. J. Hanratty (Consultant)
22. H. W. Hoffman
23. A. L. Lotts
24. E. C. Keith
25. T. S. Kress
26. D. G. Morris
27. C. B. Mullins
28-32. L. J. Ott
33. A. G. Sutton
34. H. E. Trammell
35. J. D. White
36-40. J. E. Wolfe
41. G. L. Yoder
42. ORNL Patent Office
43. Central Research Library
44. Document Reference Section
45-46. Laboratory Records Department
47. Laboratory Records (RC)

External Distribution

48-49. Director, Division of Reactor Safety Research, Nuclear Regulatory Commission, Washington, DC 20555
50. Office of Assistant Manager for Energy Research and Development, DOE, ORO, Oak Ridge, TN 37830
51-52. Technical Information Center, DOE, Oak Ridge, TN 37830
53-152. Given distribution as shown in category AN (10-NTIS)